frontiers | Research Topics

Nanobody-based cancer immunotherapy and immunoimaging

Edited by
Zahra Sharifzadeh, Mohammad Ali Shokrgozar and Hans De Haard

Published in
Frontiers in Immunology
Frontiers in Molecular Biosciences

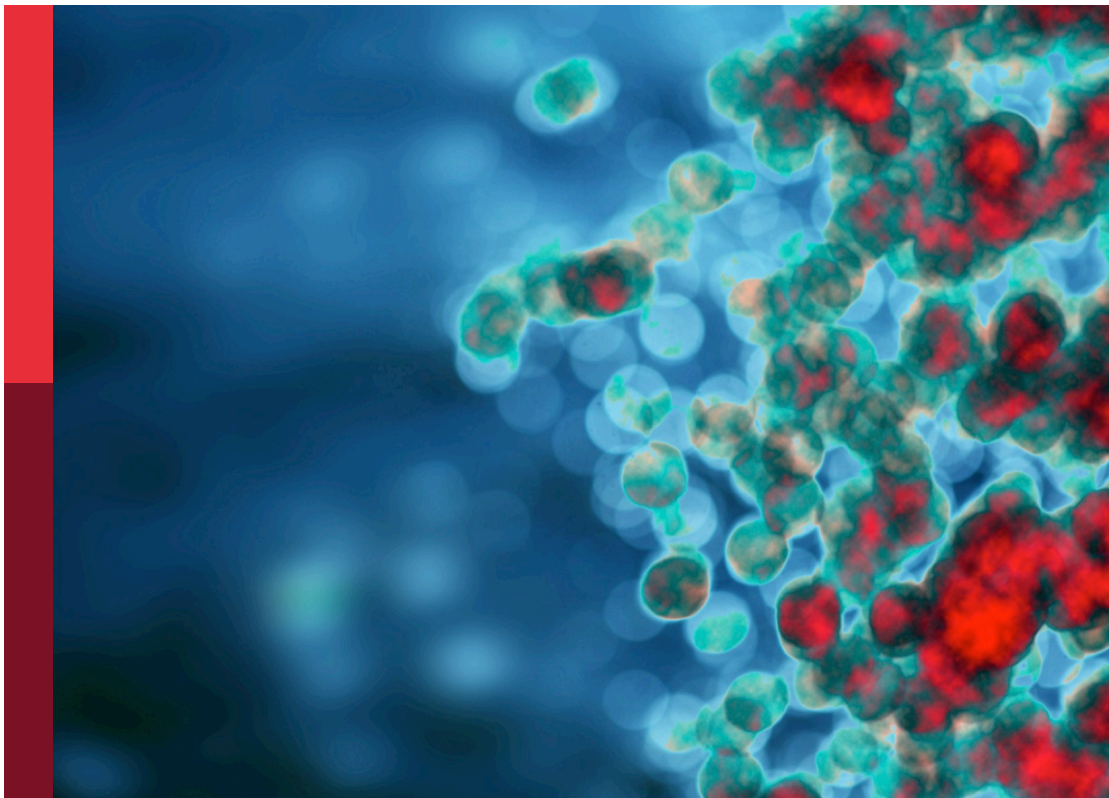

ISSN 1664-8714
ISBN 978-2-8325-2576-0
DOI 10.3389/978-2-8325-2576-0

About Frontiers

Frontiers is more than just an open access publisher of scholarly articles: it is a pioneering approach to the world of academia, radically improving the way scholarly research is managed. The grand vision of Frontiers is a world where all people have an equal opportunity to seek, share and generate knowledge. Frontiers provides immediate and permanent online open access to all its publications, but this alone is not enough to realize our grand goals.

Frontiers journal series

The Frontiers journal series is a multi-tier and interdisciplinary set of open-access, online journals, promising a paradigm shift from the current review, selection and dissemination processes in academic publishing. All Frontiers journals are driven by researchers for researchers; therefore, they constitute a service to the scholarly community. At the same time, the *Frontiers journal series* operates on a revolutionary invention, the tiered publishing system, initially addressing specific communities of scholars, and gradually climbing up to broader public understanding, thus serving the interests of the lay society, too.

Dedication to quality

Each Frontiers article is a landmark of the highest quality, thanks to genuinely collaborative interactions between authors and review editors, who include some of the world's best academicians. Research must be certified by peers before entering a stream of knowledge that may eventually reach the public - and shape society; therefore, Frontiers only applies the most rigorous and unbiased reviews. Frontiers revolutionizes research publishing by freely delivering the most outstanding research, evaluated with no bias from both the academic and social point of view. By applying the most advanced information technologies, Frontiers is catapulting scholarly publishing into a new generation.

What are Frontiers Research Topics?

Frontiers Research Topics are very popular trademarks of the *Frontiers journals series*: they are collections of at least ten articles, all centered on a particular subject. With their unique mix of varied contributions from Original Research to Review Articles, Frontiers Research Topics unify the most influential researchers, the latest key findings and historical advances in a hot research area.

Find out more on how to host your own Frontiers Research Topic or contribute to one as an author by contacting the Frontiers editorial office: frontiersin.org/about/contact

Nanobody-based cancer immunotherapy and immunoimaging

Topic editors

Zahra Sharifzadeh — Department of Immunology, Pasteur Institute of Iran, Iran

Mohammad Ali Shokrgozar — Pasteur Institute of Iran, Iran

Hans De Haard — argenx BVBA, Belgium

Citation

Sharifzadeh, Z., Shokrgozar, M. A., De Haard, H., eds. (2023). *Nanobody-based cancer immunotherapy and immunoimaging*. Lausanne: Frontiers Media SA.

doi: 10.3389/978-2-8325-2576-0

Table of contents

frontiers | Frontiers in Immunology

TYPE Editorial
PUBLISHED 16 May 2023
DOI 10.3389/fimmu.2023.1213386

OPEN ACCESS

EDITED AND REVIEWED BY
Katy Rezvani,
University of Texas MD Anderson Cancer Center, United States

*CORRESPONDENCE
Zahra Sharifzadeh
zsharifzadeh@gmail.com

RECEIVED 27 April 2023
ACCEPTED 10 May 2023
PUBLISHED 16 May 2023

CITATION
Jafari M, Maali A, Shokrgozar MA and Sharifzadeh Z (2023) Editorial: Nanobody-based cancer immunotherapy and immunoimaging.
Front. Immunol. 14:1213386.
doi: 10.3389/fimmu.2023.1213386

Editorial: Nanobody-based cancer immunotherapy and immunoimaging

Mahdie Jafari[1], Amirhosein Maali[1], Mohammad Ali Shokrgozar[2] and Zahra Sharifzadeh[1]*

[1]Department of Immunology, Pasteur Institute of Iran, Tehran, Iran, [2]National Cell Bank of Iran, Pasteur Institute of Iran, Tehran, Iran

KEYWORDS

nanobodies, single domain antibodies, cancer, immunotherapy, immunoimaging

Editorial on the Research Topic
Nanobody-based cancer immunotherapy and immunoimaging

Nanobody, the single domain antibody fragment derived from camelid antibodies, is known as the smallest naturally occurring antibody domain capable to attach to antigens with higher affinity and specificity compared to conventional antibodies (1). Considering their excellent properties, nanobodies have been extensively used in the field of immunotherapy and immunoimaging, especially for cancer diseases (2). The smaller size of nanobodies, compared to other antibody formats, enables them to efficiently penetrate into the tumor site which in turn provides more accessibility to tumor cells for therapeutics and imaging agents. Also, their remarkable stability and solubility together with reduced immunogenicity makes them ideal candidates for tumor targeting (3).

Nanobodies have been used to target cancer cells trough binding to specific cancer antigens. However, they are unable to trigger nanobody-mediated antibody-dependent cellular cytotoxicity (ADCC) and complement-dependent cytotoxicity (CDC) due the the lack of Fc domain. Zhong et al. addressed this problem through fusing a nanobody targeting Claudin18.2 antigen with human IgG1 Fc. They showed the promising therapeutic potential of this humanized nanobody/IgG1-Fc fusion protein on Caludin18.2-positive cancer cells through ADCC and CDC. Moreover, the anti-Caludin18.2 fusion nanobody showed better tumor penetration and faster tumor uptake than a chimeric IgG1 monoclonal antibody.

In addition to direct tumor-targeting, nanobodies are exploited in cell-mediated cancer immunotherapy. In this regard, Maali et al. reviewed the application of nanobodies in bridging between tumor and immune cells through bi- and multi-specific T and NK cells' engagers. Targeting tumor cells with engineered T and NK cells harboring nanobody-based chimeric antigen receptors (CARs) has been discussed as the most successful application of nanobodies in cell-mediated immunotherapy. Also, authors reviewed the different nanobody-based strategies used to enhance anti-tumor functions of macrophages. Finally, the role of nanobodies in reversing the T cell exhaustion and managing the adverse effects of different immune cell therapies is discussed. As a nanobody-based cell therapy, Nasiri et al. successfully developed second generation CAR-T cells to target CD19-positive tumor cells. They showed that the nanobody-redirected CAR-T cells had

expansion, cytotoxicity and proinflammatory cytokine secretion rates comparable to those of their scFv-based counterparts.

As mentioned above, nanobodies may act as the blockers of antigens, receptors, or intracellular mediators. In an interesting approach, Demeules et al. studied the *in vivo* purinergic checkpoint inhibition by different specific nanobodies expressed through adeno-associated viral vectors. Nanobody-mediated blocking of P2X7, a ligand-gated cation channel, significantly inhibited tumor growth in P2X7-expressing tumor models. Moreover, a bispecific nanobody-based biologic targeting CD73 (an ecto-enzyme catalyzing extracellular ATP into immunosuppressive adenosine) and PD-L1 successfully inhibited the growth and metastasis of tumor cells. Also, Keller et al. employed the intracellular expression of a nanobody specific to the GTP-bound conformation of RHOA subfamily GTPases to distrupt the RHOA/ROCK signaling pathway. They established that this functional intracellular nanobody resulted in the loss of cellular contraction properties in metastatic melanoma cells which may have implication in cancer therapy. Genetically modifying nanobodies has enabled a new generation of receptor-specific probes that target EGFR. Comez et al. discovered two nanobodies that bind to the same receptor site as EGF and other ligands that bind to EGFR. Using the NanoBRET technology, they could monitor the G protein-coupled receptor ligand binding and conformational changes of EGFR. This study proved the hopeful function of nanobodies for studying the role of the EGFR in health and disease.

Regarding their small size, single domain nature and improved stability, nanobodies represent promising candidates for facilitated delivery to the brain. Zheng et al. reviewed the application of nanobodies as research tools, diagnostic agents and therapies in brain diseases, focusing on brain tumors, Alzheimer's disease, and Parkinson's disease. In this study, they provide an overview of the different methods for transportation of nanobodies to the brain. The natural methods of brain-blood-barrier (BBB) penetration include passive diffusion, active efflux, carrier-mediated transport and transcytosis. Other strategies of cerebral delivery of nanobodies employ the structures with the ability to pass the brain as well as some means that temporarily increase the BBB permeability.

CD38 is a tumor antigen which is overexpressed in multiple myeloma, and has emerged as an ideal therapeutic target for cancer therapeutics. Hambach et al. reviewed the application of nanobody-based biologics including heavy chain antibodies, bispecific or trispecific killer cell engagers (BiKEs or TriKEs), CAR-NK cells, and nanobody-displaying adeno-associated viral vectors in efficient targeting of CD38-expressing myeloma cells. Detection of multiple myeloma in patients treated with daratumumab, a CD38-specific monoclonal antibody, is difficult due to the overlapping binding sites of daratumumab and CD38-specific imaging antibodies. Pape et al. developed a nanobody that identifies a unique, non-overlapping epitope on CD38 and labeled it with Alexa Fluor 680. This nanobody could preferentially bind to CD38 on myeloma cells, allowing selective imaging of CD38-expressing xenografts in daratumumab-pretreated mice.

In recent years, oncolytic viruses (Ovs) have emerged as a worthwhile treatment option in cancer therapy. Jafari et al. reviewed the role of combining oncolytic virotherapy and antibody-based therapeutic approaches in cancer. They discussed the benefits of OVs' combination with antibodies, nanobodies, CAR T cells, and antigen presenting cells to reduce side effects and boost anti-tumor efficacy. The results of ongoing clinical trials can help researchers create innovative combination therapy systems and bring forth ground-breaking treatments for patients. Kadkhodazadeh et al. investigated whether the SpyTag-SpyCatcher system can modulate adenovirus (Ad) tropism and induce covalent virus-adaptor molecule interactions. SpyCatcher was genetically fused with a VEGFR2-specific nanobody to develop a retargeted Ad vector. The recombinant Ad vector, which included a SpyTag peptide in its HI loop, could efficiently target VEGFR2-expressing cells via the primary Ad receptor-independent pathway. The results indicated that this functionalized Ad vector has therapeutic promise for cancer. This viral vector may target additional ligands for theranostic purposes and reduce the hepatotoxicity of systemic Ad delivery.

Considering the advantages of nanobodies and their applications, as well as the research cited regarding the use of nanobodies in the treatment and detection of different diseases, particularly cancer, it can be concluded that nanobodies could definitely be employed as an effective therapeutic and diagnostic agent.

Author contributions

All authors listed have made a substantial, direct, and intellectual contribution to the work and approved it for publication.

Acknowledgments

We are grateful to all authors who contributed to this Research Topic.

Conflict of interest

The authors declare that the research was conducted in the absence of any commercial or financial relationships that could be construed as a potential conflict of interest.

Publisher's note

References

1. Kijanka M, Dorresteijn B, Oliveira S, van Bergen en Henegouwen PM. Nanobody-based cancer therapy of solid tumors. *Nanomed (London England)* (2015) 10(1):161–74. doi: 10.2217/nnm.14.178

2. Lecocq Q, De Vlaeminck Y, Hanssens H, D'Huyvetter M, Raes G, Goyvaerts C, et al. Theranostics in immuno-oncology using nanobody derivatives. *Theranostics* (2019) 9(25):7772–91. doi: 10.7150/thno.34941

3. Verhaar ER, Woodham AW, Ploegh HL. Nanobodies in cancer. *Semin Immunol* (2021) 52:101425. doi: 10.1016/j.smim.2020.101425

frontiers | Frontiers in Immunology

ORIGINAL RESEARCH
published: 28 June 2022
doi: 10.3389/fimmu.2022.885424

OPEN ACCESS

Edited by:
Mohammad Ali Shokrgozar, Pasteur institute of Iran, Iran

Reviewed by:
Serge Muyldermans, Vrije University Brussel, Belgium
Lifei Hou, Boston Children's Hospital and Harvard Medical School, United States
Susan Hagen, Beth Israel Medical Center, United States
Cai Huang, AB Therapeutics Inc, United States
Pingzhu Zhou, Boston Children's Hospital and Harvard Medical School, United States
Heng Zheng, China Pharmaceutical University, China

***Correspondence:**
Yanshan Huang
yanshanhuang@doerbio.com
Weilin Wang
wam@zju.edu.cn

†*These authors have contributed equally to this work*

Specialty section:
This article was submitted to Cancer Immunity and Immunotherapy, a section of the journal Frontiers in Immunology

Received: *28 February 2022*
Accepted: *30 May 2022*
Published: *28 June 2022*

Citation:
Zhong W, Lu Y, Ma Z, He Y, Ding Y, Yao G, Zhou Z, Dong J, Fang Y, Jiang W, Wang W and Huang Y (2022) Development of a Humanized VHH Based Recombinant Antibody Targeting Claudin 18.2 Positive Cancers. Front. Immunol. 13:885424. doi: 10.3389/fimmu.2022.885424

Development of a Humanized VHH Based Recombinant Antibody Targeting Claudin 18.2 Positive Cancers

Weixiang Zhong[1†], Yimin Lu[2†], Zhe Ma[3], Yinjun He[4], Yongfeng Ding[2], Gaofeng Yao[3], Zhenxing Zhou[3], Jiali Dong[3], Yongliang Fang[3], Weiqin Jiang[5], Weilin Wang[6] and Yanshan Huang[3*]*

[1] *Department of Pathology, The First Affiliated Hospital, School of Medicine, Zhejiang University, Hangzhou, China,* [2] *Department of Surgical Oncology, The First Affiliated Hospital, School of Medicine, Zhejiang University, Hangzhou, China,* [3] *Department of Innovative Drug Discovery and Development, Zhejiang Doer Biologics Co., Ltd., Hangzhou, China,* [4] *School of Medicine, Zhejiang University, Hangzhou, China,* [5] *Department of Medical Oncology, The First Affiliated Hospital, School of Medicine, Zhejiang University, Hangzhou, China,* [6] *Department of Hepatobiliary and Pancreatic Surgery, The Second Affiliated Hospital, School of Medicine, Zhejiang University, Hangzhou, China*

Claudin 18.2 (CLDN18.2), a tight junction (TJ) family protein controlling molecule exchange between cells, is frequently over-expressed in gastric cancer, pancreatic adenocarcinomas and in a fraction of non–small cell lung cancer cases. The tumor properties indicate that CLDN18.2 could be an attractive drug target for gastric and pancreatic cancers. In this study, we present effective strategies for developing anti-CLDN18.2 therapeutic candidates, based on variable domain of heavy chain of heavy chain antibodies (VHHs). CLDN18.2-specific VHHs were isolated by panning a phage display library from an *alpaca* immunized with a stable cell line highly expressing CLDN18.2. Humanized VHHs fused with human IgG1 Fc, as potential therapeutic candidates, exhibited desirable binding specificity and affinity to CLDN18.2. *In vitro* experiments showed that hu7v3-Fc was capable of eliciting both antibody-dependent cellular cytotoxicity (ADCC) and complement-dependent cytotoxicity (CDC) on CLDN18.2 positive tumor cells. In the mouse xenograft model, the anti-tumor efficacy of hu7v3-Fc was significantly more potent than Zolbetuximab, the benchmark anti-CLDN18.2 monoclonal antibody. Moreover, *in vivo* biodistribution using zirconium-89 (^{89}Zr) labeled antibodies demonstrated that hu7v3-Fc (^{89}Zr-hu7v3-Fc) exhibited a better tumor penetration and a faster tumor uptake than Zolbetuximab (^{89}Zr-Zolbetuximab), which might be attributed to its smaller size and higher affinity. Taken together, anti-CDLN18.2 hu7v3-Fc is a promising therapeutic agent for human CLDN18.2 positive cancers. Furthermore, hu7v3 has emerged as a potential module for novel CLDN18.2 related therapeutics.

Keywords: Claudin 18.2, VHH, gastric cancer, pancreatic cancer, ADCC, CDC

INTRODUCTION

Gastric cancer (GC) and pancreatic cancer (PC), both accounted for 12.4% of all cancer mortalities in 2020 (1), are among the leading causes of cancer-related deaths worldwide. Due to insufficient early symptoms, patients with gastric cancer and pancreatic cancer are usually diagnosed at advanced stages with poor prognosis. Although various therapeutic approaches, such as chemotherapies, immunotherapies and targeted therapies, have been developed, the 5-year survival rates for patients with advanced GC and PC are still dismal (2, 3).

Claudin 18 (CLDN18) is a member of the claudin family with four transmembrane domains. CLDN18 has two extracellular loops, loop 1 and loop 2. CLDN18 has two splice variants in human, CLDN18.1 and CLDN18.2, which differ by 21 amino acids among the first 69 amino acids at the N-terminus but only 8 amino acids in the extracellular domain 1 (4). In normal healthy tissues, CLDN18.1 is strictly expressed on epithelial cells of lung tissue, while CLDN18.2 is confined to differentiated epithelial cells in stomach, such as mucous cells, parietal cells and chief cells (5, 6). However, CLDN18.2 is abnormally expressed in multiple cancers, including diffuse-type GC (7), PC (5, 8, 9), esophageal adenocarcinomas (10) and a small proportion of non–small cell lung cancer (11).

The variable domains of heavy chain of heavy chain antibodies (VHHs) represent the smallest naturally derived antigen-recognizing domains. Because of the significantly smaller in size than conventional monoclonal antibodies, VHHs could have a better tumor penetration and a faster tumor uptake than conventional monoclonal antibodies (12). Moreover, VHHs are highly stable and could be easily employed as building blocks for multiple formats of bi-specific antibodies and tri-specific antibodies with high affinity and avidity (13, 14). Thus, VHHs have certain advantages over conventional IgG in antibody drug development.

Here in this study, we present effective strategies for developing anti-CLDN18.2 VHH antibodies with high affinity and specificity. hu7v3-Fc, one of the humanized candidates fused with human IgG1 Fc, showed antibody-dependent cellular cytotoxicity (ADCC) and complement-dependent cytotoxicity (CDC) on CLDN18.2 positive tumor cells *in vitro*. Meanwhile in the mouse xenograft model, hu7v3-Fc demonstrated strong efficacy of anti-tumor and nuclides targeted delivery ability, indicating that it is a promising therapeutic agent for human CLDN18.2 positive cancers.

MATERIALS AND METHODS

Cell Lines and Culture Conditions

CHO-K1, CHO-CLDN18.1-GFP (CLDN18.1 and GFP co-expressing) and CHO-CLDN18.2-GFP (CLDN18.2 and GFP co-expressing) cells were cultured in CD02 medium (Quacell) at 37°C in a 5% CO_2 incubator with constant agitation at 120 rpm. ADCC bioassay effector cells were maintained in 90% RPMI1640 medium (BasalMedia) with L-glutamine and 10% fetal bovine serum (FBS, ExcellBio), 100 μg/mL hygromycin (Invivogen), 250 μg/mL G-418 sulfate solution (Invivogen), sodium pyruvate (1 mM, Gibco) and MEM non-essential amino acids (0.1 mM, Gibco), at 37°C in a humid incubator with 5% CO_2. SNU-620 (human gastric cancer cell line with endogenous CLDN18.2 expression) and NUGC4-CLDN18.2 (human gastric cancer cell line with exogenous CLDN18.2 expression) cells were grown in RPMI1640 medium supplemented with 10% FBS. MIA PaCa-2-CLDN18.2 cells (human pancreatic cancer cell line with exogenous CLDN18.2 expression) were grown in DMEM high glucose medium supplemented with 10% FBS.

Phage Library Construction

A healthy female *alpaca* was immunized with 1.0×10^7 CHO-CLDN18.2-GFP cells, with Freund's adjuvant (Sigma) as an immunopotentiator. A total of three immunizations were performed with an interval of 21 days between each immunization. Next, 30 mL of *alpaca* whole blood was harvested in a vacuum blood collection tube a week after the final immunization. Lymphocytes were then isolated using separation medium (Ficoll-Paque Plus, Sigma). Extracted total RNA (Trizol, Ambion) was used as a template for synthesizing cDNA by reverse transcription (Super Scrip III First Strain, Invitrogen). Synthesized cDNA was used as a template for the NEST polymerase chain reaction (PCR) to amplify the VHH sequences. The amplification primers for the first round of PCR were 5′-CTTGGTGGTCCTGGCTGC-3′ and 5′-ggtacgtgctgttgaactgttcc-3′. The products from the first round of PCR were used as a template for the second round. The forward and reverse primers used in the second round PCR were 5′-CATGCCATGACTGTGGCCCAGGCGGCCCAGKTGCAGC TCGTGGAGTC-3′ and 5′-CATGCCATGACTCG CGGCCGGCCTGGCCGTCTTGTGGTTTTGGTGTCTTGGG-3′, respectively. Amplified VHH fragment products were collected with a gel extraction kit (BioMIGA). Purified fragments were digested by *Sfi*I (NEB) and then ligated to phagemid pCom3xss (Addgene, #63890). The ligation products were transformed into an *Escherichia coli*–competent strain, ER2738, by electroporation.

Bio-panning of CLDN18.2 VHH

The cloned VHH repertoire was expressed at the tip of M13 virions with the assistance of M13KO7 helper phage (NEB). CHO-K1 and CHO-CLDN18.2-GFP cells were used in the first round of bio-panning to eliminate non-specific phage binders and enrich positive phages. Briefly, 4.5×10^7 CHO-K1 cells were washed with phosphate-buffered saline (PBS) before being blocked with 2% milk powder. A phage library (approximately 5.7×10^{11} plaque-forming units) was added to the blocked CHO-K1 cells and rotated at 4°C for 1 h. Cells were pelleted to collect the supernatant which was then added to the blocked CHO-CLDN18.2-GFP cells (1.5×10^7 cells) and incubated at 4°C for 1 h. To elute bound phages, cells were pelleted and washed before being resuspended in 1 mL of 0.1 M Glycine-HCl (pH 2.2) with 1 mg/mL bovine serum albumin (BSA, Sango Biotechnology). After centrifugation, the supernatant was collected and neutralized with 1 M Tris-HCl (pH 8.0). The solution containing the enriched phage particles with CLDN18.2-specific VHH was used to infect 5 mL of logarithmic phase

ER2738. Negative screening (by CHO-K1 cells and CHO-CLDN18.1-GFP cells) and positive screening (by CHO-CLDN18.2-GFP cells) was performed for another two rounds of panning before anti-CLDN18.2 phages were enriched. Eighty clones were randomly picked and cultured in a deep 96-well plate at 37°C. Cultures were then infected with M13KO7 helper phages to rescue and express the VHH at the tip of phage particles.

The cellular enzyme-linked immunosorbent assay was used to determine positive clones. The supernatant from the phage clones was diluted with 3% BSA. 50 μL of diluted phages were added to 96-well microtiter plates containing 50 μL of BSA-blocked CHO-K1, CHO-CLDN18.1-GFP, and CHO-CLDN18.2-GFP cells (5×10^5 cells each well). Mouse anti-M13 phage-horseradish peroxidase conjugate (Sinobiological) was used as a detection antibody, and tetramethylbenzidine was used as a visualizing agent. The reactions were terminated by 2 M H_2SO_4, and absorption was measured at 450 nm by a VersaMax microplate reader (Molecular Devices). Eighteen putative positive clones were further sequenced and eight unique clones were obtained finally.

Humanization, Expression and Purification

Anti-CLDN18.2 VHHs were humanized as described previously (15). Briefly, complementarity determining regions (CDR1, CDR2 and CDR3) of the $NbBcII10_{FGLA}$ (PDB:3EAK) scaffold were replaced with the corresponding region of anti-CLDN18.2 VHHs, according to the International ImMunoGeneTics information system (IMGT) amino acid numbering. Furthermore, crucial amino acid residues of FR2 were substituted to mimic the human DP-47 reference sequence, in order to improve the physicochemical properties.

The DNA fragment coding for the human IgG1 Fc (16), containing the full hinge region (EPKSSDKTHTCPPCP), was fused to the DNA fragment coding for the full length of VHH and cloned into the pcDNA3.1 expression plasmid. VHH-Fc encoding plasmids were introduced into HEK293F cells with polyethyleneimine (Polysciences, Inc.). The transfected cells were cultured for 7 days and supernatant was harvested. The desired products were further purified with Protein A affinity column (BestChrom). The benchmark Zolbetuximab were expressed and purified following the patent US9751934B2.

Immunohistochemistry

The frozen tissue section slides were fixed in acetone for 15 minutes and subsequently washed by PBS. Endogenous peroxidases and non-specific binding were blocked by incubating with 3% hydrogen peroxide for 10 minutes and with 3% BSA, respectively. Slides were incubated with primary antibodies for 30 minutes at room temperature, followed by a 30-minute incubation with horseradish peroxidase-conjugated goat anti human IgG antibodies (Thermofisher). Antibody binding was visualized by incubating with the peroxidase substrate 3,3'-diaminobenzidine (DAB, GeneTech) for 5 minutes. After counterstaining with hematoxylin (Sangon Biotechnology), tissue sections were analyzed using light microscopy (Nikon).

Antibody-Dependent Cellular Cytotoxicity Assay

The reporter-based surrogate ADCC bioassay was carried out with Jurkat cells, engineered to express FcγRIIIa and an NFAT response element driving expression of firefly luciferase, as effector cells. Briefly, 1.5×10^5 ADCC bioassay effector cells (E) were mixed with 3×10^4 CHO-CLDN18.2-GFP target cells (T) to make the final E:T = 5:1, for a final volume of 50 μL in a U-bottom plate. Test antibodies were then serially diluted into a final volume of 25 μL and added to the assay system before placed in a CO_2 incubator for 20 h. Finally, 75 μL of BIO-Glo Luciferase Assay Reagent (Promega) was added to the assay system to measure luminescence using a SpectraMax i3 (Molecular Devices).

Peripheral blood mononuclear cells (PBMCs) were used as effector cells and SNU-620 cells were used as target cells in PBMC-based assays. Briefly, 5.0×10^5 PBMCs were mixed with 2×10^4 SNU-620 cells to make the final E:T ratio 25:1, for a final volume of 100 μL in a U-bottom plate. Test antibodies were then serially diluted into a final volume of 50 μL and added to the assay system before incubated for 20 h. The culture supernatants were collected and applied to LDH release assay (Promega).

Complement-Dependent Cytotoxicity Assay

Complement-dependent cytotoxicity was assessed by flow cytometry. Briefly, CHO-CLDN18.2-GFP and NUGC-CLDN18.2 were harvested and resuspended in Opti-MEM medium (Thermofisher). Cell density was adjusted to 1×10^6 cells/ml and 50 μl of cells was seeded into each well. 50 μl of test antibodies at various concentration and 50 μl of human AB serum (15%, Schbio) used as a source of the complement were added into each well. The plate was placed at 37°C in a 5% CO_2 incubator for 2 hours. Thereafter, add 50 μl of propidium iodide (PI, Thermofisher) into each well and analyze the cells using a flow cytometer immediately.

Xenograft Tumor Model

To establish human gastric cancer or pancreatic cancer xenograft models, six-eight weeks old female CB17 SCID mice (Vital River Laboratory) were subcutaneously injected with 1×10^7 SNU-620 cells or 1×10^7 MIA PaCa-2-CLDN18.2 cells, mixed with Matrigel Matrix (Corning) with a ratio of 1:1. The mice were randomly divided into five groups: PBS as a vehicle control, 5.7 mg/kg Zolbetuximab as a positive control, 0.3 mg/kg, 1.0 mg/kg and 3.0 mg/kg hu7v3-Fc as the experimental groups, when the tumor volumes reached 170 mm^3 or 236 mm^3. Test antibodies were given by intraperitoneal injection three times per week (TIW) for five weeks.

Tumor volume were measured twice per week with a vernier caliper and determined according to the following equation: Tumor volume (mm^3) = 1/2 length × width^2. After the mice were sacrificed, the tumors were dissected and photographed.

In vivo Biodistribution Studies

In vivo biodistribution studies were performed using a SUN-620 xenograft mouse model to compare the tumor update between

hu7v3-Fc and Zolbetuximab. Both hu7v3-Fc and Zolbetuximab were radiolabeled with zirconium-89 (^{89}Zr), formulated, and administered to mouse respectively (17). Mice were anesthetized and sacrificed at 4, 24, 48, 72, 96, 120 h, respectively. The amounts of radioactivity in interest tissues (Brain, heart, liver, spleen, lung, kidney, muscle, bone and the tumor) were measured with a gamma counter. Radioactivity uptake was calculated as the percentage of the injected dose per gram of tissue (%ID/g).

Statistical Analysis

All statistical analyses were performed with Graphpad Prism 6 software. Experimental data were expressed as mean ± SD or mean ± SEM. Two-group comparisons were analyzed by Student's *t* test. $p < 0.05$ was considered significant.

RESULTS

Library Construction and Bio-panning

As a membrane protein with four transmembrane domains, it is challenging to prepare purified recombinant CLDN18.2 protein in its native conformation. In this study, we constructed a phage display library after immunization of an *alpaca* with CHO-CLDN18.2-GFP cells, which overexpress the full length of CLDN18.2. VHH gene segments were cloned into a phagemid vector, resulting in a phage library of 1.23×10^8 size.

After three rounds of bio-panning, eighty clones were randomly picked for CLDN18.2-binding test, and 18 potential positive clones were identified. After sequence analysis, eight unique sequences were successfully obtained. Compared with conventional VH region, of which the framework region 2 (FR2) has highly conserved hydrophobic amino acids (Val42, Gly49, Leu50 and Trp52) (18), the four amino residues are substituted for more hydrophilic amino acids (Tyr42, Glu/Gln49, Arg50 and Leu/Phe52) in our isolated VHHs (**Figure 1A**). Meanwhile, all the clones have longer CDR3 loops with 14~16 amino acids, which is a typical feature of VHHs (19). Using the anti-CLDN18.2-7 as an example, all the VHHs were further humanized as described previously (15). To increase stability, solubility, and affinity, crucial amino acid residues were substituted to obtain an optimum version of humanized VHH, anti-CLDN18.2-hu7v3 (**Supplementary Figure S1**). The humanized VHH was fused to the Fc domain of human IgG1 to produce a homodimer chimeric protein, anti-CLDN18.2-hu7v3-Fc (simplified as hu7v3-Fc), capable of bivalent binding, ADCC and CDC activities (**Figure 1B**). Three of the Fc fusion proteins, hu7v3-Fc, hu28v3-Fc and hu69v3-Fc, showed higher affinity to CLDN18.2 than others (**Supplementary Figure S2**). As hu28v3-Fc and hu69v3-Fc showed lower solubility and stronger aggregation (data not shown), we chose hu7v3-Fc as a leading drug candidate.

Characterization of hu7v3-Fc

The specificity of hu7v3-Fc to recognize CLDN18.2 membrane protein was evaluated. In flow cytometry assays, the Zolbetuximab (benchmark) and human IgG1 isotype were employed as a positive control and a negative control, respectively. As shown

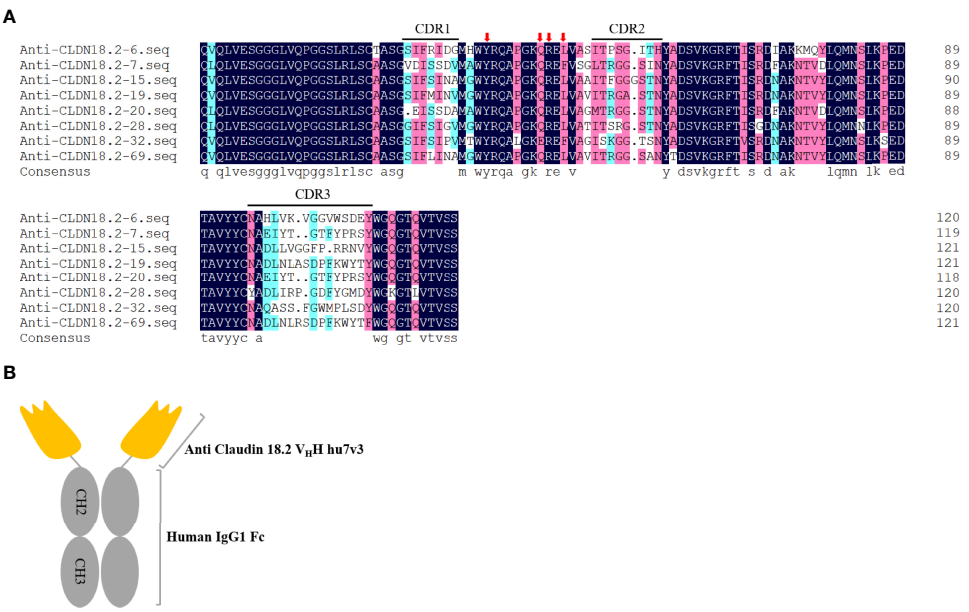

FIGURE 1 | Isolation of anti-CLDN18.2 VHH variants. **(A)** Amino acid sequences of anti-CLDN18.2 VHHs. Sequences are presented using one-letter amino acid abbreviations. DNAMAN was used to generate the alignment. Complementarity determining regions (CDRs) are shown. Four hydrophilic amino acids (Tyr42, Glu/Gln49, Arg50 and Leu/Phe52) critical for humanization are indicated with red arrows. **(B)** Schematic composition of hu7v3-Fc structure in this study. Anti CLDN18.2 VHH hu7v3 is indicated in orange, and the human IgG1 Fc domain including the hinge, CH2 and CH3 domains is indicated in gray.

in **Figure 2A**, MFI signals of hu7v3 and Zolbetuximab on CHO-CLDN18.2-GFP cells were significantly higher than that on CHO-CLDN18.1 cells, indicating an excellent specificity of hu7v3 to CLDN18.2 positive cells.

Because the expression of CLDN18.2 is strictly confined to the differentiated epithelial cells of the gastric mucosa, the binding specificity of hu7v3-Fc was also assessed with IHC. As demonstrated in **Figure 2B** and **Supplementary Figure S3**, only stomach antrum and stomach body tissue specimens showed strong positive staining for hu7v3-Fc, whereas other tissue specimens did not react with hu7v3-Fc. The binding affinity to CLDN18.2 was furtherly analyzed. As calculated from dose-responsive curves, hu7v3-Fc, with a K_D value of 1.32×10^{-9} M, shows a higher affinity to CLDN18.2 than Zolbetuximab (**Supplementary Figure S4**).

ADCC and CDC Efficacy of hu7v3-Fc

To determine the ability of hu7v3-Fc to trigger ADCC, reporter-based surrogate assay was performed, using engineered Jurkat cells expressing FcγRIIIa and NFAT response element-driven firefly luciferase as effector cells. PBMC-based LDH release assay was also performed. In the surrogate assay, the ADCC of hu7v3-Fc (EC_{50} = 0.007 nM) was 12.4-fold greater than that of Zolbetuximab (EC_{50} = 0.087 nM) against CHO-CLDN18.2-GFPs (**Figure 3A**). In the PBMC-based assay, the gastric cell line SNU-620 cells which endogenously express CLDN18.2 were used the target cells. The activity of hu7v3-Fc (EC_{50} = 2.583 ng/ml) to mediate ADCC was 82.7-fold higher than that of Zolbetuximab (EC_{50} = 397.0 ng/ml), while the human IgG1 isotype failed to produce an obvious dose-dependent signal curve (**Figure 3B**), indicating the CLDN18.2 specific mechanism of action of hu7v3-Fc.

The CDC capacity of hu7v3-Fc was assessed using human AB serum as a source of complement and NUGC4-CLDN18.2 and CHO-CLDN18.2-GFP, both over-express CLDN18.2 (**Supplementary Figure S5A**), as target cells. Of note, flow cytometry analysis demonstrated that hu7v3-Fc and Zolbetuximab exhibited similar CDC activities on both target

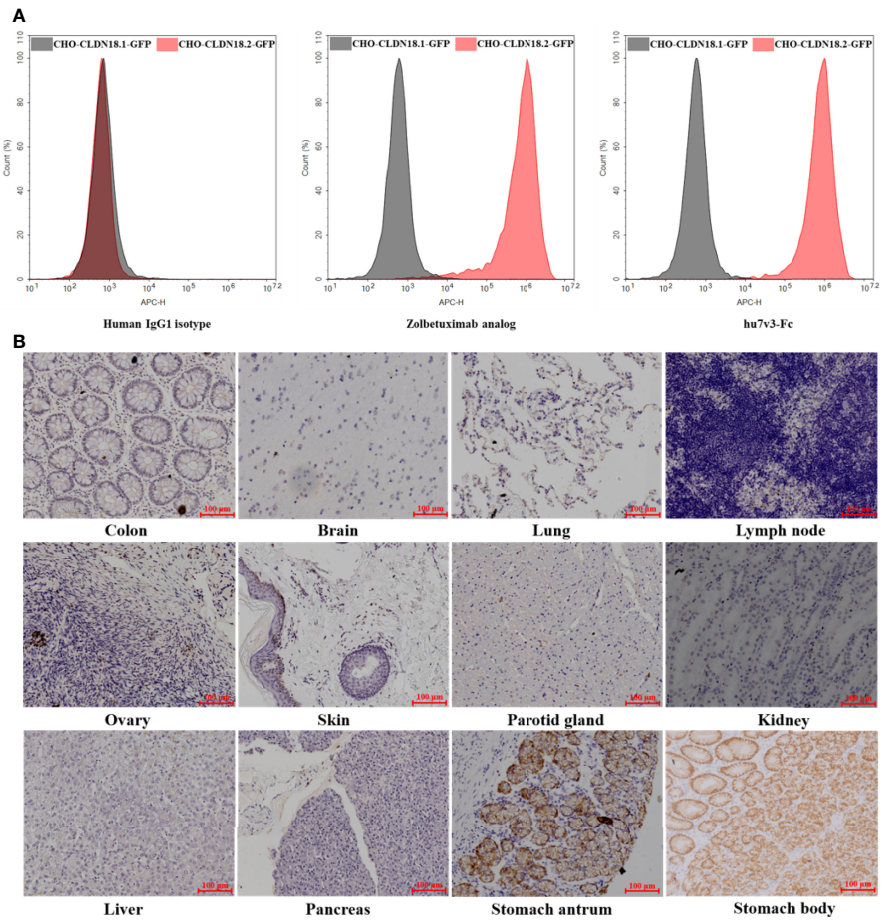

FIGURE 2 | Characterization of anti-CLDN18.2 hu7v3-Fc. **(A)** Flow cytometric analysis to determine the specificity of hu7v3-Fc to CLDN18.2. Zolbetuximab was employed as the positive control antibody, and human IgG1 isotype as the negative control antibody. CLDN18.1 and CLDN18.2 was co-expressed with GFP in CHO-CLDN18.1-GFP and CHO-CLDN18.2-GFP cells, respectively. **(B)** IHC analysis to determine the specificity of hu7v3-Fc to CLDN18.2. Frozen sections of colon, brain, lung, lymph node, ovary, skin parotid gland, kidney, liver, pancreas, stomach antrum and stomach body were obtained from healthy tissue in The First Affiliated Hospital of Zhejiang University.

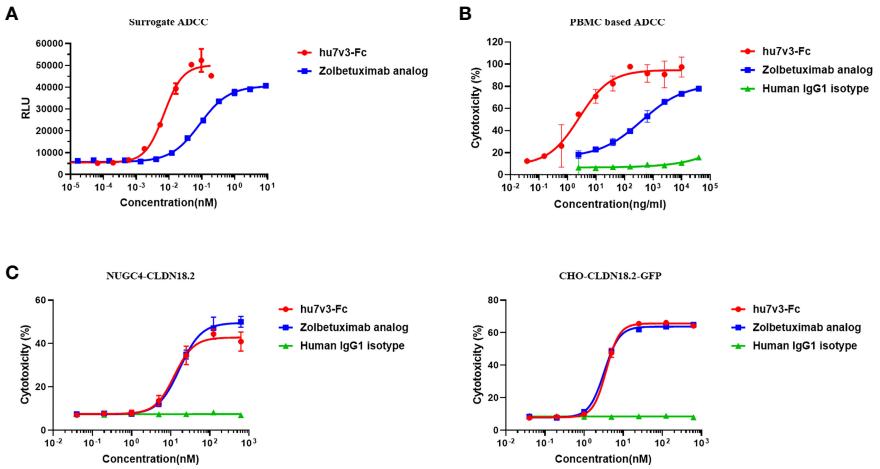

FIGURE 3 | Cytotoxicity analysis of hu7v3-Fc. **(A)** The surrogate ADCC analysis of hu7v3-Fc. Jurkat cells, engineered to express FcγRIIIa and NFAT response element-driven firefly luciferase were used as the effector cells, and CHO-CLDN18.2-GFP cells were used as target cells. The effector to target ratio was 5:1. **(B)** PBMC based ADCC analysis of hu7v3-Fc. Human PBMCs isolated form whole blood were used as the effector cells, and SNU-620 were used as the target cells. The effector to target ratio was equal to 25:1. **(C)** CDC analysis of hu7v3-Fc. Human AB serum was used as a source of the complement, with NUGC4-CLDN18.2 (left) cells and CHO-CLDN18.2-GFP (right) cells as the target cells, respectively.

cells, while the IgG1 isotype control showed no obvious CDC activity (**Figure 3C**). Although hu7v3 opsonized cells are better at binding to C1q, this binding does not translate directly to a higher CDC activity (**Supplementary Figure S5.B**).

Antitumor Activity of hu7v3-Fc *in vivo*

Next, we evaluated the antitumor effect of hu7v3-Fc using a human gastric cancer cell line SNU-620 cells xenograft model. The results indicated that SNU-620 tumor growth was significantly suppressed in mice even treated with low dosage of hu7v3-Fc (0.3 mg/kg), compared with PBS-treated group of mice. Meanwhile, the inhibitory effect of 3 mg/kg hu7v3-Fc on tumor growth was stronger than that of equal molar dosage (5.7 mg/kg) of Zolbetuximab (tumor growth inhibition (TGI): 104.5% vs 84.5%, $p < 0.05$) (**Figure 4A** and **Supplementary Table 1**).

A human pancreatic cancer cell line MIA PaCa-2-CLDN cells derived xenograft model was also created to assess the antitumor efficacy of hu7v3-Fc. As shown in **Figure 4C** and **Supplementary Table 2**, all the dosages of hu7v3-Fc (0.3 mg/kg, 1.0 mg/kg, 3.0 mg/kg) have stronger anti-tumor effects than Zolbetuximab (5.7 mg/kg). There were no significant differences in the body weight between the five groups (**Figures 4B, D**), suggesting that hu7v3-Fc is a safe and promising therapeutic candidate.

Biodistribution Studies

Biodistribution studies with ^{89}Zr-hu7v3-Fc and ^{89}Zr-Zolbetuximab were investigated in a SUN-620 subcutaneous xenograft model. *In vivo* biodistribution at 4, 24, 48, 72, 96, 120 h post-injection was showed in **Figures 5A, B**. Compared with ^{89}Zr-Zolbetuximab, ^{89}Zr-hu7v3-Fc showed faster tumor uptake and better tumor penetration at all time points, and its accumulation in tumor tissue reached a plateau (49.43 ± 9.86 ID %/g) at 72 h. Meanwhile, ^{89}Zr-hu7v3-Fc revealed higher tumor-to-muscle ratio and comparable tumor-to-liver ratio to ^{89}Zr-Zolbetuximab (**Supplementary Figure S6**).

DISCUSSION

Globally, Gastric cancer is the 4th most common malignancy and the 2nd leading cause of cancer mortality (20, 21); while pancreatic cancer is the 12th most common malignant disease and the 7th leading cause of cancer death (22). Even with effective early diagnosis, many patients are diagnosed with advanced or metastatic disease. Among the patients with advanced or metastatic stage, the survival outcomes are still dismal; the 5-year survival rate is less 20% for gastric cancer (23) and is only 2% for pancreatic cancer (24). Therefore, there are urgent unmet clinical needs for both of gastric cancer and pancreatic cancer.

In normal tissue, Claudin 18.2 is strictly expressed in gastric mucosa. However, the expression of CLDN18.2 is frequently ectopic activated in a diversity of human cancers (4), such as gastric cancer and pancreatic cancer. These characteristics suggest CLDN18.2 can be an ideal molecule for targeted therapy. Up to now, there were no approved antibody drugs against Claudin 18.2. Zolbetuximab, a chimeric IgG1 monoclonal antibody, is the first-in-class antibody drug under clinical development that specifically binds to CLDN18.2 and mediates cell death by triggering ADCC and CDC activities (25). Phase II clinical trial revealed that, for the overall population, both progression-free survival (PFS) and overall survival (OS) were significantly improved in zolbetuximab combined with EOX group, as compared with those in EOX alone group (median PFS: 7.5 months vs 5.3 months, $p < 0.0005$; median OS: 13.0 months vs 8.3 months, $p < 0.0005$) (26). The most

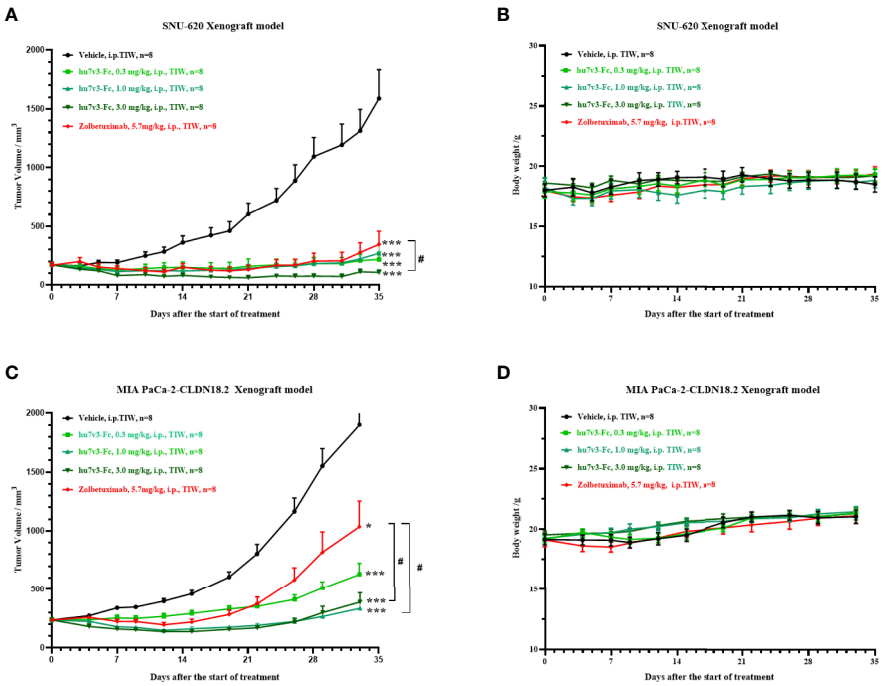

FIGURE 4 | *In vivo* tumor inhibition efficacy of anti-CLDN18.2 7v3-Fc. **(A, C)** Tumor growth curves of SNU-620 and MIA PaCa-2-CLDN18.2 bearing mice injected with different formulations, respectively. **(B, D)** Body weight changes of SNU-620 and MIA PaCa-2-CLDN18.2 bearing mice injected with different formulations, respectively.Data are shown as mean ± SEM, n = 8, *p < 0.05, ***p < 0.001 (vs Vehicle); #p< 0.05 (vs Zolbetuximab).

adverse events related to therapy include grade 1-2 of nausea, vomiting, neutropenia and anaemia, indicating the safety of CLDN18.2-targeting strategy in gastric cancer. Meanwhile, preclinical studies demonstrated that zolbetuximab mediated antitumor activity *via* inducing ADCC and CDC in pancreatic cancer models (27). Other alternative CLDN18.2-targeting therapeutic agents, such as CAR-T (NCT03890198, NCT03159819), bispecific antibody (NCT04260191) and ADC (NCT05009966, NCT04805307), are also ongoing.

Since the discovery of heavy chain only antibodies from camelid family in 1993, the application field of the VHHs has been rapidly growing. Being significantly smaller in size than the conventional monoclonal antibodies, VHHs usually have a better tumor penetration and a faster tumor uptake than conventional monoclonal antibody, as we demonstrated in **Figure 5**. This is a big advantage of VHHs compared to conventional monoclonal antibody drugs. Moreover, their longer CDR3 loops allows them to access the buried or

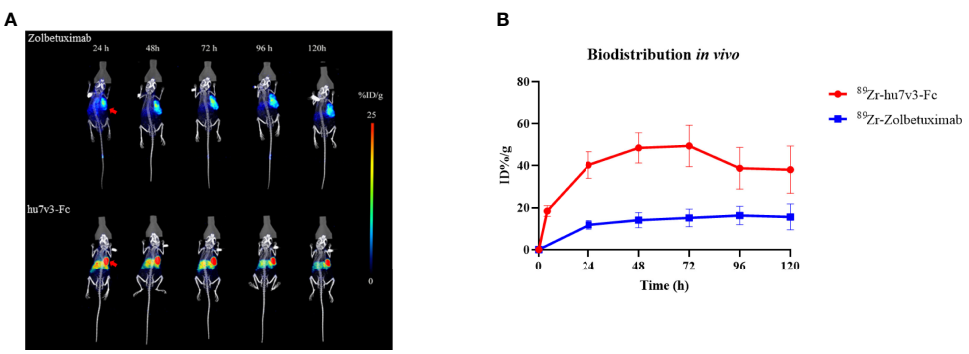

FIGURE 5 | *In vivo* tumor location of ^{89}Zr labeled 7v3-Fc. **(A)** ^{89}Zr PET-CT imaging in mice bearing subcutaneously SNU-620 tumors showed specific tumor location. Red arrowheads indicate the location of tumors. **(B)** Time-radioactivity curves derived from PET-CT imaging after injection with ^{89}Zr labeled hu7v3-Fc and Zolbetuximab. Data are displayed with Mean ± SD (n = 3).

hidden epitopes in proteins, such as the active sites of enzymes (28). Furthermore, VHHs can be building blocks for multiple bi-specific antibodies and tri-specific antibodies which can target multiple antigens and are of properties that are not offered by combination of two or three monoclonal antibodies (13, 14). Caplacizumab, the first VHH-based medicine, has been approved by FDA for adults with acquired thrombotic thrombocytopenic purpura (aTTP) in 2019 (29). VHHs labeled with different isotopes or fluorophores have been applied for tumor imaging (30), such as epidermal growth factor receptors (EGFRs) positive cancers. VHHs can be expressed as multi-specific formats simultaneously targeting multiple proteins with high affinity and their serum half-life can be prolonged by PEGylation, by fusion with long-lived serum albumin or IgG-Fc (31); or by fusion with an affinity reagent that recognizes and binds such long-lived serum proteins (32). Additionally, fusions of targeting VHHs to human IgG1 Fc can be used to recruit effector functions of ADCC and CDC (33). Altogether, development of VHH-based therapeutic agents is now in the ascendant with broad medical needs.

The use of synthetic peptide conjugated with carrier protein such as keyhole limpet hemocyanin (KLH) or BSA is the most popular strategy to generate antibodies (34). However, anti-peptides antibodies usually fail to recognize the native-state structure of membrane protein on the living cells. As most currently available VHHs recognize conformational epitopes rather than linear peptides (35), in our study, CHO-K1 cells engineered to express CLDN18.2 were used as immunogen in an *alpaca*. By cloning the VHH repertoire from the blood lymphocytes, expressing this repertoire on phages and bio-panning phages on CLDN18.2 expressing cells, eight CLDN18.2 positive VHHs were retrieved.

To improve affinity, circulation half-life, capacity to mediate anti-tumor cytotoxicity such as ADCC and CDC, the humanized anti-CLDN18.2 VHH 7v3 was fused to human IgG1 Fc to generate a bivalent fusion protein hu7v3-Fc. Flow cytometric assays and IHC staining demonstrated that hu7v3-Fc binds to CLDN18.2 with high affinity and specificity. In the cytotoxic assays, hu7v3-Fc was stronger than Zolbetuximab in the capacity to induce ADCC. Although hu7v3-Fc opsonized cells revealed a higher affinity to C1q, it mediated a CDC potency comparable to that by Zolbetuximab. The uncorrelation between C1q binding ability and CDC potency may stem from the nature of the assay methods. As the C1q binding assay was subjected to multiple cycles of washing step, Zolbetuximab because of its lower affinity is susceptible to be washed away form cell surface. In the CDC assay, Zolbetuximab could retained on the cell surface as no washing steps. Additionally, the possibility that hu7v3 and Zolbetuximab recognize different epitopes, thus affecting the CDC activity, cannot be ruled out.

In the mouse xenograft models, hu7v3-Fc was shown to be an promising therapeutic agent targeting CLDN18.2. In addition, hu7v3-Fc (around 75 kDa) is considerably smaller than Zolbetuximab (around 150 kDa). As a result, hu7v3-Fc exhibited faster tumor uptake, better tumor penetration and higher tumor-to-muscle ratio than Zolbetuximab, which may translate to improved therapeutic efficacy in cancer patients. It is worth noting that Zolbetuximab was prepared according to the patent US9751934B, any differences in production cell line, culture conditions and formulation, may attribute to the efficacy of the final product. Additionally, we performed long term toxicity study of hu7v3-Fc in SD rats and cynomolgus monkeys (data not shown), and found gastric atrophy/mixed cell inflammation/epithelial hyperplasia in hu7v3 treated animals during the dosing phase. However, a trend of recovery was observed at the end of the recovery period.

In summary, by whole cell immunization of an *alpaca*, a series of VHHs binding to CLDN18.2 with high specificity and affinity were discovered. The lead molecule, anti-CLDN18.2 hu7v3-Fc, demonstrated enhanced *in vitro* and *in vivo* anti-tumor activities, compared to the benchmark Zolbetuximab in CLDN18.2-positive gastric and pancreatic tumor cells. Additionally, these VHHs-based CAR-T and bispecific antibody for cancer therapy are under ongoing development. Future study will be conducted on incorporation of combination therapies, including chemotherapy, checkpoint blockade and cytokine therapies to further improve treatment of CLDN18.2 positive solid tumors.

DATA AVAILABILITY STATEMENT

The original contributions presented in the study are publicly available. This data can be found here: http://getentry.ddbj.nig.ac.jp/ under the accession numbers LC705046 ~LC705053.

ETHICS STATEMENT

The studies involving human participants were reviewed and approved by Clinical Research Ethics Commit of the First Affiliated Hospital, College of Medicine, Zhejiang University. The patients/participants provided their written informed consent to participate in this study. The animal study was reviewed and approved by Animal Ethics Committee of Zhejiang Academy of Medical Science and Hangzhou Normal University.

AUTHOR CONTRIBUTIONS

WZ and YL designed the study, analyzed the data, performed the experiments and wrote the manuscript. ZM, GY, ZZ and JD performed the immunization and isolation of VHH. YH and YD performed the IHC. WJ and YF supervised the project. Funding acquisition was carried out by WW. WW and YSH designed the study, supervised the project and wrote the manuscript. All authors contributed to the article and approved the submitted version.

FUNDING

The work was supported by the National Natural Science Foundation of China (81802350).

ACKNOWLEDGMENTS

We thank Dr. Cai Huang and Yuan Wang for their critical reading of this manuscript. We also would like to appreciate Peng Fang, Chenglong Yan, and Shanyou Yu, from Norroy Biosciences Co., Ltd., for their assistance with ^{89}Zr labeling of antibodies.

SUPPLEMENTARY MATERIAL

The Supplementary Material for this article can be found online at: https://www.frontiersin.org/articles/10.3389/fimmu.2022.885424/full#supplementary-material

REFERENCES

1. Sung H, Ferlay J, Siegel RL, Laversanne M, Soerjomataram I, Jemal A, et al. Global Cancer Statistics 2020: GLOBOCAN Estimates of Incidence and Mortality Worldwide for 36 Cancers in 185 Countries. *CA Cancer J Clin* (2021) 71(3):209–49. doi: 10.3322/caac.21660
2. Ansari D, Tingstedt B, Andersson B, Holmquist F, Sturesson C, Williamsson C, et al. Pancreatic Cancer: Yesterday, Today and Tomorrow. *Future Oncol* (2016) 12(16):1929–46. doi: 10.2217/fon-2016-0010
3. Yu X, Hu F, Li C, Yao Q, Zhang H, Xue Y. Clinicopathologic Characteristics and Prognosis of Proximal and Distal Gastric Cancer. *Onco Targets Ther* (2018) 11:1037–44. doi: 10.2147/OTT.S157378
4. Sahin U, Koslowski M, Dhaene K, Usener D, Brandenburg G, Seitz G, et al. Claudin-18 Splice Variant 2 Is a Pan-Cancer Target Suitable for Therapeutic Antibody Development. *Clin Cancer Res* (2008) 14(23):7624–34. doi: 10.1158/1078-0432.CCR-08-1547
5. Woll S, Schlitter AM, Dhaene K, Roller M, Esposito I, Sahin U, et al. Claudin 18.2 Is a Target for IMAB362 Antibody in Pancreatic Neoplasms. *Int J Cancer* (2014) 134(3):731–9. doi: 10.1002/ijc.28400
6. Hagen SJ, Ang LH, Zheng Y, Karahan SN, Wu J, Wang YE, et al. Loss of Tight Junction Protein Claudin 18 Promotes Progressive Neoplasia Development in Mouse Stomach. *Gastroenterology* (2018) 155(6):1852–67. doi: 10.1053/j.gastro.2018.08.041
7. Kim SR, Shin K, Park JM, Lee HH, Song KY, Lee SH, et al. Clinical Significance of CLDN18.2 Expression in Metastatic Diffuse-Type Gastric Cancer. *J Gastric Cancer* (2020) 20(4):408–20. doi: 10.5230/jgc.2020.20.e33
8. Karanjawala ZE, Illei PB, Ashfaq R, Infante JR, Murphy K, Pandey A, et al. New Markers of Pancreatic Cancer Identified Through Differential Gene Expression Analyses: Claudin 18 and Annexin A8. *Am J Surg Pathol* (2008) 32(2):188–96. doi: 10.1097/PAS.0b013e31815701f3
9. Lee JH, Kim KS, Kim TJ, Hong SP, Song SY, Chung JB, et al. Immunohistochemical Analysis of Claudin Expression in Pancreatic Cystic Tumors. *Oncol Rep* (2011) 25(4):971–8. doi: 10.3892/or.2011.1132
10. Moentenich V, Gebauer F, Comut E, Tuchscherer A, Bruns C, Schroeder W, et al. Claudin 18.2 Expression in Esophageal Adenocarcinoma and Its Potential Impact on Future Treatment Strategies. *Oncol Lett* (2020) 19(6):3665–70. doi: 10.3892/ol.2020.11520
11. Micke P, Mattsson JS, Edlund K, Lohr M, Jirstrom K, Berglund A, et al. Aberrantly Activated Claudin 6 and 18.2 as Potential Therapy Targets in Non-Small-Cell Lung Cancer. *Int J Cancer* (2014) 135(9):2206–14. doi: 10.1002/ijc.28857
12. Yang EY, Shah K. Nanobodies: Next Generation of Cancer Diagnostics and Therapeutics. *Front Oncol* (2020) 10:1182. doi: 10.3389/fonc.2020.01182
13. Nosenko MA, Atretkhany KN, Mokhonov VV, Efimov GA, Kruglov AA, Tillib SV, et al. VHH-Based Bispecific Antibodies Targeting Cytokine Production. *Front Immunol* (2017) 8:1073. doi: 10.3389/fimmu.2017.01073
14. Titong A, Gallolu Kankanamalage S, Dong J, Huang B, Spadoni N, Wang B, et al. First-In-Class Trispecific VHH-Fc Based Antibody With Potent Prophylactic and Therapeutic Efficacy Against SARS-CoV-2 and Variants. *Sci Rep* (2022) 12(1):4163. doi: 10.1038/s41598-022-07952-4
15. Vincke C, Loris R, Saerens D, Martinez-Rodriguez S, Muyldermans S, Conrath K. General Strategy to Humanize a Camelid Single-Domain Antibody and Identification of a Universal Humanized Nanobody Scaffold. *J Biol Chem* (2009) 284(5):3273–84. doi: 10.1074/jbc.M806889200
16. Lazar GA, Dang . W, Karki S, Vafa O, Peng JS, Hyun L, et al. Engineered Antibody Fc Variants With Enhanced Effector Function. *Proc Natl Acad Sci USA* (2006) 103(11):4005–10. doi: 10.1073/pnas.0508123103
17. Tang Y, Hu Y, Liu W, Chen L, Zhao Y, Ma H, et al. A Radiopharmaceutical [(89)Zr]Zr-DFO-Nimotuzumab for immunoPET With Epidermal Growth Factor Receptor Expression *In Vivo*. *Nucl Med Biol* (2019) 70:23–31. doi: 10.1016/j.nucmedbio.2019.01.007
18. Asaadi Y, Jouneghani FF, Janani S, Rahbarizadeh F. A Comprehensive Comparison Between Camelid Nanobodies and Single Chain Variable Fragments. *Biomark Res* (2021) 9(1):87. doi: 10.1186/s40364-021-00332-6
19. Muyldermans S. Single Domain Camel Antibodies: Current Status. *J Biotechnol* (2001) 74(4):277–302. doi: 10.1016/S1389-0352(01)00021-6
20. Karimi P, Islami . F, Anandasabapathy S, Freedman ND, Kamangar F. Gastric Cancer: Descriptive Epidemiology, Risk Factors, Screening, and Prevention. *Cancer Epidemiol Biomarkers Prev* (2014) 23(5):700–13. doi: 10.1158/1055-9965.EPI-13-1057
21. Sitarz R, Skierucha M, Mielko J, Offerhaus GJA, Maciejewski R, Polkowski WP, et al. Gastric Cancer: Epidemiology, Prevention, Classification, and Treatment. *Cancer Manag Res* (2018) 10:239–48. doi: 10.2147/CMAR.S149619
22. Yadav D, Lowenfels AB. The Epidemiology of Pancreatitis and Pancreatic Cancer. *Gastroenterology* (2013) 144(6):1252–61. doi: 10.1053/j.gastro.2013.01.068
23. Yura M, Takahashi T, Fukuda K, Nakamura R, Wada N, Fukada J, et al. A Highly Advanced Gastric Cancer Maintaining a Clinical Complete Response After Chemoradiotherapy Comprising S-1 and Cisplatin. *Case Rep Gastroenterol* (2018) 12(3):578–85. doi: 10.1159/000492206
24. Von Hoff DD, Ervin T, Arena FP, Chiorean EG, Infante J, Moore M, et al. Increased Survival in Pancreatic Cancer With Nab-Paclitaxel Plus Gemcitabine. *N Engl J Med* (2013) 369(18):1691–703. doi: 10.1056/NEJMoa1304369
25. Sahin U, Schuler M, Richly H, Bauer S, Krilova A, Dechow T, et al. A Phase I Dose-Escalation Study of IMAB362 (Zolbetuximab) in Patients With Advanced Gastric and Gastro-Oesophageal Junction Cancer. *Eur J Cancer* (2018) 100:17–26. doi: 10.1016/j.ejca.2018.05.007
26. Sahin U, Tureci O, Manikhas G, Lordick F, Rusyn A, Vynnychenko I, et al. FAST: A Randomised Phase II Study of Zolbetuximab (IMAB362) Plus EOX Versus EOX Alone for First-Line Treatment of Advanced CLDN18.2-Positive Gastric and Gastro-Oesophageal Adenocarcinoma. *Ann Oncol* (2021) 32(5):609–19. doi: 10.1016/j.annonc.2021.02.005
27. Tureci, Mitnacht-Kraus R, Woll S, Yamada T, Sahin U, et al. Characterization of Zolbetuximab in Pancreatic Cancer Models. *Oncoimmunology* (2019) 8(1):e1523096. doi: 10.1080/2162402X.2018.1523096
28. Lauwereys M, Arbabi Ghahroudi M, Desmyter A, Kinne J, Holzer W, De Genst E, et al. Potent Enzyme Inhibitors Derived From Dromedary Heavy-Chain Antibodies. *EMBO J* (1998) 17(13):3512–20. doi: 10.1093/emboj/17.13.3512
29. Scully M, Cataland SR, Peyvandi F, Coppo P, Knobl P, Kremer Hovinga JA, et al. Caplacizumab Treatment for Acquired Thrombotic Thrombocytopenic Purpura. *N Engl J Med* (2019) 380(4):335–46. doi: 10.1056/NEJMoa1806311
30. Bao G, Tang M, Zhao J, Zhu X, et al. Nanobody: A Promising Toolkit for Molecular Imaging and Disease Therapy. *EJNMMI Res* (2021) 11(1):6. doi: 10.1186/s13550-021-00750-5
31. Chanier T, Chames P. Nanobody Engineering: Toward Next Generation Immunotherapies and Immunoimaging of Cancer. *Antibodies (Basel)* (2019) 8(1). doi: 10.3390/antib8010013

32. Holt LJ, Basran A, Jones K, Chorlton J, Jespers LS, Brewis ND, et al. Anti-Serum Albumin Domain Antibodies for Extending the Half-Lives of Short Lived Drugs. *Protein Eng Des Sel* (2008) 21(5):283–8. doi: 10.1093/protein/gzm067
33. Harmsen MM, De Haard HJ. Properties, Production, and Applications of Camelid Single-Domain Antibody Fragments. *Appl Microbiol Biotechnol* (2007) 77(1):13–22. doi: 10.1007/s00253-007-1142-2
34. Lateef SS, Gupta S, Jayathilaka LP, Krishnanchettiar S, Huang JS, Lee BS, et al. An Improved Protocol for Coupling Synthetic Peptides to Carrier Proteins for Antibody Production Using DMF to Solubilize Peptides. *J Biomol Tech* (2007) 18(3):173–6.
35. Braun MB, Traenkle B, Koch PA, Emele F, Weiss F, Poetz O. Peptides in Headlock–a Novel High-Affinity and Versatile Peptide-Binding Nanobody for Proteomics and Microscopy. *Sci Rep* (2016) 6:19211. doi: 10.1038/srep19211

Conflict of Interest: ZM, GY, ZZ, JD, YF, and YSH are current or former employees of Zhejiang Doer Biologics Co., Ltd. YSH is a shareholder of Zhejiang Doer Biologics Co., Ltd.

The remaining authors declare that the research was conducted in the absence of any commercial or financial relationships that could be construed as a potential conflict of interest.

Publisher's Note: All claims expressed in this article are solely those of the authors and do not necessarily represent those of their affiliated organizations, or those of the publisher, the editors and the reviewers. Any product that may be evaluated in this article, or claim that may be made by its manufacturer, is not guaranteed or endorsed by the publisher.

frontiers | Frontiers in Immunology

TYPE Original Research
PUBLISHED 18 August 2022
DOI 10.3389/fimmu.2022.980539

OPEN ACCESS

EDITED BY
Zahra Sharifzadeh,
Pasteur Institute of Iran, Iran

REVIEWED BY
Serge Muyldermans,
Vrije University Brussel, Belgium
Oliver Hantschel,
Philipps-University of Marburg, Germany

*CORRESPONDENCE
Stéphanie Cabantous
stephanie.cabantous@inserm.fr
Aurélien Olichon
aurelien.olichon@inserm.fr

SPECIALTY SECTION
This article was submitted to Cancer Immunity and Immunotherapy, a section of the journal Frontiers in Immunology

RECEIVED 28 June 2022
ACCEPTED 29 July 2022
PUBLISHED 18 August 2022

CITATION
Keller L, Tardy C, Ligat L, Le Pennec S, Bery N, Koraïchi F, Chinestra P, David M, Gence R, Favre G, Cabantous S and Olichon A (2022) Tripartite Split-GFP Assay to Identify Selective Intracellular Nanobody That Suppresses GTPase RHOA Subfamily Downstream Signaling. *Front. Immunol.* 13:980539. doi: 10.3389/fimmu.2022.980539

Tripartite split-GFP assay to identify selective intracellular nanobody that suppresses GTPase RHOA subfamily downstream signaling

Laura Keller[1,2], Claudine Tardy[1], Laetitia Ligat[3], Soazig Le Pennec[1], Nicolas Bery[1], Faten Koraïchi[1], Patrick Chinestra[1], Mélissa David[1], Rémi Gence[1], Gilles Favre[1,2], Stéphanie Cabantous[2]* and Aurélien Olichon[1,4]*

[1]Centre de Recherche en Cancérologie de Toulouse (CRCT), Université de Toulouse, Institut National de la Santé et de la Recherche Médicale (INSERM), Centre National de la Recherche Scientifique (CNRS), Université Toulouse III-Paul Sabatier, Centre de Recherches en Cancérologie de Toulouse (CRCT), Toulouse, France, [2]Laboratoire de Biologie Médicale Oncologique, IUCT-Oncopôle, Toulouse, France, [3]Le Pôle Technologique du Centre de Recherches en Cancérologie de Toulouse, Plateau de Protéomique, Toulouse, France, [4]Institut National de la Santé et de la Recherche Médicale (INSERM), Unité Mixte de Recherche (UMR) 1188 Diabète athérothrombose Réunion Océan Indien (DéTROI), Université de La Réunion, Saint Denis de La Réunion, France

Strategies based on intracellular expression of artificial binding domains present several advantages over manipulating nucleic acid expression or the use of small molecule inhibitors. Intracellularly-functional nanobodies can be considered as promising macrodrugs to study key signaling pathways by interfering with protein-protein interactions. With the aim of studying the RAS-related small GTPase RHOA family, we previously isolated, from a synthetic phage display library, nanobodies selective towards the GTP-bound conformation of RHOA subfamily proteins that lack selectivity between the highly conserved RHOA-like and RAC subfamilies of GTPases. To identify RHOA/ROCK pathway inhibitory intracellular nanobodies, we implemented a stringent, subtractive phage display selection towards RHOA-GTP followed by a phenotypic screen based on F-actin fiber loss. Intracellular interaction and intracellular selectivity between RHOA and RAC1 proteins was demonstrated by adapting the sensitive intracellular protein-protein interaction reporter based on the tripartite split-GFP method. This strategy led us to identify a functional intracellular nanobody, hereafter named RH28, that does not cross-react with the close RAC subfamily and blocks/disrupts the RHOA/ROCK signaling pathway in several cell lines without further engineering or functionalization. We confirmed these results by showing, using SPR assays, the high specificity of the RH28 nanobody towards the GTP-bound conformation of RHOA subfamily GTPases. In the metastatic melanoma cell line WM266-4, RH28 expression triggered an elongated cellular phenotype associated with a loss of cellular contraction properties, demonstrating the efficient intracellular blocking of RHOA/B/C proteins downstream interactions

without the need of manipulating endogenous gene expression. This work paves the way for future therapeutic strategies based on protein-protein interaction disruption with intracellular antibodies.

KEYWORDS

RHOA GTPase, tripartite split-GFP, nanobodies, RHO-ROCK signaling, single domain antibody (sdAb)

Introduction

Recombinant antibody technology has so far provided genetically encoded high affinity reagents for common immunological assays used in fundamental and applied research (1–3). Peculiar applications such as tracing or modulating intracellular proteins in living cells are ascribed to special antibody fragments or alternative scaffolds that rely on single chain binding domains (4). Among antibody fragments that can be used inside the cell, nanobodies have emerged as promising molecular tools (5, 6). For instance, nanobodies from immunized animals or from synthetic scaffolds were efficiently engineered to specifically recognise not only an ectopic protein such as the Green Fluorescent Protein (GFP) (7, 8), or several linear epitope tags (9, 10), but also endogenous proteins (11, 12). In this regard, intracellular antibodies (also called intrabodies) present the advantage to disrupt endogenous protein functions either by functionalization through targeted protein degradation (13), ER-rerouting (14), or by competing with endogenous protein partners, thus offering an alternative strategy to small molecule inhibitors.

Proteins of the RHOA-subfamily (RHOA, RHOB and RHOC isoforms) are small GTPases belonging to the RAS superfamily. Likewise, these proteins behave like molecular switches. Upon stimuli, Guanine nucleotide Exchange Factors (GEFs) activate a fraction of RHOs (more than 95% of the cellular RHO proteins are present in the inactive GDP-bound state (15, 16)), by promoting their GTP loading. This nucleotide exchange results in a conformational change of the small GTPase, that is recognized by so-called effector proteins and triggers downstream cellular response. RHOA-subfamily small GTPases regulate key signalling pathways implicated in cell division, cell motility or other cellular processes (17, 18) and RHOA notably controls the ROCK/acto-myosin pathway that drives F-actin fiber formation and subcellular region contractility (19–21). The dysregulations of their expression and/or activity have been associated with several diseases including multiple cancers (22, 23), vascular or neurological disorders (24, 25).

The global inhibition of RHO proteins is currently achieved by RNA interference or by the use of the ADP-ribosylating bacterial exoenzyme C3 (26, 27). RNA interference can induce compensation mechanisms with other RHO proteins, making the resulting cellular phenotypes difficult to interpret with this strategy (13, 28). The ADP-ribosylating bacterial exoenzyme C3 irreversibly modifies RHO proteins leading to their subsequent degradation. Moreover, some small molecule inhibitors have been developed to prevent RHO activation, however by targeting a limited set of GEF (29). Therefore, there is an unmet need for a strategy that could specifically inhibit the active GTP-bound forms of RHO proteins, without perturbation of RHO expression or RAC activities. We hypothesized that intrabodies preferentially recognizing the conformational active state of these proteins thereby competing with endogenous effector binding, could be an efficient strategy. In this line, we previously generated from a synthetic phage display library (NaLi-H1) based on a unique nanobody scaffold, several conformational intrabodies that preferentially bind the conformational state loaded with GTP of the RAS-related RHO GTPases RHOA or RHOB (13, 30, 31). However, the clones so far selected which showed potential blocking activities did not present enough selectivity towards the RHOA subfamily over the close RAC1 subfamily, and one clone that preferentially recognised RHOB was non-blocking without being functionalized through a domain that recruits a multicomponent E3-ligase catalytic activity.

Here we present a more selective GTP-bound RHO nanobody, isolated from the synthetic nanobody library NaLi-H1, with RHOA subfamily blocking properties (31). After a competitive phage display strategy designed to enrich the library towards RHOA-GTP, we performed a phenotypic screening based on actin fiber loss associated with immunoprecipitation assays to identify a new nanobody. We further determined its intracellular selectivity as well as its effector blocking mechanism by using the tripartite split-GFP sensitive protein-protein interaction assay (32, 33). We then demonstrated that this nanobody interferes with the RHOA/ROCK actomyosin pathway, leading to a phenotypic switch from a rounded to elongated phenotype with impaired contractility. Overall, such nanobody appeared as an original and efficient tool to inhibit intracellularly GTPase activities in normal cells or in diverse pathological models.

Material and methods

Plasmids and lentiviral vectors

RHO GTPases and nanobodies were expressed as recombinant proteins from bacterial expression vectors or from mammalian expression vectors. 2SHA-RHO mutants tagged with the twin Streptag II (IBA) were expressed from a pET vector as previously described (31). Nanobodies from the NaLi-H1 library, referred to as hs2dAb for humanized synthetic single domain antibody, are expressed in a pHEN- hs2dAb-6his-myc-PIII phagemid. Hs2dAb were subcloned NcoI/NotI into the intrabody expression plasmid pIB-GFP or pIB-mCherry or pIB-IRES-MTSmCherry (13, 30, 31). Other intracellular nanobody expressing plasmids, pTRIP-TRE-Ib-myc-IRES-BFP, pIb-myc and pIb-myc-IRES-BFP, were also previously described (13). For periplasmic expression, hs2dAb-6his-myc insert was digested from pIB-GFP and inserted in a modified pHEN6-VHH-6his, thus creating a periplasmic expression vector pHEN6-hs2dAb-6his-myc-6his.

Specific plasmids were constructed for the tripartite split-GFP assays. For carboxy-terminal GFP11 tag fusions, pIb-hs2dAb-6hismyc-GFP was digested AgeI and Acc65I to remove the GFP and replaced with a PCR product encoding a Glycine Serine flexible linker followed by a carboxy-terminal GFP11 tag. For RHO-GTPases, the pGFP10-RHOA expressing CA or DN RHOA, RAC1 or CDC42 mutants were generated by site-directed mutagenesis and cloned into BspeI/XbaI sites of pcDNA_GFP10-Nter fusion vector previously described (34). For the pGFP11-RBD, the Rho Binding Domain of Rhotekin was amplified by PCR from pGST-RBD pGEX (Addgene#15247) and inserted into NotI/ClaI cloning sites of pcDNA_GFP11-Cter fusion vector previously described in 19. A pGFP11-RBD-TRE-GFP10-RHOA lentiviral vector co-expressing 10-RHOA and RBD-11 was generated by subcloning the pTRE tight RBD-11 cassette into the MluI site of an HIV-1-based lentiviral pTrip-vector carrying a tetracycline response element (TRE) (BIVICplatform, IFR 150, CHU Rangueil, Toulouse).

Cell lines, transfection method and reagents

HeLa (cervical adenocarcinoma), MRC5-SV (human immortalized fibroblasts), WM266.4 (metastatic melanoma) cell lines (ATCC) were grown in DMEM (Lonza®) supplemented with 10% FCS at 37°C in a humidified incubator with 5% CO_2. Transient transfection of DNA plasmids was performed using the Jet Prime method, as indicated by the supplier (PolyPlus Transfection®).

Western Blots were probed with the following antibodies: mouse monoclonal 26C4 anti-RHOA (1/500, O/N, 4°C, Santa Cruz Biotechnology®), goat polyclonal anti-myc tag HRP conjugated (1/3000, 1 hour, Room Temperature RT, Novus Biologicals®), mouse monoclonal anti-RAC1 (1/1000, O/N, 4°C, Millipore®), Ser19 P-Myosin light chain (1/500, O/N, 4°C Cell Signaling Technology®), GAPDH (1/2000, O/N, 4°C, Cell Signaling Technology®), mouse monoclonal Chitin Binding Domain (1/1000, O/N, 4°C NEB Biosciences®). Anti-myc tag (clone 9E10) used in immunofluorescence and flow cytometry experiments was a gift from S. Moutel. Anti-GFP10 rabbit polyclonal antibodies were obtained after rabbit immunization with synthetic peptides corresponding to GFP10 (DLPDDHYLSTQTILSKDLN) (Millegen, France®). Detection was performed using peroxidase-conjugated secondary antibodies and chemiluminescence detection kit (Biorad®) except for Ser19 P-Myosin light chain which was revealed with Amersham ECL Prime Western Blotting Detection Reagent®.

The production of stable cell lines with tetracycline inducible (Tet-on) hs2dAb expression was performed with lentiviral technology. The p-Ib-myc-IRES-BFP lentivirus was produced according to the tri-transfection procedure using the plasmids pTRIP-TRE-Ib-myc-IRES-BFP, pLvPack and pLvVSVg (Sigma®) in 293T cells for viral production. WM266.4 were previously transduced with the rtTA doxycycline-inducible transactivator, and then cells were further transduced with the IB-IRES-BFP lentivirus containing supernatant.

In order to establish the most homogeneous cell lines, for transduction efficiency, 24h after doxycycline induction, cells were then sorted on a BD Influx™ cell sorter for their cytoplasmic BFP fluorescence intensity. Flow cytometry data were analyzed with Kaluza software (Beckman Coulter®).

Subtractive phage display panning for isolating RHO-GTP specific hs2dAb

The NaLi-H1 library of humanized synthetic single domain antibody (31) was used for this study. A subtractive panning protocol was designed to isolate hs2dAb selective for the RHOA-GTP-Chitin binding domain from chitinase A1 (CBD) or twin StrepTag (2S) fusion of RHOA GTPase active mutant (RHOA L63). Constructions were expressed transiently during 24 hours in HEK293 cells and captured freshly after cell lysis on magnetic beads before incubation with the library phages. Chitin magnetic beads (NEB®) or StrepTactin coated magStrep HC (IBA®) beads were used. A phage display panning alternating rounds on chitin beads with rounds on StrepTactin beads was performed during 4 rounds. From the second round of panning, a depletion step on GDP-loaded wild type RHOA or N19 inactive mutant and on RHOB L63, RHOC L63, RAC1 L61 active mutants was included. The adequate amount of antigen coated beads was incubated for 2 hours with the phage library (10^{13} phages diluted in 1 mL of PBS + 0.1% Tween 20 + 2% non-fat milk). Phages were

previously adsorbed on empty streptavidin-coated magnetic beads (to remove nonspecific binders). Phages bound to streptavidin-coated beads or chitin beads were recovered on a magnet. Beads were washed 10 times (round 1), 15 times (round 2) and 25 times including long washes of one hour (rounds 3 and 4) with PBS-Tween 0.1%. Bound phages were eluted using triethylamine (Sigma Aldrich®) and E. coli (TG1 strain) were infected with the eluted phages. For rounds 2, 3 and 4, only 10^{12} phages were used as input.

Pull down assays

Co-precipitations of intracellular nanobodies (myc-tagged hs2dAb) with CA RHOA mutants were performed after transient co-transfection of pCBD-RHOA L63 with pIb-myc in HeLa cells. After 24 hours, cleared cell lysates containing CBD-RHO mutants in buffer (50 mM Tris pH 7.4. 500 mM NaCl, 10 mM MgCl2, 1% TritonX100, protease and phosphatase inhibitors supplemented) were incubated with chitin beads (NEB Biolabs®) for 1 hour at 4°C. Co-precipitation was revealed by RHOA antibody and myc antibody.

Co-precipitations of intrabodies (myc-tagged hs2dAb) with endogenous mammalian RHO proteins were performed after doxycycline induction of pIb-myc-IRES-BFP in WM266.4 cells. Cleared cell lysates were then incubated with His tag purification beads (Roche®) during 45 minutes at 4°C for Ni-NTA IMAC pull down. Beads were then washed thrice in washing buffer (Tris pH 7.4 50 mM, NaCl 150 mM, MgCl2 10 mM, 0.1% Tween20), and immunoprecipitates were then analyzed by Western blotting and revealed by RHOA antibody and myc antibody.

Immunofluorescence staining

Transfected cells grown on coverslips were fixed in 3.7% paraformaldehyde and permeabilized with PBS-Triton 0.1%, blocked with PBS-BSA 8%, incubated with primary antibody mouse monoclonal anti-myc tag (9E10 clone 1/800, O/N, 4°C) then Pacific blue mouse secondary antibodies (1/400, 1 hour, RT, BD Bioscience®). Alexa 568-Phalloidin (1/40, 1 hour, RT, Invitrogen®) was used to reveal actin stress fibers. All coverslips were mounted in Mowiol. Data acquisition was carried out on a Zeiss Axiovert inverted microscope and figure montage using Image J.

In cell interaction using the tripartite split-GFP assay

MRC5 cells expressing the GFP1-9 fragment (GFP1-9_MRC5) were cotransfected with plasmids expressing either GFP10 tagged constitutively active RHOA L63, RAC1 L61 or CDC42 L61 mutants or inactive RHOA N19 mutant, and with GFP11 tagged hs2dAb, RBD or PAK-BD. 20 hours after transfection, cells were fixed with 3.7% PFA (Sigma-Aldrich®) and permeabilized with 0.1% triton X100 (Sigma-Aldrich®). Cells were subsequently co-stained with 9E10 anti-myc monoclonal (1/3000, 4°C, 1h30min) antibody and with anti-GFP10 fragment antibody (1/1000, 4°C, 1h30min). Secondary antibodies were respectively mouse APC and rabbit Pacific blue (1/100, 1H, 4°C, BD Biosciences®) (1/200, 1H, 4°C BD Biosciences®). GFP fluorescence was measured using FACS MACS Quant 10 cytometer®. At least 20,000 gated events were counted for each sample and analysed using Kaluza analysis software (Beckman Coulter®). GFP fluorescence was measured using FACS MACS Quant 10 cytometer®. The geometric mean from the GFP channel was determined from the gating region corresponding to double GFP10 and GFP11 positive labelling that correlate to GFP10 RHO mutants and hs2dAb expression levels respectively.

The GFP fluorescence was also imaged on a Zeiss Axiovert inverted microscope. For immunofluorescence experiment, transfected cells were fixed in 3.7% paraformaldehyde and permeabilized with PBS-Triton 0.1%, blocked with PBS-BSA 8%, incubated with primary antibody mouse monoclonal anti-myc tag (9E10 clone 1/800, O/N, 4°C) and anti-GFP10 fragment antibody (1/1000, O/N, 4°C) then respectively with Pacific blue mouse secondary antibodies (1/400, 1 hour, RT, BD Bioscience®) and Alexa 568-anti mouse secondary antibody (1/400, 1 hour, RT, BD Bioscience®).

For intracellular competition experiments, hs2dAb N-terminally fused to mCherry were co-transfected with a tet-on inducible bidirectional promoter vector expressing GFP10-RHOAWT and GFP11-RBD in MRC5_GFP1-9 cells, a cell line referred to as triSFP-RHOA. 20 hours after transfection, GFP10-RHOAWT and GFP11-RBD expression were induced with doxycycline. 16 hours later, GFP fluorescence and hs2dAb expression were measured using FACS MACS Quant VYB cytometer. At least 20,000 gated events were counted for each sample and analysed using FlowJo analysis software.

Recombinant protein expression and purification

RHO GTPase production. 2SHA-RHO were expressed in BL21 *E.coli* cells from a pET vector. Transformed bacteria cells were used to grow 3mL LB-carbenicillin (100 µg/ml) cultures overnight at 37°C prior to inoculation in baffled flasks containing 1 L of the same media. Cells were allowed to grow at 37°C until OD600 reached 0.5-0.7. Cells were then induced with IPTG at a final concentration of 100 µM and grown for an additional 20 hours at 25°C. Cells were harvested by centrifugation at 4000g for 20 min at 4°C. The pellets were re-

suspended in lysis buffer (50 mM Tris HCl, pH 8, 150 mM NaCl, 5 mM MgCl2, 0.1% triton, 1 mM DTT, lysozyme and DNase I 1X, protease inhibitors) and lysed by sonication on ice prior to centrifugation (30 min, 15000 g, 4°C). StrepTactin SuperFlow Plus (IBA®) matrix was equilibrated in buffer A (50 mM Tris HCl, pH 8, 150 mM NaCl, 5 mM MgCl2) and was incubated with supernatant for 2 hours at 4°C. Then supernatant and matrix were loaded on a simple column in order to maximise capture of 2SHA-RHO proteins. Matrix was washed by 15 mL of washing buffer (300 mM Nacl, 50 mM tris pH8, 5 mM MgCl2, 0.1% tween20). RHO proteins were then eluted in buffer A containing 10 mM Biotin (Sigma®). Dialysis was performed overnight against buffer A containing 15% glycerol.

Nanobody purification. Hs2dAb were produced in XL1blue E.coli grown in TB-ampicillin (100 µg/mL) medium supplemented with 1% glucose in the start culture and 0.1% glucose during induction with 1 mM IPTG. After overexpression for 16h at 28°C, the cells were harvested, suspended in 15 mL ice-cold TES (Tris 100 mM pH 8, EDTA 1 mM, Sucrose 500 mM) and stored at -80°C. 30 mL of a ¼ dilution of TES buffer was added to the re-suspended pellets prior to vortex briefly and to keep for 30 min at 4°C. After centrifugation (30min, 13000g, 4°C), the periplasmic extract containing hs2dAb was purified by affinity chromatography. The protein extract was incubated 2 hours in the presence of His-Tag purification beads (Roche®) previously equilibrated with equilibration buffer (12 mM Tris pH8, 0.125 mM EDTA, 65 mM Sucrose, 300 mM NaCl, 10 mM Imidazole pH7). Beads were washed with 30 ml of washing buffer (10 mM Tris pH8, 150 mM NaCl, 10 mM Imidazole pH7). Hs2dAb were then eluted with elution buffer (500 mM Imidazole pH7, 25 mM Tris pH6.8, 300 mM NaCl) and dialysis was performed for 16 hours at 4°C in PBS 10% Glycerol. OD at 280 nm was measured in order to determine hs2dAb concentration.

Affinity measurement

Hs2dAb binding studies based on SPR technology were performed on BIAcore T200 optical biosensor instrument (GE Healthcare®). Capture of recombinant 6xHis tagged hs2dAb, expressed in XL1blue and purified as previously reported (35) was performed on a nitrilotriacetic acid (NTA) sensor chip in HBS-P+ buffer (10 mM Hepes pH 7.4, 150 mM NaCl, and 0.05% surfactant P20) (GE Healthcare). The four flow cells (Fc) of the sensor chip were used: one (Fc 1) to monitor nonspecific binding and to provide background corrections for analyses and the other three flow cells (Fc 2, 3, and 4) containing immobilized 6xHis tagged hs2dAb for measurement.

For immobilization strategies, flow cells were loaded with nickel solution (10 µL/min for 60 s) in order to saturate the NTA surface with Ni^{2+} and an extra wash was done using running buffer containing 3mM EDTA after the nickel injection. His-tagged hs2dAb in running buffer was injected in flow cells at a flow-rate of 10 µL/min. Total amount of immobilized hs2dAb was 250-300 resonance units. (RUs; 1 RU corresponds approximately to 1 pg/mm2 of protein on the sensor chip). A Single-Cycle Kinetics (SCK) analysis to determine the dissociation equilibrium constant (K_D) was carried out. SCK method prevents potential inaccuracy due to sensor chip regeneration between cycles which are necessary in the conventional Multiple Cycle Kinetics (MCK) (36). SCK binding parameters are evaluated for each injection according to the tools and fit models of the BIAevaluation software, giving similar values than MCK. As hs2dAb were smaller proteins than their respective antigens, hs2dAb were captured on the sensor chip then the recombinant GTPases were used as analytes and were injected sequentially with increased concentrations ranging between 3.125 nM to 50 nM in a single cycle without regeneration of the sensor chip between injections. Binding parameters were obtained by fitting the overlaid sensorgrams with the 1:1. Langmuir binding model of the BIAevaluation software version 1.0.

ELISA and G-LISA assays

For ELISA detection of RHO GTPases, wells of StrepTactin-coated plates (IBA®) were coated with 100 nM of recombinant CA or DN RHOA, CA RAC1 or CA CDC42 mutants as 2S-HA fused proteins (200 µl in TBS by well) during 2 hours at RT and then blocked with 5% milk in TBS-Tween 0.05% (blocking buffer) for 1 hour at RT. Several dilutions of hs2dAb in blocking buffer were applied to the ELISA plates in duplicates for 1 hour at RT. Next, we added 1 µg/ml anti-myc HRP antibody (QED Biosciences, 18824P®) in blocking buffer for 1 hour at RT and the reaction was visualized by the addition of 100 µl chromogenic substrate (Thermoscientific®, 1-step ultraTMB, 34028) for 1 min. The reaction was stopped with 50 µl H_2SO_4 1N and absorbance at 450 nm was measured using FLUOstar OPTIMA microplate reader. Plates were washed three times with washing buffer (TBS containing 0.05% (v/v) Tween 20) after each step. All steps are performed under agitation (400 rpm).

To perform competition experiments using the G-LISA® procedure, we used G-LISA® RHOA (BK124) and RAC1 (BK128) assays (Cytoskeleton) according to the manufacturer's instructions to assess if purified hs2dAb were able to compete with RBD or PAK domain. We pre-incubated 10-fold serial dilutions of NR53, RH12 or RH28 for 1 hour with 2S-HA RHOA or RAC1 before performing the G-LISA assays. Hs2dAb-6His-myc-6his inputs were controlled in an ELISA after capture on nickel coated plates as described previously (15).

Quantitative RT-PCR

RH28 and NR27 WM266.4 cells were harvested after 18 and 24 hours of induction with 1µg/ml Doxycycline, and RNA was extracted following RNeasy Plus minikit (Qiagen) procedure.

RNA concentration was measured with Nanodrop. Reverse transcription was carried out on 1 µg of RNA using RT iScript kit (Biorad). Priming for reverse transcription was done with combined oligo(dT) and random hexamers.

Quantitative PCRs were performed on cDNA using iQ SyBr Green kit (Biorad) on a ViiA-7 RT-PCR system (Applied Biosystems). RHOA transcript was quantified according to the standard $2^{-\Delta\Delta Ct}$ method after normalization to *B2M* (beta 2-microglobulin).

Primers used for determination of RHOA transcript are the following: RHOA_sens: 5'-TGGAAGATGGCATAACCTGTC and RHOA_anti-sens 5'- AACTGGTGGCTCCTCTGG; B2M_sens: 5'-ACCCCCACTGAAAAAGATGA and B2M _anti-sens 5'-ATCTTCAAACCTCCATGATG

Cell culture in a 3D matrix

Cells were embedded in a 3D matrix constituted of collagen type I (1.5 mg/ml, Corning®) in EMEM (Eagle's Minimal Essential Medium; 2 ×, Lonza®) at a concentration of 1,5 × 10^5 cells/ml. Drops (30 µl) were placed for 1 hour upside down at 37 °C to allow solidification of the matrix. The complete medium was then added and hs2dAb expression was induced by doxycycline. 6 hours later, cell morphology was observed under a Nikon inverted microscope and drops were harvested, collagenase I (100 U/mL final concentration, ThermoFisher®) added and cells centrifuged. Pelleted cells were then lysed in RIPA buffer containing phosphatase and protease inhibitors.

Gel contraction assay

A total of 0.5M cells were embedded in a 3D matrix constituted of collagen type I (3.1 mg/ml, Corning®) in EMEM (Eagle's Minimal Essential Medium; 2 ×, Lonza) and plated in a 24-wells plate. After one hour of polymerisation at 37°C, the gel was gently dissociated from the edge of the well with a 200µl-pipet tip and the expression of hs2dAb induced by adding doxycycline to the cell culture medium. The plates were scanned after 72 hours and the area of the gel and the plate were measured and quantified with ImageJ software. For each well, the percentage of gel contraction was calculated using the formula 100 − [(area of the gel/area of an empty well) × 100].

Statistical analysis

Reported values represent mean ± standard deviation (SD) of at least three independent experiments. Unless otherwise stated, student paired t-tests were performed for comparison with GraphPad Prism 9. *, p<0.05; **, p<0.01; ***, p<0.001; ****, p< 0.0001.

Results

Phenotypic screening selection of RHOA-GTP blocking intrabodies

The goal of the present study was the selection of a blocking intrabody more selective towards RHOA subfamily. After four rounds of phage display against RHOA in its GTP-bound conformation (see methods), 30 ELISA-positive families of clones were isolated (Supplementary Figure 1), including new sequences as well as a few copies of the previously identified RH12 (RHO binder H12). To screen for intracellular binders of RHOA-GTP family, this novel set of GTP-bound RHO nanobodies was subcloned into a mammalian expression vector with carboxy terminal dual 6xHis and myc tags as reporters of expression. Their ability to bind active RHOA conformation while expressed as intracellular nanobodies was first evaluated by a chitin bead co-immunoprecipitation assay after co-transfection with a CA RHOA (constitutively active RHOA L63) mutant bearing a C-terminal CBD (Chitin Binding Domain) tag (Supplementary Figure 1). We focused on 8 clones that were efficiently immunoprecipitated with the CA RHOA. As negative controls, we chose, among a set of nanobodies originating from previous phage display selections towards non-related protein targets, two clones referred to as NR27 and NR53 (31).

In order to identify a RHOA subfamily activity-blocking intrabody, we performed a phenotypic screen based on actin F-fiber staining after transfection of the nanobody candidates in HeLa cells. Indeed, in adherent cells, RHO inhibition mediated by the ADP-ribosylating bacterial exoenzyme C3 (26, 27) or after expression knockdown (37, 38) induces actin fiber loss and a dramatic morphological change. As a control of effective RHO inhibition, we treated HeLa cells with the tat-C3 exoenzyme and observed in more than 50% of the cells a stretched cellular shape with a retracted cytoplasm and elongated protrusions (Supplementary Figure 2). Among the 8 positive CA RHOA binders, 3 clones, referred to as RH28, RH29 and RH35, induced a stretched and shrunken cellular phenotype as shown in cells stained with a homogenous pattern of nanobodies expression detected in HeLa cells (Supplementary Figure 2). This cellular shape appeared similar to the one induced by recombinant tat-C3 treatment. In contrast, in NR-expressing control cells or cells with no detectable expression of RH28, RH29 or RH35 nanobodies, actin F staining revealed organisation in fibers. Therefore, we hypothesized that these 3 nanobodies might potentially be positive hits for blocking the active RHO signalling pathway.

The tripartite split-GFP assay demonstrates the intracellular biochemical selectivity of the selected intrabodies

We first confirmed the intracellular interaction between the 3 selected clones and the active RHOA conformation using the tripartite split-GFP protein-protein interaction reporter system (32). The tripartite split-GFP reporter assay was selected for its high sensitivity due to its irreversibility and lack of background fluorescence. In this assay, a GFP variant gene is separated in three parts: the β-strand 10 (GFP10) is fused to one partner of the interaction, the β-strand 11 (GFP11) fused to the second partner, and the remaining amino-terminal β-strand 1 to 9 (GFP1-9) acts as a detector moiety of the interaction, leading to the formation of a reconstituted GFP (rGFP) that becomes fluorescent after chromophore maturation (Figure 1A). The split-GFP system was previously successfully implemented to monitor active RHO or RAS GTPase interactions with their respective effector domains in cells (34). Here, the nanobodies were fused to the GFP-11 tag in amino-terminal while the CA RHOA mutant was carboxy-terminally fused to the GFP10 fragment. These constructions were expressed in a human fibroblast MRC5 cell line already validated for its stable and homogenous expression of the GFP1-9 (34). After 24 hours of co-transfection within the MRC5_GFP1-9 cell line, the expression of each moiety and rGFP fluorescence was quantified. As a positive control of intracellular RHO interaction, we used the RHOTEKIN effector RHO Binding Domain (RBD), fused to a C-terminal GFP11 tag (34). Its co-transfection with CA GFP10-RHOA led to 25% of rGFP positive cells (Figure 1B and Supplementary Figure 3). Similar percentages of rGFP positive cells were also detected in cells co-expressing the CA GFP10-RHOA for the 3 potential RHO-GTP intrabodies (23%, 21% and 17% for RH28, RH29 and RH35 respectively). Control analysis of co-expression indicated similar levels of RHO mutants and the various nanobodies in all experiments (Supplementary Figure 3). In comparison, 1% of rGFP cells could be detected when co-expressing the CA GFP10-RHOA and the negative controls NR27 or NR53, demonstrating thereby the intracellular interaction between each of the 3 intrabodies and the active form of RHOA.

Flow cytometry quantification of the reconstituted GFP (rGFP) fluorescent signal demonstrated that the high affinity, already characterized, RH12 nanobody presented a similar signal intensity and selectivity towards the active RHOA conformation. (Figure 1B and Supplementary Figure 3). We also assessed the capability of the 3 hits to selectively recognize the active RHOA conformation in the intracellular environment by testing the interaction with a DN (Dominant Negative N19) mutant of RHOA (Figures 1A, B and Supplementary Figure 3). All of them appeared selective of the active RHOA conformation since significantly lower percentages of rGFP cells were observed with the DN of RHOA (23% vs. 8.6%; 21% vs 6.6%; 17% vs. 10% respectively).

To further confirm the intracellular selectivity, we expressed in *E.coli* and purified the three nanobodies and compared their binding affinities for RHOA mutants by SPR (Supplementary Figure 4). All of them had a K_D in the sub-nanomolar range for CA RHOA but no measurable binding of DN RHOA was observed, which is consistent with the results obtained *in-cellulo*. To assess whether these hits also bind the two other isoforms of the RHOA subfamily, RHOB and RHOC, we measured their K_D values for the CA mutants (Supplementary Figure 4). RH28, RH29 and RH35 displayed nanomolar range affinities for all members of RHOA subfamily which share more than 95% amino acid identities when excluding the carboxy-terminal hypervariable domain (39).

In this assay, we also evaluate the affinities towards the CA mutants of RAC1 GTPase and found that RH29 and RH35 nanobodies, but not RH28, could also bind RAC1 with equilibrium dissociation constant in the range of 10 to 20 nM (Supplementary Figure 4). This result suggested that RH28 is the only clone highly selective towards RHOA subfamily active proteins. RH28 selectivity towards the active RHOA conformation was additionally confirmed by measuring the capacity to detect RHO GTPases in ELISA. RH28 recognized the CA mutant of RHOA while no signal was observed with CA mutants of the phylogenetically closest RHO GTPase members of RHOA subfamily, RAC1 and CDC42 (Supplementary Figure 5).

Considering potential discrepancies between *in vitro* measurements and biochemical interactions in the complexity of the intracellular environment, we assayed the selectivity of the RH28 among the 3 close subfamilies of RHO GTPases in cells by quantifying the rGFP signal obtained with RAC1 and CDC42, in their active state. As expected, the RBD tested with CA RAC1 or CA CDC42 led to a significantly lower amount of rGFP cells in comparison to the CA RHOA (28% vs. 2.6% and 28% vs. 1.7%), confirming that intracellularly, the RBD did not recognize the active forms of RAC1 nor CDC42. We validated the PAK domain as a positive control for RAC1 and CDC42 selective interaction since we observed a higher number of rGFP cells in comparison to RHOA (9.9% vs. 1.6% and 11.8% vs. 1.6%). Similarly to the natural RBD, the RH28 showed a clear selectivity towards CA RHOA and no cross reactivity with neither CA RAC1 nor CA CDC42 (26.4% vs. 4.4% and 26.4% vs. 2.8%) (Figure 2A and Supplementary Figure 6). We confirmed this result on the wild-type form of RHO GTPases (Figure 2B and Supplementary Figure 6). These results demonstrated that, in cells, the RH28 clone does not bind the closest GTPases related to RHOA even when they are expressed at a higher level than endogenous proteins. This result was also supported by the capacity of the myc tagged RH28 nanobody to immunoprecipitate the endogenous RHOA protein (data not shown). Collectively, these results led us to conclude that RH28

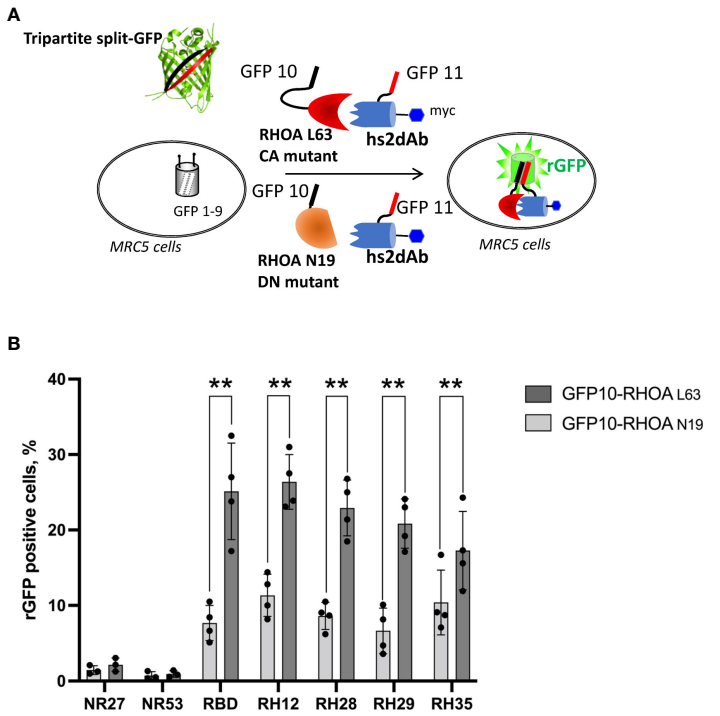

FIGURE 1
The tripartite split GFP assay demonstrates the intracellular interaction and the selective recognition of the active RHO conformation by the selected intrabodies. **(A)** Principle of the tripartite split-GFP complementation assay adapted to assess hs2dAb/RHO interaction. β-strand 10 (GFP10) and β-strand 11 (GFP11) are fused to RHOA mutants (either DN RHOA N19 or CA RHOA L63) and hs2dAb, respectively. These constructions are transfected in a MRC5 cell line that constitutively expresses the detector fragment GFP1–9 (β-strands 1–9). When protein interaction occurs, GFP10 and GFP11 strands are tethered and then spontaneously associate with GFP1–9 fragment to form a full-length GFP. If the two proteins do not interact, GFP10 and GFP11 are not tethered and entropy is too high to allow complementation with GFP1–9. **(B)** Percentage of reconstituted GFP (rGFP) fluorescent cells analyzed by flow cytometry for the indicated transfection conditions. P-values were calculated using a Student's t test. **, p<0.01.

is an artificial biomolecular domain highly selective of the GTP-bound conformation of RHOA-like subfamily. We confirmed that the RH28 domain (produced in *E.coli* and purified) performed also in conventional RHOA immunoprecipitation assays after cytochalasin D or serum stimulation (data not shown).

RH28 competes with RHOA subfamily effector binding

RHOA subfamily global inhibition was extensively studied in various cellular models using the tat-C3 exoenzyme or more selectively by RNA interference. In adherent cultured epithelial cells, the main phenotype is linked to the RHOA/ROCK pathway inhibition that lead to actomyosin contractility defect, actin fiber disorganization, and focal adhesion disassembly (40, 41). To assess if the phenotype associated with RH28 expression in the initial screen effectively reflects RHOA inhibition, we analyzed actin cytoskeleton in human fibroblast MRC5 cell line that displays high density of actin stress fibers in 2D cell culture. Phalloidin staining of cells expressing NR27 nanobody highlights the cellular shape surrounded by strong cortical actin fibers and a high density of stress fibers crossing throughout the cell. In contrast, RH28 expression abolished totally actin fibers and induced stretched elongated cells with only subtle actin staining decorating multiple protrusions at the periphery (Supplementary Figure 7), an effect that phenocopied RHOA/ROCK pathway inhibition upon either C3 or ROCK inhibitor treatments (42).

To evaluate whether the RH28-mediated actomyosin perturbation was effectively linked with RHOA inhibition, we tested the RH28 capacity to compete with CA RHOA and the RHOTEKIN RBD interaction in the triSFP RHOA activation reporter cells, a cell line previously generated to sense RHOA activity with the tripartite split-GFP assay (34). In this cellular model (MRC5_GFP1-9 expressing the CA GFP10-RHOA and GFP11-RBD under the control of doxycycline), we transiently transfected mCherry fusions of different nanobodies and the RBD (Figure 3A). Flow cytometry quantification of the rGFP

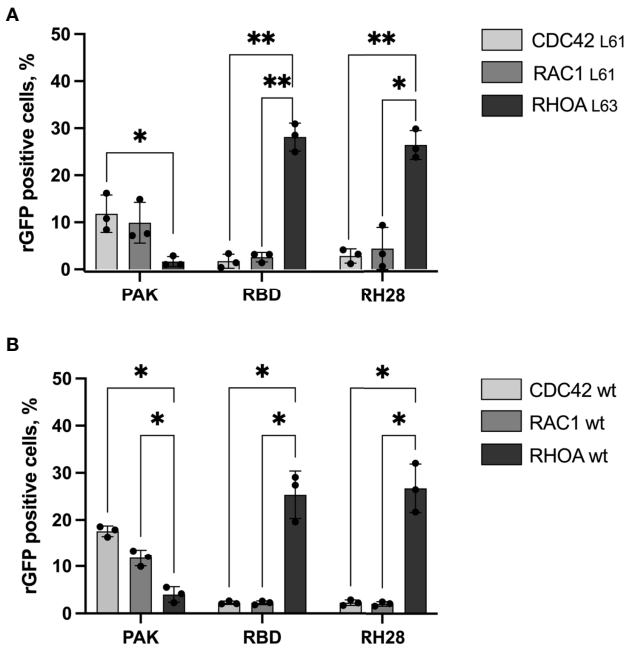

FIGURE 2
The RH28 is selective for active RHOA conformation in living cells. Percentage of reconstituted GFP (rGFP) fluorescent cells analyzed by flow cytometry for the indicated transfection conditions. **(A)** constitutively active mutants **(B)** wild-type proteins. P-values were calculated using a Student's t test.*p<0.05; **p<0.01.

fluorescence level, corresponding to CA RHOA and RBD interaction amount within each cell, was performed 48 hours after intrabody transfection in mCherry positive cells. We compared the rGFP fluorescence intensity among the different quartiles of mCherry expression levels in transfected cells (Figure 3B and Supplementary Figure 8A). As expected, we observed a decrease in rGFP fluorescence reaching 20% between the lowest and the highest quartile (rGFP geomean in mCherry last quartile 2356 vs. 3103 in first quartile) when RBD-mCherry was transiently transfected (Figure 3B). Indeed, in this assay, RBD-mCherry was supposed to behave as a direct competitor of CA-GFP10-RHOA and GFP11-RBD interaction. In the RH28-mCherry condition, we also observed significant rGFP fluorescence decrease in a similar range (rGFP geomean in mCherry last quartile 2272 vs. 3020 in first quartile) despite the fact that RH28-mCherry expression appeared lower than the RBD-mCherry (Supplementary Figure 8A). By contrast, the non-RHO nanobodies NR27 and NR53 did not affect rGFP fluorescence even for the highest expression levels in the 4th quartile, which confirms that they do not compete with RHOA activity and that the dose-dependent decay induced by RH28 is associated with its binding properties. This result suggests that the RH28 may efficiently impede the GFP11-RBD binding to CA-GFP10-RHOA, similarly to the RBD itself.

To confirm that the binding site of the RH28 interferes with the effector binding domain, we set up an *in vitro* competition assay based on the G-LISA RHO activity assay (Figure 3C and Supplementary Figure 8B). The G-LISA assay is based on the capture of GTP-bound RHO by RBD-like proteins covalently linked to the surface of the well. Like RH12, already reported as depleting the GST-RBD pull down assay (30), RH28 preincubation with 25 nM of recombinant CA 2SHA-RHOA induced a significant decrease of the signal in a concentration dependent manner (Figure 3C). We confirmed that no competition was observed on the RAC1 G-LISA assay (Supplementary Figure 8C). Altogether, these results suggest that the RH28 sterically impairs the RBD binding interface of RHOA proteins and might be a competitor of RHO effectors.

RH28 intrabody efficiently blocks RHOA/ROCK pathway in melanoma cancer cells

We finally assessed if the blocking properties of the RH28 intrabody could disturb cellular phenotype or functions. In melanoma, high level of actomyosin contractility due to RHOA/ROCK pathway has been associated with amoeboid migration of melanoma cell lines (43) as well as resistance to shear forces during extravasation (44). In this model, in order to have a better control over the expression level of intrabodies, we produced lentiviral cell lines expressing, under the control of doxycycline inducible promoter, a bicistronic gene encoding

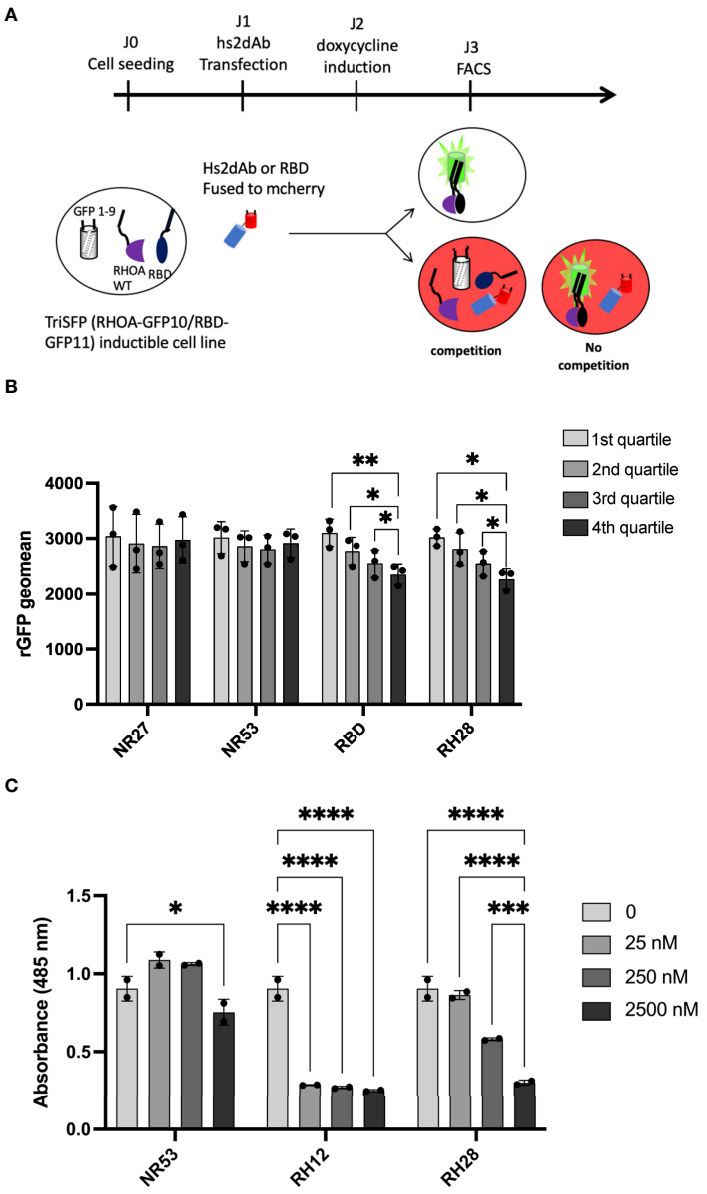

FIGURE 3
RH28 competes with RBD for active RHOA recognition. **(A)** Principle of the tripartite split-GFP complementation assay adapted to assess hs2dAb/RBD competition. Hs2dAb were transfected in the triSFP RHOA cell line, 24 hours before doxycycline induction. Among cells that express hs2dAb, a competition with RBD would lead to a decrease in the intensity of the rGFP fluorescence in mCherry positive cells. **(B)** For each hs2dAb, rGFP fluorescence intensity was quantified among the 4 different populations of mCherry positive cells (i.e., among the 4 cell populations ranked according to increasing levels of hs2dAb (or RBD) expression). **(C)** RHOA G-LISA competition assay with 10-fold dilutions of hs2dAb. Results were analyzed with two-way ANOVA model. Absorbance at 485 nm reflects RHOA-GTP captured by the coated RBD. P-values were calculated using a Student's t test. *p < 0.05; **p < 0.01; ***p < 0.001; ****p < 0.0001.

both the hs2dAb-6his-myc and a BFP fluorescent reporter through an IRES. After setting up the dose response to doxycycline to express similar level of RH28 and of the NR27 control we confirmed the functionality of the RH28 expressed in this model through RHOA immunoprecipitation experiments (Figure 4A). An increase in RHOA protein level could be observed upon RH28 expression that cannot be solely explained at the mRNA level (Supplementary Figure 9A), suggesting a potential stabilisation of RHOA induced by the RH28 nanobody. We further confirmed that the RH28 did not recognize RAC1 in this model (Supplementary Figures 9B, C). Moreover, upon RH28 expression, we observed in 2D cell culture an elongated phenotype that reminds fibroblast stretching previously observed (Supplementary Figure 7). In

10.3389/fimmu.2022.980539

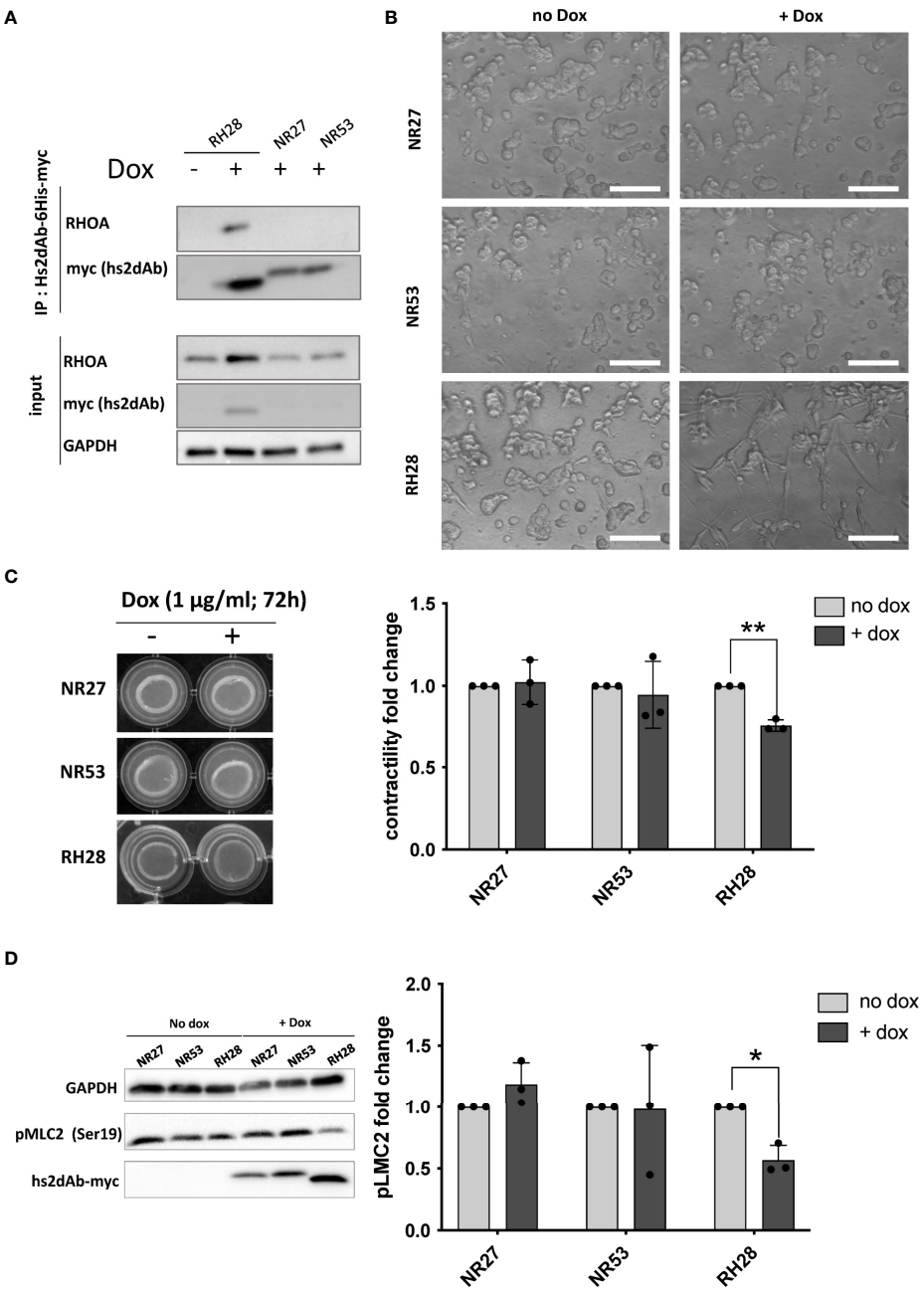

FIGURE 4
RH28 intrabody efficiently inhibits actomyosin contractility and blocks RHOA/ROCK pathway in melanoma cancer cells. **(A)** RH28 selectivity validation in WM266.4 lentiviral cell line. Expression of RH28 and NR-hs2dAb was induced or not with doxycycline at 1µg/ml. After 20 hours of induction, cells were harvested and cleared cell lysates were incubated with Ni-NTA beads for 45 min. Endogenous RHOA proteins was revealed with corresponding antibodies and hs2dAb were revealed with myc-tag antibody. **(B)** Representative images of cell line morphology in 3D collagen drops after 6 hours of hs2dAb expression. WM266.4 cell lines were seeded in collagen and phenotypes were analyzed 24 hours post doxycycline induction. At 40X magnification, elongated or rounded cell shape could be observed. Scale bar: 50 µm. **(C)** Representative images and quantification of gel contraction after 72 hours of treatment by doxycycline. **(D)** Representative immunoblot and quantification analysis of myosin light chain phosphorylation (pMLC2) status in the 3 different cell lines seeded in collagen drops. P-values were calculated using a Student's t test.*p<0.05; **p<0.01.

order to study the cellular behaviour in 3D environment in which RHO activity plays a more important role than in 2D (45, 46), cells were seeded in collagen drops. In contrast to their normal spread morphology in 2D, WM266.4 exhibited as expected a rounded phenotype in this 3D matrix (44, 47). In comparison to NR controls and to non-induced doxycycline condition, the RH28 expression uniformly induced a striking switch from rounded cells to highly elongated cells (Figure 4B). This phenotype was also associated with a defect in actomyosin contractility (24% decrease upon RH28 expression) as demonstrated by an impaired collagen retraction (Figure 4C). To confirm RHOA/ROCK pathway inhibition, we analyzed the expression of phosphorylated cofilin and phosphorylated Myosin Light Chain (pMLC) which is one canonical target defining ROCK signalling activity (48). Upon RH28 expression induction in cells grown in 3D collagen drops, elongated cell phenotype was associated with a significant decrease of phospho-MLC2 amount (Figure 4D). All together, these results demonstrate that RH28 functions in an intracellular context by blocking RHOA downstream signalling through a direct interference with RHOA-GTP effectors, leading to a specific cellular phenotype.

Discussion

Small GTPases of RHOA subfamily are master regulators of cellular processes involving actomyosin dynamics, such as cell division, cell migration or invasion. In this study we identified and characterized the nanobody RH28 as an intrabody selective towards the GTP-bound conformation of RHOA with no apparent cross reactivity towards RAC1 or CDC42. The RH28 behaves as an artificial RHO Binding Domain combining the high intracellular stability of nanobodies with inhibitory properties. This tool opens opportunities to investigate the fine-tuning of RHOA subfamily activation homeostasis in various biological contexts.

We previously generated from a synthetic phage display library based on a unique nanobody scaffold, several intracellular molecular binders of the GTP-bound RHOA or RHOB conformers (13, 30, 31). The lack of selectivity of such molecular tools targeting RHO GTPase activities or pathways is a key point in the interpretation of the cellular response. Actually, the highly conserved G domains that switch conformation between GDP or GTP loading led to the identification, in our previous work, of several conformational nanobodies. While expressed as intracellular antibodies, some hs2dAb were not able to block GTPase signalling while others were efficient blocking-nanobodies but cross-reacted with the RAC subfamily of GTPases, the close homologues of the RHOA subfamily. One pan RHO/RAC-GTP nanobody appeared inert at a moderate expression level and was engineered as an active RHO BRET biosensor (30). Another nanobody functionalised with a Fbox, referred to as F-B6 (13), was efficiently targeting RHOB-GTP for protein degradation, albeit through the dependency of the fused domain that requires a multicomponent E3-ligase catalytic activity which is not controlled by the tool itself. Of note, the nanobody referred to as RH12 with subnanomolar affinity towards RHO/RAC-GTP (31), displaces the endogenous effectors Rho Binding Domain in biochemical assays (30), induces a complex phenotype of cell border shrinkage and further toxicity that impaired cell viability (30, 31). While this nanobody mediated signalling blockade appeared encouraging to develop a macrodrug to alter RHO-GTP function, the lack of selectivity between RHOA-like and RAC1 subfamilies impeded its development as these two major RHO GTPases display opposite functions in many cellular contexts (22, 49–51).

It is challenging to translate the biochemical selectivity of molecular interaction of proteins or antibodies assessed *in vitro* to their behaviour in the intracellular complexity. Intracellular functionality of domain antibodies or alternative scaffolds have been assessed by numerous approaches, such as fluorescent two-hybrid (52) or BRET (30, 53) assays which allow, due to their reversibility, a dynamic quantification of the protein-protein interaction. However, these approaches show inherent background signal that may require tight expression control of the two components. Here, we used the tripartite split-GFP protein-protein interaction reporter assay because no signal background could emanate from the three components. Its main advantages are the absence of false positive interacting partners, and the ability to reveal low affinity interactions due to the irreversibility of the reconstituted GFP (32, 33). Moreover, the split-GFP system was previously successfully implemented to monitor active RHO or RAS GTPase interactions with their respective effector domains in cells (34). The lack of signal obtained for the RH28 with RAC1 or CDC42 active mutants thus asserts that this nanobody could not cross react with these GTPases. Nevertheless, among positive signals, this assay does not reflect conventional binding kinetic parameters of partners' interactions. It is noteworthy that the irreversibility of the rGFP induces accumulation of a signal to a certain extent, thus revealing low affinity, transient interactions, or strong interaction with a similar level of quantification. Accordingly, we observed, in previous development of the assay (32, 34) or here with the RH12 and the RBD example, that a low signal discrepancy in this assay reflects a high selectivity quantified in a reversible biochemical interaction assay such as ELISA or SPR (15). Actually, although the selectivity of the RH12 towards the active conformation of RHOA GTPases was quantitatively much higher than the one of the RHOTEKIN RBD using *in-vitro* biochemical assays (15), this strong selectivity discrepancy was eclipsed in the tripartite split-GFP measurements. Therefore, we considered here that the binding of RH28, RH29 and RH35, reflected a strong conformational selectivity towards the active form of RHOA in cells. We also analysed cross-reactivity with

RAC1 and CDC42 both *in vitro* and in cells. Although we did not formally assess the interaction with the 15 other members of RHO GTPase subfamilies, the lack of binding of the RH28 to the two RHOA-subfamily closest members may suggest that it only interacts with active RHOA/B/C proteins (39).

The phenotype induced by the RH28 expression in cells appeared more defined than the one resulting of the RH12 blockade (30, 31). Indeed, in HeLa, MRC5 or melanoma WM266-4 cell lines, cells expressing RH28 displayed a stretched elongated shape. We reasoned that this phenotype was probably correlated with the inhibition of the RHOA/ROCK pathway as the lack of contractility neither antagonizes the RAC1 mediated protrusion formation nor retracts the rear of migrating cells, thus elongating the cells by stretching them until adhesion collapsed. This phenotype was reminiscent of the ROCK inhibition by 10μM of Y27632 or other ROCK small molecule inhibitors (51), and we confirmed that this pathway was downregulated upon RH28 expression as phosphorylated Myosin Light Chain (pMLC) levels decreased. This marker of acto-myosin contraction is involved in mechanisms related to cancer cell plasticity between amoeboid or mesenchymal phenotypes, which implies different motile behaviours. Recently, high level of melanoma cell plasticity was demonstrated as a feature of MAPKi-therapy resistant melanoma (54). Several studies reported the association of RHOA or RHOB GTPases with invasive cancer resistance (54–56). ROCK inhibitors have been reported in preclinical studies to impair migration and invasion (57), to potentiate the immune system (58) or sensitize the immune checkpoint blockade response (59). Albeit the RHOA/ROCK pathway is actively targeted with numerous ROCK pharmacological inhibitors with a prospect to block invasion and metastasis in clinical trials (60), to date, none of them are approved for clinical use in cancer therapy. This may account to the lack of selectivity of ATP binding pocket kinase inhibitors that often induce side effects. The advantage of a nanobody that blocks RHOA-GTP downstream pathway may reside in the exquisite selectivity of antibody binding interface. However, the main challenge of biomolecular drugs that target intracellular activities remains their delivery as recombinant protein or mRNA inside tumor cells (61).

Data availability statement

The raw data supporting the conclusions of this article will be made available by the authors, without undue reservation.

Author contributions

Conception and design: LK, GF and AO. Development of methodology: LK and AO. Acquisition of data (including facilities): LK, CT, LL and AO. Analysis and interpretation of data: LK, CT, SC, GF and AO. Administrative, technical, or material support: FK, NB, SLP, RG, PC, SC, LL and MD. Study supervision: GF, SC and AO. Financial support: GF. All authors revised and agreed with the submission of the manuscript.

Funding

This work was financially supported by the grant Fondation pour la Recherche Médicale (FRM) (Equipe labellisée FRM [DEQ20170839117]). NB was supported by the Fondation pour la Recherche Médicale (FRM, FDT20130928310). This study used some fundings received under a collaboration contract with Cisbio Bioassays.

Acknowledgments

We acknowledge the Pôle Technologique du CRCT – Plateau Imagerie, Cytométrie and Vectorologie for assistance in cell sorting and lentiviral production. We thank P. Pellehaut for comments on the manuscript. We thank the grant Fondation pour la Recherche Médicale (FRM) (Equipe labellisée FRM [DEQ20170839117]).

Conflict of interest

Authors NB, LK, GF and AO are co-inventors on the patent PTC/EP2016/052136, concerning the discovery of RHO-GTP single-domain antibodies and their applications.

The authors declare that this study received funding from Cisbio Bioassays. The funder was not involved in the study design, collection, analysis, interpretation of data, the writing of this article or the decision to submit it for publication

Publisher's note

Supplementary material

The Supplementary Material for this article can be found online at: https://www.frontiersin.org/articles/10.3389/fimmu.2022.980539/full#supplementary-material

References

1. Hoogenboom HR. Selecting and screening recombinant antibody libraries. *Nat Biotechnol* (2005) 23:1105–16. doi: 10.1038/nbt1126

2. Helma J, Cardoso MC, Muyldermans S, Leonhardt H. Nanobodies and recombinant binders in cell biology. *J Cell Biol* (2015) 209(5):633–44. doi: 10.1083/jcb.201409074

3. Pillay TS, Muyldermans S. Application of single-domain antibodies ("Nanobodies") to laboratory diagnosis. *Ann Lab Med* (2021) 41(6):549–58. doi: 10.3343/alm.2021.41.6.549

4. Kaiser PD, Maier J, Traenkle B, Emele F, Rothbauer U. Recent progress in generating intracellular functional antibody fragments to target and trace cellular components in living cells. *Biochim Biophys Acta* (2014) 1844(11):1933–42. doi: 10.1016/j.bbapap.2014.04.019

5. Wagner TR, Rothbauer U. Nanobodies right in the middle: Intrabodies as toolbox to visualize and modulate antigens in the living cell. *Biomolecules* (2020) 10 (12):1701. doi: 10.3390/biom10121701

6. Gettemans J, De Dobbelaer B. Transforming nanobodies into high-precision tools for protein function analysis. *Am J Physiol-Cell Physiol* (2021) 320(2):C195–215. doi: 10.1152/ajpcell.00435.2020

7. Rothbauer U, Zolghadr K, Tillib S, Nowak D, Schermelleh L, Gahl A, et al. Targeting and tracing antigens in live cells with fluorescent nanobodies. *Nat Methods* (2006) 3(11):887–9. doi: 10.1038/nmeth953

8. Tang JCY, Szikra T, Kozorovitskiy Y, Teixiera M, Sabatini BL, Roska B, et al. A nanobody-based system using fluorescent proteins as scaffolds for cell-specific gene manipulation. *Cell* (2013) 154(4):928–39. doi: 10.1016/j.cell.2013.07.021

9. Traenkle B, Segan S, Fagbadebo FO, Kaiser PD, Rothbauer U. A novel epitope tagging system to visualize and monitor antigens in live cells with chromobodies. *Sci Rep* (2020) 10(1):14267. doi: 10.1038/s41598-020-71091-x

10. Götzke H, Kilisch M, Martínez-Carranza M, Sograte-Idrissi S, Rajavel A, Schlichthaerle T, et al. The ALFA-tag is a highly versatile tool for nanobody-based bioscience applications. *Nat Commun* (2019) 10(1):4403. doi: 10.1038/s41467-019-12301-7

11. Lin Y, Chen Z, Hu C, Chen ZS, Zhang L. Recent progress in antitumor functions of the intracellular antibodies. *Drug Discov Today* (2020) 25(6):1109–20. doi: 10.1016/j.drudis.2020.02.009

12. Messer A, Butler DC. Optimizing intracellular antibodies (intrabodies/nanobodies) to treat neurodegenerative disorders. *Neurobiol Dis* (2020) 134:104619. doi: 10.1016/j.nbd.2019.104619

13. Bery N, Keller L, Soulié M, Gence R, Iscache AL, Cherier J, et al. A targeted protein degradation cell-based screening for nanobodies selective toward the cellular RHOB GTP-bound conformation. *Cell Chem Biol* (2019) 26:1544–58. doi: 10.2139/ssrn.3188332

14. Marschall ALJ, Dübel S, Böldicke T. Recent advances with ER targeted intrabodies. *Adv Exp Med Biol* (2016) 917:77–93. doi: 10.1007/978-3-319-32805-8_5

15. Keller L, Tardy C, Ligat L, Gilhodes J, Filleron T, Bery N, et al. Nanobody-based quantification of GTP-bound RHO conformation reveals RHOA and RHOC activation independent from their total expression in breast cancer. *Anal Chem* (2021) 93(15):6104–11. doi: 10.1021/acs.analchem.0c05137

16. Ren XD, Schwartz MA. Determination of GTP loading on rho. *Methods Enzymol* (2000) 325:264–72. doi: 10.1016/S0076-6879(00)25448-7

17. Etienne-Manneville S, Hall A. Rho GTPases in cell biology. *Nature* (2002) 420(6916):629–35. doi: 10.1038/nature01148

18. Ridley AJ. Rho GTPase signalling in cell migration. *Curr Opin Cell Biol* (2015) 36:103–12. doi: 10.1016/j.ceb.2015.08.005

19. Pertz O, Hodgson L, Klemke RL, Hahn KM. Spatiotemporal dynamics of RhoA activity in migrating cells. *Nature* (2006) 440:1069–72. doi: 10.1038/nature04665

20. Reffay M, Parrini MC, Cochet-Escartin O, Ladoux B, Buguin A, Coscoy S, et al. Interplay of RhoA and mechanical forces in collective cell migration driven by leader cells. *Nat Cell Biol* (2014) 16(3):217–23. doi: 10.1038/ncb2917

21. Sahai E, Ishizaki T, Narumiya S, Treisman R. Transformation mediated by RhoA requires activity of ROCK kinases. *Curr Biol* (1999) 9:136–45. doi: 10.1016/S0960-9822(99)80067-0

22. Haga RB, Ridley AJ. Rho GTPases: Regulation and roles in cancer cell biology. *Small GTPases* (2016) 7(4):207–21. doi: 10.1080/21541248.2016.1232583

23. Sahai E, Marshall CJ. RHO-GTPases and cancer. *Nat Rev Cancer* (2002) 2:133–42. doi: 10.1038/nrc725

24. Flentje A, Kalsi R, Monahan TS. Small GTPases and their role in vascular disease. *Int J Mol Sci* (2019) 20(4):E917. doi: 10.3390/ijms20040917

25. Kalpachidou T, Spiecker L, Kress M, Quarta S. Rho GTPases in the physiology and pathophysiology of peripheral sensory neurons. *Cells* (2019) 8(6): E591. doi: 10.3390/cells8060591

26. Aktories K, Mohr C, Koch G. Clostridium botulinum C3 ADP-ribosyltransferase. *Curr Top Microbiol Immunol* (1992) 175:115–31. doi: 10.1007/978-3-642-76966-5_6

27. Sahai E, Olson MF. Purification of TAT-C3 exoenzyme. *Methods Enzymol.* (2006) 406:128–40. doi: 10.1016/S0076-6879(06)06011-3.

28. Boulter E, Garcia-Mata R, Guilluy C, Dubash A, Rossi G, Brennwald PJ, et al. Regulation of rho GTPase crosstalk, degradation and activity by RhoGDI1. *Nat Cell Biol* (2010) 12:477–83. doi: 10.1038/ncb2049

29. Lin Y, Zheng Y. Approaches of targeting rho GTPases in cancer drug discovery. *Expert Opin Drug Discov* (2015) 10(9):991–1010. doi: 10.1517/17460441.2015.1058775

30. Keller L, Bery N, Tardy C, Ligat L, Favre G, Rabbitts TH, et al. Selection and characterization of a nanobody biosensor of GTP-bound RHO activities. *Antibodies* (2019) 8:8. doi: 10.3390/antib8010008

31. Moutel S, Bery N, Bernard V, Keller L, Lemesre E, de Marco A, et al. NaLi-H1: A universal synthetic library of humanized nanobodies providing highly functional antibodies and intrabodies. *eLife* (2016) 5. doi: 10.7554/eLife.16228

32. Cabantous S, Nguyen HB, Pedelacq JD, Koraïchi F, Chaudhary A, Ganguly K, et al. A new protein-protein interaction sensor based on tripartite split-GFP association. *Sci Rep* (2013) 3:2854. doi: 10.1038/srep02854

33. Pedelacq JD, Cabantous S. Development and applications of superfolder and split fluorescent protein detection systems in biology. *Int J Mol Sci* (2019) 20(14): E3479. doi: 10.3390/ijms20143479

34. Koraïchi F, Gence R, Bouchenot C, Grosjean S, Lajoie-Mazenc I, Favre G, et al. High-content tripartite split-GFP cell-based assays to screen for modulators of small GTPase activation. *J Cell Sci* (2018) 131(1):jcs210419. doi: 101242/jcs.210419

35. Olichon A, Surrey T. Selection of genetically encoded fluorescent single domain antibodies engineered for efficient expression in escherichia coli. *J Biol Chem* (2007) 282(50):36314–20. doi: 10.1074/jbc.M704908200

36. Trutnau HH. New multi-step kinetics using common affinity biosensors saves time and sample at full access to kinetics and concentration. *J Biotechnol* (2006) 124(1):191–5. doi: 10.1016/j.jbiotec.2006.01.006

37. Bousquet E, Mazieres J, Privat M, Rizzati V, Casanova A, Ledoux A, et al. Loss of RhoB expression promotes migration and invasion of human bronchial cells *via* activation of AKT1. *Cancer Res* (2009) 69:6092–9. doi: 10.1158/0008-5472.CAN-08-4147

38. Vega FM, Fruhwirth G, Ng T, Ridley AJ. RhoA and RhoC have distinct roles in migration and invasion by acting through different targets. *J Cell Biol* (2011) 193 (4):655–65. doi: 10.1083/jcb.201011038

39. Olson MF. Rho GTPases, their post-translational modifications, disease-associated mutations and pharmacological inhibitors. *Small GTPases* (2018) 9 (3):203–15. doi: 10.1080/21541248.2016.1218407

40. Ridley AJ, Hall A. The small GTP-binding protein rho regulates the assembly of focal adhesions and actin stress fibers in response to growth factors. *Cell* (1992) 70(3):389–99. doi: 10.1016/0092-8674(92)90163-7

41. Uehata M, Ishizaki T, Satoh H, Ono T, Kawahara T, Morishita T, et al. Calcium sensitization of smooth muscle mediated by a rho-associated protein kinase in hypertension. *Nature* (1997) 389(6654):990–4. doi: 10.1038/40187

42. Worthylake RA, Burridge K. RhoA and ROCK promote migration by limiting membrane protrusions. *J Biol Chem* (2003) 278(15):13578–84. doi: 10.1074/jbc.M211584200

43. Rodriguez-Hernandez I, Cantelli G, Bruce F, Sanz-Moreno V. Rho, ROCK and actomyosin contractility in metastasis as drug targets. *F1000Research* (2016) 5:783. doi: 10.12688/f1000research.7909.1

44. Pinner S, Sahai E. Imaging amoeboid cancer cell motility *in vivo*. *J Microsc* (2008) 231(3):441–5. doi: 10.1111/j.1365-2818.2008.02056.x

45. Petrie RJ, Gavara N, Chadwick RS, Yamada KM. Nonpolarized signaling reveals two distinct modes of 3D cell migration. *J Cell Biol* (2012) 197(3):439–55. doi: 10.1083/jcb.201201124

46. Riching KM, Keely PJ. Rho family GTPases: Making it to the third dimension. *Int J Biochem Cell Biol* (2015) 59:111–5. doi: 10.1016/j.biocel.2014.11.007

47. Yin Z, Sadok A, Sailem H, McCarthy A, Xia X, Li F, et al. A screen for morphological complexity identifies regulators of switch-like transitions between discrete cell shapes. *Nat Cell Biol* (2013) 15(7):860–71. doi: 10.1038/ncb2764

48. Julian L, Olson MF. Rho-associated coiled-coil containing kinases (ROCK): structure, regulation, and functions. *Small GTPases* (2014) 5:e29846. doi: 10.4161/sgtp.29846

49. Bustelo XR, Sauzeau V, Berenjeno IM. GTP-binding proteins of the Rho/Rac family: regulation, effectors and functions *in vivo*. *BioEssays News Rev Mol Cell Dev Biol* (2007) 29(4):356–70. doi: 10.1002/bies.20558

50. Norman JC, Price LS, Ridley AJ, Koffer A. The small GTP-binding proteins, rac and rho, regulate cytoskeletal organization and exocytosis in mast cells by parallel pathways. *Mol Biol Cell* (1996) 7:1429–42. doi: 10.1091/mbc.7.9.1429

51. Sahai E, Marshall CJ. Differing modes of tumour cell invasion have distinct requirements for Rho/ROCK signalling and extracellular proteolysis. *Nat Cell Biol* (2003) 5:711–9. doi: 10.1038/ncb1019

52. Zolghadr K, Mortusewicz O, Rothbauer U, Kleinhans R, Goehler H, Wanker EE, et al. A fluorescent two-hybrid assay for direct visualization of protein interactions in living cells. *Mol Cell Proteomics MCP* (2008) 7(11):2279–87. doi: 10.1074/mcp.M700548-MCP200

53. Bery N, Legg S, Debreczeni J, Breed J, Embrey K, Stubbs C, et al. KRAS-specific inhibition using a DARPin binding to a site in the allosteric lobe. *Nat Commun* (2019) 10(1):2607. doi: 10.1038/s41467-019-10419-2

54. Orgaz JL, Crosas-Molist E, Sadok A, Perdrix-Rosell A, Maiques O, Rodriguez-Hernandez I, et al. Myosin II reactivation and cytoskeletal remodeling as a hallmark and a vulnerability in melanoma therapy resistance. *Cancer Cell* (2020) 37(1):85–103.e9. doi: 10.1016/j.ccell.2019.12.003

55. Calvayrac O, Mazières J, Figarol S, Marty-Detraves C, Raymond-Letron I, Bousquet E, et al. The RAS-related GTPase RHOB confers resistance to EGFR-tyrosine kinase inhibitors in non-small-cell lung cancer *via* an AKT-dependent mechanism. *EMBO Mol Med* (2017) 9(2):238–50. doi: 10.15252/emmm.201606646

56. Delmas A, Cherier J, Pohorecka M, Medale-Giamarchi C, Meyer N, Casanova A, et al. The c-Jun/RHOB/AKT pathway confers resistance of BRAF-mutant melanoma cells to MAPK inhibitors. *Oncotarget* (2015) 6(17):15250–64. doi: 10.18632/oncotarget.3888

57. Patel RA, Liu Y, Wang B, Li R, Sebti SM. Identification of novel ROCK inhibitors with anti-migratory and anti-invasive activities. *Oncogene* (2014) 33 (5):550–5. doi: 10.1038/onc.2012.634

58. Teiti I, Florie B, Pich C, Gence R, Lajoie-Mazenc I, Rochaix P, et al. *In vivo* effects in melanoma of ROCK inhibition-induced FasL overexpression. *Front Oncol* (2015) 5:156. doi: 10.3389/fonc.2015.00156

59. Kim S, Kim SA, Nam GH, Hong Y, Kim GB, Choi Y, et al. *In situ* immunogenic clearance induced by a combination of photodynamic therapy and rho-kinase inhibition sensitizes immune checkpoint blockade response to elicit systemic antitumor immunity against intraocular melanoma and its metastasis. *J Immunother Cancer* (2021) 9(1):e001481. doi: 10.1136/jitc-2020-001481

60. McLeod R, Kumar R, Papadatos-Pastos D, Mateo J, Brown JS, Garces AHI, et al. First-in-Human study of AT13148, a dual ROCK-AKT inhibitor in patients with solid tumors. *Clin Cancer Res* (2020) 26(18):4777–84. doi: 10.1158/1078-0432.CCR-20-0700

61. Bannas P, Hambach J, Koch-Nolte F. Nanobodies and nanobody-based human heavy chain antibodies as antitumor therapeutics. *Front Immunol* (2017) 8:1603. doi: 10.3389/fimmu.2017.01603

frontiers | Frontiers in Immunology

TYPE Review
PUBLISHED 13 October 2022
DOI 10.3389/fimmu.2022.1012806

OPEN ACCESS

EDITED BY
Zong Sheng Guo,
Roswell Park Comprehensive Cancer Center, United States

REVIEWED BY
Rajesh Kumar,
National Institutes of Health (NIH), United States
Zuqiang Liu,
Allegheny Health Network, United States

*CORRESPONDENCE
Zahra Sharifzadeh
zsharifzadeh@gmail.com
Shahriyar Abdoli
shahriyaran@gmail.com

SPECIALTY SECTION
This article was submitted to Cancer Immunity and Immunotherapy, a section of the journal Frontiers in Immunology

RECEIVED 05 August 2022
ACCEPTED 27 September 2022
PUBLISHED 13 October 2022

CITATION
Jafari M, Kadkhodazadeh M, Shapourabadi MB, Goradel NH, Shokrgozar MA, Arashkia A, Abdoli S and Sharifzadeh Z (2022) Immunovirotherapy: The role of antibody based therapeutics combination with oncolytic viruses. *Front. Immunol.* 13:1012806. doi: 10.3389/fimmu.2022.1012806

Immunovirotherapy: The role of antibody based therapeutics combination with oncolytic viruses

Mahdie Jafari[1], Maryam Kadkhodazadeh[2], Mina Bahrololoumi Shapourabadi[3], Nasser Hashemi Goradel[4], Mohammad Ali Shokrgozar[5], Arash Arashkia[2], Shahriyar Abdoli[6]* and Zahra Sharifzadeh[1]*

[1]Department of Immunology, Pasteur Institute of Iran, Tehran, Iran, [2]Department of Molecular Virology, Pasture Institute of Iran, Tehran, Iran, [3]HUM Immune Biotech Company, Tehran, Iran, [4]Department of Medical Biotechnology, School of Advanced Technologies in Medicine, Tehran University of Medical Sciences, Tehran, Iran, [5]National Cell Bank of Iran, Pasteur Institute of Iran, Tehran, Iran, [6]School of Advanced Medical Technologies, Golestan University of Medical Sciences, Gorgan, Iran

Despite the fact that the new drugs and targeted therapies have been approved for cancer therapy during the past 30 years, the majority of cancer types are still remain challenging to be treated. Due to the tumor heterogeneity, immune system evasion and the complex interaction between the tumor microenvironment and immune cells, the great majority of malignancies need multimodal therapy. Unfortunately, tumors frequently develop treatment resistance, so it is important to have a variety of therapeutic choices available for the treatment of neoplastic diseases. Immunotherapy has lately shown clinical responses in malignancies with unfavorable outcomes. Oncolytic virus (OV) immunotherapy is a cancer treatment strategy that employs naturally occurring or genetically-modified viruses that multiply preferentially within cancer cells. OVs have the ability to not only induce oncolysis but also activate cells of the immune system, which in turn activates innate and adaptive anticancer responses. Despite the fact that OVs were translated into clinical trials, with T-VECs receiving FDA approval for melanoma, their use in fighting cancer faced some challenges, including off-target side effects, immune system clearance, non-specific uptake, and intratumoral spread of OVs in solid tumors. Although various strategies have been used to overcome the challenges, these strategies have not provided promising outcomes in monotherapy with OVs. In this situation, it is increasingly common to use rational combinations of immunotherapies to improve patient benefit. With the development of other aspects of cancer immunotherapy strategies, combinational therapy has been proposed to improve the anti-tumor activities of OVs. In this regard, OVs were combined with other biotherapeutic platforms, including various forms of antibodies, nanobodies, chimeric antigen receptor (CAR) T cells, and dendritic cells, to reduce the side effects of OVs and enhance their efficacy. This article reviews

10.3389/fimmu.2022.1012806

the promising outcomes of OVs in cancer therapy, the challenges OVs face and solutions, and their combination with other biotherapeutic agents.

KEYWORDS

oncolytic virotherapy, cancer immunotherapy, nanobody, antibody, combination therapy, immunovirotherapy, T cells, Nk cells

1 Introduction

Cancer is rapidly becoming the leading cause of mortality worldwide. Every year, nineteen million new malignancies are diagnosed, resulting in about ten million deaths (1, 2). Because cancer is a complicated and heterogeneous disease with numerous genetic mutations, current cancer therapies frequently do not achieve the desired outcomes for the majority of malignancies, despite many promises of progress in treatment. Consequently, cancer treatment has become a challenge, so more efficient treatment procedures are required (3, 4). Traditional treatments, such as surgery, chemotherapy, hormone therapy, and radiation therapy, have not only unfavorable adverse effects on individuals in the majority of patients but also yield minimal long-term benefits (5).

Immunotherapy has been a promising approach to cancer treatment over the last two decades. It is target-specific, can be adjusted to the needs of each patient, and has fewer side effects than earlier cancer therapies. Immunotherapy drugs can be more effective against cancer when combined with other therapies, such as radiation therapy, chemotherapy and targeted drugs. As an example, several studies have shown promising results of using a mix of chemotherapy and immunotherapy as a first strike against non-small cell lung cancer (2, 5, 6). To date, various immunotherapeutic approaches have been introduced in cancer treatment, such as pro-inflammatory cytokines, cancer vaccines, adoptive T-cell therapy, antibody-based immunotherapies, and oncolytic viruses (OVs) (7, 8).

Currently, oncolytic virotherapy (OVT) is one of the most popular cancer immunotherapy approaches owing to the flexibility of viral production platforms and providing a multimodal strategy to selectively and efficiently target and destroy tumor cells (9, 10). Furthermore, OV platforms could be applied without depth knowledge of tumor antigens in various malignancies (11). OVs provide multi-mechanistic therapeutic effects against the majority of cancer types, but like with many other current cancer therapies, oncolytic virotherapy still faces challenges and hurdles before becoming an effective anticancer therapy (3). Despite some encouraging outcomes, OVT still is not completely effective in most cases because of some issues such as tumor bulk penetration, anti-viral immune responses, and unfavorable tumor microenvironment (TME) (12, 13). On the other hand, due to off-target infection and sequestrations by non-specific tissues, especially in systemic administration, there are some safety concerns about using OVs as therapeutic agents (14).

Despite this, in clinical trials of monotherapy, OVs with older generations of armings (such as GM-CSF) have elicited a potent and robust response. Newer methods, like combining OVs with immunotherapies to turn "immune-cold" tumors into "immune-hot" ones, can almost certainly make OVs more effective (3, 15, 16). The use of rational combination therapies and targeting have been raised to improve the efficacy of OVs, and these combinations may integrate multiple methodologies and technologies that can increase patient benefit from the treatment (9, 17).

Oncolytic viruses have been used in combination with other cancer treatment modalities of immunotherapy or cell therapy, such as antibodies, nanobodies, bispecific (antibody-based immunotherapies), checkpoint inhibitors, adoptive T-cell therapy, natural killer (NK) cells, and T-cell engagers (BiTE), to improve cancer treatment (10). In this review, the challenges of OVT are discussed in detail, including its low efficiency, safety issues, and delivery methods, and finally, we focus on combining OVs with other biotherapeutic strategies to overcome the challenges.

2 Intro to virotherapy: From concept to bedside

2.1 An overview of virotherapy

The concept of employing viruses to treat cancer cells has existed almost as long as viruses have been discovered (18, 19). For more than a century, viruses have been considered potential cancer-fighting agents (20–22). Since the middle of the 1800s, case reports indicated that spontaneous microbial infections in cancer patients might sometimes temporarily reduce tumor burden and, thus, many therapeutic trials have been conducted employing wild-type non-attenuated viruses in cancer therapy

(22–25). In the late 1890s, a finding that a "flu-like" condition accompanied by generalized inflammation corresponded with a reduction in tumor cells in a leukemic patient further confirmed the potential therapeutic significance of viruses, in particular (22, 26). In another case, the measles virus has been shown to be an effective natural anticancer agent in the treatment of Burkitt's lymphoblastic lymphoma (27).

For a long time, the development of selective and harmless viruses was impeded by a lack of tools for viral genome modification (16, 28, 29). It took a few decades for OVT to reach its full potential when recombinant DNA technology became widely used to increase safety (6, 22, 29). The use of a thymidine kinase (TK)-negative mutant of Herpes Simplex Virus (HSV-1) as a possible treatment for gliomas was the first report of a virus modification to reproduce only in dividing cells. TK-mutated HSV-1 has been demonstrated to reproduce preferentially in cancer cells (30–32). A mutated adenovirus (Ad), dl1520 (also known as ONYX-015), was discovered in 1996 that had the E1B55K gene deleted (33, 34). Since the E1B-55kD gene product can bind to and inactivate p53, it was assumed that the deletion of E1B-55kDa renders the mutant adenovirus unable to inactivate p53 in normal cells and, therefore, the viral replication cycle would not be completed. Moreover, the replication of ONYX-015 might be related to the indirect inactivation of the p53 pathway in tumor cells due to the loss of upstream regulators such as p14ARF (35). Nevertheless, it was shown that the p53 status can not impose a restriction on ONYX-015 replication. Actually, the loss of E1B-55K-mediated late viral RNA export results in inability of ONYX-015 to replicate in normal cells. Since, the tumor cells have a special capacity to efficiently export late viral RNA in the absence of E1B-55K, ONYX-015 would selectively replicate in cancer cells (36). As a result, clinical uses for OVs are increasingly prominent due to technological advances (37, 38).

OVs can selectively reproduce in cancer cells and propagate throughout a tumor without affecting the healthy tissues (39, 40). Despite some viruses' natural tropism for tumors, the wide range of tumor forms and histologic origins makes it challenging to link OVs to a specific malignancy (41, 42). Additionally, it is crucial to consider the tumor-specificity, possible pathogenicity, immunogenicity, druggability, and the viral stability while choosing a virus.

The administration of OVs, either systemically or locally, in cancer-bearing hosts successfully induces antiviral immunity. As a result, OV treatments activate two separate immune responses: antiviral and anticancer. While antitumor immunity is advantageous, antiviral immune responses, including innate and adaptive, are thought to be harmful to the success of OV-based therapy. Indeed, it is conceivable that antiviral immune responses might impede strong viral replication and spread, reducing direct oncolysis of cancer cells,and therefore the efficiency of OV therapy (43). As a result, the most effective "time window" for most OVs to activate anti-tumoral immunity is within the first 1-2 weeks of administration, before the virus is eliminated. One of the major challenges of OV immunotherapy is to strike a balance between the desirable induction of new anti-tumoral immunity and the competing anti-viral immunity while preventing undesired antiviral effector processes from becoming the dominant response pathway, thereby obstructing the acquisition of acquired anti-tumoral immunity. Because of this, researchers are now looking into a number of ways to treat anti-OV immune responses (44). Many studies are developing strategies to enhance OVs construction, reduce clinical toxicity, design efficient OV delivery systems, and increase efficacy by utilizing contemporary genetic engineering approaches (45). A large number of OVs are being investigated in clinical studies, and an even greater number are being evaluated in preclinical studies. The safety of virotherapy has been shown by clinical researches utilizing various OVs to treat different cancers (42, 46, 47).

2.2 Viruses that have already received regulatory approval for the treatment of cancer

Following 30 years of research and encouraging findings from several clinical trials, the OV has attracted a lot of interest, leading to an OV approved by FDA for cancer treatment (25, 38). Four OVs have been approved for use in the treatment of various malignancies. Despite being licensed in Latvia, the first OV, a picornavirus named Rigvir, was never widely used worldwide (48, 49). In 2005, the Chinese SFDA approved the use of a modified Ad, known as Oncorine (H101), in combination with chemotherapy for the treatment of head and neck cancer (50–52). Talimogene laherparepvec (T-VEC, Imlygic), an attenuated HSV containing granulocyte-macrophage colony-stimulating factor (GM-CSF), was approved by the FDA in October 2015 for the treatment of melanoma in the US (53–56). In Japan, a modified version of the HSV, called Delytact, received time-limited and conditional marketing approval for the treatment of malignant gliomas in 2021 (21, 26, 57–59). A summary of the aforementioned OVs has been presented in Table 1.

2.3 Action mechanisms of oncolytic viruses: From cytolysis to microenvironment modulation and antitumor immunostimulation

Tumor cells, due to their resistance against apoptosis, appear to be a preferred breeding ground for a wide variety of viruses (22, 60). Viral infection kills tumor cells by several mechanisms including direct cytolytic activity which is thought to be its main

TABLE 1 Global-approved oncolytic viruses (OVs).

Product	Country approved	Approval year	Virus type	Modification	Dosage
DELYTACT (teserpaturev/G47D)	Japan	2021	HSV Type I	G207's 47 gene and US11 promoter deletion	1×10^{9} PFU
Imlygic® (talimogenelaherparepvec)	United States and Europe	2015	HSV Type I	HSV1 gamma 34.5 and ICP 47 deletion and expressing GM-CSF	1×10^{6}- 1×10^{8} PFU
Oncorine (H101)	China	2005	Adenovirus serotype 5	E1B-55k and E3 deletion	5×10^{11}-1.5×10^{12} VP
Rigvir (ECHO-7)	Latvia	2004	Picornavirus	_	TCID50 10^{6}/mL

VP, Virus Particle; TCID50, Median Tissue Culture Infectious Dose; PFU, Plaque Forming Unit.

oncolytic mechanism; this activity is due to the OVs' capacity to selectively infect, replicate, and kill cancer cells (Figure 1). It is now generally accepted that virotherapy's efficacy can be attributed to a number of different processes, including alterations in the tumor's micro-and macroenvironment and intricate immune control (40, 61, 62). OVs are cytolytic due to viral propagation and host cell bursting (63), and the viral infection may trigger apoptosis in the host cell (20)

Lysed tumor cells produce endogenous danger-associated molecular patterns (DAMPs), tumor-associated antigens (TAAs), virus-derived PAMPs, and immune-stimulatory cytokines, triggering the anti-tumor immune responses (64, 65).

The key and distinguishing characteristic of OVs is their selective amplification and replication in cancer cells, leading to the death of tumor cells without affecting the normal ones. The intensity of their anti-tumor action depends on the modalities of OV-induced cancer cell death (66, 67). Immunovirotherapy, also known as OV immunotherapy or viroimmunotherapy implies an OV infection that causes an inflammatory TME by eliciting anti-tumor immune responses. Furthermore, there is evidence that OVs have the capacity to transform an immunologically "cold" TME into a "hot" one *via* the production of chemokines and cytokines. It is worth noting that a balance between helpful anti-tumor immunity and harmful anti-virus immune responses is necessary for optimizing immunovirotherapy (68, 69). In order to modify the TME, OVs may also target tumor-associated stroma cells, such as endothelial cells. Immunogenic cell death (ICD) can be caused by OVs, which promote endoplasmic stress, resulting in the release of DAMPs, such as ATP, HMGB1, ectocalreticulin, and pro-inflammatory cytokines (64). STING, TLR1, and TLR3 on immune cells sense PAMPs and DAMPs, establishing a pro-inflammatory microenvironment that stimulates the production of pro-inflammatory cytokines such as type I IFNs, interleukin (IL)-1, IL-6; TNF-a, GM-CSF, and chemokines such as CCL2, CCL3, CCL5, and CXCL10 (70, 71), leading to transformation of

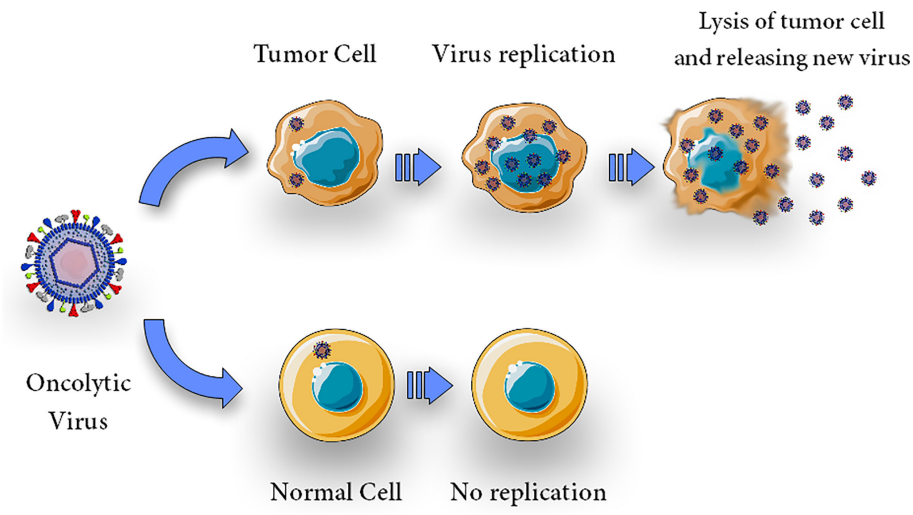

FIGURE 1
Direct cytolytic activity. Oncolytic virus can selectively infect, replicate, lyse and kill cells. Upon infection with an oncolytic virus, the oncolytic virus replicates in tumor cells and causes oncolysis but does not harm normal cells.

immunologically "cold" T-cell into "hot" T-cells (72, 73). Neutrophils and macrophages are attracted to the site of infection by CCL3 and CXCL10 chemokines, which are involved in anti-cancer responses. Aggregation of PAMPs with NK cell virus-recognition receptors causes early NK cell influx (74). Activated cytotoxic NK cells may produce cytolytic components and activate FAS-FASL, killing virus-infected cells. NK cells emit IFNs and TNF-a to excite macrophages, DCs, and T-cells. This activation of NK cells and DCs induces them to produce IFNs, TNF-a, IL-12, IL-6, and chemokines, which work both autocrinely and paracrinely to increase the initial innate response (21, 75, 76).

The tumor-specific T-cell response is the foundation of adaptive immunity against tumor cells during OV infection. Antigens presented in the context of an MHC molecule, co-stimulatory molecules, and cytokines are required for antigen presenting cells (APCs) to activate antigen-specific T-cell responses successfully (77). The released TAAs and neoantigens following tumor cell lysis by OVs are processed by APCs and are presented on their surface with MHC molecules to $CD4^+$ and $CD8^+$ T-cells (78). Also, OV-infected cells or mature APCs release various cytokines and chemokines, which aid in the recruitment and reactivation of T-cells. Both stimulated T-cells and B-cells could promote tumor regression and are capable of eradicating distant or freshly transplanted tumors without relying on an OV (79, 80).

In addition to tumor cells, the tumor's extracellular matrix (ECM) and vasculature are also affected by OVs. More than 60% of a solid tumor's mass comes from the ECM, which is a non-cellular compartment made by activated cancer-associated fibroblasts (CAFs). Collagenous matrix, proteoglycans, and hyaluronan build up in the ECM, providing an impenetrable and stiff barrier around cancerous cells. Because of these physical impediments, OVs have a tough time reaching the entire tumor mass (21). Ilkow et al. showed that interaction between CAFs and cancer cells improves vesicular stomatitis virus (VSV)-based therapies (61).

In contrast, tumor cells release transforming growth factor-beta 1 (TGF-1), which promote OV infection in CAFs. Tumor cells produce large quantities of fibroblast growth factor 2, making them vulnerable to viral infection. It has been reported that OAd not only could lyse glioblastoma cells, but also kills glioblastoma-associated stromal cells (81). Figure 2 provides a detailed anti-cacner mechanism of action of OVs.

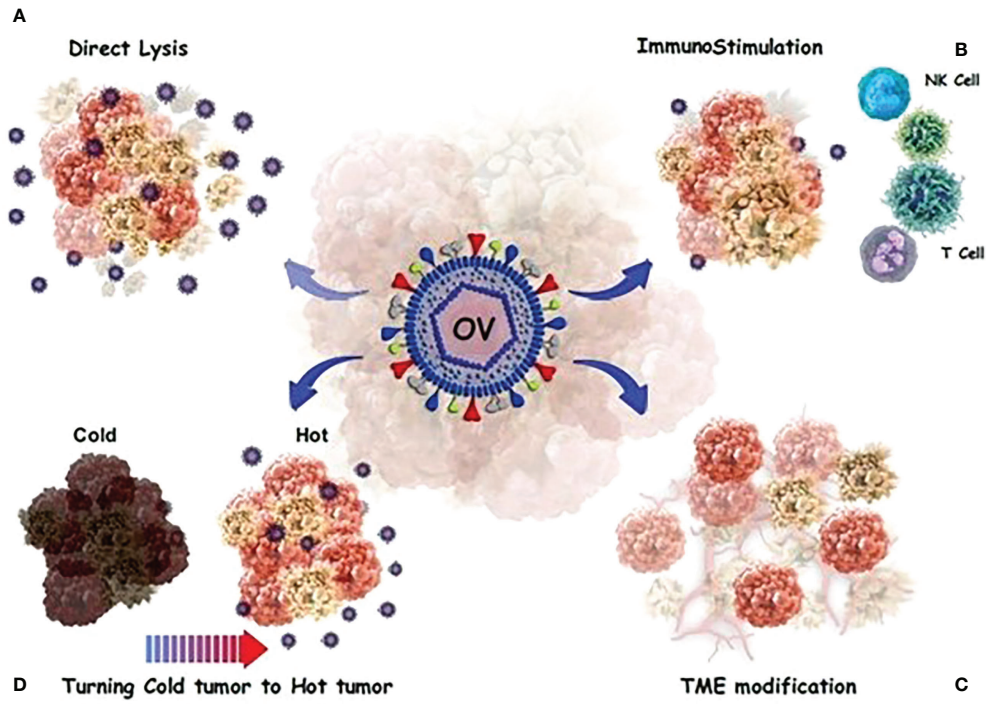

FIGURE 2
OVs have a direct or indirect toxic effect on tumor cells. **(A)** Direct oncolysis; The viruses can infect cancer cells and then replicate until the cancer cells rupture. The newborn viruses are then released to infect more cancer cells. **(B)** Neoantigens and debries from lysed cancer cells activate and recruit dendritic cells (DCs) into the tumor microenvironment and T cells migrate to the site of infection. **(C)** a number of processes occur, including the alteration of the tumor's micro-and macro-environment and the control of the immune response in a complex modulation. **(D)** OVs stimulate innate immunity and turn "cold" tumors into "hot" tumors by stimulating immune cell recruitment and activating systemic anticancer adaptive immunity to reduce tumor growth.

10.3389/fimmu.2022.1012806

3 Various types of OVs

There are two broad classes of OVs: 1) viruses that have a natural tropism for cancer cells; the naturally cancer-selective OVs utilize the abnormal signaling pathways that support their growth in cancer cells; and 2) those engineered specifically to replicate only in cancer cells (16). The activity of OVs reflects their underlying biology and the host-virus interactions that have evolved in the struggle between pathogenesis and immunity (29). The lack of an anti-viral response in cancer cells is an important mechanism of tumor selectivity for both categories. Interferons (IFNs) are secreted by normal cells in response to viral infection after intracellular pathogen recognition receptors identify viral RNA, DNA, or proteins (PRRs). Hundreds of effector genes, called IFN-stimulated genes (ISGs), are expressed as a result of this signaling cascade and aid in the elimination of the viral infection (16). Myxoma virus (MYXV; poxvirus), Newcastle disease virus (NDV; paramyxovirus), reovirus, Seneca Valley virus (SVV; picornavirus), measles virus (MV; paramyxovirus), poliovirus (PV; picornavirus), vaccinia virus (VV), Ad, HSV, and VSV are some examples of oncolytic viruses (Table 2) (63, 66, 82). Table 2 lists the different types of viruses that have been used for oncolytic purposes.

3.1 Natural tumor-replicating viruses

3.1.1 Poxviruses

One of the most important OV platforms now showing promising outcomes in clinical studies is the vaccinia virus (VV), a member of the Poxviridae family that naturally attacks malignancies (21). Tumors are a recognized target of VV strains owing to the activation of the epidermal growth factor receptor (EGFR) pathway in malignant cells (83). Researchers showed that vascular endothelial growth factor A (VEGF-A) enhances oncolytic VV cytotoxicity by studying the effect of hypoxia on VV infection (84). Tumor-derived VEGF increases VV internalization, leading to enhanced replication and cytotoxicity in both tumor cells and normal respiratory epithelial cells in an AKT-dependent manner (85). Moreover, tumor cells lack the anti-viral cytokines that protect normal cells from viral infection because of their poor interferon (IFN) response. Multiple attenuated VV mutants have been developed to improve tumor-specific targeting and safety in normal tissues (86, 87). The Pexa-Vec (JX-594), an oncolytic VV armed with GM-CSF and disruption of the TK gene, is under investigation in phase I and II clinical trials for treating renal cell carcinoma, advanced breast cancer, and advanced soft-tissue sarcoma (NCT03294083 and NCT02630368). Furthermore, an engineered vaccinia OV, RGV004, encoding a bispecific CD19/CD3 antibody, is in phase I clinical trials for the treatment of refractory/relapsed B-cell lymphoma (NCT04887025). A phase

TABLE 2 Characteristics of major oncolytic viruses.

Virus	Poxvirus	Newcastle disease Virus (NDV)	Reovirus	Measles virus	Herpes simplex virus	Adeno Viruses	Parvovirus	Poliovirus	Vesicular Stomatitis Virus	Seneca Valley Virus
Genome (Size)	dsDNA (160–190 kb)	SS (–) RNA (15 kb)	dsRNA (23 kb)	SS (–) RNA (16 kb)	dsDNA (154 kb)	dsDNA (35 kb)	ssDNA (5 kb)	SS(+) RNA (7.5 kb)	SS (–) RNA (11 kb)	SS (+) RNA (7 kb)
Virion	Complex	Enveloped	Naked	Enveloped	Enveloped	Naked	Naked	Naked	Enveloped	Naked
Replication Site	Cytoplasm	Nucleus	Cytoplasm	Nucleus	Nucleus	Nucleus	Nucleus	Cytoplasm	Cytoplasm	Cytoplasm
Receptor	Heparan, laminin, Chondroitin, integrin-1, CD98	Sialic acid	Sialic acid, JAM1	SLAMF1 (CD150), CD46, Nectin 4	HVEM, Nectin 1, Nectin 2	CAR	Sialic acid residues, P antigens	CD155	LDLR	Anthrax toxin receptor 1

I/II clinical trial showed that Pexa-vec intratumoral injection was safe and effective in treating surgically incurable metastatic melanoma (NCT00429312).

3.1.2 Newcastle disease virus

The Newcastle disease virus (NDV), belonging to the family Paramyxoviridae, is an enclosed virus and contains negative-sense single-stranded RNA (88, 89). The HN protein interacts with sialic acid receptors on the surface of host cells to bind tumor cells, and when the activated F protein joins the viral and host cell membrane, the HN protein fuses with the virus (90). As a result, the virus's genome penetrates the cytoplasm of the host. NDV can also enter cells by endocytosis and clathrin-mediated endocytosis (91). There is evidence that gene-editing technologies make it simple to introduce foreign genes with anti-tumor activities into the extensive genome of NDV (92). Numerous clinical investigations have shown that NDV has a very excellent safety profile for patients and has considerable anti-cancer activity (93). For instance, because NDV only affects the type I IFN-deficient glioblastoma cells, an inhibitor of IFN signaling eliminates the NDV resistance in type I IFN-positive cells (8, 94). In two clinical studies (NCT03889275 and NCT04613492), the drugs Durvalumab (anti-PD-L1) and attenuated NDV with the GM-CSF and IL-12 genes (MEDI5395 and MEDI9253, respectively) are being used. NDV with durvalumab, is in phase I clinical trial for treating advanced solid tumors (95).

3.1.3 Reovirus

Reovirus (RV), an unenveloped virus containing a double-stranded RNA belongs to the Reoviridae family (96). The oncolytic properties of wild-type reovirus are due to the virus's preference for replicating in cancer cells (97). Reovirus has the ability to kill cancer cells because of its preferential ability to multiply in cancer cells. Ras overexpression impairs the PKR (protein kinase RNA-activated) pathway, allowing reovirus to infect tumor cells preferentially (98–100). Reolysin (also known as Pelareorep) (101), serotype 3 RV, is the well-known oncolytic RV that as a single agent or in combination with other therapeutic strategies (29), is under investigation in clinical trials (NCT04102618, NCT04445844, and NCT04215146).

3.1.4 Measles virus

The measles virus (MV), which belongs to the genus Morbillivirus in the Paramyxoviridae family, is an enveloped virus containing negative-sense single-stranded RNA (102). Three receptors, CD46, SLAM/CD150, and poliovirus-receptor-like-4, are used by MV to infect host cells (103, 104). However, CD46 is not a tumor-selective receptor because of its expression on normal cells. MV is a hopeful OV candidate due to its good safety profile, which includes the absence of dose-limiting toxicities and spontaneous oncotropism (21, 104, 105).

Heinzerling et al. performed the first Phase I dose-escalation test with a live MV, Edmonston-Zagreb vaccine strain against cutaneous T-cell lymphoma (CTCL) (106). Clinical trials using a measles virus that expresses the human sodium/iodide symporter SLC5A5 are currently being conducted (107). The Mayo Clinic (USA) has launched a number of Phase I/II clinical studies (NCT00390299, NCT02364713, NCT02068794, NCT02700230, NCT01503177, NCT01846091) to examine the clinical safety and usefulness of MV-CEA and MV-NIS (95).

3.1.5 Picornaviruses

Picornaviruses have promising anti-cancer effects in patients (108). Picornaviruses are tumor-specific due to the overexpression of their entry receptors on cancerous cells, including CD155, integrin a1b2, intercellular adhesion molecule-1 and/or decay-accelerating factor (CVA21), anthrax toxin receptor 1 and sialic acids and anthrax toxin receptor 1 (109). Clinical studies using oncolytic picornaviruses typically go smoothly, and no off-target infections have yet been reported. Intratumoral administration of the oncolytic poliovirus PVSRIPO, the live attenuated, type I poliovirus (Sabin) vaccine harboring an internal ribosome entry site (IRES) of human rhinovirus type 2, has demonstrated initial promise in patients with recurrent glioblastoma multiforme (NCT03712358) (110). In contrast, PVSRIPO infects macrophages and DCs in culture, causing the expression of major histocompatibility complex class II (MHC II) and the generation of IFN-b and IL-12 (9, 87).

3.2 Genetically engineered (modified) oncolytic viruses

3.2.1 Herpes simplex virus

Talimogene laherparepvec (T-VEC; Imlygic), the first OV presently licensed by the FDA, is a member of the Herpesviridae family (56). In addition to T-VEC, other HSV-based OVs have been developed, such as G47δ, oHSV-IL12, G207, and rRp450 (111, 112). The majority of HSV-based vectors carry deletions in ICP34.5, a neurovirulence gene that restricts virus replication to tumor cells overexpressing the Ras gene (113). The inactivation of the ICP6 gene, which encodes a viral homolog of the cellular ribonucleotide reductase (RR), is another mechanism of HSV specificity (114, 115). The mutant virus replication is limited to actively proliferating cancer cells with high levels of RR because this enzyme is necessary for creating deoxyribonucleotides (29). The results of a Phase Ib study using T-VEC in combination with the CTLA4 checkpoint inhibitor, Ipilimumab, in people with advanced melanoma were published by Puzanov et al. (116). Additionally, the combination of OV with nivolumab has showed very promising results (12, 116–118).

3.2.2 Adenoviruses

Adenoviruses (Ads), non-enveloped viruses with icosahedral capsid and double-stranded linear DNA genomes, are members of the Adenoviridae family, specifically the genus Mastadenovirus. The capsid of Ads contains three major proteins, including Hexon, penton-base, and fiber proteins, which give them specific tropism characteristics (119). In clinical research, adenovirus serotype 5 (Ad5) is the most frequently utilized viral vector (120). Ad5 penetrates the targeted cells *via* interacting its fiber knob protein with coxsackievirus and adenovirus receptors (CARs) (118, 121).

DNX-2401 (Delta-24-RGD; tasadenoturev) is an oncolytic adenovirus, replication -competent adenovirus. A 24-base pair deletion in the E1A gene promotes tumor selectivity by preventing viral replication in normal cells with a functioning Rb pathway. An RGD-motif was added to the fiber H-loop to boost potency, allowing the virus to enter cells through v3 or v5 integrin. On tumor cells, especially glioma stem cells, these integrins are abundant (122). In preclinical models, DNX-2401 kills glioma cells through direct oncolysis and by inducing immunological responses against tumor antigens, resulting in long-term antitumor immunity and tumor regression. DNX-2401 is now being tested in clinical studies for the treatment of recurrent glioblastoma (NCT03896568) (123). Also, additional studies are being conducted to examine its effectiveness against recurrent gliomas when used in conjunction with other treatments, such as checkpoint inhibitors. In one active phase II study, DNX-2401 was injected directly into a recurrent glioblastoma or gliosarcoma followed by pembrolizumab every 3 weeks for up to 2 years or until disease progression (NCT02798406) (38).

H101 is an adenovirus with an E1B deletion that has been approved in China for the treatment of nasopharyngeal carcinoma. H101 was tested in a randomized Phase III clinical study with 160 people who had advanced squamous cell carcinomas of the head and neck or esophagus (124). The patients were randomly assigned to chemotherapy (cisplatin and 5-FU for chemotherapy-naive patients, or adriamycin and 5-FU for patients who had previously received platinum chemotherapy) with or without H101 (5×10^{11} to 1.5×10^{12} viral particles per day by intra-tumoral injection) for five consecutive days every three weeks. A total of 123 patients completed treatment, and were able to be evaluated for response. Patients who received cisplatin/5-FU + H101 exhibited a response rate of 78.8%, compared to 39.6% in the cisplatin/5-FU-only cohort. Patients who got the adriamycin/5-FU and H101 virus, as well as the adriamycin/5-FU -only group, both achieved a 50% response rate; however, these groups had a limited number of participants (n = 18). There was a substantial difference in response rate between all patients who got H101 and individuals who only received chemotherapy. The most common adverse events were fever, injection site reactions, and flu-like symptoms. Based on these findings, the Chinese regulatory agencies approved H101 in combination with chemotherapy for the treatment of nasopharyngeal cancer (10). In addition to the aformentioned viruses, several additional viruses, including parvovirus, poliovirus, vesicular stomatitis virus, Seneca valley virus, have been engineered to be used as OVs in combating cancer (21). Table 3 summarizes the types of viruses that are in different phases of clinical trials.

As a result of genetic engineering, a wide variety of potentially pathogenic viruses have been manipulated for safety and tumor-targeting applications in the past two decades. Genetic modifications including the deletion of viral genes, the use of transcription regulatory elements such as promoters and enhancers, and the alterations of viral surface proteins have been widely used to increase the effectiveness of targeted OVT (82, 125).

4 Tumor targeting strategies of oncolytic viruses

Despite the remarkable preclinical success of OVT, clinical applications remain limited. One of the most significant challenges that must be overcome is viral targeting. Various strategies have been established to achieve targeting OVs toward tumor cells. As previously described, some viruses, such as reovirus and NDV have an intrinsic tropism for tumor cells, whereas the other ones, such as Ad and HSV, should be adapted or engineered to be cancer-specific (126). Virus adaptation to cancer cells is frequently accomplished based on cancer cell modifications, including self-sufficiency in growth signals, resistance to apoptosis, neoantigen expression, and an unlimited replication potential that can be used for OVs selective infection and killing of cancer cells (127). In this regard, different approaches have been used to direct OVs into cancer cells, including modifying the virus's surface (transductional targeting), introducing specific genes downstream of specific tumor promoters or inserting genetic elements into virus genomes such as miRNA and siRNA to boost OV specificity (transcriptional targeting), and deleting virus genes that are required for replication in normal cells but have little effect on reproduction in cancer cells (33, 128, 129).

4.1 Transductional targeting

Detargeting viruses from their normal cells and retargeting them to a specific cell is a critical step in designing OVs, especially for adenovirus-based oncolytic viruses. As previously stated, Ads as one of the most utilized viruses in cancer treatment, have no innate tropism for cancer cells, whereas they exhibited a broad range of tropism for normal cells due to CAR expression in the majority of normal cells. As a result, an

unaltered virus can infiltrate and harm normal cells by systemic injection. Hence, the vector's inherent tropism should be eliminated to reduce possibly detrimental side effects. Scientists usually use two methods to solve the problem: adding ligands like peptides, antibody fragments, and nanobodies to the structure of the virus, and using bispecific adaptors. Van Erp et al. coupled transcriptional targeting by utilizing a tumor-specific promoter with transductional targeting by using an anti-CEA nanobody incorporated into Ad. CXCR4E1.B2 virus capsids. They showed that using a single specific domain for CEA which was inserted genetically into the Ad fiber could improve the specificity of infection and the ability of Ads to reproduce in cancer cells (130) Another method for modifying the surfaces and tropism of OVs is pseudotyping.

TABLE 3 Summary of clinical trials of monotherapy and combination therapy of oncolytic viruses.

	Oncolytic virus	Combination therapy	Cancer	Dosage	Clinical phase	Clinical trial No
Adenovirus	Ad-p53	Nivolumab or Pembrolizumab	Head and Neck Squamous Cell Carcinomas; Colorectal Cancer; Hepatocellular Carcinoma	5×10^{11} VP single dose	I/II	NCT02842125 NCT03004183
	Ad-CEA	Avelumab	Colorectal Cancer	1×10^{11} VP 6 doses	II	NCT03050814
	Ad-MAGEA3	Pembrolizumab	Non-Small Cell Lung	2×10^{11} VP single dose	II	NCT02879760
	ONCOS-102	Pembrolizumab	Melanoma	3×10^{11} VP 3 doses	I	NCT03003676
	LOAd703	Atezolizumab	Malignant Melanoma	1×10^{9} VP 12 doses	I/II	NCT04123470
	Ad-TK	Pembrolizumab/ valacyclovir33/ SBRT	Non-small Cell Llung Cancer; Triple-negative Breast Cancer	5×10^{11} VP single dose	II	NCT03004183
	H101	Camrelizumab	Recurrent Cervical Cancer	1.5×10^{12} VP 2-6 doses	II	NCT05234905
	CG0070		Bladder Cancer	1×10^{12} VP 3-9 doses	II	NCT02365818
Herpes simplex virus	T-VEC	Pembrolizumab	Melanoma	1×10^{8} PFU	III	NCT02263508
	OH2		Pancreatic Cancer	1×10^{7} CCID50 6 dose	I/II	NCT04637698
	T-VEC	Nivolumab/ Trabectedin	Sarcoma	1×10^{7} PFU	II	NCT03886311
	HF10	Ipilimumab	Metastatic Melanoma	1×10^{7} TCID50 6 doses	II	NCT03153085
	OrienX010	Pembrolizumab	Melanoma	3×10^{11} VP 3 doses	I	NCT03003676
	OH2		Advanced Bladder Cancer	1×10^{7} CCID50 single dose	II	NCT05248789
Newcastle disease virus	MEDI5395	Durvaluma	Advanced solid tumor	dose-expansion study to assess the safety	I	NCT03889275
Vaccinia virus	MVA-p53	Pembrolizumab	Solid tumor	5.6×10^{8} PFU 3 doses	I	NCT02432963

(Continued)

TABLE 3 Continued

	Oncolytic virus	Combination therapy	Cancer	Dosage	Clinical phase	Clinical trial No
	JX-594		Metastatic Hepatic Carcinoma	1×10^8-3×10^8 PFU single dose	I	NCT00629759
	TG4010	Nivolumab	Non-small cell lung cancer	1×10^8 PFU single dose	II	NCT02823990
	Pexa-Vec (JX-594)	Tremelimumab/ durvalumab	Refractory Colorectal cancer	3×10^8 PFU 4 doses	I/II	NCT03206073
		Ipilimumab	Advanced solid tumor	1×10^9 PFU 5 doses	I	NCT02977156
		Sorafenib	Hepatocellular Carcinoma	1×10^9 PFU 3 doses	III	NCT02562755
	Olvi-Vec	Bevacizumab/ cisplatin	Ovarian Cancer	1×10^9 PFU single dose	III	NCT05281471
	TBio-6517 (Rival-01)	Pembrolizumab	Solid tumor, Colorectal cancer	multiple doses	I/II	NCT04301011
	OVV-01		Advanced Solid Tumors	1×10^{12} VP single dose	I	NCT04787003
Vesicular stomatitis virus	VSV-IFNβ-NIS	Pembrolizumab	Non Small Cell Lung Cancer Neuroendocrine Carcinoma	5×10^{10} TCID50 single dose	II	NCT03647163
Reovirus	Reolysin	Pembrolizumab	Advanced pancreatic	4.5×10^{10} TCID50	II	NCT03723915
		Atezolizumab	Breast	4.5×10^{10} TCID50 4 doses	I	NCT04102618
			Sarcomas Metastatic to the Lung	3×10^{10} TCID50 5 doses	II	NCT00503295

VP, Virus Particle; TCID50, Median Tissue Culture Infectious Dose; PFU, Plaque Forming Unit; CCID50: Cell Culture Infectious Dose 50%.

This strategy is often done by replacing coat proteins with similar proteins from related serotypes, leading to a new tropism without changing the balance of the genome. In this regard, adenoviral fiber protein pseudotype switching is a reasonable strategy for transductional retargeting. Owing to the upregulation of CD46 on many malignant tumors, researchers replaced Ad5 fiber with the fiber of serotypes 11/35 to target tumor cells (131, 132). Another strategy that has been developed to target viruses toward tumor cells, as previously mentioned, is the use of bispecific adapters. Adaptors are molecules with two ends that bind to the viral proteins and the receptors on the cancer cells. This strategy's main advantage is the ability to use multiple adaptors to attach to the same vector without affecting the vector`s structure. Due to the overexpression of the high molecular weight melanoma-associated antigen (HMWMAA) on melanoma cells, Curiel et al. designed a bispecific adaptor, scDb MelAd, to target Ad to melanoma cells selectively. They demonstrated significantly reduced infectivity (> 50-fold) of capsid mutant Ads, restored (up to 367-fold increase), CAR-independent and HMWMAA-mediated infectivity of these mutant viruses by scDb MelAd specifically in melanoma cells, compared to a vector with wild-type fibers (133). Additionally, a universal platform for Ad5 detargeting and retargeting using the SpyTag and SpyCatcher system was developed and demonstrated that Ad5 efficiently wasredirected into VEGFR2-expressing cells using an adoptor incorporating SpyCatcher and an anti-VEGFR2 nanobody (under publication data).

4.2 Transcriptional targeting

The effectiveness of transductional techniques has been inadequate for realizing the full promise of virotherapy in the clinic. For instance, early gene therapy experiments used

therapeutic genes driven by viral promoters, such as the CMV promoter, which caused non-specific damage in normal cells and tissues as well as cancer cells. However, the use of tumor-specific promoters, which are overexpressed in tumors, stimulates the particular expression of therapeutic genes in a certain tumor, boosting their localized action and reducing mislocalization side effects (134). TTF-1 promoter, glypican-3 protein (GPC3), human secretory leukocyte protease inhibitor (hSLPI), Mucin 1 (MUC1), cyclooxygenase 2 (COX2), epithelial glycoprotein (EPG2), and human telomerase reverse transcriptase (hTERT) are the most common tumor-specific promoters used in transcriptional targeting (7). For instance, combining transcriptional targeting using the tissue-specific SLPI promoter and transductional targeting with the ovarian cancer specific adaptor protein, sCARfC6.5, which contains the coxsackie-adenovirus receptor ectodomain and a single-chain antibody specific for c-erbB-2, increased transgene expression in ovarian tumors while decreasing expression in normal tissues, including the liver, in comparison to single-approach targeting (135). As abovementioned, inserting micro-RNAs (miRNAs) into the virus genome is a new way to improve their specificity and reduce off-target effects. Many teams have used the differential landscape of miRNA expression between normal and malignant cells to hinder OVs proliferation in healthy cells. In one study, it has been demonstrated that adding several copies of a miR-124 recognition sequence into the 3′ UTR of the oncolytic HSV-1's crucial ICP4 gene prevents the virus from infecting normal cells. This phenomenon occurs because of the high expression of miR-124 in healthy neurons but not at all in glioblastoma cells (136, 137). In another study, Luo et al . employed a triple-regulated OAd containing miR143, survivin, and RGD to improve the effects of OAds. They showed that when Ad-RGD-Survivin-ZD55-miR-143 was introduced into cells, it could inhibit cell growth, migration, and invasion, as well as halt cells in the G1 phase and induce cell death (138).

Despite the use of many techniques for targeting viral vectors in cancer virotherapy and boosting the virus's efficacy in cancer treatment, when the virus must be injected systemically for the treatment of metastatic malignancies, this treatment strategy encounters a number of challenges (125) that must be overcome before the systematic administration of OVs to improve their anti-tumor activities (126). The most common challenges of delivering the virus through the bloodstream are viruses' identification as foreign agents and elimination from the body before they can reach the tumor site, known as immune-mediated clearance (127), and virus sequesteration by non-specific tissues such as the liver, lungs, and spleen (128). On the other hand, tumors are high-pressure settings with a dense and disorderly collection of cells due to thick stromal tissue and limited lymphatic drainage (42). To address these issues, scientists have designed a variety of approaches, which are described in more detail below.

4.3 Solutions to the challenges of OVs' systemic delivery

Complement activation, pre-existing immunity, or the release of inflammatory cytokines (IL-6, IL-12, and TNF) in response to vectors all contribute to OV clearance by the immune system. Some OVs, including vaccinia and HSV-1, produce anti-complement components to evade the immune system (139). HSV-1 secretes glycoprotein E, which functions as an IgG Fc receptor and efficiently inhibits IgG Fc-mediated complement activation as well as antibody-dependent cellular cytotoxicity (ADCC) (140). Pre-existing immunity canoccur due to the virus's ubiquitous nature (Ad and Reovirus), previous vaccination (vaccinia and MV), or earlier oncolytic viral treatment (141). There are currently various solutions being tested for these issues. Changing the surfaces of viral vectors by shielding with polymers such as (poly ethylene glycol (PEG), poly L-lysine, and *N*-[2-hydroxypropyl] methacrylamide (HPMA)) and lipidic vesicles often reduces their immunogenicity and increases vector persistence in the bloodstream (142). Cellular carriers, in which cells are taken from a model organism that has been infected and put back in, are another way to deliver OVs. Immune cells, stem cells, and tumor cells have been used to generate experimental OV cell carriers. Among cell carries, stem cells, according to *in vitro* and *in vivo* studies, are the most outstanding candidates for systemic delivery of OVs since they allow viruses to infect the target cells and replicate in, conceal them from the immune system, and target tumors (143, 144). In this regard, Mader et al. used mesenchymal stem cells (MSCs) to efficiently deliver oncolytic MV to ovarian cancer and protect the virus from neutralizing anti-viral antibodies. They found that using MSCs as carriers increased their localization and infiltration into tumors and transferred oncolytic MV infection to tumors, leading to enhancing mice survival (143). Immune cells, especially DCs and T-cells, have been used successfully in pre-clinical research to transfer several OVs to tumors. For instance, DCs infected with reovirus have been shown to efficiently transport and deliver their oncolytic payload into melanoma cells, even in the presence of neutralizing antibodies (145). On the other hand, OVs are removed from the bloodstream by mononuclear phagocytic cells, splenic macrophages, and hepatic Kupffer cells in the spleen and liver following systematic administration. This clearance frequently occurs following the decorating of viral particles with antibodies and complement proteins or their interaction with coagulation factors (126). However, some viruses, such as Ads, may bind directly to scavenger receptors on Kupffer cells, resulting in the release of pro-inflammatory cytokines, which may cause severe toxicities (146). The answers to these challenges are fairly similar to the methods outlined for immune response escape. In case of Ads, the hexon protein, as the most frequently structural protein, has

a critical role in liver sequestration through interaction with coagulation factor IX and scavenger receptors (147, 148). Different strategies have been developed to avoid this sequestration, such as genetic alteration in the hypervariable region (HVR) of hexon (149), pseudotyping (complete change of HVR) (150), and pharmacological agents (such as warfarin and protein obtained from snake toxin and factor X-binding protein) (151, 152). Surface PEGylation is a popular strategy for reducing non-specific tissue absorption. Kwon et al. detected a substantial 10^5 increase in tumor to liver ratio when Ad was treated with a PEGylated chitosan specific to the folate receptor compared to naked Ad (153).

4.4 Intratumoral spread of OVs in solid tumors

Tumor physiology is a major issue in cancer treatment since tumors come in a variety of forms and sizes, making it difficult to predict how and where medications, such as OVs, will be absorbed (154). Therefore, viruses transferred within the tumor can only infect and spread cells near blood vessels, leaving the rest of the tumor untreated. Therefore, researchers have focused on establishing mechanically activated transport mechanisms to promote OVs penetration and increase virus anti-cancer activity (155). Most solutions for this barrier rely on virus-encoded matrix-degrading enzymes and anti-fibrotic agents. Diop-Frimpong et al. showed that the penetration and effectiveness of intratumorally injected oncolytic HSV were improved by using Losartan, which is a clinically approved angiotensin II receptor antagonist with anti-fibrotic effects (156). In another experiment, Guedan et al. created a replicating Ad capable of producing soluble sperm hyaluronidase (PH20) (AdwtRGD-PH20). Intratumoral AdwtRGD-PH20 treatment caused hyaluronan (HA) degradation, enhanced viral dispersion, and tumor regression occurred in all of the treated tumors (157). In addition, expressing matrix metalloproteinases-1 and -8 in oncolytic HSV increased viral dispersion and treatment efficiency by breaking down tumor-associated sulfated glycosaminoglycans (158).

5 Oncolytic virotherapy in combination with cancer immunotherapeutics

Although various studies demonstrated viruses potential in eliminating tumor cells, there is currently no report that virotherapy can lead to a complete cure of cancer alone due to the previously mentioned challenges. However, there is ample evidence that OVs can be considered as the basis of combination therapy in different cancers due to their multiple mechanisms of action and their simultaneous effects on tumor cells, immune cells, and the TME (45, 159). Here, we have discussed possible combinations of OVs with different biological products that can overcome monotherapy challenges and limitations in cancer treatment.

These combinations can be classified as 1) Armed recombinant oncolytic viruses that carry the coding sequence of other therapeutic agents which are excellently discussed elsewhere by Kontermann (69), and 2) Combining OVs with other biologic therapeutics separately.

Combining viruses with either the coding sequence or the final protein form of antigen binding biologics)such as antibodies, nanobodies and CAR-T cells(can help viruses overcome some limitations, such as possible off-target side effects and non-specific uptake (Figure 3). Antibodies (Abs) are widely used in targeted therapies and mostly recognize TAAs on tumor cells. Abs are also combined with OVs to improve possibility of attachment of the virus to its target cells. As a proof to this claim, combining OVs with immune checkpoint inhibitor (ICI) antibodies is leading to promising anti-cancer results. Despite this issue, one of the main limitations of antibodies, especially for the treatment of solid tumors, is their poor tumor penetration due to physical barriers. This can be improved by using smaller antibody fragments, such as single-domain antibodies, scFv, and Fab. There are also other functional antigen-binding therapeutic formats with some notable advantages that are used in some other studies in the viro-antibody therapy field that can be translated into the clinical trial. These promising structures can be combined effectively with OVs for better therapeutic efficacy. For improving the combinational therapy outcome, nanobodies can also be used to not only assist OVs in specific targeting, but also helping viruses for more efficient penetration into solid tumors. Table 4 summarizes the various strategies of combination therapy with oncolytic viruses.

5.1 Arming oncolytic virus with antibody and its derivatives

5.1.1 OVs plus antibodies

Antibodies with different frameworks have been approved as cancer therapeutics; each has a different mode of action, such as blocking, neutralizing, and activating functions (159, 175, 176). These antibodies have been also coupled to various viruses such as Ad, MV, HSV, NDV, Reovirus, Vaccinia, and VSV in cancer combinational therapy (177–179), and some with promising results have been discussed below.

5.1.1.1 OVs plus immune checkpoint inhibitors

It has been shown that the expression of inhibitory receptors on T-cells, including programmed cell death protein 1 (PD-1)

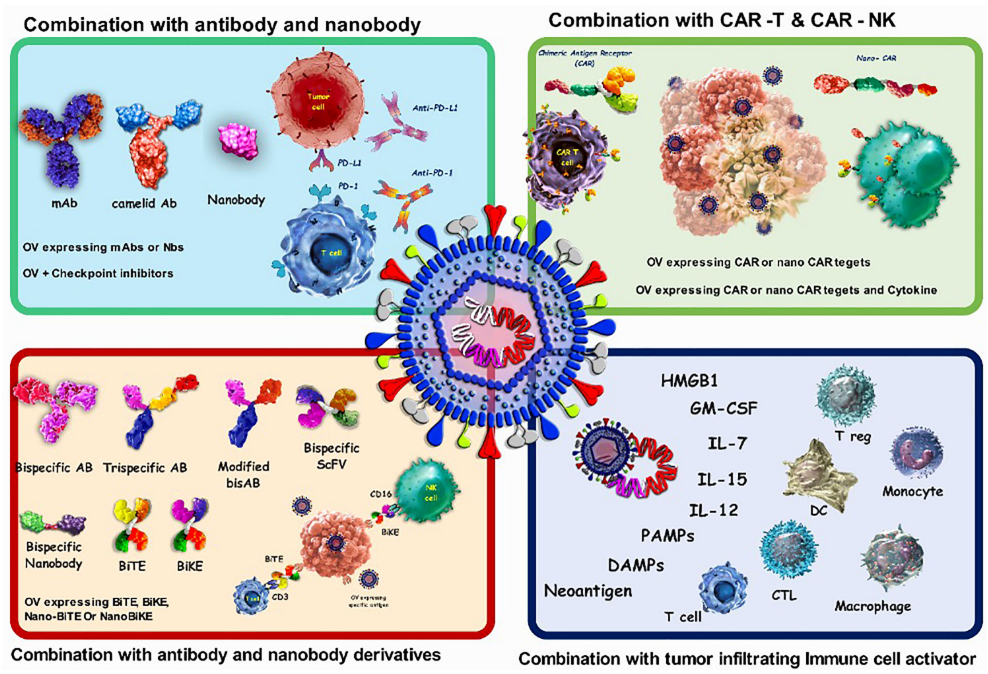

FIGURE 3
Characteristics of oncolytic virus combination therapy. OVs attack and destroy tumor cells preferentially. Lysis of tumor cells releases neoantigen, PAMPs which trigger PRRs, which then produce inflammatory cytokines and antiviral type I IFNs. Viruses can activate cell death pathways, resulting in immunogenic cell death phenotypes such as necroptosis, pyroptosis, immunogenic apoptosis, and autophagic cell death. Antibodies that target cell surface indicators of immune cells (checkpoint inhibition), cancer cells (targeted therapy), or both (bispecific antibodies) are wellestablished in cancer therapy. combination of oncolytic viruses with antibody and CAR-T cells; CAR-T cells bind to the antigen on the surface of tumor cells and kill them, but they cannot migrate deeper into the dense tumor mass to remove antigennegative tumor cells. also, CAR-NK cells show more anticancer activity than CAR-T cells because they attach to stress ligands on the surface of tumor cells. The oncolytic virus attacks and destroys tumor cells, eliminating the tumor's dense structure.

and cytotoxic T-lymphocyte-associated antigen 4 (CTLA-4), and their binding to their ligands on the target cells (PDL-1 and B7, respectively) leads to aberrant activation of T-cells. In this regard, blockade of these negative regulators by ICIs can prevent T-cells suppression and improve their optimal activity in combating tumor cells (179). Nevertheless, the clinical response of ICIs correlates with pre-existing anti-tumor immune responses, such as an elevated number of tumor-infiltrating lymphocytes (TILs) and enough expression of immune checkpoints (ligands) on the tumor cells (45, 180). It has been shown that after viral infection, the expression of immune checkpoints upregulates on the surface of tumor cells, and accordingly, one of the most compelling combinational therapies for cancer would be OVs + ICIs (45, 181). In addition, another reason that makes the combination of OVs and ICIs attractive in the treatment of cancer is their different mechanism of action, which is an important parameter from the pharmacological point of view (45).

Zamarin et al. showed that localized OVT by NDV overcomes systemic tumor resistance to ICIs by inflaming the TME. They showed that I.T. administration of NDV not only increased infiltration of the lymphocytes into the injected tumor in the B16 melanoma mice models, but also the anti-tumor effect was observed in a distant tumor without any virus injection. Also, the localized administration of NDV in combinational with systematic administration of CTLA-4 blockade exhibited more efficient anti-cancer outcomes (182). In most studies for assessment of combinational OV-ICI therapy, fully humanized IgG antibody format has been used as ICIs; FDA-approved ICIs, especially those in clinical trials and has been discussed in detail elsewhere (178, 180). For example, although immune checkpoint inhibition is a logical therapeutic candidate against glioblastoma cells due to the increased expression of PD-1 on these cells (along with IL-10 and TGF-b), anti-PD-1 alone could not sufficiently eliminate tumor cells and there was a need for synergistic interactions with OVs. So, Saha et al. showed that a triple combination using anti-CTLA-4, anti-PD-1, and G47D-mIL12 (recombinant HSV virus) cured most mice in two glioma models. This approach not only treated mice, but also protected them against tumor re-challenge. The synergistic activity was

TABLE 4 Summary of combination therapies with oncolytic viruses and other immunotherapeutic agents.

	Virus	Strategies for Antibody Gene Expression	Format	Target	Result
Combination oncolytic virus with antibody (ICI, mAb, nanobody)	Ad (Ad5/3-E1AΔ24)	Replacement of early genes (E3) with Ig chains	IgG2	Human CTLA-4	Subcutaneous xenograft mouse tumor model/intratumoral virus injection: OV-encoded antibody was detected in xenografts; 43-fold higher antibody concentration in tumor versus plasma; 81-fold higher antibody concentration detected in tumors after injection of antibody-encoding OV compared with antibody-encoding replication-deficient control virus (160).
	Influenza A virus (IAV)	Heavy chain in PB1 segment downstream of PB1 gene *via* 2A; light chain in PA segment downstream of PA gene *via* 2A	IgG and scFv	IgG and murine CTLA-4	Antibody insertion reduced titer, replication and *in vivo* morbidity and mortality of IAV Functions of OV-produced IgG was similar to hybridoma-produced Ab. Subcutaneous syngeneic bilateral mouse tumor model/intratumoral OV application: scFv-encoding OV showed superior tumor growth inhibition (both flanks) and prolonged survival compared with parental virus (161).
	HSV-1	Separate transcription unit, MMLV LTR promoter	scFv fused to mouse IgG1	Murine CTLA-4	Bilateral subcutaneous syngeneic mouse tumor model/low dose intratumoral OV injection of right flank tumor: antibody-encoding OV increasesd tumor growth inhibition of injected (117).
	NDV	Additional transcription unit downstream of P gene	scFv	Murine CTLA-4	Intradermal syngeneic mouse tumormodel/irradiation/intratumoral OV injection: antibody-encoding OV + X-ray showed similarly increased survival and tumor growth inhibition than parental virus + X-ray + systemic α-CTLA-4 when compared with α-CTLA-4 alone (162, 163).
	MV	Separate transcription unit downstream of H gene	scFv-IgG1 Fc fusion	Murine CTLA-4, murine PD-L1	Subcutaneous syngeneic mouse tumor model/intratumoral OV injection: α-CTLA-4-encoding OV reduced tumor progression, whereas α-PD-L1- encoding OV prolonged survival both compared with control virus. Both antibody-encoding OVs increased T cell infiltration, decreased Treg infiltration and resulted in splenocyte activation (164).
	VSV	Additional transcription unit between G and L genes	scFv	Human PD-L1	Subcutaneous syngeneic mouse tumor model with hPD-L1-expressing mouse tumor cells/intratumoral OV injection: Antibody-encoding-OV or combination of parental OV + intraperitoneal scFv reduced tumor growth and improved survival in comparison to monotherapies, Increase of activated CD8+ T cells in spleen of mice cured after treatment with antibody-encoding-OV compared with normal mice (165).
	Vaccinia virus	Additional transcription unit with viral H5 promoter	scFv	Human PD-L1	cell lines and activated T cells were infected: parental OV resulted in translocation of PD-L1 to cell surface in cancer cells; antibody-encoding OV delivered sufficient α-PD-L1 scFv to block cell surface detection of PD-L1 on cancer cells; OV-encoded scFv increaseed granzyme B production and prevented OV-induced decrease in perforin release by T cells (166).
	Ad (EnAd, chimeric type B Ad)	Replacement of early genes (E3) by Ig chains linked *via* IRES	IgG1	Human HER2 (Trastuzumab)	OV-encoded antibody showed direct antitumor activity and triggers ADCC *in vitro*. Subcutaneous xenograft mouse tumor model/intratumoral virus injection enhanced antitumor efficacy of antibody-encoding OV compared with parental virus or trastuzumab for Her2-positive xenografts. Higher tumor-to-blood antibody concentrations by antibody-encoding OV compared with conventional antibody application (167).
	NDV (wt velogenic Italien strain)	IgG heavy and light chains as separate, adjacent additional transcription cassettes with gene stop and gene start signal for viral transcription	IgG	CD147 (metuximab)	Orthotopic xenograft mouse tumor model/intravenous OV application: antibody-encoding OV resulted in antibody expression in tumors and tumor necrosis. Reduced intrahepatic metastasis and prolonged survival compared with parental OV (168).
	Vaccinia virus (GLV-1h68: Lister vaccine strain, triple mutant)	Separate transcription unit, viral promoters (SEL, SL [VEGF] or SEL+SL)	nanobody	VEGF (scFv) + EGFR (nanobody); VEGF (scFv) + cross-species FAP (scFv)	Subcutaneous xenograft mouse tumor model/intravenous OV injection:OVs encoding single antibodies (targeting EGFR, VEGF, or FAP) inhibited tumor growth more rapidly (one xenograft model) or stronger (other xenograft model) than control virus. OVs encoding two antibodies resulted in strongest tumor growth inhibition, significantly superior to control virus; significance not reached in comparison to single antibody-encoding OVs (169).
OVs plus bispecific antibodies	HSV-1 (G207)	Inserted as separate transcription unit with CMV promoter	BiTE or nanobody-scFv fusion	Human PD-L1 (scFv or nanobody) ×	PD-L1-positivity of T cells did not prevent expansion or effector functions after activation by purified BiTE: Co-cultures of infected tumor cell line, PBMC-derived T

(Continued)

TABLE 4 Continued

	Virus	Strategies for Antibody Gene Expression	Format	Target	Result
				human CD3 (scFv)	cells and immunosuppressive ascites fluid: BiTE-encoding OVs, not control virus, induced depletion of tumor cells (170).
	Ad (EnAd, chimeric type B Ad)	Inserted as separate transcription unit with CMV promoter	BiTE	Human folate receptor-β × human CD3	Ex vivo ascites model with total ascites cells: BiTE-encoding OV induced T cell activation and expansion, depletion of macrophages, and increase of M1 markers on remaining macrophages (repolarization) superior to parental and control viruses (171)
	MV	Additional transcription unit downstream of H gene	BiTe	Human CEA × murine or human CD3, human CD20 × murine CD3	Subcutaneous syngeneic mouse tumor models/intratumoral OV injection: BiTE-encoding OV resulted in (i) prolonged survival, in one of two models superior to control virus or direct BiTE injection; (ii) increased T cell infiltration and activation; and (iii) protective immunity (to ental tumor cells not expressing the BiTE-target. Thus indicative of antigen spread, i.e., activation of endogenous T cells specific for tumor antigens) (172).
	Vaccinia virus	Separate transcription unit, late viral promoter	BiTe	Human EphA2 × human CD3	Co-cultures of infected tumor and unstimulated T cells or PBMCs: BiTE- encoding OV, not control virus, induced T cell activation, which depended on presence of EphA2-positive cells, and T cell-dependent bystander tumor cell killing. Lung metastasis xenograft mouse tumor model/intravenous OV and/or PBMC injection: BiTE-encoding OV showed significantly delayed tumor growth compared with controls (173).
OVs plus CAR-T Cell and CAR-NK Cells	Ad	HER2 chimeric antigen receptor specific cytotoxic T lymphocytes	scFv	Metastatic HER2 Positive Solid Tumors	HER2 chimeric antigen receptor specific cytotoxic T lymphocytes (HER2 specific CAR-T cells), in combination with intra-tumor injection of CAdVEC, an oncolytic adenovirus that was designed to help the immune system including HER2 specific CAR-T cell reacted to the tumor. https://clinicaltrials.gov/
	Vaccinia virus	CD19-expressing oncolytic virus CF33-CD19	scFv	eradicate solid tumors	The combination of CD-19-directed CAR-T with CD19-encoding OV resulted in greatly improved survival of mice compared to antigen-mismatched combinations. https://www.imugene.com/
	HSV-1	IL15/IL15Rα sushi domain fusion protein	scFv	Glioblastoma	OV-IL15C plus EGFR-CAR-NK cells synergistically suppressed tumor growth and significantly improved survival compared with either monotherapy, correlating with increased intracranial infiltration and activation of NK and CD8+ T cells and elevated persistence of CAR-NK cells in an immunocompetent model. Collectively, OV-IL15C and off-the-shelf EGFR-CAR-NK cells represented promising therapeutic strategies for GBM treatment to improve the clinical management of this devastating disease (174).

associated with increased M1-like macrophages, T effector cells ($CD4^+$ and $CD8^+$), and decreased T regulatory (Treg) cells (183, 184). To emphasize the effect of combination therapy, it should be noted that while none of these agents were effective alone enough, they showed remarkable therapeutic effects in combinational strategy (184). It is worth noting that although Imlygic® has been approved for adult patients with melanoma, there are clinical trials for the assessment of Imlygic® in combination with ICIs for improving the treatment outcomes in melanoma and other cancer types (e.g., Pembrolizumab with Imlygic® or Placebo in Unresected Melanoma, NCT02263508) (181, 185). Other combinations, including this OV and ICIs for triple-negative breast cancer with metastatic liver cancer and colorectal carcinoma are also being evaluated in clinical trials (186).

5.1.1.2 OVs plus monoclonal antibodies other than ICIs

Apart from ICIs, some commercial mAbs with distinct mechanism of actions, have also been combined with OVs to improve the therapy outcome. In one study, the antitumor activity of cetuximab (an epidermal growth factor receptor inhibitor mAb) was assessed in combination with HSV. The result showed that combining cetuximab and HSV could improve distribution of the virus and lead to a synergistic antitumor effect in HT-29 tumor xenograft models (187). In another study, Zhang et al. demonstrated that combination of recombinant oncolytic HSV with Bevacizumab (BEV) (which is an antiangiogenic mAb approved for glioblastoma) in mice-bearing human GBM, was led to improvement of antiangiogenic effect of BEV while decreasing the tumor invasive-like phenotype induced by this drug (188).

5.1.2 OVs plus nanobodies

Nanobodies are the smallest natural antigen-binding constructs with a single variable domain (VHH, ~15kDa) as the antigen-binding region (189). Nanobodies have unique characteristics, such as easy selection by phage display, ease of

manipulation, high stability in harsh conditions, and reaching and recognition of specific hard-to-access epitopes, making them more attractive in combination with other agents in cancer immunotherapy, including OVs (190, 191). For instance, due to the high complexity of glioblastomas and the low accessibility of therapeutic agents to their TME, the combination of viruses and nanobodies is a promising candidate for glioblastoma treatment. In a proof-of-concept study, Gil et al. used an anti-CXCR4 nanobody for retargeting oncolytic HSV toward $CXCR4^+$ GBM cells. CXCR4 is overexpressed in various cancers, including glioblastoma, and usually correlates with a poor prognosis. The results of this study indicated that OVs plus nanobodies were highly encouraging for targeting GBM cells (192).

CD47 acts as a "don't eat me signal" to the immune system's macrophages, making it a potential therapeutic target in some cancers. Different viruses have been engineered to express anti-CD47 antibodies (193) or nanobodies (194) to have a multifaced attack on the tumor cells. In a study, anti-CD47 nanobody-expressing adenovirus reprogramed tumor immune microenvironment and showed excellent anti-tumor immunity (194). This anti-CD47 oncolytic adenovirus could induce durable tumor suppression by changing the TME condition and increasing activated TILs in the tumor site. Systemic anti-tumor effects and memory immune cells were also observed after treatment by this recombinant virus (194).

5.1.3 OVs plus bispecific or trispecific antibodies

Bispecific antibodies (bsAb) are constructs with two different antigen-binding sites with the aim of dual targeting (195). The coding sequence of bsAbs can be inserted into the viral genome to be expressed in the target tissue. Different viruses are engineered to this end, including Ad, HSV, MV and vaccinia (159, 196). Bi/trispecific antibodies can also be used in combination with viruses in various timings and dosages.

5.1.3.1 OVs plus bispecific T-cell engagers

Viruses have been successfully combined with T-cell retargeting bsAb, also called Bispecific T-cell Engager or BiTe (197), to retarget T cells to the targeted tumor cells. In one study, a recombinant adenovirus encoding bsCD3-EpCAM bispecific antibody (bsAb) could effectively activate T-cells in malignant peritoneal and pleural exudates despite the immunosuppressive environment (198). Also, in another study, NDV-BiTe constructs (e.g., antiHN scFv/antiCD3 scFv and antiHN scFv/antiCD28 scFv) were successfully designed and expressed to be evaluated for thier remarkable potentials in tumor immunotherapy especially in breast and colorectal cancers (199, 200).

5.1.3.2 OVs plus natural killer cell engagers

Emerging role of NKs cells in cancer therapy becomes clearer every day and its combination with virotherapy has accelerated the progress of therapeutic processes in cancer. Viruses can also be combined with bispecific NK engagers (201) to retarget NK cells to their targeted tumor cells.

As an examples for this type of combination, Bahrololoumi et al. constructed a bsAb (antiHN scFv/antiCD16 scFv) and a trispecific antibody(antiHN scFv/IL-15/antiCD16 scFv) to bind to the haemagglutinin neuraminidase (HN), a viral protein that is expressed on the surface of the NDV infected tumor cell, and the CD16 activating receptor on the surface of the NK cells for redirecting NK cells toward the tumor cells (201, 202). NDV-Ulster is a non-lytic strain of NDV that was used to inflame the tumoral microenvironment in this study, and also in NDV-based autologous tumor cell vaccines for stimulating the immune response in the patient's body (93, 178, 203, 204).

5.1.3.3 OVs plus trispecific antibodies

Trispecific antibody (Trike) is a single engineered antibody platform that recognizes and binds to three different targets and is expected to boost immune response significantly (205). There are different studies that combine these trifunctional engagers with OVs with the aim of cancer viro-immunotherpy. In one study, researchers constructed a trispecific immunocytokine (anti-NDV/IL2/anti-CD28) for efficiently targeting tumor cells. This trike could bind to the HN of the NDV infected tumor cells from one side and to the CD28 receptor on the T cells from the other side, while IL-2 promoted T cells function (206, 207). Ravirala et al, showed that combination of oncolytic HSV with bi/tri specific antibodies which could bind to the NKG2D and epidermal growth factor (EGF) from each side, while the trispecific one also contained IL-2 sequence, could significantly enhance infiltration and activation of NK and T cells in the tumor site (208). Various bi/trispecific antibodies that were combined with different viruses have been extensively reviewed elsewhere (209).

5.2 OVs plus CAR-T and CAR-NK cells

Chimeric antigen receptor (CAR)-T cells are T cells that have been genetically engineered to express an artificial receptor to direct them toward a specific target in an MHC-independent manner. The external domain of CAR-T cells consists of an extracellular target antigen binding domain which is usually a single-chain fragment variable (scFv) from a specific monoclonal antibody, attached to the transmembrane and signaling domains of this artificial receptor by a hinge (210). Although some scFv-based CAR-T cell products are currently approved by FDA for B-cell malignancies with encouraging results, this approach still faces some limitations, such as

trafficking and tumor infiltration, antigen escape, immunosuppressive microenvironment, and CAR-T cell-associated toxicities (211). As a consequence, CAR-T cells do not exhibit profound anti-tumor effects in solid tumors. The use of VHH-based CAR-T cells (Nanobody CAR-T cells) may could resolve the abovementioned problems (212, 213). There are different antigens that are targeted through Nanobody-based CAR-T cells, such as vascular endothelial growth factor receptor 2 (VEGFR2) (214), human epidermal growth factor receptor 2 (HER2) (215), tumor-associated glycoprotein 72 (TAG-;72) (216), prostate-specific membrane antigen (PSMA) (217–219), glypican 2 (GPC2), epidermal growth factor receptor (EGFR), B-;cell maturation antigen (BCMA), PD-;L1, and EIIIB (212, 220). It has been shown that the combination of CAR-T cells (scFv or VHH-based) with virotherapy can help CAR-T cells overcome their challenges in combat against solid tumors (such as immunosuppressive TME and heterogeneity of the antigens) and increase the immune response dramatically. For instance, Nishio et al. showed that armed oncolytic Ad (with RANTES and IL-15) could increase the efficacy of GD2 targeting CAR-T cell in a neuroblastoma solid tumor model (221). Furthermore, there is evidence that pre-treatment of solid tumors with OVs before the administration of CAR-T cells may lead to better ICD (222, 223). For example, combining recombinant oncolytic Ads containing a coding sequence of different cytokines, such as IL-2, RANTES and TNF-α, could lead to better accumulation and survival of CAR-T cells (223). Some of the combinations, such as Ad/HER-2 targeting CAR-T cell (NCT03740256) and VZV/GD2 targeting CAR-T cell (NCT01953900) therapy, are examples of such combinations being evaluated in clinical trials.

In the case of CAR-NK cells, in combination with HSV and to treat brain cancer metastases, EGFR CAR-NK cells were used intracranially in mice. This combination resulted in significantly longer survival of tumor-bearing mice when compared to monotherapies (224).

OVs attack and destroy tumor cells preferentially. Lysis of tumor cells releases neoantigen, PAMPs which trigger PRRs, which then produce inflammatory cytokines and antiviral type I IFNs. Viruses can activate cell death pathways, resulting in immunogenic cell death phenotypes such as necroptosis, pyroptosis, immunogenic apoptosis, and autophagic cell death. Antibodies that target cell surface indicators of immune cells (checkpoint inhibition), cancer cells (targeted therapy), or both (bispecific antibodies) are well-established in cancer therapy. combination of oncolytic viruses with antibody and CAR-T cells; CAR-T cells bind to the antigen on the surface of tumor cells and kill them, but they cannot migrate deeper into the dense tumor mass to remove antigennegative tumor cells. also, CAR-NK cells show more anticancer activity than CAR-T cells because they attach to stress ligands on the surface of tumor cells. The oncolytic virus attacks and destroys tumor cells, eliminating the tumor's dense structure.

5.3 Other combinations with OVs

5.3.1 OVs plus autologous DC or T cells

OVs can also be combined with cell therapy to treat different tumors, including solid tumors. For instance, the combination of NDV and dendritic cells (DC (as an exciting platform is being used in the IOZK clinic in Cologne Germany (Immun-Onkologisches Zentrum Köln). Their studies and practices in the IOZK indicated that DCs loaded with the lysate of NDV-infected tumor cells (viral oncolysate, VOL) triggered potent anti-tumor immunity by promoting the secretion of IFN-γ and IL-2 from T-cells. This combinational therapy is now available in the IOZK clinic and patients can benefit from the advantages of this kind of cancer combinational treatment (200, 225). Activation of naïve human T-cells by co-incubating with NDV-infected irradiated autologous tumor cells (ATV-NDV) which can be further modified with bi-specific or tri-specific antibodies can also offer a promising multimodal anti-cancer approach (226).

Altogether, strong evidence confirm that different therapeutic agents can have a measurable therapeutic effect in cancer treatment, but due to the specific and complex biology of cancer and its TME, the therapeutic outcome of these agents lonely, do not contribute to the final treatment of cancer patients. Thus, this is where rational combination therapy of these factors with each other, especially with OVs is much needed.

5.3.2 OVs plus tumor-infiltrating lymphocytes

It has been demonstrated that weak functionality of natural TILs in the tumor site is strongly related to tumor progression (227). OVs can set the scene by inflaming the tumor microenvironment for better functionality of TILs. Feist et al, showed that local injection of poxvirus into a solid tumor in mice, could lead to activation and accumulation of TILs in the tumor site which had a low immunogenicity before virus infection (228). In another study, it was shown that virotherapy with a type of oncolytic adenovirus, could increase the TILs and significantly reduce the tumor size in the immunocompetent mouse model (229). It has also been shown that infecting the tumor with recombinant oncolytic HSV, could unleash the full potential of TILs which led to tumor regression and antitumor immunological memory (230).

6 Conclusions

OVT success, specifically FDA- and regional-approved OVs, has made waves in (pre)clinical areas, attracting both society and the scientific community's attention. However, some of challenges have limited OVs application as immunotherapy, and their combination with other biotherapeutic platforms has been

proposed in cancer therapy. To date, hundreds of combinations of OVs with other biotherapeutic platforms, including antibodies, nanobodies, ICIs, CAR-T cells, and DCs, have been investigated in clinical trials to understand which and how best to provoke anti-cancer immune responses. Some considerations could improve the efficacy of OVs, either as monotherapy or combination therapy. First, the dosage, targeted mechanisms, administration schedule, delivery technologies, and types of OVs could be considered because of their indispensable roles in the outcome of cancer immunotherapy and priming TME in combinational regimens. Second, understanding the interaction between immune cells/system, tumor cells/TME, and OVs and the combinational agents should help make new therapeutic combinations possible. Third, defining reliable biomarkers to distinguish "hot tumors" from "cold ones" can help scientists determine subsequent therapies. Finally, providing beneficial impacts of OVs and their combinational regimens on patients' life quality requires the contribution of molecular biologists, pharmacologists, immunologists, and clinicians. Indeed, current clinical trials results can help scientists develop new systems of combination therapy and deliver innovative treatments to patients.

Author contributions

ZS conceived the presented idea and SA developed the theory. MJ took the lead in writing the manuscript and she was in charge of overall direction and planning. MJ, MK and MBS wrote the manuscript with input from all authors. NH contributed to the writing of the results and to the editing of the manuscript. MAS and AA contributed to the final version of the manuscript. All authors discussed the results and contributed to the final manuscript.

Acknowledgments

We gratefully acknowledge the Immunology Department of Pasteur Institute of Iran for their technical assistance.

Conflict of interest

Author MBS was employed by HUM Immune Biotech.

The remaining authors declare that the research was conducted in the absence of any commercial or financial relationships that could be construed as a potential conflict of interest.

Publisher's note

References

1. Siegel RL, Miller KD, Fuchs HE, Jemal A. Cancer statistics, 2022. *CA Cancer J Clin* (2022) 72(1):7–33. doi: 10.3322/caac.21708

2. Hemminki O, Manuel J, Hemminki A. Oncolytic viruses for cancer immunotherapy. *J Hematol Oncol* (2020) 13(1):84. doi: 10.1186/s13045-020-00922-1

3. Rahman MM, Mcfadden G. Oncolytic Viruses : Newest frontier for cancer immunotherapy. *Cancers* (2021) 13(21):5452. doi: 10.3390/cancers13215452

4. Grossman DC, Curry SJ, Owens DK, Barry MJ, Caughey AB, Davidson KW, et al. Behavioral counseling to prevent skin cancer: US preventive services task force recommendation statement. *JAMA* (2018) 319(11):1134–42. doi: 10.1001/jama.2018.1623

5. Spaas M, Lievens Y. Is the combination of immunotherapy and radiotherapy in non-small cell lung cancer a feasible and effective approach? *Front Med* (2019) 6 (November). doi: 10.3389/fmed.2019.00244

6. Zhang S, Rabkin SD. The discovery and development of oncolytic viruses: Are they the future of cancer immunotherapy? *Expert Opin Drug Discov* (2021) 16 (4):391–410. doi: 10.1080/17460441.2021.1850689

7. Koch MS, Lawler SE, Chiocca EA. HSV-1 oncolytic viruses from bench to Bedside : An overview of current clinical trials. *Cancers* (2020) 12(12):3514. doi: 10.3390/cancers12123514

8. Malogolovkin A, Gasanov N, Egorov A, Weener M, Ivanov R, Karabelsky A. Combinatorial approaches for cancer treatment using oncolytic Viruses : Projecting the perspectives through clinical trials outcomes. *Viruses* (2021) 13 (7):1271. doi: 10.3390/v13071271

9. Cerqueira OLD, Antunes F, Assis NG, Cardoso EC, Clavijo-Salomón MA, Domingues AC, et al. Perspectives for combining viral oncolysis with additional immunotherapies for the treatment of melanoma. *Front Mol Biosci* (2022) 9:777775. doi: 10.3389/fmolb.2022.777775

10. Kaufman HL, Kohlhapp FJ, Zloza A. Oncolytic viruses: A new class of immunotherapy drugs. *Nat Rev Drug Discovery* (2015) 14(9):642–62. doi: 10.1038/nrd4663

11. Jin K-T, Du W-L, Liu Y-Y, Lan H-R, Si J-X, Mou X-Z. Oncolytic virotherapy in solid tumors: The challenges and achievements. *Cancers (Basel)* (2021) 13 (4):588. doi: 10.3390/cancers13040588

12. Jin K, Du W, Liu Y, Lan H, Si J, Mou X. Oncolytic virotherapy in solid Tumors : The challenges and achievements. *Cancers* (2021) 13(4):588. doi: 10.3390/cancers13040588

13. Vähä-Koskela MJV, Heikkilä JE, Hinkkanen AE. Oncolytic viruses in cancer therapy. *Cancer Lett* (2007) 254(2):178–216. doi: 10.1016/j.canlet.2007.02.002

14. Coelho JF, Ferreira PC, Alves P, Cordeiro R, Fonseca AC, Góis JR, et al. Drug delivery systems: Advanced technologies potentially applicable in personalized treatments. *EPMA J* (2010) 1(1):164–209. doi: 10.1007/s13167-010-0001-x

15. Oh C-M, Chon HJ, Kim C. Combination immunotherapy using oncolytic virus for the treatment of advanced solid tumors. *Int J Mol Sci* (2020) 21(20):7743. doi: 10.3390/ijms21207743

16. Malfitano AM, Di Somma S, Iannuzzi CA, Pentimalli F, Portella G. Virotherapy: From single agents to combinatorial treatments. *Biochem Pharmacol* (2020) 177:113986. doi: 10.1016/j.bcp.2020.113986

17. Finck A, Gill SI, June CH. Cancer immunotherapy comes of age and looks for maturity. *Nat Commun* (2020) 11(1):3325. doi: 10.1038/s41467-020-17140-5

18. Larson C, Oronsky B, Scicinski J, Fanger GR, Stirn M, Oronsky A, et al. Going viral: a review of replication-selective oncolytic adenoviruses. *Oncotarget* (2015) 6(24):19976–89. doi: 10.18632/oncotarget.5116

19. Beijerinck MW. Concerning a contagium viwm fluidum as cause of the spot disease of tobacco leaves. *Phytopathol Class.* (1898) 7(1):33–52.

20. Xie F, Zheng L. Oncolytic viruses and their application to cancer treatment. *Int Arch Clin Pharmacol* (2019) 5(1):1–6. doi: 10.23937/2572-3987.1510020

21. Tian Y, Xie D, Yang L. Engineering strategies to enhance oncolytic viruses in cancer immunotherapy. *Signal Transduct Target Ther* (2022) 7(1):117. doi: 10.1038/s41392-022-00951-x

22. Kelly E, Russell SJ. History of oncolytic Viruses : Genesis to genetic engineering. *Mol Ther* (2007) 15(4):651–9. doi: 10.1038/sj.mt.6300108

23. Bouard D, Alazard-Dany D, Cosset F-L. Viral vectors: from virology to transgene expression. *Br J Pharmacol* (2009) 157(2):153–65. doi: 10.1038/bjp.2008.349

24. Dock G. The influence of complicating diseases upon leukaemia. *Am J Med Sci* (1904) 127(4):563. doi: 10.1097/00000441-190412740-00001

25. Davola ME, Mossman KL, Davola ME, Mossman KL. Oncolytic viruses : how " lytic " must they be for therapeutic efficacy? *Oncoimmunology* (2019) 8(6):1–7. doi: 10.1080/2162402X.2019.1596006

26. Rahman MM, McFadden G. Oncolytic viruses: Newest frontier for cancer immunotherapy. *Cancers (Basel).* (2021) 13(21):5452. doi: 10.3390/cancers13215452

27. Bluming AZ, Ziegler JL. Regression of burkitt's lymphoma in association with measles infection. *Lancet (London England).* (1971) 2(7715):105–6. doi: 10.1016/S0140-6736(71)92086-1

28. Chhabra N, Kennedy J. A review of cancer immunotherapy toxicity II: adoptive cellular therapies, kinase inhibitors, monoclonal antibodies, and oncolytic viruses. *J Med Toxicol* (2021) 18(1):1–13. doi: 10.1007/s13181-021-00835-6

29. Lawler SE, Speranza MC, Cho CF, Chiocca EA. Oncolytic viruses in cancer treatment a review. *JAMA Oncol* (2017) 3(6):841–9. doi: 10.1001/jamaoncol.2016.2064

30. Abdoli S, Roohvand F, Teimoori-Toolabi L, Shayan S, Shokrgozar MA. Cytotoxic effect of dual fluorescent-labeled oncolytic herpes simplex virus type 1 on mouse tumorigenic cell lines. *Res Pharm Sci* (2019) 14(1):27–35. doi: 10.4103/1735-5362.251850

31. Valyi-Nagy T, Gesser RM, Raengsakulrach B, Deshmane SL, Randazzo BP, Dillner AJ, et al. A thymidine kinase-negative HSV-1 strain establishes a persistent infection in SCID mice that features uncontrolled peripheral replication but only marginal nervous system involvement. *Virology* (1994) 199(2):484–90. doi: 10.1006/viro.1994.1150

32. Russell SJ, Peng K-W. Oncolytic virotherapy: a contest between apples and oranges. *Mol Ther* (2017) 25(5):1107–16. doi: 10.1016/j.ymthe.2017.03.026

33. Heise C, Sampson-Johannes A, Williams A, Mccormick F, Von Hoff DD, Kirn DH. ONYX-015, an E1B gene-attenuated adenovirus, causes tumor-specific cytolysis and antitumoral efficacy that can be augmented by standard chemotherapeutic agents. *Nat Med* (1997) 3(6):639–45. doi: 10.1038/nm0697-639

34. Toth K, Wold WSM. Increasing the efficacy of oncolytic adenovirus vectors. *Viruses* (2010) 2(9):1844–66. doi: 10.3390/v2091844

35. Ries SJ, Brandts CH, Chung AS, Biederer CH, Hann BC, Lipner EM, et al. Loss of p14ARF in tumor cells facilitates replication of the adenovirus mutant dl1520 (ONYX-015). *Nat Med* (2000) 6(10):1128–33. doi: 10.1038/80466

36. O'Shea CC, Johnson L, Bagus B, Choi S, Nicholas C, Shen A, et al. Late viral RNA export, rather than p53 inactivation, determines ONYX-015 tumor selectivity. *Cancer Cell* (2004) 6(6):611–23. doi: 10.1016/j.ccr.2004.11.012

37. Boagni DA, Ravirala D, Zhang SX. Current strategies in engaging oncolytic viruses with antitumor immunity. *Mol Ther Oncolytics* (2021) 22(September):98–113. doi: 10.1016/j.omto.2021.05.002

38. Ripp J, Hentzen S, Saeed A. Oncolytic viruses as an adjunct to immune checkpoint inhibition. *Front Biosci* (2022) 27(5):151. doi: 10.31083/j.fbl2705151

39. Wong B, Bergeron A, Alluqmani N, Maznyi G, Chen A, Arulanandam R, et al. Dependency of EGFR activation in vanadium-based sensitization to oncolytic virotherapy. *Mol Ther Oncolytics* (2022) 25:146–59. doi: 10.1016/j.omto.2022.04.004

40. Ricca JM, Oseledchyk A, Walther T, Liu C, Mangarin L, Merghoub T, et al. Pre-existing immunity to oncolytic virus potentiates its immunotherapeutic efficacy. *Mol Ther* (2018) 26(4):1008–19. doi: 10.1016/j.ymthe.2018.01.019

41. Russell SJ, Peng K-W. Viruses as anticancer drugs. *Trends Pharmacol Sci* (2007) 28(7):326–33. doi: 10.1016/j.tips.2007.05.005

42. Zheng M, Huang J, Tong A, Yang H. Oncolytic viruses for cancer Therapy : Barriers and recent advances. *Mol Ther Oncolytics* (2019) 15(37):234–47. doi: 10.1016/j.omto.2019.10.007

43. Gujar S, Pol JG, Kim Y, Lee PW, Kroemer G. Antitumor benefits of antiviral immunity: An underappreciated aspect of oncolytic virotherapies. *Trends Immunol* (2018) 39(3):209–21. doi: 10.1016/j.it.2017.11.006

44. Lemos de Matos A, Franco LS, McFadden G. Oncolytic viruses and the immune system: The dynamic duo. *Mol Ther Methods Clin Dev* (2020) 17:349–58. doi: 10.1016/j.omtm.2020.01.001

45. Bommareddy PK, Shettigar M, Kaufman HL. Integrating oncolytic viruses in combination cancer immunotherapy. *Nat Rev Immunol* (2018) 18(8):498–513. doi: 10.1038/s41577-018-0014-6

46. de Graaf JF, de Vor L, Fouchier RAM, van den Hoogen BG. Armed oncolytic viruses: A kick-start for anti-tumor immunity. *Cytokine Growth Factor Rev* (2018) 41:28–39. doi: 10.1016/j.cytogfr.2018.03.006

47. Allegrezza MJ, Conejo-Garcia JR. Targeted therapy and immunosuppression in the tumor microenvironment. *Trends Cancer* (2017) 3(1):19–27. doi: 10.1016/j.trecan.2016.11.009

48. Alberts P, Olmane E, Brokāne L, Krastiņa Z, Romanovska M, Kupčs K, et al. Long-term treatment with the oncolytic ECHO-7 virus rigvir of a melanoma stage IV M1c patient, a small cell lung cancer stage IIIA patient, and a histiocytic sarcoma stage IV patient-three case reports. *Apmis* (2016) 124(10):896–904. doi: 10.1111/apm.12576

49. Alberts P, Tilgase A, Rasa A, Bandere K, Venskus D. The advent of oncolytic virotherapy in oncology: The rigvir® story. *Eur J Pharmacol* (2018) 837:117–26. doi: 10.1016/j.ejphar.2018.08.042

50. Yu W, Fang H. Clinical trials with oncolytic adenovirus in China. *Curr Cancer Drug Targets.* (2007) 7(2):141–8. doi: 10.2174/156800907780058817

51. Goradel NH, Alizadeh A, Hosseinzadeh S, Taghipour M, Ghesmati Z, Arashkia A, et al. Oncolytic virotherapy as promising immunotherapy against cancer: mechanisms of resistance to oncolytic viruses. *Futur Oncol* (2021) 18(2):245–59. doi: 10.2217/fon-2021-0802

52. Goradel NH, Mohajel N, Malekshahi ZV, Jahangiri S, Najafi M, Farhood B, et al. Oncolytic adenovirus: A tool for cancer therapy in combination with other therapeutic approaches. *J Cell Physiol* (2019) 234(6):8636–46. doi: 10.1002/jcp.27850

53. Harrington KJ, Puzanov I, Hecht JR, Hodi FS, Szabo Z, Murugappan S, et al. Clinical development of talimogene laherparepvec (T-VEC): A modified herpes simplex virus type-1–derived oncolytic immunotherapy. *Expert Rev Anticancer Ther* (2015) 15(12):1389–403. doi: 10.1586/14737140.2015.1115725

54. Wang Y, Jin J, Wu Z, Hu S, Hu H, Ning Z, et al. Stability and anti-tumor effect of oncolytic herpes simplex virus type 2. *Oncotarget* (2018) 9(37):24672–83. doi: 10.18632/oncotarget.25122

55. Dharmadhikari N, Mehnert JM, Kaufman HL. Oncolytic virus immunotherapy for melanoma. *Curr Treat Options Oncol* (2015) 16(3):1–5. doi: 10.1007/s11864-014-0326-0

56. Bommareddy PK, Patel A, Hossain S, Kaufman HL. Talimogene laherparepvec (T-VEC) and other oncolytic viruses for the treatment of melanoma. *Am J Clin Dermatol* (2017) 18(1):1–15. doi: 10.1007/s40257-016-0238-9

57. Ekeke CN, Russell KL, Joubert K, Bartlett DL, Luketich JD, Soloff AC, et al. Fighting fire with Fire : Oncolytic virotherapy for thoracic malignancies. *Ann Surg Oncol* (2021) 28(5):2715–27. doi: 10.1245/s10434-020-09477-4

58. Koch MS, Lawler SE, Chiocca EA. HSV-1 oncolytic viruses from bench to bedside: An overview of current clinical trials. *Cancers (Basel)* (2020) 12(12):3514. doi: 10.3390/cancers12123514

59. Chaurasiya S, Fong Y, Warner SG. Oncolytic virotherapy for Cancer. *Clin Exp* (2021) 9(4):419. doi: 10.3390/biomedicines9040419

60. Garber K. China Approves world's first oncolytic virus therapy for cancer treatment. vol. 98. *J Natl Cancer Institute. US* (2006) 8(5):298–300. doi: 10.1093/jnci/djj111

61. Ilkow CS, Marguerie M, Batenchuk C, Mayer J, Ben Neriah D, Cousineau S, et al. Reciprocal cellular cross-talk within the tumor microenvironment promotes oncolytic virus activity. *Nat Med* (2015) 21(5):530–6. doi: 10.1038/nm.3848

62. Desjardins A, Vlahovic G, Friedman HS. Vaccine therapy, oncolytic viruses, and gliomas. *Oncol (willist Park NY).* (2016) 30(3):211–8.

63. Chiocca EA, Rabkin SD. Oncolytic viruses and their application to cancer immunotherapy. *Cancer Immunol Res* (2014) 2(4):295–300. doi: 10.1158/2326-6066.CIR-14-0015

64. Guo ZS, Lu B, Guo Z, Giehl E, Feist M, Dai E, et al. Vaccinia virus-mediated cancer immunotherapy: cancer vaccines and oncolytics. *J Immunother Cancer* (2019) 7(1):6. doi: 10.1186/s40425-018-0495-7

65. Bartlett DL, Liu Z, Sathaiah M, Ravindranathan R, Guo Z, He Y, et al. Oncolytic viruses as therapeutic cancer vaccines. *Mol Cancer* (2013) 12(1):103. doi: 10.1186/1476-4598-12-103

66. Cattaneo R, Miest T, Shashkova EV, Barry MA. Reprogrammed viruses as cancer therapeutics: targeted, armed and shielded. *Nat Rev Microbiol* (2008) 6 (7):529–40. doi: 10.1038/nrmicro1927

67. Hemminki O, Hemminki A. A century of oncolysis evolves into oncolytic immunotherapy. *Oncoimmunol* (2016) 5(2):e1074377. doi: 10.1080/2162402X.2015.1074377

68. Russell SJ, Barber GN. Oncolytic viruses as antigen-agnostic cancer vaccines. *Cancer Cell* (2018) 33(4):599–605. doi: 10.1016/j.ccell.2018.03.011

69. Kontermann RE. Viro-antibody therapy : engineering oncolytic viruses for genetic delivery of diverse antibody-based biotherapeutics. *InMabs* (2021) 13 (1):1982447. doi: 10.1080/19420862.2021.1982447

70. Kleijn A, Kloezeman J, Treffers-Westerlaken E, Fulci G, Leenstra S, Dirven C, et al. The *in vivo* therapeutic efficacy of the oncolytic adenovirus Delta24-RGD is mediated by tumor-specific immunity. *PloS One* (2014) 9(5):e97495. doi: 10.1371/journal.pone.0097495

71. Melchjorsen J. Learning from the messengers: innate sensing of viruses and cytokine regulation of immunity - clues for treatments and vaccines. *Viruses* (2013) 5(2):470–527. doi: 10.3390/v5020470

72. Kakiuchi Y, Kuroda S, Kanaya N, Kumon K, Tsumura T, Hashimoto M, et al. Local oncolytic adenovirotherapy produces an abscopal effect *via* tumor-derived extracellular vesicles. *Mol Ther* (2021) 29(10):2920–30. doi: 10.1016/j.ymthe.2021.05.015

73. Ma J, Ramachandran M, Jin C, Quijano-Rubio C, Martikainen M, Yu D, et al. Characterization of virus-mediated immunogenic cancer cell death and the consequences for oncolytic virus-based immunotherapy of cancer. *Cell Death Dis* (2020) 11(1):1–5. doi: 10.1038/s41419-020-2236-3

74. Jiang H, Clise-Dwyer K, Ruisaard KE, Fan X, Tian W, Gumin J, et al. Delta-24-RGD oncolytic adenovirus elicits anti-glioma immunity in an immunocompetent mouse model. *PloS One* (2014) 9(5):e97407. doi: 10.1371/journal.pone.0097407

75. Ramelyte E, Tastanova A, Balázs Z, Ignatova D, Turko P, Menzel U, et al. Oncolytic virotherapy-mediated anti-tumor response: a single-cell perspective. *Cancer Cell* (2021) 39(3):394–406.e4. doi: 10.1016/j.ccell.2020.12.022

76. Mardi A, Shirokova AV, Mohammed RN, Keshavarz A, Zekiy AO, Thangavelu L, et al. Biological causes of immunogenic cancer cell death (ICD) and anti – tumor therapy ; combination of oncolytic virus – based immunotherapy and CAR T – cell therapy for ICD induction. *Cancer Cell Int* (2022) 22(1):1–21. doi: 10.1186/s12935-022-02585-z

77. Ranki T, Joensuu T, Jäger E, Karbach J, Wahle C, Kairemo K, et al. Local treatment of a pleural mesothelioma tumor with ONCOS-102 induces a systemic antitumor CD8(+) T-cell response, prominent infiltration of CD8(+) lymphocytes and Th1 type polarization. *Oncoimmunology* (2014) 3(10):e958937. doi: 10.4161/21624011.2014.958937

78. Todo T, Martuza RL, Rabkin SD, Johnson PA. Oncolytic herpes simplex virus vector with enhanced MHC class I presentation and tumor cell killing. *Proc Natl Acad Sci USA* (2001) 98(11):6396–401. doi: 10.1073/pnas.101136398

79. Helmink BA, Reddy SM, Gao J, Zhang S, Basar R, Thakur R, et al. B cells and tertiary lymphoid structures promote immunotherapy response. *Nature* (2020) 577 (7791):549–55. doi: 10.1038/s41586-019-1922-8

80. Gujar SA, Marcato P, Pan D, Lee PWK. Reovirus virotherapy overrides tumor antigen presentation evasion and promotes protective antitumor immunity. *Mol Cancer Ther* (2010) 9(11):2924–33. doi: 10.1158/1535-7163.MCT-10-0590

81. Marchini A, Daeffler L, Pozdeev VI, Angelova A, Rommelaere J. Immune conversion of tumor microenvironment by oncolytic viruses: the protoparvovirus h-1PV case study. *Front Immunol* (2019) 10:1848. doi: 10.3389/fimmu.2019.01848

82. Tsun A, Miao XN, Wang CM, Yu DC. Oncolytic immunotherapy for treatment of cancer. *Prog Cancer Immunother* (2016) 241–283. doi: 10.1007/978-94-017-7555-7_5

83. Arulanandam R, Batenchuk C, Angarita FA, Ottolino-Perry K, Cousineau S, Mottashed A, et al. VEGF-mediated induction of PRD1-BF1/Blimp1 expression sensitizes tumor vasculature to oncolytic virus infection. *Cancer Cell* (2015) 28 (2):210–24. doi: 10.1016/j.ccell.2015.06.009

84. Breitbach CJ, De Silva NS, Falls TJ, Aladl U, Evgin L, Paterson J, et al. Targeting tumor vasculature with an oncolytic virus. *Mol Ther* (2011) 19(5):886–94. doi: 10.1038/mt.2011.26

85. Hiley CT, Chard LS, Gangeswaran R, Tysome JR, Briat A, Lemoine NR, et al. Vascular endothelial growth factor a promotes vaccinia virus entry into host cells *via* activation of the akt pathway. *J Virol* (2013) 87(5):2781–90. doi: 10.1128/JVI.00854-12

86. Luker KE, Hutchens M, Schultz T, Pekosz A, Luker GD. Bioluminescence imaging of vaccinia virus : Effects of interferon on viral replication and spread. *Virology* (2005) 341(2):284–300. doi: 10.1016/j.virol.2005.06.049

87. Naumenko VA, Stepanenko AA, Lipatova AV, Vishnevskiy DA, Chekhonin VP. Infection of non-cancer cells : A barrier or support for oncolytic virotherapy? *Mol Ther Oncolytics* (2022) 24:663–82. doi: 10.1016/j.omto.2022.02.004

88. Reichard KW, Lorence RM, Cascino CJ, Peeples ME, Walter RJ, Fernando MB, et al. Newcastle Disease virus selectively kills human tumor cells. *J Surg Res* (1992) 52(5):448–53. doi: 10.1016/0022-4804(92)90310-V

89. Lorence RM, Reichard KW, Katubig BB, Reyes HM, Phuangsab A, Mitchell BR, et al. Complete regression of human neuroblastoma xenografts in athymic mice after local Newcastle disease virus therapy. *J Natl Cancer Inst* (1994) 86 (16):1228–33. doi: 10.1093/jnci/86.16.1228

90. Ganar K, Das M, Sinha S, Kumar S. Newcastle Disease virus: current status and our understanding. *Virus Res* (2014) 184:71–81. doi: 10.1016/j.virusres.2014.02.016

91. Tan L, Zhang Y, Zhan Y, Yuan Y, Sun Y, Qiu X, et al. Newcastle Disease virus employs macropinocytosis and Rab5a-dependent intracellular trafficking to infect DF-1 cells. *Oncotarget* (2016) 7(52):86117–33. doi: 10.18632/oncotarget.13345

92. Meng Q, He J, Zhong L, Zhao Y. Advances in the study of antitumour immunotherapy for Newcastle disease virus. *Int J Med Sci* (2021) 18(11):2294–302. doi: 10.7150/ijms.59185

93. Zamarin D, Palese P. Oncolytic Newcastle disease virus for cancer therapy: old challenges and new directions. *Future Microbiol* (2012) 7(3):347–67. doi: 10.2217/fmb.12.4

94. Schirrmacher V. Immunobiology of Newcastle disease virus and its use for prophylactic vaccination in poultry and as adjuvant for therapeutic vaccination in cancer patients. *Int J Mol Sci* (2017) 18(5):1103. doi: 10.3390/ijms18051103

95. Malogolovkin A, Gasanov N, Egorov A, Weener M, Ivanov R, Karabelsky A. Combinatorial approaches for cancer treatment using oncolytic viruses: projecting the perspectives through clinical trials outcomes. *Viruses* (2021) 13(7):1271. doi: 10.3390/v13071271

96. Millward S, Graham AF. Structural studies on reovirus: discontinuities in the genome. *Proc Natl Acad Sci* (1970) 65(2):422–9. doi: 10.1073/pnas.65.2.422

97. Norman KL, Lee PW. Reovirus as a novel oncolytic agent. *J Clin Invest.* (2000) 105(8):1035–8. doi: 10.1172/JCI9871

98. Fernandes J. Oncogenes: The passport for viral oncolysis through PKR inhibition. *biomark Cancer* (2016) 8:BIC.S33378. doi: 10.4137/BIC.S33378

99. Strong JE, Coffey MC, Tang D, Sabinin P, Lee PW. The molecular basis of viral oncolysis: usurpation of the ras signaling pathway by reovirus. *EMBO J* (1998) 17(12):3351–62. doi: 10.1093/emboj/17.12.3351

100. Gollamudi R, Ghalib MH, Desai KK, Chaudhary I, Wong B, Einstein M, et al. Intravenous administration of reolysin, a live replication competent RNA virus is safe in patients with advanced solid tumors. *Invest New Drugs* (2010) 28 (5):641—649. doi: 10.1007/s10637-009-9279-8

101. Chakrabarty R, Tran H, Selvaggi G, Hagerman A, Thompson B, Coffey M. The oncolytic virus, pelareorep, as a novel anticancer agent: a review. *Invest New Drugs* (2015) 33(3):761–74. doi: 10.1007/s10637-015-0216-8

102. Horikami SM, Moyer SA. Structure, transcription, and replication of measles virus. *Curr Top Microbiol Immunol* (1995) 191:35–50. doi: 10.1007/978-3-642-78621-1_3

103. Bhattacharjee S, Yadava PK. Measles virus: Background and oncolytic virotherapy. *Biochem Biophys Rep* (2018) 13:58–62. doi: 10.1016/j.bbrep.2017.12.004

104. Leber MF, Neault S, Jirovec E, Barkley R, Said A, Bell JC, et al. Engineering and combining oncolytic measles virus for cancer therapy. *Cytokine Growth Factor Rev* (2020) 56:39–48. doi: 10.1016/j.cytogfr.2020.07.005

105. Mühlebach MD. Measles virus in cancer therapy. *Curr Opin Virol* (2020) 41:85–97. doi: 10.1016/j.coviro.2020.07.016

106. Heinzerling L, Künzi V, Oberholzer PA, Kündig T, Naim H, Dummer R. Oncolytic measles virus in cutaneous T-cell lymphomas mounts antitumor immune responses *in vivo* and targets interferon-resistant tumor cells. *Blood* (2005) 106(7):2287–94. doi: 10.1182/blood-2004-11-4558

107. Msaouel P, Dispenzieri A, Galanis E. Clinical testing of engineered oncolytic measles virus strains in the treatment of cancer: an overview. *Curr Opin Mol Ther* (2009) 11(1):43–53.

108. Fallaux FJ, Bout A, van der Velde I, van den Wollenberg DJ, Hehir KM, Keegan J, et al. New helper cells and matched early region 1-deleted adenovirus vectors prevent generation of replication-competent adenoviruses. *Hum Gene Ther* (1998) 9(13):1909–17. doi: 10.1089/hum.1998.9.13-1909

109. Walton RW, Brown MC, Sacco MT, Gromeier M. Engineered oncolytic poliovirus PVSRIPO subverts MDA5-dependent innate immune responses in cancer cells. *J Virol* (2018) 92(19):e00879–18. doi: 10.1128/JVI.00879-18

110. Desjardins A, Gromeier M, Herndon JE, Beaubier N, Bolognesi DP, Friedman AH, et al. Recurrent glioblastoma treated with recombinant poliovirus. *N Engl J Med* (2018) 379(2):150–61. doi: 10.1056/NEJMoa1716435

111. Aldrak N, Alsaab S, Algethami A, Bhere D, Wakimoto H, Shah K, et al. Oncolytic herpes simplex virus-based therapies for cancer. *Cells* (2021) 10(6):1541. doi: 10.3390/cells10061541

112. Farassati F, Yang AD, Lee PW. Oncogenes in ras signalling pathway dictate host-cell permissiveness to herpes simplex virus 1. *Nat Cell Biol* (2001) 3(8):745–50. doi: 10.1038/35087061

113. Abdoli S, Roohvand F, Teimoori-Toolabi L, Shokrgozar MA, Bahrololoumi M, Azadmanesh K. Construction of various γ34.5 deleted fluorescent-expressing oncolytic herpes simplex type 1 (oHSV) for generation and isolation of HSV-based vectors. *Iran BioMed J* (2017) 21(4):206–17. doi: 10.18869/acadpub.ibj.21.4.206

114. Jugovic P, Hill AM, Tomazin R, Ploegh H, Johnson DC. Inhibition of major histocompatibility complex class I antigen presentation in pig and primate cells by herpes simplex virus type 1 and 2 ICP47. *J Virol* (1998) 72(6):5076–84. doi: 10.1128/JVI.72.6.5076-5084.1998

115. Kanai R, Zaupa C, Sgubin D, Antoszczyk SJ, Martuza RL, Wakimoto H, et al. Effect of γ34.5 deletions on oncolytic herpes simplex virus activity in brain tumors. *J Virol* (2012) 86(8):4420–31. doi: 10.1128/JVI.00017-12

116. Puzanov I, Milhem MM, Minor D, Hamid O, Li A, Chen L, et al. Talimogene laherparepvec in combination with ipilimumab in previously untreated, unresectable stage IIIB-IV melanoma. *J Clin Oncol Off J Am Soc Clin Oncol* (2016) 34(22):2619–26. doi: 10.1200/JCO.2016.67.1529

117. Thomas S, Kuncheria L, Roulstone V, Kyula JN, Mansfield D, Bommareddy PK, et al. Development of a new fusion-enhanced oncolytic immunotherapy platform based on herpes simplex virus type 1. *J Immunother Cancer* (2019) 7(1):214. doi: 10.1186/s40425-019-0682-1

118. Macedo N, Miller DM, Haq R, Kaufman HL. Clinical landscape of oncolytic virus research in 2020. *Journal for immunotherapy of cancer* (2020) 8 (2):e001486. doi: 10.1136/jitc-2020-001486

119. Vellinga J, van der Heijdt S, Hoeben RC. The adenovirus capsid: major progress in minor proteins. *J Gen Virol* (2005) 86(Pt 6):1581–8. doi: 10.1099/vir.0.80877-0

120. Arnberg N. Adenovirus receptors: implications for targeting of viral vectors. *Trends Pharmacol Sci* (2012) 33(8):442–8. doi: 10.1016/j.tips.2012.04.005

121. Koski A, Kangasniemi L, Escutenaire S, Pesonen S, Cerullo V, Diaconu I, et al. Treatment of cancer patients with a serotype 5/3 chimeric oncolytic adenovirus expressing GMCSF. *Mol Ther* (2010) 18(10):1874–84. doi: 10.1038/mt.2010.161

122. Fueyo J, Alemany R, Gomez-Manzano C, Fuller GN, Khan A, Conrad CA, et al. Preclinical characterization of the antiglioma activity of a tropism-enhanced adenovirus targeted to the retinoblastoma pathway. *J Natl Cancer Inst* (2003) 95 (9):652–60. doi: 10.1093/jnci/95.9.652

123. Lang FF, Conrad C, Gomez-Manzano C, Yung WKA, Sawaya R, Weinberg JS, et al. Phase I study of DNX-2401 (Delta-24-RGD) oncolytic adenovirus: Replication and immunotherapeutic effects in recurrent malignant glioma. *J Clin Oncol Off J Am Soc Clin Oncol* (2018) 36(14):1419–27. doi: 10.1200/JCO.2017.75.8219

124. Xia Z-J, Chang J-H, Zhang L, Jiang W-Q, Guan Z-Z, Liu J-W, et al. Phase III randomized clinical trial of intratumoral injection of E1B gene-deleted adenovirus (H101) combined with cisplatin-based chemotherapy in treating squamous cell cancer of head and neck or esophagus. *Ai zheng= Aizheng= Chin J Cancer* (2004) 23(12):1666–70.

125. Liu T-C, Galanis E, Kirn D. Clinical trial results with oncolytic virotherapy: a century of promise, a decade of progress. *Nat Clin Pract Oncol* (2007) 4(2):101–17. doi: 10.1038/ncponc0736

126. Russell SJ, Peng K, Bell JC. Oncolytic virotherapy. *Nat Biotechnol* (2012) 30 (7):658–70. doi: 10.1038/nbt.2287

127. Kew Y, Levin VA. Advances in gene therapy and immunotherapy for brain tumors. *Curr Opin Neurol* (2003) 16(6):665–70. doi: 10.1097/00019052-200312000-00004

128. Martuza RL, Malick A, Markert JM, Ruffner KL, Coen DM. Experimental therapy of human glioma by means of a genetically engineered virus mutant. *Sci (80-).* (1991) 252(5007):854–6. doi: 10.1126/science.1851332

129. Stojdl DF, Lichty B, Knowles S, Marius R, Atkins H, Sonenberg N, et al. Exploiting tumor-specific defects in the interferon pathway with a previously unknown oncolytic virus. *Nat Med* (2000) 6(7):821–5. doi: 10.1038/77558

130. Van Erp EA, Kaliberova LN, Kaliberov SA, Curiel DT. Retargeted oncolytic adenovirus displaying a single variable domain of camelid heavy-chain-only antibody in a fiber protein. *Mol Ther* (2015) 2:15001. doi: 10.1038/mto.2015.1

131. Liu Y, Wang H, Yumul R, Gao W, Gambotto A, Morita T, et al. Transduction of liver metastases after intravenous injection of Ad5/35 or Ad35 vectors with and without factor X-binding protein pretreatment. *Hum Gene Ther* (2009) 20(6):621–9. doi: 10.1089/hum.2008.142

132. Wang H, Liu Y, Li Z, Tuve S, Stone D, Kalyushniy O, et al. *In vitro* and *in vivo* properties of adenovirus vectors with increased affinity to CD46. *J Virol* (2008) 82(21):10567–79. doi: 10.1128/JVI.01308-08

133. Nettelbeck DM, Rivera AA, Kupsch J, Dieckmann D, Douglas JT, Kontermann RE, et al. Retargeting of adenoviral infection to melanoma: combining genetic ablation of native tropism with a recombinant bispecific single-chain diabody (scDb) adapter that binds to fiber knob and HMWMAA. *Int J Cancer* (2004) 108(1):136–45. doi: 10.1002/ijc.11563

134. Montaño-Samaniego M, Bravo-Estupiñan DM, Méndez-Guerrero O, Alarcón-Hernández E, Ibáñez-Hernández M. Strategies for targeting gene therapy in cancer cells with tumor-specific promoters. *Front Oncol* (2020) 10:605380. doi: 10.3389/fonc.2020.605380

135. Barker SD, Dmitriev IP, Nettelbeck DM, Liu B, Rivera AA, Alvarez RD, et al. Combined transcriptional and transductional targeting improves the specificity and efficacy of adenoviral gene delivery to ovarian carcinoma. *Gene Ther* (2003) 10(14):1198–204. doi: 10.1038/sj.gt.3301974

136. Mazzacurati L, Marzulli M, Reinhart B, Miyagawa Y, Uchida H, Goins WF, et al. Use of miRNA response sequences to block off-target replication and increase the safety of an unattenuated, glioblastoma-targeted oncolytic HSV. *Mol Ther* (2015) 23(1):99–107. doi: 10.1038/mt.2014.177

137. Gaur A, Jewell DA, Liang Y, Ridzon D, Moore JH, Chen C, et al. Characterization of microRNA expression levels and their biological correlates in human cancer cell lines. *Cancer Res* (2007) 67(6):2456–68. doi: 10.1158/0008-5472.CAN-06-2698

138. Luo Q, Song H, Deng X, Li J, Jian W, Zhao J, et al. A triple-regulated oncolytic adenovirus carrying microRNA-143 exhibits potent antitumor efficacy in colorectal cancer. *Mol Ther* (2020) 16:219–29. doi: 10.1016/j.omto.2020.01.005

139. Ferguson MS, Lemoine NR, Wang Y. Systemic delivery of oncolytic viruses: hopes and hurdles. *Adv Virol* (2012) 2012:805629. doi: 10.1155/2012/805629

140. Lubinski JM, Lazear HM, Awasthi S, Wang F, Friedman HM. The herpes simplex virus 1 IgG fc receptor blocks antibody-mediated complement activation and antibody-dependent cellular cytotoxicity in vivo. *J Virol* (2011) 85(7):3239–49. doi: 10.1128/JVI.02509-10

141. Croyle MA, Le HT, Linse KD, Cerullo V, Toietta G, Beaudet A, et al. PEGylated helper-dependent adenoviral vectors: highly efficient vectors with an enhanced safety profile. *Gene Ther* (2005) 12(7):579–87. doi: 10.1038/sj.gt.3302441

142. Capasso C, Hirvinen M, Cerullo V. Beyond gene delivery: Strategies to engineer the surfaces of viral vectors. *Biomedicines* (2013) 1(1):3–16. doi: 10.3390/biomedicines1010003

143. Mader EK, Maeyama Y, Lin Y, Butler GW, Russell HM, Galanis E, et al. Mesenchymal stem cell carriers protect oncolytic measles viruses from antibody neutralization in an orthotopic ovarian cancer therapy model. *Clin Cancer Res* (2009) 15(23):7246–55. doi: 10.1158/1078-0432.CCR-09-1292

144. Thorne SH, Negrin RS, Contag CH. Synergistic antitumor effects of immune cell-viral biotherapy. *Sci (80-).* (2006) 311(5768):1780–4. doi: 10.1126/science.1121411

145. Ilett EJ, Bárcena M, Errington-Mais F, Griffin S, Harrington KJ, Pandha HS, et al. Internalization of oncolytic reovirus by human dendritic cell carriers protects the virus from neutralization. *Clin Cancer Res* (2011) 17(9):2767–76. doi: 10.1158/1078-0432.CCR-10-3266

146. Haisma HJ, Boesjes M, Beerens AM, van der Strate BWA, Curiel DT, Plddemann A, et al. *Scavenger receptor A: New route adenovirus 5. Mol Pharm* (2009) 6(2):366–74. doi: 10.1021/mp8000974

147. Roberts DM, Nanda A, Havenga MJE, Abbink P, Lynch DM, Ewald BA, et al. Hexon-chimaeric adenovirus serotype 5 vectors circumvent pre-existing anti-vector immunity. *Nature* (2006) 441(7090):239–43. doi: 10.1038/nature04721

148. Khare R, Reddy VS, Nemerow GR, Barry MA. Identification of adenovirus serotype 5 hexon regions that interact with scavenger receptors. *J Virol* (2012) 86 (4):2293–301. doi: 10.1128/JVI.05760-11

149. Prill J-M, Espenlaub S, Samen U, Engler T, Schmidt E, Vetrini F, et al. Modifications of adenovirus hexon allow for either hepatocyte detargeting or targeting with potential evasion from kupffer cells. *Mol Ther* (2011) 19(1):83–92. doi: 10.1038/mt.2010.229

150. Zhang Z, Krimmel J, Zhang Z, Hu Z, Seth P. Systemic delivery of a novel liver-detargeted oncolytic adenovirus causes reduced liver toxicity but maintains the antitumor response in a breast cancer bone metastasis model. *Hum Gene Ther* (2011) 22(9):1137–42. doi: 10.1089/hum.2011.003

151. Parker AL, Waddington SN, Nicol CG, Shayakhmetov DM, Buckley SM, Denby L, et al. Multiple vitamin K-dependent coagulation zymogens promote adenovirus-mediated gene delivery to hepatocytes. *Blood* (2006) 108(8):2554–61. doi: 10.1182/blood-2006-04-008532

152. Atoda H, Ishikawa M, Mizuno H, Morita T. Coagulation factor X-binding protein from deinagkistrodon acutus venom is a gla domain-binding protein. *Biochemistry* (1998) 37(50):17361–70. doi: 10.1021/bi981177x

153. Kwon O-J, Kang E, Choi J-W, Kim SW, Yun C-O. Therapeutic targeting of chitosan–PEG–folate-complexed oncolytic adenovirus for active and systemic cancer gene therapy. *J Control Release* (2013) 169(3):257–65. doi: 10.1016/j.jconrel.2013.03.030

154. Minchinton AI, Tannock IF. Drug penetration in solid tumours. *Nat Rev Cancer* (2006) 6(8):583–92. doi: 10.1038/nrc1893

155. Hill C, Carlisle R. Achieving systemic delivery of oncolytic viruses. *Expert Opin Drug Deliv.* (2019) 16(6):607–20. doi: 10.1080/17425247.2019.1617269

156. Diop-Frimpong B, Chauhan VP, Krane S, Boucher Y, Jain RK. Losartan inhibits collagen I synthesis and improves the distribution and efficacy of nanotherapeutics in tumors. *Proc Natl Acad Sci* (2011) 108(7):2909–14. doi: 10.1073/pnas.1018892108

157. Guedan S, Rojas JJ, Gros A, Mercade E, Cascallo M, Alemany R. Hyaluronidase expression by an oncolytic adenovirus enhances its intratumoral spread and suppresses tumor growth. *Mol Ther* (2010) 18(7):1275–83. doi: 10.1038/mt.2010.79

158. Mok W, Boucher Y, Jain RK. Matrix metalloproteinases-1 and-8 improve the distribution and efficacy of an oncolytic virus. *Cancer Res* (2007) 67(22):10664–8. doi: 10.1158/0008-5472.CAN-07-3107

159. Kontermann RE, Ungerechts G, Nettelbeck DM. Viro-antibody therapy: engineering oncolytic viruses for genetic delivery of diverse antibody-based biotherapeutics. *MAbs* (2021) 13(1):1982447. doi: 10.1080/19420862.2021.1982447

160. Dias JD, Hemminki O, Diaconu I, Hirvinen M, Bonetti A, Guse K, et al. Targeted cancer immunotherapy with oncolytic adenovirus coding for a fully human monoclonal antibody specific for CTLA-4. *Gene Ther* (2012) 19(10):988–98. doi: 10.1038/gt.2011.176

161. Hamilton JR, Vijayakumar G, Palese P. A recombinant antibody-expressing influenza virus delays tumor growth in a mouse model. *Cell Rep* (2018) 22(1):1–7. doi: 10.1016/j.celrep.2017.12.025

162. Vijayakumar G, Palese P, Goff PH. Oncolytic Newcastle disease virus expressing a checkpoint inhibitor as a radioenhancing agent for murine melanoma. *EBioMedicine* (2019) 49:96–105. doi: 10.1016/j.ebiom.2019.10.032

163. Vijayakumar G, McCroskery S, Palese P. Engineering Newcastle disease virus as an oncolytic vector for intratumoral delivery of immune checkpoint inhibitors and immunocytokines. *J Virol* (2020) 94(3):e01677–19. doi: 10.1128/JVI.01677-19

164. Engeland CE, Grossardt C, Veinalde R, Bossow S, Lutz D, Kaufmann JK, et al. CTLA-4 and PD-L1 checkpoint blockade enhances oncolytic measles virus therapy. *Mol Ther* (2014) 22(11):1949–59. doi: 10.1038/mt.2014.160

165. Wu C, Wu M, Liang M, Xiong S, Dong C. A novel oncolytic virus engineered with PD-L1 scFv effectively inhibits tumor growth in a mouse model. *Cell Mol Immunol* (2019) 16(9):780–2. doi: 10.1038/s41423-019-0264-7

166. Kleinpeter P, Fend L, Thioudellet C, Geist M, Sfrontato N, Koerper V, et al. Vectorization in an oncolytic vaccinia virus of an antibody, a fab and a scFv against programmed cell death -1 (PD-1) allows their intratumoral delivery and an improved tumor-growth inhibition. *Oncoimmunology* (2016) 5(10):e1220467. doi: 10.1080/2162402X.2016.1220467

167. Liikanen I, Tähtinen S, Guse K, Gutmann T, Savola P, Oksanen M, et al. Oncolytic adenovirus expressing monoclonal antibody trastuzumab for treatment of HER2-positive cancer. *Mol Cancer Ther* (2016) 15(9):2259–69. doi: 10.1158/1535-7163.MCT-15-0819

168. Wei D, Li Q, Wang X-L, Wang Y, Xu J, Feng F, et al. Oncolytic Newcastle disease virus expressing chimeric antibody enhanced anti-tumor efficacy in orthotopic hepatoma-bearing mice. *J Exp Clin Cancer Res* (2015) 34:153. doi: 10.1186/s13046-015-0271-1

169. Huang T, Wang H, Chen NG, Frentzen A, Minev B, Szalay AA. Expression of anti-VEGF antibody together with anti-EGFR or anti-FAP enhances tumor regression as a result of vaccinia virotherapy. *Mol Ther Oncolytics* (2015) 2:15003. doi: 10.1038/mto.2015.3

170. Khalique H, Baugh R, Dyer A, Scott EM, Frost S, Larkin S, et al. Oncolytic herpesvirus expressing PD-L1 BiTE for cancer therapy: exploiting tumor immune suppression as an opportunity for targeted immunotherapy. *J Immunother Cancer* (2021) 9(4):e001292. doi: 10.1136/jitc-2020-001292

171. Scott EM, Jacobus EJ, Lyons B, Frost S, Freedman JD, Dyer A, et al. Bi- and tri-valent T cell engagers deplete tumour-associated macrophages in cancer patient samples. *J Immunother Cancer* (2019) 7(1):1–18. doi: 10.1186/s40425-019-0807-6

172. Schönung M, Meyer J, Nöllke P, Olshen AB, Hartmann M, Murakami N, et al. International consensus definition of DNA methylation subgroups in juvenile myelomonocytic LeukemiaDNA methylation subgroups in JMML. *Clin Cancer Res* (2021) 27(1):158–68. doi: 10.1158/1078-0432.CCR-20-3184

173. Yu F, Hong B, Song X-T. A T-cell engager-armed oncolytic vaccinia virus to target the tumor stroma. *Cancer Transl Med* (2017) 3(4):122. doi: 10.4103/ctm.ctm_13_17

174. Ma R, Lu T, Li Z, Teng K-Y, Mansour AG, Yu M, et al. An oncolytic virus expressing IL15/IL15Rα combined with off-the-Shelf EGFR-CAR NK cells targets glioblastoma. *Cancer Res* (2021) 81(13):3635–48. doi: 10.1158/0008-5472.CAN-21-0035

175. Lu RM, Hwang YC, Liu IJ, Lee CC, Tsai HZ, Li HJ, et al. Development of therapeutic antibodies for the treatment of diseases. *J BioMed Sci* (2020) 27(1):1–30. doi: 10.1186/s12929-019-0592-z

176. Goulet DR, Atkins WM. Considerations for the design of antibody-based therapeutics. *J Pharm Sci* (2020) 109(1):74–103. doi: 10.1016/j.xphs.2019.05.031

177. Briolay T, Petithomme T, Fouet M, Nguyen-Pham N, Blanquart C, Boisgerault N. Delivery of cancer therapies by synthetic and bio-inspired nanovectors. *Mol Cancer* (2021) 20(1):1–24. doi: 10.1186/s12943-021-01346-2

178. Russell L, Peng KW, Russell SJ, Diaz RM. Oncolytic viruses: Priming time for cancer immunotherapy. *BioDrugs* (2019) 33(5):485–501. doi: 10.1007/s40259-019-00367-0

179. Sivanandam V, LaRocca CJ, Chen NG, Fong Y, Warner SG. Oncolytic viruses and immune checkpoint inhibition: The best of both worlds. *Mol Ther - Oncolytics* (2019) 13:93–106. doi: 10.1016/j.omto.2019.04.003

180. Chiu M, Armstrong EJL, Jennings V, Foo S, Crespo-Rodriguez E, Bozhanova G, et al. Combination therapy with oncolytic viruses and immune checkpoint inhibitors. *Expert Opin Biol Ther* (2020) 20(6):635–52. doi: 10.1080/14712598.2020.1729351

181. Senior M. Checkpoint inhibitors go viral. *Nat Biotechnol* (2019) 37(1):12–7. doi: 10.1038/nbt.4327

182. Zamarin D, Holmgaard RB, Subudhi SK, Park JS, Mansour M, Palese P, et al. Localized oncolytic virotherapy overcomes systemic tumor resistance to immune checkpoint blockade immunotherapy. *Sci Transl Med* (2014) 6 (226):226ra32. doi: 10.1126/scitranslmed.3008095

183. Saha D, Martuza RL, Rabkin SD. Oncolytic herpes simplex virus immunovirotherapy in combination with immune checkpoint blockade to treat glioblastoma. *Immunotherapy* (2018) 10(9):779–86. doi: 10.2217/imt-2018-0009

184. Saha D, Martuza RL, Rabkin SD. Curing glioblastoma : Oncolytic HSV-IL12 and checkpoint blockade. *Oncoscience* (2017) 4(July):67–9. doi: 10.18632/oncoscience.359

185. Harrington K, Freeman DJ, Kelly B, Harper J, Soria JC. Optimizing oncolytic virotherapy in cancer treatment. *Nat Rev Drug Discovery* (2019) 18 (9):689–706. doi: 10.1038/s41573-019-0029-0

186. Nettelbeck DM, Leber MF, Altomonte J, Angelova A, Beil J, Berchtold S, et al. Virotherapy in germany–recent activities in virus engineering, preclinical development, and clinical studies. *Viruses* (2021) 13(8):1–29. doi: 10.3390/v13081420

187. Wu Z, Ichinose T, Naoe Y, Matsumura S, Villalobos IB, Eissa IR, et al. Combination of cetuximab and oncolytic virus canerpaturev synergistically inhibits human colorectal cancer growth. *Mol Ther - Oncolytics* (2019) 13(June):107–15. doi: 10.1016/j.omto.2019.04.004

188. Zhang W, Fulci G, Buhrman JS, Stemmer-Rachamimov AO, Chen JW, Wojtkiewicz GR, et al. Bevacizumab with angiostatin-armed oHSV increases antiangiogenesis and decreases bevacizumab-induced invasion in U87 glioma. *Mol Ther* (2012) 20(1):37–45. doi: 10.1038/mt.2011.187

189. Yang EY, Shah K. Nanobodies: Next generation of cancer diagnostics and therapeutics. *Front Oncol* (2020) 10(July). doi: 10.3389/fonc.2020.01182

190. Rahbarizadeh F, Ahmadvand D, Sharifzadeh Z. Nanobody; an old concept and new vehicle for immunotargeting. *Immunol Invest.* (2011) 40(3):299–338. doi: 10.3109/08820139.2010.542228

191. Najmeddin A, Bahrololoumi M, Behdani M, Dorkoosh F. Nanobodies as powerful pulmonary targeted biotherapeutics against SARS-CoV-2, pharmaceutical point of view. *BBA-General Subj.* (2021) 1865(11):129974. doi: 10.1016/j.bbagen.2021.129974

192. Gil JS, Dubois M, Neirinckx V, Lombard A, Coppieters N, D'Arrigo P, et al. Nanobody-based retargeting of an oncolytic herpesvirus for eliminating CXCR4+ GBM cells: a proof-of-principle. *Mol Ther - Oncolytics* (2022) 26:35-48. doi: 10.1016/j.omto.2022.06.002

193. Xu B, Tian L, Chen J, Wang J, Ma R, Dong W, et al. An oncolytic virus expressing a full-length antibody enhances antitumor innate immune response to glioblastoma. *Nat Commun* (2021) 12(1):1–7. doi: 10.1038/s41467-021-26003-6

194. Zhang B, Shu Y, Hu S, Qi Z, Chen Y, Innovation C. *An oncolytic adenovirus armed with a nanobody against CD47 reprograms tumor immune microenvironment and drives durabl antitumor immunity*. Available at SSRN 3914649.

195. Labrijn AF, Janmaat ML, Reichert JM, Parren PWHI. Bispecific antibodies: a mechanistic review of the pipeline. *Nat Rev Drug Discovery* (2019) 18(8):585–608. doi: 10.1038/s41573-019-0028-1

196. Heidbuechel JPW, Engeland CE. Oncolytic viruses encoding bispecific T cell engagers: a blueprint for emerging immunovirotherapies. *J Hematol Oncol* (2021) 14(1):1–24. doi: 10.1186/s13045-021-01075-5

197. Haas C, Lulei M, Fournier P, Arnold A, Schirrmacher V. A tumor vaccine containing anti-CD3 and anti-CD28 bispecific antibodies triggers strong and

durable antitumor activity in human lymphocytes. *Int J Cancer* (2006) 118(3):658–67. doi: 10.1002/ijc.21390

198. Freedman JD, Hagel J, Scott EM, Psallidas I, Gupta A, Spiers L, et al. Oncolytic adenovirus expressing bispecific antibody targets T-cell cytotoxicity in cancer biopsies. *EMBO Mol Med* (2017) 9(8):1067–87. doi: 10.15252/emmm.201707567

199. Schirrmacher V. Oncolytic Newcastle disease virus as a prospective anti-cancer therapy. a biologic agent with potential to break therapy resistance. *Expert Opin Biol Ther* (2015) 15(12):1757–71. doi: 10.1517/14712598.2015.1088000

200. Schirrmacher V, van Gool S, Stuecker W. Breaking therapy resistance: An update on oncolytic Newcastle disease virus for improvements of cancer therapy. *Biomedicines* (2019) 7(3):66. doi: 10.3390/biomedicines7030066

201. Bahrololoumi M, Momburg F, Roohvand F, Jarahian M. International immunopharmacology bi / tri-specific antibodies (HN-Fc-CD16 and HN-Fc-IL-15-CD16) cross-linking natural killer (NK) -CD16 and Newcastle disease virus (NDV) -HN , enhanced NK activation for cancer immunotherapy. *Int Immunopharmacol* (2021) 96:107762. doi: 10.1016/j.intimp.2021.107762

202. Bahrololoumi Shapourabadi M, Roohvand F, Arashkia A, Mohajel N, Abdoli S, Shahosseini Z, et al. Expression and purification of a bispecific antibody against CD16 and hemagglutinin neuraminidase (HN) in e. coli for cancer immunotherapy. *Rep Biochem Mol Biol* (2020) 9(1):50–7. doi: 10.29252/rbmb.9.1.50

203. Schirrmacher V, Haas C, Bonifer R, Ahlert T, Gerhards R, Ertel C. Human tumor cell modification by virus infection: An efficient and safe way to produce cancer vaccine with pleiotropic immune stimulatory properties when using Newcastle disease virus. *Gene Ther* (1999) 6(1):63–73. doi: 10.1038/sj.gt.3300787

204. Schirrmacher V, Fournier P. Newcastle Disease virus: A promising vector for viral therapy, immune therapy, and gene therapy of cancer. *Gene Therapy of Cancer* (2009) 2009:565–605.

205. Garfall AL, June CH. Three is a charm for an antibody to fight cancer microbial clues to a liver disease. *Nature* (2019) 575:450–1. doi: 10.1038/d41586-019-03495-3

206. Aigner M, Janke M, Lulei M, Beckhove P, Fournier P, Schirrmacher V. An effective tumor vaccine optimized for costimulation *via* bispecific and trispecific fusion proteins. *Int J Oncol* (2008) 32(4):777–89. doi: 10.3892/ijo.32.4.777

207. Fournier P, Schirrmacher V. Bispecific antibodies and trispecific immunocytokines for targeting the immune system against cancer: Preparing for the future. *BioDrugs* (2013) 27(1):35–53. doi: 10.1007/s40259-012-0008-z

208. Ravirala D, Mistretta B, Gunaratne PH, Pei G, Zhao Z, Zhang X. Co-Delivery of novel bispecific and trispecific engagers by an amplicon vector augments the therapeutic effect of an HSV-based oncolytic virotherapy. *J Immunother Cancer* (2021) 9(7):1–14. doi: 10.1136/jitc-2021-002454

209. Guo ZS, Lotze MT, Zhu Z, Storkus WJ, Song XT. Bi- and tri-specific T cell engager-armed oncolytic viruses: Next-generation cancer immunotherapy. *Biomedicines* (2020) 8(8):1–16. doi: 10.3390/biomedicines8070204

210. Miliotou AN, Papadopoulou LC. CAR T-cell therapy: A new era in cancer immunotherapy. *Curr Pharm Biotechnol* (2018) 19(1):5–18. doi: 10.2174/1389201019666180418095526

211. Sterner RC, Sterner RM. CAR-T cell therapy : current limitations and potential strategies. *Blood Cancer J* (2021) 11(4):69. doi: 10.1038/s41408-021-00459-7

212. Safarzadeh Kozani P, Naseri A, Mirarefin SMJ, Salem F, Nikbakht M, Evazi Bakhshi S, et al. Nanobody-based CAR-T cells for cancer immunotherapy. *biomark Res* (2022) 10(1):1–18. doi: 10.1186/s40364-022-00371-7

213. Gamboa L, Zamat AH, Vanover D, Thiveaud CA, Peck HE, Phuengkham H, et al. Sensitizing solid tumors to CAR-mediated cytotoxicity using synthetic antigens. *bioRxiv* (2021). doi: 10.1101/2021.12.11.472238

214. Hajari Taheri F, Hassani M, Sharifzadeh Z, Behdani M, Arashkia A, Abolhassani M. T Cell engineered with a novel nanobody-based chimeric antigen receptor against VEGFR2 as a candidate for tumor immunotherapy. *IUBMB Life* (2019) 71(9):1259–67. doi: 10.1002/iub.2019

215. Jamnani FR, Rahbarizadeh F, Shokrgozar MA, Ahmadvand D, Mahboudi F, Sharifzadeh Z. Targeting high affinity and epitope-distinct oligoclonal nanobodies to HER2 over-expressing tumor cells. *Exp Cell Res* (2012) 318 (10):1112–24. doi: 10.1016/j.yexcr.2012.03.004

216. Sharifzadeh Z, Rahbarizadeh F, Shokrgozar MA, Ahmadvand D, Mahboudi F, Jamnani FR, et al. Genetically engineered T cells bearing chimeric nanoconstructed receptors harboring TAG-72-specific camelid single domain antibodies as targeting agents. *Cancer Lett* (2013) 334(2):237–44. doi: 10.1016/j.canlet.2012.08.010

217. Hassani M, Hajari Taheri F, Sharifzadeh Z, Arashkia A, Hadjati J, van Weerden WM, et al. Construction of a chimeric antigen receptor bearing a nanobody against prostate a specific membrane antigen in prostate cancer. *J Cell Biochem* (2019) 120(6):10787–95. doi: 10.1002/jcb.28370

218. Evazalipour M, D'Huyvetter M, Tehrani BS, Abolhassani M, Omidfar K, Abdoli S, et al. Generation and characterization of nanobodies targeting PSMA for molecular imaging of prostate cancer. *Contrast Media Mol Imaging.* (2014) 9 (3):211–20. doi: 10.1002/cmmi.1558

219. Hassani M, Hajari Taheri F, Sharifzadeh Z, Arashkia A, Hadjati J, van Weerden WM, et al. Engineered jurkat cells for targeting prostate-specific membrane antigen on prostate cancer cells by nanobody-based chimeric antigen receptor. *Iran BioMed J* (2020) 24(2):81–8. doi: 10.29252/ibj.24.2.81

220. Bao C, Gao Q, Li LL, Han L, Zhang B, Ding Y, et al. The application of nanobody in CAR-T therapy. *Biomolecules* (2021) 11(2):1–18. doi: 10.3390/biom11020238

221. Nishio N, Diaconu I, Liu H, Cerullo V, Caruana I, Hoyos V, et al. Armed oncolytic virus enhances immune functions of chimeric antigen receptor-modified T cells in solid tumors. *Cancer Res* (2014) 74(18):5195–205. doi: 10.1158/0008-5472.CAN-14-0697

222. Rezaei R, Esmaeili H, Ghaleh G, Farzanehpour M, Dorostkar R, Ranjbar R, et al. Combination therapy with CAR T cells and oncolytic viruses : a new era in cancer immunotherapy. *Cancer Gene Ther* (2021) 1:1–14. doi: 10.1038/s41417-021-00359-9

223. Guedan S, Alemany R. CAR-T cells and oncolytic viruses: Joining forces to overcome the solid tumor challenge. *Front Immunol* (2018) 9. doi: 10.3389/fimmu.2018.02460

224. Chen X, Han J, Chu J, Zhang L, Zhang J, Chen C, et al. A combinational therapy of EGFR-CAR NK cells and oncolytic herpes simplex virus 1 for breast cancer brain metastases. *Oncotarget* (2016) 7(19):27764–77. doi: 10.18632/oncotarget.8526

225. Schirrmacher V, Stücker W, Lulei M, Bihari A-S, Sprenger T. Long-term survival of a breast cancer patient with extensive liver metastases upon immune and virotherapy: A case report. *Immunotherapy* (2015) 7(8):855–60. doi: 10.2217/imt.15.48

226. Schirrmacher V, Fournier P. Multimodal cancer therapy involving oncolytic Newcastle disease virus, autologous immune cells and bispecific antibodies. *Front Oncol* (2014) 4:1–5. doi: 10.3389/fonc.2014.00224

227. Sato E, Olson SH, Ahn J, Bundy B, Nishikawa H, Qian F, et al. Intraepithelial CD8+ tumor-infiltrating lymphocytes and a high CD8+/regulatory T cell ratio are associated with favorable prognosis in ovarian cancer. *Proc Natl Acad Sci USA* (2005) 102(51):18538–43. doi: 10.1073/pnas.0509182102

228. Feist M, Zhu Z, Dai E, Ma C, Liu Z, Giehl E, et al. Oncolytic virus promotes tumor-reactive infiltrating lymphocytes for adoptive cell therapy. *Cancer Gene Ther* (2021) 28(1–2):98–111. doi: 10.1038/s41417-020-0189-4

229. Morales-Molina A, Rodríguez-Milla MÁ, Gimenez-Sanchez A, Perisé-Barrios AJ, García-Castro J. Cellular virotherapy increases tumor-infiltrating lymphocytes (Til) and decreases their pd-1+ subsets in mouse immunocompetent models. *Cancers (Basel).* (2020) 12(7):1–17. doi: 10.3390/cancers12071920

230. Ye K, Li F, Wang R, Cen T, Liu S, Zhao Z, et al. An armed oncolytic virus enhances the efficacy of tumor-infiltrating lymphocyte therapy by converting tumors to artificial antigen presenting cells in situ. *Mol Ther* (2022) 30(12):1–19. doi: 10.1016/j.ymthe.2022.06.010

frontiers | Frontiers in Immunology

TYPE Original Research
PUBLISHED 19 October 2022
DOI 10.3389/fimmu.2022.1012534

OPEN ACCESS

EDITED BY
Zahra Sharifzadeh,
Pasteur Institute of Iran, Iran

REVIEWED BY
Xiongwen Lv,
Anhui Medical University, China
Michael Sitkovsky,
Northeastern University, United States

*CORRESPONDENCE
Sahil Adriouch
sahil.adriouch@univ-rouen.fr

SPECIALTY SECTION
This article was submitted to Cancer Immunity and Immunotherapy, a section of the journal Frontiers in Immunology

RECEIVED 05 August 2022
ACCEPTED 03 October 2022
PUBLISHED 19 October 2022

CITATION
Demeules M, Scarpitta A, Hardet R, Gondé H, Abad C, Blandin M, Menzel S, Duan Y, Rissiek B, Magnus T, Mann AM, Koch-Nolte F and Adriouch S (2022) Evaluation of nanobody-based biologics targeting purinergic checkpoints in tumor models *in vivo*. *Front. Immunol.* 13:1012534. doi: 10.3389/fimmu.2022.1012534

Evaluation of nanobody-based biologics targeting purinergic checkpoints in tumor models *in vivo*

Mélanie Demeules[1], Allan Scarpitta[1], Romain Hardet[1], Henri Gondé[1], Catalina Abad[1], Marine Blandin[1], Stephan Menzel[2,3,4], Yinghui Duan[5], Björn Rissiek[5], Tim Magnus[5], Anna Marei Mann[2], Friedrich Koch-Nolte[2] and Sahil Adriouch[1*]

[1]University of Rouen, INSERM, U1234, Pathophysiology Autoimmunity and Immunotherapy (PANTHER), Normandie Univ, Rouen, France, [2]Institute of Immunology, University Medical Center Hamburg-Eppendorf, Hamburg, Germany, [3]Core Facility Nanobodies, University of Bonn, Bonn, Germany, [4]Mildred Scheel Cancer Career Center HaTriCS4, University Medical Center Hamburg-Eppendorf, Hamburg, Germany, [5]Department of Neurology, University Medical Center Hamburg-Eppendorf, Hamburg, Germany

Adenosine triphosphate (ATP) represents a danger signal that accumulates in injured tissues, in inflammatory sites, and in the tumor microenvironment. ATP promotes tumor growth but also anti-tumor immune responses notably *via* the P2X7 receptor. ATP can also be catabolized by CD39 and CD73 ecto-enzymes into immunosuppressive adenosine. P2X7, CD39 and CD73 have attracted much interest in cancer as targets offering the potential to unleash anti-tumor immune responses. These membrane proteins represent novel purinergic checkpoints that can be targeted by small drugs or biologics. Here, we investigated nanobody-based biologics targeting mainly P2X7, but also CD73, alone or in combination therapies. Blocking P2X7 inhibited tumor growth and improved survival of mice in cancer models that express P2X7. P2X7-potentiation by a nanobody-based biologic was not effective alone to control tumor growth but enhanced tumor control and immune responses when used in combination with oxaliplatin chemotherapy. We also evaluated a bi-specific nanobody-based biologic that targets PD-L1 and CD73. This novel nanobody-based biologic exerted a potent anti-tumor effect, promoting tumor rejection and improving survival of mice in two tumor models. Hence, this study highlights the importance of purinergic checkpoints in tumor control and open new avenues for nanobody-based biologics that may be further exploited in the treatment of cancer.

KEYWORDS

P2X7, purinergic signaling, tumor microenvironment (TME), anti-tumor immune responses, nanobody, nanobody-based biologics, AAV vectors

10.3389/fimmu.2022.1012534

Introduction

Adenosine triphosphate (ATP) release into the extracellular space (eATP) represents a well-known danger signal acting through two main families of plasma membrane receptors: G protein-coupled receptors, named P2Y receptors, and ATP-gated ion channels, termed P2X receptors (1). Among the latter family, P2X7 forms a homotrimeric receptor that has attracted much interest in the fields of inflammation and cancer. P2X7, a non-selective ligand-gated cation channel, is expressed at the cell surface of various leukocytes, in particular monocytes, macrophages and regulatory T cells (2–5). P2X7 is known to be central in inflammation for its ability to activate the NLRP3 inflammasome and trigger IL-1β and IL-18 release (3, 6–9). Prolonged activation of P2X7 leads to the opening of a membrane pore allowing the entry of large molecules of up to 900 Da. Whether this membrane permeabilization is due to dilatation of the P2X7 channel itself or to the activation of non-selective pores like pannexin-1, gasdermin D or anoctamin 6, may depend on the cellular context, the lipid composition of the membrane, and on the level of expression of these proteins (10–12). Whatever the exact molecular mechanism that leads to pore formation, P2X7 can induce a major perturbation of intracellular ion balance and thereby modify cellular activities, cellular function, and cell fate. In the context of cancer, P2X7 has been assigned various and contrasting roles as a driver of cancer cell growth (13) and metastatic dissemination, or as a promoter of immune mediated tumor eradication (14, 15). High concentrations of eATP, released in the vicinity of stressed or damaged cells during inflammation, but also within the tumor site, represent a "danger signal" than can influence the activity and function of immune cells. P2X7 is also found at the surface of numerous tumor cell types an as been proposed to confer a selective advantage to tumor cells through their tonic stimulation, leading to higher concentration of mitochondrial calcium, fueling growth and invasiveness (16, 17). eATP plays a complex role within the tumor microenvironment (TME) depending on multiple factors such as its concentration, the abundance of ecto-ATPases, the expression level of P2X7, and the nature of the P2X7 variant expressed by immune and tumor cells (18, 19).

On T lymphocytes, P2X7 induces the shedding of CD62L and CD27 by metalloproteases (5, 20–23), and controls the differentiation, proliferation and survival of T cells and of tissue resident memory T cells (24, 25). Also, FoxP3$^+$ regulatory T cells (Tregs) are known to express P2X7 at high levels, and its activation controls their phenotype, their suppressive functions, as well as their survival (4, 5). Taken together, activation of P2X7 on myeloid and lymphoid cells converge to promote and amplify inflammation as well as the emergence of an adaptive T cell response (3, 6, 26).

In the TME, P2X7 blockade induces modification in the expression of ecto-enzymes involved in the control of the purinergic signaling cascade, including modifications in the expression of the 5'-ecto-nucleotidase CD73 that control accumulation of immunosuppressive adenosine (27). This strongly suggests that P2X7 expression and function may control the entire eATP/adenosine balance in the TME and may exert a broad impact on tumor proliferation and dissemination. Yet, other studies also suggested a key role of P2X7 in anti-tumor immunity and have linked the release of its ligand, ATP, to the occurrence of immunogenic cell death and to stimulation of anti-tumor immune responses (28, 29). Hence, P2X7 either on its own or together with other key players of the purinergic signaling cascade such as CD39 and CD73, play an important role in tumor immunogenicity at least during the early phase of cancer development (29–31). Antagonistic antibodies targeting CD39 that are in clinical development exert their therapeutic effect partly in relation with P2X7 (32, 33). CD73-blocking antibodies, which also hold promise in clinics, were shown to improve anti-tumor immune responses and to prevent metastasis when used alone or in combination with other therapeutic strategies (34, 35). Indeed, CD73 blockade may decrease accumulation of adenosine, a potent anti-inflammatory molecule that inhibit anti-tumor immune responses and favor tumor growth (36–38). This protumoral effect of adenosine rely on different mechanisms, such as the expression of the inhibitory A2a adenosine receptors by T cells limiting their activation and expansion in the adenosine riche TME (36, 37). These discoveries has led to preclinical and clinical validations that have better delineate the factors that contribute to improve anti-tumor immune responses in therapeutic strategies aiming to inhibit adenosine signaling in the tumor context (39–42).

Taking together, this suggest that targeting P2X7 and/or multiple key purinergic players in the TME, may be beneficial for the treatment of tumors. Here we used an AAVnano methodological approach that we previously described (43, 44) to evaluate the anti-tumor effects of P2X7 blocking, or conversely P2X7 potentiation, in different tumor models *in vivo*. Further, we developed novel nanobody-based biologics targeting other key immune and/or purinergic checkpoints of the TME and evaluated their efficacy either alone, or in combination with a P2X7-potentiating nanobody-based biologic. Interestingly, we demonstrated that a bi-specific construct targeting PD-L1 and CD73 exerts a potent anti-tumor effect, promoting tumor rejection and improving mice survival in two tumor models. Hence, this study highlight the importance of the purinergic signaling in the tumor context and suggests that key purinergic players represent attractive novel anti-tumor checkpoints that may be further exploited in future treatments.

Material and methods

Mice, reagents, antibodies

C57BL/6JRj wild-type mice obtained from Janvier Labs were used for all experiments. Mice were housed in a specific pathogen-free facility and were aged of 8 weeks at the beginning of experiments. All animal experimental protocols were approved by the French Ministry of Education and Research, after consultation of the ethical committee (n° APAFIS#27682). Adenosine 5'-tri-phosphate disodium salt was purchased from Sigma Aldrich (A2383). Red blood cell (RBC) lysis/fixation Solution, True-Nuclear Transcription factor buffer set, and antibodies to CD45 (clone 30-F11), CD4 (RM'-5), CD8 (53-6.7), CD25 (PC-61), CD19 (1D3/CD19), FoxP3 (MF-14), CD27 (LG.3A10), CD62L (MEL-14), P2X7R (1F11), CD39 (Duha59), CD73 (CXCR3-176), TIGIT (1G9), TIM3 (RMT3-23), CD49b (DX5), NK1.1 (PK136), CX3CR1 (SAO11F11), PD-1 (29F1A12), CD11c (N418), CD11b (M1170), CD44 (IM7), XCR1 (ZET), P2X7 (1F11) and purified CD16/D32 (TruStain FcX) were obtained from Biolegend or Sony Biotechnology.

Cell cultures

Mouse B16F10 melanoma (ATCC CRL-6375), mouse Lewis Lung Carcinoma (LLC, ATCC CRL-1642) and mouse thymoma (EG7, ATCC CRL-2113) cell lines were maintained in culture using standard procedures and were regularly tested for the absence of mycoplasma contamination. B16F10 and LLC were grown in DMEM glutamax medium, FBS 10%, penicillin (100 U/ml) streptomycin (100 mg/ml) and pyruvate 1 mM, (all purchased from ThermoFisher Scientific, Gibco). EG7 were grown in RPMI medium, FBS 10%, penicillin (100 U/ml) streptomycin (100 mg/ml) and pyruvate 1 mM, (all purchased from ThermoFisher Scientific, Gibco).

Flow cytometry analyses

For evaluation of P2X7 expression tumor cells were collected, and single-cell suspensions were prepared and washed using standard procedures. Cells were stained with fluorochrome-conjugated anti-P2X7 (clone 1F11) or related isotype controls.

For evaluation of P2X7-dependent shedding of CD27 and CD62L upon ex vivo exposure to ATP, blood samples were collected, washed, resuspended into PBS (without Ca^{2+} and Mg^{2+}) and divided into 3 tubes. Cells were then treated with 30 µM ATP, 150 µM ATP or left untreated. After incubation for 15 min at 37°C, cells were washed in cold D-PBS containing 10% FBS and stained on ice with fluorochrome-conjugated antibodies before one-step fixation and RBC lysis (using RBC Lysis/Fixation Solution, Sony Biotechnology). The percentages of cells co-expressing CD27 and CD62L were then evaluated by flow cytometry.

For the evaluation of the cells infiltrating the tumor, the B16F10 tumor was excised, and the cell suspension was filtered through a 100 µM nylon filter (cell strainer, BD Biosciences). Single cell suspensions were prepared and washed using standard procedures. Cells were stained with fluorochrome-conjugated antibodies before one-step fixation and RBC lysis. Cells were then analyzed by flow cytometry.

Flow cytometry data acquisitions were performed using an LSRFortessa or a FACSCanto-I (BD Biosciences) apparatus and subsequent analyses were performed using FlowJo software (v10.8.1,Tree Star, Ashland, OR).

Nanobody-based biologics, production of AAV vectors, and muscle transduction

All nanobody-based biologics were based on nanobodies generated and selected as described before (9, 45). The construct 14D5-dimHLE used to potentiate P2X7 function was based on a nanobody dimer ("dim" format) fused to the Alb8 anti-albumin nanobody (to confer half-life extension "HLE"). This construct contains the coding sequences for to two 14D5 nanobodies, fused together using a 35-GS linker (GGGGS)x7, and the coding sequence for an anti-albumin nanobody Alb8 fused *via* a 9-GS linker (GGGGSGGGS) (9, 45). Similarly, PD-L1-dimHLE, CD73-dimHLE and CD73/PD-L1-dimHLE were designed as monospecific or bi-specific nanobody-based biologics based on the same strategy with the published sequence of an anti-PD-L1 blocking nanobody (clone B3) (46) or the sequence of a CD73-blocking nanobody (clone SB121). The CD73-specific nanobody SB121 was generated from an immunized alpaca and reformatted into a dimHLE using established protocols described earlier (47–49). The construct 13A7-hcAb used to inhibit P2X7 function was designed as a heavy-chain antibody (hcAb) by fusing the sequence corresponding to the nanobody 13A7 to the hinge and Fc regions of a mutated mouse IgG1 antibody carrying the "LSF" mutations (T252L, T254S, T256F) described previously to confer higher affinity to the neonatal Fc receptor (FcRn) and thereby an extended half-life *in vivo* (50, 51). For AAV vectors production, all constructs were cloned into a pFB plasmid under the control of a CBA promoter (for AAV1 constructs encoding 14D5-dimHLE and 13A7-hcAb) or under the related CASI promoter (for AAV8 constructs encoding PD-L1-dimHLE, CD73-dimHLE and CD73/PD-L1-dimHLE). Production, purification, and titration of recombinant AAV1 and AAV8 were performed by Virovek (Hayward, California, USA) using the baculovirus expression system in Sf9 insect cells. For muscle transduction, mice hind legs were shaved under anesthesia and 100 µL diluted AAV were injected into muscles using a total dose of 10^{11} viral genomes (vg) per mouse.

Experiments in murine models

For muscle transduction, mice hind legs were shaved under anesthesia and 100 µL PBS-diluted AAV were injected into 4 muscle sites (gastrocnemius and/or quadriceps) to reach a total dose of 10^{11} viral genomes (vg) per mouse. 21 days later B16F10 ($5x10^5$), LLC ($5x10^5$) or EG7 (10^6) cells were subcutaneously injected into the right flank of each mouse. The animals were randomized, and the operator was blinded to the group of allocation. Tumors were measured using a digital caliper, and their volumes were estimated using the formula V= length × width × [(length + width)/2]. In some experiments, 5mg/kg oxaliplatin was injected seven days after tumor inoculation.

Statistics

All data are presented as mean ± standard error of the mean (SEM). Statistical comparisons between experimental groups were performed using one-way ANOVA and Tukey's multiple comparisons *post hoc* tests. Two-Way ANOVA with Dunnett's multiple comparisons *post hoc* tests was used for statistical analysis of tumor growth curves. Statistical analysis of the survival was performed using Log-Rank tests. All statistical analyses were performed with the GraphPad Prism software (V8, GraphPad, San Diego, Ca, USA). For all, the threshold for statistical significance was set at $p<0.05$ (*$p<0.05$, **$p<0.01$, ***$p<0.001$ and **** $p<0.0001$).

Results

Injection of AAV vectors coding for nanobody-based biologics that target P2X7 significantly blocks or potentiates P2X7 functions *in vivo*

In this study, we used the AAVnano methodological approach (43, 44), to evaluate the anti-tumor effect of nanobody-based biologics designed to block or to potentiate P2X7 functions. Using this methodology, we previously reported that a single intramuscular (i.m.) injection of the corresponding AAVnano vector elicits production of the modulating nanobody-based biologics over several weeks (43, 44) with a relatively stable pharmacokinetic profile, thereby allowing evaluation of the targeted pathway *in vivo* (Figure 1A). We generated AAV vectors coding for a P2X7-antagonistic heavy chain antibody format designated 13A7-hcAb (i.e., nanobody 13A7 fused to the hinge and Fc-region of a mouse IgG1) or a bivalent, half-life extended, P2X7-potentiating nanobody dimer format designated 14D5-dimHLE (i.e. composed of a dimer of nanobody 14D5, fused to a third nanobody specific for albumin) (9) (Figure 1B). AAV1 vectors coding for these constructs were injected i.m. in the hind-leg muscles of C57BL/6 mice, 21 days before tumor cell inoculation. First, to evaluate the functionality of the nanobody-based constructs produced *in vivo*, we collected blood samples before tumor inoculation in each experiment, and evaluated P2X7 functionality at the surface of circulating peripheral blood leucocytes. For that, blood samples were incubated with different concentrations of ATP ex vivo, and P2X7-dependent shedding of CD62L and CD27 were monitored on T cells (4, 5, 20, 52, 53). As expected from a P2X7-antagonistic biologic, $CD8^+$ T cells (Figure 1C), $CD4^+$ T cells (Figure 1D) and $CD4^+$ $CD25^+$ regulatory T cells (Tregs) (Figure 1E) from mice injected with AAV1 coding for 13A7-hcAb were protected from ATP-induced shedding of CD62L/CD27. Conversely, T cells from mice injected with AAV1 vector coding for the P2X7-potentiating 14D5-dimHLE construct showed enhanced sensitivity in this assay, notably at the lowest ATP dose of 30 µM (Figures 1C–E). Hence, these results confirm the blocking effect of 13A7-hcAb, and conversely the potentiating effect of 14D5-dimHLE, which were produced *in vivo* upon a single i.m. injection of the corresponding AAVnano vectors.

Nanobody-based biologic that inhibit P2X7 functions have a beneficial anti-tumor effect in P2X7-expressing tumor models

To evaluate the effects of the blocking and the potentiating nanobody-based biologics in a tumor context, we took advantage of our AAVnano methodology to induce their continuous expression *in vivo*. However, as expression of P2X7 in tumor cells has been reported to influence tumor growth *per se*, owing to a trophic effect of P2X7 tonic stimulation, we first verified the levels of P2X7 expression at the surface of each tumor model. The results demonstrated that Lewis lung carcinoma (LLC) cells express very low surface levels of P2X7, while the melanoma B16F10 cells display intermediate P2X7 levels, and the EG7 thymoma cells express the highest levels (Figure 2A). These tumor cells were inoculated in groups of animals that received AAV1 vectors coding for either 13A7-hcAb or 14D5-dimHLE three weeks before and the tumor volumes were measured on the following days (Figure 2B). For the LLC model with low levels of P2X7, we observed no significant effect of the nanobody-based biologics on tumor growth, but a tendency of better tumor control in the group that received the AAV vector coding for 14D5-dimHLE (Figure 2C), also resulting in a slightly better survival in this group (Figure 2D). In the B16F10 melanoma model, the potentiating 14D5-dimHLE biologic had no obvious effect on tumor growth and mice survival, while the antagonistic 13A7-hcAb significantly reduced tumor growth (Figure 2E) and slightly improved survival, although not significantly (Figure 2F). In the EG7 thymoma model with the highest level of P2X7, we observed again that the P2X7-potentiating biologic

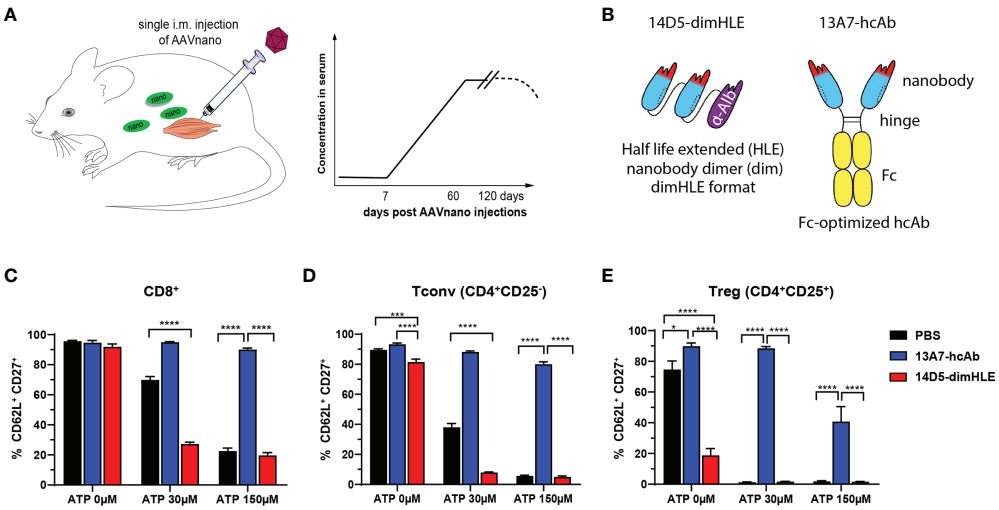

FIGURE 1
AAVnano methodology used to block or to potentiate P2X7 activity *in vivo* **(A)** AAVnano methodology is based on the single i.m. injection of AAVnano vectors coding for a nanobody-based biologic. This is anticipated to induce long-term and stable *in vivo* production of the designed biologics *in vivo* (43). **(B)** Schemes illustrating the format of the different nanobody-based biologics used in this work. The 14D5-dimHLE is composed of a dimer of the P2X7-potentiating 14D5 nanobody, coupled to a third albumin-specific nanobody (Alb8) conferring extended half-life (HLE). The 13A7-hcAb is composed of an antagonistic nanobody targeting P2X7, coupled to the hinge and the Fc-region of a mouse IgG1, carrying "LSF" mutations (T252L, T254S, T256F) to confer higher affinity to the neonatal Fc receptor (FcRn) involved in extending antibody half-life *in vivo* (50). **(C–E)** The ability of the corresponding AAVnano vectors to induce functional modulation (i.e. inhibition or potentiation) of P2X7 functions *in vivo*, was assessed 20 days after their i.m. injection. For that, blood samples were collected and incubated *in vitro* with 0, 30 or 150 µM ATP. P2X7-dependent shedding of CD62L and CD27 was evaluated at the surface of $CD8^+$, $CD4^+CD25^-$ (Tconv), and $CD4^+CD25^+$ (Tregs) lymphocyte subsets, known to express different level of P2X7 and to display increasing sensitivity to ATP. One representative experiment out of at least two is shown with n=7 mice per group. The statistical comparisons between groups were performed using one-way ANOVA. *p<0.05, ***p<0.001, ****p<0.0001.

had no effect on the early phase of tumor growth. However, as also observed in the melanoma model, blocking P2X7 with the 13A7-hcAb biologic significantly decreased tumor growth and improved mice survival (Figures 2G, H). Interestingly, a gradation of the beneficial effect of the blocking 13A7-hcAb biologic can be noticed, apparently in relation with the surface expression of P2X7 in each of these tumor models (Figures 2A, C, E, G). Taken together, these results suggest that inhibition of P2X7 significantly reduces tumor growth when P2X7 is expressed at the surface of the tumor cells.

Potentiation of P2X7 functions *in vivo* with the 14D5-dimHLE biologic influences the composition of immune infiltrates in a melanoma model

Next, we turned to the B16F10-Ova melanoma model with the aim to also study the composition of immune infiltrates, and possibly to detect antigen-specific anti-tumor T cells that could emerge if an adaptive immune response is induced by nanobody-based therapies. As before, groups of mice received AAVnano vectors coding for 14D5-dimHLE or 13A7-hcAb. The monitored tumor growth was in line with the previous results obtained with the B16F10 model and showed again that 13A7-hcAb inhibits tumor growth in the early phase of tumor progression, although not significantly, while 14D5-dimHLE did not induce any conspicuous effect (Figure 3A). Next, 14 days after tumor inoculation, the tumor was resected to study the composition of the immune infiltrates in the different groups. We observed that the nanobody-based biologic 14D5-dimHLE alter the composition of the lymphoid compartment in the TME significantly as compared to control mice (Figure 3B). Indeed, 14D5-dimHLE biologic decreased the proportion of $CD4^+$ T cells and increased the proportion of $CD8^+$ T cells (Figure 3C). 13A7-hcAb biologic in contrast did not significantly modify the lymphoid compartment but reduced the proportion of $CD11b^+$ $CD11c^-$ myeloid cells (Figures 3B, C). Both 13A7-hcAB and 14D5-dimHLE biologics decreased the percentage of $CD4^+$ T cells expressing the exhaustion marker TIGIT, and more importantly, of those expressing the immunosuppressive enzymes CD39 and CD73, two important purinergic checkpoints (Figure 3D). These ecto-enzymes tended also to be less expressed at the surface of Tregs, although with a higher variability. Although the composition of the TME was modified by the biologics treatment, with a reduction of immunosuppressive cells This was apparently not enough to reject the tumor in agreement with the absence of detectable $CD8^+$ T cells recognizing the tumor-derived ovalbumin (Ova)

10.3389/fimmu.2022.1012534

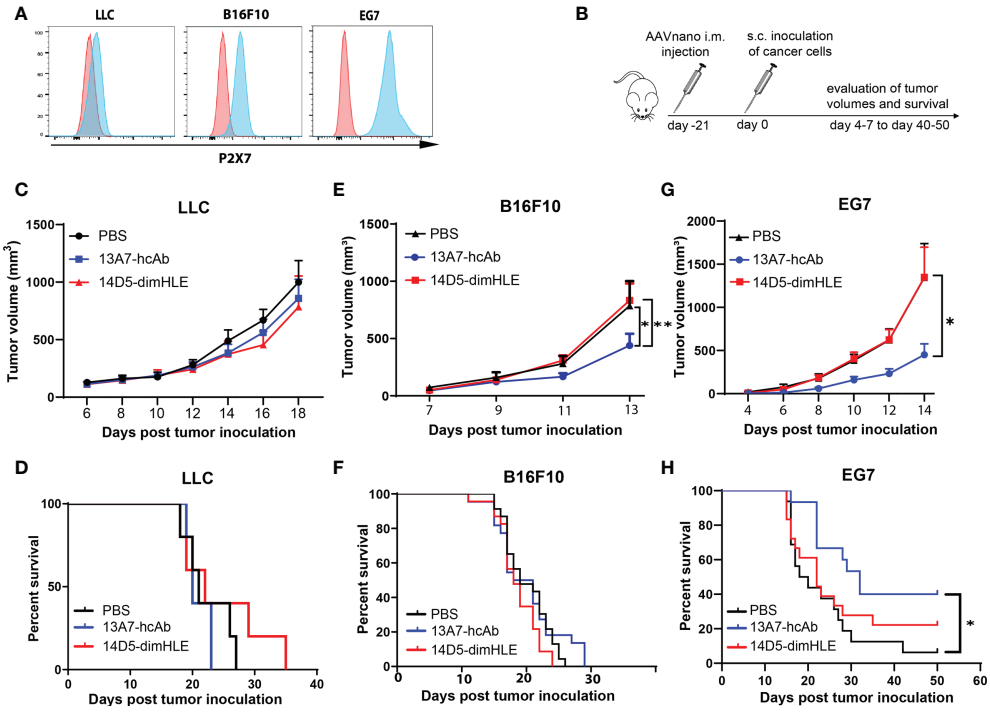

FIGURE 2
Antagonistic nanobody-based biologics directed against P2X7 inhibit the subcutaneous growth of tumor cell lines expressing P2X7 *in vivo* **(A)** P2X7 cell surface levels of LLC carcinoma, B16F10 melanoma, and EG7 thymoma cell lines were evaluated by flow cytometry using a fluorochrome-conjugated P2X7-specific antibody (blue histograms) and compared to the background staining obtained using a fluorochrome-coupled isotype control antibody (red histograms). **(B)** Protocol used to evaluate the *in vivo* effect of P2X7-blocking or P2X7-potentiating biologics on tumor growth. Mice were injected i.m. with 10^{11} vg/mouse of the indicated AAVnano vectors, namely AAV-13A7-hcAb (coding for the P2X7-blocking nanobody-based biologic), or AAV-14D5-dimHLE (coding for the P2X7-potentiating nanobody-based biologic). 21 days later, mice were inoculated with the indicated cancer cells in the right flank of the animal and tumor volumes were monitored over time. **(C, E, G)** Mean tumor volumes in groups of mice (n = 10) injected with the LLC carcinoma, B16F10 melanoma, or EG7 thymoma tumor model. **(D, F, H)** Corresponding survival curves are shown for each tumor model. Experiments were repeated at least 2 times with similar results. The statistical comparisons between tumor volumes were performed using two-way ANOVA. The statistical analyses of survival rates were performed using Log-Rank tests. *p<0.05, **p<0.01.

antigen (data not shown). These results indicate that both P2X7-targeting biologics can influence the composition of the TME, even the potentiating 14D5-dimHLE biologic that did not show any effect on the tumor growth in this model. Taken together, this suggests that although P2X7 potentiation induces a more favorable TME for the emergence and for the activation of anti-tumor immune cells, targeting P2X7 alone was clearly not enough to control tumor progression in this aggressive melanoma model.

P2X7 potentiating and blocking biologics in combination with an immunogenic chemotherapy improve tumor control in the EG7 tumor model

We next evaluated our P2X7-targeting biologics in combination with an immunogenic chemotherapy treatment. We reasoned that such a treatment should indeed increase the concentration of ATP in the TME and may therefore synergize with P2X7 targeting. We chose the EG7 model, as it was previously shown to be sensitive to oxaliplatin and to induce an immunogenic cell death that relies on ATP release *in vivo* (28). Notably, we expected that the potentiating 14D5-dimHLE nanobody-based biologic would favor the emergence of anti-tumor immune responses and promote tumor control when given in combination with oxaliplatin. To evaluate this hypothesis, we injected as before the AAVnano vectors coding for both biologics three weeks before EG7 tumor inoculation. A single dose of oxaliplatin was then injected 7 days after tumor inoculation when the mean volume of tumors reached 50 mm^3 (Figure 4A). As expected, oxaliplatin used at 5 mg/kg decreased tumor growth but did not induce complete tumor rejection. When combined with the 14D5-dimHLE potentiating biologic, a better tumor control was observed and, importantly, tumor

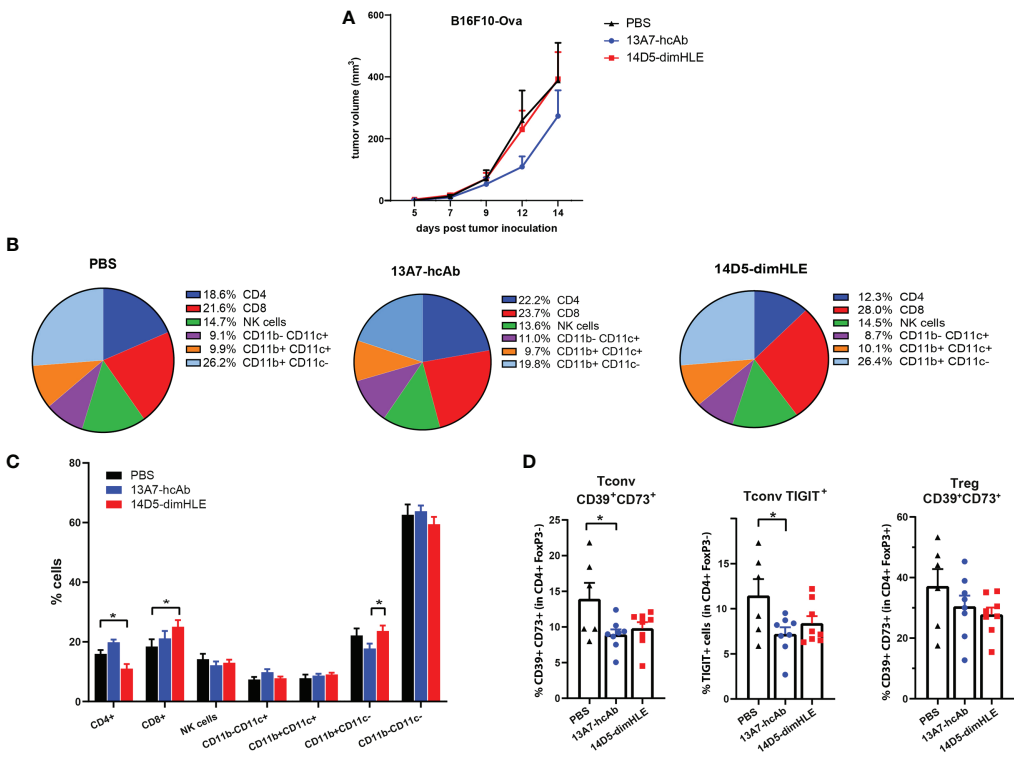

FIGURE 3
Modification of immune cell infiltrates within the tumor microenvironment in response to *in vivo* generated biologics targeting P2X7. **(A)** Tumor growth curves of B16F10-Ova melanoma cells are shown for group of mice treated as in Figure 2B. **(B, C)** Relative percentages of tumor infiltrating myeloid and lymphoid CD45$^+$ cells were determined by flow cytometry 14 days after tumor inoculation in groups of mice (n=6-7) treated with AAV-13A7-hcAb, AAV-14D5-dimHLE, or with PBS. **(D)** Percentages of CD39$^+$CD73$^+$ cells (left panel) or TIGIT$^+$ (middle panel) cells within the conventional CD4$^+$FoxP3$^-$ T cells (Tconv), and the percentages of CD39$^+$CD73$^+$ cells within the CD4$^+$FoxP3$^+$ Tregs subset (right panel) were determined by flow cytometry. The statistical comparisons between tumor volumes were performed using 2-way ANOVA. The statistical comparisons between tumor infiltrating cell subpopulations were performed using one-way ANOVA. *p<0.05.

rejections in most mice (Figure 4B). Taking advantage of the expression of the Ova antigen by this tumor cell line, we also monitored the emergence of anti-Ova CD8$^+$ specific T cell in the blood of these mice, 14 and 22 days post tumor inoculation. The data indeed suggest that the combination of oxaliplatin and 14D5-dimHLE results in more robust CD8$^+$ T cells stimulation than in the other groups (Figure 4C). This was also the case when evaluating the anti-Ova IgG responses, suggesting a higher level of immune stimulation in this group (Figure 4D). Interestingly, we also noticed a better tumor control in the group of mice that received oxaliplatin together with the P2X7-blocking 13A7-hcAb biologic (Figure 4B). As the EG7 tumor cell line expresses high levels of P2X7, we assume that this effect was related to the inhibition of the tonic stimulation of P2X7. This is in agreement with the lower stimulation of immune cells in this group in comparison with the previous one (Figures 4C, D). Taken together, these data suggest that both P2X7-targeting biologics, the blocking 13A7-hcAbs as well as the potentiating 14D5-dimHLE, can improve tumor control in combination with oxaliplatin chemotherapy, although with different mechanisms of action.

A bispecific biologic targeting both CD73 and PD-L1 more effectively inhibits tumor growth *in vivo* than monotherapies with P2X7-specific biologics

We next evaluated other nanobody-based biologics using our method, either alone or in combination with 14D5-dimHLE treatment. As CD73 has emerged as a key purinergic checkpoint in the TME, we designed a CD73-specific construct based on nanobody clone SB121, which displays an antagonistic effect on the enzymatic activity of CD73 *in vitro*. Like 14D5-dimHLE, the CD73-targeting construct, termed anti-CD73-dimHLE, contains a nanobody dimer (SB121), coupled to an anti-albumin nanobody to increase its half-life *in vivo*. For comparison, we

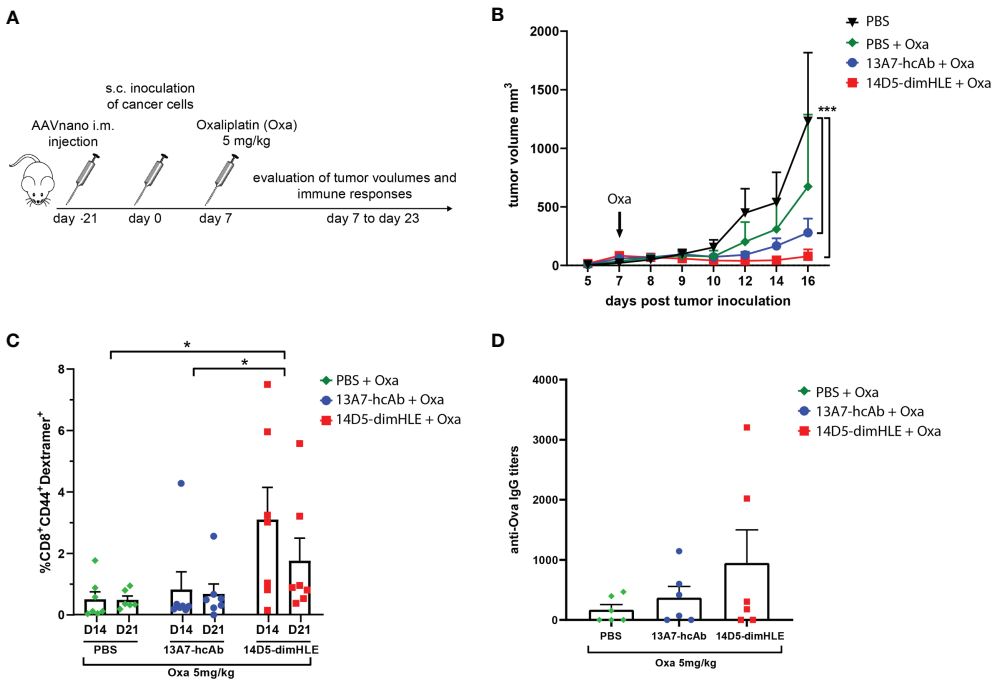

FIGURE 4
Treatment with P2X7-targeting biologics combined with oxaliplatin chemotherapy **(A)** Protocol used to evaluate the *in vivo* effect of P2X7-targeting biologics on tumor growth when combined with oxaliplatin chemotherapy. AAVnano coding for the P2X7-blocking 13A7-hcAb, or for the P2X7-potentiating 14D5-dimHLE were injected i.m. 21 days before s.c. injection of EG7-Ova thymoma cells. Oxaliplatin (5 mg/kg) was injected once at day 7 post tumor inoculation. **(B)** Mean tumor volumes overtime in each group of animals (n=7). **(C)** Percentages of Ova-specific $CD8^+$ cells in peripheral blood were determined by flow cytometry at days 14 and 22 post tumor inoculation. **(D)** Anti-Ova IgG titers were determined by ELISA in sera collected 23 days post tumor inoculation. Statistical comparisons between tumor volumes were performed using two-way ANOVA, and statistical comparisons between the levels of anti-Ova immune responses were performed using one-way ANOVA *p<0.05, ***p<0.001.

also designed a nanobody-based construct that targets the well-known PD-L1 immune checkpoint, that we termed anti-PDL1-dimHLE. For that, we used the same dimHLE format but with nanobody clone B3, previously demonstrated to specifically block the interaction between PD-L1 and its cognate receptor PD-1 (46). Finally, we also designed a bispecific construct targeting both, CD73 and PD-L1, as both proteins are overexpressed by the tumor cells and/or by the immune infiltrates that compose the TME (54). We reasoned that this bispecific construct, termed anti-CD73/PDL1-HLE, might not only improve T cell activation by inhibiting the PD-1/PD-L1 axis, but also inhibit the accumulation of anti-inflammatory adenosine in the TME, which represents another non-redundant immunosuppressive mechanism. Evaluation of the monospecific and the bispecific nanobody-based biologics was again performed using our AAVnano method using the EG7 thymoma model (Figure 5) as well as the more aggressive and less immunogenic B16F10 melanoma model (Figure 6). For that, AAV8 vectors coding for either anti-CD73-dimHLE, anti-PDL1-dimHLE or anti-CD73/PDL1-HLE were generated and injected i.m. in different groups of mice. For comparison, an additional group was injected with the AAVnano vector coding for 14D5-dimHLE, the P2X7-potentiating biologic. As before, EG7 or B16F10 tumor cell lines were inoculated 3 weeks later (Figures 5A and 6A). Like in the previous experiments, the 14D5-dimHLE biologic alone did not promote tumor control of EG7 nor of B16F10 tumors, and was statistically indistinguishable from the untreated control group, both in terms of tumor growth and survival (Figures 5B, C and 6B, C). Similarly, the anti-CD73-dimHLE biologic did not inhibited tumor growth nor survival in both tumor models. In contrast, the bispecific anti-CD73/PDL1-HLE biologic significantly enhanced the control of tumor growth in the B16F10 melanoma model, or even led to complete tumor rejection in the EG7 model, as well as improved mice survival in both tumor models (Figures 5B, C and 6B, C). Interestingly, in both tumor models, this novel bispecific construct also tended to be more efficient than the anti-PDL1-dimHLE biologic, in terms of reduction of tumor growth as well as in terms of mice survival.

Finally, we also evaluated each of the three biologics (anti-CD73-dimHLE, anti-PDL1-dimHLE, and anti-CD73/PDL1-

10.3389/fimmu.2022.1012534

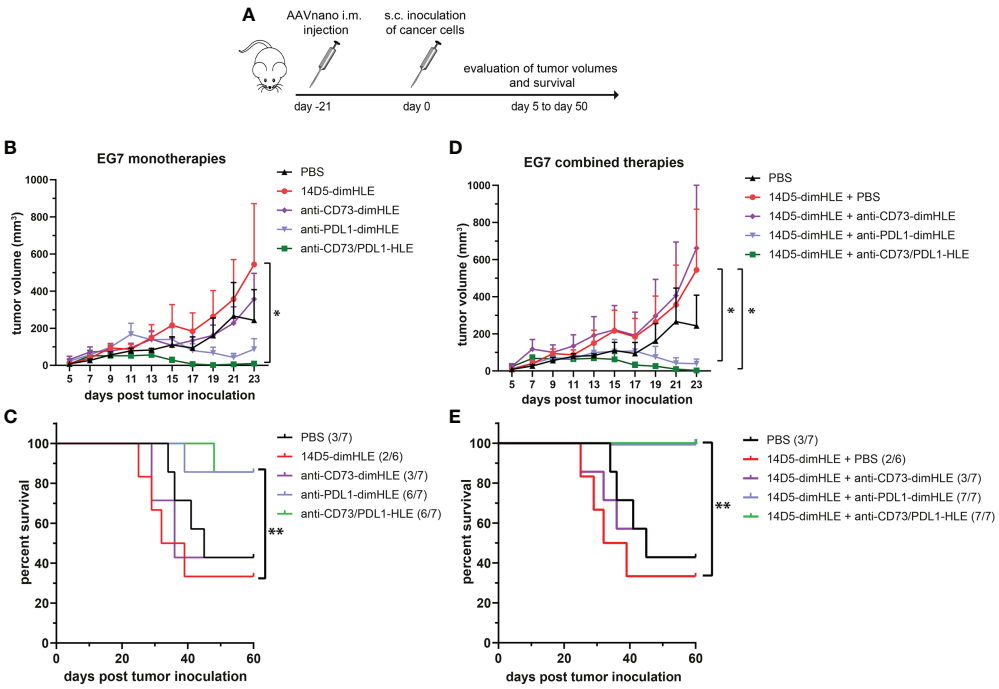

FIGURE 5
A bispecific biologic targeting both CD73 and PD-L1 more effectively inhibits the subcutaneous growth of EG7 melanoma cells *in vivo* than monotherapies with P2X7-specific biologics. **(A)** Protocol used to evaluate the *in vivo* effect of nanobody-based biologics targeting P2X7, CD73, and/or PD-L1. The AAVnano coding for the P2X7-potentiating 14D5-dimHLE, for the CD73-inhibiting anti-CD73-dimHLE, for the PD-L1 blocking anti-PDL1-dimHLE, or the bispecific biologic targeting both CD73 and PD-L1 (anti-CD73/PDL1-HLE), were injected i.m. 21 days before s.c. injection of EG7 thymoma cells. These biologics were either evaluated alone **(B, C)**, or in combination with the 14D5-dimHLE P2X7-potentiating biologic **(D, E)**. In that case, the AAVnano vectors coding for 14D5-dimHLE were injected i.m. into the gastrocnemius while the AAVnano vectors coding for the additional biologics were injected i.m. into the quadriceps. Mean tumor volumes overtime **(B, D)** and survival **(C, E)**, were followed in the different group of mice (n=7), as indicated. The statistical comparisons between tumor volumes were performed using two-way ANOVA, and the statistical analyses of survival were performed using Log-Rank tests. *p<0.05, **p<0.01.

HLE), in combination with the 14D5-dimHLE. For that, an AAV1 vector coding for 14D5-dimHLE was injected in the gastrocnemius while the AAV8 vector coding for the second biologic was injected in the quadriceps to induce concomitant expression of two biologics at the same time. As in the previous experiment, EG7 or B16F10 tumor cell lines were inoculated 3 weeks later (Figures 5A and 6A). In both tumor models, the anti-CD73-dimHLE did not significantly synergize with the 14D5-dimHLE biologic, neither on the control of tumor growth nor in terms of mice survival (Figures 5D, E and 6D, E). In contrast, tumor growth was better controlled and mice survival was significantly improved in the groups that received anti-PDL1-dimHLE, or anti-CD73/PDL1-HLE, in addition to the 14D5-dimHLE biologic, suggesting at least that the beneficial effects of anti-PDL1-dimHLE, and of anti-CD73/PDL1-HLE are maintained in the presence of the P2X7-potentiating biologic. However, as compared to the data obtained for each individual construct, the results did not show a better anti-tumor effect in combination with 14D5-dimHLE biologic. In fact, this was difficult to evaluate in the less aggressive EG7 tumor model as both mono and combined therapy led to near complete tumor rejection and survival of almost all the mice in these cohorts (Figures 5B vs D, C vs E). However, when comparing the data in the more aggressive B16F10 melanoma model, the combined therapy tended to be slightly less efficient than anti-PDL1-dimHLE or anti-CD73/PDL1-HLE given alone (Figures 6B vs D, C vs E). This would suggest that, by favoring the stimulation of P2X7 on the surface of the tumor cells, the potentiating 14D5-dimHLE in the long run displays a net effect that is rather in favor of tumor progression than in favor of the anti-tumor immune response. This may suggest that short term P2X7 potentiation, by means of direct injection of the recombinant 14D5-dimHLE biologic, may be better suited than its continuous stimulation, to tip the balance in favor of the activation of the immune system. However, this would have to be tested in future experiments in a broader range of tumor types that express, or not, P2X7. Nevertheless, from the present data, we concluded that targeting both, CD73 and PD-L1, with bispecific nanobody-based biologics represent a promising approach in cancer treatment.

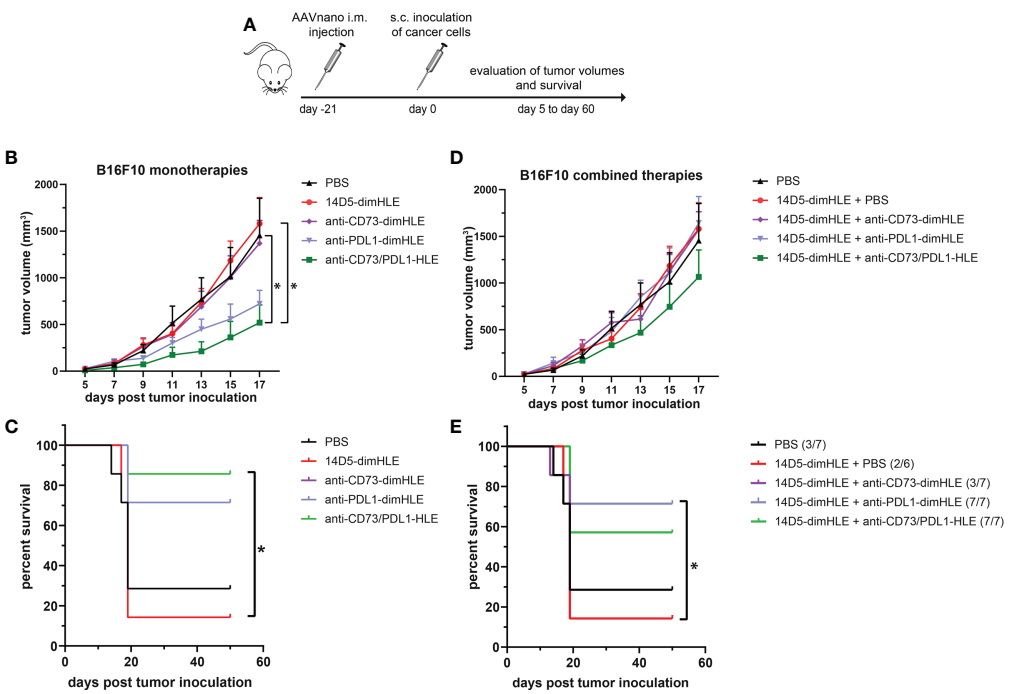

FIGURE 6
A bispecific biologic targeting both CD73 and PD-L1 more effectively inhibits the subcutaneous growth of B16F10 melanoma cells *in vivo* than monotherapies with P2X7-specific biologics **(A)** Protocol used to evaluate the *in vivo* effect of nanobody-based biologics targeting P2X7, CD73, and/or PD-L1. The AAVnano coding for the P2X7-potentiating 14D5-dimHLE, for the CD73-inhibiting CD73-dimHLE, for the PD-L1 blocking PDL1-dimHLE, or the bispecific CD73/PDL1-HLE, were injected i.m. 21 days before s.c. injection of B16F10 melanoma cells. These biologics were either evaluated alone **(B, C)**, or in combination with the 14D5-dimHLE P2X7-potentiating biologics **(D, E)**. In that case, the AAVnano vectors coding for 14D5-dimHLE were injected i.m. into the gastrocnemius while the AAVnano vectors coding for the additional biologics were injected i.m. into quadriceps. Mean tumor volumes overtime **(B, D)** and survival **(C, E)**, were followed in the different group of mice (n=7), as indicated. The statistical comparisons between tumor volumes were performed using two-way ANOVA, and the statistical analyses of survival were performed using Log-Rank tests. *p<0.05.

Discussion

The TME is a dynamic environment and the privileged site where cancer cells are in close contact with the host. The biochemical and cellular composition of the TME is of paramount importance for the regulation of cancer cells metabolism, proliferation, motility and dissemination. The TME can facilitate anti-tumor immune responses but may conversely foster the generation of an immunosuppressive environment that facilitates tumor growth. The biochemical composition of the TME is a result of the activity of the cancer and host cells. Over the last few years, the abundance of eATP was identified as a prominent TME characteristic (29, 55). Cell stress and cell death lead to loss of plasma membrane integrity and represent important sources of eATP in the TME (11). Hypoxia itself is a potent stimulus for ATP release, even in the absence of cell damage. Various cells also release ATP, either as part of their normal metabolism or when responding to activation, metabolic or mechanical stress, or signals that induce cell death. This has been documented for numerous cells, including cancer cells, dendritic cells, tumor-infiltrating neutrophils, tumor-associated macrophages or platelets (29, 31, 32, 55). Once released in the TME, eATP binds to P2Y and P2X receptors. Among the P2 receptors, the role of the P2X7 receptor has been widely implicated in several types of cancer and suggested to be involved in the complex dialog between cancer and immune cells within the TME (31). The balance between ATP release and its degradation by a variety of ecto-enzymes determines the concentration of eATP and of its catabolites in the TME. eATP is indeed catabolized to ADP and AMP, and then to the immunosuppressive adenosine that exerts its effect *via* the widely expressed P1 receptors. Generation of adenosine from eATP is essentially controlled by the sequential activity of CD39 and CD73. These ecto-enzymes are expressed by many cell types in the TME, including cancer cells, cancer-associated fibroblasts (CAFs), cytotoxic T cells, Tregs, NK cell subsets, M2-like tumor associated macrophages (TAMs), or myeloid-derived suppressor cells (MDSCs) (29). Accumulation of adenosine in

the TME exert a potent immunosuppressive function, notably through the inhibitory A2a adenosine receptors expressed by T cells that restraint their activation and expansion in the adenosine riche TME (36–38). Preclinical and clinical studies have further highlight the potential offered by therapeutic strategies aiming to inhibit adenosine signaling in cancer, and the "purinergic signature" that favor their application (39–42).

In this study, we used the AAVnano method approach (43, 44) to evaluate the anti-tumor potential of several nanobody-based biologics in different tumor models. Nanobodies, as for classical antibodies, offer excellent target specificity that may prevent unwanted off-target effects possibly observed with small chemical drugs. We selected nanobodies that specifically bind mouse P2X7 and but not the close P2X4 and P2X1 paralogs (9, 45). We chose to express our nanobody-based biologics directly *in vivo* upon AAV vector-mediated gene transfer. AAV vectors are widely used in gene therapy settings and represent an efficient and safe approach to transfer genes of interest into muscle cells and to elicit long-term systemic *in situ* production of transgenic proteins, including selected antibodies that confer protection from infectious diseases (56, 57). In our experimental approach, we previously demonstrated that a single i.m. administration of the AAVnano vector (10^{11} vg/mouse) coding for our engineered nanobody-based biologics was sufficient to elicit *in vivo* production of saturating levels of biologics that persist for several months. We validated here, prior to the tumor inoculation, that the blocking or the potentiating P2X7-specific biologics were produced *in vivo* and were able to completely block P2X7 (i.e., for the 13A7-hcAb biologic) or to potentiate its activity notably at low ATP concentration, (i.e., for the 14D5-dimHLE construct) (Figure 1, and data not shown). As a hallmark associated with P2X7 receptor activation, we used a sensitive *ex vivo* assay based on metalloprotease-dependent shedding of CD27 and CD62L from the T cell surface (5, 20–23). Our data demonstrate that a single i.m. injection of AAVnano coding for the P2X7-antagonistic 13A7-hcAb protects T cells from ATP-induced CD27 and CD62L shedding (Figures 1C–E) while the AAVnano coding for the P2X7-potentiating 14D5-dimHLE sensitized T cells to ATP-induced shedding of CD27 and CD62L (Figures 1C–E). We next used our AAVnano methodological approach to evaluate the net consequence of either blocking, or potentiating, P2X7 in different tumor models. The tumor models were selected for their differential levels of P2X7 surface expression, ranging from very low, in the lung carcinoma model LLC, intermediate in the B16F10 melanoma model, to relatively high expression in the EG7 thymoma model (Figure 2A). As P2X7 tonic stimulation in the context of the ATP-rich TME has been associated with tumor growth and invasiveness, it appeared indeed to be an important factor to consider in our study. Importantly, none of these cancer cell lines is rapidly going into cell death by concentrations of ATP below the millimolar range, while this is the case for mouse T cells (not shown). This indicates, as suggested by different studies, that the P2X7 receptor in cancer cells does not behave as a cytolytic receptor. This may be explained by the expression of particular splice variants, or mutated versions of the receptor, that remain to be characterized in our tumor lines. However, this was studied in a wide variety of human cancer cells, where P2X7 variants that have lost their cytolytic properties but have retained the capacity to trigger calcium influx in response to ATP (31, 58–62). Therefore, blocking P2X7 is expected to inhibit tonic tumor cells stimulation and tumor progression. Our results are in complete agreement with this hypothesis. We demonstrate that blocking P2X7 in the LLC lung carcinoma model had no effect on the tumor progression and mice survival, in line with the very low surface expression of P2X7 in this tumor line (Figures 2A, C, D). For the two other tumor models, our data point to a gradation of the beneficial effect of the 13A7-hcAb biologic, in direct relation with the surface expression of P2X7 in each of these tumor models. Indeed, the P2X7-blocking 13A7-hcAb biologic more potently inhibits tumor growth in the EG7 tumor model, which displays the highest P2X7 surface level, than in the B16F10 model that expresses an intermediate level of P2X7 (Figures 2A, C, E, F). Taken together, these results suggest that inhibition of P2X7 significantly reduces tumor growth and improves survival, when P2X7 is expressed at the surface of the tumor cells.

To better understand the biological effects of the nanobody-based biologics targeting P2X7 on the composition of the TME, we next studied the frequency and the phenotype of the cells present in the tumor infiltrates. For that, we resected the tumor and analyzed the cell profiles by flow cytometry. We observed that the nanobody-based biologic 14D5-dimHLE, that was paradoxically not associated with any beneficial effect on tumor growth nor on mice survival, significantly alters the composition of the lymphoid compartment in the TME as compared to control mice (Figures 3B, C). Notably, the 14D5-dimHLE biologic was found to increase the proportion of $CD8^+$ T cells, which may indicate the stimulation of tumor-specific T cells (Figure 3C). This treatment was also associated with a decrease in the expression of the exhaustion marker TIGIT, and of CD39 and CD73, two ecto-enzymes considered as targetable purinergic checkpoints (32–35). This suggests that P2X7 potentiation by the 14D5-dimHLE biologic contributes to the induction of a more favorable TME, which possibly is less immunosuppressive, but that this treatment alone is not sufficient for the emergence of a potent and effective anti-tumor immune response. As this result has been obtained in the B16F10 melanoma model expressing intermediate levels of P2X7, higher tonic stimulation of P2X7 at the surface of the tumor cells, facilitated by the 14D5-dimHLE biologic, probably also contributed to the global effect of this biologic *in vivo*. This may be addressed in future studies using for instance a B16F10 melanoma model deficient for P2X7

expression, to better delineate the potential beneficial effect of P2X7 stimulation on immune cells, from its detrimental effect on the tumor cells themselves.

As the 14D5-dimHLE biologic does not promote beneficial effects when used alone, we next evaluated whether potentiation of P2X7 can enhance anti-tumor immune responses when combined with immunogenic oxaliplatin chemotherapy, that may increase the release of ATP in the tumor, or with anti-immune checkpoints therapy, or antagonism of CD73 involved in the formation of the immunosuppressive adenosine. We first evaluated the combination therapy based on a single injection of oxaliplatin in animals that have been injected beforehand with AAVnano vectors coding for the 14D5-dimHLE biologic (Figure 4A). We observed that this combination resulted in a significant decrease in EG7 tumor growth (Figure 4B), associated with an increase in tumor-specific cellular and humoral immune responses (Figures 4C–D). These data suggest that P2X7 potentiation in the context of an immunogenic chemotherapy reinforce the immune responses. The mechanism may involve stimulation and migration of dendritic cells, as well as Treg cell death, which both involve P2X7 and can contribute together to the emergence of effective adaptive anti-tumor immune responses (4, 26, 28, 29).

We then evaluated the 14D5-dimHLE P2X7-potentiating biologic in combination with a nanobody-based biologics targeting CD73, another important purinergic checkpoint, or PD-L1, a prototypic immune checkpoint. Another construct was designed to target both CD73 and PD-L1 at the same time using a bispecific nanobody-based biologic. We evaluated theses biologics as monotherapy and in combination with 14D5-dimHLE in the EG7 thymoma model and in the less immunogenic B16F10 melanoma model considered to be more aggressive. We did not observe any beneficial effect of these treatments when combined with 14D5-dimHLE, as compared to their evaluation as monotherapy (Figures 5 and 6). In fact, it was not possible to faithfully evaluate the possible beneficial effect of the combination involving anti-PDL1-dimHLE or anti-CD73/PDL1-HLE biologics as both treatments were already very effective alone to induce tumor control. Nevertheless, the treatment based on anti-CD73-dimHLE and 14D5-dimHLE, either as monotherapy, or combined, was not effective to control tumor growth nor to improve mice survival. This may at least partly reflect the P2X7-dependant trophic stimulation of EG7 and B16F10 cancer cells. Blocking CD73 may indeed increase the accumulation of ATP in the TME and 14D5-dimHLE may further enhance P2X7 activity at the surface of these cancer cells, tipping the balance in favor of tumor growth. Whether this is a plausible explanation may deserve further investigations, involving for instance the assessment of eATP concentration in the TME and its evolution upon treatment with these biologics.

In the course of our evaluations, we tested for the first time a bispecific biologic targeting CD73 and PD-L1, that we termed anti-CD73/PDL1-HLE. Here, we aimed to combine a nanobody targeting the prototypical PD-L1 immune checkpoint with a nanobody targeting CD73 that is considered as an emerging targetable purinergic checkpoint. This anti-CD73/PDL1-HLE biologic improved the control of tumor growth in the aggressive B16F10 melanoma model, or even induced complete tumor rejection in the EG7 model, as well as improved mice survival in both tumor models (Figures 5B, C and 6B, C). Interestingly, in both tumor models, this novel bispecific biologic also tended to be more efficient than the anti-PDL1-dimHLE biologic, in terms of reduction of tumor growth as well as in terms of mice survival. The mechanism remains to be fully explored, but possibly rely on the inhibition of two complementary non-redundant mechanisms that contribute together to the progressive formation of the immunosuppressive TME. In line, previous studies demonstrated that antibodies directed against CD73 enhance antitumor immune responses, when used in combination with anti-immune checkpoints (34, 35, 63). Also, as both CD73 and PD-L1 are overexpressed in the TME, this bispecific biologic may advantageously accumulate around the tumor to exert its beneficial effect but this remains to be fully investigated. We conclude, however, from our present data that targeting both, CD73 and PD-L1, with bispecific nanobody-based biologics represents a promising approach in cancer treatment.

Data availability statement

The raw data supporting the conclusions of this article will be made available by the authors, without undue reservation.

Ethics statement

The animal study was reviewed and approved by French Ministry of Education and Research, after consultation of the ethical committee.

Author contributions

MD, FK-N, and SA conceived and design the study. MD, AS, RH, HG, CA, MB, SM, YD, BR, TM, AM, FK-N and SA developed the methodology. All authors contributed to the planning, acquisition of data, or to the interpretation of the results. MD, CA, FK-N, and SA wrote the manuscript. All authors revised and approved the manuscript.

Funding

The present work was funded by a grant No ANR-18-CE92-0046-01 from Agence National de la Recherche (ANR) to SA, and by grants No 310/13, SFB1328-A13, SFB1328-Z02 from the Deutsche Forschungsgemeinschaft (DFG) to FK-N, BR, and TM.

Acknowledgments

The authors would like to thank Rachid Zoubairi, Gaetan Riou, Laetitia Jean and Chantal Barou, from Rouen, and Birte Albrecht and Dorte Wendt, from Hamburg, for excellent technical assistance.

Conflict of interest

The authors declare that the research was conducted in the absence of any commercial or financial relationships that could be construed as a potential conflict of interest.

FK-N is a co-inventor on a patent application on P2X7-specific nanobodies. FK-N, SM, YD, BR, and TM are co-inventors on a patent application on CD73-specific nanobodies.

Publisher's note

References

1. Burnstock G. Purinergic signalling. *Br J Pharmacol* (2006) 147 Suppl 1:S172–81. doi: 10.1038/sj.bjp.0706429

2. Bartlett R, Stokes L, Sluyter R. The P2x7 receptor channel: Recent developments and the use of P2x7 antagonists in models of disease. *Pharmacol Rev* (2014) 66(3):638–75. doi: 10.1124/pr.113.008003

3. Di Virgilio F, Dal Ben D, Sarti AC, Giuliani AL, Falzoni S. The P2x7 receptor in infection and inflammation. *Immunity* (2017) 47(1):15–31. doi: 10.1016/j.immuni.2017.06.020

4. Hubert S, Rissiek B, Klages K, Huehn J, Sparwasser T, Haag F, et al. Extracellular nad+ shapes the Foxp3+ regulatory T cell compartment through the Art2-P2x7 pathway. *J Exp Med* (2010) 207(12):2561–8. doi: 10.1084/jem.20091154

5. Rissiek B, Haag F, Boyer O, Koch-Nolte F, Adriouch S. P2x7 on mouse T cells: One channel, many functions. *Front Immunol* (2015) 6:204. doi: 10.3389/fimmu.2015.00204

6. Adinolfi E, Giuliani AL, De Marchi E, Pegoraro A, Orioli E, Di Virgilio F. The P2x7 receptor: A main player in inflammation. *Biochem Pharmacol* (2018) 151:234–44. doi: 10.1016/j.bcp.2017.12.021

7. Orioli E, De Marchi E, Giuliani AL, Adinolfi E. P2x7 receptor orchestrates multiple signalling pathways triggering inflammation, autophagy and Metabolic/Trophic responses. *Curr Med Chem* (2017) 24(21):2261–75. doi: 10.2174/0929867324666170303161659

8. Hofman P, Cherfils-Vicini J, Bazin M, Ilie M, Juhel T, Hebuterne X, et al. Genetic and pharmacological inactivation of the purinergic P2rx7 receptor dampens inflammation but increases tumor incidence in a mouse model of colitis-associated cancer. *Cancer Res* (2015) 75(5):835–45. doi: 10.1158/0008-5472.CAN-14-1778

9. Danquah W, Meyer-Schwesinger C, Rissiek B, Pinto C, Serracant-Prat A, Amadi M, et al. Nanobodies that block gating of the P2x7 ion channel ameliorate inflammation. *Sci Transl Med* (2016) 8(366):366ra162. doi: 10.1126/scitranslmed.aaf8463

10. Peverini L, Beudez J, Dunning K, Chataigneau T, Grutter T. New insights into permeation of Large cations through atp-gated P2x receptors. *Front Mol Neurosci* (2018) 11:265. doi: 10.3389/fnmol.2018.00265

11. Di Virgilio F, Giuliani AL, Vultaggio-Poma V, Falzoni S, Sarti AC. Non-nucleotide agonists triggering P2x7 receptor activation and pore formation. *Front Pharmacol* (2018) 9:39. doi: 10.3389/fphar.2018.00039

12. Di Virgilio F, Schmalzing G, Markwardt F. The elusive P2x7 macropore. *Trends Cell Biol* (2018) 28(5):392–404. doi: 10.1016/j.tcb.2018.01.005

13. Di Virgilio F, Sarti AC, Falzoni S, De Marchi E, Adinolfi E. Extracellular atp and P2 purinergic signalling in the tumour microenvironment. *Nat Rev Cancer* (2018) 18(10):601–18. doi: 10.1038/s41568-018-0037-0

14. Adinolfi E, Capece M, Franceschini A, Falzoni S, Giuliani AL, Rotondo A, et al. Accelerated tumor progression in mice lacking the atp receptor P2x7. *Cancer Res* (2015) 75(4):635–44. doi: 10.1158/0008-5472.CAN-14-1259

15. Adinolfi E, De Marchi E, Orioli E, Pegoraro A, Di Virgilio F. Role of the P2x7 receptor in tumor-associated inflammation. *Curr Opin Pharmacol* (2019) 47:59–64. doi: 10.1016/j.coph.2019.02.012

16. Adinolfi E, Callegari MG, Ferrari D, Bolognesi C, Minelli M, Wieckowski MR, et al. Basal activation of the P2x7 atp receptor elevates mitochondrial calcium and potential, increases cellular atp levels, and promotes serum-independent growth. *Mol Biol Cell* (2005) 16(7):3260–72. doi: 10.1091/mbc.e04-11-1025

17. Adinolfi E, Cirillo M, Woltersdorf R, Falzoni S, Chiozzi P, Pellegatti P, et al. Trophic activity of a naturally occurring truncated isoform of the P2x7 receptor. *FASEB J* (2010) 24(9):3393–404. doi: 10.1096/fj.09-153601

18. Young CNJ, Gorecki DC. P2rx7 purinoceptor as a therapeutic target-the second coming? *Front Chem* (2018) 6:248. doi: 10.3389/fchem.2018.00248

19. Schwarz N, Drouot L, Nicke A, Fliegert R, Boyer O, Guse AH, et al. Alternative splicing of the n-terminal cytosolic and transmembrane domains of P2x7 controls gating of the ion channel by adp-ribosylation. *PloS One* (2012) 7(7):e41269. doi: 10.1371/journal.pone.0041269

20. Scheuplein F, Schwarz N, Adriouch S, Krebs C, Bannas P, Rissiek B, et al. Nad+ and atp released from injured cells induce P2x7-dependent shedding of Cd62l and externalization of phosphatidylserine by murine T cells. *J Immunol* (2009) 182(5):2898–908. doi: 10.4049/jimmunol.0801711

21. Schwarz N, Fliegert R, Adriouch S, Seman M, Guse AH, Haag F, et al. Activation of the P2x7 ion channel by soluble and covalently bound ligands. *Purinergic Signal* (2009) 5(2):139–49. doi: 10.1007/s11302-009-9135-5

22. Sommer A, Kordowski F, Buch J, Maretzky T, Evers A, Andra J, et al. Phosphatidylserine exposure is required for Adam17 sheddase function. *Nat Commun* (2016) 7:11523. doi: 10.1038/ncomms11523

23. Seman M, Adriouch S, Scheuplein F, Krebs C, Freese D, Glowacki G, et al. Nad-induced T cell death: Adp-ribosylation of cell surface proteins by Art2 activates the cytolytic P2x7 purinoceptor. *Immunity* (2003) 19(4):571–82. doi: 10.1016/s1074-7613(03)00266-8

24. Stark R, Wesselink TH, Behr FM, Kragten NAM, Arens R, Koch-Nolte F, et al. T Rm maintenance is regulated by tissue damage *Via* P2rx7. *Sci Immunol* (2018) 3(30). doi: 10.1126/sciimmunol.aau1022

25. Rissiek B, Lukowiak M, Raczkowski F, Magnus T, Mittrucker HW, Koch-Nolte F. *In vivo* blockade of murine Artc2.2 during cell preparation preserves the vitality and function of liver tissue-resident memory T cells. *Front Immunol* (2018) 9:1580. doi: 10.3389/fimmu.2018.01580

26. Adriouch S, Hubert S, Pechberty S, Koch-Nolte F, Haag F, Seman M. Nad+ released during inflammation participates in T cell homeostasis by inducing Art2-mediated death of naive T cells in vivo. *J Immunol* (2007) 179(1):186–94. doi: 10.4049/jimmunol.179.1.186

27. De Marchi E, Orioli E, Pegoraro A, Sangaletti S, Portararo P, Curti A, et al. The P2x7 receptor modulates immune cells infiltration, ectonucleotidases expression and extracellular atp levels in the tumor microenvironment. *Oncogene* (2019) 38(19):3636–50. doi: 10.1038/s41388-019-0684-y

28. Ghiringhelli F, Apetoh L, Tesniere A, Aymeric L, Ma Y, Ortiz C, et al. Activation of the Nlrp3 inflammasome in dendritic cells induces il-1beta-Dependent adaptive immunity against tumors. *Nat Med* (2009) 15(10):1170–8. doi: 10.1038/nm.2028

29. Kepp O, Bezu L, Yamazaki T, Di Virgilio F, Smyth MJ, Kroemer G, et al. Atp and cancer immunosurveillance. *EMBO J* (2021) 40(13):e108130. doi: 10.15252/embj.2021108130

30. de Andrade Mello P, Coutinho-Silva R, Savio LEB. Multifaceted effects of extracellular adenosine triphosphate and adenosine in the tumor-host interaction and therapeutic perspectives. *Front Immunol* (2017) 8:1526. doi: 10.3389/fimmu.2017.01526

31. Lara R, Adinolfi E, Harwood CA, Philpott M, Barden JA, Di Virgilio F, et al. P2x7 in cancer: From molecular mechanisms to therapeutics. *Front Pharmacol* (2020) 11:793. doi: 10.3389/fphar.2020.00793

32. Li XY, Moesta AK, Xiao C, Nakamura K, Casey M, Zhang H, et al. Targeting Cd39 in cancer reveals an extracellular atp- and inflammasome-driven tumor immunity. *Cancer Discov* (2019) 9(12):1754–73. doi: 10.1158/2159-8290.CD-19-0541

33. Yan J, Li XY, Roman Aguilera A, Xiao C, Jacoberger-Foissac C, Nowlan B, et al. Control of metastases *Via* myeloid Cd39 and nk cell effector function. *Cancer Immunol Res* (2020) 8(3):356–67. doi: 10.1158/2326-6066.CIR-19-0749

34. Allard B, Longhi MS, Robson SC, Stagg J. The ectonucleotidases Cd39 and Cd73: Novel checkpoint inhibitor targets. *Immunol Rev* (2017) 276(1):121–44. doi: 10.1111/imr.12528

35. Perrot I, Michaud HA, Giraudon-Paoli M, Augier S, Docquier A, Gros L, et al. Blocking antibodies targeting the Cd39/Cd73 immunosuppressive pathway unleash immune responses in combination cancer therapies. *Cell Rep* (2019) 27 (8):2411–25 e9. doi: 10.1016/j.celrep.2019.04.091

36. Huang S, Apasov S, Koshiba M, Sitkovsky M. Role of A2a extracellular adenosine receptor-mediated signaling in adenosine-mediated inhibition of T-cell activation and expansion. *Blood* (1997) 90(4):1600–10. doi: 10.1182/blood.v90.4.1600.1600_1600_1610

37. Ohta A, Gorelik E, Prasad SJ, Ronchese F, Lukashev D, Wong MK, et al. A2a adenosine receptor protects tumors from antitumor T cells. *Proc Natl Acad Sci U.S.A.* (2006) 103(35):13132–7. doi: 10.1073/pnas.0605251103

38. Ohta A, Sitkovsky M. Role of G-Protein-Coupled adenosine receptors in downregulation of inflammation and protection from tissue damage. *Nature* (2001) 414(6866):916–20. doi: 10.1038/414916a

39. Fong L, Hotson A, Powderly JD, Sznol M, Heist RS, Choueiri TK, et al. Adenosine 2a receptor blockade as an immunotherapy for treatment-refractory renal cell cancer. *Cancer Discov* (2020) 10(1):40–53. doi: 10.1158/2159-8290.Cd-19-0980

40. Sitkovsky MV. Lessons from the A2a adenosine receptor antagonist-enabled tumor regression and survival in patients with treatment-refractory renal cell cancer. *Cancer Discov* (2020) 10(1):16–9. doi: 10.1158/2159-8290.Cd-19-1280

41. Sitkovsky MV. Sufficient numbers of anti-tumor T cells is a condition of maximal efficacy of anti-Hypoxia-A2-Adenosinergic drugs during cancer immunotherapy. *Curr Opin Pharmacol* (2020) 53:98–100. doi: 10.1016/j.coph.2020.07.011

42. Willingham SB, Hotson AN, Miller RA. Targeting the A2ar in cancer; early lessons from the clinic. *Curr Opin Pharmacol* (2020) 53:126–33. doi: 10.1016/j.coph.2020.08.003

43. Demeules M, Scarpitta A, Abad C, Gonde H, Hardet R, Pinto-Espinoza C, et al. Evaluation of P2x7 receptor function in tumor contexts using raav vector and nanobodies (Aavnano). *Front Oncol* (2020) 10:1699. doi: 10.3389/fonc.2020.01699

44. Koch-Nolte F, Eichhoff A, Pinto-Espinoza C, Schwarz N, Schafer T, Menzel S, et al. Novel biologics targeting the P2x7 ion channel. *Curr Opin Pharmacol* (2019) 47:110–8. doi: 10.1016/j.coph.2019.03.001

45. Danquah W, Koch-Nolte F, Stortelers C, Toon L. Inventors; P2x7 receptor antagonists and agonists. (2013). Available at: https://patents.google.com/patent/WO2013178783A1/

46. Ingram JR, Dougan M, Rashidian M, Knoll M, Keliher EJ, Garrett S, et al. Pd-L1 is an activation-independent marker of brown adipocytes. *Nat Commun* (2017) 8(1):647. doi: 10.1038/s41467-017-00799-8

47. Stahler T, Danquah W, Demeules M, Gonde H, Hardet R, Haag F, et al. Development of antibody and nanobody tools for P2x7. *Methods Mol Biol* (2022) 2510:99–127. doi: 10.1007/978-1-0716-2384-8_6

48. Eden T, Menzel S, Wesolowski J, Bergmann P, Nissen M, Dubberke G, et al. A cdna immunization strategy to generate nanobodies against membrane proteins in native conformation. *Front Immunol* (2017) 8:1989. doi: 10.3389/fimmu.2017.01989

49. Koch-Nolte F, Reyelt J, Schossow B, Schwarz N, Scheuplein F, Rothenburg S, et al. Single domain antibodies from llama effectively and specifically block T cell ecto-Adp-Ribosyltransferase Art2.2 in vivo. *FASEB J* (2007) 21(13):3490–8. doi: 10.1096/fj.07-8661com

50. Ghetie V, Popov S, Borvak J, Radu C, Matesoi D, Medesan C, et al. Increasing the serum persistence of an igg fragment by random mutagenesis. *Nat Biotechnol* (1997) 15(7):637–40. doi: 10.1038/nbt0797-637

51. Scheuplein F, Rissiek B, Driver JP, Chen YG, Koch-Nolte F, Serreze DV. A recombinant heavy chain antibody approach blocks Art2 mediated deletion of an inkt cell population that upon activation inhibits autoimmune diabetes. *J Autoimmun* (2010) 34(2):145–54. doi: 10.1016/j.jaut.2009.08.012

52. Gu B, Bendall LJ, Wiley JS. Adenosine triphosphate-induced shedding of Cd23 and l-selectin (Cd62l) from lymphocytes is mediated by the same receptor but different metalloproteases. *Blood* (1998) 92(3):946–51. doi: 10.1182/blood.V92.3.946

53. Moon H, Na HY, Chong KH, Kim TJ. P2x7 receptor-dependent atp-induced shedding of Cd27 in mouse lymphocytes. *Immunol Lett* (2006) 102 (1):98–105. doi: 10.1016/j.imlet.2005.08.004

54. Beavis PA, Stagg J, Darcy PK, Smyth MJ. Cd73: A potent suppressor of antitumor immune responses. *Trends Immunol* (2012) 33(5):231–7. doi: 10.1016/j.it.2012.02.009

55. Giuliani AL, Sarti AC, Di Virgilio F. Extracellular nucleotides and nucleosides as signalling molecules. *Immunol Lett* (2019) 205:16–24. doi: 10.1016/j.imlet.2018.11.006

56. Balazs AB, Ouyang Y, Hong CM, Chen J, Nguyen SM, Rao DS, et al. Vectored immunoprophylaxis protects humanized mice from mucosal hiv transmission. *Nat Med* (2014) 20(3):296–300. doi: 10.1038/nm.3471

57. Saunders KO, Wang L, Joyce MG, Yang ZY, Balazs AB, Cheng C, et al. Broadly neutralizing human immunodeficiency virus type 1 antibody gene transfer protects nonhuman primates from mucosal simian-human immunodeficiency virus infection. *J Virol* (2015) 89(16):8334–45. doi: 10.1128/JVI.00908-15

58. Benzaquen J, Dit Hreich SJ, Heeke S, Juhel T, Lalvee S, Bauwens S, et al. P2rx7b is a new theranostic marker for lung adenocarcinoma patients. *Theranostics* (2020) 10(24):10849–60. doi: 10.7150/thno.48229

59. Benzaquen J, Heeke S, Janho Dit Hreich S, Douguet L, Marquette CH, Hofman P, et al. Alternative splicing of P2rx7 pre-messenger rna in health and diseases: Myth or reality? *BioMed J* (2019) 42(3):141–54. doi: 10.1016/j.bj.2019.05.007

60. Giuliani AL, Colognesi D, Ricco T, Roncato C, Capece M, Amoroso F, et al. Trophic activity of human P2x7 receptor isoforms a and b in osteosarcoma. *PloS One* (2014) 9(9):e107224. doi: 10.1371/journal.pone.0107224

61. Pegoraro A, De Marchi E, Adinolfi E. P2x7 variants in oncogenesis. *Cells* (2021) 10(1). doi: 10.3390/cells10010189

62. Vangsted AJ, Klausen TW, Gimsing P, Abildgaard N, Andersen NF, Gang AO, et al. Genetic variants in the P2rx7 gene are associated with risk of multiple myeloma. *Eur J Haematol* (2014) 93(2):172–4. doi: 10.1111/ejh.12353

63. Neo SY, Yang Y, Record J, Ma R, Chen X, Chen Z, et al. Cd73 immune checkpoint defines regulatory nk cells within the tumor microenvironment. *J Clin Invest* (2020) 130(3):1185–98. doi: 10.1172/JCI128895

frontiers | Frontiers in Immunology

TYPE Original Research
PUBLISHED 27 October 2022
DOI 10.3389/fimmu.2022.1010270

OPEN ACCESS

EDITED BY
Zahra Sharifzadeh,
Pasteur Institute of Iran, Iran

REVIEWED BY
Olga Mulas,
Università di Cagliari, Italy
Weijun Wei,
Shanghai Jiao Tong University, China
Mattia D'Agostino,
University of Turin, Italy

*CORRESPONDENCE
Peter Bannas
p.bannas@uke.de

†These authors share senior authorship

SPECIALTY SECTION
This article was submitted to Cancer Immunity and Immunotherapy, a section of the journal Frontiers in Immunology

RECEIVED 02 August 2022
ACCEPTED 03 October 2022
PUBLISHED 27 October 2022

CITATION
Pape LJ, Hambach J, Gebhardt AJ, Rissiek B, Stähler T, Tode N, Khan C, Weisel K, Adam G, Koch-Nolte F and Bannas P (2022) CD38-specific nanobodies allow *in vivo* imaging of multiple myeloma under daratumumab therapy. *Front. Immunol.* 13:1010270. doi: 10.3389/fimmu.2022.1010270

CD38-specific nanobodies allow *in vivo* imaging of multiple myeloma under daratumumab therapy

Luca Julius Pape[1,2], Julia Hambach[1,2], Anna Josephine Gebhardt[1,2], Björn Rissiek[3], Tobias Stähler[2], Natalie Tode[2], Cerusch Khan[1,2], Katja Weisel[4], Gerhard Adam[1], Friedrich Koch-Nolte[2†] and Peter Bannas[1*†]

[1]Department of Diagnostic and Interventional Radiology and Nuclear Medicine, University Medical Center Hamburg-Eppendorf, Hamburg, Germany, [2]Institute of Immunology, University Medical Center Hamburg-Eppendorf, Hamburg, Germany, [3]Department of Neurology, University Medical Center Hamburg-Eppendorf, Hamburg, Germany, [4]Department of Oncology, Hematology and Bone Marrow Transplantation, University Medical Center Hamburg-Eppendorf, Hamburg, Germany

Rationale: Recent studies have demonstrated the feasibility of CD38-specific antibody constructs for *in vivo* imaging of multiple myeloma. However, detecting multiple myeloma in daratumumab-pretreated patients remains difficult due to overlapping binding epitopes of the CD38-specific imaging antibody constructs and daratumumab. Therefore, the development of an alternative antibody construct targeting an epitope of CD38 distinct from that of daratumumab is needed. We report the generation of a fluorochrome-conjugated nanobody recognizing such an epitope of CD38 to detect myeloma cells under daratumumab therapy *in vitro*, *ex vivo*, and *in vivo*.

Methods: We conjugated the CD38-specific nanobody JK36 to the near-infrared fluorescent dye Alexa Fluor 680. The capacity of $JK36^{AF680}$ to bind and detect CD38-expressing cells pretreated with daratumumab was evaluated on CD38-expressing tumor cell lines *in vitro*, on primary myeloma cells from human bone marrow biopsies *ex vivo*, and in a mouse tumor model *in vivo*.

Results: Fluorochrome-labeled nanobody $JK36^{AF680}$ showed specific binding to CD38-expressing myeloma cells pretreated with daratumumab *in vitro* and *ex vivo* and allowed for specific imaging of CD38-expressing xenografts in daratumumab-pretreated mice *in vivo*.

Conclusions: Our study demonstrates that a nanobody recognizing a distinct, non-overlapping epitope of CD38 allows the specific detection of myeloma cells under daratumumab therapy *in vitro*, *ex vivo*, and *in vivo*.

KEYWORDS

CD38, daratumumab, multiple myeloma, nanobody, fluorescence imaging, flow cytometry

Introduction

CD38 is a major target for the therapy of multiple myeloma (MM). Daratumumab is a CD38-specific monoclonal antibody with high efficacy as monotherapy or combination therapy for relapsed and newly diagnosed multiple myeloma (1–4). Daratumumab therapy has been integrated into international treatment guidelines and has become the standard of care (5). Reliable and accurate assessment of treatment response is needed even in the presence of therapeutic daratumumab plasma levels. Unfortunately, this presents a diagnostic challenge since daratumumab interferes both with flow cytometry (6–9) as well as with free light chain assays (10) and serum immunofixation electrophoresis (11).

Myeloma manifestations can alternatively be detected *in vivo* by cross-sectional imaging techniques such as whole-body computed tomography, magnetic resonance imaging (12), and ^{18}F-FDG-positron emission tomography (PET) (13–15). These imaging techniques detect medullary and extramedullary myeloma lesions with high sensitivity (16). However, these techniques do not allow monitoring of CD38 expression or prediction of susceptibility to daratumumab treatment since they are not antigen-specific to CD38.

Immuno-positron emission tomography using radiolabeled CD38-specific antibodies overcomes this challenge, thereby enabling the detection and visualization of CD38-expressing myeloma cells *in vivo* (17–20). Unfortunately, detecting multiple myeloma in daratumumab-pretreated patients remains difficult due to overlapping binding epitopes of currently available CD38-specific imaging antibody constructs and daratumumab. Therefore, the development of alternative antibody constructs targeting a different epitope of CD38 is needed.

Nanobodies are single variable immunoglobulin domains derived from camelid heavy-chain antibodies (21). CD38-specific nanobodies can be used either for the treatment of multiple myeloma by generation of nanobody-based heavy-chain antibodies (hcAbs) (22–26), nanobody-based CARs (27), and nanobody-based BiKEs (28), or for *in vivo* imaging of multiple myeloma (29). Their small molecular size (Figures 1A, B), low immunogenicity, and ease of formatting make them ideally suited for *in vivo* imaging purposes (21, 30–33).

The aim of our study was to generate a fluorochrome-conjugated nanobody recognizing an epitope of CD38 distinct from that of daratumumab to detect tumor cells under daratumumab therapy *in vitro*, *ex vivo*, and *in vivo*.

Materials and methods

Cell lines

Three human multiple myeloma cell lines (LP-1, U266, RPMI-8226), two human Burkitt lymphoma cell lines (Daudi and CA-46), and a murine B cell lymphoma cell line (YAC-1) were obtained from the German Collection of Microorganisms and Cell Culture (DSMZ, Braunschweig, Germany). Human cell lines were chosen due to their uniform expression of CD38. Stable expression of *Photinus pyralis* luciferase (Promega, Madison, WI, USA) in Daudi luc, CA-46 luc, YAC-1 luc, and LP-1 luc cell lines was achieved by lentiviral transduction as

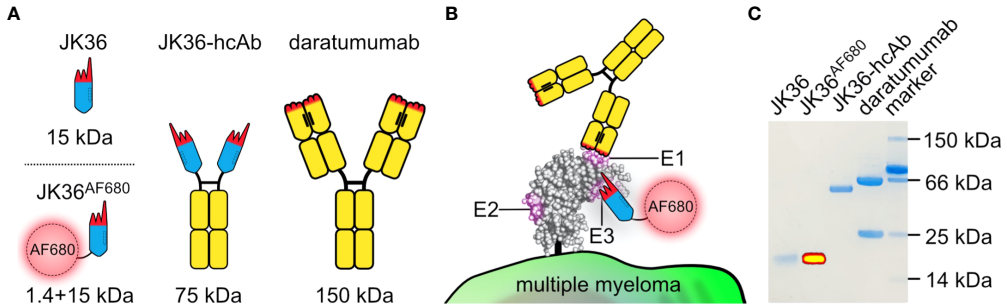

FIGURE 1
Structure, binding sites, and purity of JK36^{AF680} nanobody, JK36 heavy chain antibody, and daratumumab. **(A)** Comparison of different antibody constructs targeting CD38. The framework of single-domain antibody (nanobody) JK36 is indicated in blue with the CDR-regions indicated in red. Heavy-chain antibody JK36-hcAb consists of two heavy chains each containing nanobody JK36 fused to the hinge (black), CH2, and CH3 domains (yellow) of human IgG1. The conventional human IgG1 mAb daratumumab is also indicated in black and yellow. The hydrophobic interface between the two variable domains of daratumumab is replaced by a corresponding hydrophilic region in JK36, accounting for the excellent solubility of this VHH domain in absence of a light chain. **(B)** Daratumumab (epitope E1) and JK36^{AF680} (epitope E3) recognize two distinct, non-overlapping epitopes (E1 and E3) of CD38. Epitope 2 (E2) is recognized by nanobody JK2 (not shown) and was used in our study for control staining of CD38. **(C)** 1 µg of purified JK36^{AF680}, JK36-hcAb, and daratumumab were size-fractionated by SDS-PAGE and visualized by Coomassie staining. Superimposed fluorescent signals (yellow) were recorded using a near-infrared fluorescence *in vivo* imaging system.

10.3389/fimmu.2022.1010270

described previously (25, 34). YAC-1 luc cells were stably transfected with human CD38 using the expression vector pEF-DEST51 (29), yielding YAC-1 CD38+ cells. Untransfected YAC-1 cells served as negative controls.

Production and labeling of antibody constructs

Human CD38-specific nanobody JK36 was generated from an immunized llama as described previously (29, 35). His/myc-tagged nanobody JK36 was produced in HEK293-6E cells and purified from supernatants using immobilized metal affinity chromatography (29). Nanobody JK36 was labeled with the fluorescent dye Alexa Fluor 680 ($JK36^{AF680}$) according to the manufacturer's instructions using succinimidyl esters (Invitrogen, Karlsbad, CA, USA).

Heavy chain antibodies (hcAbs) JK36-hcAb and isotype control L-15-hcAb were generated by subcloning the coding region of nanobody JK36 and isotype control nanobody L-15 upstream of the coding region for the hinge, CH2, and CH3 domains of human IgG1 in the pCSE2.5 vector (kindly provided by Thomas Schirrmann, University of Braunschweig, Braunschweig, Germany) (24). HcAbs were produced in HEK293-6E cells and purified from supernatants by affinity chromatography using protein A sepharose (36, 37). Daratumumab (Darzalex) was purchased from Janssen-Cilag, Neuss, Germany.

The purity of antibody constructs was assessed by SDS-PAGE and InstantBlue™ Coomassie staining. Alexa Fluor 680-labeling of nanobody JK36 was controlled by imaging fluorescence levels using the IVIS-200 *in vivo* imaging device (PerkinElmer, Waltham, MA, USA).

Monoclonal antibody $HIT2^{PerCP/Cy5.5}$ was purchased from Becton Dickinson, Franklin Lakes, NJ, USA (25).

Flow cytometry

For CD38-expression analyses, CD38-positive cells and CD38-negative control cells were incubated with $JK36^{AF680}$ (0,2 µl in 100 µl PBS/BSA) at 4 °C for 30 min. Cells were washed twice and analyzed using a FACS Canto II flow cytometer and FlowJo software (Becton Dickinson, Franklin Lakes, NJ, USA).

CD38 pretreatment (i.e., cross-blockade) analyses were performed by pre-incubating cells with an excess (200 nM) of daratumumab or JK36-hcAb at 4 °C for 30 min. Cells were then incubated with nanobody $JK36^{AF680}$ (1:500 in PBS/BSA) to detect unblocked epitopes using flow cytometry.

Biolayer interferometry

The extracellular domain of human CD38 (aa 46-300) was produced, purified, and biotinylated as described previously (22, 28). Biolayer interferometry analysis was performed at 20°C in kinetic buffer (PBS containing 1% bovine serum albumin, and 0.005% (v/v) polysorbate 80 (Tween 80, Sigma-Aldrich, St. Louis, MO, USA)). For individual antibodies, concentrations of 500 nM per antibody were used while antibody combinations were analyzed at a concentration of 250 nM per antibody to allow for complete saturation of CD38. Biolayer interferometry measurements were carried out using a BLItz system (FortéBio, Fremont, CA, USA).

Streptavidin-coated biosensors were placed in wells containing only kinetic buffer for 30 seconds to establish a baseline signal. Sensors were then transferred to wells containing the biotinylated extracellular domain of human CD38 for 90 seconds to allow for association of CD38 to the sensor. This was followed by 30 seconds of dissociation in kinetic buffer. CD38-coated sensors were subsequently dipped into wells containing the blocking antibody daratumumab for 90 seconds to saturate epitope E1. Sensors were then moved to wells containing both the blocking antibody daratumumab and a second antibody (daratumumab, JK36-hcAb, or L-15-hcAb) for 90 seconds. This permitted assessment of binding of the second antibody to CD38 in the presence of the blocking antibody as opposed to solely evaluating binding to CD38. This protocol considers any possible inhibitory effects that excess unbound daratumumab might have on secondary antibody binding. A final washing step in kinetic buffer was performed for 90 seconds to monitor the dissociation of CD38-bound antibodies. The resulting dataset was plotted using GraphPad Prism 9.3.1 (GraphPad Software, CA, USA).

Fluorescence microscopy

YAC-1 CD38+ cells were incubated with an excess of daratumumab (3 µg/100 µl), JK36-hcAb (3 µg/100 µl), or no blocking agent at 4 °C for 20 min. Cells were washed once with PBS/0,02% BSA. Cells were then resuspended in 100 µl PBS/BSA containing $JK36^{AF680}$ at a dilution of 1:500 and diamidino-phenylindole (DAPI) at a dilution of 1:5000 (v/v) and incubated at 4 °C for 20 min to stain CD38 and nuclei, respectively. Stained cells were washed twice before resuspension in 100 µl of PBS/BSA. Twenty µl of each sample was subsequently placed on a glass microscopy slide without addition of a fixative agent. Cell samples were then captured using a Zeiss Axio Observer microscope with a 40x EC Plan-

Apochromat Oil lens. Microscopic images were analyzed using ZEN Pro 3.4 software (Zeiss, Oberkochen, Germany) and Affinity Designer 1.10.5 (Serif, Nottingham, UK).

Flow cytometric analysis of primary human bone marrow samples

Aspiration of fresh bone marrow was approved by the Institutional Review Board (PV5505). Fresh bone marrow aspirates were collected from nine newly diagnosed, untreated multiple myeloma patients. Ficoll-Paque density gradient centrifugation (Sigma-Aldrich, St. Louis, MO, USA) was carried out to isolate bone marrow mononuclear cells (BM-MNCs). Remaining erythrocytes were depleted by resuspending the resulting cell pellet in red cell lysis buffer (NH4Cl + KHCO3 + EDTA).

BM-MNCs were stained using PacO and a panel of fluorochrome-labeled antibodies targeting CD19, CD38, CD39, CD45, CD55, CD56, CD59, CD138, CD229, CD319 and analyzed by flow cytometry to determine the degree of bone marrow infiltration with malignant plasma cells (27). Multiple myeloma cells were identified by high expression of CD38.

Blocking assays were carried out by incubating BM-MNCs without (positive control) or with 100 nM of daratumumab or JK36-hcAb in PBS/BSA at 4 °C for 30 min. After one washing step, detection nanobody JK36^{AF680} was added for another 30 min. Mean fluorescence intensities (MFI) of bound nanobody JK36^{AF680} were assessed by flow cytometry. Relative fluorescence intensities (%) of multiple myeloma cells labeled with nanobody JK36^{AF680} were calculated as follows:

$$relative\ \ fluorescence\ \ intensity_{sample}\ [\%] = \frac{MFI\ \ (AF680)_{sample}}{MFI\ \ (AF680)_{positive\ \ control}} x100\,\%$$

Significant differences in relative fluorescence intensities were calculated by using one-way ANOVA (GraphPad Prism 9.3.1).

In vivo and *ex vivo* imaging

Animal experiments were approved by the local animal welfare commission (N069/2018). Six-week-old female NMRI Foxn1nu mice were acquired from Charles River (Charles River Laboratories, Sulzfeld, Germany) and kept in their cages for two weeks. Eight-week-old mice were kept on an alfalfa-free diet for one week prior to *in vivo* imaging experiments to reduce autofluorescence of the intestine (38).

Tumors were generated by subcutaneously injecting mice with 1x10^7 CD38-negative YAC-1 cells on the left shoulder and 5x10^6 CD38-positive YAC-1 cells on the right shoulder in 0.2 µl of 50% RPMI and 50% Matrigel (Becton Dickinson, Franklin Lakes, NJ, USA). This established murine lymphoma model (29) was chosen because the reliable subcutaneous growth of YAC-1 cells allows for intraindividual comparison of antigen-positive and antigen-negative tumors using near-infrared fluorescence imaging. This would not have been feasible using a disseminated human myeloma model. Numbers of injected cells were adjusted to account for the slightly slower growth rate of CD38-negative vs. CD38-positive YAC-1 cells. Tumor locations at shoulder level were chosen to maximize the distance to the kidneys and liver, which had shown high fluorescence signals in previous studies (29, 33). After six days, mice (total, n=30) were intravenously injected with either 100 µl of isotonic saline containing 500 µg of daratumumab (n=10 mice) (Janssen Biotech, Horsham, PA, USA), 250 µg of JK36-hcAb (n=10 mice), or no blocking agent (n=10 mice). After 24 hours, mice were intravenously injected with 50 µg of JK36^{AF680}.

In vivo near-infrared fluorescence imaging was performed under isoflurane anesthesia before and 2, 4, 6, 12, and 24 hours after injection of JK36^{AF680} using a small animal imaging system (IVIS-200, PerkinElmer, Waltham, MA, USA) (29). After qualitative imaging *in vivo*, quantitative off-line analyses were performed by placing ROIs around CD38-positive tumors, CD38-negative tumors (negative control), and the hind limb (background signal). Total radiant efficiency was determined with Living Image 4.2 software (PerkinElmer) and the background value was subtracted. Tumor-to-background ratios were calculated by dividing the tumor uptake value by the background value. Radiant efficiencies and tumor-to-background ratios were compared between treatment groups using a mixed-effect analysis with Tukey's multiple comparison test (GraphPad Prism 9.3.1).

For *ex vivo* validation of *in vivo* measurements, three mice from each treatment group were sacrificed six hours after injection. Tumors and organs (muscle, spleen, lungs, liver, kidneys, stomach, intestine) were dissected and imaged *ex vivo* with the IVIS-200 system.

Ex vivo flow cytometric analyses of cells from explanted subcutaneous tumors

Single cell suspensions from explanted and dissected CD38-positive and CD38-negative tumors were generated by passage through a cell strainer with a pore size of 70 µm (Corning Life Sciences, Corning, NY, USA).

Cell surface levels of CD38 on resuspended tumor cells were determined using hcAb JK2 rabbit IgG, which binds a third epitope of CD38 distinct from that of both daratumumab and JK36-hcAb. Bound JK2-hcAb was detected with a rabbit IgG-specific, R-phycoerythrin-conjugated secondary antibody (Cat.-No. 711-116-152, Jackson ImmunoResearch, Ely, UK) (29).

Quantification of *in vivo* injected and tumor-bound blocking antibodies daratumumab and JK36-hcAb was performed by labeling resuspended tumor cells with an R-phycoerythrin-conjugated human IgG-specific secondary antibody (Cat.-No. 709-116-149, Jackson ImmunoResearch). Mean fluorescence intensities were obtained by flow cytometry to determine and compare binding (i.e. blocking efficiencies) of daratumumab and JK36-hcAb.

Quantification of *in vivo* injected and tumor-bound imaging nanobody JK36^{AF680} was performed by flow cytometric analysis of resuspended tumor cells. Mean fluorescence intensities of CD38-labeling efficiencies with JK36^{AF680} were compared between groups of mice pre-treated with either daratumumab, JK36-hcAb, or saline.

To determine the maximum achievable labeling efficiency of CD38 with JK36^{AF680}, cells were labeled *ex vivo* with saturating doses (100 nM) of JK36^{AF680}.

CD38-positive and CD38-negative YAC-1 luc cells from cell culture were incubated as described above and served as controls.

Results

Purity of nanobody JK36, JK36-hcAb, and daratumumab was confirmed by SDS-PAGE analyses. Successful labeling of purified nanobody JK36 with Alexa Fluor 680 (JK36^{AF680}) was verified by imaging of the SDS-PAGE gel with the *in vivo* imaging system (Figure 1C).

Simultaneous binding of nanobody JK36 and daratumumab to purified CD38

Biolayer interferometry was used to determine whether nanobody JK36 and daratumumab bind simultaneously to CD38. After binding of biotinylated CD38 to a streptavidin-coated sensor, blocking antibody daratumumab and secondary antibodies (JK36-hcAb, daratumumab, or isotype control L-15-hcAb) were added sequentially (Figure 2).

The results show an increase in signal intensities upon the addition of the blocking antibody daratumumab. After adding the secondary antibody JK36-hcAb, a strong increase in signal intensity was observed, indicating simultaneous binding of daratumumab and JK36-hcAb. In contrast, adding daratumumab as a secondary antibody did not lead to further signal increase, indicating saturated binding of daratumumab as the primary antibody to CD38. Isotype control L-15-hcAb also did not lead to a signal increase, indicating specific binding of JK36-hcAb to CD38.

These results demonstrate that nanobody JK36 and daratumumab bind independently and simultaneously to CD38.

Specific binding of nanobody JK36^{AF680} to daratumumab-pretreated myeloma cells *in vitro* and *ex vivo*

In vitro binding of nanobody JK36^{AF680} to daratumumab-pretreated cells was assessed using five human (LP-1, U266, RPMI-8226, CA46, Daudi) lymphoma cell lines, and one murine lymphoma cell line transfected with human CD38 (YAC-1 CD38+) (Figure 3A). CD38-specific monoclonal antibody HIT2$^{PerCP/Cy5.5}$ was used as control. Cells were incubated without or with saturating doses of daratumumab and then stained with nanobody JK36^{AF680} or monoclonal antibody HIT2$^{PerCP/Cy5.5}$ followed by flow cytometry.

The results show that both nanobody JK36^{AF680} and monoclonal antibody HIT2$^{PerCP/Cy5.5}$ bound to all six CD38-expressing cell lines. Pretreatment with daratumumab almost completely blocked binding of HIT2$^{PerCP/Cy5.5}$, indicating that daratumumab and HIT2 bind to overlapping epitopes on CD38. Pretreatment with daratumumab did not block binding of JK36^{AF680}, confirming independent binding of nanobody JK36 and daratumumab. Pretreatment of cells with heavy chain antibody JK36-hcAb completely blocked the binding of nanobody JK36^{AF680}, confirming specific binding to human CD38.

Ex vivo binding of nanobody JK36^{AF680} to daratumumab-pretreated primary myeloma cells was assessed using cell

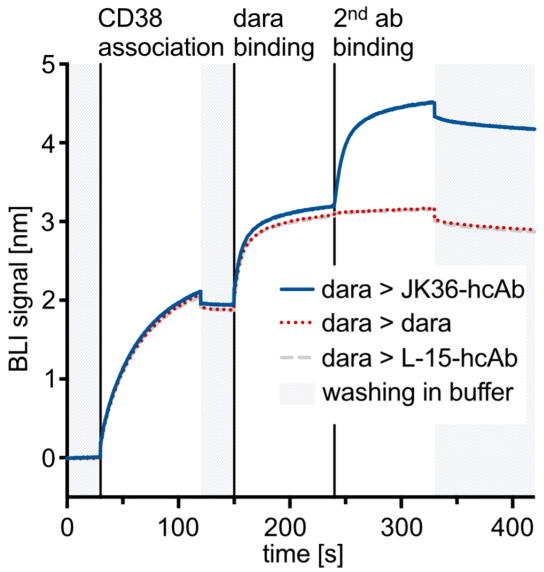

FIGURE 2
Biolayer interferometry sensograms demonstrating simultaneous binding of nanobody-based JK36-hcAb and daratumumab to purified CD38. Streptavidin-coated biosensors were used to capture the biotinylated extracellular domain of CD38. Sensors were then dipped into wells containing daratumumab in excess before being transferred to wells containing both daratumumab and secondary antibodies at the indicated time points. An increase in signal indicates binding to the sensor. Dissociation was allowed by washing in buffer and is indicated in grey.

10.3389/fimmu.2022.1010270

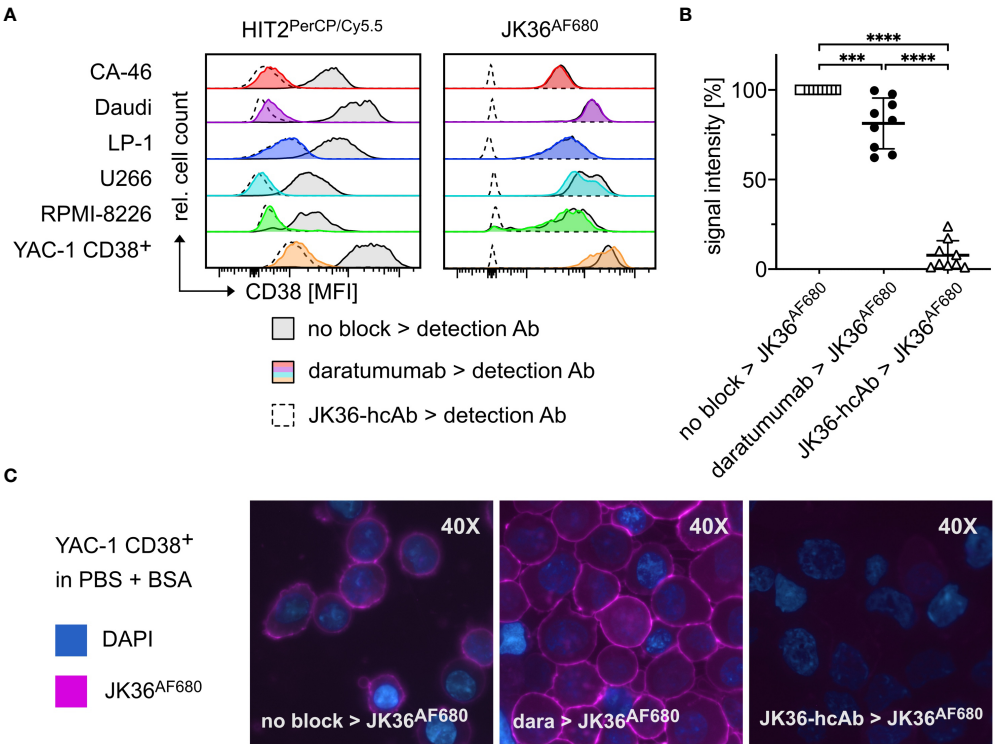

FIGURE 3
Specific binding of nanobody JK36^{AF680} to daratumumab-pretreated myeloma cells *in vitro* and *ex vivo*. **(A)** FACS analyses of CD38+ CA-46, Daudi, LP-1, U266, RPMI-8226, and YAC-1 CD38+ cells. Cells were saturated with daratumumab before detection of CD38 with the CD38-specific diagnostic antibody HIT2$^{PerCP/Cy5.5}$ (left) or the CD38-specific nanobody JK36^{AF680} (right). Cells saturated with JK36-hcAb served as negative controls since previous experiments had shown complete blocking of both JK36^{AF680} and HIT2$^{PerCP/Cy5.5}$ binding after incubation with JK36-hcAb. Untreated cells were used as positive controls and indicate CD38 expression of the cell line. **(B)** Bone marrow aspirates of human multiple myeloma patients were pre-incubated without (open rectangles, positive control) or with saturating doses of daratumumab (black circles) or JK36-hcAb (open triangles, negative control). CD38 was then labeled using JK36^{AF680} and cells were analyzed by flow cytometry for comparison of epitope blocking by daratumumab and JK36-hcAb. Signal intensities were compared using one-way ANOVA with Tukey's multiple comparisons test (****= p<0.0001, ***=p<0.001). Depicted are means ± SD. Results are representative of nine independent experiments. **(C)** Fluorescence microscopy analyses of YAC-1 CD38+ cells. Cells were incubated with PBS/BSA (left panel), daratumumab (middle panel), or JK36-hcAb (right panel) before the addition of JK36^{AF680}. DAPI was used to stain nuclei. Results are representative of three independent experiments.

suspensions from human bone marrow biopsies from patients with multiple myeloma (Figure 3B). The results confirmed specific labeling of daratumumab-pretreated primary myeloma cells with nanobody JK36^{AF680}. Again, pretreatment of cells with heavy chain antibody JK36-hcAb completely blocked the binding of nanobody JK36^{AF680}.

Fluorescence microscopy of JK36^{AF680}-labeled YAC-1 CD38 + cells revealed prominent staining of the cell surface (Figure 3C). Pretreatment with daratumumab did not affect cell surface labeling with JK36^{AF680}, while pretreatment with JK36-hcAb completely blocked binding of JK36^{AF680}.

These results demonstrate that nanobody JK36^{AF680} can be used for the specific detection of daratumumab-pretreated CD38-expressing cells *in vitro* and *ex vivo* and therefore warrants further evaluation for imaging of CD38-expressing tumors *in vivo*.

Nanobody JK36^{AF680} allows specific imaging of daratumumab-pretreated CD38-positive tumors *in vivo*

In vivo imaging experiments using nanobody JK36^{AF680} were performed in mice carrying tumors derived from subcutaneously injected YAC-1 cells. All mice were bearing two subcutaneous tumors for comparative analyses of *in vivo* imaging signals: one CD38-positive tumor on the right shoulder and one CD38-negative control tumor on the left shoulder. *In vivo* near-infrared fluorescence imaging with nanobody JK36^{AF680} was performed in mice pretreated for 24 hours with either isotonic saline (positive control), daratumumab, or JK36-hcAb (negative or specificity control) (Figure 4).

The results demonstrate specific binding of nanobody JK36^{AF680} to CD38-positive tumors in both saline-pretreated

and daratumumab-pretreated mice as early as two hours after injection. Pretreatment of mice with JK36-hcAb resulted in a strong reduction in imaging signals from CD38-positive tumors, confirming specific binding of JK36^{AF680} to CD38 *in vivo*.

At early time points after injection of JK36^{AF680}, strong signals were also observed in the kidneys in all animals, reflecting passage of nanobody JK36 through the renal filtration barrier. Additionally, CD38-negative tumors showed signal intensities slightly above background signals at early time points, likely reflecting perfusion of tumors with blood containing unbound JK36^{AF680}. The unspecific signal from CD38-negative tumors and kidneys decreased over time, while signal intensities remained high in the CD38-positive tumors for six hours, confirming specific binding of JK36^{AF680} only to tumors expressing CD38.

ROI analyses confirmed a rapidly increasing signal in CD38-positive tumors and little if any signal in CD38-negative tumors and background tissue (Figure 5A). At all time points, there was no statistically significant difference in signal intensities of CD38-positive tumors between saline-pretreated and daratumumab-pretreated mice. Pretreatment with JK36-hcAb resulted in a significant decrease in CD38-positive tumor signal intensities.

Calculation of tumor-to-background ratios (T/B-ratio) confirmed a rapidly increasing T/B-ratio of CD38-positive tumors after injection of JK36^{AF680} in both saline-pretreated and daratumumab-pretreated mice (Figure 5B). The T/B-ratio of CD38-positive tumors reached a maximum of 3.12 ± 1.43 after six hours in saline pretreated animals, compared to 2.54 ± 1.04 in daratumumab-pretreated animals (p=0.5049). Also, there was no statistically significant difference in T/B-ratios of CD38-positive tumors between saline-pretreated and daratumumab-pretreated mice at all other time points. CD38-negative tumors revealed significantly lower T/B-ratios when compared to CD38-positive tumors in all three treatment groups, again confirming specific binding of nanobody JK36^{AF680} to human CD38.

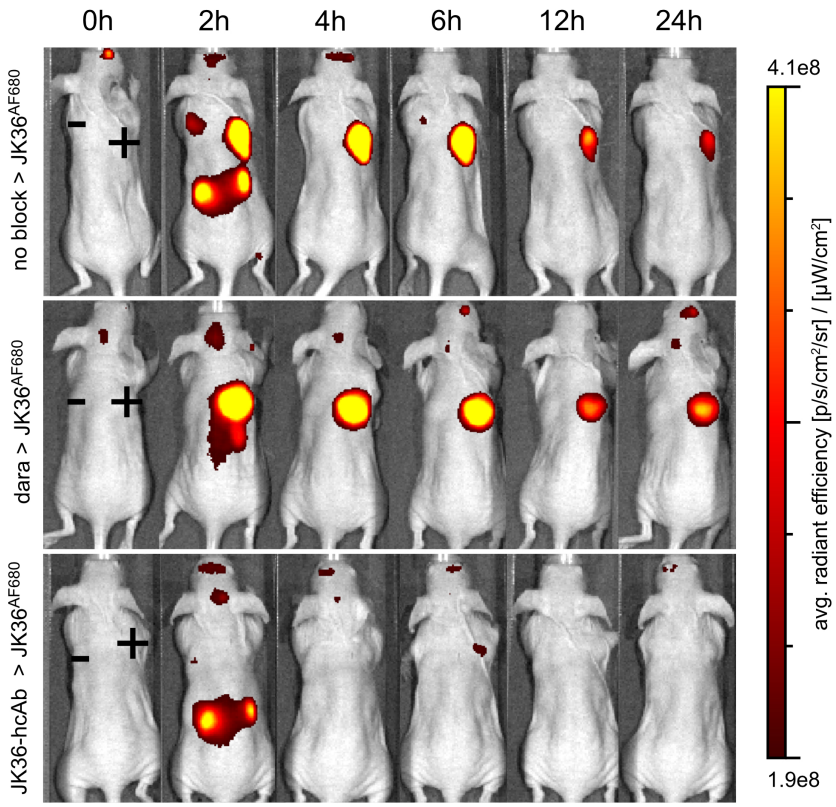

FIGURE 4
Specific *in vivo* imaging of subcutaneous CD38+ tumors using nanobody JK36^{AF680} in saline-, daratumumab-, and JK36-hcAb-pretreated mice. All mice were analyzed six days after subcutaneous injection of CD38-positive YAC-1 cells on the right shoulder (+) and CD38-negative YAC-1 cells on the left shoulder (-). Prior to imaging, mice were pretreated for 24 hours with either isotonic saline (n=10, positive control, top row), daratumumab (n=10, middle row), or JK36-hcAb (n=10, specificity control, bottom row). Near-infrared fluorescence *in vivo* imaging was performed before (0h) and at the indicated time points after the injection of 50 µg of nanobody JK36^{AF680}. Signal intensities of all injected mice and imaging time points are all equally leveled to allow direct and fair visual comparison.

10.3389/fimmu.2022.1010270

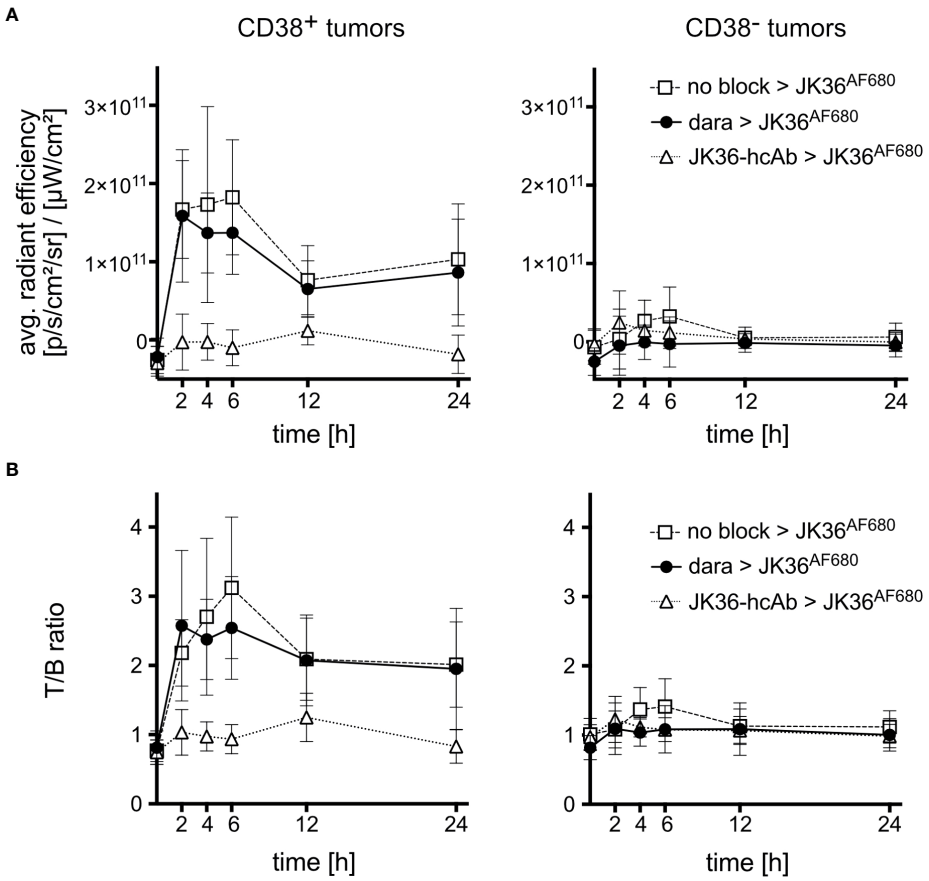

FIGURE 5
Average radiant efficiencies and tumor-to-background ratios of CD38-positive and CD38-negative tumors *in vivo*. Mice were pretreated for 24 hours with either isotonic saline (n=10, positive control, open rectangles), daratumumab (n=10, black circles), or JK36-hcAb (n=10, specificity control, open triangles). Near-infrared fluorescence *in vivo* imaging was performed before and at the indicated time points after injection of nanobody JK36^{AF680}. **(A)** Average radiant efficiencies were determined from circular regions of interest (ROIs) drawn around CD38-positive and CD38-negative tumors. Signal intensities were corrected for background signal. **(B)** Tumor-to-background ratios were obtained by dividing tumor signals by background signals obtained from ROIs drawn around normal tissue (hind leg). At all time points, there was no statistically significant difference in signal intensities and T/B-ratios of CD38-positive tumors between saline-pretreated and daratumumab-pretreated mice, as indicated by overlapping 95%-confidence intervals.

Ex vivo analyses of cells from explanted tumors

Ex vivo near-infrared fluorescence imaging of dissected individual organs six hours post-injection confirmed specific uptake of JK36^{AF680} in CD38-positive tumors in both saline-pretreated and daratumumab-pretreated mice (Figure 6A). JK36-hcAb-pretreated animals showed no specific uptake of JK36^{AF680}. Signals in most other tissues, including CD38-negative tumors, returned to background levels, with low fluorescent signals still detectable in the kidneys. While the liver itself showed only background fluorescence, fluorescent signals in the gallbladder likely reflect biliary excretion of fluorochromes.

Ex vivo flow cytometric analyses of CD38-positive tumors was performed six hours post-injection to quantify the relative amount of *in vivo* injected and still tumor-bound JK36^{AF680} (Figure 6B). Flow cytometry of tumor cells suspensions showed specific labeling of CD38-positive cells with JK36^{AF680} in both saline-pretreated and daratumumab-pretreated mice and no specific labeling of CD38-negative tumor cells. The *ex vivo* observed flow cytometric fluorescence signal obtained by *in vivo* injection of JK36^{AF680} was low in saline-pretreated and daratumumab-pretreated groups, while there was no binding of JK36^{AF680} to JK36-hcAb pretreated cells.

Additional *ex vivo* staining using JK36^{AF680} resulted in strong labeling of CD38-positive cells obtained from saline-pretreated mice. In contrast, additional *ex vivo* staining with JK36^{AF680} of daratumumab-pretreated and JK36-hcAb-

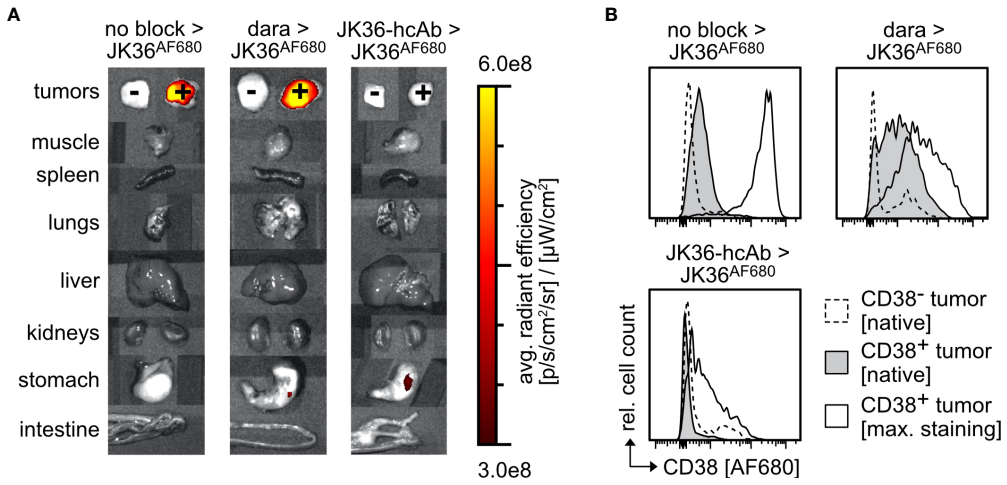

FIGURE 6
Ex vivo analyses of cells from CD38$^+$ and CD38$^-$ tumors explanted from mice 6 hours and 24 hours post-injection of JK36^{AF680}. **(A)** Fluorescence levels of individual tumors and organs explanted from mice pretreated with isotonic saline, daratumumab, or JK36-hcAb 6 hours after injection of JK36^{AF680}. **(B)** Histograms depicting median fluorescence intensities of the AF680 channel in mice after pretreatment with isotonic saline, daratumumab, or JK36-hcAb, obtained from tumors explanted 24 hours after injection of JK36^{AF680}. Dashed histograms represent native AF680 signals of the CD38$^-$ control tumor, grey histograms represent native AF680 signals of the CD38$^+$ tumor, open histograms represent the maximum AF680 signal obtained after *ex vivo* staining of CD38$^+$ tumor cells with JK36^{AF680}. Each panel is a representative example of n=10 per treatment group. Cell debris was initially excluded by setting an appropriate FSC-A threshold before gating on single cells. YAC-1 cells were then identified by co-expression of CD38 (using nanobody JK2, identifying the remaining free epitope of CD38) and GFP.

pretreated mice resulted in weaker staining, possibly reflecting downregulation of CD38 due to therapeutic effects of daratumumab and JK36-hcAb *in vivo* during the 24 hours of pretreatment and six hours imaging period.

Discussion

Our study demonstrates that a nanobody recognizing a distinct, non-overlapping epitope of CD38 allows the detection of myeloma cells pretreated with daratumumab. Nanobody JK36^{AF680} specifically detected CD38-expressing tumor cells *in vitro*, *ex vivo*, and *in vivo* irrespective of daratumumab treatment status.

JK36^{AF680} therefore represents a promising tool to overcome current clinical challenges in the assessment of treatment response in daratumumab-pretreated multiple myeloma patients (6, 10, 11). The possibility to detect and monitor CD38-expressing myeloma cells in daratumumab-pretreated patients is of increasing importance considering the increasingly broader indications for daratumumab treatment (39, 40).

Previous studies demonstrated the feasibility of fluorophore- or radionuclide-labeled daratumumab for *in vivo* imaging purposes of CD38-expressing myeloma cells (19, 20, 41). However, targeting the same epitope as daratumumab is only effective in daratumumab-naive patients. It would instead be expedient to use other labeled antibody constructs that target an epitope of CD38 distinct from that of daratumumab. This would allow not only to image untreated patients but also daratumumab-pretreated patients.

Instead of using a conventional monoclonal antibody, we used nanobody JK36^{AF680}, recognizing a distinct, non-overlapping epitope of CD38 for demonstrating the feasibility of specific imaging of daratumumab-pretreated CD38-expressing tumors. Key advantages of using nanobodies over conventional antibodies for *in vivo* diagnostic purposes include greater ease of production (42) as well as more favorable imaging kinetics: nanobodies allow for excellent tumor-to-background ratios as early as 6 hours post-injection and for same-day *in vivo* imaging (33, 41), owing to the rapid elimination of excess unbound nanobodies by renal filtration. Furthermore, the risk of allergic infusion reactions is reduced when using nanobodies as opposed to conventional antibodies, owing to their low immunogenicity (43). This possibly explains the lack of infusion reactions in patients receiving caplacizumab, the first FDA-approved nanobody (44).

Additionally, a recent study revealed that our nanobody JK36 detects myeloma cells from daratumumab-treated patients with greater sensitivity than a commercially available CD38-specific multi-epitope reagent (6). Here we show that JK36 also detects CD38-expressing tumor cells with greater sensitivity

than monoclonal antibody HIT2$^{PerCP/Cy5.5}$ which is currently being used in flow cytometric assays (45–47) to assess treatment response in patients receiving daratumumab.

Isatuximab, the second FDA-approved CD38-specific monoclonal antibody, binds to a different epitope of CD38 than daratumumab (48). Further studies are warranted to evaluate the feasibility of nanobody-based imaging of multiple myeloma under isatuximab therapy, possibly using a different nanobody than JK36.

An inherent limitation of our study is the use of near-infrared fluorescent dyes for *in vivo* imaging. The signal intensity of fluorochromes such as AlexaFluor680 decreases with increasing tissue depth, precluding cross-sectional imaging of human patients (49). This limitation, however, could be overcome by coupling nanobody JK36 to a radionuclide such as ^{68}Ga ^{64}Cu or ^{99}Tc, which would allow imaging by PET or SPECT (17, 19, 50, 51).

Since CD38 is not only expressed on myeloma cells but also on other cells (52), some level of on-target off-tissue signal is expected when using CD38-specific nanobodies for *in vivo* imaging purposes. This, however, is not a limitation of nanobody JK36 but rather a ubiquitous phenomenon when employing antibody-based imaging strategies.

In summary, we have demonstrated that a nanobody recognizing an epitope on CD38 distinct from that of daratumumab allows the specific detection of myeloma cells pretreated with daratumumab *in vitro*, *ex vivo*, and *in vivo*. Future studies using radiolabeled nanobody JK36 are warranted to investigate the potential for clinical imaging of daratumumab-pretreated human multiple myeloma patients.

Data availability statement

The raw data supporting the conclusions of this article will be made available by the authors, without undue reservation.

Ethics statement

The studies involving human participants were reviewed and approved by Hamburger Ärztekammer. The patients/participants provided their written informed consent to participate in this study. The animal study was reviewed and approved by Behörde für Justiz und Verbraucherschutz.

Author contributions

PB and FK-N conceived the project. All authors carried out experiments or analyzed data. LP, PB, and FK-N wrote the manuscript. All authors contributed to the article and approved the submitted version.

Funding

Supported by grants from the Deutsche Forschungsgemeinschaft to PB (BA 5893/7), FK-N (No. 31016 and SFB1328-Z02), and BR (SFB1328-Z02). LP was financially supported by the Else-Kröner-Fresenius-Stiftung iPRIME scholarship (2021_EKPK.10), UKE, Hamburg.

Acknowledgments

We thank Fabienne Seyfried, Institute of Immunology, and Michael Horn, University Cancer Center Hamburg, for their excellent technical assistance. We thank the UCCH *In Vivo* Optical Imaging Core Facility and the UKE Microscopic Imaging Facility (UMIF) for their excellent support.

Conflict of interest

FK-N receives a share of antibody sales via MediGate GmbH, a wholly-owned subsidiary of the University Medical Center Hamburg-Eppendorf. PB and FK-N are co-inventors on a patent application on CD38-specific nanobodies.

The remaining authors declare that the research was conducted in the absence of any commercial or financial relationships that could be construed as a potential conflict of interest.

Publisher's note

References

1. Palumbo A, Chanan-Khan A, Weisel K, Nooka AK, Masszi T, Beksac M, et al. Daratumumab, bortezomib, and dexamethasone for multiple myeloma. *N Engl J Med* (2016) 375(8):754–66. doi: 10.1056/NEJMoa1606038

2. Facon T, Kumar S, Plesner T, Orlowski RZ, Moreau P, Bahlis N, et al. Daratumumab plus lenalidomide and dexamethasone for untreated myeloma. *N Engl J Med* (2019) 380(22):2104–15. doi: 10.1056/NEJMoa1817249

3. Lonial S, Weiss BM, Usmani SZ, Singhal S, Chari A, Bahlis NJ, et al. Daratumumab monotherapy in patients with treatment-refractory multiple myeloma (SIRIUS): an open-label, randomised, phase 2 trial. *Lancet* (2016) 387 (10027):1551–60. doi: 10.1016/S0140-6736(15)01120-4

4. Usmani SZ, Nahi H, Plesner T, Weiss BM, Bahlis NJ, Belch A, et al. Daratumumab monotherapy in patients with heavily pretreated relapsed or refractory multiple myeloma: final results from the phase 2 GEN501 and SIRIUS trials. *Lancet Haematol* (2020) 7(6):e447–55. doi: 10.1016/S2352-3026(20) 30081-8

5. Dimopoulos MA, Moreau P, Terpos E, Mateos MV, Zweegman S, Cook G, et al. Multiple myeloma: EHA-ESMO clinical practice guidelines for diagnosis, treatment and follow-up(†). *Ann Oncol* (2021) 32(3):309–22. doi: 10.1016/ j.annonc.2020.11.014

6. Oberle A, Brandt A, Alawi M, Langebrake C, Janjetovic S, Wolschke C, et al. Long-term CD38 saturation by daratumumab interferes with diagnostic myeloma cell detection. *Haematologica* (2017) 102(9):e368–70. doi: 10.3324/ haematol.2017.169235

7. Mizuta S, Kawata T, Kawabata H, Yamane N, Mononobe S, Komai T, et al. VS38 as a promising CD38 substitute antibody for flow cytometric detection of plasma cells in the daratumumab era. *Int J Hematol* (2019) 110(3):322–30. doi: 10.1007/s12185-019-02685-z

8. Chopra S, Dunham T, Syrbu SI, Karandikar NJ, Darbro BW, Holman CJ. Utility of flow cytometry and fluorescence *In situ* hybridization in follow-up monitoring of plasma cell myeloma. *Am J Clin Pathol* (2021) 156(2):198–204. doi: 10.1093/ajcp/aqaa224

9. Courville EL, Yohe S, Shivers P, Linden MA. VS38 identifies myeloma cells with dim CD38 expression and plasma cells following daratumumab therapy, which interferes with CD38 detection for 4 to 6 months. *Am J Clin Pathology*. (2019) 153(2):221–8. doi: 10.1093/ajcp/aqz153

10. Rosenberg AS, Bainbridge S, Pahwa R, Jialal I. Investigation into the interference of the monoclonal antibody daratumumab on the free light chain assay. *Clin Biochem* (2016) 49(15):1202–4. doi: 10.1016/j.clinbiochem.2016.07.016

11. van de Donk NW, Otten HG, El Haddad O, Axel A, Sasser AK, Croockewit S, et al. Interference of daratumumab in monitoring multiple myeloma patients using serum immunofixation electrophoresis can be abrogated using the daratumumab IFE reflex assay (DIRA). *Clin Chem Lab Med* (2016) 54(6):1105–9. doi: 10.1515/cclm-2015-0888

12. Bannas P, Hentschel HB, Bley TA, Treszl A, Eulenburg C, Derlin T, et al. Diagnostic performance of whole-body MRI for the detection of persistent or relapsing disease in multiple myeloma after stem cell transplantation. *Eur Radiol* (2012) 22(9):2007–12. doi: 10.1007/s00330-012-2445-y

13. Mosebach J, Thierjung H, Schlemmer HP, Delorme S. Multiple myeloma guidelines and their recent updates: Implications for imaging. *Rofo* (2019) 191 (11):998–1009. doi: 10.1055/a-0897-3966

14. Rajkumar SV, Dimopoulos MA, Palumbo A, Blade J, Merlini G, Mateos MV, et al. International myeloma working group updated criteria for the diagnosis of multiple myeloma. *Lancet Oncol* (2014) 15(12):e538–48. doi: 10.1016/S1470-2045(14)70442-5

15. Derlin T, Peldschus K, Münster S, Bannas P, Herrmann J, Stübig T, et al. Comparative diagnostic performance of 18F-FDG PET/CT versus whole-body MRI for determination of remission status in multiple myeloma after stem cell transplantation. *Eur Radiology* (2013) 23(2):570–8. doi: 10.1007/s00330-012-2600-5

16. Derlin T, Bannas P. Imaging of multiple myeloma: Current concepts. *World J Orthop* (2014) 5(3):272–82. doi: 10.5312/wjo.v5.i3.272

17. Wang C, Chen Y, Hou YN, Liu Q, Zhang D, Zhao H, et al. ImmunoPET imaging of multiple myeloma with [(68)Ga]Ga-NOTA-Nb1053. *Eur J Nucl Med Mol Imaging*. (2021) 48(9):2749–60. doi: 10.1007/s00259-021-05218-1

18. Kang L, Jiang D, England CG, Barnhart TE, Yu B, Rosenkrans ZT, et al. ImmunoPET imaging of CD38 in murine lymphoma models using (89)Zr-labeled daratumumab. *Eur J Nucl Med Mol Imaging* (2018) 45(8):1372–81. doi: 10.1007/ s00259-018-3941-3

19. Kang L, Li C, Yang Q, Sutherlin L, Wang L, Chen Z, et al. (64)Cu-labeled daratumumab F(ab')2 fragment enables early visualization of CD38-positive lymphoma. *Eur J Nucl Med Mol Imaging* (2021) 49:1470–81. doi: 10.1007/ s00259-021-05593-9

20. Ulaner GA, Sobol NB, O'Donoghue JA, Kirov AS, Riedl CC, Min R, et al. CD38-targeted immuno-PET of multiple myeloma: From xenograft models to first-in-Human imaging. *Radiology* (2020) 295(3):606–15. doi: 10.1148/ radiol.2020192621

21. Wesolowski J, Alzogaray V, Reyelt J, Unger M, Juarez K, Urrutia M, et al. Single domain antibodies: promising experimental and therapeutic tools in infection and immunity. *Med Microbiol Immunol* (2009) 198(3):157–74. doi: 10.1007/s00430-009-0116-7

22. Baum N, Eggers M, Koenigsdorf J, Menzel S, Hambach J, Staehler T, et al. Mouse CD38-specific heavy chain antibodies inhibit CD38 GDPR-cyclase activity and mediate cytotoxicity against tumor cells. *Front Immunol* (2021) 12:703574. doi: 10.3389/fimmu.2021.703574

23. Baum N, Fliegert R, Bauche A, Hambach J, Menzel S, Haag F, et al. Daratumumab and nanobody-based heavy chain antibodies inhibit the ADPR cyclase but not the NAD(+) hydrolase activity of CD38-expressing multiple myeloma cells. *Cancers (Basel)* (2020) 13(1):76. doi: 10.3390/cancers13010076

24. Schutze K, Petry K, Hambach J, Schuster N, Fumey W, Schriewer L, et al. CD38-specific biparatopic heavy chain antibodies display potent complement-dependent cytotoxicity against multiple myeloma cells. *Front Immunol* (2018) 9:2553. doi: 10.3389/fimmu.2018.02553

25. Schriewer L, Schutze K, Petry K, Hambach J, Fumey W, Koenigsdorf J, et al. Nanobody-based CD38-specific heavy chain antibodies induce killing of multiple myeloma and other hematological malignancies. *Theranostics* (2020) 10(6):2645–58. doi: 10.7150/thno.38533

26. Bannas P, Koch-Nolte F. Perspectives for the development of CD38-specific heavy chain antibodies as therapeutics for multiple myeloma. *Front Immunol* (2018) 9:2559. doi: 10.3389/fimmu.2018.02559

27. Hambach J, Riecken K, Cichutek S, Schutze K, Albrecht B, Petry K, et al. Targeting CD38-expressing multiple myeloma and burkitt lymphoma cells in vitro with nanobody-based chimeric antigen receptors (Nb-CARs) 9(1):321. *Cells* (2020) 9(2). doi: 10.3390/cells9020321

28. Hambach J, Fumey W, Staehler T, Gebhardt AJ, Adam G, Weisel K, et al. Half-life extended nanobody-based CD38-specific bispecific killercell engagers induce killing of multiple myeloma cells. *Front Immunol* (2022) 13:838406. doi: 10.3389/fimmu.2022.838406

29. Fumey W, Koenigsdorf J, Kunick V, Menzel S, Schutze K, Unger M, et al. Nanobodies effectively modulate the enzymatic activity of CD38 and allow specific imaging of CD38(+) tumors in mouse models in vivo. *Sci Rep* (2017) 7(1):14289. doi: 10.1038/s41598-017-14112-6

30. Ackaert C, Smiejkowska N, Xavier C, Sterckx YGJ, Denies S, Stijlemans B, et al. Immunogenicity risk profile of nanobodies. *Front Immunol* (2021) 12. doi: 10.3389/fimmu.2021.632687

31. Bannas P, Well L, Lenz A, Rissiek B, Haag F, Schmid J, et al. *In vivo* near-infrared fluorescence targeting of T cells: comparison of nanobodies and conventional monoclonal antibodies. *Contrast Media Mol Imaging*. (2014) 9 (2):135–42. doi: 10.1002/cmmi.1548

32. Bannas P, Lenz A, Kunick V, Fumey W, Rissiek B, Schmid J, et al. Validation of nanobody and antibody based in vivo tumor xenograft NIRF-imaging experiments in mice using ex vivo flow cytometry and microscopy. *J Vis Exp* (2015) 98):e52462. doi: 10.3791/52462

33. Bannas P, Lenz A, Kunick V, Well L, Fumey W, Rissiek B, et al. Molecular imaging of tumors with nanobodies and antibodies: Timing and dosage are crucial factors for improved *in vivo* detection. *Contrast Media Mol Imaging* (2015) 10 (5):367–78. doi: 10.1002/cmmi.1637

34. Weber K, Mock U, Petrowitz B, Bartsch U, Fehse B. Lentiviral gene ontology (LeGO) vectors equipped with novel drug-selectable fluorescent proteins: new building blocks for cell marking and multi-gene analysis. *Gene Ther* (2010) 17 (4):511–20. doi: 10.1038/gt.2009.149

35. Koch-Nolte F, Glowacki G, Bannas P, Braasch F, Dubberke G, Ortolan E, et al. Use of genetic immunization to raise antibodies recognizing toxin-related cell surface ADP-ribosyltransferases in native conformation. *Cell Immunol* (2005) 236 (1-2):66–71. doi: 10.1016/j.cellimm.2005.08.033

36. Zhang J, Liu X, Bell A, To R, Baral TN, Azizi A, et al. Transient expression and purification of chimeric heavy chain antibodies. *Protein Expr Purif* (2009) 65 (1):77–82. doi: 10.1016/j.pep.2008.10.011

37. Danquah W, Meyer-Schwesinger C, Rissiek B, Pinto C, Serracant-Prat A, Amadi M, et al. Nanobodies that block gating of the P2X7 ion channel ameliorate inflammation. *Sci Transl Med* (2016) 8(366):366ra162. doi: 10.1126/ scitranslmed.aaf8463

38. Inoue Y, Izawa K, Kiryu S, Tojo A, Ohtomo K. Diet and abdominal autofluorescence detected by *in vivo* fluorescence imaging of living mice. *Mol Imaging* (2008) 7(1):21–7. doi: 10.2310/7290.2008.0003

39. Cowan AJ, Allen C, Barac A, Basaleem H, Bensenor I, Curado MP, et al. Global burden of multiple myeloma: A systematic analysis for the global burden of disease study 2016. *JAMA Oncol* (2018) 4(9):1221–7. doi: 10.1001/jamaoncol.2018.2128

40. Nooka AK, Kaufman JL, Hofmeister CC, Joseph NS, Heffner TL, Gupta VA, et al. Daratumumab in multiple myeloma. *Cancer* (2019) 125(14):2364–82. doi: 10.1002/cncr.32065

41. Cho N, Ko S, Shokeen M. Preclinical development of near-Infrared-Labeled CD38-targeted daratumumab for optical imaging of CD38 in multiple myeloma. *Mol Imaging Biol* (2021) 23(2):186–95. doi: 10.1007/s11307-020-01542-4

42. Muyldermans S. Nanobodies: Natural single-domain antibodies. *Annu Rev Biochem* (2013) 82(1):775–97. doi: 10.1146/annurev-biochem-063011-092449

43. Cortez-Retamozo V, Lauwereys M, Hassanzadeh Gh G, Gobert M, Conrath K, Muyldermans S, et al. Efficient tumor targeting by single-domain antibody fragments of camels. *Int J Cancer* (2002) 98(3):456–62. doi: 10.1002/ijc.10212

44. Pascual Izquierdo MC, Mingot-Castellano ME, Kerguelen Fuentes AE, García-Arroba Peinado J, Cid J, Jiménez M, et al. Real-world effectiveness of caplacizumab vs standard of care in immune thrombotic thrombocytopenic purpura. *Blood Adv* (2022). doi: 10.1182/bloodadvances.2022008028

45. Pojero F, Flores-Montero J, Sanoja L, Perez JJ, Puig N, Paiva B, et al. Utility of CD54, CD229, and CD319 for the identification of plasma cells in patients with clonal plasma cell diseases. *Cytometry B Clin Cytom* (2016) 90(1):91–100. doi: 10.1002/cyto.b.21269

46. Broijl A, de Jong ACM, van Duin M, Sonneveld P, Kühnau J, van der Velden VHJ. VS38c and CD38-multiepitope antibodies provide highly comparable minimal residual disease data in patients with multiple myeloma. *Am J Clin Pathol* (2022) 157(4):494–7. doi: 10.1093/ajcp/aqab163

47. Rawstron AC, Child JA, de Tute RM, Davies FE, Gregory WM, Bell SE, et al. Minimal residual disease assessed by multiparameter flow cytometry in multiple myeloma: Impact on outcome in the medical research council myeloma IX study. *J Clin Oncol* (2013) 31(20):2540–7. doi: 10.1200/JCO.2012.46.2119

48. Lee HT, Kim Y, Park UB, Jeong TJ, Lee SH, Heo Y-S. Crystal structure of CD38 in complex with daratumumab, a first-in-class anti-CD38 antibody drug for treating multiple myeloma. *Biochem Biophys Res Commun* (2021) 536:26–31. doi: 10.1016/j.bbrc.2020.12.048

49. Mérian J, Gravier J, Navarro F, Texier I. Fluorescent nanoprobes dedicated to in vivo imaging: From preclinical validations to clinical translation. *Molecules* (2012) 17(5):5564–91. doi: 10.3390/molecules17055564

50. Duray E, Lejeune M, Baron F, Beguin Y, Devoogdt N, Krasniqi A, et al. A non-internalised CD38-binding radiolabelled single-domain antibody fragment to monitor and treat multiple myeloma. *J Hematol Oncol* (2021) 14(1):183. doi: 10.1186/s13045-021-01171-6

51. Krishnan A, Adhikarla V, Poku EK, Palmer J, Chaudhry A, Biglang-Awa VE, et al. Identifying CD38+ cells in patients with multiple myeloma: first-in-human imaging using copper-64-labeled daratumumab. *Blood Adv* (2020) 4 (20):5194–202. doi: 10.1182/bloodadvances.2020002603

52. Krejcik J, Casneuf T, Nijhof IS, Verbist B, Bald J, Plesner T, et al. Daratumumab depletes CD38+ immune regulatory cells, promotes T-cell expansion, and skews T-cell repertoire in multiple myeloma. *Blood* (2016) 128 (3):384–94. doi: 10.1182/blood-2015-12-687749

frontiers | Frontiers in Immunology

TYPE Review
PUBLISHED 02 November 2022
DOI 10.3389/fimmu.2022.1005800

OPEN ACCESS

EDITED BY
Zahra Sharifzadeh,
Pasteur Institute of Iran, Iran

REVIEWED BY
Rintu Thomas,
Baylor College of Medicine,
United States
Mehdi Yousefi,
Tabriz University of Medical Sciences,
Iran

*CORRESPONDENCE
Friedrich Koch-Nolte
nolte@uke.de

†These authors share senior authorship

SPECIALTY SECTION
This article was submitted to
Cancer Immunity
and Immunotherapy,
a section of the journal
Frontiers in Immunology

RECEIVED 28 July 2022
ACCEPTED 21 October 2022
PUBLISHED 02 November 2022

CITATION
Hambach J, Mann AM, Bannas P and
Koch-Nolte F (2022) Targeting
multiple myeloma with nanobody-
based heavy chain antibodies,
bispecific killer cell engagers, chimeric
antigen receptors, and nanobody-
displaying AAV vectors.
Front. Immunol. 13:1005800.
doi: 10.3389/fimmu.2022.1005800

Targeting multiple myeloma with nanobody-based heavy chain antibodies, bispecific killer cell engagers, chimeric antigen receptors, and nanobody-displaying AAV vectors

Julia Hambach[1,2], Anna Marei Mann[1], Peter Bannas[2†] and Friedrich Koch-Nolte[1*†]

[1]Institute of Immunology, University Medical Center Hamburg-Eppendorf, Hamburg, Germany, [2]Department of Diagnostic and Interventional Radiology and Nuclear Medicine, University Medical Center Hamburg-Eppendorf, Hamburg, Germany

Nanobodies are well suited for constructing biologics due to their high solubility. We generated nanobodies directed against CD38, a tumor marker that is overexpressed by multiple myeloma and other hematological malignancies. We then used these CD38-specific nanobodies to construct heavy chain antibodies, bispecific killer cell engagers (BiKEs), chimeric antigen receptor (CAR)-NK cells, and nanobody-displaying AAV vectors. Here we review the utility of these nanobody-based constructs to specifically and effectively target CD38-expressing myeloma cells. The promising results of our preclinical studies warrant further clinical studies to evaluate the potential of these CD38-specific nanobody-based constructs for treatment of multiple myeloma.

KEYWORDS

nanobody, multiple myeloma, CAR, heavy chain antibodies, BiKE, AAV, VHH, CD38

Introduction

Nanobodies are highly soluble, single variable immunoglobulin domains derived from heavy chain antibodies (hcAbs) that naturally occur in llamas and other camelids (Figure 1A). Due to a splice site mutation, hcAbs lack the CH1 domain of a conventional antibody and do not pair with a light chain (1). Nanobodies contain a hydrophilic region in place of the hydrophobic patch that mediates pairing of VH and VL domains in conventional antibodies (2). Nanobodies thus display a much higher solubility and better developability than individual variable domains or single chain variable fragments (scFv)

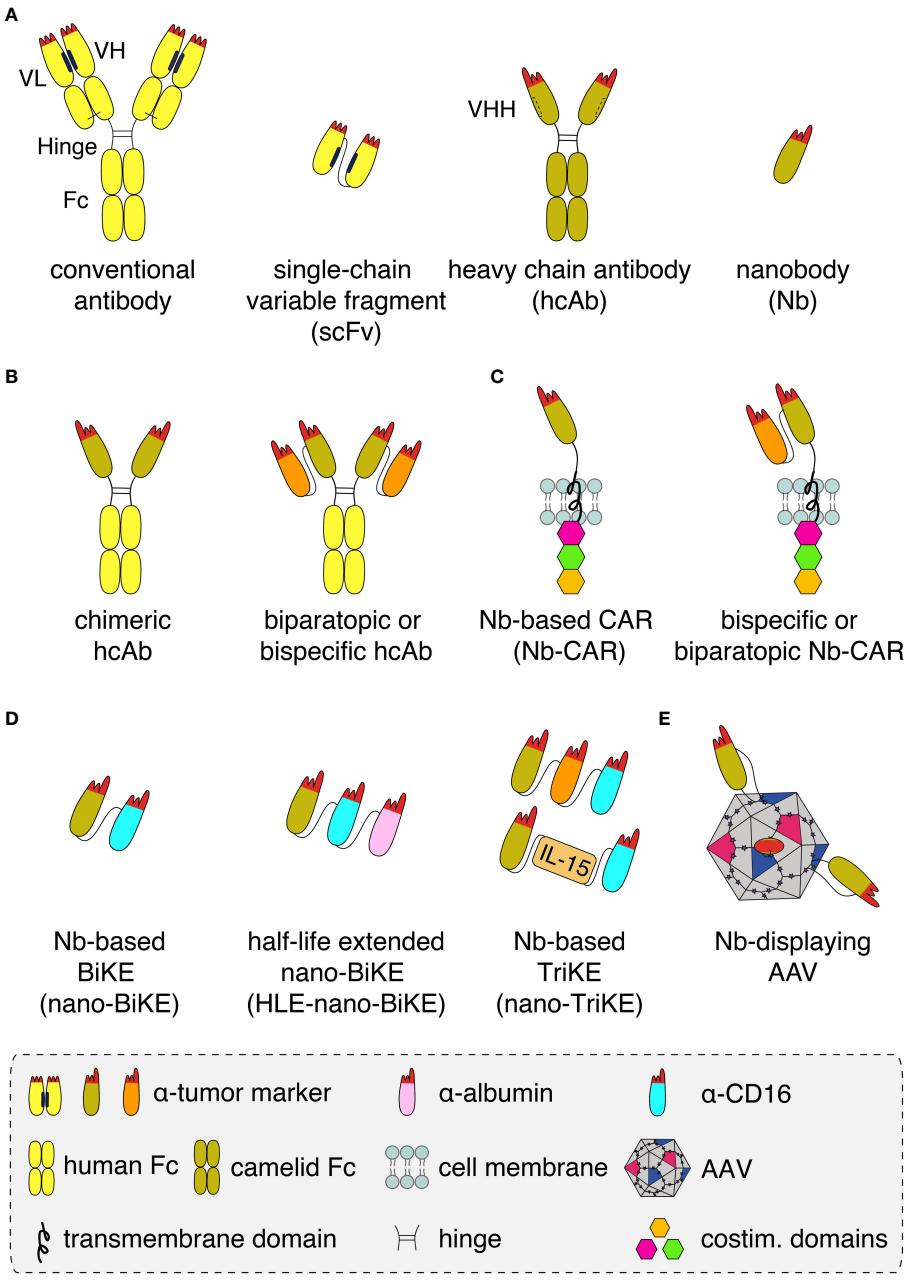

FIGURE 1
Schematics of nanobody-based biologics **(A)** Conventional antibodies (yellow) contain light and heavy chains that pair *via* hydrophobic regions (black bars) in the framework of the VL and VH domains and by a disulphide bond (light black line) between the CL and CH1 domains. The complementarity-determining regions (red) of VH and VL together form the antigen-binding paratope. A recombinant antigen-binding module, i.e. a single chain variable fragment (scFv), can be derived from a conventional antibody by genetically fusing the VH and VL domains *via* a peptide linker. Heavy chain antibodies (hcAb, olive) derived from llamas lack the light chain and the CH1 domain. A hydrophilic patch (dashed bar) of the VHH domain in place of the corresponding hydrophobic region of a VH domain accounts for the excellent solubility of recombinant VHH domains, i.e. nanobodies (Nb), that allows easy fusion to other proteins and/or Nbs. **(B)** Nanobodies can be converted into hcAbs of any isotype by genetic fusion to hinge, CH2 and CH3 domains, e.g. of human IgG1. Genetic fusion to a second nanobody that recognizes either a second epitope on the same target antigen or a distinct target (orange), results in a biparatopic or a bispecific hcAb, respectively. **(C)** Genetic fusion of one or two nanobodies to a transmembrane domain and to cytosolic costimulatory domains yields a monomeric, biparatopic or bispecific chimeric antigen receptor (CAR) that can be transduced into T cells or NK cells. **(D)** Fusion of one or two tumor marker-specific nanobodies to a nanobody recognizing the Fc-receptor of NK cells (CD16, light blue) yields bispecific or trispecific killer cell engagers (nano-BiKEs or nano-TriKEs). As an alternative to a second tumor-specific nanobody, IL-15 can be fused to a tumor marker-specific nanobody and a CD16-specific nanobody to generate a nano-TriKE. Half-life extension (HLE) of these molecules can be achieved by genetic fusion to an albumin-specific nanobody (magenta). **(E)** Genetic fusion of a membrane protein-specific nanobody into an exposed surface loop of the VP1 capsid protein yields a targeted nanobody-displaying adeno-associated viral vector (AAV) that specifically transduces cells expressing the target antigen.

derived from conventional antibodies. These properties make them particularly suited for specific and efficient targeting of tumor antigens *in vivo* (3, 4).

Nanobodies can be used in a LEGO brick like fashion for the construction of a wide variety of nanobody-based biologics, including biparatopic and bispecific reagents (Figures 1B–E). Caplacizumab, the first nanobody-based therapeutic approved for clinical use in 2019, is a genetic fusion of two identical nanobodies against the van Willebrandt factor linked *via* a peptide linker. Caplacizumab is approved for the treatment of acquired thrombotic thrombocytopenic purpura (5). Ciltacel, a nanobody-based therapeutic that recently received fast-track approval by the FDA for the therapy of multiple myeloma, is a biparatopic chimeric antigen receptor (CAR) containing two genetically linked nanobodies fused to the transmembrane and signal transduction modules of different T cell membrane proteins (Figure 1C). The two nanobodies recognize non-overlapping epitopes of B cell maturation antigen (BCMA), a cell surface receptor of the TNF superfamily expressed by mature B cells and often overexpressed by multiple myeloma cells (6–9). Remarkably, in order to achieve complete remission, tenfold lower cell numbers are required for CAR-T cells expressing this nanobody-based biparatopic receptor compared to CAR-T cells expressing a single BCMA-specific nanobody. This is thought to reflect the higher affinity, higher stability, and/or lower unspecific off-target binding of the BCMA-specific nanobodies compared to scFvs and conventional VHs (10, 11).

Multiple myeloma is a hematological malignancy that is characterized by the uncontrollable expansion of malignant plasma cells in the bone marrow (12–14). Survival of myeloma patients has improved with new drugs and autologous stem cell transplantation. Despite this progress, the majority of myeloma patients relapse (15–18), underlining the need for more effective treatment options with higher specificity and fewer side effects (15, 19, 20).

CD38 is a type II transmembrane glycoprotein whose extracellular domain is an enzyme that hydrolyzes NAD+. Multiple myeloma cells and other hematological malignancies overexpress CD38. This makes it an interesting target for immunotherapy. Since CD38 is part of the purinergic-signaling cascade that converts NAD+ into immunosuppressive adenosine, the overexpression of CD38 on tumor cells is thought to contribute to an anti-inflammatory tumor microenvironment (21, 22).

Daratumumab and isatuximab are CD38-specific monoclonal antibodies that have been approved for the treatment of multiple myeloma in newly diagnosed and relapsed myeloma patients (23). Genmab isolated daratumumab from human immunoglobulin transgenic mice immunized with CD38 (24, 25). Isatuximab is a chimeric CD38 specific antibody developed by Sanofi from immunized mice (26). Other CD38 specific antibodies such as TAK-079 and MOR202 have also entered clinical trials (23). We have generated CD38-specific nanobodies from immunized llamas (27). Here, we focus on the reformatting of CD38-specific nanobodies into potential immunotherapeutics. The insights gained may be applied also to nanobodies directed against other tumor targets.

CD38-specific nanobody-based antibody constructs

We have generated nanobodies from llamas using genetic immunization that bind to three independent epitopes of CD38 (27, 28). For both, daratumumab and isatuximab, we have identified nanobodies that bind independent epitopes, i.e. they stain cells that are already covered with daratumumab or isatuximab (27, 29). Such nanobodies are useful for detecting CD38 on the cell surface in patients undergoing daratumumab or isatuximab therapy (30).

We used these CD38-specific nanobodies to generate CD38-specific nanobody-based heavy chain antibodies (hcAbs), chimeric antigen receptor CAR-NK cells, bispecific killer cell engagers (BiKEs), and nanobody-displaying adeno-associated viruses (AAVs) (Figures 1B–E) (27, 29, 31–34). Some of these have been radiolabeled and tested as tools for the *in vivo* imaging of multiple myeloma (35). Similarly, the group of Yong Juan Zhao has selected a panel of CD38-specific nanobodies from immunized Bactrian camels (36). One of these, 1G3, was used to generate CD38-specific nanobody-based CAR-T cells (36). Caers et al. radiolabeled some of our nanobodies and the nanobodies by Zhao et al. as a tool for studying fratricide of NK cells under daratumumab therapy (37).

Nanobody-based heavy chain antibodies (hcAbs)

Binding of therapeutic antibodies to a target cell can induce various effector functions including antibody-dependent cellular cytotoxicity (ADCC), complement dependent cytotoxicity (CDC), antibody-dependent cellular phagocytosis (ADCP), and antibody-induced apoptosis (38). ADCC was shown to be a major mode of action of daratumumab (39, 40). In ADCC, the Fc-part of an antibody bound to the target cell is recognized by the Fc-receptor CD16 on an NK cell (Figure 2A). This activates the NK cell to release perforins, which ultimately lyse the target cell by forming pores.

Genetic fusion of a nanobody with the hinge and Fc-domains of human IgG1 generates a chimeric heavy chain antibody (hcAb) (Figures 1B, 2A) (41, 42). We generated such CD38-specific nanobody-based hcAbs and evaluated their potential to induce ADCC and CDC (29, 32). These hcAbs

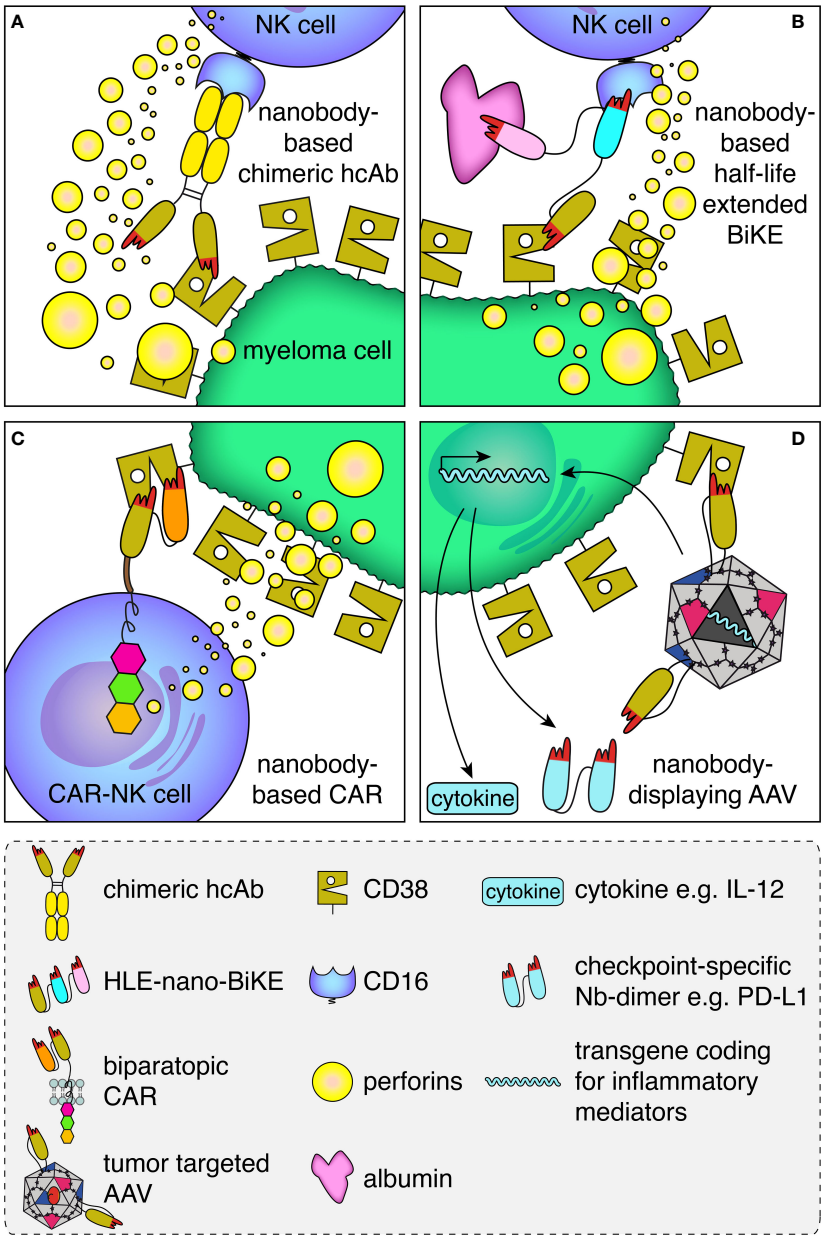

FIGURE 2
Schematic illustration of the mode of action of the CD38-specific nanobody-based hcAbs, BiKEs, CARs and nanobody-displaying AAVs. **(A)** Antibody-dependent cellular cytotoxicity (ADCC) by an NK cell against a myeloma cell is mediated by a CD38-specific nanobody-based heavy chain antibody. A nanobody-based CD38-specific heavy chain antibody (hcAb) bound to a tumor-antigen (CD38, olive) on the plasma membrane of a multiple myeloma cell is recognized by an Fc-receptor (CD16, blue) of an NK cell. Cross-linking of CD16 on the NK cell induces the release of perforins, which form pores and kill the myeloma cell. **(B)** A half-life extended (HLE)-nano-BIKE crosslinks CD38 on the tumor cell and CD16 on the NK cell, causing release of perforins and killing of the myeloma cell. A third, albumin-specific nanobody (magenta) binds to albumin in the plasma and thereby extends the half-life of the construct by slowing renal filtration. **(C)** An NK cell transduced with a biparatopic nanobody-based chimeric antigen receptor (CAR) binds to CD38. Cross-linking of multiple nano-CARs on the NK cell surface triggers the release of perforins and lysis of the myeloma cell. **(D)** A membrane protein-specific CD38-specific nanobody inserted in the capsid of an AAV mediates specific transduction of tumor cells expressing the cognate target. Expression of the transgene encoding a pro-inflammatory cytokine (e.g. IL-12) and/or a checkpoint blocking nanobody dimer (e.g. α-PDL-1) helps to convert an immunosuppressive into an inflammatory tumor microenvironment.

showed potent ADCC toward CD38 expressing tumor cell lines *in vitro* and to multiple myeloma cells from patient bone marrow samples *ex vivo* independent of the bound epitope, but failed to induce CDC of these cells. In a xenograft model, mice treated with the hcAbs showed significantly improved survival. This is consistent with results with the CD38-specific antibody MOR202, which also did not induce CDC *in vitro* but performed well in clinical trials, although not as well as daratumumab (43).

The relative roles of ADCC and CDC in the overall success of therapeutic antibodies in multiple myeloma are as of yet unknown. It is more likely that a combination of effects underlies therapeutic efficacy. However, our results imply that ADCC may be more important than CDC, at least in a xenograft model *in vivo*. The ability of therapeutic antibodies to induce effector functions can be manipulated through directed mutagenesis of specific amino acids in the Fc-part of the antibody. For example, introduction of the single point mutation E345A, a so-called hexabody mutation, into CD38-specific IgG1 hcAbs, conferred the capacity to potently induce CDC (29).

Effective CDC can also be triggered when two hcAbs that bind to different epitopes on CD38 are combined, although neither can trigger CDC independently. This is likely due to cross-linking of CD38 on the tumor cell. Based on this observation, we generated tetravalent biparatopic hcAbs. In these constructs, two different CD38-specific nanobodies connected by a GS linker are genetically fused to the hinge, CH2 and CH3 domain of IgG1, generating tetravalent hcAbs (Figure 1B). These hcAbs also triggered effective CDC against CD38-expressing cell lines.

Antibody-mediated modulation of the enzyme function of CD38 may also contribute to changing a "cold" into a "hot" tumor microenvironment (22, 44). Some of our hcAbs, i.e. those that bound to epitope 2, indeed inhibited the GDPR-cyclase activity of CD38, as had been reported also for daratumumab and isatuximab (22, 27). However, none of these antibodies affected the NAD-hydrolase activity, i.e. the main enzymatic activity of CD38.

CD38 is not only expressed by tumor cells, but also by regulatory B and T cells as well as by myeloid suppressor cells and NK cells. Simultaneous targeting of CD38 on regulatory cells might contribute to a less immunosuppressive tumor milieu and to the expansion of effector T cells (38). In contrast, targeting of NK cells, as evidenced by a reduction of CD38-expressing NK cell numbers during daratumumab treatment may contribute to tumor relapse (38). Therefore, it is desirable to design better antibody-constructs that specifically target myeloma cells and spare healthy cells.

To increase the specificity of hcAbs further, the principle of a biparatopic hcAb could be extended to a bispecific hcAb, in which two nanobodies with specificities for two different tumor markers are combined in one construct. This might hamper tumor escape from immunotherapy by antigen loss. By selectively using nanobodies with a low affinity for their target, it might be possible to generate hcAbs that only bind when both target antigens are expressed on the target cell.

In conclusion, hcAbs represent a promising new type of anti-tumor biologic. Our CD38-specific chimeric hcAbs and biparatopic hcAbs showed effectivity *in vitro*, *ex vivo*, and *in vivo*, deserving further verification in clinical trials.

Nanobody-based bispecific killer cell engagers (BiKEs)

Bispecific engagers such as bispecific T cell engagers (BiTEs) or bispecific killer cell engagers (BiKEs) are designed to recruit cytotoxic immune cells to tumor cells. In a classical BiTE, a tumor antigen specific scFv is linked to an scFv specific for CD3 (part of the T cell receptor complex) *via* a peptide linker (45, 46). Binding of the BiTEs to the cell surface of tumor cells expressing the target antigen, subsequently recruits T cells *via* multivalent binding of the CD3-specific scFvs on the BiTE-coated tumor cell surface. Formation of an immunological synapse between the target cell and the T cell induces activation of the T cell. The activated T cell releases perforins that cause lysis of the tumor cell (46). Similarly, bispecific NK cell engagers (BiKEs) feature a tumor cell-specific scFv linked to an scFv that is specific for CD16 (the high affinity Fc-receptor) on an NK cell in place of the CD3-specific scFv (47).

Nanobodies seem particularly suited for the construction of BiTEs and BiKEs because of their better solubility and reformatability (Figure 2B) (2). Several groups have constructed chimeric BiTEs and BiKEs that contain a tumor-antigen-specific nanobody fused to an scFv for targeting either CD16 or CD3 (48–50). Others have constructed BiKEs that contain two nanobodies (51–53). For example, Van Faassen et al. generated a series of nanobody-only BiKEs directed against CD19, HER2 and EGFR that showed good killing efficacy against cells displaying the respective target on the cell surface (54).

The small size of BiTEs and BiKEs, whether composed of scFvs or of nanobodies, lies below the size of the renal filtration barrier, leading to rapid renal excretion. Various strategies have been used to extend the half-life of BiKEs and BiTEs *in vivo*. For example, fusion to hinge and Fc-domain of IgG or to an albumin-specific binding element can impede renal filtration and increase the *in vivo* half-life of BiKEs or BiTEs. Such constructs are called half-life extended (HLE-BiKE) (55–57). Using CD38-, CD16- and albumin-specific nanobodies, we recently developed CD38-specific half-life extended nanobody-based BiKEs (HLE-nano BiKEs) (33). These recruited CD16-expressing NK92 cells to exert potent cytotoxicity against CD38-expressing tumor cell lines *in vitro* and primary multiple myeloma cells *ex vivo*, independent of the epitope bound on CD38. In our preclinical set up, HLE-nano BiKEs induced

NK92-mediated cytolysis even more effectively than daratumumab. Biolayer interferometry analyses confirmed simultaneous binding of all three nanobodies to their respective target. Importantly, simultaneous binding of albumin did not interfere with BiKE-mediated killing. Moreover, we encountered no problems with aggregation during production, purification, and concentration of our HLE-nano BiKEs, which in contrast is often observed with scFv-based constructs (58–60).

For BiKEs, the CD16-specific binding element used may influence the effectiveness of the BiKE. A number of CD16-specific nanobodies (54, 61) that show a range of affinities for CD16a could mediate different effectiveness as a binding element in the BiKE. Van Faassen et al. developed a nanobody that not only binds CD16a, which is expressed on NK cells, monocytes, and macrophages, but also CD16b, which is expressed on neutrophils and is important for phagocytosis (54). These authors also investigated the influence of the order of nanobodies in the BiKE and the linker length (54). They found no significant differences in killing between BiKEs containing the same nanobodies with different linker lengths or arrangements of nanobodies.

BiKE-mediated NK cell cytotoxicity and antibody mediated cellular cytotoxicity (ADCC) both activate NK cells *via* CD16. In case of antibodies, the binding affinity of CD16 to the Fc-part of the antibody may influence the effectivity of ADCC (62). Therapeutic antibodies may also be affected by the prevalence of physiological IgG in plasma (63). Thus, antibodies present in serum may already occupy high affinity Fc-receptors on immune cells. To overcome this competition, high levels of therapeutic antibodies or antibodies engineered for increased affinity to CD16 may be needed. Such problems are likely circumvented by BiKEs that contain a nanobody that binds to CD16 independent of its occupancy by IgG. Fusion of an additional tumor-specific binding module or a co-stimulatory interleukin such as IL-15 converts a bispecific engager into a trispecific engager, also called TriKE (45, 64, 65). TriKEs have shown increased efficiency compared to BiKEs (66, 67).

Given their excellent solubility, stability, and their ease of production, we propose further *in vivo* evaluation of nanobody-based BiKEs and TriKEs versus scFv-based bispecific engagers for the therapy of multiple myeloma.

Nanobody-based chimeric antigen receptors (CARs)

T cells or NK cells equipped with a chimeric antigen receptor (CAR) can bind to tumor antigens independent of their native T cell or Fc-receptor and thereby induce CAR-dependent cellular cytotoxicity (CAR-DCC) (Figure 2C). CARs of the first generation featured a binding element such as a tumor marker-specific scFv fused *via* an extracellular linker to a transmembrane domain and a cytosolic immunoreceptor tyrosine-based activation motif (ITAM) of CD3. The introduction of additional ITAMs of other costimulatory receptors such as 41BB, OX40 or CD28 led to the development of second and third generation CARs (68).

In CAR-T therapy, T cells of the patient are genetically modified by transduction with a lentiviral vector to express a tumor marker-specific CAR and are then expanded *ex vivo*. The expanded cells are transplanted back to the patient, often inducing a storm-like release of cytokines due to massive activation of the transplanted T cells. The side effects of this cytokine storm often require management of the patient on an intensive care unit. Another drawback of CAR-T cell-based therapies is the dependence on the quality of the graft (69, 70). Since cells are harvested from already diseased and often heavily pre-treated patients, the fitness and quantity of cells obtained from a patient may be reduced.

NK cell-based CAR cells represent an alternative in this regard. NK cells show fewer side effects during transplantation than T cells (71). In addition, NK cells from established cell cultures or allogeneic transplants show lower graft-versus-host effects (72, 73). This may allow the use of CAR-NK cells as an "off-the-shelf" therapy, since new CAR cells do not have to be individually produced for each patient (74).

Although widely used, scFvs exhibit inherent structural properties that limit their applicability *in vivo*. The VH and VL domains associate *via* a hydrophobic interface that is inherently instable. Dissociation of the domains at this interface may impede expression levels of the CAR on the cell surface. Moreover, the exposed hydrophobic surfaces of the VH and VL domains may account for nonspecific binding to off target cells (11). This may lead to early depletion of CAR-T cells and may result in a decreased success of therapy. The inherent instability of scFv also hampers the construction of CARs composed of two or more scFvs, i.e. bispecific or biparatopic tandem CARs, as the VH and VL of the two scFvs could mismatch.

As in the case of BiTEs and BiKEs, high solubility and easy reformatability render nanobodies particularly suited for the construction of CARs (Figure 2C). The introduction of nanobodies as binding domain for these artificial receptors led to the development of CARs with fine-tuned binding properties (11). Moreover, due to their small size, it is possible to insert more than one nanobody into the CAR (10, 75, 76). This gives researchers the opportunity to further refine the specificity and affinity of a nanobody-based CAR. For example, tandem linkage of two nanobodies that bind to independent epitopes of BCMA resulted in BCMA-specific biparatopic CARs with higher affinities for the target and exceptionally high effectivity of the derived CAR-T cells (10, 11).

With respect to CD38, several scFv-based CAR-T and NK cells have been developed (77–79), some of which are currently under clinical evaluation (clinical trials NCT03473496,

NCT03464916, NCT04861480. June 2022, clinicaltrials.gov). Some of these were affinity-optimized to more specifically target cells that highly express CD38 rendering a very potent CD38-specific CAR. Recently, we and others have used CD38-specific nanobodies for the construction of nanobody-based CARs (31, 36). The nanobody-based CAR-T cells developed by An et al. displayed significant cytotoxicity and cytokine production *in vitro* as well as *in vivo* in a xenograft mouse model (36). We expressed our nanobody-based CARs on NK92 cells as a basis for "off-the-shelf" CAR-NK cells. These nanobody-based CAR-NK cells also showed potent cytotoxicity against CD38+ cells *in vitro* and *ex vivo*. The effectiveness of the CAR-NK cells was interestingly independent of the epitope on CD38 bound by the nanobody.

Since healthy cells also express CD38, it would be advantageous to develop CAR cells that specifically kill CD38 overexpressing myeloma cells. Conceivably, one could introduce one or more additional nanobodies that recognize another membrane protein expressed on the surface of the myeloma cell such as CD138, CD319 or CD229. Such a bispecific CAR might improve tumor cell binding of CAR-T or CAR-NK cells over binding of healthy cells that only express one of the two target proteins.

Nanobody-based CARs are easier to engineer genetically than scFvs. Nanobody-based CARs can be designed for their affinity, avidity, and specificity through their LEGO brick-like structure. Therefore, nanobody-based CAR cells represent a promising technology to combat multiple myeloma.

Nanobody-displaying AAV vectors

Adeno-associated viral vectors (AAVs) are well-established tools for gene therapy (80, 81). AAVs are non-replicative, non-enveloped, small ssDNA viruses. Typically the nucleotide sequences coding for the viral capsid and replication genes are replaced by the nucleotide sequence of a gene of interest to be delivered to the transduced target cells. This sequence may encode a fluorescent reporter, a protein or RNA modulator, a toxin, an antibody or nanobody/hcAb, an inflammatory cytokine, a microRNA or a CRISPR/Cas9 targeting module (82–86). However, AAVs often show a broad tropism, hampering delivery of the gene of interest to a specific cell type such as a tumor cell (87). Mutations of and peptide insertions into the capsid proteins have been used to reduce binding of the AAV vector to ubiquitously expressed targets (e.g. glycoproteins) and to increase the selectivity for certain cells and tissues (88). More specific targeting technologies have also been developed to direct the AAV capsid to specific cell surface receptors, e.g. by genetic fusion or chemical ligation of an AAV capsid protein to the ligand of a cell surface receptor (89–91). For example, HER2-specific design ankyrin repeat proteins (DARPins) have been used for the improved transduction of HER2-expressing cells through AAV2 (92).

Here too, the high solubility and easy reformatability could render nanobodies particularly suited as targeting modules for AAVs, e.g. to myeloma cells overexpressing CD38. To this end, we inserted a CD38-specific nanobody into the exposed GH2/GH3 surface loop of the VP1 viral capsid protein of AAV2 (34). Since the N terminus of a nanobody is located close to the antigen-binding paratope while the C terminus is on the opposite side, we used a short linker on the C terminus and a longer linker on the N terminus to allow an upright orientation of the nanobody on the capsid surface (Figure 2D). All CD38-specific nanobodies tested as well as several other nanobodies targeting structurally distinct membrane proteins were successfully inserted in this way. This suggests that this strategy likely is suited for a broad range of nanobodies and target membrane proteins. For each of the inserted nanobodies, we observed a 10- to 500-fold enhanced AAV transduction of target-transfected HEK cells and other target-protein-expressing cells. Remarkably, AAVs displaying a CD38-specific nanobody also specifically transduced CD38-expressing myeloma cells in primary bone marrow samples of multiple myeloma patients. We analyzed the transduction efficiency *via* a GFP reporter as transgene - for future applications the nanobody-displaying AAVs could encode inflammatory mediators, e.g. pro-inflammatory cytokines or nanobody dimers that block immune checkpoint proteins like PD-L1 (Figure 2D).

In conclusion we propose that nanobodies represent a means to combine the benefits of AAV-mediated gene transfer with specific targeting of myeloma cells. Nanobody-displaying AAVs pave the way for a wide range of applications as vectors for delivery of immunomodulatory substances such as cytokines or checkpoint inhibitors to the tumor microenvironment.

Discussion

Nanobodies display an inherent robustness and high solubility that has been shaped by millions of years of evolution in the camelid lineages. In contrast, single variable immunoglobulin domains (VH or VL) derived from conventional human antibodies often show a tendency to aggregate in the absence of its natural partner (93, 94). This is attributed to hydrophobic surface patches in the framework regions where VH and VL naturally associate. In the context of a natural antibody the pairing and covalent linkage of the adjacent CH1 and CL domains additionally stabilizes the association of VH and VL domains. Conversely, the pairing of VH and VL domains generally is less stable in the context of a recombinant scFv, where a VH and VL domains are genetically fused *via* a peptide linker. These inherent structural features likely account for the much better developability of nanobody-based biologics than of scFv-based biologics.

Two nanobody-based biologics have been granted FDA approval for clinical use: Caplacizumab, a homodimer of two identical van Willebrandt factor-specific nanobodies connected by a peptide linker and Ciltacel a chimeric antigen receptor composed of a heterodimer of two different BCMA-specific nanobodies that target non-overlapping epitopes of BCMA. The size of Caplacizumab is much smaller than that of a conventional antibody and lies below the size of the renal filtration barrier. Consequently, Caplacizumab exhibits a short half-life *in vivo* and is intended for short-term treatment of blood clotting disorders. The BCMA-specific biparatopic nanobody of Ciltacel, in contrast, is expressed as a cell surface receptor on transduced T-cells and is intended for long-term treatment of BCMA-expressing multiple myeloma.

The entry of nanobodies into the clinic likely has been slowed by concerns regarding the potential immunogenicity of the camelid VHH domain in human patients. In general, immunogenicity of variable immunoglobulin domains is much less of a concern than that of constant immunoglobulin domains and other proteins. Humans carry ~50-150 distinct VH and VL encoding gene fragments. Somatic hypermutation during natural immune responses generates millions of variants of the germline VH and VL domains. During pregnancy, such variants are transferred across the placenta from the mother to the fetus. This likely accounts for the high natural tolerance against VH and VL domains of other species.

To mitigate immunogenicity concerns, framework residues in nanobodies intended for clinical use in humans, usually are "humanized" (95). This involves substitutions of amino acid residues on the surface of the VHH domain by corresponding residues commonly found in human VH domains. Owing to the natural similarity of VHH domains to human VH3 domains, this is often possible without compromising the stability or functionality of the nanobody, perhaps with the exception of the hydrophilic residues at the former interface to the VL domain.

The astounding efficacy of the nanobody-based Ciltacel (96) compared to CARs based on scFvs raises a number of questions that need be addressed in future studies. Is a biparatopic CAR generally more efficient than a monovalent CAR? Do the epitopes recognized by the nanobodies influence the efficacy? Could the efficacy of a CAR be increased by combining two nanobodies directed against distinct cell surface receptors such as CD38 and BCMA that are co-expressed by the target cell? It also remains to be seen whether the astounding efficacy of the nanobody-based CARs can be reached also with nanobody-based CARs targeting other cell surface proteins (11, 97).

In this review we focused on the applicability of CD38-specific nanobody-based constructs for the treatment of multiple myeloma. Targeting CD38 with such constructs could also be a promising alternative for the treatment of other CD38 positive malignancies. CD38 is also often highly expressed in other hematological malignancies, e.g. acute myeloid leukemia (AML) (98), and chronic lymphocytic leukemia (CLL) (99). Moreover, CD38 over- expression by cancer-associated fibroblast has been suggested to promote a pro-tumoral activity in melanoma (100). Expression of CD38 by lung cancer and other solid tumors may also contribute to an oncogenic tumor microenvironment by promoting the enzymatic conversion of NAD+ to immunosuppressive adenosine (101, 102). CD38-specific nanobody-based constructs that inhibit its enzyme activity would be targeting the "Achilles heel" of such tumors.

Most tumors are heterogeneous, and tumor cells that do not express or loose expression of the target membrane protein of a therapeutic antibody would have a growth advantage (103, 104). In such cases, simultaneous targeting of two or more tumor cell membrane proteins would impede escape and lower the rate of recurrence (105). The specificity of nanobody-based constructs for tumor cells might be enhanced by simultaneous targeting of multiple tumor-specific antigens through integration of additional nanobodies into the construct. The small size of nanobodies and ease of reformatability facilitate the construction of bispecific hcAbs, BiKEs, CARs, and nanobody-displaying AAV vectors (29, 33, 53).

CD38 is also expressed by in multiple different cell types of innate and acquired immunity, including both, tumor promoting cells and cells with cytotoxic activity (21, 23). Targeting of regulatory T cells and B cells, and myeloid derived suppressor cells would be beneficial, whereas targeting of NK cells and activated cytotoxic T cells would be counter-productive (78, 106, 107). As in case of tumor heterogeneity, by combining nanobodies with low affinity for two targets that are co-expressed by tumor cells but not by NK or T cells, e.g. CD38 and BCMA, it might be possible to specifically deplete only cells expressing both target antigens and thus to develop nanobody-based antibody constructs with lower off-target effects.

The results of our own studies with CD38-specific nanobodies illustrate the utility of nanobody-based heavy chain antibodies, BiKEs, CARs and nanobody-displaying AAV vectors to specifically and effectively target CD38-expressing myeloma cells. The promising results of our preclinical studies warrant further clinical studies to evaluate the potential of these CD38-specific nanobody-based constructs for treatment of multiple myeloma.

Author contributions

All authors conceived the topic, PB and FK-N acquired funding, JH and FK-N wrote the manuscript. All authors contributed to the article and approved the submitted version.

Funding

This work was supported by grants from the Deutsche Forschungsgemeinschaft to PB (BA 5893/7) and FK-N (No310/16, SFB1328- Z02, BMBF-COMMUTE).

Acknowledgments

We thank Fabienne Seyfried, Birte Albrecht, and Josephine Gebhardt for excellent technical assistance.

Conflict of interest

PB and FK-N are co-inventors on a patent application on CD38-specific nanobodies. AM and FK-N are co-inventors on a patent application on nanobody-displaying AAV vectors. FK-N receives a share of antibody and protein sales *via* MediGate GmbH, a wholly owned subsidiary of the University Medical Center Hamburg-Eppendorf.

The remaining author declares that the research was conducted in the absence of any commercial or financial relationships that could be construed as a potential conflict of interest.

MediGate GmbH was not involved in the study design, collection, analysis, interpretation of data, the writing of this article, or the decision to submit it for publication.

Publisher's note

References

1. Flajnik MF, Deschacht N, Muyldermans S. A case of convergence: Why did a simple alternative to canonical antibodies arise in sharks and camels? *PloS Biol* (2011) 9(8):e1001120. doi: 10.1371/journal.pbio.1001120

2. Bannas P, Hambach J, Koch-Nolte F. Nanobodies and Nanobody-based human heavy chain antibodies as antitumor therapeutics. *Front Immunol* (2017) 8:1603. doi: 10.3389/fimmu.2017.01603

3. Bannas P, Lenz A, Kunick V, Well L, Fumey W, Rissiek B, et al. Molecular imaging of tumors with nanobodies and antibodies: Timing and dosage are crucial factors for improved *in vivo* detection. *Contrast Media Mol Imaging* (2015) 10 (5):367–78. doi: 10.1002/cmmi.1637

4. Bannas P, Well L, Lenz A, Rissiek B, Haag F, Schmid J, et al. *In vivo* near-infrared fluorescence targeting of T cells: comparison of nanobodies and conventional monoclonal antibodies. *Contrast Media Mol Imaging* (2014) 9 (2):135–42. doi: 10.1002/cmmi.1548

5. Peyvandi F, Scully M, Kremer Hovinga JA, Cataland S, Knöbl P, Wu H, et al. Caplacizumab for acquired thrombotic thrombocytopenic purpura. *New Engl J Med* (2016) 374(6):511–22. doi: 10.1056/NEJMoa1505533

6. Tan CR, Shah UA. Targeting BCMA in Multiple Myeloma. *Curr Hematol Malig Rep* (2021) 16(5):367–83. doi: 10.1007/s11899-021-00639-z

7. Yu B, Jiang T, Liu D. BCMA-targeted immunotherapy for multiple myeloma. *J Hematol Oncol* (2020) 13(1):125. doi: 10.1186/s13045-020-00962-7

8. Wei W, Zhang Y, Zhang D, Liu Q, An S, Chen Y, et al. Annotating BCMA expression in multiple myelomas. *Mol Pharm* (2022) 19(10):3492–501. doi: 10.1021/acs.molpharmaceut.1c00628

9. Xu J, Chen LJ, Yang SS, Sun Y, Wu W, Liu YF, et al. Exploratory trial of a biepitopic CAR T-targeting B cell maturation antigen in relapsed/refractory multiple myeloma. *Proc Natl Acad Sci U S A* (2019) 116(19):9543–51. doi: 10.1073/pnas.1819745116

10. Zhao WH, Liu J, Wang BY, Chen YX, Cao XM, Yang Y, et al. A phase 1, open-label study of LCAR-B38M, a chimeric antigen receptor T cell therapy directed against B cell maturation antigen, in patients with relapsed or refractory multiple myeloma. *J Hematol Oncol* (2018) 11(1):141. doi: 10.1186/s13045-018-0681-6

11. Bao C, Gao Q, Li LL, Han L, Zhang B, Ding Y, et al. The Application of Nanobody in CAR-T Therapy. *Biomolecules.* (2021) 11(2):238. doi: 10.3390/biom11020238

12. Kazandjian D. Multiple myeloma epidemiology and survival: A unique malignancy. *Semin Oncol* (2016) 43(6):676–81. doi: 10.1053/j.seminoncol.2016.11.004

13. Ackley J, Ochoa MA, Ghoshal D, Roy K, Lonial S, Boise LH. Keeping Myeloma in Check: The Past, Present and Future of Immunotherapy in Multiple Myeloma. *Cancers (Basel)* (2021) 13(19):4787. doi: 10.3390/cancers13194787

14. Derlin T, Bannas P. Imaging of multiple myeloma: Current concepts. *World J Orthop* (2014) 5(3):272–82. doi: 10.5312/wjo.v5.i3.272

15. Giuliani N, Accardi F, Marchica V, Dalla Palma B, Storti P, Toscani D, et al. Novel targets for the treatment of relapsing multiple myeloma. *Expert Rev Hematol* (2019) 12(7):481–96. doi: 10.1080/17474086.2019.1624158

16. Derlin T, Peldschus K, Münster S, Bannas P, Herrmann J, Stübig T, et al. Comparative diagnostic performance of ^{18}F-FDG PET/CT versus whole-body MRI for determination of remission status in multiple myeloma after stem cell transplantation. *Eur Radiol* (2013) 23(2):570–8. doi: 10.1007/s00330-012-2600-5

17. Sung H, Ferlay J, Siegel RL, Laversanne M, Soerjomataram I, Jemal A, et al. Global cancer Statistics 2020: GLOBOCAN estimates of incidence and mortality worldwide for 36 cancers in 185 countries. *CA: A Cancer J Clin* (2021) 71(3):209–49. doi: 10.3322/caac.21660

18. Bannas P, Hentschel HB, Bley TA, Treszl A, Eulenburg C, Derlin T, et al. Diagnostic performance of whole-body MRI for the detection of persistent or relapsing disease in multiple myeloma after stem cell transplantation. *Eur Radiol* (2012) 22(9):2007–12. doi: 10.1007/s00330-012-2445-y

19. Pawlyn C, Davies FE. Toward personalized treatment in multiple myeloma based on molecular characteristics. *Blood.* (2019) 133(7):660–75. doi: 10.1182/blood-2018-09-825331

20. Rajkumar SV. Multiple myeloma: Every year a new standard? *Hematol Oncol* (2019) 37 Suppl 1(Suppl 1):62–5. doi: 10.1002/hon.2586

21. Costa F, Dalla Palma B, Giuliani N. CD38 Expression by myeloma cells and its role in the context of bone marrow microenvironment: Modulation by therapeutic agents. *Cells.* (2019) 8(12):1632. doi: 10.3390/cells8121632

22. Baum N, Fliegert R, Bauche A, Hambach J, Menzel S, Haag F, et al. Daratumumab and Nanobody-Based Heavy Chain Antibodies Inhibit the ADPR Cyclase but not the NAD(+) Hydrolase Activity of CD38-Expressing Multiple Myeloma Cells. *Cancers (Basel)* (2020) 13(1):2645–58. doi: 10.3390/cancers13010076

23. van de Donk N, Richardson PG, Malavasi F. CD38 antibodies in multiple myeloma: back to the future. *Blood.* (2018) 131(1):13–29. doi: 10.1182/blood-2017-06-740944

24. de Weers M, Tai YT, van der Veer MS, Bakker JM, Vink T, Jacobs DC, et al. Daratumumab, a novel therapeutic human CD38 monoclonal antibody, induces killing of multiple myeloma and other hematological tumors. *J Immunol* (2011) 186(3):1840–8. doi: 10.4049/jimmunol.1003032

25. Chim CS, Kumar S, Wong VKC, Ngai C, Kwong YL. 3-weekly daratumumab-lenalidomide/pomalidomide-dexamethasone is highly effective in relapsed and refractory multiple myeloma. *Hematology.* (2021) 26(1):652–5. doi: 10.1080/16078454.2021.1965737

26. Mikhael J, Belhadj-Merzoug K, Hulin C, Vincent L, Moreau P, Gasparetto C, et al. A phase 2 study of isatuximab monotherapy in patients with multiple myeloma who are refractory to daratumumab. *Blood Cancer J* (2021) 11(5):89. doi: 10.1038/s41408-021-00478-4

27. Fumey W, Koenigsdorf J, Kunick V, Menzel S, Schütze K, Unger M, et al. Nanobodies effectively modulate the enzymatic activity of CD38 and allow specific imaging of CD38(+) tumors in mouse models in vivo. *Sci Rep* (2017) 7(1):14289. doi: 10.1038/s41598-017-14112-6

28. Koch-Nolte F, Glowacki G, Bannas P, Braasch F, Dubberke G, Ortolan E, et al. Use of genetic immunization to raise antibodies recognizing toxin-related cell surface ADP-ribosyltransferases in native conformation. *Cell Immunol* (2005) 236 (1-2):66–71. doi: 10.1016/j.cellimm.2005.08.033

29. Schütze K, Petry K, Hambach J, Schuster N, Fumey W, Schriewer L, et al. CD38-specific biparatopic heavy chain antibodies display potent complement-dependent cytotoxicity against multiple myeloma Cells. *Front Immunol* (2018) 9:2553. doi: 10.3389/fimmu.2018.02553

30. Oberle A, Brandt A, Alawi M, Langebrake C, Janjetovic S, Wolschke C, et al. Long-term CD38 saturation by daratumumab interferes with diagnostic myeloma cell detection. *Haematologica*. (2017) 102(9):e368–e70. doi: 10.3324/haematol.2017.169235

31. Hambach J, Riecken K, Cichutek S, Schütze K, Albrecht B, Petry K, et al. Targeting CD38-expressing multiple myeloma and burkitt lymphoma Cells *In vitro* with nanobody-based chimeric antigen receptors (Nb-CARs). *Cells*. (2020) 9 (2):321. doi: 10.3390/cells9020321

32. Schriewer L, Schütze K, Petry K, Hambach J, Fumey W, Koenigsdorf J, et al. Nanobody-based CD38-specific heavy chain antibodies induce killing of multiple myeloma and other hematological malignancies. *Theranostics*. (2020) 10(6):2645–58. doi: 10.7150/thno.38533

33. Hambach J, Fumey W, Stähler T, Gebhardt AJ, Adam G, Weisel K, et al. Half-life extended nanobody-based CD38-specific bispecific killercell engagers induce killing of multiple myeloma cells. *Front Immunol* (2022) 13:838406. doi: 10.3389/fimmu.2022.838406

34. Eichhoff AM, Börner K, Albrecht B, Schäfer W, Baum N, Haag F, et al. Nanobody-enhanced targeting of AAV gene therapy vectors. *Mol Ther Methods Clin Dev* (2019) 15:211–20. doi: 10.1016/j.omtm.2019.09.003

35. Duray E, Lejeune M, Baron F, Beguin Y, Devoogdt N, Krasniqi A, et al. A non-internalised CD38-binding radiolabelled single-domain antibody fragment to monitor and treat multiple myeloma. *J Hematol Oncol* (2021) 14(1):183. doi: 10.1186/s13045-021-01171-6

36. An N, Hou YN, Zhang QX, Li T, Zhang QL, Fang C, et al. Anti-Multiple Myeloma activity of nanobody-based anti-CD38 chimeric antigen receptor T cells. *Mol Pharm* (2018) 15(10):4577–88. doi: 10.1021/acs.molpharmaceut.8b00584

37. Lejeune M, Duray E, Peipp M, Clémenceau B, Baron F, Beguin Y, et al. Balancing the CD38 expression on effector and target cells in daratumumab-mediated NK Cell ADCC against Multiple Myeloma. *Cancers (Basel)* (2021) 13 (12):3072. doi: 10.3390/cancers13123072

38. Saltarella I, Desantis V, Melaccio A, Solimando AG, Lamanuzzi A, Ria R, et al. Mechanisms of resistance to anti-cd38 daratumumab in multiple myeloma. *Cells*. (2020) 9(1):167. doi: 10.3390/cells9010167

39. Pereira NA, Chan KF, Lin PC, Song Z. The "less-is-more" in therapeutic antibodies: Afucosylated anti-cancer antibodies with enhanced antibody-dependent cellular cytotoxicity. *MAbs*. (2018) 10(5):693–711. doi: 10.1080/19420862.2018.1466767

40. Weng WK, Levy R. Two immunoglobulin G fragment C receptor polymorphisms independently predict response to rituximab in patients with follicular lymphoma. *J Clin Oncol* (2003) 21(21):3940–7. doi: 10.1200/JCO.2003.05.013

41. Bannas P, Koch-Nolte F. Perspectives for the development of CD38-specific heavy chain antibodies as therapeutics for multiple myeloma. *Front Immunol* (2018) 9:2559. doi: 10.3389/fimmu.2018.02559

42. Tintelnot J, Baum N, Schultheiß C, Braig F, Trentmann M, Finter J, et al. Nanobody targeting of epidermal growth factor receptor (EGFR) ectodomain variants overcomes resistance to therapeutic egfr antibodies. *Mol Cancer Ther* (2019) 18(4):823–33. doi: 10.1158/1535-7163.MCT-18-0849

43. Chim CS, Kumar SK, Orlowski RZ, Cook G, Richardson PG, Gertz MA, et al. Management of relapsed and refractory multiple myeloma: novel agents, antibodies, immunotherapies and beyond. *Leukemia*. (2018) 32(2):252–62. doi: 10.1038/leu.2017.329

44. Baum N, Eggers M, Koenigsdorf J, Menzel S, Hambach J, Staehler T, et al. Mouse CD38-specific heavy chain antibodies inhibit cd38 gdpr-cyclase activity and mediate cytotoxicity against tumor cells. *Front Immunol* (2021) 12:703574. doi: 10.3389/fimmu.2021.703574

45. Allen C, Zeidan AM, Bewersdorf JP. BiTEs, DARTS, BiKEs and TriKEs-are antibody based therapies changing the future treatment of AML? *Life (Basel)* (2021) 11(6):465. doi: 10.3390/life11060465

46. Einsele H, Borghaei H, Orlowski RZ, Subklewe M, Roboz GJ, Zugmaier G, et al. The BiTE (bispecific T-cell engager) platform: Development and future potential of a targeted immuno-oncology therapy across tumor types. *Cancer*. (2020) 126(14):3192–201. doi: 10.1002/cncr.32909

47. Tay SS, Carol H, Biro M. TriKEs and BiKEs join CARs on the cancer immunotherapy highway. *Hum Vaccin Immunother* (2016) 12(11):2790–6. doi: 10.1080/21645515.2016.1198455

48. Vallera DA, Oh F, Kodal B, Hinderlie P, Geller MA, Miller JS, et al. A HER2 tri-specific nk cell engager mediates efficient targeting of human ovarian cancer. *Cancers (Basel)* (2021) 13(16):3994. doi: 10.3390/cancers13163994

49. Mandrup OA, Ong SC, Lykkemark S, Dinesen A, Rudnik-Jansen I, Dagnæs-Hansen NF, et al. Programmable half-life and anti-tumour effects of bispecific T-cell engager-albumin fusions with tuned FcRn affinity. *Commun Biol* (2021) 4 (1):310. doi: 10.1038/s42003-021-01790-2

50. Tapia-Galisteo A, Sánchez Rodríguez Í, Aguilar-Sopeña O, Harwood SL, Narbona J, Ferreras Gutierrez M, et al. Trispecific T-cell engagers for dual tumor-targeting of colorectal cancer. *Oncoimmunology*. (2022) 11(1):2034355. doi: 10.1080/2162402X.2022.2034355

51. Dong B, Zhou C, He P, Li J, Chen S, Miao J, et al. A novel bispecific antibody, BiSS, with potent anti-cancer activities. *Cancer Biol Ther* (2016) 17 (4):364–70. doi: 10.1080/15384047.2016.1139266

52. Rozan C, Cornillon A, Pétiard C, Chartier M, Behar G, Boix C, et al. Single-domain antibody–based and linker-free bispecific antibodies targeting fcγriii induce potent antitumor activity without recruiting regulatory t cells. *Mol Cancer Ther* (2013) 12(8):1481–91. doi: 10.1158/1535-7163.MCT-12-1012

53. Els Conrath K, Lauwereys M, Wyns L, Muyldermans S. Camel single-domain antibodies as modular building units in bispecific and bivalent antibody constructs. *J Biol Chem* (2001) 276(10):7346–50. doi: 10.1074/jbc.M007734200

54. van Faassen H, Jo DH, Ryan S, Lowden MJ, Raphael S, MacKenzie CR, et al. Incorporation of a novel cd16-specific single-domain antibody into multispecific natural killer cell engagers with potent ADCC. *Mol Pharm* (2021) 18(6):2375–84. doi: 10.1021/acs.molpharmaceut.1c00208

55. Rotman M, Welling MM, van den Boogaard ML, Moursel LG, van der Graaf LM, van Buchem MA, et al. Fusion of hIgG1-Fc to 111In-anti-amyloid single domain antibody fragment VHH-pa2H prolongs blood residential time in APP/PS1 mice but does not increase brain uptake. *Nucl Med Biol* (2015) 42(8):695–702. doi: 10.1016/j.nucmedbio.2015.03.003

56. Molloy ME, Austin RJ, Lemon BD, Aaron WH, Ganti V, Jones A, et al. Preclinical characterization of hpn536, a trispecific, t-cell-activating protein construct for the treatment of mesothelin-expressing solid tumors. *Clin Cancer Res* (2021) 27(5):1452–62. doi: 10.1158/1078-0432.CCR-20-3392

57. Giffin MJ, Cooke K, Lobenhofer EK, Estrada J, Zhan J, Deegen P, et al. AMG 757, a Half-life extended, DLL3-targeted bispecific t-cell engager, shows high potency and sensitivity in preclinical models of small-cell lung cancer. *Clin Cancer Res* (2021) 27(5):1526–37. doi: 10.1158/1078-0432.CCR-20-2845

58. Bates A, Power CA. David Vs. Goliath: The structure, function, and clinical prospects of antibody fragments. *Antibodies (Basel)* (2019) 8(2):28. doi: 10.3390/antib8020028

59. van der Linden RH, Frenken LG, de Geus B, Harmsen MM, Ruuls RC, Stok W, et al. Comparison of physical chemical properties of llama VHH antibody fragments and mouse monoclonal antibodies. *Biochim Biophys Acta* (1999) 1431 (1):37–46. doi: 10.1016/S0167-4838(99)00030-8

60. Wörn A, Plückthun A. Stability engineering of antibody single-chain Fv fragments. *J Mol Biol* (2001) 305(5):989–1010. doi: 10.1006/jmbi.2000.4265

61. Behar G, Sibéril S, Groulet A, Chames P, Pugnière M, Boix C, et al. Isolation and characterization of anti-FcgammaRIII (CD16) llama single-domain antibodies that activate natural killer cells. *Protein Eng Des Sel* (2008) 21(1):1–10. doi: 10.1093/protein/gzm064

62. Congy-Jolivet N, Bolzec A, Ternant D, Ohresser M, Watier H, Thibault G. Fc gamma RIIIa expression is not increased on natural killer cells expressing the Fc gamma RIIIa-158V allotype. *Cancer Res* (2008) 68(4):976–80. doi: 10.1158/0008-5472.CAN-07-6523

63. Preithner S, Elm S, Lippold S, Locher M, Wolf A, da Silva AJ, et al. High concentrations of therapeutic IgG1 antibodies are needed to compensate for inhibition of antibody-dependent cellular cytotoxicity by excess endogenous immunoglobulin G. *Mol Immunol* (2006) 43(8):1183–93. doi: 10.1016/j.molimm.2005.07.010

64. Felices M, Lenvik TR, Davis ZB, Miller JS, Vallera DA. Generation of BiKEs and TriKEs to Improve NK Cell-Mediated Targeting of Tumor Cells. *Methods Mol Biol* (2016) 1441:333–46. doi: 10.1007/978-1-4939-3684-7_28

65. Sarhan D, Brandt L, Felices M, Guldevall K, Lenvik T, Hinderlie P, et al. 161533 TriKE stimulates NK-cell function to overcome myeloid-derived suppressor cells in MDS. *Blood Adv* (2018) 2(12):1459–69. doi: 10.1182/bloodadvances.2017012369

66. Vallera DA, Felices M, McElmurry R, McCullar V, Zhou X, Schmohl JU, et al. IL15 trispecific killer engagers (trike) make natural killer cells specific to CD33+

targets while also inducing persistence, *in vivo* expansion, and enhanced function. *Clin Cancer Res* (2016) 22(14):3440–50. doi: 10.1158/1078-0432.CCR-15-2710

67. Cheng Y, Zheng X, Wang X, Chen Y, Wei H, Sun R, et al. Trispecific killer engager 161519 enhances natural killer cell function and provides anti-tumor activity against CD19-positive cancers. *Cancer Biol Med* (2020) 17(4):1026–38. doi: 10.20892/j.issn.2095-3941.2020.0399

68. Hong M, Clubb JD, Chen YY. Engineering CAR-T cells for next-generation cancer therapy. *Cancer Cell* (2020) 38(4):473–88. doi: 10.1016/j.ccell.2020.07.005

69. Morgan MA, Büning H, Sauer M, Schambach A. Use of cell and genome modification technologies to generate improved "off-the-shelf" CAR T and CAR NK cells. *Front Immunol* (2020) 11:1965. doi: 10.3389/fimmu.2020.01965

70. Xie G, Dong H, Liang Y, Ham JD, Rizwan R, Chen J. CAR-NK cells: A promising cellular immunotherapy for cancer. *EBioMedicine*. (2020) 59:102975. doi: 10.1016/j.ebiom.2020.102975

71. Hodgins JJ, Khan ST, Park MM, Auer RC, Ardolino M. Killers 2.0: NK cell therapies at the forefront of cancer control. *J Clin Invest* (2019) 129(9):3499–510. doi: 10.1172/JCI129338

72. Lupo KB, Matosevic S. Natural Killer Cells as Allogeneic Effectors in adoptive cancer immunotherapy. *Cancers (Basel)* (2019) 11(6):769. doi: 10.3390/cancers11060769

73. Suck G, Odendahl M, Nowakowska P, Seidl C, Wels WS, Klingemann HG, et al. NK-92: an 'off-the-shelf therapeutic' for adoptive natural killer cell-based cancer immunotherapy. *Cancer Immunology Immunother* (2016) 65(4):485–92. doi: 10.1007/s00262-015-1761-x

74. Klingemann H, Boissel L, Toneguzzo F. Natural killer cells for immunotherapy - advantages of the NK-92 cell line over blood NK cells. *Front Immunol* (2016) 7:91. doi: 10.3389/fimmu.2016.00091

75. Mei H, Li C, Jiang H, Zhao X, Huang Z, Jin D, et al. A bispecific CAR-T cell therapy targeting BCMA and CD38 in relapsed or refractory multiple myeloma. *J Hematol Oncol* (2021) 14(1):161. doi: 10.1186/s13045-021-01170-7

76. Tang Y, Yin H, Zhao X, Jin D, Liang Y, Xiong T, et al. High efficacy and safety of CD38 and BCMA bispecific CAR-T in relapsed or refractory multiple myeloma. *J Exp Clin Cancer Res* (2022) 41(1):2. doi: 10.1186/s13046-021-02214-z

77. Poels R, Drent E, Lameris R, Katsarou A, Themeli M, van der Vliet HJ, et al. Preclinical evaluation of invariant natural killer t cells modified with cd38 or bcma chimeric antigen receptors for multiple myeloma. *Int J Mol Sci* (2021) 22(3):1096. doi: 10.3390/ijms22031096

78. Drent E, Themeli M, Poels R, de Jong-Korlaar R, Yuan H, de Bruijn J, et al. A Rational strategy for reducing on-target off-tumor effects of cd38-chimeric antigen receptors by affinity optimization. *Mol Ther* (2017) 25(8):1946–58. doi: 10.1016/j.ymthe.2017.04.024

79. Mihara K, Yoshida T, Takei Y, Sasaki N, Takihara Y, Kuroda J, et al. T cells bearing anti-CD19 and/or anti-CD38 chimeric antigen receptors effectively abrogate primary double-hit lymphoma cells. *J Hematol Oncol* (2017) 10(1):116. doi: 10.1186/s13045-017-0488-x

80. Mingozzi F, High KA. Therapeutic *in vivo* gene transfer for genetic disease using AAV: progress and challenges. *Nat Rev Genet* (2011) 12(5):341–55. doi: 10.1038/nrg2988

81. Colella P, Ronzitti G, Mingozzi F. Emerging issues in AAV-mediated in vivo gene therapy. *Mol Ther Methods Clin Dev* (2018) 8:87–104. doi: 10.1016/j.omtm.2017.11.007

82. Balazs AB, Ouyang Y, Hong CM, Chen J, Nguyen SM, Rao DS, et al. Vectored immunoprophylaxis protects humanized mice from mucosal HIV transmission. *Nat Med* (2014) 20(3):296–300. doi: 10.1038/nm.3471

83. Yang Y, Wang L, Bell P, McMenamin D, He Z, White J, et al. A dual AAV system enables the Cas9-mediated correction of a metabolic liver disease in newborn mice. *Nat Biotechnol* (2016) 34(3):334–8. doi: 10.1038/nbt.3469

84. Demeules M, Scarpitta A, Abad C, Gondé H, Hardet R, Pinto-Espinoza C, et al. Evaluation of P2X7 receptor function in tumor contexts using raav vector and nanobodies (AAVnano). *Front Oncol* (2020) 10:1699. doi: 10.3389/fonc.2020.01699

85. Griciuc A, Federico AN, Natasan J, Forte AM, McGinty D, Nguyen H, et al. Gene therapy for Alzheimer's disease targeting CD33 reduces amyloid beta accumulation and neuroinflammation. *Hum Mol Genet* (2020) 29(17):2920–35. doi: 10.1093/hmg/ddaa179

86. GuhaSarkar D, Neiswender J, Su Q, Gao G, Sena-Esteves M. Intracranial AAV-IFN-β gene therapy eliminates invasive xenograft glioblastoma and improves survival in orthotopic syngeneic murine model. *Mol Oncol* (2017) 11(2):180–93. doi: 10.1002/1878-0261.12020

87. Herrmann AK, Grimm D. High-Throughput Dissection of AAV-Host Interactions: The fast and the curious. *J Mol Biol* (2018) 430(17):2626–40. doi: 10.1016/j.jmb.2018.05.022

88. Börner K, Kienle E, Huang LY, Weinmann J, Sacher A, Bayer P, et al. Pre-arrayed Pan-AAV peptide display libraries for rapid single-round screening. *Mol Ther* (2020) 28(4):1016–32. doi: 10.1016/j.ymthe.2020.02.009

89. Ponnazhagan S, Mahendra G, Kumar S, Thompson JA, Castillas MJr. Conjugate-based targeting of recombinant adeno-associated virus type 2 vectors by using avidin-linked ligands. *J Virol* (2002) 76(24):12900–7. doi: 10.1128/JVI.76.24.12900-12907.2002

90. Landegger LD, Pan B, Askew C, Wassmer SJ, Gluck SD, Galvin A, et al. A synthetic AAV vector enables safe and efficient gene transfer to the mammalian inner ear. *Nat Biotechnol* (2017) 35(3):280–4. doi: 10.1038/nbt.3781

91. Ried MU, Girod A, Leike K, Büning H, Hallek M. Adeno-associated virus capsids displaying immunoglobulin-binding domains permit antibody-mediated vector retargeting to specific cell surface receptors. *J Virol* (2002) 76(9):4559–66. doi: 10.1128/JVI.76.9.4559-4566.2002

92. Münch RC, Janicki H, Völker I, Rasbach A, Hallek M, Büning H, et al. Displaying high-affinity ligands on adeno-associated viral vectors enables tumor cell-specific and safe gene transfer. *Mol Ther* (2013) 21(1):109–18. doi: 10.1038/mt.2012.186

93. Gil D, Schrum AG. Strategies to stabilize compact folding and minimize aggregation of antibody-based fragments. *Adv Biosci Biotechnol* (2013) 4(4a):73–84. doi: 10.4236/abb.2013.44A011

94. Jäger M, Plückthun A. Domain interactions in antibody Fv and scFv fragments: effects on unfolding kinetics and equilibria. *FEBS Letters* (1999) 462 (3):307–12. doi: 10.1016/S0014-5793(99)01532-X

95. Vincke C, Loris R, Saerens D, Martinez-Rodriguez S, Muyldermans S, Conrath K. General strategy to humanize a camelid single-domain antibody and identification of a universal humanized nanobody scaffold. *J Biol Chem* (2009) 284 (5):3273–84. doi: 10.1074/jbc.M806889200

96. Zhao W-H, Wang B-Y, Chen L-J, Fu W-J, Xu J, Liu J, et al. Four-year follow-up of LCAR-B38M in relapsed or refractory multiple myeloma: a phase 1, single-arm, open-label, multicenter study in China (LEGEND-2). *J Hematol Oncol* (2022) 15(1):86. doi: 10.1186/s13045-022-01301-8

97. Hanssens H, Meeus F, De Veirman K, Breckpot K, Devoogdt N. The antigen-binding moiety in the driver's seat of CARs. *Med Res Rev* (2022) 42 (1):306–42. doi: 10.1002/med.21818

98. Naik J, Themeli M, de Jong-Korlaar R, Ruiter RWJ, Poddighe PJ, Yuan H, et al. CD38 as a therapeutic target for adult acute myeloid leukemia and T-cell acute lymphoblastic leukemia. *Haematologica*. (2019) 104(3):e100-e3. doi: 10.3324/haematol.2018.192757

99. Paulus A, Malavasi F, Chanan-Khan A. CD38 as a multifaceted immunotherapeutic target in CLL. *Leuk Lymphoma* (2022), 1–11. doi: 10.1080/10428194.2022.2090551

100. Ben Baruch B, Mantsur E, Franco-Barraza J, Blacher E, Cukierman E, Stein R. CD38 in cancer-associated fibroblasts promotes pro-tumoral activity. *Lab Invest* (2020) 100(12):1517–31. doi: 10.1038/s41374-020-0458-8

101. Chen L, Diao L, Yang Y, Yi X, Rodriguez BL, Li Y, et al. CD38-Mediated immunosuppression as a mechanism of tumor cell escape from pd-1/pd-l1 blockade. *Cancer Discovery* (2018) 8(9):1156–75. doi: 10.1158/2159-8290.CD-17-1033

102. Dwivedi S, Rendón-Huerta EP, Ortiz-Navarrete V, Montaño LF. CD38 and regulation of the immune response cells in cancer. *J Oncol* (2021) 2021:6630295. doi: 10.1155/2021/6630295

103. Zah E, Nam E, Bhuvan V, Tran U, Ji BY, Gosliner SB, et al. Systematically optimized BCMA/CS1 bispecific CAR-T cells robustly control heterogeneous multiple myeloma. *Nat Commun* (2020) 11(1):2283. doi: 10.1038/s41467-020-16160-5

104. Yang Q, Parker CL, McCallen JD, Lai SK. Addressing challenges of heterogeneous tumor treatment through bispecific protein-mediated pretargeted drug delivery. *J Control Release* (2015) 220(Pt B):715–26. doi: 10.1016/j.jconrel.2015.09.040

105. Ruella M, Barrett DM, Kenderian SS, Shestova O, Hofmann TJ, Perazzelli J, et al. Dual CD19 and CD123 targeting prevents antigen-loss relapses after CD19-directed immunotherapies. *J Clin Invest* (2016) 126(10):3814–26. doi: 10.1172/JCI87366

106. Krejcik J, Casneuf T, Nijhof IS, Verbist B, Bald J, Plesner T, et al. Daratumumab depletes CD38+ immune regulatory cells, promotes T-cell expansion, and skews T-cell repertoire in multiple myeloma. *Blood*. (2016) 128 (3):384–94. doi: 10.1182/blood-2015-12-687749

107. Krejcik J, Frerichs KA, Nijhof IS, van Kessel B, van Velzen JF, Bloem AC, et al. Monocytes and granulocytes reduce cd38 expression levels on myeloma cells in patients treated with daratumumab. *Clin Cancer Res* (2017) 23(24):7498–511. doi: 10.1158/1078-0432.CCR-17-2027

frontiers | Frontiers in Immunology

TYPE Review
PUBLISHED 08 November 2022
DOI 10.3389/fimmu.2022.978513

OPEN ACCESS

EDITED BY
Zahra Sharifzadeh,
Pasteur Institute of Iran, Iran

REVIEWED BY
Tae Hyun Kang,
Kookmin University, South Korea
Björn Rissiek,
University Medical Center Hamburg-Eppendorf, Germany
Fatemeh Kazemi-Lomedasht,
Pasteur Institute of Iran (PII), Iran

*CORRESPONDENCE
Fang Zheng
Fang.zheng@xjtu.edu.cn
Geert Raes
Geert.Raes@vub.be

SPECIALTY SECTION
This article was submitted to Cancer Immunity and Immunotherapy, a section of the journal Frontiers in Immunology

RECEIVED 26 June 2022
ACCEPTED 30 September 2022
PUBLISHED 08 November 2022

CITATION
Zheng F, Pang Y, Li L, Pang Y, Zhang J, Wang X and Raes G (2022) Applications of nanobodies in brain diseases.
Front. Immunol. 13:978513.
doi: 10.3389/fimmu.2022.978513

Applications of nanobodies in brain diseases

Fang Zheng[1*], Yucheng Pang[1], Luyao Li[1], Yuxing Pang[2], Jiaxin Zhang[1], Xinyi Wang[1] and Geert Raes[3,4*]

[1]The Key Laboratory of Environment and Genes Related to Disease of Ministry of Education, Health Science Center, Xi'an Jiaotong University, Xi'an, China, [2]School of Electronic Science and Engineering, University of Electronic Science and Technology of China, Chengdu, China, [3]Research Group of Cellular and Molecular Immunology, Vrije Universiteit Brussel, Brussels, Belgium, [4]Myeloid Cell Immunology Lab, Vlaams Instituut voor Biotechnologie (VIB) Center for Inflammation Research, Brussels, Belgium

Nanobodies are antibody fragments derived from camelids, naturally endowed with properties like low molecular weight, high affinity and low immunogenicity, which contribute to their effective use as research tools, but also as diagnostic and therapeutic agents in a wide range of diseases, including brain diseases. Also, with the success of Caplacizumab, the first approved nanobody drug which was established as a first-in-class medication to treat acquired thrombotic thrombocytopenic purpura, nanobody-based therapy has received increasing attention. In the current review, we first briefly introduce the characterization and manufacturing of nanobodies. Then, we discuss the issue of crossing of the brain-blood-barrier (BBB) by nanobodies, making use of natural methods of BBB penetration, including passive diffusion, active efflux carriers (ATP-binding cassette transporters), carrier-mediated influx *via* solute carriers and transcytosis (including receptor-mediated transport, and adsorptive mediated transport) as well as various physical and chemical methods or even more complicated methods such as genetic methods *via* viral vectors to deliver nanobodies to the brain. Next, we give an extensive overview of research, diagnostic and therapeutic applications of nanobodies in brain-related diseases, with emphasis on Alzheimer's disease, Parkinson's disease, and brain tumors. Thanks to the advance of nanobody engineering and modification technologies, nanobodies can be linked to toxins or conjugated with radionuclides, photosensitizers and nanoparticles, according to different requirements. Finally, we provide several perspectives that may facilitate future studies and whereby the versatile nanobodies offer promising perspectives for advancing our knowledge about brain disorders, as well as hopefully yielding diagnostic and therapeutic solutions.

KEYWORDS

nanobody, brain disease, Alzheimer's disease, Parkinson's disease, brain infection, brain tumor, stroke, theragnostics

1 Introduction

1.1 Antibodies and nanobodies

Antibodies form a basic Y-shaped structure consisting of two heavy chains and two light chains, of which different regions have different functions such as antigen-binding (Fab) and regulating the activity of immune cells (Fc), as shown in Figure 1. In addition, the half-life of IgG is prolonged by the binding and dissociation of the Fc part of IgG to the neonatal Fc receptor (FcRn) (1), and the affinity of the antibody to the antigen is most affected by the complementary determinant regions of the variable region.

In 1993, Hamers-Casterman et al. found a natural heavy chain antibody (HCAb) in camels containing only γ heavy chain and missing the first domain of its constant region (CH1) (Figure 1) (2). Subsequent studies have found that this HCAb is common in all camelids (3). The variable region of the HCAb that retains antigen-binding activity, namely the variable domain of heavy chain of heavy-chain antibody (VHH), has a molecular weight of only about 15 kDa (1/10 of that of conventional antibodies) and a size in the nanometer scale, while it retains an antigen binding affinity that is often in the low nanomolar range. Therefore, VHH was called nanobody (Nb) by its original developer, Belgian biopharmaceutical company Ablynx. Due to the small size of nanobodies (Nbs), they can be easily cleared by glomerular filtration and because they also lack an Fc-tail and the associated interaction with FcRn, their serum half-life is very short (4). The short serum half-life as compared to full size antibodies has major advantages for applications such as *in vivo* imaging, since it allows to obtain a rapid clearance from untargeted tissues, with a low background signal and high target-to-background ratio and thus high contrast within hours after tracer injection as compared to up to several days for full-size antibodies, and also limits the background radiation to untargeted organs and thus the radiotoxicity (5). On the other hand, as will also be discussed in section 2.2., protein engineering technology to combine multiple Nbs or make fusions with other proteins can be used to increase the Nb serum half-life for other applications, where a longer serum-half-life may be preferred, for example to obtain a sustained therapeutic effect. But this will then also again increase the size of these constructs and so it is necessary to make a trade-off between size and serum half-life, depending on the individual applications in research, diagnostics and therapy. It is worth mentioning that heavy chain antibodies have been found not only in camelids, but also in some cartilaginous fishes (such as nurse shark), named immunoglobulin new or nurse shark antigen receptor (IgNAR) to distinguish them from HCAb in camelids. In addition, their structures are different. For example,

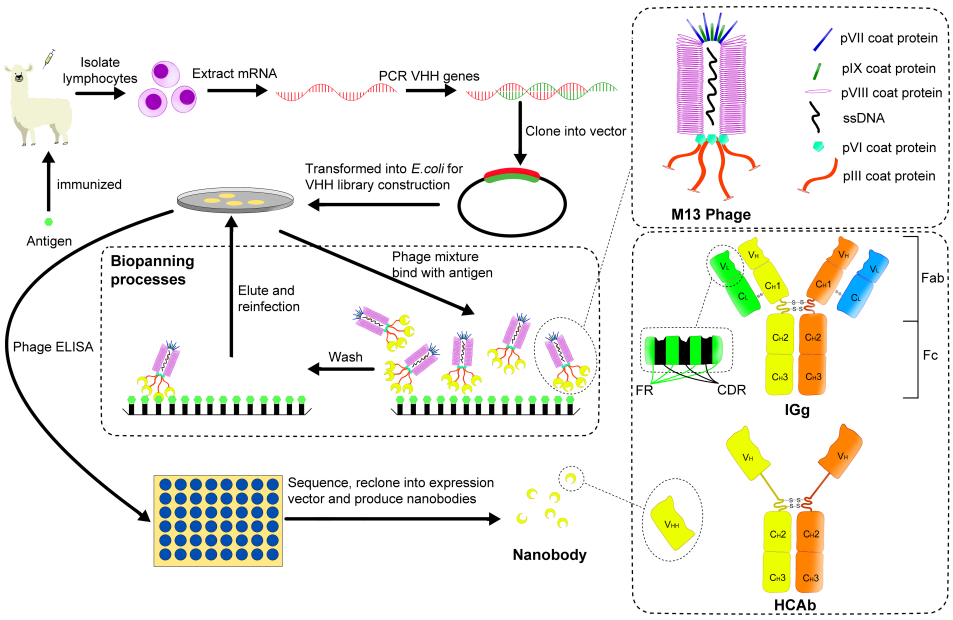

FIGURE 1
A brief process for building an immune library and screening for nanobody using M13 phage display. The coat structure of M13 phage is shown in the upper right panel, and the structure difference between general IgG and HCAb in camelids is shown in the lower right panel. After using a specific antigen to immunize a camelid, mRNA is extracted from its lymphocytes. Then PCR technology is used to obtain the corresponding DNA fragments, which are cloned into a phage display vector. After several cycles of biopanning, the required phages are screened for antigen binding via ELISA. Finally, the obtained nanobodies are sequenced and expressed for example in *E.coli*.

the variable domain of IgNAR (VNAR) only contains two CDRs, CDR1 and CDR3, and its CDR3 is usually longer than the corresponding region in IgG (6).

1.2 Screening and preparation of nanobodies

At present, the selection of Nbs is mainly realized by constructing a phage display library and screening high-performance antibodies from it.

For the construction of an immune library, the specific antigens (either as protein or *via* DNA vaccination) mixed with standard adjuvants such as Gerbu are injected into the camelid such as Bactrian camel, dromedary, llama and alpaca. These immunizations are performed typically eight times in two months and the corresponding HCAbs undergo affinity maturation (7, 8). Then an aliquot of peripheral blood is collected to obtain the lymphocytes and the mRNA in the lymphocytes is isolated and reverse transcribed into cDNA. Next, the cDNA can be amplified by PCR, cloned in frame to a surface protein gene on the phage vector, and then transferred into host cells such as *E. coli*. As a result, a small library containing the required VHH gene fragments (typically about 10^6 individual transformants) is obtained (9). For reference, Pardon et al. provided comprehensive and detailed methods of immunization and the construction of immune libraries (10).

Phage display is a widely used display platform (11). The phages used include many types (T7, T4, M13, etc.), among which the filamentous phage of the M13 type is most commonly used. The M13 phage's coat proteins include five types, as shown in Figure 1. Among all the coat proteins, the pIII protein is usually used as the display platform for Nb screening.

To select VHH's binding the antigen with high affinity, progeny phages are typically subjected to two to three cycles of biopanning, whereby they are incubated on a microtitration plate which has antigen fixed on it. After washing of unwanted phages that are not immobilized on the antigen, the selected phages are eluted and used to re-infect the host. Finally, the individual clones are analyzed for antigen-binding by standard enzyme-linked immunosorbent assay (ELISA) and the corresponding genes are sequenced to complete the initial screening of Nbs (9). Among the identified Nbs, selection of the lead compounds is later on performed using functional assays, depending on the desired properties and applications. Since Nbs have no complex structure, they can be expressed in large quantities in hosts such as prokaryotic cells. The entire process of constructing an immune library and screening target antibodies by phage display is shown in Figure 1.

In addition to immune libraries, natural libraries (12) and synthetic/semi-synthetic libraries (13) have also been proposed for generation of Nbs. These libraries are not dependent on immune responses in experimental animals, but usually, the content of the libraries needs to be much higher than that of immune libraries, especially for natural libraries (~ 10^9 individual clones) (3). In addition to phage display, the methods for screening the required Nbs from libraries also include cell surface display (14), ribosome display (15), mRNA/cDNA display (16), and high-throughput DNA sequencing and mass spectrometric identification (17), etc. There are also different suitable methods for different constructed libraries (9).

Nbs can be used as a good tool for research, diagnosis, and treatment. However, they need to be chemically functionalized to achieve certain functions in specific scenarios. Like for other proteins, chemical functionalization methods for Nbs can include natural amino acid residue methods, labeling methods, and non-natural amino acid methods (18). Using these methods, Nbs can be linked to fluorescent proteins (FP) or other detection moieties for imaging or to therapeutic moieties such as radionuclides, toxins or small molecule drugs as antibody-drug conjugates (ADC) for targeted therapy. In addition, Nbs can be formatted into a variety of other forms, such as the polyvalent Nb (polymer formed by the same Nbs) or multi-specific Nb (polymer formed by different Nbs). Compared with monovalent Nbs, these can have stronger apparent affinity or avidity for antigen (19, 20).

1.3 Brain-related applications of nanobodies as research tools

Thanks to their special structure, Nbs have many advantages compared to ordinary antibodies, such as high solubility (21, 22), high stability (23, 24), high antigen-binding ability (25), low immunogenicity (26), and strong tissue penetration (27). Based on these advantages, in addition to their clinical applications, which will be discussed later, Nbs can also be an excellent tool for basic brain research. In particular, to image the cell structure and reaction processes, Nbs tagged with fluorescent molecules are an excellent imaging tool in microscopy. Nbs were for example used to reveal an extra-synaptic population of synaptosomal-associated protein-25 (SNAP-25) and Syntaxin 1A in hippocampal neurons. Using a new technology called subdiffractional tracking of internalized molecules (sdTIM), based on a pulse-chase of fluorescently tagged ligands destined to undergo endocytic transport, the activity-dependent internalization of Atto647N-tagged anti-green fluorescent protein (GFP) Nbs bound to pHluorin-tagged synaptic protein vesicle-associated membrane protein 2 (VAMP2) was used to study the dynamics of endocytic pathways of synaptic vesicles (28). Similarly, antagonistic Nbs to vesicle glutamate transporters (VGLUTs) were linked to fluorescent molecules to study their inhibitory effect on neurotransmitter glutamate transport, improving the understanding of neurotransmitter transport processes (29). Nbs against activity-regulated

cytoskeleton-associated (Arc) protein were used as a new tool for studying the dynamics and function of Arc protein, providing a new approach for studying the long-term plasticity, memory, and cognitive flexibility of synapses (30). In addition to small-scale imaging, a whole-body immunolabeling approach called Nb (VHH)-boosted 3D imaging of solvent-cleared organs (vDISCO) has been proposed. Hereby, the signal of endogenous fluorescent proteins expressed in the central nervous system of transgenic mice can be enhanced more than 100 times using Nbs targeting these fluorescent proteins that have in turn been tagged with potent dyes such as Atto594, Atto488 or Alexa647, allowing head-to-toe light slice microscopy (panoramic imaging) and subcellular detail imaging of transparent mice. This technology was used to image neuronal changes in different pathological conditions (31). To further improve the imaging quality of Nbs, in addition to fluorescent molecules, the combination of Nbs with quantum dots (QD) (32), single-walled carbon nanotubes (SWCNT) (33) and other materials also showed exciting results. SWCNT emit light in the near-infrared band without bleaching or scintillation, which is very advantageous for imaging deep tissues.

Nbs also have powerful functions as molecular linking tools, one of which is that the ribosomes in neurons retrogradely labeled with GFP can be targeted with anti-GFP Nbs, and this method allows immunoprecipitation of the mRNA being translated in the presence of GFP (34). For example, to study the dopamine pathways, researchers built a pseudorabies virus (PRV) strain, in which the spread of the virus and expression of GFP are activated only after exposure to cyclization recombination enzyme (Cre). Once activated in Cre-expressing neurons, the virus serially labels chains of presynaptic neurons. To further study edge dopamine neurons and their molecular characteristics of presynaptic input, researchers used the previously mentioned approach to immunoprecipitate ribosomes to retrograde trace infected neurons and identify important inputs to the mesolimbic dopamine pathway (35). In addition to the application in immunoprecipitation, Tang, J,CY et al. developed a method for gene manipulation using GFP and anti-GFP Nbs, called Cre recombinase dependent on GFP (CRE-DOG). In this set-up, GFP acts as a scaffold that aggregates modular transcription domains and assembles a hybrid transcription complex to activate the target gene, where GFP recognition is mediated by paired anti-GFP Nbs (36). Using similar ideas, the team also developed a GFP-dependent transcription system (37), termed flippase dependent on GFP (FLP-Dog) (38), and other gene manipulation methods, providing reliable tools for photogenetics and other technologies.

Of course, Nbs can also be used to study the role of certain molecules in diseases by taking advantage of antagonistic Nbs which can block the function of the targeted antigens. For example, von Willebrand factor (VWF) is an important factor affecting ischemic stroke. Through the construction of a targeted Nb, the specific role of von Willebrand factor in ischemic stroke could be studied and the mechanism of VWF mediated by its A1 domain could be determined (39). Finally, the Nb specificity can be used to identify specific molecules expressed in disease. For example, Jovcevska, I et al. enriched phage-displayed Nb libraries from protein extracts of glioblastoma cell lines NCH644 and NCH421K. Through bioinformatics analysis, several molecules, including dihydropyrimidinase-related protein 2 (DPYSL2), were identified that are expressed differentially in glioblastoma as compared to normal tissues, providing promising reference biomarkers for follow-up research and treatment (40).

2 Transport of nanobodies to the brain

Antibodies usually perform their functions by binding to target molecules, which means that we need to deliver Nbs to the brain in order to have functionality in the brain. The blood-brain-barrier (BBB) is the biggest obstruction to drug delivery in the brain, and whether the BBB is crossed naturally by the Nb or not determines how the drug needs to be administered. In general, administration methods which themselves cross the BBB, such as intrathecal injection, can usually result in a higher concentration of drugs in the brain, but have the risk of greater tissue injury. On the other hand, drug delivery across the BBB after intravenous injection, is characterized by low tissue damage, but usually also lower concentration of drugs in the target organ. Both methods have their advantages and disadvantages. Nowadays, minimally invasive or even non-invasive diagnosis and treatment methods have received most attention. How to reduce the damage of drug administration and make it pass the BBB efficiently is one of the focuses of research. Compared with ordinary antibodies, Nbs have a 10 times smaller size and thus they should at least in theory have a better chance of penetrating the BBB, which may offer advantages for non-invasive or minimally invasive treatment.

2.1 Natural methods of BBB penetration

Barrier structures in the human body protect import organs, such as the blood-testosterone barrier, blood-eye barrier, blood-placenta barrier, etc. Among them, the BBB, which protects the central nervous system (CNS), is the barrier structure that is most difficult to pass in the human body. The average microvascular surface area per gram of tissue is 150 to 200 square centimeters, and the average BBB area of an adult is 12 to 18 square meters. The production and maintenance of BBB function mainly depends on the interaction between brain-microvessel endothelial cells (BMECs), and astrocytes and

pericytes. These structures, capillary basal membrane, microglia, and neurons are collectively called neurovascular units (NVU) (as shown in Figure 2) (27, 41). In physiology, the BBB allows molecules to pass through in several ways. The first way is passive diffusion. Fat solubility and molecular weight determine the efficiency of passive diffusion. When the molecular weight of a molecule is greater than 400Da, fat solubility does not increase the efficiency of its penetration through the BBB. At the same time, a high polar surface area (PSA) greater than 80 Å2 and the tendency to form more than 6 hydrogen bonds are also considered limiting factors for the entry of compounds into the central nervous system. The second pathway is active efflux. ATP-binding cassette proteins (ABC proteins) are expressed in the endocortical membrane of the blood-brain barrier. They lead to drug resistance characteristics of the CNS through the active efflux of foreign molecules and endogenous metabolites. The third pathway is carrier-mediated transport (CMT) through specific carrier proteins. Amino acids, fatty acids, and other substances cross through the BBB in this way. The fourth pathway is transcytosis, which includes receptor-mediated transcytosis (RMT), whereby larger molecules initiate transcytosis either by binding to specific receptors, and adsoptive-mediated transcytosis (AMT), which is based on adsorption with a positive charge to specific sites in the cell membrane (41).

2.2 BBB penetration by nanobodies after systemic administration *via* blood

Nbs use similar physiological mechanisms to pass through the BBB as those described above (Figure 2). Thereby it should be taken into account that the concentration of the Nb that can be obtained in the brain, depends not only on the ability of the Nb to cross the BBB but also on its pharmacokinetic characteristics. Studies using multivalent constructs of Nbs to increase their avidity or using Nb constructs of which the serum half-life had been increased *via* PEGylation or fusion with another Nb targeting serum albumin, have revealed that affinity and circulation time affect the uptake of Nbs in the brain (20, 42). In addition, the fusion of Nbs with an Fc segment can also increase circulating plasma half-life and increase brain uptake (43). It is important, however, to note that fusing Fc segments and Nbs alone may not necessarily be sufficient to increase brain uptake, since in another study fusing Fc segments to extend the time window for brain uptake did not increase BBB crossing, which may be related to molecular weight, species differences, or whether the Nbs themselves penetrate the BBB (44).

A first method *via* which some Nbs can cross the BBB is *via* RMT. The first Nbs described to cross the BBB *via* RMT were FC5 and FC44 (45). FC5 binds to BMECs' luminal α (2, 3)-sialoglycoprotein receptor to trigger clathrin-mediated endocytosis (46), FC44 binds to a protein of about 36kDa on BMECs, of which the identity needs further study (45). Compared with Nbs EG2 and A20.1 (targeting extracellular domain of EGFRvIII and *C. difficile* toxin A, respectively), FC5 and FC44 passed through an *in vitro* BBB model (SV-ARBEC) more easily (50-100 folds) and also had a better CSF/serum concentration ratio (20-40 folds) *in vivo* (47). Fusing the FC5 Nb to a human Fc segment, improved serum pharmacokinetics and resulted in an enhanced pharmacological action of chemically coupled agents. A bivalent fusion of FC5 with Fc exhibited a significantly increased transcytosis rate across the cerebral epithelial monolayer as compared to a monovalent fusion (43). Nbs targeting insulin-like growth factor receptors have been studied as tools for brain delivery of biologics. In one study, three Nbs targeting the extracellular domain of the human insulin-like growth factor-1 receptor (IGF1R) showed transmigration across an *in vitro* cell line-BBB model (SV-ARBEC). *In vivo*, fusions of these Nbs with mouse Fc segment showed enhanced brain uptake *via* RMT as compared to a control mFc. One of the IGF1R Nb-mFc coupled with the non-BBB crossing analgesic neuropeptide galanin also showed a dose-dependent analgesic effect (48). More recently, Nbs targeting the transferrin receptor have been produced as tools to deliver a biologically active peptide to the brain *via* RMT. Peripheral injection of such Nbs coupled with neurotensin, a neuropeptide that causes hypothermia when present in the brain but is unable to reach the brain from the periphery, resulted in hypothermia in mice (49). Finally, also an anti-prion Nb, known as PrioV3, was reported to be capable of crossing the BBB *in vitro* and *in vivo via* RMT (50).

A limited number of Nbs have been reported to pass through the BBB spontaneously *via* AMT. These Nbs generally have higher pI (27), such as a Nb targeting GFAP (pI=9.4) (51), R3QV targeting Aβ42 (pI>8.3) and A2 targeting Phosphorylated Tau protein (pI>9.5) (19).

A third approach is to deliver Nbs across the BBB using structures that can cross the BBB, such as glutathione targeted PEGylated liposomes (52), multi-walled carbon nanotubes (MWCNTs) (53), or Fe_3O_4 nanoparticles (54). On the other hand, Nbs can themselves be used to improve the targeting of liposomes in the brain (55). It is worth noting that cell penetrating peptides (CPPs), may also be useful for increasing Nb penetration into the brain. Fusing Nbs to CPPs has allowed the generation of cell-permeable Nbs, that can enter into living cells *via* non-endocytic delivery (56). Although the internalization process of this short amino acid sequence with positive charge is still controversial, it has shown the ability to help scFv targeting PrP^{Sc} and α-synuclein penetrating the BBB, which should also be applicable to Nbs (57, 58).

In addition, a temporary increase in BBB permeability through physical and chemical means can also improve the ability of Nbs to pass through the BBB. Studies have shown that intra-arterial administration can increase the uptake of Nbs in

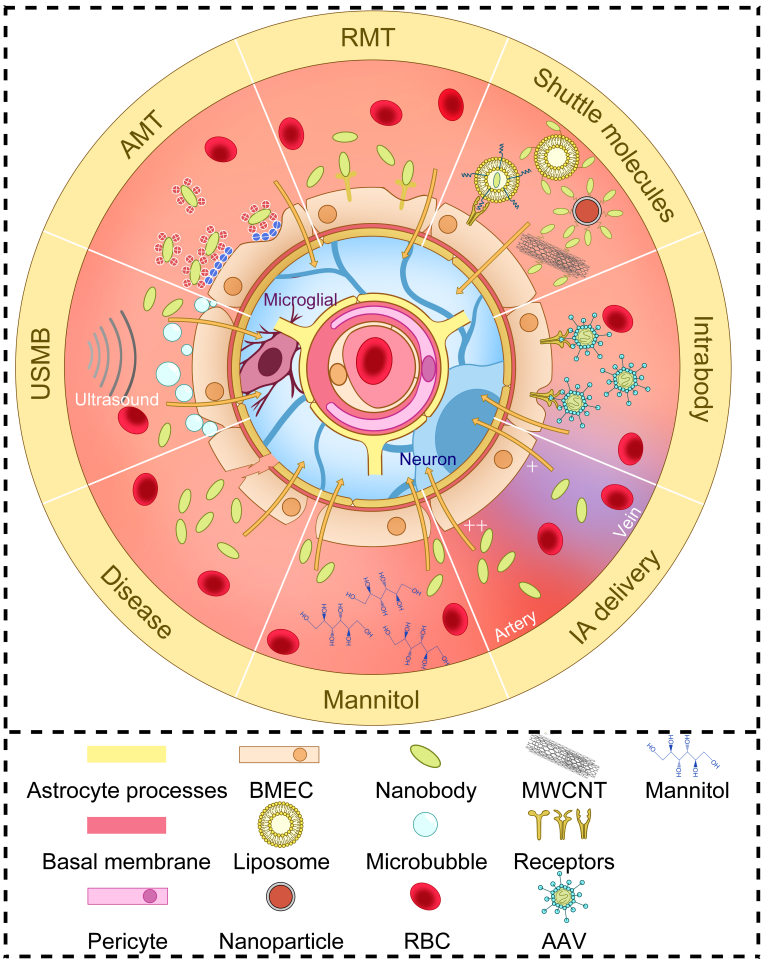

FIGURE 2
The structure of neurovascular units and several ways to increase BBB delivery of nanobodies. Brain-microvessel endothelial cells (BMECs), astrocytes, pericytes, capillary basal membrane, microglia, and neurons make up neurovascular Units (NVU). The efficiency of nanobodies crossing the BBB depends on altering BBB permeability or some physiological mechanisms of BBB crossing. AMT, adsorptive-mediated transcytosis; RMT, receptor-mediated transcytosis; USMB, ultrasound and microbubble; MWCNT, multi-walled carbon nanotubes; AAV, adeno-associated virus vectors; RBC, red blood cell; IA, intra-arterial.

the brain (59). Mannitol, as a hyperosmotic agent, can also improve the ability of several Nb fusion molecules to cross the BBB by weakening the junctions of BMECs (48, 51, 59). In a recent study, the combination of ultrasound and microbubbles (USMB) was found to enhance the permeability of drugs through an *in vitro* epithelial cell (MDCK II) barrier. USMB treatment increased epithelial cell permeability to large molecular weight molecules (between 4 and 20 kDa) by 3-7 times while promoting the intracellular accumulation of the same molecules. USMB doubled the paracellular permeability of an anti-CXCR4 Nb and increased its binding to retinoblastoma cells five-folds, suggesting a possible novel way to improve the delivery of drugs to organs protected by tissue barriers such as the BBB (60). The increase in brain temperature is also one of the factors affecting the structural stability of the BBB (27). Finally, when the BBB is damaged by disease, the ability of Nbs to pass through the BBB is naturally enhanced. This is why many studies on disease-related Nbs show that they can spontaneously enter the brain under pathological conditions where the BBB integrity is compromised (51, 61).

2.3 Other administration methods of nanobodies used for brain targeting

Less commonly used administration methods for Nbs include intranasal, intrathecal/intraventricular administration, and other local administration methods. For example, intracerebroventricular injection of Aβ -secretase 1(BACE1)-inhibiting Nb was reported to induce acute reduction of Aβ load

in blood and brain of transgenic AD model mice (62). Intrathecal administration, which induces less damage than intraventricular injection and has been extensively studied in stroke and neurodegenerative disease models to deliver larger molecules across the BBB (63), may also be an interesting approach to deliver Nbs in the brain in the future. Pizzo et al. have analyzed how IgG and Nbs distribute throughout the rat brain in a size-dependent manner after intrathecal administration. Both spread in the brain surface, and along the perivascular space around all types of blood vessels studied, whereby the percentage brain area accessed was strikingly greater for the smaller sdAb than for the larger IgG (64).

Drugs delivered by intranasal administration can cross the BBB by intracellular or paracellular pathways of the olfactory nerve and trigeminal nerve (65), which is a good method of local administration for drugs that cannot cross the BBB. Notably, intranasally administered Nb against Transthyretin (TTR) was found to cross the BBB. However, in that case also target-mediated effects occurred, whereby in wild-type mice, the anti-TTR Nb was specifically internalized in a receptor-mediated process by motor neurons, whereas in TTR deficient mice, the Nb was internalized by all cells, for late lysosomal degradation (66).

In a completely different approach from the protein-based methods, gene transfer strategies with adeno-associated virus (AAV) vectors can deliver Nbs directly to the CNS in a manner that rather transports genes, and thus has long-term effects (67).

3 Diagnostic and therapeutic applications of nanobodies in brain diseases

3.1 Alzheimer's disease

Alzheimer's disease (AD) is a degenerative disease of the CNS. In addition to macroscopic manifestations of brain atrophy, pathological phenomena in AD patients' brain tissues include tau-containing neurofibrillary tangles, amyloid β-protein (Aβ) plaques, activated glia or enlarged endosomes, which can be observed by microscopy. Also covert changes such as loss of synaptic homeostasis, loss of integrity of neurons or neuronal networks occur (68). The current diagnosis and treatment of AD are based on biomarkers related to its pathology and clinical manifestations of cognitive impairment. Although the etiology of AD is unknown, symptoms of cognitive impairment in AD can be detected by neuropsychological testing. However, multiple brain diseases may cause similar symptoms, so using biomarkers to achieve differential diagnosis and clinical staging is a solution. The biomarker diagnosis of AD is summarized as the ATN framework, i.e., "Aβ", "Tau" and "neurodegeneration", including A: Aβ-PET (Positron Emission Computed Tomography) of the brain, Aβ42 in body fluids or Aβ40/Aβ42, T: Tau-PET, P-Tau181 or P-Tau217, N: FDG (Fluorodeoxyglucose)-PET or MRI (showing brain atrophy and distinguishing it from other diseases such as cerebral hemorrhage), Total Tau, Neurofilament light (NfL), etc. (68). Aβ, P-Tau, and NfL in body fluids can be simply detected by ELISA. The tracers used for Aβ-PET are ^{11}C Pittsburgh Compound-B (PIB), ^{18}F-Flutemetamol, ^{18}F-Florbetapir and ^{18}F-Forbetaben. The tracers used for Tau-PET is ^{18}F-Flortaucipir (68–70). Although antibodies are widely used in ELISA and other technologies, antibodies have at present not been used in the imaging diagnosis of AD, and no image-related antibody tracer has entered clinical trials. Some preclinical imaging studies have started to report the use of Nbs for detecting AD-related biomarkers. For example, despite a brain uptake yet too low for effective *in vivo* imaging, ^{99m}Tc-labeled Nb pa2H targeting Aβ resulted in a small yet significant higher cerebral uptake in APP/PS1 mice (71). R3QV, a Nb binding the central 17~28 residues of Aβ, and Nb A2 targeting the C-terminal of pTau protein, both have been reported to cross the BBB (19). Site-specific labeling of R3QV with the contrastophore gadolinium was used to design imaging probes for magnetic resonance imaging (MRI) (72). In addition, gadolinium-based nanoparticles were also chelated with radionuclies ($^{68}Ga^{3+}$ or $^{111}In^{3+}$) or covalently bound with near-infrared pigments (such as Cyanine5.5) to be used *in vivo* (73).

Notably, Nbs targeting Aβ oligomers (PrioAD12 and PrioAD13) detected accumulation of Aβ oligomers in the retina, which originated in peripheral blood and preceded cognitive decline and brain deposition of oligomers. This provides an idea for early detection of AD *via* an "eye test" (74, 75). In addition to the identification of typical pathological molecules, the identification of different forms of aggregation of the Aβ molecule is also of interest because they appear in AD at different stages of the disease. The V31-1 Nb recognizes the C-terminal of Aβ42 and only recognizes monomers and oligomers in Western Blot (WB) and dot-blot analysis (76). Similarly, Nbs A4 and E1 exhibit strong affinity for Aβ oligomers (77, 78). Another Nb, B10, showed recognition of the Aβ fibril without recognition of the protein fragment Aβ1-40 or weakly of the Aβ oligomers, indicating recognition of conformational epitopes (79). In addition, Rutgers et al. constructed eight Nbs targeting Aβ (ni3A, ni8B, va2E, vaE2, va1G, pa4D, pa11E, pa2H), among which pa4D, pa11E, and pa2H can recognize Aβ in the vascular and parenchymal depositions, while the other Nbs can only recognize Aβ in the vascular depositions. This suggests that there may be differences between Aβ epitopes in blood vessels and brain (80). Among various tested Aβ-targeting Nbs, VHH ni3A showed the highest transmigration efficiency in an *in vitro* blood-brain barrier model (co-culture of bovine brain capillary endothelial cells and rat's

astrocytes) through active transport (81). Tau protein is also one of the targets for AD, for example using Nb F8-2 targeting the C-terminal of Tau protein (82).

Currently, the treatment methods of AD are not very effective. In addition to conventional treatment of complications and improvement of living habits, cholinesterase inhibitors such as Donepezil and Rivastamine and similar drugs can only improve the functional abnormalities caused by cholinergic neuron damage in AD patients. Disease-modifying therapies targeting AD pathological molecules have been widely studied, and many antibody drugs have entered clinical trials (68, 83). On 2 November 2019, the State Medical Products Administration of the People's Republic of China (SDA) conditionally approved Oligomannate, an acid oligosaccharide extracted from Marine brown algae, for marketing with the pharmacological action of preventing Aβ fibrils from forming and depolymerizing the formed fibrils. The U.S. Food and Drug Administration (FDA) announced On June 7, 2021 that it has approved Biogen's Aducanumab for the treatment of early-stage Alzheimer's disease (AD). Although its therapeutic efficacy is still debated, there is no doubt that it has led to the development of AD antibody drugs and disease-modifying therapies.

The use of Nbs to treat AD has also been investigated. Nbs can play a therapeutic role by inhibiting fibrils aggregation and blocking Aβ -induced neurotoxicity. Aβ oligomers were found to be primarily toxic molecules rather than mature Aβ fibrils or Aβ monomers. Nbs A4, E1, V31-1 can bind to Aβ oligomers, inhibit their aggregation into Aβ fibrils and block Aβ oligomer induced neurotoxicity to SH-SY5Y neuroblastoma cells (76–78). Similarly, B10AP prevents the formation of mature Aβ amyloid fibrils by preventing the formation of fibrils in the protofibrils stage (the stage before the formation of mature Aβ fibrils) (79). In addition to inhibiting fiber aggregation, direct degradation of Aβ is also a feasible method. Asec-1A could inhibit the toxicity of Aβ aggregation to SH-SY5Y neuroblastoma cells by hydrolyzing Aβ at the α-secretase site (84, 85). In addition, the fusion of Nbs that can cross the BBB with therapeutic molecules was also evaluated. In a longitudinal study with treatment for 5 weeks using a BBB crossing Nb (FC5) fused to an amyloid-β oligomer-binding peptide (ABP) *via* a mouse IgG Fc fragment, PET showed a significant reduction in brain Aβ levels, MRI showed correction of hippocampal atrophy and increased CSF Aβ ratio of 42/40 and decreased Nfl concentration was found (86). Although Aβ is the primary target for the treatment of AD, improvement in Tau pathology is also of therapeutic significance. VHH Z70 recognizes the PHF6 sequence, known for its nucleation capacity, and effectively inhibits Tau aggregation *in vitro* and spread and aggregation in FRET biosensor reporter cells. Local expression of VHH Z70 in the brain using a lentiviral vector infection also reduced tau spread in the Tau pathological mouse model THY-Tau 30 (87). As a method of treatment, AAV-mediated delivery of Nbs into the brain has also been evaluated, namely for the Nb targeting BACE1 (beta-secretase 1), a target in Alzheimer's disease (67). Nbs related to the diagnosis and treatment of AD are summarized in Supplementary Table 1.

3.2 Parkinson's disease

Parkinson's disease (PD) is a neurodegenerative disease of which the incidence increases with age. Its etiology is complex and is explained by gene environment interactions. The current COVID-19 pandemic has raised concerns that COVID-19 may increase the risk of PD sickness, because COVID-19 leads to low body temperature and may cause neural degeneration following nasal entry into the brain (88). Currently it is believed that the pathophysiological characteristics of PD are the accelerated death of dopaminergic neurons caused by the complex interaction of abnormal α-synuclein aggregation with lewy bodies, mitochondrial dysfunction, lysosomes or vesicle transport, synaptic transport problems and neuroinflammation. Macroscopic manifestations are symptoms caused by the loss of dopamine cells in the substantia nigra striatum, such as typical bradykinesia and less common depression and anxiety, etc. The symptoms of disease are usually treated by levodopa (a precursor of dopamine) (88).

At present, the diagnosis of PD mainly depends on symptoms, that is, it does not meet the absolute exclusion criteria, there are at least two supportive criteria, and there are no red flags (89). However, diagnosis or scale dependent on clinical manifestations cannot avoid some subjectivity, and diagnosis combined with biomarkers will improve this shortcoming and be more conducive to early diagnosis.

Nbs developed so far in the context of PD mainly target α-synuclein, including NbSyn2 and NbSyn87 (90–93), which both target the C terminal of α-synuclein, but the sequence targeted by NbSyn2 is closer to the C terminal, and has less impact on the aggregation of α-synuclein (93). Studies have shown that selective phosphorylation of α-synuclein will significantly change the affinity of NbSyn87 binding to it (94). Recently, Nbα-syn01, a Nb targeting the n-terminal of α-synuclein, has also emerged, and preferentially recognizes α-synuclein fibrils rather than monomers (95). However, as far as PD diagnosis is concerned, so far there have not been any Nb studies related to brain imaging of diagnostic biomarkers.

Concerning medical treatment for PD, the ideas for reducing the pathological aggregation of α-synuclein can be divided into two ways: the first is to inhibit the aggregation of α-synuclein into fibrils, and the second is to degrade α-synuclein. Studies have shown that both NbSyn2 and NbSyn87 can inhibit the formation of α-synuclein fibrils *in vitro*, and their presence reduces high forster resonance energy transfer (FRET) α-synuclein oligomer with greater toxicity, which in turn reduces cell death, microglial activation and other injury responses (96). Nba-syn01 can also inhibit the α-synuclein-seeded aggregation

in vitro and reduce its toxicity to SH-SY5Y cells (95). Since α-synuclein in PD is mainly aggregated inside cells, its degradation becomes more difficult. Constructing Nbs as intrabodies will allow them to be expressed in cells. Meanwhile, fusion of intrabodies with PEST amino acid sequences rich in prolyl(P), glutamine(E), aspartic acid(D), serine(S) and threonyl(T) residues can improve the intracellular solubility of intrabodies and induce proteasome degradation (97). As such, NbSyn87PEST intrabodies could degrade α-synuclein aggregation in cell culture and reduce its cytotoxicity (98). In subsequent studies, adeno-associated virus vectors were injected into the substantia nigra through stereotaxic injections and it was found that NbSyn87PEST intrabodies could significantly reduce the pathological aggregation of α-synuclein. However, compared with human sourced scFv VH14, NbSyn87PEST showed no significant dopaminergic tone maintenance in the striatum, and there was a certain inflammatory response (99).

In addition to targeting α-synuclein, targeting other PD-related proteins is also a treatment method. For example, since PD is usually associated with mutations of Leucine-rich repeat kinase 2 (LRRK2) that increase its activity, a variety of Nbs targeting different sites of LRRK2 have been developed as inhibitors (100, 101). Nbs associated with PD diagnosis and treatment are summarized in Supplementary Table 2.

Recent studies have found that the pathology of PD occurs in blood, skin and other tissues. Although the specificity and sensitivity of its diagnosis using peripheral markers are not all high, this provides ideas for the development of diagnosis in the future (102). In addition to the typical PD-related molecules, damage-related molecules common to some diseases can also be used as therapeutic or diagnostic targets, such as Nbs targeting caspase-3 and Mitochondrial Rho GTPase 1 (Miro1). Nbs against the former can resist cell damage caused by oxidative stress in a variety of brain diseases, while the latter is associated with mitochondrial homeostasis and is a potential biomarker or therapeutic target after visualization or regulation by Nbs (103, 104).

3.3 Brain tumor

3.3.1 Glioblastoma

Isocitrate dehydrogenase (IDH)-wildtype glioblastoma (GB), previously termed as primary glioblastoma, is the most common and malignant glioma occurring in adults (105), with a peak incidence in the age group of 75 to 79 years old (106), especially among Caucasians (107). Current standard treatment for GB upon initial diagnosis is surgical resection followed by the postoperative Stupp protocol, namely radiation and concomitant chemotherapy with temozolomide (108). Although the application of the Stupp protocol since 2005 has significantly enhanced therapeutic effects, the median survival of patients still doesn't exceed two years (109), for which the essential reasons lie in the nature of the tumor. This WHO grade IV diffuse glioma is characterized by heightened invasiveness, intra- and inter-tumor heterogeneity, relative resistance to therapy, and high recurrence rate, mainly due to the mobility of glioblastoma stem cells (GSCs). It has a profoundly immunosuppressive microenvironment mediated by myeloid-derived suppressor cells (MDSCs), and further affects the systemic immune status even without distant metastases. Furthermore, gliomas exhibit a low mutational burden and offer few therapeutic targets to the immune system, severely limiting the efficacy of immunotherapy (110). Given the lack of visual signals of all the tumor cells, part of the cancer tissues remain inevitably after surgery. Meanwhile, functional areas of the brain are frequently involved, which poses challenges for surgeons to achieve the balance between maximizing the extent of resection and minimizing neurological morbidity. Further, the BBB remains a formidable hurdle for drug delivery.

Although the molecular parameters of glioma have become important criteria for GB classification and grading (105), current clinical diagnosis still mainly relies on imaging examination including CT, MRI and PET/SPECT. However, CT/MRI can only observe the anatomical features of the tumor, and the relatively high uptake of glucose by the cerebral cortex makes the imaging specificity of 18F-FDG for brain tumors not high (111). Not only this, the full course of glioma treatment requires highly sensitive, non-invasive imaging strategies to demarcate tumor boundaries, guide surgery, evaluate therapeutic effects, and identify recurrence.

Given the difficulties in the diagnosis and treatment of GBs, Nbs are attracting attention. A dual-target Nb aiming at EGFR/EGFRvIII (wild type and mutant EGFR) -overexpressed in GB cells, was labelled with Cy5.5 (a near infrared dye) for optical imaging (112). Further, the Cy5.5-labelled Nb was attached to small unilamellar vesicles loaded with the MRI contrast agent Gd, achieving MRI/NIR bimodal imaging (55). However, considering the heterogeneity of GB, researchers have tried to find target binding antigens in the tumor microenvironment, including the overexpressed insulin-like growth factor binding protein 7 (IGFBP7) in the blood vessels of brain tumors (54), as well as signal regulatory protein alpha (SIRPα) significantly expressed by microglia- and monocyte-derived tumor-associated macrophages (TAMs) (113). A recent study reported that anti-SIRPα Nb labeled with ^{99m}Tc can qualitatively display intracranial tumors (113).

A basic idea of applying Nbs for GB treatment is to antagonize key antigens in the progression of glioma. Zottel A et al. first validated eight novel antigens of GB and then examined the effects of four Nbs and their different combinations on glioma cells *in vitro*. Among them, Nb225 (anti-TUFM) and Nb79 (anti-vimentin) showed good tumor suppressive effect, with no harm to normal astrocytes (114). As an alternative, Nbs have been used as the targeting moiety of

immunotoxins, setting the stage for the cytotoxic part to come into play. Some studies have used bivalent anti-EGFR Nb coupled with pseudomonas exotoxin (PE) to potentiate killing of GB tumor cells and tumor stem cells by pro–apoptotic tumor necrosis factor–related apoptosis–inducing ligand (TRAIL). Hereby, the receptor-targeted toxin upregulated TRAIL death receptors and suppressed the expression of anti–apoptotic proteins, thus overcoming TRAIL resistance in BG tumor cells and tumor stem cells (115, 116). It is worth noting that a recent study by Porčnik A et al. focused on the molecular signatures and driver genes behind the cellular subpopulations of GB, and managed to relate tumor invasion with the expression pattern of the transcription factor TRIM28 in the core and rim of the tumor (117). Based on these findings, they generated Nb237 to antagonize TRIM28 for reducing the invasiveness of GB cells, and obtained favorable results *in vivo* using zebra fish embryos xenografted with GB cells.

In recent years, photoimmunotherapy (PIT) has achieved great progress. It combines near-infrared light, which is harmless to the human body, and immunotherapy to selectively kill cancer cells overexpressing specific antigens through the activation of the light-activated substance IRDye700DX. Researchers are also trying to apply this new strategy in the treatment of GB. It was reported that US28, a foreign viral GPCR encoded by human cytomegalovirus and expressed by tumor cells, enhanced GB growth (118). Thus, a US28-targeting bivalent Nb was developed, and further labelled with IRDye700DX for PIT (119). An EGFR antibody-photosensitizer conjugate AkaluxTM has been commercially approved for head and neck malignancies (NCT02422979). Using Nbs as targeting substances, PIT may open a new chapter in glioma treatment.

3.3.2 Brain metastases

Brain metastases (BMs), the major type of adult brain tumor, occur when primary tumor cells migrate through blood, lymphatic or directly invade the brain. The most common primary tumors giving rise to BMs are lung cancer, breast cancer and melanoma, with proportions of 40%-50%, 15%-20%, and 5%-20% respectively (120). With the progress of radiotherapy and molecular targeted therapy, consensus has been reached, that an individualized treatment plan should be developed for patients with BM, using the optimal sequential use of surgery, stereotactic radiosurgery, whole-brain radiation therapy, targeted therapy, and immunotherapy (121). However, given the difficulty of treatment, prevention of BMs should be the focus, especially among the high-risk groups, including patients with stage III/IV non-small cell lung cancer (NSCLC), HER2+ breast cancer, and melanoma.

As compared to studies on Nbs for the theragnostics of GB, research on the use of Nbs in the context of BMs is relatively mature, probably because people have a better understanding of the pathological mechanism of the primary tumors and can continue to use their well-developed Nbs. A notable example is the attempt to utilize 2Rs15d for detecting and treating the BMs of HER2pos breast cancer. 2Rs15d binds to the domain I of HER2, different from the epitope recognized by trastuzumab and pertuzumab (C-terminus of domain IV) (122) and maintains its affinity to HER2 under conditions where the individual is receiving HER2-targeted drug therapy, which enables 2Rs15d derivatives to be used either as imaging probes for monitoring the treatment effect or serve as an add-on treatment. In an early study, 18F labeled 2Rs15d injected intravenously into mice bearing intracranial HER2-expressing BT474M1 tumors, successfully visualized the HER2pos brain tumor *via* PET, with tumor-to-tissue ratios greater than 10:1 in major organs except for kidney (123). When radiolabeled with 111In, similar results were also observed in mice bearing either intracranial SKOV3.IP1 or 231Br tumors *via* μSPECT/CT (124). Quantum dots (QDs), also known as semiconductor nanocrystals (semiconductor nanocrystals), have unique optical properties compared with traditional dyes, and can detect target molecules with extremely low concentrations, thereby significantly improving detection sensitivity. According to one study, anti-HER2 Nb fluorescently labelled with QDs could efficiently assess micro-metastases even in thick tissue sections using single- and two-photon imaging (125). Besides, in this study, breast cancer cells were first transplanted into the peripheral organs and tissues of animals to better simulate the process of BMs. Overall, these results demonstrated the potential of Nb-based imaging agents in BMs detection.

Further, radiolabeled 2Rs15d has exhibited therapeutic potential. The same study where 111In-2Rs15d was introduced, also coupled 2Rs15d with α–particle emitting 225Ac or β–particle emitting 131I (31). Mice bearing intracranial tumors receiving either 225Ac-2Rs15d or 131I -2Rs15d both had a longer median survival. Thereby, an α-radionuclide such as 225Ac, an excellent therapeutic candidate, may expand treatment options in addition to β–particle radiotherapy. It is worth noting that 131I can release β-particles and γ-rays simultaneously, showing theragnostic value.

Moreover, taking advantage of Nbs, efforts have been made to tackle BMs of NSCLC. Precision medicine is the most distinctive feature of lung cancer diagnosis and treatment. Targeted therapy has become the core method for the treatment of advanced (NSCLC), especially for relatively well-researched targets such as EGFR and ALK. However, this also faces a serious problem: resistance mutations of tumors. For example, EGFRT790M is the major cause of the failure of first-generation EGFR TKI, represented by gefitinib. In addition, when tumors metastasize to the brain, drugs that do not easily penetrate the BBB also lose their usefulness. To address the core challenges of NSCLC BM and drug resistance, Yin W et al. constructed a sophisticated liposomal system, T12/P-Lipo (126), in which they attached a transferrin receptor (TfR)-binding

peptide T12 and an anti-PDL1 Nb to the surface of the liposome. PD-1/PD-L1 monoclonal antibody is a representative immune checkpoint inhibitor (ICI). Although PD-L1 is not upregulated in primary brain tumors, it is highly expressed in NSCLC cancer cells, the surrounding TAMs and tumor vascular epithelial cells. Hence, anti-PDL1 Nbs can be effectively used as targeting ligands for nanocarriers. Regarding the latter, simvastatin (SV) and gefitinib (Gef) were loaded into the engineered liposome, whereby SV could promote the repolarization of TAM from M2 to M1, thereby re-sensitizing EGFRT790M cells to Gef. The therapeutic efficacy of T12/P-Lipo was thus evidenced in the BMs model of H1975 NSCLC(Supplementary Table 3).

3.4 Other brain diseases

Antibodies or antibody fragments such as Nbs are rarely used in infectious diseases of the central nervous system. In a recent study, Nbs VHHG9 and VHHF3 targeting Neisseria adhesin A (NadA), which can antagonize the interaction between recombinant NadA and cell receptors, were developed. The preincubation of Neisseria meningitidis with VHHF3 and VHHG9 could significantly reduce the adhesion of *neisseria meningitidis* to human microvascular endothelial cells *in situ* and prevent it from crossing a BBB model (human BMECs) *in vitro*, providing a new treatment idea (127). Rabies is also an infectious disease in which the CNS is mainly affected. After infection, the virus invades the CNS through the peripheral nervous system, presenting symptoms such as hydrophobia and mania. There is a high risk of death from respiratory or circulatory failure without early treatment, so post-exposure treatment of rabies is very important. The use of antibodies to neutralize the virus is a very effective way to reduce the cost of post-exposure treatment. A variety of Nbs with high affinity and low cost have been developed. For example, Nbs were linked with a coil-coil peptide derived from the human cartilage oligomeric matrix protein (COMP48) to form homogenous pentavalent multimers called combodies 26424 and 26434] (128) or bi-specific Nbs were developed that can target albumin to increase blood half-life, which were then combined with post-exposure vaccine prophylaxis (129, 130).

Prion diseases are rare CNS degenerative diseases of specific etiology. They can be classified as sporadic, genetic, or acquired (infection), such as Creutzfeldt-Jakob disease, fatal familial insomnia, and Kuru disease. They are characterized by accumulation and aggregation of prions or abnormally folded proteins. Compared with the typical α-helix in normal PrP^{c} (Cellular Prion protein), the abnormally folded isoform PrP^{sc} has a large number of β-folds and is partially resistant to proteases, rapidly converting normal proteins into abnormal proteins (131). Due to the special pathological manifestations and specific pathological molecules of the disease, the diagnosis is relatively clear (such as brain MRI and immunohistochemical detection of PrP^{sc} deposition, etc.), but there is no clear treatment plan. At present, research on the use of Nbs in the field of prion diseases has mainly been focused on studying of the molecular interaction and developing a potential treatment. For example, NB-PRP-01 targeting PrP^{c} was reported to be co-crystallized with PrP^{c} (132). The mechanism of PrP transformation was studied by the crystallization of Nb484 and full-length human PrP (133). It was further found that Nb484 could bind to the hydrophobic region of mouse PrP, inhibit its transformation and showed no neurotoxicity in cultured sections (134). Nbs that simultaneously could cross the BBB and have therapeutic effects will have the best therapeutic significance. For example, PrioV3 Antibody has been found to traverse *in vitro* or *in vivo* the BBB and inhibit PrP^{SC} accumulation in ScN2a Cells and ScGT1 cell lines, to which Nbs themselves have not been shown to be neurotoxic (50, 74).

Concerning degenerative diseases of the central nervous system other than AD and PD, Nbs can also play a beneficial role in Huntington's disease. Similar to AD and PD, Huntington's disease is caused by a genetic mutation, in this case one that causes abnormal Huntingtin proteins to accumulate in nerve cells and affect nerve cell function. The basal ganglia is usually the first to be affected, causing the chorea symptoms. In 2015, the first Nb targeting the N-terminal domain of Huntingtin protein was developed and reported to show good affinity for human mutant and wild-type Huntingtin protein (135). The use of Nbs as an intrabody may be a good development direction given the intracellular aggregation of Huntington's protein, and other sources of intrabody have been shown to be feasible early on (136).

There are also many diseases of the nervous system characterized by an inflammatory response, such as multiple sclerosis. Multiple sclerosis (MS) is a primary demyelinating disease of unknown etiology, which may be related to genetic, environmental, infection and other factors. The lesions are extensive, including significantly reduced oligodendrocyte and astrocyte proliferation. The current idea of treatment for MS is to reduce inflammation and promote myelin regeneration. Since multiple cytokines are involved in the mechanism of MS and there are no typical pathological molecules like in degenerative diseases, antibodies to treat MS usually target various cytokines and immune cell surface antigens. At present, the targets of Nbs that have been evaluated as a treatment option for MS are TNFR1 and CXCL10. The anti-TNFR1 Nb TROS was shown to inhibit inflammation *in vitro* and *in vivo* (137), TROS also reduced neuroinflammation, preserved myelin and neurons in the MS model (mog35-55 induced experimental autoimmune encephalomyelitis, EAE) (138). The Nb 3Nb12 against CXCL10 was reported to block the CXCL10-CXCR3 binding and effectively inhibit the chemotaxis of CXCR3-Transfected HEK293T cells, which provides support for subsequent studies on treatment and diagnosis (139).

ALX-0681, with commercial name caplacizumab, is a Nb targeting the A1 domain of vWF, and is able to instantly inhibit the formation of microthrombi, significantly reducing the risk of thrombosis in acquired thrombocytopenic purpura (aTTP) (140). It was approved by the European Commission (EC) in 2018 for the treatment of adult patients with aTTP. Intriguingly, ALX-0681 was developed as an advanced variant of ALX-0081, also a bivalent vWF-targeting Nb. Before ALX-0681 went into clinical trials, ALX-0081 had been investigated in patients with risk to develop thromboembolism. Although it failed in a comparative Phase II randomized trial since it did not perform better in reducing bleeding events compared with abciximab (NCT01020383) (141), there was one study which demonstrated its capability in reducing brain infarction (142). Specifically, ALX-0081 was considered to block GPIb-vWF interaction, thus preventing the complete occlusion of cerebral blood vessels, promoting reperfusion, meanwhile mitigating the risk of bleeding. In a number of clinical trials of caplacizumab, stroke as a major event was used to evaluate the drug effect (143, 144), however, whether caplacizumab can be used as an antithrombotic drug in the context of cerebral infarction remains unclear. In view that the current drug treatment for thrombotic stroke comprising anti-platelets, anti-coagulation and thrombolysis, but this cannot avoid the risk of brain hemorrhage, we believe that the application of anti-vWF Nbs is worth exploring (Supplementary Table 4).

4 Discussion and outlook

As molecules with small molecular weight, high affinity and low immunogenicity, Nbs can be applied in a wide range of fields and also offer specific advantages as compared to ordinary full-size antibodies. For brain-related research, Nbs can be used to develop a variety of microscopy imaging tracers for specific targets, and Nbs can also serve as linkage molecules in genetic regulators of specific genes.

Nbs are not only tools to study brain disease-related molecules, but also can be developed into diagnostic reagents and therapeutic drugs. At present, although there is no lack of innovation in the use of Nbs for AD, PD, prion and other brain diseases, most compounds under development are still in an early research and preclinical phase. Studies of the therapeutic effect of the Nbs will need to go beyond counteracting toxicity to cultured nerve cells and address the effect on various pathological and neurological manifestations in the disease models. Thereby, successful crossing of the BBB remains an important attention point for diagnostic or therapeutic targeting in brain diseases. Yet, examples we have given such as that Nbs targeting the extracellular domain of the human insulin-like growth factor-1 receptor (IGF1R) coupled with the non-BBB crossing analgesic neuropeptide galanin also showed a dose-dependent analgesic effect, point to conditions where Nbs can indeed cross the BBB *in vivo* and exert a biological effect. Recent findings on autophagy dysregulation in AD, may offer an interesting possible new direction. It has been found that lysosomal acidification leads to a decrease in enzyme activity, which in turn reduces the ability to decompose Aβ (145). In addition, few research has been done on the treatment with Nbs related to microglia, a crucial cell in central nervous system diseases. Recent studies have shown that once activated by Aβ, microglia reach a chronic tolerant phase as a result of broad defects in energy metabolism and subsequently diminished immune responses, including cytokine secretion and phagocytosis. Interferon-gamma treatment reversed the defective glycolytic metabolism and inflammatory functions of microglia and thereby mitigated the AD pathology of 5XFAD mice (146). Microglia and their modulators may also be targeted with Nbs, either as tracers for imaging or even for therapeutics in case the suitable targets can be identified.

With regard to brain tumors, although Nbs and Nb-derived conjugates have many advantages for GB diagnosis and treatment, there are also some potential pitfalls. For instance, in case of systemic administration, effects on organs such as kidneys, liver or spleen may cause dose-limiting toxicities. In addition, chemical modification of Nbs may change their affinity, so it is necessary to verify the affinity and specificity of the Nbs before and after labeling or fusion with other compounds such as toxins. Moreover, the above literature provides valuable clues for the clinical application of Nbs, but before these schemes can be finally applied to the clinic many obstacles and difficulties still need to be overcome, the most important of which are the tumor heterogeneity of GB, and the individualized selection of the targets. Multi-target combination treatment strategies of immunotherapy and targeted therapy may be an important research direction to solve this problem in the future. Secondly, the evaluation of the treatment response of immunotherapy is also another problem. A robust imaging and molecular biology evaluation system will need to be established to predict and monitor the efficacy of therapy in individual patients, and there also Nbs may play a role. Also for the early detection of BMs, Nb-based molecular imaging holds great application prospects and, as a targeting molecule, Nb also greatly assists in drug delivery and radioimmunotherapy, allowing relatively mature treatments for peripheral lesions to have the opportunity to work in the brain. The ultimate requirement will mainly be clinical dose-response studies to address whether sufficient amounts of the Nbs can be obtained across the BBB to effectively eliminate cancer cells in the brain, under conditions with acceptable toxicity, both in the brain and in peripheral organs.

It is worth to mention that, in the current review, we have mainly focused on the use of Nbs as research tools and tracers for *in vivo* imaging and therapy. In addition, Nbs can also be used as tracers in microcantilever sensors (147) and organic transistors (148, 149) for early detection of diseases or pathogen detection. At the same time, the lower cost of producing Nbs compared to monoclonal antibodies makes them suitable for manufacturing *in vitro* diagnostic kits. At present, the research

and development of high-sensitivity detection devices for the detection of brain diseases is still in a relatively early stage and warrants further studies. But biosensors using Nbs definitively show promising potential for rapid, low-cost and large-scale screening for brain diseases such as AD in the future (150).

Overall, there is still a lot of innovation to be explored in the application of Nbs in the field of brain diseases.

Author contributions

FZ, YCP, LL, YXP, JZ, and XW wrote this manuscript. FZ and GR revised this manuscript. All authors contributed to the article and approved the submitted version.

Funding

FZ was supported by National Natural Science Foundation of China(No. 38170187, Basic research program of Natural Science in Shaanxi Province (NO. 2021JM-007), Science Foundation of the Chinese Academy of Medical Sciences (2021-JKCS-008), LL, YCP, and XW were supported by national college students' science and technology innovation project (SJ202110698176).

Acknowledgments

We apologize for not including all of the publications by our colleagues.

Conflict of interest

GR is shareholder of Precirix and Abscint and is inventor on various patent applications covering diagnostic and/or therapeutic use of Nbs. FZ is shareholder of Shaanxi Shaanxi Haisinuowei Technology Co. LTD and is inventor on various patent applications covering diagnostic and/or therapeutic use of Nbs.

The remaining authors declare that the research was conducted in the absence of any commercial or financial relationships that could be construed as a potential conflict of interest.

Publisher's note

Supplementary material

The Supplementary Material for this article can be found online at: https://www.frontiersin.org/articles/10.3389/fimmu.2022.978513/full#supplementary-material

References

1. Burmeister WP, Huber AH, Bjorkman PJ. Crystal structure of the complex of rat neonatal fc receptor with fc. *Nature* (1994) 372(6504):379–83. doi: 10.1038/372379a0

2. Hamers-Casterman C, Atarhouch T, Muyldermans S, Robinson G, Hamers C, Songa EB, et al. Naturally occurring antibodies devoid of light chains. *Nature* (1993) 363(6428):446–8. doi: 10.1038/363446a0

3. Muyldermans S. Nanobodies: Natural single-domain antibodies. *Annu Rev Biochem* (2013) 82:775–97. doi: 10.1146/annurev-biochem-063011-092449

4. Fan K, Jiang B, Guan Z, He J, Yang D, Xie N, et al. Fenobody: A ferritin-displayed nanobody with high apparent affinity and half-life extension. *Anal Chem* (2018) 90(9):5671–7. doi: 10.1021/acs.analchem.7b05217

5. D'Huyvetter M, Vos J, Caveliers V, Vaneycken I, Heemskerk J, Duhoux FP, et al. Phase I trial of (131)I-Gmib-Anti-Her2-Vhh1, a new promising candidate for Her2-targeted radionuclide therapy in breast cancer patients. *J Nucl Med* (2021) 62 (8):1097–105. doi: 10.2967/jnumed.120.255679

6. Kovaleva M, Ferguson L, Steven J, Porter A, Barelle C. Shark variable new antigen receptor biologics - a novel technology platform for therapeutic drug development. *Expert Opin Biol Ther* (2014) 14(10):1527–39. doi: 10.1517/14712598.2014.937701

7. De Genst E, Handelberg F, Van Meirhaeghe A, Vynck S, Loris R, Wyns L, et al. Chemical basis for the affinity maturation of a camel single domain antibody. *J Biol Chem* (2004) 279(51):53593–601. doi: 10.1074/jbc.M407843200

8. Muyldermans SA. Guide to: Generation and design of nanobodies. *FEBS J* (2021) 288(7):2084–102. doi: 10.1111/febs.15515

9. Liu W, Song H, Chen Q, Yu J, Xian M, Nian R, et al. Recent advances in the selection and identification of antigen-specific nanobodies. *Mol Immunol* (2018) 96:37–47. doi: 10.1016/j.molimm.2018.02.012

10. Pardon E, Laeremans T, Triest S, Rasmussen SG, Wohlkonig A, Ruf A, et al. A general protocol for the generation of nanobodies for structural biology. *Nat Protoc* (2014) 9(3):674–93. doi: 10.1038/nprot.2014.039

11. hie H, Meyer T, Schirrmann T, Hust M, Dubel S. Phage display derived therapeutic antibodies. *Curr Pharm Biotechnol* (2008) 9(6):439–46. doi: 10.2174/138920108786786349

12. Yan J, Wang P, Zhu M, Li G, Romao E, Xiong S, et al. Characterization and applications of nanobodies against human procalcitonin selected from a novel naive nanobody phage display library. *J Nanobiotechnology* (2015) 13:33. doi: 10.1186/s12951-015-0091-7

13. De Genst E, Saerens D, Muyldermans S, Conrath K. Antibody repertoire development in camelids. *Dev Comp Immunol* (2006) 30(1-2):187–98. doi: 10.1016/j.dci.2005.06.010

14. Fleetwood F, Devoogdt N, Pellis M, Wernery U, Muyldermans S, Stahl S, et al. Surface display of a single-domain antibody library on gram-positive bacteria. *Cell Mol Life Sci* (2013) 70(6):1081–93. doi: 10.1007/s00018-012-1179-y

15. Hanes J, Jermutus L, Pluckthun A. Selecting and evolving functional proteins in vitro by ribosome display. *Methods Enzymol* (2000) 328:404–30. doi: 10.1016/S0076-6879(00)28409-7

16. Wang H, Liu R. Advantages of mrna display selections over other selection techniques for investigation of protein-protein interactions. *Expert Rev Proteomics* (2011) 8(3):335–46. doi: 10.1586/epr.11.15

17. Fridy PC, Li Y, Keegan S, Thompson MK, Nudelman I, Scheid JF, et al. A robust pipeline for rapid production of versatile nanobody repertoires. *Nat Methods* (2014) 11(12):1253–60. doi: 10.1038/nmeth.3170

18. Schumacher D, Helma J, Schneider AFL, Leonhardt H, Hackenberger CPR. Nanobodies: Chemical functionalization strategies and intracellular applications. *Angew Chem Int Ed Engl* (2018) 57(9):2314–33. doi: 10.1002/anie.201708459

19. Li T, Vandesquille M, Koukouli F, Dudeffant C, Youssef I, Lenormand P, et al. Camelid single-domain antibodies: A versatile tool for in vivo imaging of extracellular and intracellular brain targets. *J Control Release* (2016) 243:1–10. doi: 10.1016/j.jconrel.2016.09.019

20. Glassman PM, Walsh LR, Villa CH, Marcos-Contreras OA, Hood ED, Muzykantov VR, et al. Molecularly engineered nanobodies for tunable pharmacokinetics and drug delivery. *Bioconjug Chem* (2020) 31(4):1144–55. doi: 10.1021/acs.bioconjchem.0c00003

21. Muyldermans S. Applications of nanobodies. *Annu Rev Anim Biosci* (2021) 9:401–21. doi: 10.1146/annurev-animal-021419-083831

22. Salvador JP, Vilaplana L, Marco MP. Nanobody: Outstanding features for diagnostic and therapeutic applications. *Anal Bioanal Chem* (2019) 411(9):1703–13. doi: 10.1007/s00216-019-01633-4

23. Dumoulin M, Conrath K, Van Meirhaeghe A, Meersman F, Heremans K, Frenken LG, et al. Single-domain antibody fragments with high conformational stability. *Protein Sci* (2002) 11(3):500–15. doi: 10.1110/ps.34602

24. Perez JM, Renisio JG, Prompers JJ, van Platerink CJ, Cambillau C, Darbon H, et al. Thermal unfolding of a llama antibody fragment: A two-state reversible process. *Biochemistry* (2001) 40(1):74–83. doi: 10.1021/bi0009082

25. Stijlemans B, Conrath K, Cortez-Retamozo V, Van Xong H, Wyns L, Senter P, et al. Efficient targeting of conserved cryptic epitopes of infectious agents by single domain antibodies. *Afr Trypanosomes as Paradigm. J Biol Chem* (2004) 279 (2):1256–61. doi: 10.1074/jbc.M307341200

26. Cortez-Retamozo V, Backmann N, Senter PD, Wernery U, De Baetselier P, Muyldermans S, et al. Efficient cancer therapy with a nanobody-based conjugate. *Cancer Res* (2004) 64(8):2853–7. doi: 10.1158/0008-5472.CAN-03-3935

27. Ruiz-Lopez E, Schuhmacher AJ. Transportation of single-domain antibodies through the blood-brain barrier. *Biomolecules* (2021) 11(8):1131. doi: 10.3390/biom11081131

28. Joensuu M, Padmanabhan P, Durisic N, Bademosi AT, Cooper-Williams E, Morrow IC, et al. Subdiffractional tracking of internalized molecules reveals heterogeneous motion states of synaptic vesicles. *J Cell Biol* (2016) 215(2):277–92. doi: 10.1083/jcb.201604001

29. Schenck S, Kunz L, Sahlender D, Pardon E, Geertsma ER, Savtchouk I, et al. Generation and characterization of anti-vglut nanobodies acting as inhibitors of transport. *Biochemistry* (2017) 56(30):3962–71. doi: 10.1021/acs.biochem.7b00436

30. Ishizuka Y, Mergiya TF, Baldinotti R, Xu J, Hallin EI, Markusson S, et al. Development and validation of arc nanobodies: New tools for probing arc dynamics and function. *Neurochem Res* (2022) 47(9):2656–66. doi: 10.1101/2022.01.20.477070

31. Cai R, Pan C, Ghasemigharagoz A, Todorov MI, Forstera B, Zhao S, et al. Panoptic imaging of transparent mice reveals whole-body neuronal projections and skull-meninges connections. *Nat Neurosci* (2019) 22(2):317–27. doi: 10.1038/s41593-018-0301-3

32. Modi S, Higgs NF, Sheehan D, Griffin LD, Kittler JT. Quantum dot conjugated nanobodies for multiplex imaging of protein dynamics at synapses. *Nanoscale* (2018) 10(21):10241–9. doi: 10.1039/C7NR09130C

33. Mann FA, Lv Z, Grosshans J, Opazo F, Kruss S. Nanobody-conjugated nanotubes for targeted near-infrared in vivo imaging and sensing. *Angew Chem Int Ed Engl* (2019) 58(33):11469–73. doi: 10.1002/anie.201904167

34. Ekstrand MI, Nectow AR, Knight ZA, Latcha KN, Pomeranz LE, Friedman JM. Molecular profiling of neurons based on connectivity. *Cell* (2014) 157(5):1230–42. doi: 10.1016/j.cell.2014.03.059

35. Pomeranz LE, Ekstrand MI, Latcha KN, Smith GA, Enquist LW, Friedman JM. Gene expression profiling with cre-conditional pseudorabies virus reveals a subset of midbrain neurons that participate in reward circuitry. *J Neurosci* (2017) 37(15):4128–44. doi: 10.1523/JNEUROSCI.3193-16.2017

36. Tang JC, Rudolph S, Dhande OS, Abraira VE, Choi S, Lapan SW, et al. Cell type-specific manipulation with gfp-dependent cre recombinase. *Nat Neurosci* (2015) 18(9):1334–41. doi: 10.1038/nn.4081

37. Tang JC, Szikra T, Kozorovitskiy Y, Teixiera M, Sabatini BL, Roska B, et al. A nanobody-based system using fluorescent proteins as scaffolds for cell-specific gene manipulation. *Cell* (2013) 154(4):928–39. doi: 10.1016/j.cell.2013.07.021

38. Tang JC, Drokhlyansky E, Etemad B, Rudolph S, Guo B, Wang S, et al. Detection and manipulation of live antigen-expressing cells using conditionally stable nanobodies. *Elife* (2016) 5:e15312. doi: 10.7554/eLife.15312

39. Denorme F, Martinod K, Vandenbulcke A, Denis CV, Lenting PJ, Deckmyn H, et al. The Von willebrand factor A1 domain mediates thromboinflammation, aggravating ischemic stroke outcome in mice. *Haematologica* (2021) 106(3):819–28. doi: 10.3324/haematol.2019.241042

40. Jovcevska I, Zupanec N, Urlep Z, Vranic A, Matos B, Stokin CL, et al. Differentially expressed proteins in glioblastoma multiforme identified with a nanobody-based anti-proteome approach and confirmed by oncofinder as possible tumor-class predictive biomarker candidates. *Oncotarget* (2017) 8 (27):44141–58. doi: 10.18632/oncotarget.17390

41. Kadry H, Noorani B, Cucullo L. A blood-brain barrier overview on structure, function, impairment, and biomarkers of integrity. *Fluids Barriers CNS* (2020) 17(1):69. doi: 10.1186/s12987-020-00230-3

42. Su S, Esparza TJ, Nguyen D, Mastrogiacomo S, Kim JH, Brody DL. Pharmacokinetics of single domain antibodies and conjugated nanoparticles using a hybrid near infrared method. *Int J Mol Sci* (2021) 22(16):8695. doi: 10.3390/ijms22168695

43. Farrington GK, Caram-Salas N, Haqqani AS, Brunette E, Eldredge J, Pepinsky B, et al. A novel platform for engineering blood-brain barrier-crossing bispecific biologics. *FASEB J* (2014) 28(11):4764–78. doi: 10.1096/fj.14-253369

44. Rotman M, Welling MM, van den Boogaard ML, Moursel LG, van der Graaf LM, van Buchem MA, et al. Fusion of Higg1-fc to 111in-Anti-Amyloid single domain antibody fragment vhh-Pa2h prolongs blood residential time in App/Ps1 mice but does not increase brain uptake. *Nucl Med Biol* (2015) 42(8):695–702. doi: 10.1016/j.nucmedbio.2015.03.003

45. Muruganandam A, Tanha J, Narang S, Stanimirovic D. Selection of phage-displayed llama single-domain antibodies that transmigrate across human blood-brain barrier endothelium. *FASEB J* (2002) 16(2):240–2. doi: 10.1096/fj.01-0343fje

46. Abulrob A, Sprong H, Van Bergen EHP, Stanimirovic D. The blood-brain barrier transmigrating single domain antibody: Mechanisms of transport and antigenic epitopes in human brain endothelial cells. *J Neurochem* (2005) 95 (4):1201–14. doi: 10.1111/j.1471-4159.2005.03463.x

47. Haqqani AS, Caram-Salas N, Ding W, Brunette E, Delaney CE, Baumann E, et al. Multiplexed evaluation of serum and csf pharmacokinetics of brain-targeting single-domain antibodies using a nanolc-Srm-Ilis method. *Mol Pharm* (2013) 10 (5):1542–56. doi: 10.1021/mp3004995

48. Alata W, Yogi A, Brunette E, Delaney CE, van Faassen H, Hussack G, et al. Targeting insulin-like growth factor-1 receptor (Igf1r) for brain delivery of biologics. *FASEB J* (2022) 36(3):e22208. doi: 10.1096/fj.202101644R

49. Wouters Y, Jaspers T, De Strooper B, Dewilde M. Identification and in vivo characterization of a brain-penetrating nanobody. *Fluids Barriers CNS* (2020) 17 (1):62. doi: 10.1186/s12987-020-00226-z

50. Jones DR, Taylor WA, Bate C, David M, Tayebi MA. Camelid anti-prp antibody abrogates prp replication in prion-permissive neuroblastoma cell lines. *PloS One* (2010) 5(3):e9804. doi: 10.1371/journal.pone.0009804

51. Li T, Bourgeois JP, Celli S, Glacial F, Le Sourd AM, Mecheri S, et al. Cell-penetrating anti-gfap vhh and corresponding fluorescent fusion protein vhh-gfp spontaneously cross the blood-brain barrier and specifically recognize astrocytes: Application to brain imaging. *FASEB J* (2012) 26(10):3969–79. doi: 10.1096/fj.11-201384

52. Rotman M, Welling MM, Bunschoten A, de Backer ME, Rip J, Nabuurs RJ, et al. Enhanced glutathione pegylated liposomal brain delivery of an anti-amyloid single domain antibody fragment in a mouse model for alzheimer's disease. *J Control Release* (2015) 203:40–50. doi: 10.1016/j.jconrel.2015.02.012

53. Zhu S, Huang AG, Luo F, Li J, Li J, Zhu L, et al. Application of virus targeting nanocarrier drug delivery system in virus-induced central nervous system disease treatment. *ACS Appl Mater Interfaces* (2019) 11(21):19006–16. doi: 10.1021/acsami.9b06365

54. Iqbal U, Albaghdadi H, Luo Y, Arbabi M, Desvaux C, Veres T, et al. Molecular imaging of glioblastoma multiforme using anti-Insulin-Like growth factor-binding protein-7 single-domain antibodies. *Br J Cancer* (2010) 103 (10):1606–16. doi: 10.1038/sj.bjc.6605937

55. Iqbal U, Albaghdadi H, Nieh MP, Tuor UI, Mester Z, Stanimirovic D, et al. Small unilamellar vesicles: A platform technology for molecular imaging of brain tumors. *Nanotechnology* (2011) 22(19):195102. doi: 10.1088/0957-4484/22/19/195102

56. Herce HD, Schumacher D, Schneider AFL, Ludwig AK, Mann FA, Fillies M, et al. Cell-permeable nanobodies for targeted immunolabelling and antigen manipulation in living cells. *Nat Chem* (2017) 9(8):762–71. doi: 10.1038/nchem.2811

57. Spencer B, Williams S, Rockenstein E, Valera E, Xin W, Mante M, et al. Alpha-synuclein conformational antibodies fused to penetratin are effective in models of lewy body disease. *Ann Clin Transl Neurol* (2016) 3(8):588–606. doi: 10.1002/acn3.321

58. Skrlj N, Drevensek G, Hudoklin S, Romih R, Curin Serbec V, Dolinar M. Recombinant single-chain antibody with the Trojan peptide penetratin positioned in the linker region enables cargo transfer across the blood-brain barrier. *Appl Biochem Biotechnol* (2013) 169(1):159–69. doi: 10.1007/s12010-012-9962-7

59. Lesniak WG, Chu C, Jablonska A, Behnam AB, Zwaenepoel O, Zawadzki M, et al. Pet imaging of distinct brain uptake of a nanobody and similarly-sized pamam dendrimers after intra-arterial administration. *Eur J Nucl Med Mol Imaging* (2019) 46(9):1940–51. doi: 10.1007/s00259-019-04347-y

60. Rousou C, de Maar J, Qiu B, van der Wurff-Jacobs K, Ruponen M, Urtti A, et al. The effect of microbubble-assisted ultrasound on molecular permeability across cell barriers. *Pharmaceutics* (2022) 14(3):494. doi: 10.3390/pharmaceutics14030494

61. Caljon G, Caveliers V, Lahoutte T, Stijlemans B, Ghassabeh GH, Van Den Abbeele J, et al. Using microdialysis to analyse the passage of monovalent nanobodies through the blood-brain barrier. *Br J Pharmacol* (2012) 165(7):2341–53. doi: 10.1111/j.1476-5381.2011.01723.x

62. Dorresteijn B, Rotman M, Faber D, Schravesande R, Suidgeest E, van der Weerd L, et al. Camelid heavy chain only antibody fragment domain against beta-site of amyloid precursor protein cleaving enzyme 1 inhibits beta-secretase activity in vitro and in vivo. *FEBS J* (2015) 282(18):3618–31. doi: 10.1111/febs.13367

63. Calias P, Banks WA, Begley D, Scarpa M, Dickson P. Intrathecal delivery of protein therapeutics to the brain: A critical reassessment. *Pharmacol Ther* (2014) 144(2):114–22. doi: 10.1016/j.pharmthera.2014.05.009

64. Pizzo ME, Wolak DJ, Kumar NN, Brunette E, Brunnquell CL, Hannocks MJ, et al. Intrathecal antibody distribution in the rat brain: Surface diffusion, perivascular transport and osmotic enhancement of delivery. *J Physiol* (2018) 596(3):445–75. doi: 10.1113/JP275105

65. Soleimanizadeh A, Dinter H, Schindowski K. Central nervous system delivery of antibodies and their single-domain antibodies and variable fragment derivatives with focus on intranasal nose to brain administration. *Antibodies (Basel)* (2021) 10(4):47. doi: 10.3390/antib10040047

66. Gomes JR, Cabrito I, Soares HR, Costelha S, Teixeira A, Wittelsberger A, et al. Delivery of an anti-transthyretin nanobody to the brain through intranasal administration reveals transthyretin expression and secretion by motor neurons. *J Neurochem* (2018) 145(5):393–408. doi: 10.1111/jnc.14332

67. Marino M, Zhou L, Rincon MY, Callaerts-Vegh Z, Verhaert J, Wahis J, et al. Aav-mediated delivery of an anti-Bace1 vhh alleviates pathology in an alzheimer's disease model. *EMBO Mol Med* (2022) 14(4):e09824. doi: 10.15252/emmm.201809824

68. Knopman DS, Amieva H, Petersen RC, Chetelat G, Holtzman DM, Hyman BT, et al. Alzheimer Disease. *Nat Rev Dis Primers* (2021) 7(1):33. doi: 10.1038/s41572-021-00269-y

69. Curtis C, Gamez JE, Singh U, Sadowsky CH, Villena T, Sabbagh MN, et al. Phase 3 trial of flutemetamol labeled with radioactive fluorine 18 imaging and neuritic plaque density. *JAMA Neurol* (2015) 72(3):287–94. doi: 10.1001/jamaneurol.2014.4144

70. Jie C, Treyer V, Schibli R, Mu L. Tauvid: The first fda-approved pet tracer for imaging tau pathology in alzheimer's disease. *Pharm (Basel)* (2021) 14(2):110. doi: 10.3390/ph14020110

71. Nabuurs RJ, Rutgers KS, Welling MM, Metaxas A, de Backer ME, Rotman M, et al. *In vivo* detection of amyloid-beta deposits using heavy chain antibody fragments in a transgenic mouse model for alzheimer's disease. *PloS One* (2012) 7(6):e38284. doi: 10.1371/journal.pone.0038284

72. Vandesquille M, Li T, Po C, Ganneau C, Lenormand P, Dudeffant C, et al. Chemically-defined camelid antibody bioconjugate for the magnetic resonance imaging of alzheimer's disease. *MAbs* (2017) 9(6):1016–27. doi: 10.1080/19420862.2017.1342914

73. Pansieri J, Plissonneau M, Stransky-Heilkron N, Dumoulin M, Heinrich-Balard L, Rivory P, et al. Multimodal imaging gd-nanoparticles functionalized with Pittsburgh compound b or a nanobody for amyloid plaques targeting. *Nanomedicine (Lond)* (2017) 12(14):1675–87. doi: 10.2217/nnm-2017-0079

74. David MA, Jones DR, Tayebi M. Potential candidate camelid antibodies for the treatment of protein-misfolding diseases. *J Neuroimmunol* (2014) 272(1-2):76–85. doi: 10.1016/j.jneuroim.2014.05.001

75. Habiba U, Descallar J, Kreilaus F, Adhikari UK, Kumar S, Morley JW, et al. Detection of retinal and blood abeta oligomers with nanobodies. *Alzheimers Dement (Amst)* (2021) 13(1):e12193. doi: 10.1002/dad2.12193

76. Lafaye P, Achour I, England P, Duyckaerts C, Rougeon F. Single-domain antibodies recognize selectively small oligomeric forms of amyloid beta, prevent abeta-induced neurotoxicity and inhibit fibril formation. *Mol Immunol* (2009) 46(4):695–704. doi: 10.1016/j.molimm.2008.09.008

77. Zameer A, Kasturirangan S, Emadi S, Nimmagadda SV, Sierks MR. Anti-oligomeric abeta single-chain variable domain antibody blocks abeta-induced toxicity against human neuroblastoma cells. *J Mol Biol* (2008) 384(4):917–28. doi: 10.1016/j.jmb.2008.09.068

78. Kasturirangan S, Li L, Emadi S, Boddapati S, Schulz P, Sierks MR. Nanobody specific for oligomeric beta-amyloid stabilizes nontoxic form. *Neurobiol Aging* (2012) 33(7):1320–8. doi: 10.1016/j.neurobiolaging.2010.09.020

79. Habicht G, Haupt C, Friedrich RP, Hortschansky P, Sachse C, Meinhardt J, et al. Directed selection of a conformational antibody domain that prevents mature amyloid fibril formation by stabilizing abeta protofibrils. *Proc Natl Acad Sci U.S.A.* (2007) 104(49):19232–7. doi: 10.1073/pnas.0703793104

80. Rutgers KS, van Remoortere A, van Buchem MA, Verrips CT, Greenberg SM, Bacskai BJ, et al. Differential recognition of vascular and parenchymal beta amyloid deposition. *Neurobiol Aging* (2011) 32(10):1774–83. doi: 10.1016/j.neurobiolaging.2009.11.012

81. Rutgers KS, Nabuurs RJ, van den Berg SA, Schenk GJ, Rotman M, Verrips CT, et al. Transmigration of beta amyloid specific heavy chain antibody fragments across the in vitro blood-brain barrier. *Neuroscience* (2011) 190:37–42. doi: 10.1016/j.neuroscience.2011.05.076

82. Dupre E, Danis C, Arrial A, Hanoulle X, Homa M, Cantrelle FX, et al. Single domain antibody fragments as new tools for the detection of neuronal tau protein in cells and in mice studies. *ACS Chem Neurosci* (2019) 10(9):3997–4006. doi: 10.1021/acschemneuro.9b00217

83. Scheltens P, De Strooper B, Kivipelto M, Holstege H, Chetelat G, Teunissen CE, et al. Alzheimer's disease. *Lancet* (2021) 397(10284):1577–90. doi: 10.1016/S0140-6736(20)32205-4

84. Kasturirangan S, Brune D, Sierks M. Promoting alpha-secretase cleavage of beta-amyloid with engineered proteolytic antibody fragments. *Biotechnol Prog* (2009) 25(4):1054–63. doi: 10.1002/btpr.190

85. Kasturirangan S, Boddapati S, Sierks MR. Engineered proteolytic nanobodies reduce abeta burden and ameliorate abeta-induced cytotoxicity. *Biochemistry* (2010) 49(21):4501–8. doi: 10.1021/bi902030m

86. Kang MS, Shin M, Ottoy J, Aliaga AA, Mathotaarachchi S, Quispialaya K, et al. Preclinical in vivo longitudinal assessment of Kg207-m as a disease-modifying alzheimer's disease therapeutic. *J Cereb Blood Flow Metab* (2022) 42(5):788–801. doi: 10.1177/0271678X211035625

87. Danis C, Dupre E, Zejneli O, Caillierez R, Arrial A, Begard S, et al. Inhibition of tau seeding by targeting tau nucleation core within neurons with a single domain antibody fragment. *Mol Ther* (2022) 30(4):1484–99. doi: 10.1016/j.ymthe.2022.01.009

88. Bloem BR, Okun MS, Klein C. Parkinson's disease. *Lancet* (2021) 397(10291):2284–303. doi: 10.1016/S0140-6736(21)00218-X

89. Postuma RB, Berg D, Stern M, Poewe W, Olanow CW, Oertel W, et al. Mds clinical diagnostic criteria for parkinson's disease. *Mov Disord* (2015) 30(12):1591–601. doi: 10.1002/mds.26424

90. Vuchelen A, O'Day E, De Genst E, Pardon E, Wyns L, Dumoulin M, et al. (1)H, (13)C and (15)N assignments of a camelid nanobody directed against human alpha-synuclein. *Biomol NMR Assign* (2009) 3(2):231–3. doi: 10.1007/s12104-009-9182-4

91. De Genst EJ, Guilliams T, Wellens J, O'Day EM, Waudby CA, Meehan S, et al. Structure and properties of a complex of alpha-synuclein and a single-domain camelid antibody. *J Mol Biol* (2010) 402(2):326–43. doi: 10.1016/j.jmb.2010.07.001

92. Guilliams T, El-Turk F, Buell AK, O'Day EM, Aprile FA, Esbjorner EK, et al. Nanobodies raised against monomeric alpha-synuclein distinguish between fibrils at different maturation stages. *J Mol Biol* (2013) 425(14):2397–411. doi: 10.1016/j.jmb.2013.01.040

93. El-Turk F, Newby FN, De Genst E, Guilliams T, Sprules T, Mittermaier A, et al. Structural effects of two camelid nanobodies directed to distinct c-terminal epitopes on alpha-synuclein. *Biochemistry* (2016) 55(22):3116–22. doi: 10.1021/acs.biochem.6b00149

94. El TF, De Genst E, Guilliams T, Fauvet B, Hejjaoui M, Di Trani J, et al. Exploring the role of post-translational modifications in regulating alpha-synuclein interactions by studying the effects of phosphorylation on nanobody binding. *Protein Sci* (2018) 27(7):1262–74. doi: 10.1002/pro.3412

95. Hmila I, Vaikath NN, Majbour NK, Erskine D, Sudhakaran IP, Gupta V, et al. Novel engineered nanobodies specific for n-terminal region of alpha-synuclein recognize lewy-body pathology and inhibit in-vitro seeded aggregation and toxicity. *FEBS J* (2022) 289(15):4657–73. doi: 10.1111/febs.16376

96. Iljina M, Hong L, Horrocks MH, Ludtmann MH, Choi ML, Hughes CD, et al. Nanobodies raised against monomeric a-synuclein inhibit fibril formation and destabilize toxic oligomeric species. *BMC Biol* (2017) 15(1):57. doi: 10.1186/s12915-017-0390-6

97. Joshi SN, Butler DC, Messer A. Fusion to a highly charged proteasomal retargeting sequence increases soluble cytoplasmic expression and efficacy of diverse anti-synuclein intrabodies. *MAbs* (2012) 4(6):686–93. doi: 10.4161/mabs.21696

98. Butler DC, Joshi SN, Genst E, Baghel AS, Dobson CM, Messer A. Bifunctional anti-Non-Amyloid component alpha-synuclein nanobodies are protective in situ. *PloS One* (2016) 11(11):e0165964. doi: 10.1371/journal.pone.0165964

99. Chatterjee D, Bhatt M, Butler D, De Genst E, Dobson CM, Messer A, et al. Proteasome-targeted nanobodies alleviate pathology and functional decline in an alpha-Synuclein-Based parkinson's disease model. *NPJ Parkinsons Dis* (2018) 4:25. doi: 10.1038/s41531-018-0062-4

100. Leemans M, Galicia C, Deyaert E, Daems E, Krause L, Paesmans J, et al. Allosteric modulation of the gtpase activity of a bacterial Lrrk2 homolog by conformation-specific nanobodies. *Biochem J* (2020) 477(7):1203–18. doi: 10.1042/BCJ20190843

101. Singh RK, Soliman A, Guaitoli G, Stormer E, von Zweydorf F, Dal Maso T, et al. Nanobodies as allosteric modulators of parkinson's disease-associated Lrrk2. *Proc Natl Acad Sci USA* (2022) 119(9):e2112712119. doi: 10.1073/pnas.2112712119

102. Chahine LM, Beach TG, Brumm MC, Adler CH, Coffey CS, Mosovsky S, et al. *In vivo* distribution of alpha-synuclein in multiple tissues and biofluids in Parkinson disease. *Neurology* (2020) 95(9):e1267–e84. doi: 10.1212/WNL.0000000000010404

103. McGonigal K, Tanha J, Palazov E, Li S, Gueorguieva-Owens D, Pandey S. Isolation and functional characterization of single domain antibody modulators of caspase-3 and apoptosis. *Appl Biochem Biotechnol* (2009) 157(2):226–36. doi: 10.1007/s12010-008-8266-4

104. Fagbadebo FO, Kaiser PD, Zittlau K, Bartlick N, Wagner TR, Froehlich T, et al. A nanobody-based toolset to monitor and modify the mitochondrial gtpase Miro1. *Front Mol Biosci* (2022) 9:835302. doi: 10.3389/fmolb.2022.835302

105. Figarella-Branger D, Appay R, Metais A, Tauziede-Espariat A, Colin C, Rousseau A, et al. [the 2021 who classification of tumours of the central nervous system]. *Ann Pathol* (2021) 42(5):367–82. doi: 10.1016/j.annpat.2021.11.005

106. Chen B, Chen C, Zhang Y, Xu J. Recent incidence trend of elderly patients with glioblastoma in the united states, 2000-2017. *BMC Cancer* (2021) 21(1):54. doi: 10.1186/s12885-020-07778-1

107. Tamimi AF, Juweid M. "Epidemiology and Outcome of Glioblastoma." In: De Vleeschouwer S, editor. *Glioblastoma*. (Brisbane, Australia: Codon Publications) (2017) 143–53. doi: 10.15586/codon.glioblastoma.2017.ch8

108. Stupp R, Mason WP, van den Bent MJ, Weller M, Fisher B, Taphoorn MJ, et al. Radiotherapy plus concomitant and adjuvant temozolomide for glioblastoma. *N Engl J Med* (2005) 352(10):987–96. doi: 10.1056/NEJMoa043330

109. Alzial G, Renoult O, Paris F, Gratas C, Clavreul A, Pecqueur C. Wild-type isocitrate dehydrogenase under the spotlight in glioblastoma. *Oncogene* (2022) 41(5):613–21. doi: 10.1038/s41388-021-02056-1

110. Himes BT, Geiger PA, Ayasoufi K, Bhargav AG, Brown DA, Parney IF. Immunosuppression in glioblastoma: Current understanding and therapeutic implications. *Front Oncol* (2021) 11:770561. doi: 10.3389/fonc.2021.770561

111. Berti V, Mosconi L, Pupi A. Brain: Normal variations and benign findings in fluorodeoxyglucose-Pet/Computed tomography imaging. *PET Clin* (2014) 9(2):129–40. doi: 10.1016/j.cpet.2013.10.006

112. Iqbal U, Trojahn U, Albaghdadi H, Zhang J, O'Connor-McCourt M, Stanimirovic D, et al. Kinetic analysis of novel mono- and multivalent vhh-fragments and their application for molecular imaging of brain tumours. *Br J Pharmacol* (2010) 160(4):1016–28. doi: 10.1111/j.1476-5381.2010.00742.x

113. De Vlaminck K, Romao E, Puttemans J, Pombo AAR, Kancheva D, Scheyltjens I, et al. Imaging of glioblastoma tumor-associated myeloid cells using nanobodies targeting signal regulatory protein alpha. *Front Immunol* (2021) 12:777524. doi: 10.3389/fimmu.2021.777524

114. Zottel A, Jovcevska I, Samec N, Mlakar J, Sribar J, Krizaj I, et al. Anti-vimentin, anti-tufm, anti-Nap1l1 and anti-Dpysl2 nanobodies display cytotoxic effect and reduce glioblastoma cell migration. *Ther Adv Med Oncol* (2020) 12:1758835920915302. doi: 10.1177/1758835920915302

115. van de Water JA, Bagci-Onder T, Agarwal AS, Wakimoto H, Roovers RC, Zhu Y, et al. Therapeutic stem cells expressing variants of egfr-specific nanobodies have antitumor effects. *Proc Natl Acad Sci USA*. (2012) 109(41):16642–7. doi: 10.1073/pnas.1202832109

116. Karakas N, Stuckey D, Revai-Lechtich E, Shah K. Il13ralpha2 and egfrtargeted pseudomonas exotoxin potentiates the trailmediated death of gbm cells. *Int J Mol Med* (2021) 48(1):145. doi: 10.3892/ijmm.2021.4978

117. Porcnik A, Novak M, Breznik B, Majc B, Hrastar B, Samec N, et al. Trim28 selective nanobody reduces glioblastoma stem cell invasion. *Molecules* (2021) 26(17):5141. doi: 10.3390/molecules26175141

118. Heukers R, Fan TS, de Wit RH, van Senten JR, De Groof TWM, Bebelman MP, et al. The constitutive activity of the virally encoded chemokine receptor Us28 accelerates glioblastoma growth. *Oncogene* (2018) 37(30):4110–21. doi: 10.1038/s41388-018-0255-7

119. De Groof TWM, Mashayekhi V, Fan TS, Bergkamp ND, Sastre TJ, van Senten JR, et al. Nanobody-targeted photodynamic therapy selectively kills viral gpcr-expressing glioblastoma cells. *Mol Pharm* (2019) 16(7):3145–56. doi: 10.1021/acs.molpharmaceut.9b00360

120. Kaufmann TJ, Smits M, Boxerman J, Huang R, Barboriak DP, Weller M, et al. Consensus recommendations for a standardized brain tumor imaging protocol for clinical trials in brain metastases. *Neuro Oncol* (2020) 22(6):757–72. doi: 10.1093/neuonc/noaa030

121. Suh JH, Kotecha R, Chao ST, Ahluwalia MS, Sahgal A, Chang EL. Current approaches to the management of brain metastases. *Nat Rev Clin Oncol* (2020) 17(5):279–99. doi: 10.1038/s41571-019-0320-3

122. Vaneycken I, Devoogdt N, Van Gassen N, Vincke C, Xavier C, Wernery U, et al. Preclinical screening of anti-Her2 nanobodies for molecular imaging of breast cancer. *FASEB J* (2011) 25(7):2433–46. doi: 10.1096/fj.10-180331

123. Zhou Z, Vaidyanathan G, McDougald D, Kang CM, Balyasnikova I, Devoogdt N, et al. Fluorine-18 labeling of the Her2-targeting single-domain antibody 2rs15d using a residualizing label and preclinical evaluation. *Mol Imaging Biol* (2017) 19(6):867–77. doi: 10.1007/s11307-017-1082-x

124. Puttemans J, Dekempeneer Y, Eersels JL, Hanssens H, Debie P, Keyaerts M, et al. Preclinical targeted alpha- and beta(-)-Radionuclide therapy in Her2-positive brain metastasis using camelid single-domain antibodies. *Cancers (Basel)* (2020) 12(4):1017. doi: 10.3390/cancers12041017

125. Ramos-Gomes F, Bode J, Sukhanova A, Bozrova SV, Saccomano M, Mitkovski M, et al. Single- and two-photon imaging of human micrometastases and disseminated tumour cells with conjugates of nanobodies and quantum dots. *Sci Rep* (2018) 8(1):4595. doi: 10.1038/s41598-018-22973-8

126. Yin W, Zhao Y, Kang X, Zhao P, Fu X, Mo X, et al. Bbb-penetrating codelivery liposomes treat brain metastasis of non-small cell lung cancer with Egfr (T790m) mutation. *Theranostics* (2020) 10(14):6122–35. doi: 10.7150/thno.42234

127. Kulkarni A, Mochnacova E, Majerova P, Curlik J, Bhide K, Mertinkova P, et al. Single domain antibodies targeting receptor binding pockets of Nada restrain adhesion of neisseria meningitidis to human brain microvascular endothelial cells. *Front Mol Biosci* (2020) 7:573281. doi: 10.3389/fmolb.2020.573281

128. Boruah BM, Liu D, Ye D, Gu TJ, Jiang CL, Qu M, et al. Single domain antibody multimers confer protection against rabies infection. *PloS One* (2013) 8(8):e71383. doi: 10.1371/journal.pone.0071383

129. Terryn S, Francart A, Lamoral S, Hultberg A, Rommelaere H, Wittelsberger A, et al. Protective effect of different anti-rabies virus vhh constructs against rabies disease in mice. *PloS One* (2014) 9(10):e109367. doi: 10.1371/journal.pone.0109367

130. Terryn S, Francart A, Rommelaere H, Stortelers C, Van Gucht S. Post-exposure treatment with anti-rabies vhh and vaccine significantly improves protection of mice from lethal rabies infection. *PloS Negl Trop Dis* (2016) 10(8):e0004902. doi: 10.1371/journal.pntd.0004902

131. Baldwin KJ, Correll CM. Prion disease. *Semin Neurol* (2019) 39(4):428–39. doi: 10.1055/s-0039-1687841

132. Abskharon RN, Soror SH, Pardon E, El HH, Legname G, Steyaert J, et al. Combining in-situ proteolysis and microseed matrix screening to promote crystallization of prpc-nanobody complexes. *Protein Eng Des Sel* (2011) 24(9):737–41. doi: 10.1093/protein/gzr017

133. Abskharon RN, Giachin G, Wohlkonig A, Soror SH, Pardon E, Legname G, et al. Probing the n-terminal beta-sheet conversion in the crystal structure of the human prion protein bound to a nanobody. *J Am Chem Soc* (2014) 136(3):937–44. doi: 10.1021/ja407527p

134. Abskharon R, Wang F, Wohlkonig A, Ruan J, Soror S, Giachin G, et al. Structural evidence for the critical role of the prion protein hydrophobic region in forming an infectious prion. *PloS Pathog* (2019) 15(12):e1008139. doi: 10.1371/journal.ppat.1008139

135. Schut MH, Pepers BA, Klooster R, van der Maarel SM, El KM, Verrips T, et al. Selection and characterization of llama single domain antibodies against n-terminal huntingtin. *Neurol Sci* (2015) 36(3):429–34. doi: 10.1007/s10072-014-1971-6

136. Colby DW, Chu Y, Cassady JP, Duennwald M, Zazulak H, Webster JM, et al. Potent inhibition of huntingtin aggregation and cytotoxicity by a disulfide bond-free single-domain intracellular antibody. *Proc Natl Acad Sci USA* (2004) 101(51):17616–21. doi: 10.1073/pnas.0408134101

137. Steeland S, Puimege L, Vandenbroucke RE, Van Hauwermeiren F, Haustraete J, Devoogdt N, et al. Generation and characterization of small single domain antibodies inhibiting human tumor necrosis factor receptor 1. *J Biol Chem* (2015) 290(7):4022–37. doi: 10.1074/jbc.M114.617787

138. Steeland S, Van Ryckeghem S, Van Imschoot G, De Rycke R, Toussaint W, Vanhoutte L, et al. Tnfr1 inhibition with a nanobody protects against eae development in mice. *Sci Rep* (2017) 7(1):13646. doi: 10.1038/s41598-017-13984-y

139. Sadeghian-Rizi T, Behdani M, Khanahmad H, Sadeghi HM, Jahanian-Najafabadi A. Generation and characterization of a functional nanobody against inflammatory chemokine Cxcl10, as a novel strategy for the treatment of multiple sclerosis. *CNS Neurol Disord Drug Targets* (2019) 18(2):141–8. doi: 10.2174/1871527317666181114134518

140. Callewaert F, Roodt J, Ulrichts H, Stohr T, van Rensburg WJ, Lamprecht S, et al. Evaluation of efficacy and safety of the anti-vwf nanobody alx-0681 in a preclinical baboon model of acquired thrombotic thrombocytopenic purpura. *Blood* (2012) 120(17):3603–10. doi: 10.1182/blood-2012-04-420943

141. Bartunek J, Barbato E, Heyndrickx G, Vanderheyden M, Wijns W, Holz JB. Novel antiplatelet agents: Alx-0081, a nanobody directed towards Von willebrand factor. *J Cardiovasc Transl Res* (2013) 6(3):355–63. doi: 10.1007/s12265-012-9435-y

142. Momi S, Tantucci M, Van Roy M, Ulrichts H, Ricci G, Gresele P. Reperfusion of cerebral artery thrombosis by the gpib-vwf blockade with the nanobody alx-0081 reduces brain infarct size in Guinea pigs. *Blood* (2013) 121 (25):5088–97. doi: 10.1182/blood-2012-11-464545

143. Peyvandi F, Scully M, Kremer HJA, Knobl P, Cataland S, De Beuf K, et al. Caplacizumab reduces the frequency of major thromboembolic events, exacerbations and death in patients with acquired thrombotic thrombocytopenic purpura. *J Thromb Haemost* (2017) 15(7):1448–52. doi: 10.1111/jth.13716

144. Scully M, Cataland SR, Peyvandi F, Coppo P, Knobl P, Kremer HJA, et al. Caplacizumab treatment for acquired thrombotic thrombocytopenic purpura. *N Engl J Med* (2019) 380(4):335–46. doi: 10.1056/NEJMoa1806311

145. Lee JH, Yang DS, Goulbourne CN, Im E, Stavrides P, Pensalfini A, et al. Faulty autolysosome acidification in alzheimer's disease mouse models induces autophagic build-up of abeta in neurons, yielding senile plaques. *Nat Neurosci* (2022) 25(6):688–701. doi: 10.1038/s41593-022-01084-8

146. Baik SH, Kang S, Lee W, Choi H, Chung S, Kim JI, et al. A breakdown in metabolic reprogramming causes microglia dysfunction in alzheimer's disease. *Cell Metab* (2019) 30(3):493–507.e6. doi: 10.1016/j.cmet.2019.06.005

147. Rao D, Mei K, Yan T, Wang Y, Wu W, Chen Y, et al. Nanomechanical sensor for rapid and ultrasensitive detection of tumor markers in serum using nanobody. *Nano Res* (2021) 15(2):1003–12. doi: 10.1007/s12274-021-3588-4

148. Filipiak MS, Rother M, Andoy NM, Knudsen AC, Grimm S, Bachran C, et al. Highly sensitive, selective and label-free protein detection in physiological solutions using carbon nano tube transistors with nano body receptors. *SENSORS AND ACTUATORS B-CHEMICAL* (2018) 255:1507–16. doi: 10.1016/j.snb.2017.08.164

149. Guo K, Wustoni S, Koklu A, Diaz-Galicia E, Moser M, Hama A, et al. Rapid single-molecule detection of covid-19 and mers antigens *Via* nanobody-functionalized organic electrochemical transistors. *Nat BioMed Eng* (2021) 5 (7):666–77. doi: 10.1038/s41551-021-00734-9

150. Ren X, Yan J, Wu D, Wei Q, Wan Y. Nanobody-based apolipoprotein e immunosensor for point-of-Care testing. *ACS Sens* (2017) 2(9):1267–71. doi: 10.1021/acssensors.7b00495

frontiers | Frontiers in Immunology

TYPE Original Research
PUBLISHED 23 November 2022
DOI 10.3389/fimmu.2022.1006718

OPEN ACCESS

EDITED BY
Zahra Sharifzadeh,
Pasteur Institute of Iran, Iran

REVIEWED BY
Theam Soon Lim,
Universiti Sains Malaysia (USM), Malaysia
Stephanie Cabantous,
Institut National de la Santé et de la Recherche Médicale (INSERM), France

*CORRESPONDENCE
Stephen J. Hill
stephen.hill@nottingham.ac.uk
Laura E. Kilpatrick
laura.kilpatrick@nottingham.ac.uk

SPECIALTY SECTION
This article was submitted to Cancer Immunity and Immunotherapy, a section of the journal Frontiers in Immunology

RECEIVED 29 July 2022
ACCEPTED 31 October 2022
PUBLISHED 23 November 2022

CITATION
Comez D, Glenn J, Anbuhl SM, Heukers R, Smit MJ, Hill SJ and Kilpatrick LE (2022) Fluorescently tagged nanobodies and NanoBRET to study ligand-binding and agonist-induced conformational changes of full-length EGFR expressed in living cells.
Front. Immunol. 13:1006718.
doi: 10.3389/fimmu.2022.1006718

Fluorescently tagged nanobodies and NanoBRET to study ligand-binding and agonist-induced conformational changes of full-length EGFR expressed in living cells

Dehan Comez[1,2], Jacqueline Glenn[1,2], Stephanie M. Anbuhl[3,4], Raimond Heukers[3,4], Martine J. Smit[3], Stephen J. Hill[1,2]* and Laura E. Kilpatrick[2,5]*

[1]Division of Physiology, Pharmacology and Neuroscience, School of Life Sciences, University of Nottingham, Nottingham, United Kingdom, [2]Centre of Membrane Proteins and Receptors (COMPARE), University of Birmingham and University of Nottingham, The Midlands Nottingham, Nottingham, United Kingdom, [3]Division of Medicinal Chemistry, Amsterdam Institute of Molecular and Life Sciences (AIMMS) Vrije Universiteit (VU), Amsterdam, Netherlands, [4]QVQ Holding BV, Utrecht, Netherlands, [5]Division of Bimolecular Science and Medicinal Chemistry, Biodiscovery Institute, School of Pharmacy, University of Nottingham, Nottingham, United Kingdom

Introduction: The Epidermal Growth Factor Receptor is a member of the Erb receptor tyrosine kinase family. It binds several ligands including EGF, betacellulin (BTC) and TGF-α, controls cellular proliferation and invasion and is overexpressed in various cancer types. Nanobodies (VHHs) are the antigen binding fragments of heavy chain only camelid antibodies. In this paper we used NanoBRET to compare the binding characteristics of fluorescent EGF or two distinct fluorescently labelled EGFR directed nanobodies (Q44c and Q86c) to full length EGFR.

Methods: Living HEK293T cells were stably transfected with N terminal NLuc tagged EGFR. NanoBRET saturation, displacement or kinetics experiments were then performed using fluorescently labelled EGF ligands (EGF-AF488 or EGF-AF647) or fluorescently labelled EGFR targeting nanobodies (Q44c-HL488 and Q86c-HL488).

Results: These data revealed that the EGFR nanobody Q44c was able to inhibit EGF binding to full length EGFR, while Q86c was able to recognise agonist bound EGFR and act as a conformational sensor. The specific binding of fluorescent Q44c-HL488 and EGF-AF488 was inhibited by a range of EGFR ligands (EGF> BTC>TGF-α).

10.3389/fimmu.2022.1006718

Discussion: EGFR targeting nanobodies are powerful tools for studying the role of the EGFR in health and disease and allow real time quantification of ligand binding and distinct ligand induced conformational changes.

KEYWORDS

EGFR, nanobody, BRET, NanoBiT, fluorescence

Introduction

The epidermal growth factor receptor (EGFR) is a glycoprotein of 170 kDa, encoded by a gene located on chromosome 7p11.2 (1). It has a cysteine-rich extracellular region, a single transmembrane spanning region and an intracellular domain with tyrosine kinase activity (2). Its extracellular portion is subdivided into four distinct regions with domains I and III containing the sites for EGF binding and the cysteine-rich domains II and IV containing N-linked glycosylation sites. The first step of EGFR activation has been proposed to involve ligand-induced dimerization of EGFR, leading to stimulation of its intracellular kinase domain and autophosphorylation of EGFR at multiple intracellular tyrosine residues (3). This results in the recruitment of downstream signalling proteins such as Src homology domain-containing adaptor protein C (Shc), growth factor receptor-bound protein 2 (Grb2) and phospholipase Cγ (PLCγ) (1, 2, 4).

X-ray crystallography using purified extracellular regions of EGFR produced the original elegant scheme for ligand-induced EGFR dimerization (5). Binding of EGF to domains I and III stabilizes an extended conformation and exposes a dimerization interface in domain II, promoting self-association with a K_D in the micromolar range (5–10). However, this model does not capture the complex ligand-binding characteristics seen for cell surface full-length EGFRs in intact cells, where there is increasing evidence of negative cooperativity (7) and distinct affinity states for ligand-binding and intracellular signalling (4, 8–10).

Insight into the structural origins of EGF/EGFR binding complexity has been provided by studies of the Drosophila EGFR (dEGFR), which, unlike its human counterpart, retains its negative cooperativity when the soluble extracellular regions are isolated and purified (11). This work has shown that single ligand occupied asymmetric dimers can form (7, 11, 12). Mutations that block EGFR dimerization (Y251A and R285S) do not reduce ligand affinity (9) but do abolish EGFR signalling (6, 13). Furthermore, extracellular EGFR-activating mutations (R84K and A265V or A265D) enhance ligand-binding affinity without directly promoting EGFR dimerization, suggesting that these particular oncogenic mutations alter the allosteric linkage between dimerization and ligand binding (9).

EGFR is activated by seven different growth factors (14), which fall into two groups based on receptor-binding affinity (10). The high-affinity ligands are EGF, transforming growth factor-α (TGFα), betacellulin (BTC) and heparin binding EGF-like growth factor (HB-EGF) and the low-affinity ligands are epiregulin, epigen and amphiregulin (10). Individual EGFR ligands also induce qualitatively and quantitatively different downstream signals (15–17). Recent crystallographic and cellular studies have shown that two EGFR ligands, epiregulin and epigen, drive the purified EGFR extracellular domains into dimers, each resulting in different structures (10). The resulting ligand-induced dimers were weaker and more short-lived than those induced by EGF itself, suggesting that epiregulin and epigen are both partial agonists of EGFR dimerization (10). Unexpectedly, this weakened dimerization elicited more sustained responses than EGF, provoking responses in breast cancer cells associated with differentiation rather than proliferation (10). In addition, recent cryo-EM structures of full-length EGFR bound to EGF or TGFα have revealed differential stabilization of quaternary structures of EGFR dimers where the membrane proximal tips of domain IV are either juxtaposed or separated (18). EGF and TGFα differ in their ability to maintain the conformation with the membrane-proximal tips separated (18).

Heavy-chain antibodies have been described in species belonging to the camelid family that can target EGFR (19). Heavy chain antibodies are composed of two identical heavy chains and do not contain a light chain (19). Their antigen-binding part is therefore composed of a single immunoglobulin (Ig) variable region (VHH or nanobody) that can be easily incorporate into, and expressed from, a plasmid and genetically engineered to generate novel receptor specific probes. This approach has revealed nanobodies that bind to a similar site to EGF on the receptor (20, 21) and others that bind to EGFR but do not compete for EGF binding and are non-activating (20, 22). EgB4 is an example of the latter category of EGFR nanobody that has previously been used to evaluate gross movements of the extracellular domains of EGFR with respect to a fluorescent membrane dye (23). We have recently demonstrated for G protein-coupled receptors that receptor-specific nanobodies can be used to monitor ligand binding and

conformation changes using NanoBRET technology (24). In the present study we have used N-terminal nanoluciferase-tagged EGFR and NanoBRET to investigate the pharmacological properties of a fluorescent derivative of EgB4 (Q86c-HL488) and a second fluorescent nanobody that binds to the EGF-binding site (Q44c-HL488) in a similar manner to the previously described 7D12 (21).

Materials and methods

Materials

Epidermal Growth Factor fluorescently labelled with Alexa Fluor 488 (E13345) or Alexa Fluor 647 (E35351) were purchased from Thermo Fischer Scientific (Waltham, USA). Human recombinant TGF-alpha (239-A-100), human recombinant betacellulin (261-CE-010), human recombinant epiregulin (1195-EP-025), human recombinant amphiregulin (262-AR-100), human recombinant epigen (6629-EP-025) and human recombinant EGF (236-EG-200) were purchased from R&D Systems (Minnesota, USA). Purified LgBiT, FuGENE HD Transfection Reagent and furimazine were purchased from Promega Corporation. Opti-MEM reduced serum medium was purchased from Gibco (31985062). Q44c and Q86c, containing an unpaired cysteine in the C-terminal tag, were provided by QVQ (Utrecht, The Netherlands).

DNA constructs

cDNA encoding N terminal fusions of EGFR to NanoLuc or HiBiT were a kind gift from Promega Corporation, with the EGFR ORF originally obtained from the Kazusa DNA Research Institute (Kisarazu, Japan). For N-terminal NanoLuc tagged constructs, EGFR lacking its native signal sequence, was cloned into a pNKF1-secN CMV vector fusing the signal peptide sequence of IL-6 onto the N terminus of NanoLuc. The resulting vector encoded NanoLuc fused to the N-terminus of EGFR *via* a Gly-Ser-Ser-Gly (AIA) linker (termed NLuc-EGFR). For N-terminal HiBiT tagged constructs, HiBiT (VSGWRLFKKIS) was inserted after the signal peptide from IL-6 and fused to EGFR using a GSSG linker (termed HiBiT-EGFR).

Cell culture

Human embryonic kidney (HEK293) cells stably expressing N-terminal NanoLuc-tagged EGFR (NLuc-EGFR) and wildtype HEK293 cells were cultured in Dulbecco's Modified Eagle Medium-high glucose (DMEM; D6429, Sigma Aldrich) containing 10% fetal calf serum (FCS; F7524, Sigma Aldrich) at 37^0C/5% CO_2. Cells were passaged at 70% confluency using phosphate buffer saline (PBS; D8537, Sigma Aldrich) and trypsin (0.25% w/v in versene; T4174, Sigma Aldrich). All stable and transient transfections were performed using FuGENE HD (Promega Corporation) at a reagent to cDNA ratio of 3:1 following manufacturer's instructions. We confirm that these cell lines are mycoplasma free.

Nanobody production, purification and conjugation

Nanobodies were produced in *Saccharomyces cerevisiae* (strain *VWK18 gal1*) as described previously (25). Purification was performed using a CaptureSelect™ C-tagXL column (#494307205, Thermo Fisher Scientific) and pH elution (20 mM citric acid, 150 mM NaCl, pH=3). After dialyzing against PBS, protein purity and integrity was verified by SDS PAGE under reducing conditions, and protein concentration was determined by UV Vis measurement at 280 nm. Q44c and Q86c were site-directionally conjugated to HiLyte™ Fluor 488 C2 maleimide (AS-81164, Anaspec, Fremont, USA) using the unpaired thiol in the tag (later called Q44c-HL488 and Q86c-HL488). First, thiols were reduced using 2.75-times molar excess of Tris(2-carboxyethyl)phosphine (TCEP) (0797C437, Sigma-Aldrich) for 3 hours at 37°C. Then, a 4-times molar excess of HiLyte™ Fluor 488 C2 maleimide dissolved in DMSO was added. After 5 minutes of incubation at room temperature, the remaining TCEP and dye were removed using 2 Zeba™ desalting spin columns (89882, Thermo Fischer Scientific). Degree of labelling was determined using UV-VIS spectrometry and was >0.5. The amount of free dye was assessed upon size separation by SDS-PAGE followed by a fluorescence scan (Ex: 475 nm, Em ≥ 520 nm, D-Digit Scanner, LI-COR Biosciences, Lincoln, USA) and was<5%.

NanoBRET ligand and nanobody saturation binding assays

HEK293 cells stably expressing NLuc-EGFR were seeded onto poly-D-lysine coated (Sigma Aldrich; 0.1 mg·mL^{-1}) 96-well flat bottom, μCLEAR® white CELLSTAR® TC plates (Greiner Bio-One 655098, Stonehouse, UK) in 100 μL DMEM, at a density of 40,000 cells/well. Plates were incubated at 37°C /5% CO_2 overnight. The next day, culture media was removed, and each well washed with 100 μL of HEPES buffered Salt Solution (HBSS) (2 mM of sodium pyruvate, 146 mM of NaCl, 5 mM of KCl, 1 mM of $MgSO_4.7H_2O$, 10 mM of HEPES, 1.3 mM of $CaCl_2.2H_2O$, 1.5 mM $NaHCO_3$, 10 mM D-glucose; pH 7.45) containing 0.2% BSA. After this washing step, fluorescently labelled EGF ligands (0-100nM) or nanobodies (0-200nM) were added to the appropriate wells in increasing

concentrations (in the presence or absence of 100nM EGF) in 50 µL total volume of HBSS per well. Cells were incubated in the dark at 37°C for 30 minutes. 12.5 nM final concentration of furimazine was added to each well and cells were incubated for a further 5 minutes. Fluorescence and luminescence emissions were simultaneously detected using a PHERAstar FS dual plate reader (BMG Labtech, Offenburg, Germany). When using red fluorescently labelled EGF (EGF-AF647) emissions were detected using an optic module fitted with a 460 nm (80 nm) bandpass filter for collecting luminescence (NLuc) emissions and a >610 nm long pass filter for fluorescence emissions (AF647). For green fluorescently labelled EGF (AF488) or labelled nanobodies (Q44-HL488 or Q86-HL488) emissions were detected using an optic module fitted with a 475 nm (30 nm) band-pass filter for collecting luminescence emissions and a 535 nm (30 nm) band pass filter for fluorescence emissions (AF488). Raw BRET ratios were calculated by dividing fluorescence emissions by luminescence emissions, and the results were plotted using GraphPad Prism 9.2 (GraphPad Software, La Jolla, CA).

NanoBRET nanobody displacement assay

HEK293 cells stably expressing NLuc-EGFR (40,000/well) were plated onto poly-D-lysine-coated white 96-well plates as described above. After overnight incubation at 37^0C/5% CO_2, cells were washed with HBSS containing 0.2% BSA. Increasing concentrations of non-fluorescent ligands or nanobodies were simultaneously added alongside a fixed concentration of fluorescent EGF (EGF-AF488 or EGF-AF647) or nanobody (HL488 tagged) to each well in a 50 µL final volume of HBSS containing 0.2% BSA. Cells were incubated for 30 minutes at 37°C/5% CO_2 in the dark. A 12.5 nM final concentration of furimazine was added to each well. Fluorescence and luminescence were measured simultaneously using a PHERAstar FS dual plate reader as described previously.

Nanobody kinetics assay

HEK293 cells stably expressing NLuc-EGFR (40.000/well) were plated onto poly-D-lysine-coated white 96-well plates as described above and incubated overnight at 37^0C/5% CO_2. The next day cells were washed with 100 µL of HBSS containing 0.2% BSA. 45 µL of HBSS containing furimazine (12.5 nM final concentration) was added to each well. Baseline BRET measurements were undertaken using a PHERAstar FS dual plate reader for 15 minutes at 37°C every 60 seconds. After baseline measurement, fluorescent nanobodies (3.125 – 200nM) were added to the cells. Plates were read for 2 hours, every 60 seconds at 37°C. For EGF competition assays, increasing concentrations of non-fluorescent EGF (10^{-13} – 10^{-7}M) were added 30 minutes after nanobody addition and measurements continued for a further 90 minutes at 37°C using a BRET 1 plus optical module.

NanoBiT internalization assay

HEK293 cells (20,000/well) were plated onto poly-D-lysine-coated white 96-well plates as described previously and incubated at 37°C/5% CO_2 overnight. The next day cells were transfected with 100 ng per well of HiBiT-EGFR cDNA with FuGENE HD Transfection Reagent using a 3:1 DNA/FuGENE HD ratio in OptiMEM following manufacturer's instructions. Cells were then incubated at 37°C/5% CO_2 overnight. The next day culture media was removed, and cells were washed with HBSS once. Cells were incubated with 100nM EGF, Q44 or Q86 nanobodies in HBSS containing 0.02% BSA for 120, 60, 30 or 5 minutes at 37°C. Plates were then washed once using HBSS/0.02% BSA and then incubated with 10 nM of purified LgBiT and furimazine (1/400 dilution) diluted in HBSS/0.02% BSA for 20 minutes. Luminescence was then measured using a PHERAstar FS plate reader (BMG Labtech, Offenburg, Germany) using the LUM Plus optical module.

Data analysis

All data obtained from NanoBRET assays were determined from BRET ratios calculated using Microsoft Excel:

$$BRET\ \text{ratio} = \frac{\text{Emission from acceptor channel}}{\text{Emission from donor channel}}$$

Data were analysed using GraphPad Prism 9.20 (GraphPad Software, La Jolla, CA, USA). Data are presented as mean ± S.E.M. All experiments were performed in 5-6 independent experiments with triplicate wells (see figure legends for details). Drug additions were randomly allocated to wells within each 96-well plate. Statistical significance was defined as $P<0.05$.

Saturation binding curves were fit to the following equation:

$$Total\ \ Binding = \ B_{MAX} \cdot \frac{[L]}{[L] + \ K_D} + M \,.[L] + C$$

where [L] is the concentration of fluorescent ligand (nanobody or EGF), B_{MAX} is the level of maximal specific binding, K_D is the equilibrium dissociation constant of the labelled ligand in the same units as [L], M is the slope of the non-specific binding component, C represents the background BRET ratio (in the absence of fluorescent ligand). In the case of EGF-AF488 or EGF-AF647, total and non-specific binding (obtained in the presence of 100 nM EGF) were fitted simultaneously with shared parameters for M and C. In the case of Q86c-HL488, total binding curves obtained in the presence or absence of 100 nM EGF were fitted simultaneously to the above equation with shared parameters for M and C.

Competition binding data were fit to following equation:

$$\%\ Inhibition\ of\ specific\ binding = \frac{(100 \times [A])}{([A] \times IC_{50})}$$

where [A] is the concentration of unlabelled ligand and IC_{50} is the concentration of ligand required to inhibit 50% of the specific binding of the fluorescent ligand. In the case of EGF-AF488 and EGF-AF647 competition experiments, the IC_{50} values were then used to calculate the K_i values using the Cheng-Prussoff equation:

$$K_i = \frac{IC_{50}}{1 + \frac{[L]}{K_D}}$$

where [L] is the concentration of fluorescent ligand in nM, and K_D is the dissociation constant of that fluorescent ligand in nM.

In the case of Q86c-HL488 binding experiments where increasing concentrations of EGFR ligands produced a marked increase in the level of specific binding, the data were fit to the following equation:

$$\%\ Increase\ in\ specific\ binding = \frac{(100 \times [A])}{([A] \times EC_{50})}$$

where [A] is the concentration of unlabelled EGFR ligand and EC_{50} is the concentration of ligand required to produce 50% of the maximum increase in the specific binding of the fluorescent ligand.

For HiBiT internalization experiments, all data were normalised to relative luminescence units obtained for buffer only (HBSS/0.02% BSA; 100%) for each individual experiment. Normalised data across experimental replicates were then pooled and statistical significance was determined using one way ANOVA and defined as $P<0.05$.

Results

Effect of Q44c and Q86c on EGF ligand binding to NLuc-EGFR

Initial studies were undertaken to investigate the effect of unlabelled Q44c and Q86c on the binding of fluorescent analogues of EGF to the full-length EGFR receptor expressed in living HEK293 cells. Both EGF-AF488 and EGF-AF647 exhibited saturable binding to the N-terminal nanoluciferase-tagged EGFR (NLuc-EGFR) that was displaceable by 100 nM unlabelled EGF (Figures 1A, C). The mean K_D values obtained for EGF-AF488 and EGF-AF647 were 2.30 ± 0.09 nM (n=5) and 3.49 ± 0.21 nM (n=5) respectively. Furthermore, increasing concentrations of unlabelled EGF were able to potently inhibit the specific binding of different concentrations of EGF-AF488 (Figure 1B) and EGF-AF647 (Figure 1D) yielding pKi values for unlabelled EGF of 9.35 ± 0.02 (n=5) and 9.61 ± 0.06 (n=5) respectively. Consistent with Q44c binding to the same epitope

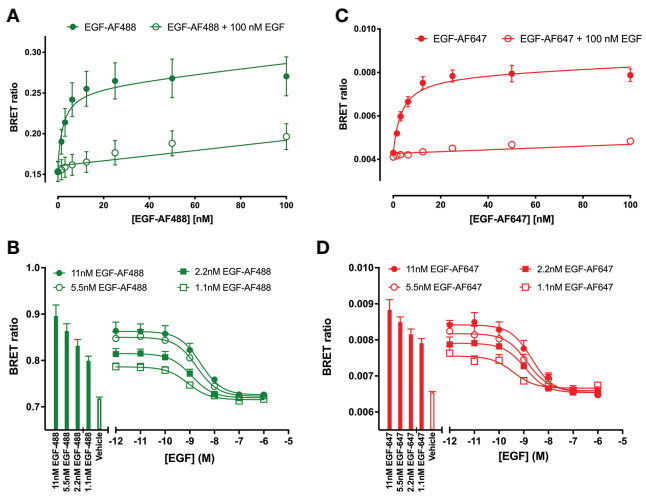

FIGURE 1
Quantification of fluorescent EGF binding to HEK293 cells stably expressing a full-length N-terminal nanoluficerase (NanoLuc) tagged-EGFR measured using NanoBRET. Saturation binding of fluorescently labelled **(A)** EGF-AF488 and **(C)** EGF-AF647 in the absence (closed circles) or presence (open circles) of 100 nM unlabelled EGF added simultaneously and incubated for 30 minutes at 37°C. Saturation experiments were performed in HBSS containing 0.2 % BSA. Displacement of various fixed concentrations of **(B)** EGF-AF488 or **(D)** EGF-AF647 by increasing concentrations of unlabelled EGF. Both ligands were added simultaneously, and cells incubated for 60 minutes at 37°C. The NLuc substrate furimazine (12.5 nM) was added and plates incubated for 5 minutes then luminescence and fluorescence emissions were measured using a BMG Pherastar. Displacement experiments were performed in HBSS containing 0.1 % BSA. Closed bars represent fluorescent EGF alone, with open bars representing vehicle (HBSS/0.1% BSA). Data are combined mean ± SEM from five independent experiments, where each experiment was performed in triplicate.

as EGF on the EGFR, this nanobody was able to potently displace the binding of both 3 nM EGF-AF488 (pIC_{50} = 8.63 ± 0.05, n=5; Figure 2A) and 3 nM EGF-AF647 (pIC_{50} = 8.61 ± 0.15, n=5; Figure 2B). In contrast, Q86c showed no significant effect on the binding of both fluorescent EGF analogues at concentrations up to 100 nM (Figures 2A, B).

Binding of fluorescent nanobodies Q44c-HL488 and Q86c-HL488 to NLuc-EGFR

Next, the ability of fluorescently labelled Q44c and Q86c to bind to full-length N-terminal nanoluciferase-EGFR was investigated using NanoBRET. Genetic introduction of a C-terminal cysteine residue into the nanobody sequence allowed a directional attachment of a fluorophore (HiLyte Fluor488; HL488) to both nanobodies without affecting their binding properties. Both Q44c-HL488 and Q86c-HL488 were able to bind to NLuc-EGFR and demonstrated a clear saturability of specific binding. Analysis of the ligand-binding isotherms assuming that there was both a saturable component of specific binding and a linear component of non-specific binding revealed K_D values of 14.94 ± 1.04 nM (n=5) and 3.21 ± 1.10 nM (n=5) for Q44c-HL488 and Q86c-HL 488 respectively (Figure 3). In the presence of 100 nM EGF, the specific binding of Q44c-HL488 was completely prevented leaving only the expected linear non-specific component of binding

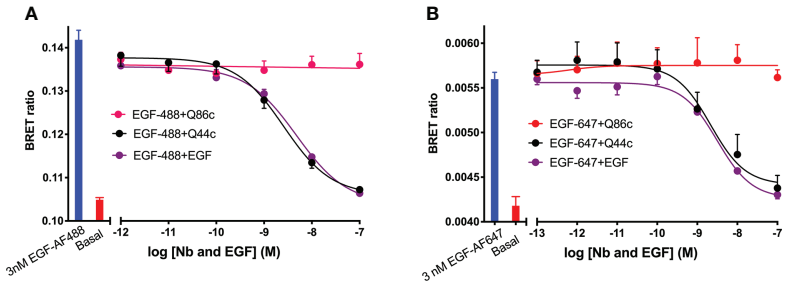

FIGURE 2
Displacement of **(A)** EGF-AF488 (3 nM) or **(B)** EGF-AF647 (3 nM) by unlabelled-EGFR nanobodies Q44c, Q86c and unlabelled EGF. NanoBRET experiments were performed using HEK293 cells stably expressing full-length N-terminal nanoluciferase-EGFR. Fluorescently labelled EGF and competing unlabelled ligands were added simultaneously and incubated for 30 minutes at 37°C. Experiments were performed in HBSS containing 0.2% BSA. The NLuc substrate furimazine (12.5 nM) was added and plates incubated for 5 minutes then luminescence and fluorescence emissions were measured using a BMG Pherastar. Blue bars represent BRET ratios obtained for total EGF-AF488 or EGF-AF647 binding in the absence of competing ligand, whereas red bars represent those measured for HBSS/0.2% BSA buffer alone (basal). Data are combined mean ± SEM from five independent experiments, where each experiment was performed in triplicate.

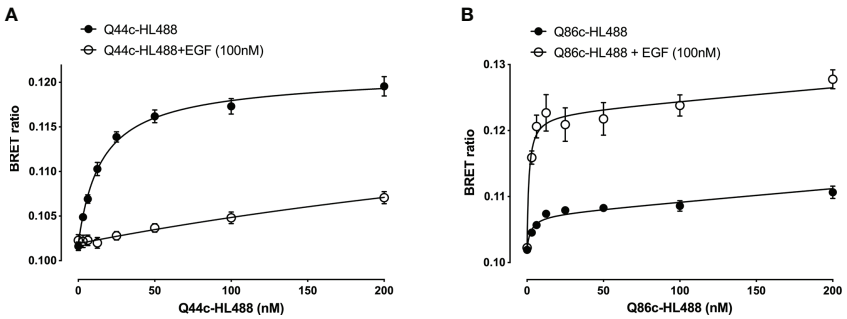

FIGURE 3
Saturation binding of fluorescently (HiLyte™ Fluor 488) labelled EGFR nanobodies **(A)** Q44c-HL488 and **(B)** Q86c-HL488 in absence (closed circles) or presence (open circles) of 100 nM EGF. NanoBRET experiments were performed using full-length N-terminal nanoluciferase-EGFR stably expressing HEK293 cells. Nanobodies and EGF were added simultaneously and incubated for 30 minutes at 37°C. Experiments were performed in HBSS containing 0.2 % BSA. The NLuc substrate furimazine (12.5 nM) was added and plates incubated for 5 minutes then luminescence and fluorescence emissions were measured using a BMG Pherastar. Data are combined mean ± SEM from five independent experiments, where each experiment was performed in triplicate.

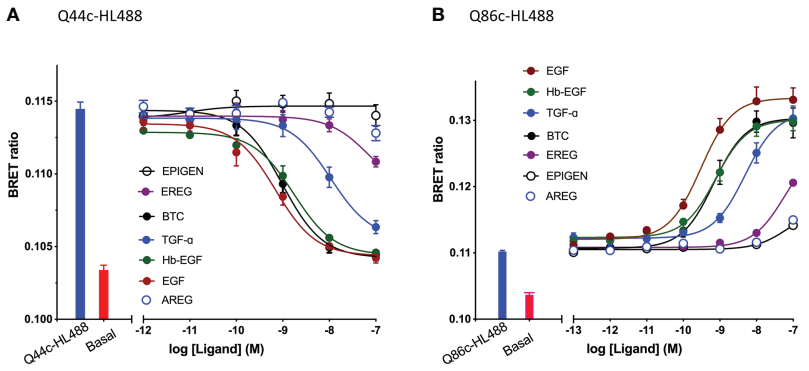

FIGURE 4
Effect of EGFR ligands on the binding of fluorescent **(A)** Q44c-HL488 (14.6 nM) and **(B)** Q86c-HL488 (12.5 nM) to full-length N-terminal nanoluciferase-EGFR stably expressed in HEK293 cells. Cells were treated with nanobodies and EGFR ligands simultaneously and incubated for 30 minutes at 37°C. Experiments were performed in HBSS containing 0.2 % BSA. The NLuc substrate furimazine (12.5 nM) was added and plates incubated for 5 minutes then luminescence and fluorescence emissions were measured using a BMG Pherastar. Blue bars represent BRET ratios obtained for total Q44c-HL488 or Q86c-HL488 in the absence of competing ligand, whereas red bars represent those measured for HBSS/0.2% BSA buffer alone (basal). Data are combined mean ± SEM from five independent experiments, where each experiment was performed in triplicate.

(Figure 3A). In marked contrast, in the presence of 100 nM EGF the specific binding of Q86c-HL488 was markedly enhanced leading to a significant increase (437.6 ± 57.3%, n=5) in the B_{MAX} value ($p<0.005$; paired t test) compared to that obtained in the absence of EGF (Figure 3B). In addition, the K_D value of Q86c-HL488 obtained in the presence of 100 nM EGF was slightly decreased (1.18 ± 0.28 nM, n=5).

The specific binding of Q44c-HL488 was inhibited by a range of EGF ligands with a rank order of potency of EGF>BTC=Hb-EGF>TGF-α>ERG>AREG and Epigen (Figure 4A and Table 1). A very similar rank order of potency was obtained with these ligands for their enhancement of the specific binding of Q86c-HL488 to NLuc-EGFR (Figure 4B and Table 1). Thus, molecules that bind with higher affinity to the EGF binding site are more efficient in modifying the binding of Q86 to EGFR. The rank order of potencies was also comparable to that obtained from inhibition of the binding of 3 nM EGF-AF488 (Table 1), although the actual EC_{50} and IC_{50} values for modulating the binding of both Q44c-HL488 and Q86c-HL488 were at lower concentrations than the pKi value calculated from displacement of EGF-AF488 binding (Table 1). This was most marked for TGF-α and probably confirms that the EC_{50} and IC_{50} values also relate to agonist efficacy and the consequences of receptor activation and conformational changes.

Kinetic analysis of the binding of both Q44c-HL488 and Q86c-HL488 to NLuc-EGFR indicated that at the higher concentrations of fluorescent nanobody used in these experiments, two components were observed in their kinetic profiles represented by a fast pronounced peak in the BRET ratio followed by a decline to a lower plateau (Figures 5A, B). This was more marked for Q86c-HL488 (Figure 5B) and might suggest a time-dependent change in receptor conformation or the onset of a component of receptor internalisation. Addition of EGF after a steady plateau of binding had been achieved with 25 nM fluorescent nanobody, yielded an expected inhibition (Figure 6A) or stimulation (Figure 6B) of Q44c-HL488 and Q86c-HL488 binding to EGFR respectively. Interestingly, the stimulatory effect of EGF on Q86c-HL488 was characterised by a slow fall to a lower plateau after the initial peak was obtained.

TABLE 1 pIC_{50} and pEC_{50} Values for the effect of EGFR ligands on the binding of 14.6 nM Q44c-HL488 or 12.5 nM Q86c-HL488 to full-length N-terminal nanoluciferase-EGFR in HEK293 Cells.

EGFR Ligand	Q44c-HL488 (pIC_{50})	Q86c-HL488 (pEC_{50})	EGF-AF488 (pKi)
EGF	9.23 ± 0.11 (n=5)	9.52 ± 0.06 (n=5)	8.86 ± 0.07 (n=5)
Hb-EGF	8.80 ± 0.13 (n=5)	9.20 ± 0.17 (n=5)	8.43 ± 0.08 (n=5)
TGF-α	7.96 ± 0.19 (n=5)	8.32 ± 0.09 (n=5)	6.83 ± 0.05 (n=5)
BTC	9.02 ± 0.14 (n=5)	9.17 ± 0.09 (n=5)	8.45 ± 0.05 (n=5)

Values are mean ± S.E.M of n individual experiments.
These values have also been compared with their pKi values determined from inhibition of binding of 3 nM EGF-AF488.

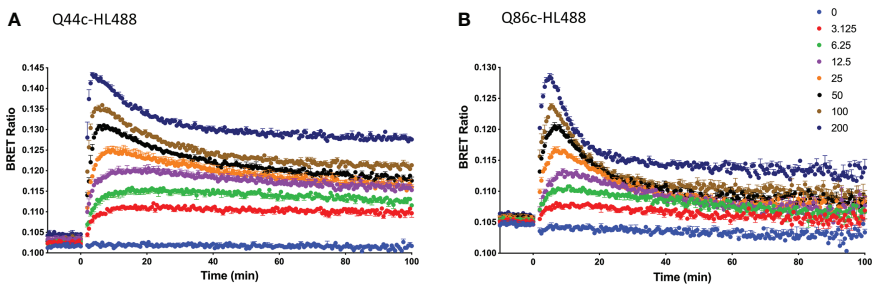

FIGURE 5
Kinetic NanoBRET experiment showing the binding of different concentrations of fluorescent **(A)** Q44c-HL488 or **(B)** Q86c-HL488 to full-length N-terminal nanoluciferase-EGFR. The concentrations of Q44c-HL488 and Q86c-HL488 are given in nM. HEK293 cells stably expressing NLuc-EGFR were treated with furimazine (12.5 nM) and luminescence and fluorescence values were read for 15 minutes (every 60 sec) at 37°C using a BMG Pherastar. Experiments were performed in HBSS containing 0.2 % BSA. Following this period, cells were treated with various concentrations of either fluorescent nanobody and the luminescence and fluorescence emissions simultaneously recorded for a further 100 min at 37°C. Data are mean ± SEM from triplicate determinations in a single experiment. This single experiment is representative of five independent experiments performed.

Interactions between Q44c and Q86c

To evaluate whether there were interactions between Q44c and Q86c in binding to full-length N-terminal nanoluciferase-EGFR we undertook competition binding experiments with their fluorescent analogues. Unlabelled Q44c had no effect on the specific binding of Q86c-HL488 under conditions where the positive effect of EGF could be clearly demonstrated (Figure 7A). Q86c did, however, produce an inhibition of Q86c-HL488 binding at the highest concentrations used. As expected, both unlabelled Q44c and EGF inhibited the binding of Q44c-HL488 consistent with the proposal that Q44c and EGF bind to the same epitope of EGFR (Figure 7B). Interestingly, Q86c was able to produce a small but significant ($p<0.05$; One-way ANOVA) enhancement of Q44c-HL488 binding (Figure 7B) reminiscent of the effect of the low affinity EGF ligands on the binding of Q86c-HL488 (Figure 4B).

Effect of unlabelled Q44c and Q86c on EGFR internalization measured using NanoBiT

To determine whether the fall to a plateau from an initial peak in the kinetic profile of Q44c-HL488 and Q86c-HL488 binding was due to the onset of receptor internalization, we studied EGFR internalization in response to unlabelled EGF, Q44c or Q86c using N-terminal HiBiT-tagged EGFR (26). In this approach, purified LgBiT is added after the agonist

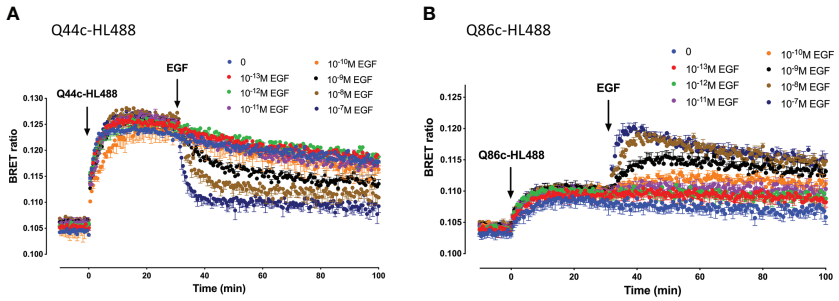

FIGURE 6
Kinetics of EGF-induced changes in the NanoBRET signal obtained with fluorescent **(A)** Q44c-HL488 or **(B)** Q86c-HL488 binding to NLuc-EGFR. HEK293 cells stably expressing full-length N-terminal nanoluciferase-EGFR were treated with furimazine (12.5 nM) and, luminescence and fluorescence values were read for 15 minutes (every 60 sec) at 37°C using a BMG Pherastar. Following this period, cells were treated with 25 nM of either respective fluorescent nanobody and luminescence and fluorescence emissions simultaneously recorded for a further 30 min at 37°C. After 30 minutes, various concentrations of EGF were added to the wells and measurements continued for a further 30 minutes at 37°C. Data are mean ± SEM from triplicate determinations in a single experiment. This single experiment is representative of five independent experiments performed.

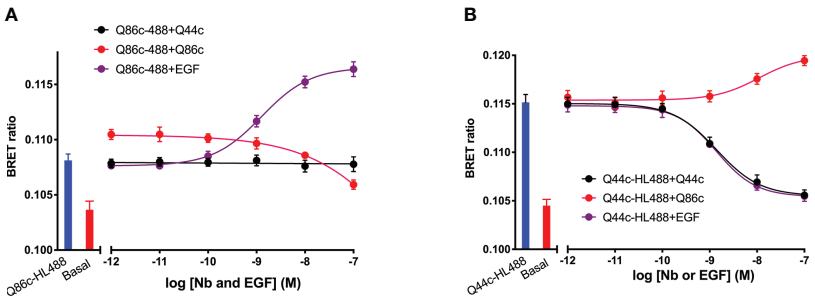

FIGURE 7
The effect of unlabelled Q44c, Q86c and EGF on the binding of fluorescent **(A)** Q44c-HL488 (14.6 nM) and **(B)** Q86c-HL488 (12.5 nM) to full-length N-terminal nanoluciferase-EGFR. NanoBRET experiments were performed using NLuc-EGFR stably expressing HEK293 cells. Cells were treated with either nanobody and EGF simultaneously and incubated for 30 minutes at 37°C. The NLuc substrate furimazine (12.5 nM) was added and plates incubated for 5 minutes then luminescence and fluorescence emissions were measured using a BMG Pherastar. Experiments were performed in HBSS containing 0.2 % BSA. Data are combined mean ± SEM from five independent experiments, where each experiment was performed in triplicate.

stimulation period. As LgBiT is itself not membrane permeable, luminescence detected from re-complemented full length nanoluciferase is indicative of the EGFR population still remaining at the cell surface after agonist stimulation. Using this approach, 100 nM EGF induced significant receptor internalization within 5 min of agonist administration which was not seen with Q86c and Q44c (Figure 8). These data suggest that the fall in luminescence at high concentrations of both Q44c-HL488 and Q86c-HL488 following attainment of the initial peak is more likely a consequence of molecular rearrangement. However, the fall in signal from Q86c-HL488 following EGF addition could be explained by EGF-induced receptor internalization.

Discussion

In the present study we have used small (*circa* 15 KDa) fluorescent camelid nanobodies targeting the human EGFR to investigate ligand-binding and conformational changes induced by agonists in living cells. Q44c-HL488 binds to ligand-free EGFR but not to EGF-occupied receptors suggesting that it

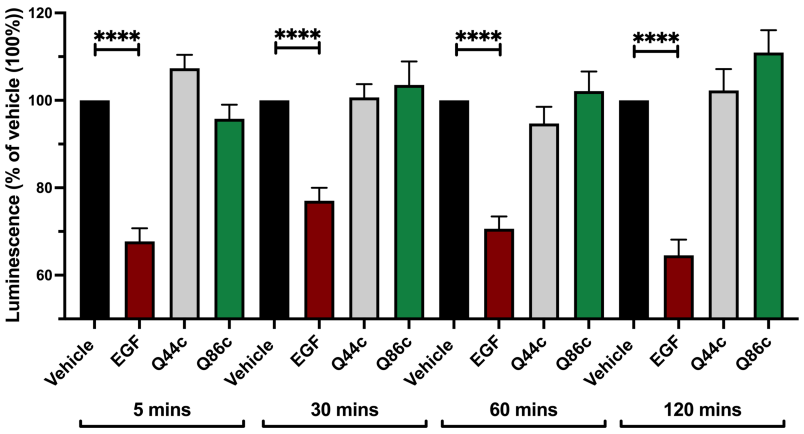

FIGURE 8
Effect of unlabelled Q44c, Q86c and EGF on EGFR internalization measured using NanoBiT. HEK293 cells transiently expressing HiBiT-EGFR cDNA, were treated with EGF (100 nM), Q44c (100 nM) or Q86c (100 nM) in HBSS/0.02% BSA for 5, 30, 60 or 120 minutes at 37°C. Purified LgBiT (10 nM) and furimazine (1:400 dilution) were then added and cells incubated for a further 20 minutes at 37°C to allow NanoBiT recomplementation (leading to the formation of full-length nanolucifierase) and furimazine oxidation to occur. Luminescence emissions were then measured using a BMG Pherastar. Data are mean ± SEM from quadruplicate observations in a single experiment pooled from 5 (120 minutes incubation) and 7 (5, 30, 60 minute incubations) independent experiments. Data were normalized to vehicle controls (100%) and statistical significance determined using a one way ANOVA (**** = P<0.0001).

binds to an epitope close to the EGF-binding site on domain III and can sterically interfere with the binding of EGF (20, 21). To test this directly, we used a N-terminal nanoluciferase-tagged variant of EGFR (NLuc-EGFR) expressed in living cells and monitored the binding of fluorescent variants of EGF and Q44c using NanoBRET (27–29). The proximity requirements (<10 nm) of the NanoBRET approach provided a very sensitive measure of specific binding to EGFR. Q44c-HL488 was able to directly bind to ligand-free EGFR with high affinity, and unlabelled Q44c was able to compete for specific EGF-AF488 binding to EGFR. The specific binding of Q44c-HL488 to EGFR was fully displaced by 100 nM unlabelled EGF and 100 nM non-fluorescent Q44c was able to fully prevent the binding of either EGF-AF488 or EGF-AF647 to NLuc-EGFR. In keeping with previous observations (10), other higher-affinity EGFR ligands (TGFα, BTC, HB-EGF) potently inhibited the binding of Q44c-HL488 whilst low-affinity ligands epiregulin, epigen and amphiregulin were considerably weaker with only epiregulin producing a small but significant displacement of Q44c-HL488 binding when used at a maximal concentration (100nM). Q44c-HL488 binding could, however, be completely prevented by unlabelled Q44c.

In marked contrast to the data obtained with Q44c-HL488, Q86c-HL488 was able to bind with high affinity to both ligand-free and EGF-occupied receptors. Also, unlabelled Q86c had no effect on the binding of EGF-AF488 or EGF-AF647 to NLuc-EGFR at concentrations up to 100nM. Similarly, EGF did not inhibit the binding of Q86c-HL488 to EGFR. EGF did, however, produce a marked enhancement (438%) of the BRET signal obtained with Q86c-HL488. This was mimicked in a concentration-dependent manner by all EGFR ligands with EGF, HB-EGF, BTC and TGF-α being the most potent, epiregulin producing a modest response and both epigen and amphiregulin producing very weak but observable stimulations at the highest concentrations employed (100 nM). The most likely explanation for this significant increase in Q86c-HL488 BRET induced by EGFR ligands is that it represents a conformational change related to the agonist-induced extended conformation of EGFR and exposure of the dimerization interface in domain II leading to receptor homodimerization (5–10). This is in keeping with the recent receptor X-ray crystal structures of Q86 (EgB4) alone and bound to the full extracellular EGFR-EGF complex in its extended active conformation (30)). It is also interesting that Q86c can induce a small enhancement of Q44c-HL488 binding (but not EGF-AF488 or EGF-AF647 binding) which suggests that there are subtle differences in the binding of EGF and Q44c to domain III of EGFR.

NanoBRET is dependent upon both close proximity (<10 nm) but also the orientation of the donor and acceptor moieties. Thus, conformation changes can have a profound impact on both the relative orientation and proximity of the donor and acceptor elements of the proteins of interest (29, 31). Furthermore, if as expected EGFR dimerization is induced (32), then there is also scope for additional BRET between the Q86c-HL488 and the N-terminal nanoluciferase on the opposing as well as the same protomer, resulting in an enhancement of the final BRET signal observed. The differences in the final BRET signal observed with high affinity and low affinity EGFR ligands might therefore reflect differences in the structure of the dimers generated (10) in addition to the affinity differences observed for binding to EGFR. Q86 (EgB4) has been shown previously to not compete for EGF-binding to EGFR (20, 22). Furthermore, in keeping with its ability to sense conformational changes in EGFR reported here, Q86 (EgB4) has previously been used to evaluate gross movements of the extracellular domains of EGFR from the plane of the cell membrane (23). This would be consistent with the detection of an extended conformation capable of forming homodimers.

The kinetic analysis of the binding of both Q44c-HL488 and Q86c-HL488 to NLuc-EGFR indicated that at the higher concentrations of nanobody used in these experiments, two components were observed in their kinetic profiles represented by a fast pronounced peak in the BRET ratio followed by a decline to a lower plateau. This would be consistent with either some limited conformation rearrangement of EGFR following binding of the nanobody or a nanobody-induced receptor internalisation. Furthermore, addition of EGF after a steady plateau of binding had been achieved yielded the expected inhibition (for Q44c-HL488 binding) or stimulation (for Q86c-HL488 binding). The two phases were most apparent for Q86c-HL488 and it is interesting that the subsequent stimulatory effect of EGF was characterised by a fall to a lower plateau after an initial rapid peak was obtained. If a conformational rearrangement is responsible for this effect then it is likely that this is a consequence of negative cooperativity (4, 7–10) across the dimer interface. For example, an overshoot of ligand binding to an extended active EGFR conformation could occur before the asymmetric dimers are formed leading to loss of nanobody or EGF from one of the protomers due to negative cooperativity across the dimer interface. Similarly, there is evidence for ligand-independent dimerization of non-active EGFRs which is dependent upon close proximity of the intracellular juxtamembrane domains (33–35). Negative cooperativity across the juxtamembrane dimer interface of non-active EGFRs could also explain the complex kinetic profiles of the binding of Q44c-HL488 and Q86c-HL488 in the absence of EGF.

The simplest explanation, however, for the fast pronounced peak in the BRET ratio followed by a decline to a lower plateau observed with EGF, Q44c-HL488 and Q86c-HL488 is that they are inducing a rapid internalization of a proportion of the cell surface receptors. In order to investigate this, we took advantage of the NanoBiT internalization assay developed by Soave et al (26). In this approach a small eleven amino acid fragment of nanoluciferase (HiBiT) (26, 36, 37) was added to the N-terminus

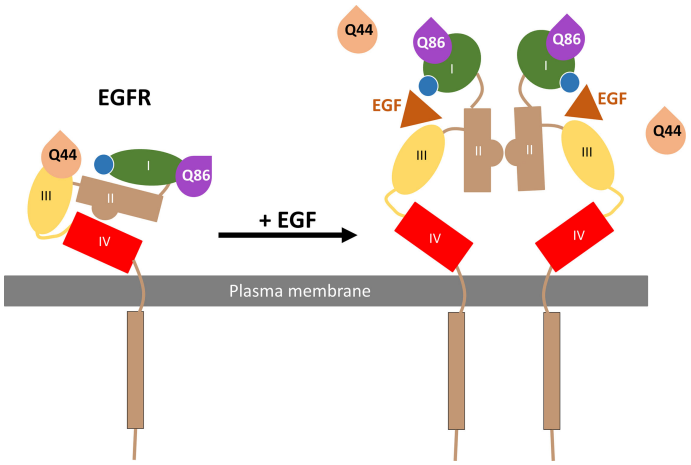

FIGURE 9
Schematic of Q44c and Q86c binding on domain III and I of the EGFR respectively. While EGF binding to the EGFR alters the EGFR conformation and causes the dissociation of Q44c, this conformational rearrangement leads to closer proximity of Q86c with the nanoluciferase tag (illustrated by the blue circle) on EGFR.

of EGFR. Following stimulation of EGFR with EGF or nanobody, the large 156 amino acid fragment (LgBiT) of nanoluciferase was added to allow complementation of full length nanoluciferase and reinstatement of the luminescence signal following addition of furimazine (26, 35). Since LgBiT is cell impermeable, luminescence provides a good measure of the population of EGFR remaining at the cell surface (26, 37). This approach was able to confirm that EGF can induce internalization of the EGFR receptor. The effect of EGF was rapid (occurring within 5 min) and sustained over the 120 min of the experiment. These data are in keeping with the well-established internalization of EGFR after agonist treatment (38–40). However, internalization was not seen with the two nanobodies Q86c and Q44c. These data suggest that the fall in luminescence at high concentrations of both Q44c-HL488 and Q86c-HL488 following attainment of the initial peak is more likely a consequence of conformational change and allosteric regulation which might alter the stability of the nanobody at its binding site. However, the fall in signal from Q86c-HL488 following EGF addition could be secondary to EGF-induced receptor internalization.

In summary, the present manuscript has used NanoBRET and NanoBiT technologies in combination with fluorescent nanobodies to demonstrate the direct binding of Q44c-HL488 and Q86c-HL488 to two different sites on the full-length EGFR receptor in living cells (Figure 9). Q44c-HL488 was able to inhibit EGF binding to full length EGFR consistent with the proposal that it binds to domains I and III of EGFR in a similar manner to 7D12 (21) (Figure 9). In contrast, Q86c-HL488 can bind to EGF-bound EGFR and act as a conformational sensor by detecting the change to an open conformation of the receptor on EGF binding (Figure 9). This conformational change reveals the dimerization domain II and facilitates EGFR dimerization. These data suggest that these two nanobodies will be powerful tools for studying the role of EGFR in both health and disease.

Data availability statement

The original contributions presented in the study are included in the article/supplementary material. Further inquiries can be directed to the corresponding authors.

Author contributions

Conceived the study: SH and LK. Generated reagents: DC, JG, SA, LK, and MS. Participated in research design: DC, SH, LK, JG, RH, SA, and MS. Conducted experiments: DC, JG, and LK. Performed data analysis: DC, SH, and LK. Wrote or contributed to the writing of the manuscript: DC, SH, LK, RH, SMA, and MJS. All authors contributed to the article and approved the submitted version.

Funding

Research was supported by MRC (grant numbers MR/N020081/1 and MR/W016176/1) and the ONCORNET 2.0 (ONCOgenic Receptor Network of Excellence and Training 2.0) PhD training programme (DC and SA) funded by the European Commission for a Marie Sklodowska Curie Actions

(H2020-MSCA grant agreement 860229). LK is funded by a University of Nottingham Anne McLaren Research Fellowship.

Acknowledgments

The authors would like to thank Promega Corporation for kindly providing the NanoLuc-EGFR and HiBiT-EGFR constructs.

Conflict of interest

RH is CSO of QVQ Holding B.V. and SA is affiliated to QVQ Holdings.

The remaining authors declare that the research was conducted in the absence of any commercial or financial relationships that could be construed as a potential conflict of interest.

Publisher's note

References

1. Singh M, Jadhav HR. Targeting non-small cell lung cancer with small molecule EGFR tyrosine kinase inhibitors. *Drug Discovery Today* (2018) 23:745–53. doi: 10.1016/j.drudis.2017.10.004

2. Lemmon MA, Schlessinger J. Cell signaling by receptor tyrosine kinases. *Cell* (2010) 141:1117–34. doi: 10.1016/j.cell.2010.06.011

3. Yarden Y, Schlessinger J. Epidermal growth factor induces rapid, reversible aggregation of the purified epidermal growth factor receptor. *Biochemistry* (1987) 26:1443–51. doi: 10.1021/bi00379a035

4. Ferguson KM, Hu C. Lemmon MA insulin and epidermal growth factor receptor family members share parallel activation mechanisms. *Protein Sci* (2020) 29:1331–44. doi: 10.1002/pro.3871

5. Burgess AW, Cho HS, Eigenbrot C, Ferguson KM, Garrett TPJ, Leahy DJ, et al. An open-and-shut case? recent insights into the activation of EGF/ErbB receptors. *Mol Cell* (2003) 12:541–52. doi: 10.1016/S1097-2765(03)00350-2

6. Dawson JP, Berger MB, Lin CC, Schlessinger J, Lemmon MA, Ferguson KM. Epidermal growth factor receptor dimerization and activation require ligand-induced conformational changes in the dimer interface. *Mol Cell Biol* (2005) 25:7734–42. doi: 10.1128/MCB.25.17.7734-7742.2005

7. Macdonald-Obermann JL, Pike LJ. The intracellular juxtamembrane domain of the epidermal growth factor (EGF) receptor is responsible for the allosteric regulation of EGF binding. *J Biol Chem* (2009) 284:13570–6. doi: 10.1074/jbc.M109.001487

8. Defize LH, Boonstra J, Meisenhelder J, Kruijer W, Tertoolen LG, Tilly BC, et al. Signal transduction by epidermal growth factor occurs through the subclass of high affinity receptors. *J Cell Biol* (1989) 109:2495–507. doi: 10.1083/jcb.109.5.2495

9. Bessman NJ, Bagchi A, Ferguson KM, Lemmon MA. Complex relationship between ligand binding and dimerization in the epidermal growth factor receptor. *Cell Rep* (2014) 9:1306–17. doi: 10.1016/j.celrep.2014.10.010

10. Freed DM, Bessman NJ, Kiyatkin A, Salazar-Cavazos E, Byrne PO, Moore JO, et al. EGFR ligands differentially stabilize receptor dimers to specify signaling kinetics. *Cell.* (2017) 171:683–95. doi: 10.1016/j.cell.2017.09.017

11. Alvarado D, Klein DE, Lemmon MA. Structural basis for negative cooperativity in growth factor binding to an EGF receptor. *Cell* (2010) 142:568–79. doi: 10.1016/j.cell.2010.07.015

12. Liu P, Cleveland TE4, Bouyain S, PO B, PA L, Leahy DJ. A single ligand is sufficient to activate EGFR dimers. *Proc Natl Acad Sci U.S.A.* (2012) 109:10861–6. doi: 10.1073/pnas.1201114109

13. Ogiso H, Ishitani R, Nureki O, Fukai S, Yamanaka M, Kim JH, et al. Crystal structure of the complex of human epidermal growth factor and receptor extracellular domains. *Cell.* (2002) 110:775–87. doi: 10.1016/S0092-8674(02)00963-7

14. Harris RC, Chung E, Coffey RJ. EGF receptor ligands. *Exp Cell Res* (2003) 284:2–13. doi: 10.1016/S0014-4827(02)00105-2

15. Knudsen SL, Mac AS, Henriksen L, van Deurs B, Grøvdal LM. EGFR signaling patterns are regulated by its different ligands. *Growth Factors* (2014) 32:155–63. doi: 10.3109/08977194.2014.952410

16. Ronan T, Macdonald-Obermann JL, Huelsmann L, Bessman NJ, Naegle KM, Pike LJ. Different epidermal growth factor receptor (EGFR) agonists produce unique signatures for the recruitment of downstream signaling proteins. *J Biol Chem* (2016) 291:5528–40. doi: 10.1074/jbc.M115.710087

17. Wilson KJ, Mill C, Lambert S, Buchman J, Wilson TR, Hernandez-Gordillo V, et al. EGFR ligands exhibit functional differences in models of paracrine and autocrine signaling. *Growth Factors.* (2012) 30:107–16. doi: 10.3109/08977194.2011.649918

18. Huang Y, Ognjenovic J, Karandur D, Miller K, Merk A, Subramaniam S, et al. A molecular mechanism for the generation of ligand-dependent differential outputs by the epidermal growth factor receptor. *Elife.* (2021) 10:e73218. doi: 10.7554/elife.73218

19. Roovers RC, Laeremans T, Huang L, De Taeye S, Verkleij AJ, Revets H, et al. Efficient inhibition of EGFR signaling and of tumour growth by antagonistic anti-EFGR nanobodies. *Cancer Immunol Immunother* (2007) 56:303–17. doi: 10.1007/s00262-006-0180-4

20. Hofman EG, Ruonala MO, Bader AN, van den Heuvel D, Voortman J, Roovers RC, et al. EGF induces coalescence of different lipid rafts. *J Cell Sci* (2008) 121:2519–28. doi: 10.1242/jcs.028753

21. Schmitz KR, Bagchi A, Roovers RC, van Bergen en Henegouwen PM, Ferguson KM. Structural evaluation of EGFR inhibition mechanisms for nanobodies/VHH domains. *Structure* (2013) 21:1214–24. doi: 10.1016/j.str.2013.05.008

22. Low-Nam ST, Lidke KA, Cutler PJ, Roovers RC, van Bergen en Henegouwen PM, Wilson BS, et al. ErbB1 dimerization is promoted by domain co-confinement and stabilized by ligand binding. *Nat Struct Mol Biol* (2011) 18:1244–9. doi: 10.1038/nsmb.2135

23. Zanetti-Domingues LC, Korovesis D, Needham SR, Tynan CJ, Sagawa S, Roberts SK, et al. The architecture of EGFR's basal complexes reveals autoinhibition mechanisms in dimers and oligomers. *Nat Commun* (2018) 9:4325. doi: 10.1038/s41467-018-06632-0

24. Soave M, Heukers R, Kellam B, Woolard J, Smit MJ, Briddon SJ, et al. Monitoring allosteric interactions with CXCR4 using NanoBiT conjugated nanobodies. *Cell Chem Biol* (2020) 27:1250–61. doi: 10.1016/j.chembiol.2020.06.006

25. Heukers R, Mashayekhi V, Ramirez-Escudero M, de Haard H, Verrips TC, van Bergen En Henegouwen PMP, et al. VHH-photosensitizer conjugates for targeted photodynamic therapy of met-overexpressing tumor cells. *Antibodies (Basel).* (2019) 8:26. doi: 10.3390/antib8020026

26. Soave M, Kellam B, Woolard J, Briddon SJ. Hill SJ NanoBiT® complementation to monitor agonist-induced adenosine A1 receptor internalization. *SLAS Discovery* (2019) 25:186–94. doi: 10.1177/2472555219880475

27. Stoddart L, Johnstone EKM, Wheal AJ, Goulding J, Robers MB, Machleidt T, et al. Application of BRET to monitor ligand binding to GPCRs. *Nat Methods* (2015) 12:661–63. doi: 10.1038/nmeth.3398

28. Kilpatrick LE, Friedman-Ohana R, Alcobia DC, Riching K, Peach CJ, Wheal A, et al. Real-time analysis of the binding of fluorescent $VEGF_{165}$a to VEGFR2 in living cells: Effect of receptor tyrosine kinase inhibitors and fate of internalized agonist-receptor complexes. *Biochem Pharmacol* (2017) 136:62–75. doi: 10.1016/j.bcp.2017.04.006

29. Lay CS, Bridges A, Goulding J, Briddon SJ, Soloviev Z, Craggs PD, et al. Probing the binding of interleukin-23 to individual receptor components and the IL-23 heteromeric receptor complex in living cells using NanoBRET. *Cell Chem Biol* (2022) 29:19–29. doi: 10.1016/j.chembiol.2021.05.002

30. Zeronian MR, Doulkeridou S, van Bergen En Henegouwen PMP, Janssen BJC. Structural insights into the non-inhibitory mechanism of the anti-EGFR EgB4 nanobody. *BMC Mol Cell Biol* (2022) 23:12. doi: 10.1186/s12860-022-00412-x

31. Schihada H, Vandenabeele S, Zabel U, Frank M, Lohse MJ, Maiellaro I. A universal bioluminescence resonance energy transfer sensor design enables high-sensitivity screening of GPCR activation dynamics. *Commun Biol* (2018) 1:105. doi: 10.1038/s42003-018-0072-0

32. Hofman EG, Bader AN, Voortman J, van den Heuvel DJ, Sigismund S, Verkleij AJ, et al. Ligand-induced EGF receptor oligomerization is kinase-dependent and enhances internalization. *J Biol Chem* (2010) 285:39481–9. doi: 10.1074/jbc.M110.164731

33. Yu X, Sharma KD, Takahashi T, Iwamoto R, Mekada E. Ligand-independent dimer formation of epidermal growth factor receptor (EGFR) is a step separable from ligand-induced EGFR signaling. *Mol Biol Cell* (2002) 13:2547–57. doi: 10.1091/mbc.01-08-0411

34. Macdonald-Obermann JL, Piwnica-Worms D, Pike LJ. Mechanics of EGFR receptor/Erbb2 kinase activation revealed by luciferase fragment complementation imaging. *Proc Natl Acad Sci U. S. A.* (2012) 109:137–42. doi: 10.1073/pnas.1111316109

35. Nevoltris D, Lombard B, Dupuis E, Mathis G, Chames P, Baty D. Conformational nanobodies reveal tethered epidermal growth factor receptor involved in EGFR/ErbB2 predimers. *ACS Nano.* (2015) 9:1388–99. doi: 10.1021/nn505752u

36. Dixon AS, Schwinn MK, Hall MP, Zimmerman K, Otto P, Lubben TH, et al. NanoLuc complementation reporter optimized for accurate measurement of protein interactions in cells. *ACS Chem Biol* (2016) 11:400–08. doi: 10.1021/acschembio.5b00753

37. Peach CJ, Kilpatrick LE, Woolard J, Hill SJ. Use of NanoBiT and NanoBRET to monitor fluorescent VEGF-a binding kinetics to VEGFR2/NRP1 heteromeric complexes in living cells. *Br J Pharmacol* (2021) 178:2393–411. doi: 10.1111/bph.15426

38. Schlessinger J. Common and distinct elements in cellular signaling *via* EGF and FGF receptors. *Science.* (2004) 306:1506–7. doi: 10.1126/science.1105396

39. Nishimura Y, Bereczky B, Ono M. The EGFR inhibitor gefitinib suppresses ligand-stimulated endocytosis of EGFR *via* the early/late endocytic pathway in non-small cell lung cancer cell lines. *Histochem Cell Biol* (2007) 127:541–53. doi: 10.1007/s00418-007-0281-y

40. Nishimura Y, Yoshioka K, Bereczky B, Itoh K. Evidence for efficient phosphorylation of EGFR and rapid endocytosis of phosphorylated EGFR *via* the early/late endocytic pathway in a gefitinib-sensitive non-small cell lung cancer cell line. *Mol Cancer.* (2008) 7:42. doi: 10.1186/1476-4598-7-42

frontiers | Frontiers in Molecular Biosciences

TYPE Original Research
PUBLISHED 05 December 2022
DOI 10.3389/fmolb.2022.1039324

OPEN ACCESS

EDITED BY
Fazli Wahid,
Pak-Austria Fachhochschule Institute of Applied Sciences and Technology, Pakistan

REVIEWED BY
Mehran Alavi,
Razi University, Iran
Vesa P. Hytönen,
University of Tampere, Finland

*CORRESPONDENCE
Kayhan Azadmanesh,
azadmanesh@pasteur.ac.ir
Arash Arashkia,
a_arashkia@pasteur.ac.ir

SPECIALTY SECTION
This article was submitted to Nanobiotechnology, a section of the journal Frontiers in Molecular Biosciences

RECEIVED 08 September 2022
ACCEPTED 22 November 2022
PUBLISHED 05 December 2022

CITATION
Kadkhodazadeh M, Mohajel N, Behdani M, Baesi K, Khodaei B, Azadmanesh K and Arashkia A (2022), Fiber manipulation and post-assembly nanobody conjugation for adenoviral vector retargeting through SpyTag-SpyCatcher protein ligation. *Front. Mol. Biosci.* 9:1039324. doi: 10.3389/fmolb.2022.1039324

Fiber manipulation and post-assembly nanobody conjugation for adenoviral vector retargeting through SpyTag-SpyCatcher protein ligation

Maryam Kadkhodazadeh[1], Nasir Mohajel[1], Mahdi Behdani[2], Kazem Baesi[3], Behzad Khodaei[4], Kayhan Azadmanesh[1]* and Arash Arashkia[1]*

[1]Department of Molecular Virology, Pasture Institute of Iran, Tehran, Iran, [2]Venom and Biotherapeutics Molecules Laboratory, Medical Biotechnology Department, Biotechnology Research Center, Pasteur Institute of Iran, Tehran, Iran, [3]Hepatitis and AIDS Department, Pasteur institute of Iran, Tehran, Iran, [4]School of Medicine, Tehran University of Medical Sciences, Tehran, Iran

For adenoviruses (Ads) to be optimally effective in cancer theranostics, they need to be retargeted toward target cells and lose their natural tropism. Typically, this is accomplished by either engineering fiber proteins and/or employing bispecific adapters, capable of bonding Ad fibers and tumor antigen receptors. This study aimed to present a simple and versatile method for generating Ad-based bionanoparticles specific to target cells, using the SpyTag-SpyCatcher system. The SpyTag peptide was inserted into the HI loop of fiber-knob protein, which could act as a covalent anchoring site for a targeting moiety fused to a truncated SpyCatcher (SpyCatcherΔ) pair. After confirming the presence and functionality of SpyTag on the Ad type-5 (Ad5) fiber knob, an adapter molecule, comprising of SpyCatcherΔ fused to an anti-vascular endothelial growth factor receptor 2 (VEGFR2) nanobody, was recombinantly expressed in *Escherichia coli* and purified before conjugation to fiber-modified Ad5 (fmAd5). After evaluating fmAd5 detargeting from its primary coxsackie and adenovirus receptor (CAR), the nanobody-decorated fmAd5 could be efficiently retargeted to VEGFR2-expressing 293/KDR and human umbilical vein endothelial (HUVEC) cell lines. In conclusion, a plug-and-play platform was described in this study for detargeting and retargeting Ad5 through the SpyTag-SpyCatcher system, which could be potentially applied to generate tailored bionanoparticles for a broad range of specific targets; therefore, it can be introduced as a promising approach in cancer nanotheranostics.

KEYWORDS

SpyTag/SpyCatcher, retargeting, adapter, fiber knob, adenovirus (Ad)

Introduction

Recently, various nano-sized viral and non-viral vectors (nanovectors) have been employed in cancer theranostics to maximize efficacy, while minimizing the side effects. Considering numerous advantages and disadvantages of the nanovectors (Supplementary Table S1), bionanoparticles can be excellent alternatives to inorganic nanoparticles owing to their higher biocompatibility and biodegradability (Chung et al., 2020). The optimal bionanoparticles for cancer theranostics should be capable of self-assembly, targeting, cell entry, and endosomal escape. Accordingly, viruses have been applied as great naturally occurring nanocarriers for theranostic applications (Somiya et al., 2017).

Among various viral vectors, adenoviruses (Ads) have been extensively used in clinical trials for gene therapy and vaccination due to their high *in vivo* stability and gene transfer efficiency (Ginn et al., 2018; Singh et al., 2019). More importantly, the safety of Ad-based vectors has been advocated in preclinical and clinical trials (Hajeri et al., 2020). Despite the strong safety profile of these vectors, besides remarkable advances in Ad vector-mediated gene therapy, their clinical application remains challenging. The challenges are mainly attributed to the broad tropism of Ad vectors due to the high affinity of Ad fiber-knob domains for cellular receptors, including the widely expressed coxsackie and adenovirus receptors (CARs) (Zhang and Bergelson, 2005). In contrast, cancer cells mainly have low/no expression of native Ad receptors (Okegawa et al., 2001). It is known that the CAR distribution influences the Ad biodistribution *in vivo*; therefore, intravenous administration of Ads may result in liver toxicity owing to the higher rate of liver transduction (Tao et al., 2001). Accordingly, Ad vectors modified with active targeting modalities have been developed to deal with the resistance of tumor cells and non-specific uptake toxicity and to facilitate efficient gene delivery with fewer side effects.

So far, various detargeting and retargeting methods have been proposed and investigated in the literature, including the modification of capsid proteins (e.g., hexon, fiber, and penton) and implementation of bispecific adapter molecules. The majority of previous studies have focused on alterations in the fiber protein, which is a crucial component of capsid, with a significant contribution to Ad tropism. Generally, the fiber protein is a homotrimeric, antenna-shaped protein, which connects with the penton base to generate penton capsomers found at the icosahedral Ad virion vertices (Krasnykh et al., 2000). Ad5 uses a two-step process to penetrate into cells. First, the knob domain of the fiber must connect with the primary CAR on target cells. Second, the penton base makes contact with integrin receptors on the cell surface, triggering viral uptake *via* receptor-mediated endocytosis (Wickham et al., 1993; Tomko et al., 1997).

While genetic modification has been a prosperous approach for virus targeting, successful incorporation of extraneous moieties into capsid proteins requires extensive protein engineering, which is both challenging and time-consuming. Besides, replacement of the capsid fiber protein mainly results in the production of structurally unstable vectors (Noureddini and Curiel, 2005; Waehler et al., 2007). Also, some targeting ligands require post-translational modifications, such as disulfide bonds that are not present in the cytoplasm or nucleoplasm of cells, where the fiber and Ad particle production occurs (Magnusson et al., 2002).

Comparatively, adapter-based systems that can couple various adapters into the same vector are flexible platforms with no impact on the vector structure. They concurrently eliminate native viral tropisms and facilitate a novel tropism toward the desired target (Dmitriev et al., 2000; Pereboev et al., 2004). However, the majority of adapter systems have drawbacks that limit their potential use in theranostics. The most significant disadvantage of adapter systems is the suboptimal stability of the vector-adapter complex because of unanticipated interactions with other elements that interrupt non-covalent binding (Waehler et al., 2007). To address this challenge, methods that can produce Ad vectors capable of binding to other molecules through covalent interactions, without any need for virus engineering, can be effective.

The SpyCatcher/SpyTag system, a protein-peptide pair forming an isopeptide bond when exposed to each other, has been introduced to create universal vectors (Zakeri et al., 2012). This system is based on the immunoglobulin-like collagen adhesion domain (CnaB2) of *Streptococcus pyogenes*, containing an internal isopeptide bond between Lys31 and Asp117 (Oke et al., 2010; Li and Fierer, 2014). This isopeptide bond is stable over a wide range of pH, temperatures, redox environments, and detergents (Dovala et al., 2016). Since its introduction in 2012, the SpyTag-SpyCatcher system has been implemented in various studies, involving bioactive hydrogels (Sun et al., 2014), thermostabilized proteins (Schoene et al., 2014), multivalent antigen-presenting vaccines derived from virus-like particles (Brune et al., 2016), and lentivirus retargeting (Kasaraneni et al., 2017).

The present study aimed to investigate whether Ad tropism can be altered by the SpyTag-SpyCatcher system, resulting in covalent binding between the virus and the targeted adapter molecule. For this purpose, the feasibility of native Ad5 fiber replacement with a recombinant fiber containing the SpyTag peptide was assessed. Besides, the ability of the modified fiber to bind to the SpyCatcher, as well as the ablation of CAR-mediated internalization of virions following bioconjugation with the SpyCatcher, was examined. Subsequently, a retargeted Ad vector was generated as a model using an adapter molecule, which was constructed through the genetic fusion of SpyCatcher with a nanobody specific to vascular endothelial growth factor

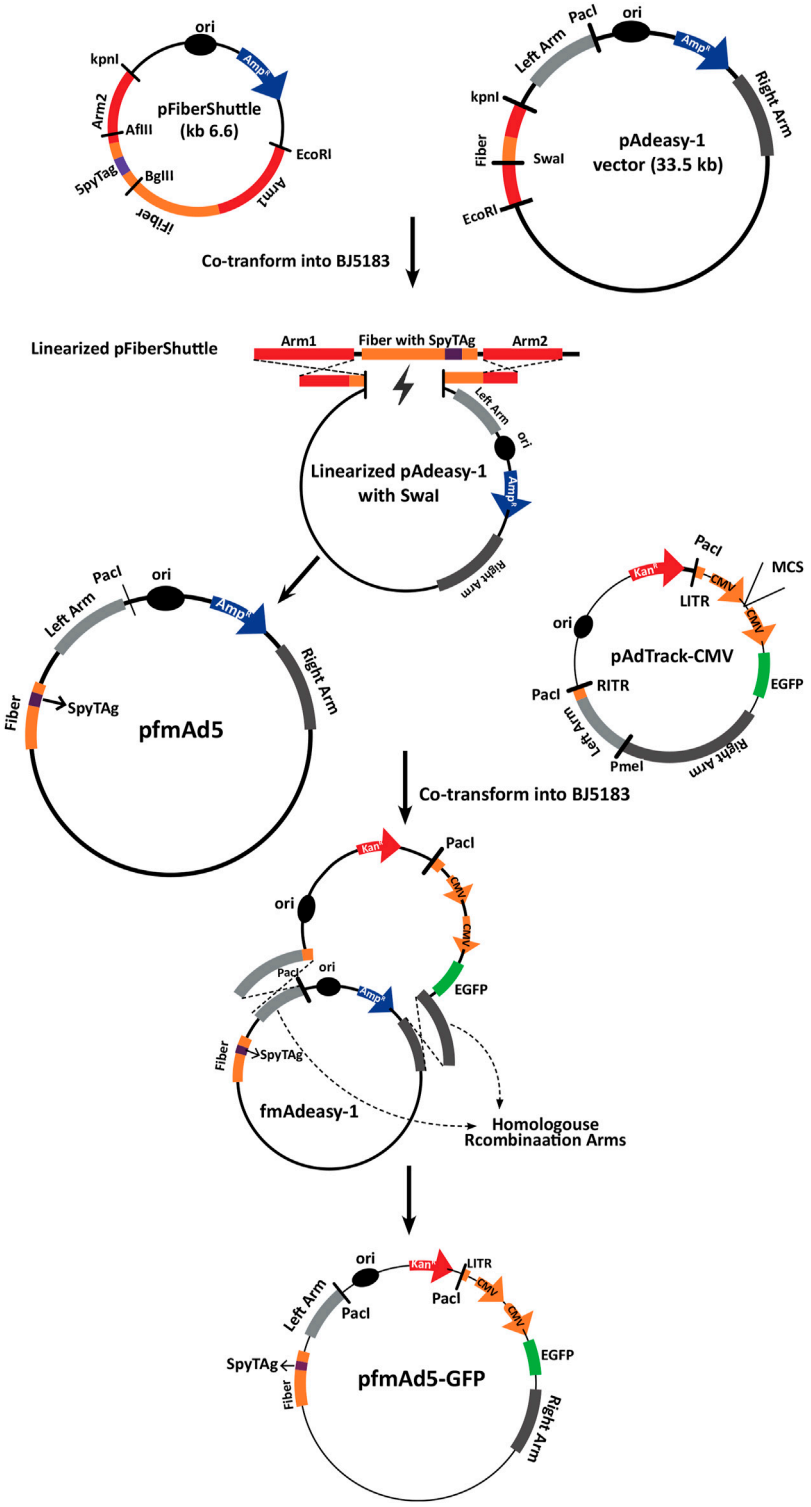

FIGURE 1
A schematic representation of the development process of pfmAd5-GFP. The pFiberShuttle and pAdeasy-1 constructs were first co-transformed into *E. coli* BJ5183 for a homologous recombination (HR) to generate pAdeasy-1 containing SpyTag. This vector was then used in HR with pAdTrack-CMV containing an *EGFP* gene to create pfmAd5-GFP. The pAd5-GFP, as the control virus, was developed using intact pAdeasy-1 and pAdTrack-CMV for HR.

receptor-2 (VEGFR2), as one of the main targets for the inhibition of tumor angiogenesis.

Based on the results, the recombinant Ad vector with a SpyTag peptide in its HI loop could robustly engage the adapter molecule to target VEGFR2-expressing cells through a CAR-independent cell entry mechanism. According to the findings, this functionalized Ad vector has great potential applications in cancer theranostics. To the best of our knowledge, this is the first study to evaluate Ad functionality following fiber modification *via* insertion of SpyTag into the HI loop and its bioconjugation with the targeting SpyCatcher-containing adapter molecule.

Materials and methods

Construction of modified Ad vector

The protocol proposed by Wu and Curiel was used to produce a pFiberShuttle vector, containing the SpyTag peptide within the knob HI loop (Wu and Curiel, 2008). Accordingly, a 3.5-kb fragment from the plasmid pAdeasy-1 (Addgene, Uniteed States), encompassing a fiber-coding gene and homologous recombination (HR) arms, was subcloned in pUC-19 between *Eco*RI-*Kpn*I restriction sites. Subsequently, a 670-bp fragment, incorporating a 13-amino-acid SpyTag coding sequence (AHIVMVDAYKPTK) following amino acid G543 in the HI loop, was ordered to be synthesized by Biomatik (Ontario, Canada). It was then subcloned between *Afl*II-*Bgl*II digestion sites of the 3.5-kb, subcloned fragment to replace the homologous segment of the intact fiber.

Additionally, to generate a fiber-modified Ad5, an E1 and E3-deleted backbone vector, that is, pAdeasy-1, was used. To facilitate recombination, the pFiberShuttle vector and the backbone should be linearized near or in the position of the fiber gene. Accordingly, a unique *Swa*I cut site was introduced into the fiber gene of pAdeasy-1 vector. For this purpose, pAdeasy-1 was first digested with *Bam*HI, and the produced 11,753-bp fragment, containing the fiber gene and a unique *Nde*I restriction site, was subcloned into the pBluescript-SK vector (Addgene, Uniteed States) (Wu and Curiel, 2008). Afterward, a pair of oligonucleotides (Supplementary Table S1) containing the *Swa*I cut site, as well as sticky ends that ligate in the *Nde*I restriction site, were synthesized and inserted into the corresponding *Nde*I cut site of the subcloned, 11,753-bp, fiber-coding fragment. Finally, the intact homologous pAdeasy-1 fragment was replaced with the modified fragment containing the *Swa*I cut site.

The fiber-modified Ad backbone vector (pfm-Ad5) was constructed by homologous recombination (HR) between the linearized pFiberShuttle vector and the modified pAdeasy-1 in *E. coli* BJ5183 (Figure 1). Polymerase chain reaction (PCR) with specific primers (Supplementary Table S1) was performed to verify the presence of SpyTag sequence in the Ad5 backbone fiber. The pfm-Ad5 vector was then used to generate the recombinant Ad, encompassing an enhanced green fluorescent protein (EGFP) expression cassette (pfmAd5-GFP) through HR with linearized pAdTrack-CMV vector (Addgene, Uniteed States) (Figure 1).

Additionally, an unmodified Ad5-GFP virus was produced following HR between unchanged pAdeasy-1 and linearized pAdTrack-CMV. To confirm HR, the recombined vectors were extracted and digested with *Pac*I, followed by transfection into the AD-293 cell line, using a Lipofectamine™ 2000 Transfection Reagent (Invitrogen, Uniteed States) to rescue fmAd5-GFP and Ad5-GFP. Following the production of fmAd5-GFP, the presence of SpyTag in the fiber protein was confirmed *via* Ad genome extraction with a QIAamp DSP Virus Kit (Qiagen, Germany), followed by PCR and fiber sequencing. The fmAd5-GFP and Ad5-GFP titers were determined by the Median Tissue Culture Infectious Dose ($TCID_{50}$) assay (Herrmann and Bucksch, 2014).

Recombinant protein expression

The DNA fragment encoding SpyCatcherΔ, a protein with 21- and 14-amino-acid truncations at the N and C termini of the original protein, respectively (Kasaraneni et al., 2017), was synthesized by Biomatik (Ontario, Canada); it also harbored a 14-amino-acid hinge sequence at its C-terminus. Subsequently, the fragment was subcloned in the pET-28a (+) bacterial expression plasmid (Novagen, Uniteed States) to generate pET28Catcher. Additionally, to generate a SpyTag-expressing plasmid, a pair of oligonucleotides (Supplementary Table S1) containing the SpyTag sequence and sticky ends for ligation into the *Kpn*I and *Sal*I cut sites was synthesized and subcloned into the pET-32a (+) plasmid (Novagen, Uniteed States). The plasmids were then transformed into *E. coli* Rosetta (DE3), and protein expression was induced by the addition of 1 mM isopropyl β-D-1-thiogalactopyranoside (IPTG) for 4 hours at 37°C in a Lysogeny broth (LB) culture medium. The expressed SpyCatcherΔ and TrxA-SpyTag proteins were then purified using Ni-NTA agarose columns (Qiagen, Germany), according to the manufacturer's protocols.

To evaluate the ability of SpyCatcherΔ to create an isopeptide bond with SpyTag, the purified SpyCatcherΔ (15.8 kDa) was incubated with TrxA-SpyTag (19.4 kDa) at a molar ratio of 1: 1 for 1 hour at room temperature. The protein bioconjugation was tested by sodium dodecyl sulfate-polyacrylamide gel electrophoresis (SDS-PAGE). Additionally, to assess the ligation of fmAd5-GFP with the SpyCatcherΔ, 5×10^9 $TCID_{50}$ of the virus was incubated with 10 μM of the purified SpyCatcherΔ for 2 hours at 37°C. Next, the mixture was denatured by boiling in a sample buffer for 5 minutes at 95°C and subsequently analyzed by SDS-PAGE. The protein was

finally blotted onto a polyvinylidene difluoride (PVDF) membrane and developed with ECL Plus Substrate for Western blotting (Thermo Fisher Scientific, Uniteed States) after sequential incubation with a locally-obtained anti-SpyCatcherΔ serum and goat anti-mouse IgG-HRP (Abcam, United Kingdom). The Ad5-GFP was used as the control virus.

To generate an adapter molecule, encompassing a VEGFR2-specific nanobody fused to the SpyCatcherΔ, the nanobody-coding gene was amplified from the p2.2-Nb plasmid (Ahani et al., 2016) and subcloned at the N-terminus of the SpyCatcherΔ-coding sequence in the pET28Catcher plasmid through a flexible SGSGSSGAS linker. The construct was then subcloned in the pHEN6C expression vector containing a C-terminal His6 tag. Next, it was transformed into *E. coli* WK6 cells and induced for protein expression and purification as previously described (Rouet et al., 2012). Finally, the ability of the adapter molecule to covalently bind to the SpyTag was examined by SDS-PAGE.

Moreover, for the Ad5 fiber knob expression, its coding sequence was amplified from pAdEasy-1 (Yang et al., 2006) and subcloned into pET-32a (+). The expression parameters were similar to those of the abovementioned proteins. Nonetheless, due to protein aggregation, phosphate-buffered saline (PBS), containing 2% glycerol and 0.01% Tween 20, was used as dialysis buffer and protein solvent for protein purification.

Cell lines

In this study, the Chinese hamster ovary cell line (CHO-K1), the human embryonic kidney cell line optimized for Ad propagation (AD-293), the A549 human lung epithelial cell line with a high expression of CARs, the 293/KDR cell line stably overexpressing VEGFR2, and human umbilical vein endothelial cells (HUVEC) as the primary VEGFR2-expressing cell line were used. The cell lines present in this study were obtained from the National Cell Bank of Pasteur Institute of Iran. The AD-293, 293/KDR, and A549 cells were grown in Dulbecco's Modified Eagles Medium (DMEM, Biosera, Philippines), containing 10% heat-inactivated fetal bovine serum (FBS; Gibco, Uniteed States) and antibiotics (100 U/mL of penicillin and 100 µg/ml of streptomycin) (Biosera, Philippines). The CHO-K1 and HUVEC cells were cultured in DMEM-F12 (Biosera, Philippines), containing 10% FBS and antibiotics as described above.

The CHO-K1 cell line, which stably expresses SpyCatcherΔ on its surface (CHO-Spy), was developed through transfection with a pDisplay plasmid (Thermo Fisher Scientific, Uniteed States), encoding SpyCatcherΔ, according to a previously described protocol (Mortensen et al., 1997). Briefly, before transfection, the susceptibility of CHO-K1 to G418 (BioBasic, Canada) was determined to be 0.4 mg/ml. Transfection was performed with a Lipofectamine 2000 Transfection Reagent. The medium was replaced 48 h after transfection, and fresh DMEM-F12, containing 0.5 mg/ml of G418, was added to the medium. Next, the cells were serially diluted into a 96-well plate and incubated for 14 days to isolate the monoclonal cell line. Twelve monoclonal cells were selected and expanded to analyze the SpyCatcherΔ expression by flow cytometry (CyFlow, Partec, Germany), using the anti-SpyCatcherΔ serum and goat anti-mouse IgG-PE antibody (Thermo Fisher Scientific, Uniteed States).

Transduction of CHO-K1 and CHO-Spy by Ad vectors

The CHO-K1 and CHO-Spy were cultured at 1.5–2×10^5 cells/well in 24-well plates and infected with fmAd5-GFP and Ad5-GFP vectors at multiplicity of infection (MOI) of 10, 50, 100, 200, 500, and 1000 $TCID_{50}$/cell for 2 hours. Subsequently, the medium was removed, and 0.5 ml of DMEM/Nutrient Mixture F-12 (DMEM/F-12), containing 2% FBS, was added to each well. The transduction efficiency was evaluated by measuring the fluorescence of cells after 48 h of incubation at 37°C, using fluorescent microscopy and flow cytometry.

CAR-binding inhibition assay

The A549 cells were first cultured in a 24-well tissue culture plate at a density of 1×10^5 cells per well. On the following day, fmAd5-GFP, at MOIs of 100 and 400, was combined with 0, 5, 10, and 20 µM of purified SpyCatcherΔ and incubated at 37°C for 2 hours, followed by the addition of SpyCatcherΔ-conjugated virus to each well and incubation for another 2 hours in a cell culture incubator. After the medium removal, 0.5 ml of DMEM, containing 2% FBS, was added to each well. The cells were harvested after 48 h, and the percentage of transduction was measured by flow cytometry.

Nanobody-conjugated virus transduction

The 293/KDR and HUVEC cells were grown at 1.5–2×10^5 cells/well in 24-well plates, and their CARs were blocked by the addition of a purified recombinant Ad5-knob protein to each well at a final concentration of 100 µg/ml. Subsequently, the Ad vectors were incubated with 10 µM of SpyCatcherΔ-nanobody adapter molecule and different ratios of the adapter and fiber (1:1, 1:100, and 1:1000) for 2 hours at 37°C. Afterward, fmAd5-GFP and Ad5-GFP (as the control vector) were added at MOIs of 10, 20, and 50 and to the HUVEC cells at MOIs of 100, 200 and 500 $TCID_{50}$/cell. Following 2 hours of incubation at 37°C, the virus-containing medium was withdrawn and replaced with a

fresh medium, containing 2% FBS. To prevent reinfection, the 293/KDR cells were cultured for 24 h at 37°C, while the HUVEC cells were cultured for 48 h. Flow cytometry was finally carried out to determine the transduction rate and fluorescence intensity.

Results

Generation of fiber-modified Ad vector

A SpyTag-decorated Ad vector, which could covalently bind to the SpyCatcher-fused targeting moiety, was generated, enabling the vector to be retargeted to various ligands, without further genetic modifications of the vector. According to previous studies, considering the crystallographic structure of the Ad fiber, two regions of the knob, that is, the C-terminus and the HI loop, were suitable for incorporating foreign motifs, as they allowed exposure and facilitated viral interaction with the target cell, with unlikely effects on key viral functions (e.g., capsid packaging and viral infection) (Belousova et al., 2002).

For Ad5 retargeting, the SpyTag-coding sequence was inserted into the HI loop of the fiber knob between G543 and D544 residues through HR (Dmitriev et al., 1998). The fmAd5-GFP and Ad5-GFP were rescued and upscaled in AD-293 cells after verifying the presence of SpyTag in the Ad fiber genome by PCR. After viral amplification, the Ad genome was extracted, and the presence of SpyTag sequence was reconfirmed by fiber sequencing (Supplementary Figure S1). To determine whether the insertion of 13-amino-acid peptides affected viral replication and titer, fmAd5-GFP and Ad5-GFP were amplified under similar conditions and titrated using the $TCID_{50}$ assay. Their titers were nearly the same, equivalent to 5×10^{10} $TCID_{50}$/mL.

Expression and purification of recombinant proteins

The original SpyTag-SpyCatcher system consisted of a 13-amino-acid SpyTag and a 138-amino-acid SpyCatcher (Li and Fierer, 2014). In this study, a modified SpyCatcher was used with 21- and 14-residue truncations at the N and C termini, respectively, as full-length SpyCatcher has been identified to interact with an unknown cell surface receptor, leading to significant background transduction (Kasaraneni et al., 2017). However, before assessing the ability of SpyCatcherΔ to bind to fiber-modified Ad containing SpyTag, its potential to bind to free SpyTag was investigated. For this purpose, SpyCatcherΔ and TrxA-SpyTag were recombinantly expressed in *E. coli* Rosetta (DE3) and purified by exploiting their His-tag for Ni-NTA chromatography.

The TrxA-SpyTag and SpyCatcherΔ were highly expressed in *E. coli* Rosetta (DE3), yielding 20 mg/L of purified protein. However, no indication of adapter molecule expression was found in *E. coli* Rosetta (DE3) cells using various pET vectors; accordingly, the pHEN6C expression vector and *E. coli* WK6 cells, which were optimized for nanobody production, were employed. The Ni-NTA chromatography was also used to purify the recombinant adapter molecule. Next, the adapter protein, comprising of the anti-VEGFR2 nanobody-SpyCatcherΔ fusion, was combined with the TrxA-SpyTag peptide to examine whether TrxA-SpyTag could bioconjugate with the adapter molecule. The complex formation was assessed using SDS-PAGE. As demonstrated in Figure 2A, the adapter molecule could form a stable linkage with TrxA-SpyTag.

Subsequently, Western blotting was performed to determine the presence of SpyTag in the fiber structure and its capability to bind to its SpyCatcherΔ pair. As shown in Figure 2B, besides the SpyCatcherΔ band (16 kDa), a band of approximately 77 kDa was observed, suggesting the bonding of Ad-modified fiber (61 kDa) with the SpyCatcherΔ. However, when the control virus, Ad5-GFP, was mixed with the SpyCatcherΔ, this 77-kDa band was absent. The Ad5 knob protein was also produced in *E. coli* Rosetta (DE3), with TrxA and His tags at its N-terminus, allowing for single-step isolation using Ni-NTA chromatography, which indicated a single ~38 kDa band on SDS-PAGE (Figure 2C). Moreover, the functionality of recombinant knob protein was assessed using 293/KDR and AD-293 cell lines. The ability of the protein to block CAR and prevent the internalization of Ad5 is presented in Supplementary Figure S2.

Establishment of the CHO-Spy cell line

The CHO-K1 cell line (CAR-negative cells) was transfected with a pDisplay vector, encoding SpyCatcherΔ and neomycin resistance genes to generate a cell line that allowed for the steady expression of SpyCatcher on its surface. Therefore, it was possible to investigate the fmAd5-GFP binding capacity to SpyCatcher on the cell surface, as well as virus internalization *via* SpyCatcher/SpyTag binding. Following G418 selection, the pool of cell clones was expanded, and flow cytometry was performed to evaluate the SpyCatcherΔ expression on the cell surface. Approximately 13% of CHO-K1 cells expressed SpyCatcherΔ. Next, a clonal selection was carried out, yielding 12 monoclonal cells. The SpyCatcherΔ expression level and cell uniformity were also assessed using flow cytometry. Three out of 12 monoclonal cells, which showed the highest expression levels and homogeneity >96%, were finally isolated. Data for one of the selected clones are depicted in Figure 3.

SpyTag-SpyCatcher-mediated viral vector transduction

The transduction efficiency of CHO-K1 and CHO-Spy cells was examined with fmAd5-GFP and Ad5-GFP to primarily

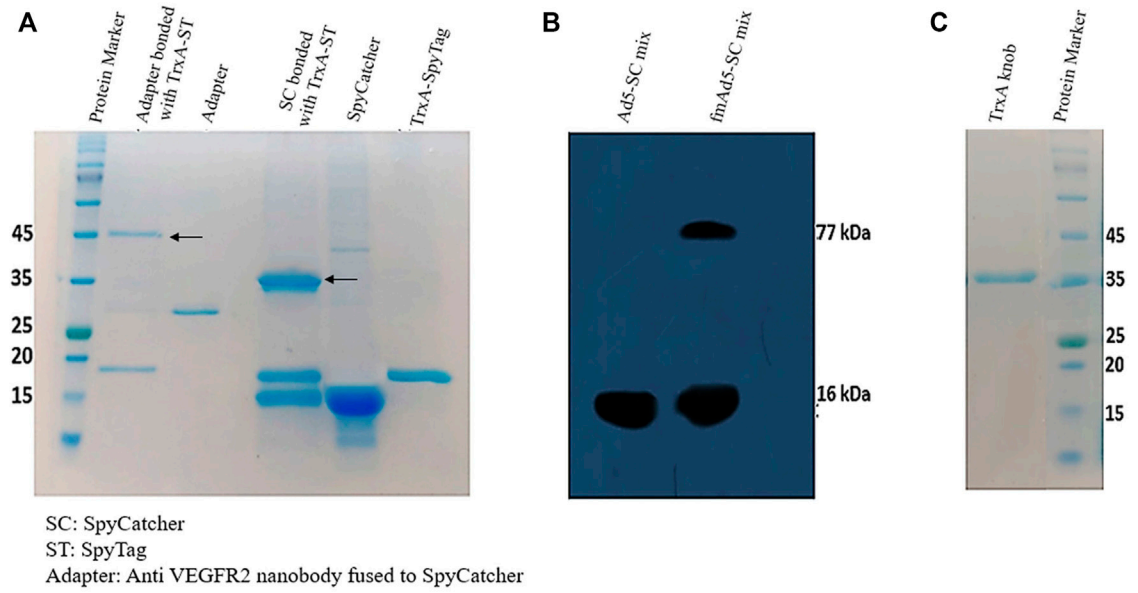

FIGURE 2
Characterization of protein expression and binding. **(A)** The SDS-PAGE analysis of SpyCatcher-TrxA-SpyTag bioconjugation. The purified TrxA-SpyTag was mixed with SpyCatcher and adapter (SpyCatcher-anti VEGFR-2 nanobody) at a molar ratio of 1:1 at room temperature for 1 hour. **(B)** Western blotting analysis to identify Ad-modified fiber bound to the SpyCatcherΔ. The vector (5×10^9 $TCID_{50}$) was incubated for 2 hours at 37°C with 10 μM of purified SpyCatcherΔ before boiling and application on 12% SDS-PAGE gel, followed by blotting to a PVDF membrane; it was finally probed with a polyclonal antibody against the SpyCatcherΔ and goat anti-mouse IgG (HRP). **(C)** The 12% SDS-PAGE analysis of the purification of recombinant knob protein fused to TrxA and His tags.

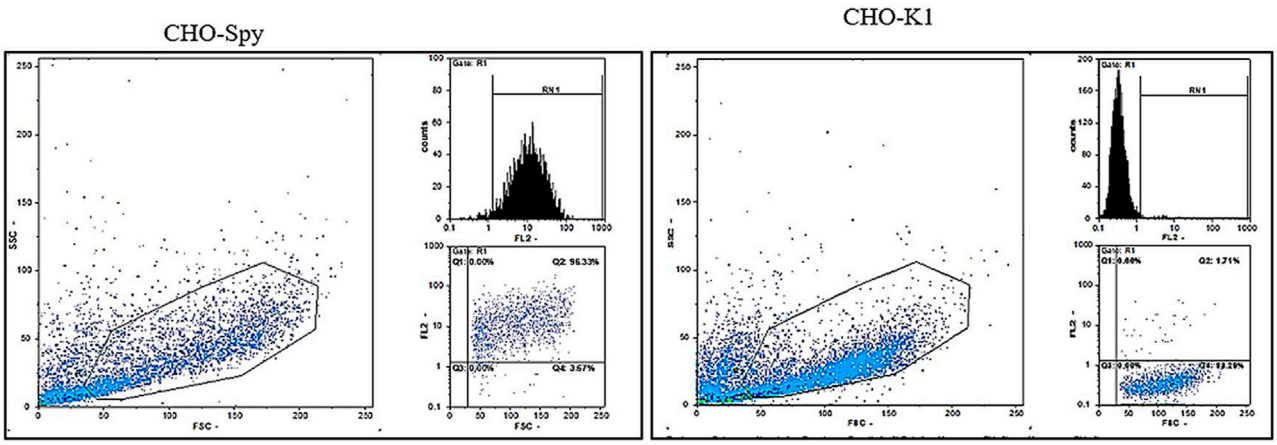

FIGURE 3
The flow cytometric analysis of SpyCatcherΔ expression after CHO-KI transfection. Following the transfection of CHO-KI cells with the pDisplay plasmid encoding SpyCatcherΔ, 12 clones were isolated, and the level of SpyCatcherΔ expression and homogeneity were determined *via* flow cytometry. Monoclonal cells expressing the SpyCatcherΔ, as well as CHO-KI cells as the negative controls, were treated with the anti-SpyCatcher serum for 1 hour, followed by incubation with the goat anti-mouse Ig-PE. Three out of 12 expanded monoclonal cells demonstrated more than 96% homogeneity and high expression levels of SpyCatcherΔ, as depicted for one of the clones on the left panel. The right panel shows the non-transfected CHO-KI cell line as the negative control.

examine the functionality of the SpyTag-harboring viral vector in binding to the cell surface-expressed SpyCatcher. It should be noted that the CHO-K1 cells do not normally express detectable levels of human CAR; consequently, they are normally non-permissive to natural Ads. The CHO-Spy cells that were able to express SpyCatcherΔ on the cell surface were also developed. The

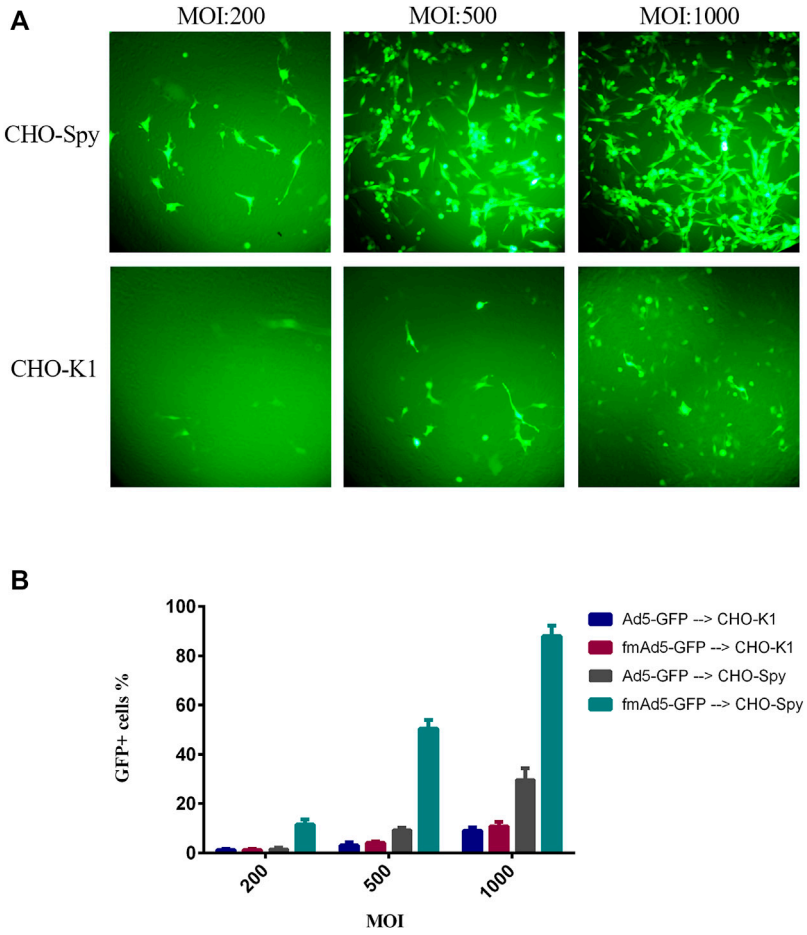

FIGURE 4
Transduction efficiency of CHO-K1 and CHO-Spy cells with fmAd5-GFP and Ad5-GFP. **(A)** The cells were infected with fiber-modified Ad-GFP at MOIs of 200, 500, and 1000 $TCID_{50}$/cell for 48 h, and the fluorescent signal of EGFP was investigated by fluorescent microscopy. **(B)** The percentage of transducted CHO-K1 and CHO-Spy cells with various MOIs of fmAd5-GFP and Ad5-GFP vectors according to flow cytometry; data are presented based on duplicate experiments, and values are presented as mean ± SEM.

transduction efficiency of both cell lines was negligible at MOIs of 10, 50, and 100 for both viral vectors at 48 h post-infection (data not shown), while at higher MOIs (200, 500, and 1000) of fmAd5-GFP and Ad5-GFP, as shown in Figure 4A, there was a significant difference in transduction efficiency between CHO-K1 and CHO-Spy with fmAd5-GFP at all MOIs. The results were confirmed using flow cytometry, which indicated the percentage of EGFP-positive cells and the mean fluorescence intensity after infection with each vector. In case of both viral vectors, CHO-K1 cells showed the lowest percentage of EGFP-positive cells and the lowest overall fluorescence intensity in the transduced cells, as expected (Figure 4B).

On the other hand, when the CHO-Spy cells were infected with the Ad5-GFP control virus, the transduction rate was slightly higher than CHO-K1 cells, but significantly lower than the fmAd5-GFP. It was hypothesized that the slight increase in the Ad5-GFP transduction rate in CHO-Spy cells might be related to the inaccurate measurement of CHO-Spy cells because of their high adhesion capability following the SpyCatcherΔ expression. In the CHO-Spy cells, transduction with fmAd5-GFP at MOI of 1000 resulted in the transduction of nearly 90% of cells *versus* 9% of CHO-K1 cells. Besides, the EGFP fluorescence intensity was twice higher, indicating the efficient transduction of fmAd5-GFP into the CHO-Spy cells through bioconjugation of the Spy-tagged viral vector with cell surface-expressed SpyCatcher. Also, differences of approximately 9–10 folds in transduction (as shown in Figure 4B) and 2-5 folds in fluorescence intensity were identified at other MOIs.

Blockade of CAR-mediated transduction

This study assessed whether SpyCatcher conjugation to fmAd5-GFP resulted in the ablation of CAR-mediated transduction of A549, as a high CAR-expressing cell line.

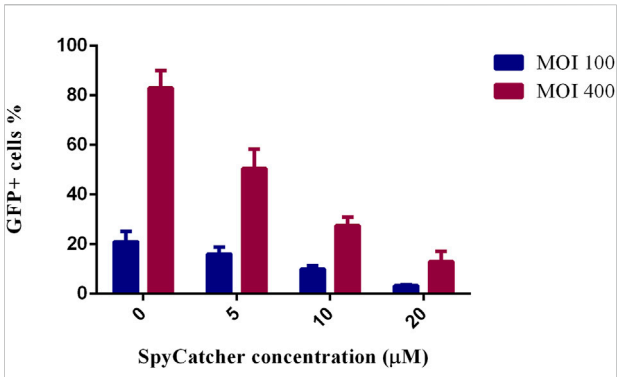

FIGURE 5
Ablation of CAR-mediated transduction of A549 cells. The percentage of GFP⁺ cells is shown after the incubation of fmAd5-GFP at MOIs of 100 and 400 by increasing the concentration of SpyCatcherΔ before infecting the A549 cells. Data are based on duplicate experiments, and values are represented as mean ± SEM.

Accordingly, fmAd5-GFP was incubated at MOIs of 100 and 400 with 0, 5, 10, and 20 μM of SpyCatcherΔ at 37°C for 2 hours before infecting the A549 cells. As shown in Figure 5, the percentage of EGFP-positive cells decreased with an increase in the SpyCatcher protein concentration. When fmAd5-GFP was incubated with 20 μM of SpyCatcher at both MOIs, the number of positive EGFP cells reduced by seven folds relative to the non-SpyCatcher control group; consequently, the SpyCatcherΔ binding to the fmAd5-GFP could effectively reduce the virus entry *via* CARs.

VEGFR2-expressing cell transduction by the retargeted viral vector

To examine the efficacy of Ad vector retargeting, the 293/KDR cell line, expressing a high level of cell-surface VEGFR2, and HUVEC as the primary VEGFR2-expressing cell line, were transduced with fmAd5-GFP, which was previously conjugated with the adapter molecule. When the 293/KDR and HUVEC cells were transduced with the adapter-conjugated fmAd5-GFP and adapter-mixed Ad5-GFP, there was a significant increase in transduction efficiency of both cell lines with the adapter-conjugated fmAd5-GFP. The flow cytometry revealed that the percentage of EGFP⁺ 293/KDR and HUVEC cells in the adapter-conjugated fmAd5-GFP-transducted group was almost three and two folds higher than the control group at all MOIs, respectively (Figure 6A).

Additionally, a serial increase in the adapter-to-fiber ratio from 1:1 to 1:1000 resulted in a progressive rise in the percentage of EGFP⁺ 293/KDR and HUVEC cells infected with adapter-conjugated fmAd5-GFP; conversely, the rate of transduction with adapter-mixed Ad5-GFP was significantly lower and also invariant (Figure 6B). However, in terms of EGFP fluorescence intensity, there was no significant difference between the adapter-conjugated fmAd5-GFP and the control groups. Based on these findings, although Ad5-GFP mixed with an adapter could partially infect VEGFR2-expressing cells, there was a remarkable increase in the transduction efficiency when the adapter-conjugated fmAd5-GFP was used for both VEGFR2-expressing cell lines.

Discussion

The current study aimed to present a bionanoparticle-based adaptable technique for modifying the natural receptor specificity of Ad5 vector, which can be used to retarget Ad5 for theranostic applications. Although Ad5 is the most common viral vector modified for gene therapy, development of a safe and efficient vector remains challenging in the clinical setting. One of the main restrictions in the clinical administration of Ads is the promiscuous native Ad tropism, which limits its systemic administration, as it can induce toxicity through non-specific uptake, while decreasing the vector bioavailability for the target cells (Waehler, et al., 2007). Therefore, detargeting and retargeting are crucial strategies for improving the efficacy of Ad-mediated tumor theranostics. To address this issue, adapters have been introduced; nevertheless, the unstable, non-covalent adapter-vector complex may decrease its efficacy.

In this regard, in a study conducted in 2006, the avidin-biotin system, as one of the strongest non-covalent protein–ligand interactions, was used to redirect Ad5 to dendritic cells. The biotin acceptor peptide (BAP) was genetically incorporated into the fiber protein to generate an Ad-BAP fusion. Because of its high-affinity interaction (10^{-15} M), this system demonstrated high potential for *in vivo* applications, although toxicity was still probable due to the presence of free biotin in the circulation (Maguire et al., 2006). Additionally, in another study, the BAP system was used to compare retargeting of Ad vector through modification of fiber, protein IX, and hexon toward various cell types. In contrast to protein IX and hexon, only fiber modification with high-affinity receptor binding ligands could lead to effective Ad retargeting, most probably due to atypical virus trafficking in case of protein IX and hexon modifications (Campos and Barry, 2006).

In the present study, the bacterial superglue, SpyTag-SpyCatcher, which has been shown to have a median breakage force more than 20 times stronger than the avidin-biotin interaction, was employed (Zakeri et al., 2012; Veggiani et al., 2014). In this system, in contrast to chemical conjugation-based techniques, the SpyTag and SpyCatcher can easily react with one another to form a stable covalent bond under various conditions. The SpyTag can also react at either the N-terminus, C-terminus, or an internal site of protein, making it more flexible than previous split protein-based systems.

In this study, a modified Ad5 vector was generated by inserting the SpyTag peptide into the HI loop of Ad5 fiber knob. The SpyTag on the knob domain acted as an anchoring site for a cell-binding

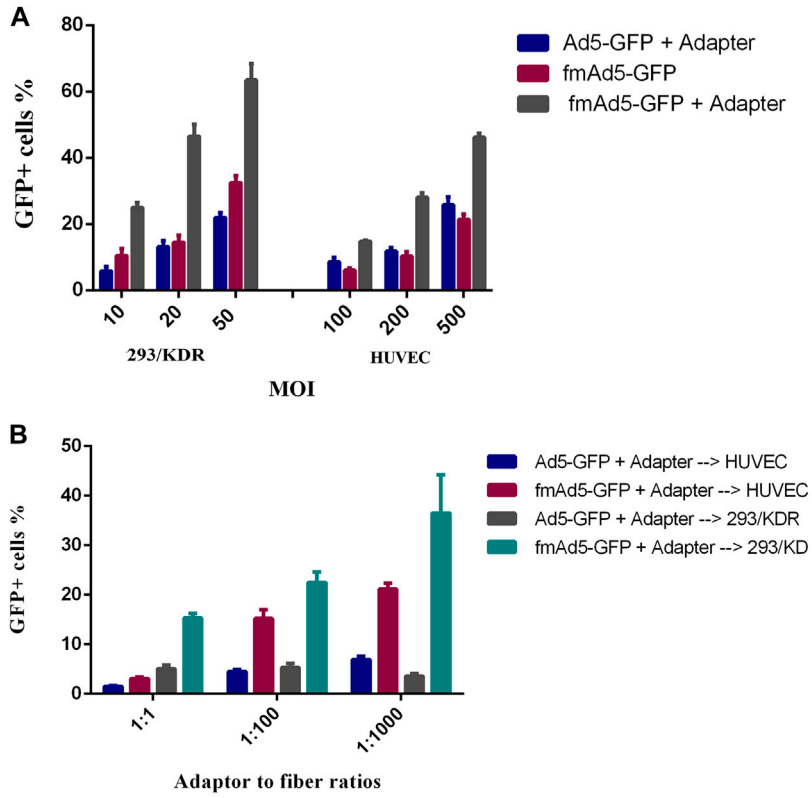

FIGURE 6
Transduction of VEGFR2-expressing cells with the retargeted adenoviral (Ad) vector. **(A)** Comparison of the transduction efficiency of adapter-mixed Ad5-GFP with adapter-conjugated fmAd5-GFP. After blocking CAR with the recombinant knob protein, the 293/KDR and HUVEC cells were transduced with different MOIs of adapter-treated Ad5-GFP or fmAd5-GFP. **(B)** After incubating the 293/KDR and HUVEC cells with the knob protein, the cells were infected with Ad vectors that were previously incubated with the adapter at various adapter-to-fiber ratios and MOIs of 20 and 200, respectively. Data are presented based on duplicate experiments, and values are presented as mean ± SEM.

protein (CBP) linked with the SpyCatcher. According to previous studies, any change in the knob can lead to fiber instability; therefore, the structure of the Ad5 fiber knob protein poses a limitation for fiber-modified Ad vector development (Dmitriev et al., 1998). However, considering the rescue of fiber-modified Ad5 containing SpyTag with an infectious unit similar to the control virus with an intact fiber, the insertion of SpyTag into the fiber knob did not affect virus packaging or propagation in our system.

To evaluate the functionality of fmAd5-GFP as a fiber-modified SpyTag-containing Ad5, the CHO-Spy cells with SpyCatcherΔ on their surface were treated with the modified virus. Following SDS-PAGE and Western blotting analysis, which confirmed the ligation ability of fmAd5-GFP with the SpyCatcher (Figure 2B), a comparison of the transduction rate of CHO-Spy *versus* CHO-K1 cells revealed that fmAd5-GFP could bind to CHO-Spy cells and transduce them almost 9–10 times more than CHO-K1 (Figure 4B). Additionally, a 2-5fold increase in the fluorescence intensity of CHO-Spy cells transducted with fmAd5-GFP (relative to CHO-K1) confirmed the efficient binding of SpyCatcher on the CHO-Spy surface with SpyTag on the modified virus (Figure 4A).

The fmAd5-GFP detargeting was examined by application of SpyCatcher-ligated modified virus on A549 as a high CAR-expressing cell line. The significant inhibition of CAR-mediated viral transduction (Figure 5) approves a hypothesis which proposes that Ad5 is remarkably less capable of transducing cells through CARs after binding with an adapter molecule, conjugated to the SpyCatcher (Waehler, et al., 2007). This observation is also comparable to the findings of a study by Dreier et al. (2013) which showed that binding of 1D3nc SHP1 (trimeric DARPins grabbing the knob from three sides) to the knob blocked all CAR-binding sites and completely impaired gene transfer into HEK-293 cells. Nevertheless, due to the uncertainty of SpyCatcher attachment to all three monomers of the knob, the degree of CAR-binding ablation was lower than the trimeric DARPin (1D3nc SHP), which could bind more firmly to all three knob monomers. Generally, non-specific transduction, particularly in hepatocytes, significantly decreased by preventing CAR binding in the modified SpyCatcher-ligated virus.

To retarget fmAd5-GFP, SpyCatcher fused to a nanobody against VEGFR2 was used in the current study. VEGFR2 has

been widely targeted for the anti-angiogenic treatment of tumors, as well as diagnosis of various cancers, such as breast and gastric cancers (Masuda et al., 2012; Lian et al., 2019; Masłowska et al., 2021). Currently, camelid nanobody-based therapeutics are being evaluated in clinical trials against various diseases, including cancers. Immunogenicity is one of the main challenges in the application of antibodies, especially when repeated injections are required. Overall, nanobodies exhibit low immunogenicity owing to their high degree of homology with the human VH domain, which can strongly mitigate the potential negative consequences (Jovčevska and Muyldermans, 2020).

Additionally, the single-domain characteristic of nanobodies facilitates their genetic manipulation, allowing for the construction of multivalent nanobodies or their fusion with other proteins. Besides, due to the production of nanobodies using low-cost expression systems, such as *E. coli,* they are appealing tools for a wide range of applications (De Vlieger et al., 2018). Therefore, in this study, we decorated fmAd5-GFP with a SpyCatcher-fused nanobody specific to VEGFR2 as a model CBP in an adapter structure. There was a significant difference in the transduction rate when a high adapter concentration or adapter-to-fiber ratio was used (Figure 6), which is consistent with earlier studies (Dreier et al., 2011). Previously, it was reported that chelating the trimeric knob by bivalent or trivalent adapters could improve the Ad retargeting specificity and efficacy at lower adapter concentrations or adapter-to-fiber ratios (Dreier et al., 2011). Accordingly, in future studies, a triple SpyCatcher adapter can be created using a trimerization motif to achieve optimal retargeting and detargeting at lower adapter concentrations or adapter-to-fiber ratios.

In conclusion, in the present study, using the SpyTag-SpyCatcher protein ligation chemistry, a readily modifiable Ad-based bionanoparticle was developed *in vitro* for retargeting, without any need for genetic manipulation of the viral vector. The results revealed that the insertion of SpyTag peptide into the HI loop of the Ad5 fiber knob did not impair the viral production process; it also did not impair the SpyTag-incorporated knob availability to bind to the adapter molecule. The modified Ad vector was significantly detargeted from its natural CAR and retargeted to VEGFR2. Although VEGFR2 was targeted as a CBP model, this viral vector could be easily modified by covalent binding to target other ligands for various theranostic applications, while significantly mitigating the side effects of systemic Ad administration, including hepatotoxicity.

Data availability statement

The original contributions presented in the study are included in the article/Supplementary Materials, and further inquiries can be directed to the corresponding authors.

Author contributions

The authors confirm contribution to the paper as follows: Study conception and design: AA, KA, NM, MK, and KB; carrying out the experiments: MK; advising the project and providing some critical materials: KB, MB; data collection: MK, AA, and KA; analysis and interpretation of results: MK, AA, KA, and NM; draft manuscript preparation: MK, BK, AA, KA, and NM. All authors reviewed the results and approved the final version of the manuscript.

Funding

This work was conducted as a Ph.D. student project and was financially supported by the Institute Pasteur of Iran (Grant No. BP_9584) and also by the Hum-Immune Biotech company.

Acknowledgments

We would like to express our gratitude to the employees of the Department of Molecular Virology of Pasteur Institute of Iran and also Younes Hoseini for his valuable advice.

Conflict of interest

The authors declare that the research was conducted in the absence of any commercial or financial relationships that could be construed as a potential conflict of interest.

Publisher's note

Supplementary material

The Supplementary Material for this article can be found online at: https://www.frontiersin.org/articles/10.3389/fmolb.2022.1039324/full#supplementary-material

References

Ahani, R., Roohvand, F., Cohan, R. A., Etemadzadeh, M. H., Mohajel, N., Behdani, M., et al. (2016). Sindbis virus-pseudotyped lentiviral vectors carrying VEGFR2-specific nanobody for potential transductional targeting of tumor vasculature. *Mol. Biotechnol.* 58 (11), 738–747. doi:10.1007/s12033-016-9973-7

Arvizo, R., Bhattacharya, R., and Mukherjee, P. (2010). Gold nanoparticles: Opportunities and challenges in nanomedicine. *Expert Opin. Drug Deliv.* 7 (6), 753–763. doi:10.1517/17425241003777010

Belousova, N., Krendelchtchikova, V., Curiel, D. T., and Krasnykh, V. (2002). Modulation of adenovirus vector tropism via incorporation of polypeptide ligands into the fiber protein. *J. Virol.* 76 (17), 8621–8631. doi:10.1128/jvi.76.17.8621-8631.2002

Brune, K. D., Leneghan, D. B., Brian, I. J., Ishizuka, A. S., Bachmann, M. F., Draper, S. J., et al. (2016). Plug-and-Display: Decoration of virus-like particles via isopeptide bonds for modular immunization. *Sci. Rep.* 6 (1), 19234–19313. doi:10.1038/srep19234

Butt, M. H., Zaman, M., Ahmad, A., Khan, R., Mallhi, T. H., Hasan, M. M., et al. (2022). Appraisal for the potential of viral and nonviral vectors in gene therapy: A review. *Genes* 13 (8), 1370. doi:10.3390/genes13081370

Campos, S. K., and Barry, M. A. (2006). Comparison of adenovirus fiber, protein IX, and hexon capsomeres as scaffolds for vector purification and cell targeting. *Virology* 349 (2), 453–462. doi:10.1016/j.virol.2006.01.032

Chung, Y. H., Cai, H., and Steinmetz, N. F. (2020). Viral nanoparticles for drug delivery, imaging, immunotherapy, and theranostic applications. *Adv. Drug Deliv. Rev.* 156, 214–235. doi:10.1016/j.addr.2020.06.024

De Vlieger, D., Ballegeer, M., Rossey, I., Schepens, B., and Saelens, X. (2018). Single-domain antibodies and their formatting to combat viral infections. *Antibodies* 8 (1), 1. doi:10.3390/antib8010001

Dmitriev, I., KashEntsEva, E., Rogers, B. E., Krasnykh, V., and Curiel, D. T. (2000). Ectodomain of coxsackievirus and adenovirus receptor genetically fused to epidermal growth factor mediates adenovirus targeting to epidermal growth factor receptor-positive cells. *J. Virol.* 74 (15), 6875–6884. doi:10.1128/jvi.74.15.6875-6884.2000

Dmitriev, I., Krasnykh, V., Miller, C. R., WangM. KashEntsEva, E., Mikheeva, G., et al. (1998). An adenovirus vector with genetically modified fibers demonstrates expanded tropism via utilization of a coxsackievirus and adenovirus receptor-independent cell entry mechanism. *J. Virol.* 72 (12), 9706–9713. doi:10.1128/JVI.72.12.9706-9713.1998

Dovala, D., Sawyer, W. S., Rath, C. M., and Metzger, L. E. (2016). Rapid analysis of protein expression and solubility with the SpyTag–SpyCatcher system. *Protein Expr. Purif.* 117, 44–51. doi:10.1016/j.pep.2015.09.021

Dreier, B., Honegger, A., Hess, C., Nagy-Davidescu, G., Mittl, P. R. E., Grutter, M. G., et al. (2013). Development of a generic adenovirus delivery system based on structure-guided design of bispecific trimeric DARPin adapters. *Proc. Natl. Acad. Sci. U. S. A.* 110 (10), E869–E877. doi:10.1073/pnas.1213653110

Dreier, B., Mikheeva, G., Belousova, N., Parizek, P., Boczek, E., Jelesarov, I., et al. (2011). Her2-specific multivalent adapters confer designed tropism to adenovirus for gene targeting. *J. Mol. Biol.* 405 (2), 410–426. doi:10.1016/j.jmb.2010.10.040

Ginn, S. L., Amaya, A. K., Alexander, I. E., Edelstein, M., and Abedi, M. R. (2018). Gene therapy clinical trials worldwide to 2017: An update. *J. Gene Med.* 20 (5), e3015. doi:10.1002/jgm.3015

Hajeri, P. B., Sharma, N. S., and Yamamoto, M. (2020). Oncolytic adenoviruses: Strategies for improved targeting and specificity. *Cancers* 12 (6), 1504. doi:10.3390/cancers12061504

Herrmann, H., and Bucksch, H. (2014) Application(S) Manual, *Dictionary geotechnical engineering/wörterbuch GeoTechnik*, Springer, Berlin, Germany, doi:10.1007/978-3-642-41714-6_12296

Jovčevska, I., and Muyldermans, S. (2020). The therapeutic potential of nanobodies. *BioDrugs.* 34 (1), 11–26. doi:10.1007/s40259-019-00392-z

Kasaraneni, N., Chamoun-Emanuelli, A. M., Wright, G., and Chen, Z. (2017). Retargeting lentiviruses via spyCatcher-spyTag chemistry for gene delivery into specific cell types. *MBio* 8 (6), 018600–e1917. doi:10.1128/mBio.01860-17

Krasnykh, V. N., Douglas, J. T., and Van Beusechem, V. W. (2000). Genetic targeting of adenoviral vectors. *Mol. Ther.* 1 (5), 391–405. doi:10.1006/mthe.2000.0062

Li, L., Fierer, J. O., Rapoport, T. A., and Howarth, M. (2014). Structural analysis and optimization of the covalent association between SpyCatcher and a peptide tag. *J. Mol. Biol.* 426 (2), 309–317. doi:10.1016/j.jmb.2013.10.021

Lian, L., Li, X. L., Xu, M. D., Li, X. M., Wu, M. Y., Zhang, Y., et al. (2019). VEGFR2 promotes tumorigenesis and metastasis in a pro-angiogenic-independent way in gastric cancer. *BMC cancer* 19 (1), 183–215. doi:10.1186/s12885-019-5322-0

Madaan, K., Kumar, S., Poonia, N., Lather, V., and Pandita, D. (2014). Dendrimers in drug delivery and targeting: Drug-dendrimer interactions and toxicity issues. *J. Pharm. Bioallied Sci.* 6 (3), 139–150. doi:10.4103/0975-7406.130965

Magnusson, M. K., Hong, S. S., Henning, P., Boulanger, P., and Lindholm, L. (2002). Genetic retargeting of adenovirus vectors: Functionality of targeting ligands and their influence on virus viability. *J. Gene Med.* 4 (4), 356–370. doi:10.1002/jgm.285

Maguire, C. A., Sapinoro, R., Girgis, N., Rodriguez-Colon, S. M., Ramirez, S. H., Williams, J., et al. (2006). Recombinant adenovirus type 5 vectors that target DC-SIGN, ChemR23 and alpha(v)beta3 integrin efficiently transduce human dendritic cells and enhance presentation of vectored antigens. *Vaccine* 24 (5), 671–682. doi:10.1016/j.vaccine.2005.08.038

Masłowska, K., Halik, P. K., Tymecka, D., Misicka, A., and Gniazdowska, E. (2021). The Role of VEGF receptors as molecular target in nuclear medicine for cancer diagnosis and combination therapy. *Cancers* 13 (5), 1072. doi:10.3390/cancers13051072

Masuda, H., Zhang, D., Bartholomeusz, C., Doihara, H., Hortobagyi, G. N., and Ueno, N. T. (2012). Role of epidermal growth factor receptor in breast cancer. *Breast Cancer Res. Treat.* 136 (2), 331–345. doi:10.1007/s10549-012-2289-9

Mortensen, R., Chestnut, J. D., Hoeffler, J. P., and Kingston, R. E. (1997). Selection of transfected mammalian cells. *Curr. Protoc. Neurosci.* 4 (1), Unit 4.6–6. doi:10.1002/0471142301.ns0406s00

Muthu, M. S., Leong, D. T., Mei, L., and Feng, S. S. (2014). Nanotheranostics - application and further development of nanomedicine strategies for advanced theranostics. *Theranostics* 4 (6), 660–677. doi:10.7150/thno.8698

Noureddini, S. C., and Curiel, D. T. (2005). Genetic targeting strategies for adenovirus. *Mol. Pharm.* 2 (5), 341–347. doi:10.1021/mp050045c

Oke, M., Carter, L. G., Johnson, K. A., Liu, H., McMahon, S. A., Yan, X., et al. (2010). The scottish structural proteomics facility: Targets, methods and outputs. *J. Struct. Funct. Genomics* 11 (2), 167–180. doi:10.1007/s10969-010-9090-y

Okegawa, T., Pong, R. C., Li, Y., Bergelson, J. M., Sagalowsky, A. I., and Hsieh, J. T. (2001). The mechanism of the growth-inhibitory effect of coxsackie and adenovirus receptor (CAR) on human bladder cancer: A functional analysis of car protein structure. *Cancer Res.* 61 (17), 6592–6600.

Pereboev, A. V., Nagle, J. M., Shakhmatov, M. A., Triozzi, P. L., Matthews, Q. L., Kawakami, Y., et al. (2004). Enhanced gene transfer to mouse dendritic cells using adenoviral vectors coated with a novel adapter molecule. *Mol. Ther.* 9 (5), 712–720. doi:10.1016/j.ymthe.2004.02.006

Riley, M. K., and Vermerris, W. (2017). Recent advances in nanomaterials for gene delivery—A review. *Nanomaterials* 7 (5), 94. doi:10.3390/nano7050094

Rouet, R., Lowe, D., Dudgeon, K., Roome, B., Schofield, P., Langley, D., et al. (2012). Expression of high-affinity human antibody fragments in bacteria. *Nat. Protoc.* 7 (2), 364–373. doi:10.1038/nprot.2011.448

Schoene, C., Fierer, J. O., Bennett, S. P., and Howarth, M. (2014). SpyTag/SpyCatcher cyclization confers resilience to boiling on a mesophilic enzyme. *Angew. Chem. Int. Ed. Engl.* 126 (24), 6101–6104. doi:10.1002/anie.201402519

Singh, S., Kumar, R., and Agrawal, B. (2019). Adenoviral vector-based vaccines and gene therapies: Current status and future prospects. *Adenoviruses* 53–91. doi:10.5772/intechopen.79697

Somiya, M., Liu, Q., and Kuroda, S. (2017). Current progress of virus-mimicking nanocarriers for drug delivery. *Nanotheranostics* 1 (4), 415–429. doi:10.7150/ntno.21723

Sun, F., Zhang, W. B., Mahdavi, A., Arnold, F. H., and Tirrell, D. A. (2014). Synthesis of bioactive protein hydrogels by genetically encoded SpyTag-SpyCatcher chemistry. *Proc. Natl. Acad. Sci. U. S. A.* 111 (31), 11269–11274. doi:10.1073/pnas.1401291111

Tao, N., Gao, G. P., ParrM., Johnston, J., BaradeT, T., Wilson, J. M., et al. (2001). Sequestration of adenoviral vector by Kupffer cells leads to a nonlinear dose response of transduction in liver. *Mol. Ther.* 3 (1), 28–35. doi:10.1006/mthe.2000.0227

Tomko, R. P., Xu, R., and Philipson, L. (1997). HCAR and MCAR: The human and mouse cellular receptors for subgroup C adenoviruses and group B coxsackieviruses. *Proc. Natl. Acad. Sci. U. S. A.* 94 (7), 3352–3356. doi:10.1073/pnas.94.7.3352

Veggiani, G., Zakeri, B., and Howarth, M. (2014). Superglue from bacteria: Unbreakable bridges for protein nanotechnology. *Trends Biotechnol.* 32 (10), 506–512. doi:10.1016/j.tibtech.2014.08.001

Waehler, R., Russell, S. J., and Curiel, D. T. (2007). Engineering targeted viral vectors for gene therapy. *Nat. Rev. Genet.* 8 (8), 573–587. doi:10.1038/nrg2141

Wickham, T. J., Mathias, P., Cheresh, D. A., and Nemerow, G. R. (1993). Integrins αvβ3 and αvβ5 promote adenovirus internalization but not virus attachment. *Cell* 73 (2), 309–319. doi:10.1016/0092-8674(93)90231-e

Wu, H., and Curiel, D. T. (2008). "Fiber-modified adenoviruses for targeted gene therapy," in *Gene therapy protocols* (Berlin, Germany: Springer), 113–132.

Yang, J., Zhao, Y., Liu, T., Chen, Y., and Yu, S. (2006). High-level expression, one-step purification of soluble Ad5-knob protein and its activity assay. *Cancer biother. Radiopharm.* 21 (3), 269–275. doi:10.1089/cbr.2006.21.269

Zakeri, B., Fierer, J. O., Celik, E., Chittock, E. C., Schwarz-Linek, U., Moy, V. T., et al. (2012). Peptide tag forming a rapid covalent bond to a protein, through engineering a bacterial adhesin. *Proc. Natl. Acad. Sci. U. S. A.* 109 (12), E690–E697. doi:10.1073/pnas.1115485109

Zhang, Y., and Bergelson, J. M. (2005). Adenovirus receptors. *J. Virol.* 79 (19), 12125–12131. doi:10.1128/JVI.79.19.12125-12131.2005

Zhao, M.-X., and Zhu, B.-J. (2016). The research and applications of quantum dots as nano-carriers for targeted drug delivery and cancer therapy. *Nanoscale Res. Lett.* 11 (1), 207–209. doi:10.1186/s11671-016-1394-9

frontiers | Frontiers in Immunology

TYPE Review
PUBLISHED 25 January 2023
DOI 10.3389/fimmu.2023.1012841

OPEN ACCESS

EDITED BY
Jose A. Garcia-Sanz,
(CSIC), Spain

REVIEWED BY
Hidde Ploegh,
Boston Children's Hospital and Harvard Medical School, United States
Paul Van Bergen En Henegouwen,
Utrecht University, Netherlands

*CORRESPONDENCE
Zahra Sharifzadeh
zsharifzadeh@gmail.com

†These authors have contributed equally to this work and share first authorship

SPECIALTY SECTION
This article was submitted to Cancer Immunity and Immunotherapy, a section of the journal Frontiers in Immunology

RECEIVED 06 August 2022
ACCEPTED 09 January 2023
PUBLISHED 25 January 2023

CITATION
Maali A, Gholizadeh M, Feghhi-Najafabadi S, Noei A, Seyed-Motahari SS, Mansoori S and Sharifzadeh Z (2023) Nanobodies in cell-mediated immunotherapy: On the road to fight cancer.
Front. Immunol. 14:1012841.
doi: 10.3389/fimmu.2023.1012841

Nanobodies in cell-mediated immunotherapy: On the road to fight cancer

Amirhosein Maali[1,2†], Monireh Gholizadeh[1,3†], Saba Feghhi-Najafabadi[1†], Ahmad Noei[1], Seyedeh Sheila Seyed-Motahari[1,4], Shafieeh Mansoori[1] and Zahra Sharifzadeh[1*]

[1]Department of Immunology, Pasteur Institute of Iran, Tehran, Iran, [2]Department of Medical Biotechnology, Faculty of Allied Medicine, Qazvin University of Medical Sciences, Qazvin, Iran, [3]Department of Medical Biotechnology, Faculty of Advanced Medical Sciences, Tabriz University of Medical Sciences, Tabriz, Iran, [4]Department of Biology, Science and Research Branch, Islamic Azad University, Tehran, Iran

The immune system is essential in recognizing and eliminating tumor cells. The unique characteristics of the tumor microenvironment (TME), such as heterogeneity, reduced blood flow, hypoxia, and acidity, can reduce the efficacy of cell-mediated immunity. The primary goal of cancer immunotherapy is to modify the immune cells or the TME to enable the immune system to eliminate malignancies successfully. Nanobodies, known as single-domain antibodies, are light chain-free antibody fragments produced from Camelidae antibodies. The unique properties of nanobodies, including high stability, reduced immunogenicity, enhanced infiltration into the TME of solid tumors and facile genetic engineering have led to their promising application in cell-mediated immunotherapy. They can promote the cancer therapy either directly by bridging between tumor cells and immune cells and by targeting cancer cells using immune cell-bound nanobodies or indirectly by blocking the inhibitory ligands/receptors. The T-cell activation can be engaged through anti-CD3 and anti-4-1BB nanobodies in the bispecific (bispecific T-cell engagers (BiTEs)) and trispecific (trispecific T-cell engager (TriTEs)) manners. Also, nanobodies can be used as natural killer (NK) cell engagers (BiKEs, TriKEs, and TetraKEs) to create an immune synapse between the tumor and NK cells. Nanobodies can redirect immune cells to attack tumor cells through a chimeric antigen receptor (CAR) incorporating a nanobody against the target antigen. Various cancer antigens have been targeted by nanobody-based CAR-T and CAR-NK cells for treating both hematological and solid malignancies. They can also cause the continuation of immune surveillance against tumor cells by stopping inappropriate inhibition of immune checkpoints. Other roles of nanobodies in cell-mediated cancer immunotherapy include reprogramming macrophages to reduce metastasis and angiogenesis, as well as preventing the severe side effects occurring in cell-mediated immunotherapy. Here, we highlight the critical functions of various immune cells, including T cells, NK cells, and macrophages in the TME, and discuss newly developed immunotherapy methods based on the targeted manipulation of immune cells and TME with nanobodies.

KEYWORDS

nanobodies, single domain antibodies, cancer immunotherapy, immune cell therapy, CAR, BiTE, BiKE, immune checkpoint

1 Introduction

For the past 20 years, cancer incidence and mortality have been increasing, making it the leading cause of death worldwide and a huge public health concern (1). Surgery, radiation, and chemotherapy, the standard cancer treatments, have a hard time eliminating cancer cells. Cell therapy, targeted therapy, and gene therapy are other cancer treatment options (2, 3). The introduction of autologous or allogeneic cellular material into a patient for therapeutic reasons is called cell therapy. The cell-based immunotherapy harness the potential of immune cells to selectively kill cancer cells (4).

In cancer immunotherapy, the host immune system is essential in the recognition and targeting of tumor cells. The unique characteristics of the tumor microenvironment (TME), such as heterogeneity, reduced blood flow, hypoxia, and acidity, can all affect how responsive the tumor cells are to treatment (5). Although the TME's makeup varies depending on the type of tumor, common components include immune cells, stromal cells, blood vessels, and extracellular matrix. The TME is not merely a silent spectator but rather an active supporter of cancer growth (6). The cancer-associated fibroblasts, mesenchymal stem cells, and cancer-associated adipocytes are the main stromal cells in the TME. They contribute to cancer angiogenesis, invasion, and metastasis mainly through the secretion of several growth factors (such as TGF-β, EGF, and VEGF, matrix metalloproteinases, and some cytokines (such as TNF-α, IL-1, and IL-6) (7). The primary goal of immunotherapy is to modify the immune cells or the TME to enable the immune system to eliminate malignancies successfully.

Monoclonal antibodies (mAbs) can bind to the activatory or inhibitory receptors expressed on immune cells and trigger changes in them that lead to the activation of the immune cells. Moreover, mAbs against tumor antigens are used to redirect the specificity of immune cells toward the malignant cells. Due to their low tumor penetrability, high manufacturing costs, and potential for developing treatment resistance, mAbs still have substantial limitations (8). Nanobodies, known as single-domain antibodies, are light chain-free antibody fragments produced from Camelidae antibodies that can be good substitutes for mAbs (9). They can promote immune cell-mediated immunotherapy either directly by bridging between tumor cells and immune cells and by targeting cancer cells using immune cell-bound nanobodies or indirectly by blocking the inhibitory ligands/receptors (Figure 1). Here, we highlight the critical functions of various immune cells, including T cells, NK cells, and macrophages, in the TME and discuss newly developed immunotherapy methods based on the targeted manipulation of immune cells and TME with nanobodies.

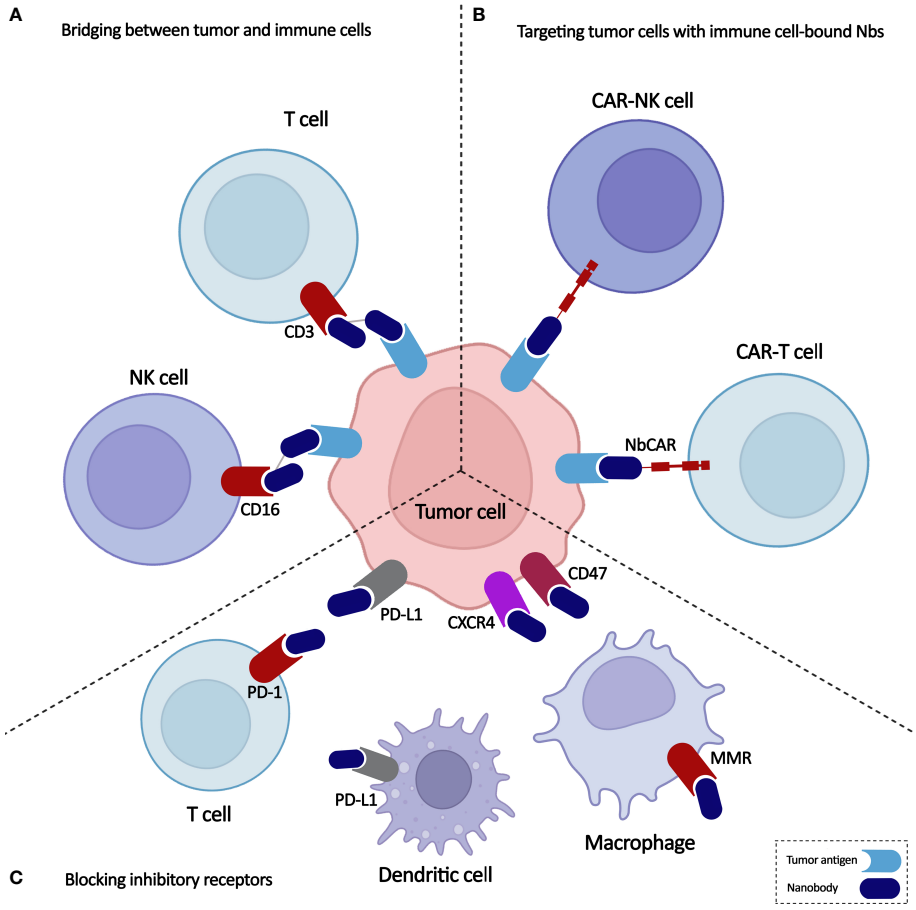

FIGURE 1
Overview on application of nanobodies in cell-based immunotherapy. Nanobodies participate in anti-cancer immune cell-mediated therapies through **(A)** bridging between tumor and immune cells, **(B)** targeting tumor cells with immune cell-bound nanobodies, and **(C)** blocking inhibitory receptors.

2 Nanobodies: The smaller variant of antibodies

It has been more than three decades since the first therapeutic antibodies, which consisted of murine-derived mAbs, were approved by the U.S. Food and Drug Administration (FDA). The major disadvantages of mAbs include their immunogenicity (especially murine-derived ones) and large size. Alternatively, antibody fragments such as the antigen-binding fragment (Fab) and single-chain variable fragment (scFv) could be used in different applications (Figure 2). However, the short serum half-life of these fragments and their aggregation-induced immunogenicity limit their utility as both diagnostic reagents and therapeutics (8). Actually, the hydrophobic interaction of VH and VL domains limits the stability and solubility of engineered antibodies and usually leads to aggregation or mispairing of variable domains. These features show that new antibody formats are needed with the same binding specificity of antibodies but with better stability and *in vivo* characteristics (10).

Single-domain antibodies (sdAbs), also known as nanobodies or VHHs (Variable domain of Heavy chain from Heavy-chain only antibodies (HCAbs)), are derived from camelid heavy-chain antibodies. Nanobodies, as the smallest natural antigen binding domains, have dimensions in the nanometer range (~2.5 nm in diameter and ~4 nm in height) and a molecular weight of about 15 kD (8). The high-affinity nanobodies against different targets, including tumor markers, could be selected from the phage-displayed libraries through the biopanning process. They are highly soluble and do not tend to associate with other hydrophobic protein surfaces. Nanobodies have a high degree of sequence identity with human type 3 VH domains (VH3) germline sequences (11, 12), a unique property that is considered to contribute to their low immunogenicity. This reduced immunogenicity allows the prolonged and repeated administration of nanobodies in patients (13).

They can be produced easily in microorganisms, mammalian cells, or plants. Nanobody expression yield is high, whether in the periplasm of *Escherichia coli* or the cytoplasm of eukaryotic cells (14).

Thanks to their small size, intravenously administered nanobodies can rapidly extravasate from the blood circulation and deliver reagents to the target location. Moreover, their monomeric single-domain nature facilitates their genetic fusion to additional proteins, reporter molecules, or proteinaceous drugs (14, 15). Although the passage of antibodies and their derivatives through the blood-brain barrier (BBB) is a major challenge for treating brain diseases (16, 17), the small size of nanobodies may increase their chance of crossing the BBB either naturally or as a result of cancer-induced BBB leakage (18, 19). However, some nanobodies have limited BBB permeability which may be improved by different delivery methods (20), such as adeno-associated virus (AAV)-based delivery (16) and carrier-mediated transport (21).

Nanobodies have been used in different applications, including biosensing, affinity-capturing of proteins, and protein crystallization. They have been especially used for cancer therapeutics by targeting surface receptors of tumor cells such as HER2 (22), CAIX (23), TAG-72 (24), DR5 (25), c-Met (26), EGFR (27), mesothelin (28), AgSK1 (29) and CD33 (30). The main mechanisms of action of these nanobodies include suppression of downstream growth signaling and promotion of apoptosis in cancer cells (31, 32). Moreover, soluble ligands secreted by tumor cells have been targeted by specific nanobodies (9). Nanobody-based targeting of tumor ligands, including EGF (33), HGF (34), and VEGF (35), has resulted in efficient inhibition of tumor growth and metastasis.

Now, about 16 therapeutic nanobodies have entered clinical trials for various disease types (36). In 2019, Caplacizumab, a bivalent nanobody targeting von Willebrand, received approval from the FDA for the treatment of patients with thrombotic thrombocytopenic purpura (37).

3 Nanobody-based T-cell immunotherapy

T cells are critical components of the immune system that can be activated against cancer cells to have a functional response. The immunosuppressive cells in the TME, as well as the expression of inhibitory receptors, render T cells dysfunctional in cancer (38). Moreover, the decrease in the immunogenicity of the tumor cells, through the reduced expression of immunogenic cancer antigens or the paucity of major histocompatibility complex (MHC) class I molecules, causes the cancer cells to escape from the T cells (39). Antibodies and nanobodies could be used to activate T cells and retarget them against cancer cells (Figure 3).

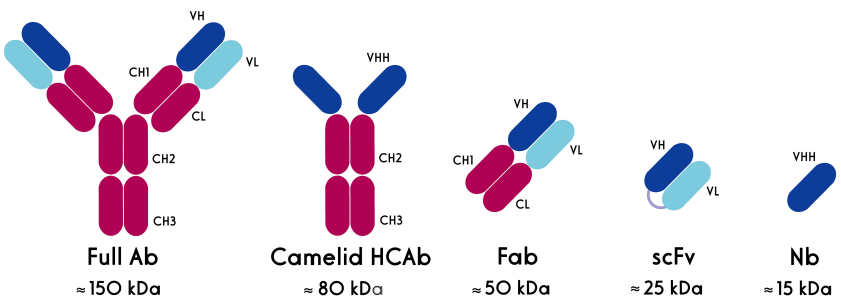

FIGURE 2
Schematic structures of conventional and heavy chain antibodies and their derivatives. HCAb: heavy chain antibody, Fab: antigen-binding fragment, scFv: single chain variable fragment, Nb, nanobody.

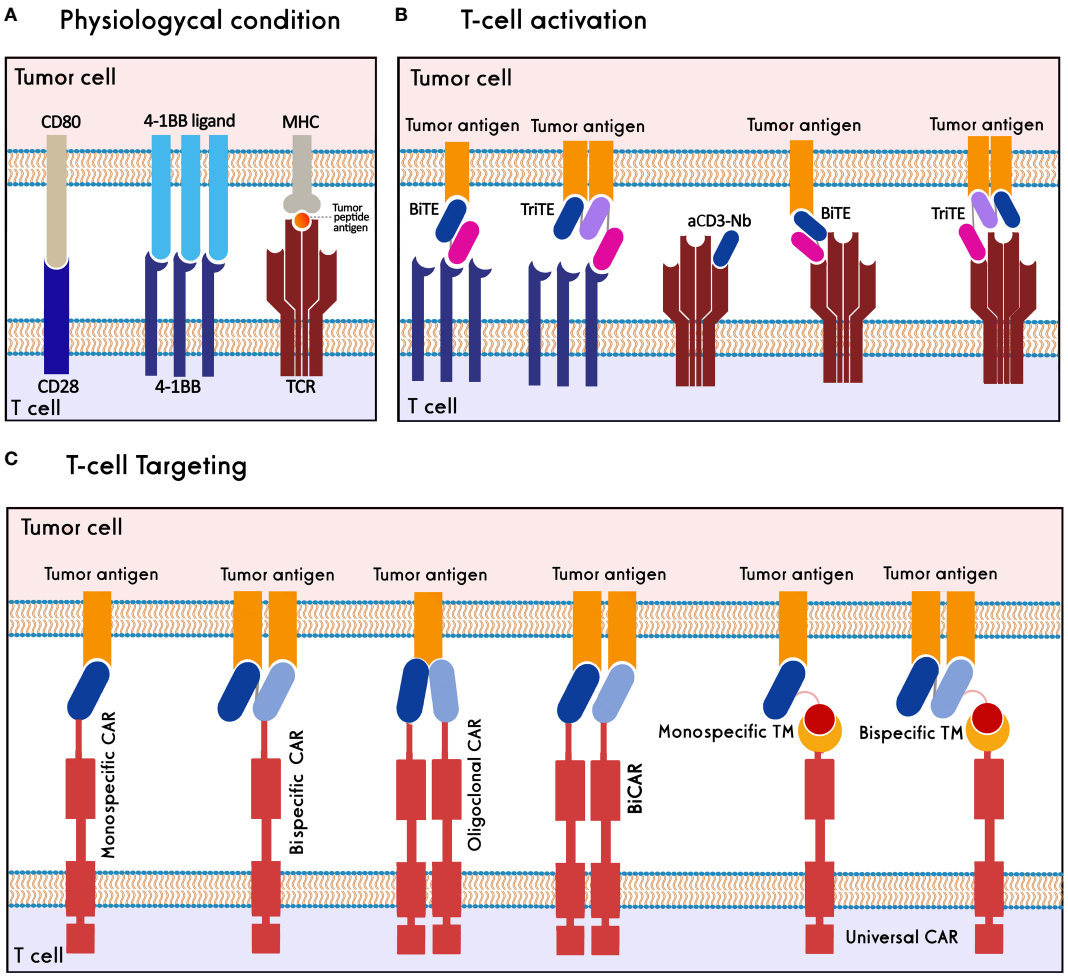

FIGURE 3
Nanobody-based T cell immunotherapy. **(A)** T cells are activated through synapsing CD3-TCR/MHC/tumor peptide antigen, CD28/CD80 and 4-1BB/4-1BB ligand. **(B)** T cells are activated against tumor cells using 4-1BB/CD3 BiTEs, 4-1BB/CD3 TriTEs, and anti-CD3-Nanobody (aCD3-Nb). **(C)** T cells target tumor antigens through monospecific CAR, bispecific CAR, oligoclonal CAR, biCAR, and monospecific-/bispecific-universal CAR-T cells.

3.1 Nanobody-based T-cell activation

In physiological conditions, stimulation of activatory molecules, i.e., CD3, CD28, and 4-1BB, activates T cells resulting in their proliferation and effector functions (40–42). Various studies show that T-cell activation can be induced through antibodies or antibody fragments specific to these activatory molecules. Heretofore, a CD19 (scFv)/CD3(scFv) bispecific T-cell engager (BiTE), blinatumomab, has been approved for clinical administration in refractory/relapsed B- acute lymphoblastic leukemia (B-ALL) and non-Hodgkin lymphoma (NHL) (43, 44).

3.1.1 CD3-based T-cell activators

The anti-CD3 nanobodies and nanobody-based CD3-targeting BiTEs have been studied as T-cell activators due to the molecular benefits of nanobodies compared to other modules. A study showed that an anti-CD3 nanobody could successfully activate T cells, raise the secretion of IL-2 and IFN-γ cytokines and suppress tumor growth in a xenograft mouse model (45). The anti-tumor property of another anti-CD3 nanobody was proved through the activation of cytotoxic T lymphocytes and inhibition of angiogenesis. In this study, angiogenic markers, i.e., VEGFR2, MMP-9, and CD31, were reduced, while activated T-cell markers such as IL-2 were increased (46).

The EgA1 anti-EGFR nanobody was used for constructing LiTE (light T-cell engager) and ATTACK (asymmetric tandem trimerbody for T-cell activation and killing cancer) bispecific engagers by combining one and three EGFR-binding nanobodies with a single CD3-binding scFv, respectively. The tetravalent BiTE, ATTACK, enhanced the binding capacity towards EGFR-expressing cells and exhibited potent target cell lysis compared to monovalent LiTE (47). Two anti-EGFR LiTEs, produced in two orientations, i.e., as EGFR (Nb)/CD3(scFv) and CD3(scFv)/EGFR(Nb), showed enhanced T-cell activation and significant inhibition of EGFR-expressing tumor cells (48). To extend the half-life of LiTE, it was fused to the human albumin sequence, which resulted in greater tumor growth suppression and a longer half-life of albumin fusion LiTE compared to the LiTE molecule without fusion (49). The anti-tumor effects of PD-L1(scFv)/CD3(scFv) and PD-L1(Nb)/CD3(scFv) BiTEs were investigated in armed oncolytic herpesvirus-1. The Nb-harboring BiTE creates a cross-linked pseudo-synapse between PD-L1 and

CD3 for simultaneous immune checkpoint blockage and T-cell activation (50). Aiming to increase the avidity of antibody fragments in T-cell engagers, MART-1_{27L}-HLA-A2(Nb)/CD3(scFv) BiTE was accumulated using human cartilage oligomeric matrix protein (COMP48) to form a multimeric module termed 'combody'. This strategy led to raising the combody affinity by 10^5-fold compared to that of the monovalent BiTE with no effect on antibody specificity (51). Moreover, for improving BiTE efficacy, a HER2-specific T-cell engager was developed by fusing two anti-HER2 nanobodies targeting non-overlapping epitopes of HER2 to an anti-CD3 Fab. This nanobody-based BiTE demonstrated potent inhibition of tumor cells compared to trastuzumab (52). A HER2(Nb)/CD3 (scFv) BiTE, termed BiHC (bispecific HER2-CD3 antibody), could significantly activate T cells and increase the cytotoxicity of $HER2^+$ tumor cells (53). Another BiTE against carcinoembryonic antigen (CEA), CEA(Nb)/CD3(Fab), showed potent T-cell activation in the xenograft model. The anti-tumor efficacy of this BiTE was increased *via* site-specific PEGylation (54). A CD3(scFv)/EGFR(Nb)/EpCAM (Nb) trispecific T-cell engager (TriTE) was developed to target colorectal cancer cells that could activate T cells and lyse colorectal cancer cells (55).

3.1.2 4-1BB-based T-cell activators

While anti-CD28 nanobody modules have not been extensively studied, various scFv-based BiTEs were developed for targeting 4-1BB as a co-stimulator of T-cell activation; however, they were withdrawn from the clinical trials due to their high toxicity. Switching to nanobody-based 4-1BB-agonistic BiTEs can be a promising approach to overcoming T-cell activation challenges. Recently, an agonistic nanobody targeting CRD4 of 4-1BB was fused to an anti-PD-L1 nanobody. This PD-L1(Nb)/4-1BB(Nb) BiTE significantly activates T-cells and inhibits tumor cell proliferation *in vitro* and *in vivo*. In a xenograft mouse model, the nanobody-based BiTE showed reduced toxicity compared to the scFv-based one (56). A trimeric CEA(Nb)/4-1BB(scFv) BiTE was developed using the murine collagen XVIII-derived homotrimerization domain (TIE^{XVIII}) which forms a hexagonal conformation (three anti-CEA nanobodies and three anti-4-1BB scFvs) (57). Also, a trimeric EGFR(Nb)/4-1BB(scFv) BiTE was constructed by this strategy (58). Both trimeric BiTEs significantly recognize 4-1BB and the corresponding tumor antigen, activate T-cells and inhibit target antigen-expressing tumor cells. Due to the multimeric formation potential of nanobody-based BiTEs and TriTEs, it is possible to evaluate co-targeting more tumor antigens and stimulatory domains, providing higher tumor specificity and lower toxicity compared to scFv and other modules.

In brief, nanobodies could provide the ability to design molecules capable of multiple binding to T cells' activating receptors. Also, the nanobody-based T-cell activators are more efficient in infiltrating solid tumors due to their reduced molecular size. Since a HER2-targeting nanobody has entered into clinical trials (NCT04467515) and HER2(Nb)/CD3(scFv) BiTE has shown promising preclinical results, it seems that the nanobody-based anti-HER2 BiTEs have a greater chance to progress to clinical trials for treating $HER2^+$ breast cancers.

3.2 Nanobody-based T-cell targeting

Chimeric antigen receptors (CARs) are synthetic protein molecules that redirect T cells to target tumor cells. Conventional CAR-T Cells comprise an extracellular domain of an antigen-binding scFv, a hinge domain, a transmembrane domain, an intracellular domain, and one or more costimulatory domains (59). Based on the positive characteristics of nanobodies, they were employed to establish nanobody-based CAR-T cells (NbCAR-T cells) for targeting several cancer types. So far, various strategies have been used to produce NbCAR-T cells with improved safety and efficacy, including monomeric, oligoclonal, bispecific, multispecific, and universal NbCARs. In the following, these different strategies and different tumor antigens studied in pre-clinical and clinical studies are reviewed (Table 1).

3.2.1. Monospecific NbCAR-T cells

3.2.1.1. Targeting hematologic malignancies by monospecific NbCAR-T cells

The most common hematologic malignancies are derived from B cells (89). Up to now, four CD19-CAR-T cell products to treat B-ALL and B-NHL and two BCMA-targeted CAR-T products to treat multiple myeloma have been approved by the FDA. The most important tumor antigens targeted by NbCAR-T cells against B cell malignancies include CD19, CD22, CD20, CD33, and CD72. Multiple myeloma, the second most common hematologic malignancy, has been targeted by NbCAR-T cells against BCMA and CD38 (65).

Three second-generation CD33-NbCARs could kill the target tumors and increase the levels of IL-2 and IFN-γ cytokines, while they had no effects on negative target tumor cells. The comparison of constructs, including 4-1BB or CD28 costimulatory domains, showed that 4-1BB-based constructs, unlike CD28-based ones, could control the new $CD33^+$ THP1 tumor cells added to the medium after 7 days. Moreover, CD20-NbCAR-T cells with a 4-1BB costimulatory domain could also completely destroy subcutaneous tumors in less than 20 days (66). Three third-generation CD22-NbCAR-T cells have been individually developed using three different high-affinity nanobodies. Among them, the CD22MN-NbCAR-T cells, which harbored the nanobody with the least affinity, could effectively inhibit the tumor burden in laboratory mice. This implies that the high affinity of the targeting moiety does not correlate with strong cytotoxicity of NbCAR-T cells (67).

The CD72-NbCAR-T showed potent cytotoxic activity and strong degranulation against $CD72^+$ cells and primary B-ALL samples, comparable to CD19-CAR-T cells. These CD72-specific CAR-T cells were effective even on the cells knocked out for CD19, although CD19-CAR-T activity was reduced (68). The CD7-NbCAR-T cells were able to eliminate abnormal T cells and overcome the fratricide of CAR-T cells. CD7-NbCAR-T cells need to be further investigated as a suitable therapeutic potential for the treatment of patients with T-cell malignancies. An allogeneic CD7-NbCAR-T has been designed, which avoids the expression of the CD7 cell surface to minimalize fratricide. Evaluation of its safety and efficacy proved that all side effects were both reversible and controllable except in one patient (70).

10.3389/fimmu.2023.1012841

TABLE 1 List of nanobody-based CAR-T cells.

Functional type	Target	CAR Structure	Tumor type	Reference
Monospecific	BCMA	BCMA.Nb-CD8α-CD8αTM-4-1BB-CD3 ζ	Hematologic malignancies	(60–62)
Bi-epitopic	BCMA	BCMA.Nb-BCMA.Nb-CD8α-CD8αTM-4-1BB-CD3ζ	Hematologic malignancies	(63, 64)
Monospecific	CD38	CD38.Nb-CD8α-CD8αTM-4-1BB-CD3ζ	Hematologic malignancies	(65)
Monospecific	CD33	CD33.Nb-CD8α-CD8αTM-4-1BB-CD3ζ CD33.Nb-CD8α-CD8αTM-CD28-CD3ζ	Hematologic malignancies	(66)
Monospecific	CD20	CD20.Nb-CD8α-CD8αTM-4-1BB-CD3ζ	Hematologic malignancies	(66)
Monospecific	CD22	CD22.Nb-mutFc-CD8ATM-ICOS-4-1BB- CD3ζ	Hematologic malignancies	(67)
Monospecific	CD72	CD72.Nb-CD8α-CD8αTM-4-1BB-CD3ζ	Hematologic malignancies	(68)
Monospecific	CD7	–	Hematologic malignancies	(69, 70)
Monospecific	MUC1	MUC1.Nb-CH3CH2hinge- CD28TM-CD28-CD3 ζ MUC1.Nb-CH3CH2(hinge)$_2$-CD28TM-CD28-CD3ζ MUC1.Nb-CH3CH2hinge-CD28TM-CD28-OX40-CD3 ζ MUC1.Nb-CH3CH2(hinge)$_2$-CD28TM-CD28-OX40-CD3ζ	Solid tumor	(71)
Monospecific	MUC1	MUC1.Nb-IgG3Hinge-FC-CD28TM-CD28-CD3ζ	Solid tumor	(72)
Monospecific	MUC1	MUC1.Nb-IgG3-Fc&Hinge-CD28TM-CD28-CD3ζ MUC1Nb-IgG3-Fc&Hinge-Hinge-CD28TM-CD28-CD3ζ MUC1Nb-FCRIIHinge-CD28TM-CD28-CD3ζ	Solid tumor	(73)
Monospecific	MUC1	MUC1.Nb-IgG3hinge-CD28TM-CD28-CD3ζ	Solid tumor	(74)
Monospecific	PMSA	PMSA.Nb-IgG1hinge-Fc-CD28TM-CD28-CD3ζ	Solid tumor	(75, 76)
Monospecific	VEGFR2	VEGFR2.Nb-IgG1-Fc-CD28-CD28-CD3ζ	Solid tumor	(77)
Oligoclonal	TAG-72	TAG-72.Nb-IgG3-Fc&Hinge-CD28TM-CD28-CD3ζ TAG-72.Nb-IgG3-Fc&Hinge-Hinge-CD28TM-CD28-CD3ζ TAG-72.Nb-IgG3-Fc&Hinge-CD28TM-CD28-OX40-CD3ζ TAG-72.Nb-IgG3-Fc&Hinge-Hinge-CD28TM-CD28-OX40-CD3ζ	Solid tumor	(78)
Oligoclonal	HER2	HER2.Nb-IgG3-Fc&Hinge-CD28-CD28-CD3ζ HER2.Nb-IgG3-Fc&Hinge-Hinge-CD28-CD28-CD3ζ HER2.Nb-IgG3-Fc&Hinge-CD28-CD28-OX40-CD3ζ HER2.Nb-IgG3-Fc&Hinge-Hinge-CD28-CD28-OX40-CD3ζ	Solid tumor	(79)
Bispecific	CD20&HER2	CD20.Nb-IgG1-Fc-CD28TM-CD28-CD3ζ HER2.Nb-IgG1-Fc-CD28TM-CD28-CD3ζ CD20.Nb-HER2.Nb-IgG1-Fc-CD28TM-CD28-CD3ζ	Solid tumor	(80)
Bispecific	CD19&CD20	CD19.Nb-IgG4.hinge-CD8TM-4-1BB-CD3ζ CD20.Nb-IgG4.hinge-CD8TM-4-1BB-CD3ζ CD20.Nb-CD19Nb-IgG4.hinge-CD8TM-4-1BB-CD3ζ	Hematologic malignancies	(81)
Bispecific &Split	CD13&TIM3	Nb-IgG4mutant (IgG4m) hinge- CD8TM- 4-1BB, and CD3ζ CD13.Nb-CD3ζ, TIM3.scFv-CD28-4-1BB	Hematologic malignancies	(82)
Trispecific	CD19&CD20 &CD22	CD22.Nb-CD20.Nb-CD19.Nb-CD8α- 4-1BB-CD3ζ	Hematologic malignancies	(83)
Trispecific	CD33&CD123 &CLL1	TanCAR-a hinge spacer-CD8TM-41BBz–CD3ζ	Hematologic malignancies	(84)
Universal	EGFR	anti-E5B9-CD28- CD28 TM-CD28-CD3ζ	Solid tumor	(85)
Universal	EGFR	anti-E5B9-CD28-CD28 TM-CD28-CD3ζ	Solid tumor	(86)
Universal	EGFR	anti-E5B9-CD28-CD28.TM-CD28-CD3ζ	Solid tumor	(87)
Universal	CD105	CD105.Nb(C184)-CD8α.hinge-CD8α.TM-4-1BB-CD3ζ	Solid tumor	(88)

The monovalent humanized NbCAR-T cells developed against BCMA antigen showed 88.89% progression-free survival in R/R (relapsed/refractory) multiple myeloma patients (60). Unlike the scFv-CARs, these NbCARs were evenly distributed on the membrane surface of T cells. They could recognize and kill tumors with high BCMA expression more powerfully than tumors with low BCMA expression (63). A bi-epitopic NbCAR-T (LCAR-B38M) targeting two different epitopes of BCMA showed ORRs (overall response rates) and CRs (complete responses) varied from 80% to 94.8% and from 56% to 76%, respectively (62, 64). The CD38-NbCAR-T cells exposed to $CD38^+$ tumors could proliferate effectively, kill the target cells, and reduce the tumor size in an *in vivo* evaluation. There were few cytotoxic effects against normal $CD38^+$ cells, such as B cells, adult T cells, and NK cells (65). In

spite of the low expression of CD38 on T cells (90), just a small percentage of T cells were killed by CD38-NbCAR-T. The transduced T cells were effectively proliferated and lived for a long time without functional defects (65).

3.2.1.2 Targeting solid tumors by monospecific NbCAR-T cells

Unlike CAR-T cell therapy against hematological malignancies, limited clinical success has been observed in CAR-T cell therapy against solid tumors due to facing several challenges, including tumor antigen heterogeneity, trafficking and infiltration into tumor tissue, and immunosuppressive TME (88). The most important solid tumor antigens targeted by NbCAR-T cells include MUC1, prostate-specific membrane antigen (PSMA), HER2, and CD105.

Two designed MUC1-NbCAR and pFKC8 (containing human caspase 8 and two modified domains of FKBP12) constructs were co-transfected into Jurkat T cells. After the addition of dimerizer, transfected T cells were reduced by 91% (71). MUC1-NbCAR-T cells could produce IL-2 cytokine, proliferate and lyse $MUC1^+$ cells (72, 74). The introduction of phiC31 integrase in MUC1-NbCAR-T cells led to efficient and stable transduction of constructs into the Jurkat cells (73). Immunohistological evaluation of the prostate samples proved that the higher the expression of PMSA, the more severe cancer (91). The PSMA-NbCAR-T cells could express the CD69 activation marker, produce the IL-2 cytokine, and inhibit $PSMA^+$ tumor growth (75).

3.2.1.3 Targeting tumor stroma and vasculature by monospecific NbCAR-T cells

Cancer cells often create the vascular system around the tumor to grow more rapidly. Since the expression of VEGF and VEGFR in tumors is related to their angiogenesis and metastasis (92), tumor vasculature has been a major target for CAR-T cells. The VEGFR2-NbCAR-T cells could efficiently lyse the $VEGFR2^+$ tumor cells and produce IFN-γ and IL-2 cytokines (77). EIIIB, a fibronectin splice variant, is overexpressed by the tumor stroma and neovasculature, which makes it a potential target candidate for CAR-T cell therapy. EIIIB-NbCAR-T cells could delay the tumor growth, interfere with the blood supply to the tumor and enhance immune cells infiltration into the TME (93).

3.2.2 Oligoclonal NbCAR-T cells

Numerous studies have shown that T cells can target tumor antigens with an oligoclonal pattern in tumor tissues, thus reducing the likelihood of antigen escape (94). Two different studies used this approach: one to design TAG72-NbCAR-T cells (78) and another one to develop HER2-NbCAR-T cells (79). When TAG72-NbCAR-expressing oligoclonal T cells were stimulated by the $TAG72^+$ tumor cells, they resulted in the proliferation of CAR-T cells dependent on the target antigen and secretion of IL-2 cytokine. The designed system may avoid CAR immunogenicity and prevent the escape of the tumor cells (78). The function evaluation of the HER2-NbCAR-T cell exhibited that their cytokine secretion, proliferation, and cytotoxic activity were higher than their monoclonal counterparts (79).

3.2.3. Bi- and multispecific NbCAR-T cells

One of the major drawbacks of monospecific CAR-T cells is the recurrence of the disease due to a mutation that results in the removal or reduction of the relevant tumor antigen expression. This drawback can be eliminated by designing CAR-T cells targeting more than one tumor antigen. Based on this theory, researchers have shown that the use of bispecific, tandem, and a combination of two single CAR-T cells can reduce these drawbacks (95, 96).

Three NbCAR-T cells, one tandem form (a single CAR structure consisting of two distinct antigen recognition domains targeting two tumor antigens), and two distinct monospecific forms, were designed against HER2 and CD20 tumor antigens. The efficiency of the tandem CD20-HER2-NbCAR-T cells was better than that of two monospecific NbCAR-T cells, and the efficiency of the CD20-NbCAR-T cell was the lowest. It was assumed that the distance between the CD20-Nb domain to the cell membrane of T cells was much longer than the distance between the HER2-Nb to the T cell's membrane. Therefore, it is possible that inhibitory phosphatases enter this large immunological synapse and disrupt the activity of T cells (80). Three CAR-T constructs (CD20-NbCAR-T, CD19-NbCAR-T, and tandem CD20-CD19-NbCAR-T) were exposed to the primary cancer cells obtained from patient-derived (PD) tumor samples. These NbCAR-T cells could lyse the primary cancer cells and showed increased expression of CD69 (81). A bispecific and split CAR-T (BissCAR) was produced against CD13, and TIM3 antigens of AML cells, in which CD13-Nb was linked to CD3ζ signaling and anti-TIM3-scFv was linked to two costimulatory domains, CD28 and 4-1BB. BissCAR produced more cytokines when exposed to $CD13^+TIM3^+$ cells (mimicking leukemic stem cells) compared to $CD13^+TIM3^-$ cells (mimicking normal hematopoietic stem cells (HSCs)) because both activating and stimulatory signals were activated. BissCAR injection into NSG mice with PD AML resulted in complete tumor elimination with reduced toxicity to HSCs (82).

A trispecific NbCAR-T (triNbCAR-T), LCAR-AIO, simultaneously targets three different tumor antigens, including CD19, CD20, and CD22, to treat patients with recurrent B cell malignancies. Compared to CD19-scFvCAR-T, LCAR-AIO showed greater cytokine production and lytic activity against target cells. When LCAR-AIO was exposed to cells whose CD19 tumor antigens had been knocked out, it maintained its lytic activity, which means these cells may prevent tumor escape in $CD19^-$ patients. Compared to its monospecific counterparts, LCAR-AIO showed better T-cell proliferation, longer shelf life, and superior tumor eradication efficiency in an NCG murine model (83). In another study, triNbCAR-T cells targeting CD33, CD123, and CLL1 tumor antigens could exhibit cytolytic activity equal to or greater than their monospecific counterparts and high levels of IFN-γ and IL-2 cytokines when exposed to $CD33^+$ or $CD123^+$ only tumors, whereas they produced lower levels of these cytokines when exposed to CLL^+ only tumors (84).

3.2.4 Universal NbCAR-T cells

Despite of obtained remarkable successes, all of the FDA-approved CAR-T cells are being made from autologous T cells and target only one cancer antigen. These autologous CAR-T cells with a fixed antigen specificity have several negative points, involving high cost and long-lasting manufacturing, an inherent risk of product

failure, and limited efficacy due to tumor antigen escape (97). Also, conventional CAR-T cell therapies may cause some side effects, such as on-target/off-tumor reactions, cytokine release syndrome (CRS), and neurotoxicity, which threaten the life of patients (98). Because these engineered CAR-T cells are inherently active, their activities and specificities are permanent and not easily controllable. Therefore, two universal systems were designed to solve these problems: i) universal CAR-T cells and ii) universal T cells (97).

3.2.4.1 Universal nanobody-based CAR-T cells

These universal CAR-T cells separate the conventional CARs into two modules: i) the signaling module or uniCAR module, which harbors a binding moiety to a specific epitope combined with the intracellular signaling domains *via* a hinge and the transmembrane regions, and ii) a target module (TM), which is a bispecific fusion molecule with one binding domain directed against a tumor-associated antigen (TAA) and a part (can be an scFv, an epitope, or a small molecule) specifically recognized by the signaling module (99). To date, four diverse types of universal CAR-T cells have been developed: (i) antibody-dependent cellular cytotoxicity receptors, (ii) bispecific protein-mediated linkage, (iii) anti-tag CARs, and (iv) tag-specific interactions (100). These adaptor CAR (adCAR) platforms can switch on/off the CAR-T cells to control their activity (101). Moreover, there is the capability to simultaneously or sequentially target different TAAs (99).

The Nb-adCAR-T cells were produced based on the E5B9 peptide tag, derived from nuclear antigen La-SS-B, and anti-E5B9 scFv to split the intracellular signaling domain from the antigen-binding domain (86). These engineered T cells could target and lyse $EGFR^+$ tumor cells in a TM concentration-dependent manner. Although the deletion of TM participating in the Nb-adCAR-T cell complex was delayed, free TM was deleted more rapidly (85). Because of the higher avidity of the bivalent anti-EGFR TMs, they could direct the Nb-adCAR-T cells to tumor cells with low EGFR expression levels, while the monovalent TMs could only direct the Nb-adCAR-T cells to tumor cells with high EGFR expression levels (86). In another study, the EGFR-scFv-TM was compared with the EGFR-Nb-TM. The quantities of different cytokines were similar in the presence of both Nb- and scFv-TMs. The scFv-TMs could induce the lysis of tumor cells with low EGFR expression levels more efficiently than the Nb-TMs, which may increase the risk of targeting healthy tissues (87).

3.2.4.2 Universal T cells

Universal T cells are prepared by disrupting MHC loci (HLA-A) or TRAC loci of the endogenous α or β subunits at the genomic level (97). Universal CD105-NbCAR-T cells were designed by CRISPR/Cas9 method for solid tumor immunotherapy. In a human tumor xenograft model, universal CD105-NbCAR-T cells repressed the growth of $CD105^+$ tumors, decreased tumor weight, and increased the lifespan of mice (88).

Since nanobodies can be easily reformatted into multi-domain structures, NbCAR-T cells are easier to engineer compared to scFv-based CARs. According to the clinical trial studies such as CD19/20 bispecific NbCAR-T cells against B cell lymphoma (NCT03881761) and BCMA-NbCAR-T cells (NCT03664661) and LCAR-B38M-NbCAR-T cells against multiple myeloma, it seems that NbCAR-T cells targeting blood cancers have the more likelihood to reach FDA approval.

4 Nanobody-based NK cell immunotherapy

Nanobody-mediated NK cell immunotherapy is a promising tool for non-specific tumor cell recognizing and targeting, focusing on the nature of NK cells (Figure 4). In physiological conditions, NK cells target tumor cells through the downregulation of HLA on tumor cells (102). They could be engineered with CARs to target different tumor antigens. Moreover, NK cells may be triggered using appropriate mAbs and antibody fragments, including nanobodies, to eliminate cancer cells.

4.1 Nanobody-based NK cell activators: BiKEs, TriKEs, and TetraKEs

The activation of NK cells occurs through antibody binding to CD16, a primary activator domain on NK cells. Furthermore, when CD16 is targeted, the NK cells act as cytotoxic effectors through CD16-mediated antibody-dependent cellular cytotoxicity (ADCC) (10, 103). Various soluble anti-CD16 nanobodies are established and characterized to activate NK cells again in tumor cells (in mono-, bi-, tri-, and tetraspecific manners) (104).

Bispecific and trispecific killer cell engagers (BiKEs and TriKEs) are antibody-based small molecules that create an immune synapse between the tumor and NK cells. BiKEs target a tumor antigen and another functional element on the NK cell membrane, e.g., CD16, NKG2D, and NKp46, while TriKEs target one more element (commonly a tumor antigen or IL-15).

Various preclinical studies have examined the anti-tumor potency of BiKEs and TriKEs. A CD16(Nb)/CEA(Nb) BiKE was developed for the simultaneous targeting of CD16 and CEA^+ ovarian and colorectal cancer cells. This anti-CEA BiKE showed significant NK cell activation and suppressed cancer progression in a mouse xenograft model (105). Another anti-CEA BiKE comprising anti-CD16 and anti-CEA nanobodies could effectively recruit NK cells and showed significant *in vivo* tumor growth inhibition (106). A llama anti-CD16 nanobody was fused to three different nanobodies targeting CD19, HER2, and EGFR cancer antigens to create anti-CD16/CD19, anti-CD16/HER2, and anti-CD16/EGFR BiKEs, respectively. They induced significant target-specific activation and ADCC response in NK cells against target antigen-expressing tumor cells (107). The anti-CD16/CD30 BiKE, which targets the lymphoma antigen CD30, was enrolled in a clinical trial on relapsed/refractory Hodgkin's lymphoma (HL) patients, which showed a high overall response rate in patients with $CD30^+$ T-cell malignancies (NCT03192202). This CD30/CD16 BiKE was developed in a tetravalent manner, providing more half-life than the bivalent form (108, 109).

IL-15, physiologically secreted by activated monocytes/macrophages, activates NK cells *via* synapsing to IL-15R expressed on the NK cell membrane and stimulated NK cell expansion. CD16 (Nb)/IL-15/CLEC12A(scFv) TriKE was designed for targeting acute

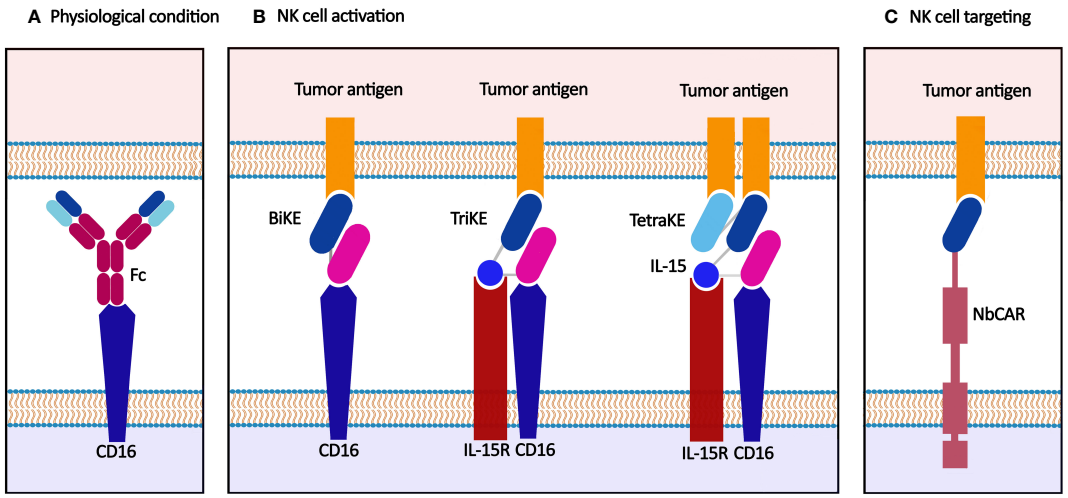

FIGURE 4
Nanobody-based NK cell immunotherapy. **(A)** NK cells are activated through synapsing Fc and CD16 in physiological conditions. **(B)** BiKE, TriKE, and TetraKE target tumor antigen(s) and IL-15R, another functional element on the NK cell membrane, e.g., CD16. **(C)** CAR-NK cell recognizes the tumor antigen and exerts anti-tumor effects.

myeloid leukemia (AML) *via* IL-15-activated NK cells. This camelied/human TriKE successfully targeted CLEC12A expressed on leukemic hematopoietic stem cells in AML patients with no bonding to normal hematopoietic stem cells (110). Moreover, CD16(Nb)/IL-15/HER2 (scFv) TriKE could significantly activate the NK cells and inhibit the proliferation of HER2$^+$ cancer cells *in vitro* (SKOV3 and SKBR3 cells) and *in vivo* (xenograft NGS mice models) (111).

Considering valuable properties of nanobodies, novel NK cell engagers may be developed by substituting scFv modules with existing nanobodies against different tumor antigens. For example, anti-EpCAM nanobody-based TriKEs could be developed for stimulating NK cells' cytotoxicity in colorectal cancer using EpCAM-specific nanobodies (112, 113). Also, an anti-CD33 nanobody which was developed for targeting AML cells (30), could be used instead of anti-CD33 scFv in CD16(scFv)/IL-15/CD33(scFv) TriKE. This trivalent engager could significantly activate NK cells and induce NK-mediated ADCC against CD33 antigen expressed on AML cells and myeloid-derived suppressor cells (MDSCs) (114). Furthermore, CD16(scFv)/CD19/CD22(scFv) TriKE was developed for targeting CD19 and CD22 (leukemia/lymphoma antigens) and CD16, simultaneously (115). Since anti-CD19 and anti-CD22 nanobodies have been developed for targeting leukemia/lymphoma cells (67, 116), they can be used in nanobody-based NK cell engagers. Also, the scFv modules applied in CD16/IL-15/CD133/EpCAM TetraKE can be substituted with their nanobody counterparts for effective targeting of carcinoma antigens simultaneously (117, 118).

In conclusion, nanobodies are potent tools for activating NK cells through NK cell-activating receptors, especially CD16. The scFv-based NK cell engagers have given promising results in clinical trials targeting CD30 (NCT04101331), CD33 (NCT03214666), BCMA (NCT04434469), EGFR (NCT04259450), and HER2 (NCT04143711). Considering that nanobodies targeting HER2 (NCT04467515) and BCMA (as NbCAR-T cells) (NCT03664661) have reached clinical trials, nanobody-based NK cell engagers targeting HER2 and BCMA have more chance to be effective against HER2$^+$ solid tumors and multiple myeloma, respectively.

4.2 Nanobody-based targeting of NK cells

CAR-NK cells target tumor antigens expressed on the surface of tumor cells and simultaneously benefit from the NK cells' cytotoxic effects. CAR-NK cells have advantages over CAR-T cells; including lower on-target/off-tumor toxicity due to their shorter lifespan than CAR-T cells, lower CRS and neurotoxicity due to their limited cytokine secretion profile, activation by their natural cytotoxicity receptors in a CAR-independent manner, killing tumor cells through CD16-mediated ADCC, and availability of allogeneic sources of NK cells, i.e., NK92 cell lines, peripheral blood mononuclear cells, umbilical cord blood, and induced pluripotent stem cells (iPSCs) (119). Nanobodies are utilized in the extracellular recognition domain of the chimeric receptors in CAR-NK cells. Compared to scFvs, nanobodies have a more efficient surface expression level and less cross-reactivity in CAR-NK cells. Also, nanobody-based CAR-NK cells have fewer recipient immunogenic responses than CAR-NKs targeted with murine-derived scFvs. Furthermore, multidomain applications of nanobodies are more retained due to the smaller size than scFv (120).

In a study, monovalent anti-CD7 nanobody (VHH6) and bivalent (VHH6-VHH6) nanobodies were fused to a CAR construct and expressed on the surface of NK-92MI cells. The results indicated the enhanced activation and cytotoxicity of CAR-NK cells that led to significant inhibition of T-ALL cells (121). In another study, an anti-CD38 nanobody was used for targeting CD38$^+$ MM/Burkitt lymphoma cells by CAR-NK cells. These cells could successfully lyse the primary human multiple myeloma cells and deplete CD38$^+$ myeloma cells in human bone marrow-derived samples (122).

In another strategy, TCR-like nanobodies were applied to target intracellular tumor antigens presented by the HLA molecules. In an

NK cell-based anti-melanoma experiment, GPA7, a TCR-like nanobody, was fused to the intracellular domain of CD3ζ to target the melanoma-associated gp100/HLA-A2 complex expressed in melanoma cells. The engineered NK92 cells could effectively recognize melanoma cells and inhibit their growth in a mouse xenograft model (123). Nanobody conjugation to NK cells was used for the simulation of CAR therapy. NK92 cells were conjugated with an anti-EGFR nanobody through the glycoengineering approach. The conjugated NK cells could target EFGR-overexpressing tumors and exhibit potent cytotoxic activity toward them (124).

Since then, there have been multiple clinical trials on CD7- and CD38-targeting CAR-T cells to treat a number of different blood and bone marrow cancers (125). Moreover, a phase I/II trial was conducted to evaluate the safety and efficacy of anti-CD7 CAR-NK cells in $CD7^+$ leukemia and lymphoma patients (NCT02742727). Based on the hopeful outcomes of treatment with CAR-T and CAR-NK cells targeting CD7 and CD38 markers, as well as the success *in vtiro* development of nanobody-based CAR-NK cells against these tumor antigens, it seems that nanobody-based CD7 and CD38 CAR-NK cells will advance to clinical stage investigations for the treatment of leukemia, lymphoma, and myeloma.

5 Nanobody-based targeting of macrophages

Macrophages are highly plastic immune cells that comprise phenotypically different populations in various cancers (126). They have exhibited dual functions based on the microenvironmental cues in cancer development, including preventing tumor growth in the early stages and promoting it in the later ones (127). One of the most important reasons for macrophage targeting in cancer immunotherapy is their high ability to infiltrate (comprise >50% of the tumor mass) into the TME (128). Although T cells are the main immune cells for the removal of tumor cells, they have low infiltration and are often suppressed by TME inhibitory factors (129).

Macrophages are functionally divided into two subtypes: classically activated macrophages (M1) and alternatively activated macrophages (M2). M1 macrophages have anti-tumor activity and secrete pro-inflammatory cytokines such as IL-1β, IL-6, IL-12, IL-23, TNF-α nitric oxide, and CXCL9 and CXCL0 (130, 131). LPS and T helper (Th) 1 cytokine, like IFN-γ polarize macrophages towards the M1 phenotype (132, 133). M1 cells, in turn, have a positive influence on Th1 cells and boost anti-tumor responses. Anti-inflammatory responses of macrophages are relevant to the M2 phenotype. IL-4 released by Th2 cells and the production of IL-4, IL-10, or IL-13 by tumor cells polarize macrophages into an M2 phenotype (131, 134). Tumor-associated macrophages (TAMs) localize in the TME, usually have an M2 phenotype, and comprise the most number of immune cells in TME (135). TAMs remodel the TME by releasing the inhibitory cytokines, including TGF-β and IL-10, and expressing immune checkpoint ligands to inhibit infiltration and anti-tumor activity of other immune cells, especially cytotoxic T cells. A subset of TAMs that overexpresses macrophage mannose receptors (MMR, CD206) under hypoxic conditions refers to $MMR^{high}MHC\text{-}II^{low}$ TAMs. They are strongly involved in angiogenesis and immunosuppression of the TME (136). Therefore, targeting macrophages, especially TAMs, can be a promising opportunity for boosting immunotherapy of various malignancies.

Different macrophage-based strategies have been used to enhance cancer immunotherapy, including TAMs depletion, M2 repolarization, blocking of checkpoint immune ligands/receptors on macrophages and "don't eat me" signaling, and preventing infiltration of macrophages into the TME (Figure 5).

Recently, the use of nanobodies to target macrophages have been exhibited improved therapeutic effects combined with high safety compared to mAbs in multiple malignancies. For instance, simultaneous inhibition of the CCL2 and CCL5, which are necessary chemokines for attracting TAMs to the TME and upregulated on hepatocellular carcinoma tumor cells, by a bispecific nanobody (BisCCL2/5i) demonstrated more survival benefits than the combination of two full-length antibodies or two small molecules against CCL2 and CCL5 *in vivo*. Delivery of the BisCCL2/5i mRNA encapsulated in an approved lipid nanoparticle led to not only a reduction of more than 50% of M2 macrophages and mitigation of intratumoral macrophages trafficking but also significantly polarized M2-TAMs to an M1-phenotype leading to the increased M1/M2 ratio and improved T-cell infiltration. Combination therapy using BisCCL2/5i nanobody and a trimeric PD-L1 inhibitor triggered a robust anti-tumor response and long-term survival in primary and metastatic liver malignancies (137).

The binding of CD47 on cancer cells to signal regulatory protein-a (SIRPa) on macrophages results in the escape of cancer cells from phagocytosis (138). Blockade of the CD47/SIRPa pathway can enhance macrophage-mediated phagocytosis (MMP), increase the frequency of TAMs in TME, and reduce tumor growth (139). Clinical mAbs that target CD47 have some side effects (e.g., RBC hemagglutinin, platelet aggregation) that may limit their application (140). The pre-clinical studies showed that HuNb1-IgG4, a fusion protein containing an anti-human CD47 nanobody and a human IgG4 Fc fragment, could overcome these drawbacks. This nanobody showed a low affinity for RBCs that led to less toxicity while being able to specifically recognize the human CD47 and bound to it with a higher affinity than B6H12 (an anti-CD47 mAb). HuNb1-IgG4 nanobody exhibited superior anti-tumor efficacy compared to the clinical anti-CD47 mAbs (141).

Since Fc moiety may have non-specific binding and induce immunogenicity *in vivo*, replacing it with a nanocarrier may improve the application of macrophages-targeted nanobodies. The use of the nanobody-fused nanogels (as a drug nanocarrier) can be an efficient strategy to specifically deplete TAMs by the nanobody moiety and simultaneously deliver a drug surrounded by the nanogel into the TME. For example, the polymeric nanogel-conjugated anti-MMR nanobodies could specifically target $MHC\text{-}II^{low}/MMR^{high}$ TAMs in the complex environment of tumor cells (136).

The coupling of nanobodies to the other molecules, including small molecules or pro-inflammatory cytokines, can effectively reverse the immunosuppressive microenvironment of tumors following M2-macrophage repolarization. For example, administration of an IFN-γ-/or IL-2-fused high-affinity anti-PD-L1 nanobody to mice bearing pancreatic tumors showed a phenotype shift in intratumoral macrophages toward M1-macrophage with approximately 50% reduction of tumor burden as well as enhanced

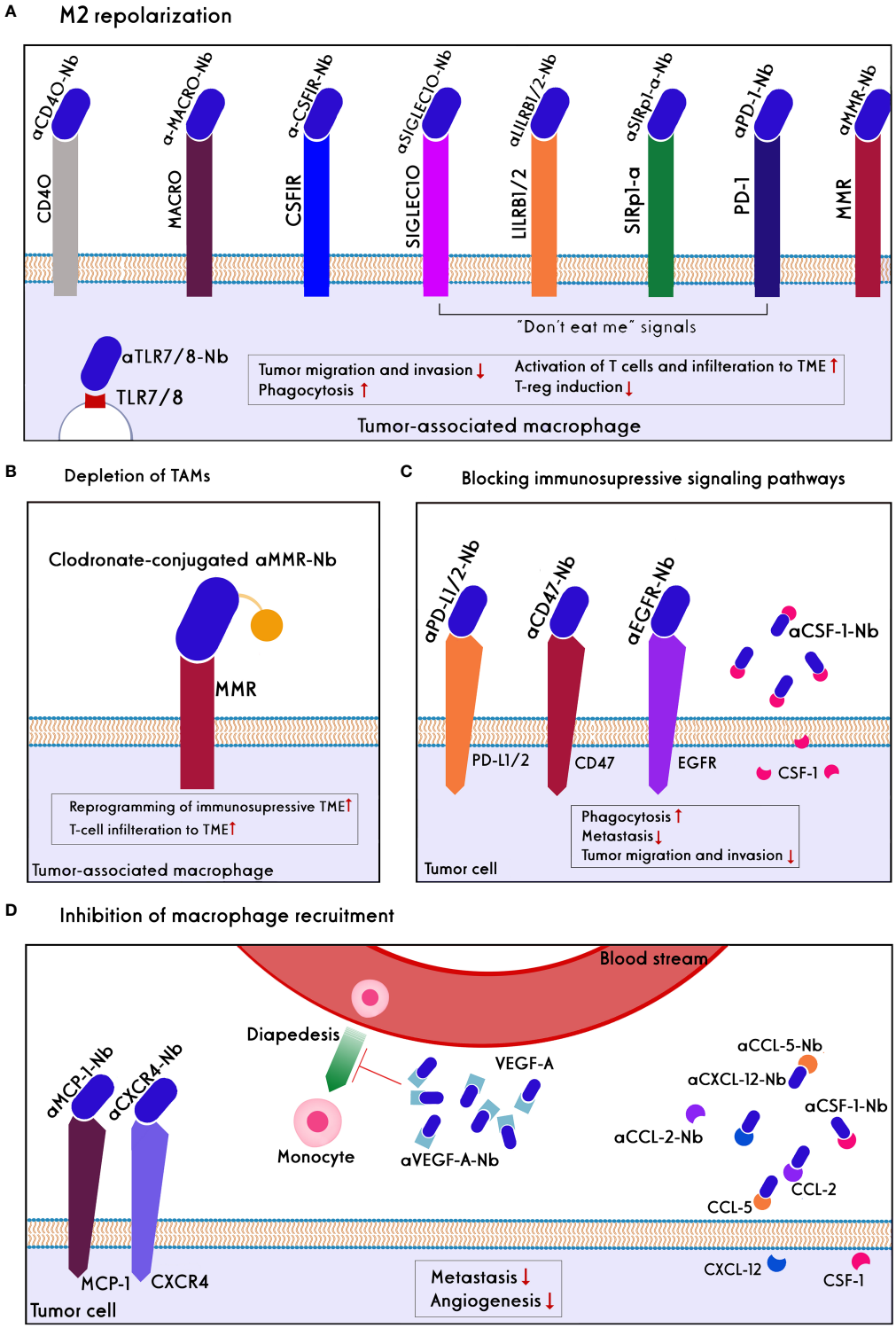

FIGURE 5
Approaches of nanobody/antibody-based targeting of Macrophages. Direct targeting strategies include: **(A)** M2 repolarization: CD40 and TLR7/8 agonists, the blockades of MACRO, CSF1R, MMR, and blocking of 'don't eat me' signals such as PD1, SIRP-a, LILRB1/and 2, and SIGLEC10 on TAMs lead to repolarization of M2 to M1 phenotype in the TME. As a result, tumor migration, invasion, and Treg induction decline, whereas phagocytosis, T-cell activation, and tumor infiltration increase. **(B)** TAMs depletion using anti-MMR conjugated clodronate, as a bisphosphonate, increase reprogramming of immunosuppression of TME and T-cell infiltration. Indirect targeting strategies include: **(C)** blocking of immunosuppressive signaling pathways: inhibition of CSF-1 ligand secreted by tumor cells, blocking of don't eat me signals like CD47 and PDL1/2 on the tumor cells, as well as blocking EGFR on the tumor cells prevent scape of the tumors from phagocytosis and decrease metastasis, tumor migration, and invasion. **(D)** Inhibition Macrophage recruitment: Chemokine of MCP-1 on the tumor cells, soluble chemoattractants such as CCL2, CLL5, CXCL12, CSF-1, VEGF-A has secreted by tumor cells and bystander cells to recall macrophages to the TME. Anti-VEGF-A nanobody/antibody reduces angiogenesis. Nanobodies/antibodies against these chemokines prevent the diapedesis of monocytes into the TME and then their differentiation to the immunosuppressive TAMs. Also, the blockade of the CXCL12/CXCL4 axis reduces metastasis.

infiltration of $CD8^+$ T cells into TME (142). In another study, a small molecule named imidazoquinoline (IMDQ) was linked to an anti-MMR nanobody. IMDQ have known as a TLR7/8 agonist, which strongly stimulates the inflammatory phenotype of macrophages. *In vivo* studies showed that the use of IMDQ-Linked anti-MMR nanobody resulted in skewed MHC-$II^{low}MMR^{high}$ TAMs towards M1-phenotype without its uptake by the other MMR^+ immune cells such as B cells, dendritic cells (DCs), and monocytes. As a consequence, the anti-tumor function of T cells was augmented, and the tumor burden significantly declined (143).

Although the reprogramming of macrophages can provide a great opportunity for restoring stroma, their effective activation is a major problem for cancer immunotherapy. Simultaneous repolarization of TAMs and blocking of the CD47/SIRPα signaling axis can overwhelm this challenge. It was demonstrated that the cell membrane-coated magnetic nanoparticles engineered to overexpress high-affinity variants of SIRPα mAbs could successfully block the CD47-SIRPα pathway. Moreover, the magnetic nanoparticles promoted M2 TAM repolarization and delivered the cell membrane into tumor sites (144). As a result, the local tumor growth was controlled well, and distant tumor metastasis declined by 50%. The insufficient penetration of nanoparticles into the TME due to the undesirable clearance by the macrophages, as well as their sequestering by monocytes, neutrophils, and RBCs, is a challenge for their translation into the clinic. Nanobodies targeting colony-stimulating factors or CD47 can be suitable substitutes in macrophage-based cancer immunotherapy.

Pre-clinical studies have demonstrated that the reprogramming of macrophages from M2 to M1 phenotype through blocking the surface markers of macrophages such as CCL2, CCL5, PD-L1, as well as blocking the CD47/SIRPa signaling can effectively activate innate and adaptive immune systems to eliminate cancer cells. Moreover, blocking the other vital TAMs receptors (e.g., CSF-1R) and inhibitory receptors (e.g., LILRB1, LILRB2, CTLA-4) by nanobodies can improve the anti-tumor immunity in the TME through reprogramming of macrophages (145, 146). Furthermore, it has been suggested that CAR macrophages can improve anti-tumor functions *in vitro* and *in vivo* models (145). Whether using the nanobody-containing CARs (instead of scFv) can boost the anti-cancer efficiency of the CAR macrophages should be investigated in future studies.

Despite the growing application of nanobodies and increased clinical trials of macrophage-targeted therapies, there is limited literature on targeting macrophages with nanobodies. An anti-MMR nanobody radiolabeled with ^{68}Ga-NOTA has entered phase II clinical trials for imaging of MMR-expressing macrophages in head and neck squamous cell carcinoma as well as HL and NHL. The promising results of mAbs that target TAMs for cancer immunotherapy can be expanded to the corresponding nanobodies. A phase I/II clinical study has shown that anti-Clever-1 (bexmarilimab), a novel humanized IgG4-antibody that targets Clever-1 receptor on the TAMs surface, can reprogram M2 TAM to M1 phenotype (147). This antibody has shown considerable anti-tumor activity in patients with advanced solid tumors, including melanoma, gastric, breast, and hepatocellular cancers. Given the desired characteristics of nanobodies, the development of an anti-Clever-1 nanobody could be a suitable candidate for reprogramming TAMs in refractory solid tumors. Moreover, it expects that the identification of new targets on TAMs can increase the application of nanobodies in macrophage-mediated immunotherapy.

6 Nanobody-based immune checkpoint Inhibition

The term "immune checkpoints" (ICs) refers to a group of co-stimulatory and co-inhibitory molecules that are essential for immunological homeostasis and host survival. Under normal physiological circumstances, a balance between the signals from these molecules enables self-tolerance and safeguards the host from tissue damage during an immune response to a foreign antigen (148). In the case of malignancy, immune checkpoint components are co-opted, inhibiting cytotoxic T cells from launching an efficient anti-tumor response (149). Checkpoint inhibitors are medications that stop ICs from binding to their ligands, leading to eliminating T-cell inhibition and boosting the immune system's ability to fight cancer. CTLA-4, programmed death receptor 1 (PD-1), PD-L1, T-cell immunoglobulin and mucin domain-containing 3 (TIM-3), T-cell immunoreceptor with immunoglobulin and immunoreceptor tyrosine-based inhibitory motif (ITIM) domain (TIGIT), and lymphocyte-activation gene 3 (LAG-3) are the receptors that have been the most thoroughly researched (150) (Figure 6).

The mAb-based immune checkpoint inhibition has proven to be effective in inhibiting tumor growth. The FDA approved various checkpoint inhibitors as cancer treatments, including mAbs that target PD-1, such as nivolumab (Opdivo®), pembrolizumab (Keytruda®), and cemiplimab (Libtayo®); mAbs against PD-L1, such as atezolizumab (Tecentriq®), avelumab (Bavencio®), and durvalumab (Imfinzi®); and anti-CTLA-4 mAb ipilimumab (Yervoy®). The utility of mAbs has been constrained by factors like high production costs, low tissue penetration, and immune-related side effects (151, 152). The nanobodies' superior properties, compared to mAbs, make them useful tools for successful immune checkpoint inhibition (152).

T, B, and NK cells frequently express the cell surface receptor PD-1. It has been discovered that the PD-1/PD-L1 pathway is important in the escape of cancer from immune surveillance. In many cancers, PD-1 is expressed on effector T cells and exhausted T cells in TME; and PD-L1 is found on the tumor cell surface. One of the most effective strategies to activate anti-tumor immune responses in the tumor environment has been blocking the PD-1/PD-L1 pathway (153). KN035 is a nanobody that can strongly bind to PD-L1 molecules and successfully disrupt the interaction between PD-L1 and PD1. It can successfully contend with other PD-L1 antibodies for the five hotspot areas where PD-L1 binds to PD-1. KN035 can also successfully stimulate peripheral blood mononuclear cells (PBMCs) *in vitro* and trigger interferon release (154). K2, another PD-L1-specific nanobody, could prevent the interaction between PD1 and PD-L1 and improve dendritic cells' capacity to promote T-cell activation and cytokine generation. In contrast to anti-PD-L1 mAbs, this nanobody has a high ability to bind PD-L1 on both immune and non-immune cells and to increase activation of functional antigen-specific cytotoxic T cells. Therefore, treatment with K2 nanobody and dendritic cell vaccination may be more

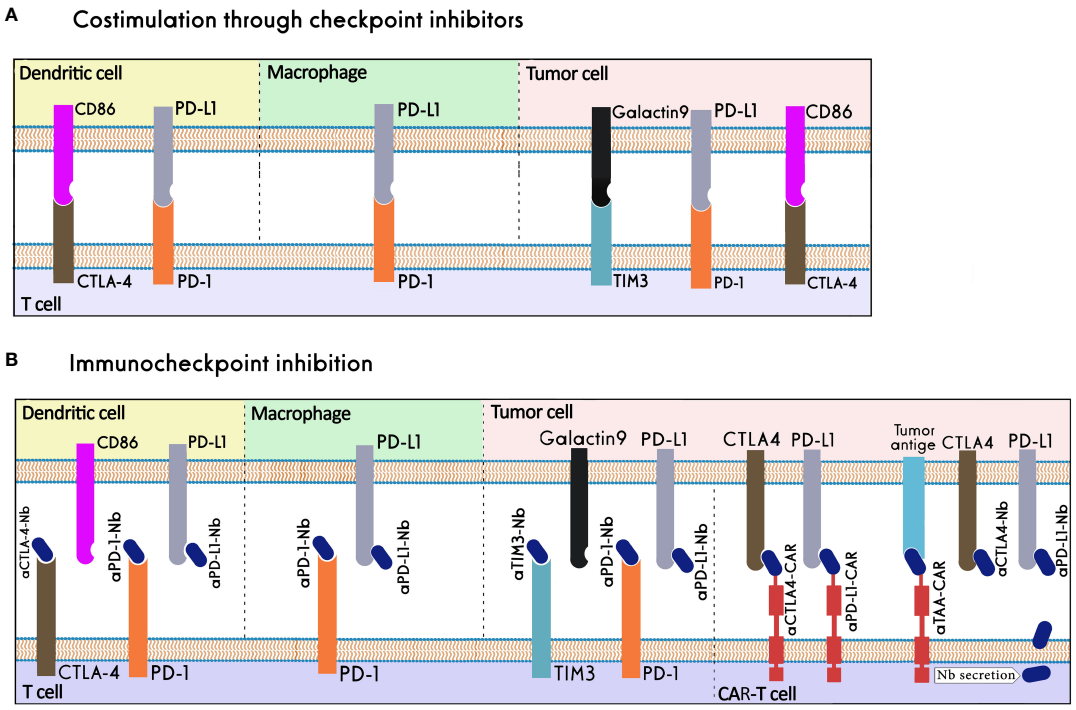

FIGURE 6
Nanobody-based Immune checkpoint Inhibition. **(A)** Immune checkpoints in physiological conditions. **(B)** Immune checkpoints in the tumor microenvironment, nanobodies can inhibit immune checkpoints by binding to them or their ligands, work as the binding domain in CAR-T cells, or be secreted in the tumor microenvironment by CAR-T cells.

effective against cancer diseases than PD-L1 mAbs (155). Moreover, an anti-PD1 nanobody, Nb97, was used to create the Nb97-Nb97-HSA fusion protein that demonstrated more efficacy in stimulating the immune function than a humanized Nb97-Fc (156). In order to draw the appropriate leukocyte populations in the TME, a PD-L1-blocking nanobody was fused to a charge-engineered chemokine CCL21. Using a microfluidic platform mimicking the TME, it was demonstrated the chemokine-nanobody fusion could selectively target PD-L1$^+$ tumor cells and recruit effector cells to the TME (157). A unique anti-PD-L1/CXCR4 bispecific nanobody could successfully penetrate the tumor tissues in a xenograft mouse model and inhibit the growth of pancreatic cancer cells much better than the combination therapy using anti-PD-L1 and anti-CXCR4 nanobodies (158).

A bispecific antibody consisting of an anti-PD-L1 antibody and an anti-TIGIT nanobody could bridge between PD-L1$^+$ tumor cells and T/NK cells leading to simultaneous blockade of PD-L1/PD-1 and TIGIT, enhanced infiltration of cytotoxic T lymphocytes (CTLs) and NK cells; and tumor growth inhibition in a mouse model (159). Moreover, a PD-L1/4-1BB bispecific nanobody can concurrently bind PD-L1 on tumor target cells and 4-1BB on effector cells. It can block the PD-L1/PD-1 pathway and induce 4-1BB signaling at the same time, leading to high antitumor potency with minimal toxicity (56).

A key inhibitory regulator of immunological responses is CTLA-4. Following T-cell activation, CTLA-4 rapidly expresses on T cells and has a higher affinity than CD28 for binding to B7 molecules. By increasing the threshold of signals needed for full T-cell activation, CTLA-4 may make it impossible for T cells to begin responding, and it may also cause them to stop responding already (148). Using phage display, four CTLA-4-specific nanobodies were isolated that had a strong binding capacity and were able to detect particular CTLA-4 epitopes. The survival of mice with melanoma increased after receiving the anti-CTLA-4 nanobody (Nb16) treatment because of the significant tumor growth inhibition (160). Moreover, this anti-CTLA-4 nanobody could increase the anti-tumor activities of cytotoxic T cells and prolong the survival of NOD/SCID mice bearing melanoma cells (151). The immunosuppression caused by the CTLA-4 pathway may limit the effectiveness of cellular therapy based on the tumor antigen-presenting dendritic cells and cytokine-induced killer cells (DC-CIK). An anti-CTLA-4 nanobody was used to suppress CTLA-4 signaling in order to counteract the negative co-stimulation from T cells. The DC-CIK cells displayed increased proliferation and IFN-γ production *in vitro* following stimulation with anti-CTLA-4, which intensified their lethal effect on the tumor cells (161). Another strategy to prevent ICs is to give nanobodies locally using CAR-T cells as cargo. The CAR-T cells that secrete anti-PD-L1 or anti-CTLA-4 nanobodies have better proliferation and persistence compared with nonsecreting CAR-T cells (162).

Alternative ICs, including TIM3, can be considered as a potential therapeutic target to obtain more effective anti-tumor responses in patients not responding to PD1/PDL1 and CTLA4 inhibitors (163). An anti-human TIM-3 nanobody was produced with an inhibitory impact equivalent to or superior to that of anti-TIM-3 antibodies. This nanobody demonstrated a high binding capacity to TIM-3 and a high anti-proliferative effect on the acute myeloid leukemia cell line HL-60 by disrupting the galectin/TIM-3 signal (164).

Considering their excellent tissue penetration properties, nanobodies are attractive candidates for blocking inhibitory receptors of immune

cells in the dense environment of solid tumor tissues. A nanobody targeting CTLA-4 has entered a phase I clinical trial for treating advanced/metastatic solid tumors (NCT04126590). In addition, anti-mesothelin CAR-T cells secreting PD-1 nanobodies are under clinical evaluation for mesothelioma, ovarian, colorectal, and non-small-cell lung cancers (NCT04489862, NCT05373147, NCT04503980).

7 The potential role of nanobodies in managing adverse effects of immune cell therapy

Despite the clinical success of BiTEs and CAR-T cells in the treatment of B-cell malignancies, CRS and its subsequent inflammatory effects reduce the effectiveness of these therapies in patients (165). Pyroptosis is an inflammatory cell death that is caused by pore-forming proteins such as Gasdermins (E and D). These proteins are activated by inflammatory caspases and cause pores in the cell membrane that results in releasing their cytosolic content containing high amounts of danger-associated molecular patterns (DAMPs). The DAMPs contribute to the initiation of the inflammasome activation and subsequent activation of macrophages, which produce high levels of proinflammatory cytokines such as IL-1β and IL-6, the main drivers of inflammatory events during CRS (166, 167). All types of inflammasomes require an adapter protein called ASC (apoptosis-associated speck-like protein containing a CARD, caspase recruitment domain) to be activated (Figure 7) which includes a pyrin domain (PYD) and a CARD. The main feature of inflammasome activation is the formation of ASC speck as a result of the oligomerization of ASC (PYD) filaments and their cross-linking with CARD, which creates a micrometer-sized structure (168). The blockage in these pathways can lead to disruption in inflammation.

A nanobody was developed against the CARD domain of human ASC protein to investigate how the inflammasome is activated under physiological conditions. *In vitro* studies have shown that this nanobody not only prevents the interaction between CARD and PYD but also inhibits the activation of various types of inflammasomes which indicates the importance of ASC protein in the construction of different types of inflammasomes (169). It was proved that this nanobody was able to inhibit the inflammatory function of post-pyroptotic inflammasomes, making nanobodies the first biological agents capable of disassembling precursors of inflammasomes *in vitro*. Nanobodies against human and mouse ASC could effectively inhibit ASC-Speck activity after pore formation in pyroptotic cells, whereas they did not interfere with the initial secretion of cytokine IL-1β before pyroptosis, which is necessary for host defense against infections (170).

P2X7 is a ligand-gated ion channel that detects extracellular ATP and initiates a pro-inflammatory signaling cascade that results in NLRP3 inflammasome activation and secretion of pro-inflammatory cytokines. The P2X7 ion channel is prominently expressed by monocytes and T cells and responds to extracellular ATP from damaged cells during sterile inflammation. Specific small-molecule inhibitors for P2X7 were developed for the treatment of inflammatory diseases by Pfizer (CE-224,535) and Astrazeneca (AZ-10606120 and AZD9056) (171, 172).

Studies show limitations of small molecule inhibitors, including short half-life *in vivo*, narrow therapeutic window, or toxic metabolites (173).

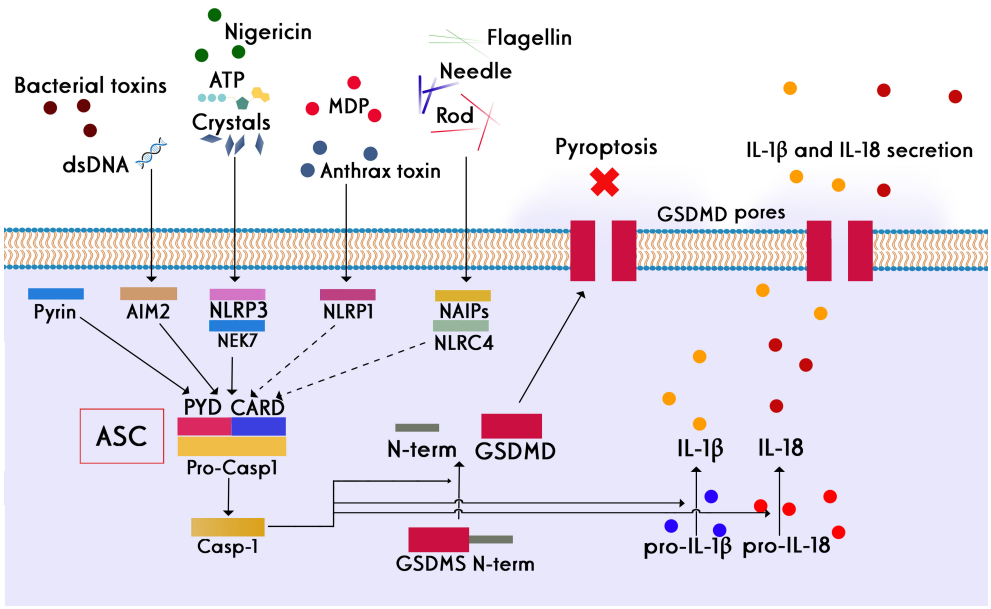

FIGURE 7
Different stimuli involved in the activation of different subsets of the inflammasome family and the canonical role of ASC in inflammasome assembly. Four key inflammasomes, namely NLRP1, NLRP3, NLRC4, and AIM2, have been best characterized. Following the activation of inflammasomes, inflammatory caspases are converted from the pro-active to the active form. The main consequence of this event is the creation of the active form of the pro-inflammatory cytokine interleukin 1 beta, which is one of the main drivers of inflammation. Apoptosis inhibitory proteins (NAIPs) function as direct receptors for bacterial flagellin and the needle and rod subunits. NLRP3 activation also requires NIMA-related kinase 7 (NEK7), which binds to the NLRP3 leucine-rich repeats (LRRs) and is required for its oligomerization. Many stimuli, such as bacterial lipopolysaccharide (LPS), crystals, extracellular ATP, and dsDNA, can activate the inflammasome complex. In addition to creating the active form of gasdermins, the consequence of inflammasome activation is the secretion of significant amounts of pro-inflammatory cytokines, such as IL-1β and IL-6, by macrophages, which are the main drivers of inflammatory events during CRS.

Due to the unique propensity of nanobodies to bind to functional crevices on proteins, these molecules can resolve the need for special bindings to ion channels (174). Highly potent nanobodies were isolated against mouse and human P2X7 ion channels, which showed higher specificity and lower toxicity in comparison to small molecule antagonists. The anti-mouse P2X7 nanobody could efficiently decrease inflammation in an experimental mouse model of glomerulonephritis. Compared with small-molecule inhibitors of P2X7, the anti-human P2X7 nanobody showed much more potency in preventing the IL-1β release, making it a viable biological option for controlling inflammatory cases associated with high content of cell damage and extracellular ATP (175). Another important player involved in the pathogenesis of CRS and neurotoxicity effects induced by CAR-T treatment is the pro-inflammatory cytokine IL-6. Inhibition of IL-6 signaling by tocilizumab, a mAb against IL-6 receptor (IL-6R), has been approved by the FDA as a biological treatment for the CAR-T-related CRS (176).

Unlike other cytokines, IL-6 can activate the signaling cascade by binding to a membrane receptor (mIL-6R; classical signaling) or to its soluble receptor (sIL-6R; trans-signaling) (177). A half-life extended bispecific nanobody was developed against IL-6R and HSA (human serum albumin) under the name ALX-0061. Different studies on this molecule proved its ability to inhibit IL-6 signaling equivalent to the tocilizumab antibody. ALX-0061 nanobody showed increased half-life and complete inhibition of inflammation in a monkey model of collagen-induced arthritis. Considering the promising results of this molecule in preclinical experiments, it is expected to be used as a biotherapeutic in the control of chronic inflammation and autoimmune diseases (178).

8 Conclusion

Antibodies are being widely explored for the activation of immune cells, including T cells, NK cells, and macrophages. Moreover, the retargeting of immune cells toward cancer cells has been achieved through tumor antigen-specific antibodies. Interestingly, antibodies could reverse the immunosuppressive state of the TME by immune checkpoint blockade. The superior properties of nanobodies compared to conventional antibodies make them ideal candidates for targeted modulation of immune cells in cancer therapies. Thanks to their high stability, enhanced infiltration into the TME of solid tumors and facile genetic engineering, nanobodies can act as complements to immune cell-mediated therapies. However, the fast clearance of nanobodies from circulation may preclude their utility for therapeutic applications. To improve their *in vivo* half-life, nanobodies can be modified by different approaches such as PEGylation, PASylation, addition of albumin-binding domains, and fusion to Fc domain of human antibodies.

The role of nanobodies in cell-mediated immunotherapy can be categorized into three types: bridging between tumor and immune cells, targeting tumor cells with immune cell-bound nanobodies, and blocking the inhibitory receptors expressed on immune cells (Figure 1). The nanobody-based bi- and multispecific cell engagers can make a bridge between tumor cells and immune effector cells leading to cell-mediated cytotoxicity. As T and NK cells' engagers, nanobodies have shown promising preclinical results in multiple myeloma and breast cancer, which provide insights to develop more specific nanobodies against the surface antigens of cancer and immune cells. The most successful application of nanobodies in cell-mediated immunity has been redirecting immune cells to attack tumor cells through a chimeric receptor incorporating a nanobody against the target antigen. Various cancer antigens have been targeted by nanobody-based CAR-T and CAR-NK cells for treating both hematological and solid malignancies. However, considering their clinical trials results, anti-BCMA NbCAR-T cells may be the first nanobody-based engineered immune cells to reach the market for treating multiple myeloma. Finally, by blocking the immune cells' inhibitory receptors, nanobodies can aid them to exert more efficient anti-tumor functions. As the potent immune checkpoint inhibitors, nanobodies can reverse the T cell exhaustion and restore anti-tumor immunity. Moreover, the anti-tumor functions of macrophages can be enhanced through nanobody-mediated blockade of the CD47/SIRPa pathway, reprogramming of macrophages from M2 to M1 phenotype and depletion of TAMs from the TME. Nanobodies against the inflammatory cytokines and proteins involved in pyroptosis can be used to prevent the severe side effects occurring in CAR-T cell therapy and might enable a safer anti-cancer immune cell therapy.

Taken together, nanobodies are appealing as potential therapeutics to effectively modulate the immune cells' functions, manage the inflammatory side effects of immune cell therapy and restore the immune surveillance to cancer patients.

Author contributions

ZS supervised and revised this manuscript. AM, MG, SF-N, AN, SS, and SM contributed to data collection, literature review, and manuscript drafting. All authors contributed to the article and approved the submitted version.

Acknowledgments

We gratefully acknowledge the Immunology Department of Pasteur Institute of Iran for their technical assistance.

Conflict of interest

The authors declare that the research was conducted in the absence of any commercial or financial relationships that could be construed as a potential conflict of interest.

Publisher's note

References

1. Sung H, Ferlay J, Siegel RL, Laversanne M, Soerjomataram I, Jemal A, et al. Global cancer statistics 2020: GLOBOCAN estimates of incidence and mortality worldwide for 36 cancers in 185 countries. *CA: Cancer J Clin* (2021) 71(3):209–49. doi: 10.3322/caac.21660

2. Dong Y, Wan Z, Gao X, Yang G, Liu L. Reprogramming immune cells for enhanced cancer immunotherapy: Targets and strategies. *Front Immunol* (2021) 12:609762. doi: 10.3389/fimmu.2021.609762

3. Cuciniello R, Filosa S, Crispi S. Novel approaches in cancer treatment: preclinical and clinical development of small non-coding RNA therapeutics. *J Exp Clin Cancer Res CR* (2021) 40(1):383. doi: 10.1186/s13046-021-02193-1

4. El-Kadiry AE, Rafei M, Shammaa R. Cell therapy: Types, regulation, and clinical benefits. *Front Med* (2021) 8:756029. doi: 10.3389/fmed.2021.756029

5. Kumar M, Thangavel C, Becker RC, Sadayappan S. Monoclonal antibody-based immunotherapy and its role in the development of cardiac toxicity. *Cancers* (2020) 13 (1):86. doi: 10.3390/cancers13010086

6. Anderson NM, Simon MC. The tumor microenvironment. *Curr Biol CB* (2020) 30 (16):R921–r5. doi: 10.1016/j.cub.2020.06.081

7. Guo S, Deng CX. Effect of stromal cells in tumor microenvironment on metastasis initiation. *Int J Biol Sci* (2018) 14(14):2083–93. doi: 10.7150/ijbs.25720

8. Yang EY, Shah K. Nanobodies: Next generation of cancer diagnostics and therapeutics. *Front Oncol* (2020) 10:1182. doi: 10.3389/fonc.2020.01182

9. Verhaar ER, Woodham AW, Ploegh HL. Nanobodies in cancer. *Semin Immunol* (2021) 52:101425. doi: 10.1016/j.smim.2020.101425

10. Bannas P, Hambach J, Koch-Nolte F. Nanobodies and nanobody-based human heavy chain antibodies as antitumor therapeutics. *Front Immunol* (2017) 8:1603. doi: 10.3389/fimmu.2017.01603

11. Finlay WJ, Almagro JC. Natural and man-made V-gene repertoires for antibody discovery. *Front Immunol* (2012) 3:342. doi: 10.3389/fimmu.2012.00342

12. Vincke C, Loris R, Saerens D, Martinez-Rodriguez S, Muyldermans S, Conrath K. General strategy to humanize a camelid single-domain antibody and identification of a universal humanized nanobody scaffold. *J Biol Chem* (2009) 284(5):3273–84. doi: 10.1074/jbc.M806889200

13. Klarenbeek A, El Mazouari K, Desmyter A, Blanchetot C, Hultberg A, de Jonge N, et al. Camelid ig V genes reveal significant human homology not seen in therapeutic target genes, providing for a powerful therapeutic antibody platform. *mAbs* (2015) 7(4):693–706. doi: 10.1080/19420862.2015.1046648

14. Hu Y, Liu C, Muyldermans S. Nanobody-based delivery systems for diagnosis and targeted tumor therapy. *Front Immunol* (2017) 8:1442. doi: 10.3389/fimmu.2017.01442

15. Hassanzadeh-Ghassabeh G, Devoogdt N, De Pauw P, Vincke C, Muyldermans S. Nanobodies and their potential applications. *Nanomed (London England)* (2013) 8 (6):1013–26. doi: 10.2217/nnm.13.86

16. Marino M, Zhou L, Rincon MY, Callaerts-Vegh Z, Verhaert J, Wahis J, et al. AAV-mediated delivery of an anti-BACE1 VHH alleviates pathology in an alzheimer's disease model. *EMBO Mol Med* (2022) 14(4):e09824. doi: 10.15252/emmm.201809824

17. Edavettal S, Cejudo-Martin P, Dasgupta B, Yang D, Buschman MD, Domingo D, et al. Enhanced delivery of antibodies across the blood-brain barrier *via* TEMs with inherent receptor-mediated phagocytosis. *Med (New York NY)* (2022) 3(12):860–82.e15. doi: 10.1016/j.medj.2022.09.007

18. Li T, Bourgeois JP, Celli S, Glacial F, Le Sourd AM, Mecheri S, et al. Cell-penetrating anti-GFAP VHH and corresponding fluorescent fusion protein VHH-GFP spontaneously cross the blood-brain barrier and specifically recognize astrocytes: application to brain imaging. *FASEB J* (2012) 26(10):3969–79. doi: 10.1096/fj.11-201384

19. Li T, Vandesquille M, Koukouli F, Dudeffant C, Youssef I, Lenormand P, et al. Camelid single-domain antibodies: A versatile tool for *in vivo* imaging of extracellular and intracellular brain targets. *J Control Release* (2016) 243:1–10. doi: 10.1016/j.jconrel.2016.09.019

20. Ruiz-Lopez E, Schuhmacher AJ. Transportation of single-domain antibodies through the blood-brain barrier. *Biomolecules* (2021) 11(8):1131. doi: 10.3390/biom11081131

21. Iqbal U, Albaghdadi H, Luo Y, Arbabi M, Desvaux C, Veres T, et al. Molecular imaging of glioblastoma multiforme using anti-insulin-like growth factor-binding protein-7 single-domain antibodies. *Br J cancer* (2010) 103(10):1606–16. doi: 10.1038/sj.bjc.6605937

22. Hussack G, Raphael S, Lowden MJ, Henry KA. Isolation and characterization of camelid single-domain antibodies against HER2. *BMC Res notes* (2018) 11(1):866. doi: 10.1186/s13104-018-3955-8

23. Araste F, Ebrahimizadeh W, Rasooli I, Rajabibazl M, Mousavi Gargari SL. A novel VHH nanobody against the active site (the CA domain) of tumor-associated, carbonic anhydrase isoform IX and its usefulness for cancer diagnosis. *Biotechnol lett* (2014) 36 (1):21–8. doi: 10.1007/s10529-013-1340-1

24. Sharifzadeh Z, Rahbarizadeh F, Shokrgozar MA, Ahmadvand D, Mahboudi F, Rahimi Jamnani F, et al. Development of oligoclonal nanobodies for targeting the tumor-associated glycoprotein 72 antigen. *Mol Biotechnol* (2013) 54(2):590–601. doi: 10.1007/s12033-012-9601-0

25. Huet HA, Growney JD, Johnson JA, Li J, Bilic S, Ostrom L, et al. Multivalent nanobodies targeting death receptor 5 elicit superior tumor cell killing through efficient caspase induction. *mAbs* (2014) 6(6):1560–70. doi: 10.4161/19420862.2014.975099

26. Slørdahl TS, Denayer T, Moen SH, Standal T, Børset M, Ververken C, et al. Anti-c-MET nanobody - a new potential drug in multiple myeloma treatment. *Eur J haematol* (2013) 91(5):399–410. doi: 10.1111/ejh.12185

27. Chen T, Liu X, Hong H, Wei H. Novel single-domain antibodies against the EGFR domain III epitope exhibit the anti-tumor effect. *J Trans Med* (2020) 18(1):376. doi: 10.1186/s12967-020-02538-y

28. Tang Z, Feng M, Gao W, Phung Y, Chen W, Chaudhary A, et al. A human single-domain antibody elicits potent antitumor activity by targeting an epitope in mesothelin close to the cancer cell surface. *Mol Cancer Ther* (2013) 12(4):416–26. doi: 10.1158/1535-7163.MCT-12-0731

29. Rashidi SK, Mousavi Gargari SL, Ebrahimizadeh W. Targeting colorectal cancer cell lines using nanobodies; AgSK1as a potential target. *Iranian J Biotechnol* (2017) 15 (2):78–86. doi: 10.15171/ijb.1472

30. Romão E, Krasniqi A, Maes L, Vandenbrande C, Sterckx YG, Stijlemans B, et al. Identification of nanobodies against the acute myeloid leukemia marker CD33. *Int J Mol Sci* (2020) 21(1):310. doi: 10.3390/ijms21010310

31. Yan Y, Cheng X, Li L, Zhang R, Zhu Y, Wu Z, et al. A novel small molecular antibody, HER2-nanobody, inhibits tumor proliferation in HER2-positive breast cancer cells *In vitro* and in vivo. *Front Oncol* (2021) 11:669393. doi: 10.3389/fonc.2021.669393

32. Rossotti MA, Henry KA, van Faassen H, Tanha J, Callaghan D, Hussack G, et al. Camelid single-domain antibodies raised by DNA immunization are potent inhibitors of EGFR signaling. *Biochem J* (2019) 476(1):39–50. doi: 10.1042/BCJ20180795

33. Guardiola S, Varese M, Sánchez-Navarro M, Vincke C, Teixidó M, García J, et al. Blocking EGFR activation with anti-EGF nanobodies *via* two distinct molecular recognition mechanisms. *Angewandte Chemie (International ed English)* (2018) 57 (42):13843–7. doi: 10.1002/anie.201807736

34. Vosjan MJ, Vercammen J, Kolkman JA, Stigter-van Walsum M, Revets H, van Dongen GA. Nanobodies targeting the hepatocyte growth factor: potential new drugs for molecular cancer therapy. *Mol Cancer Ther* (2012) 11(4):1017–25. doi: 10.1158/1535-7163.MCT-11-0891

35. Kazemi-Lomedasht F, Behdani M, Bagheri KP, Habibi-Anbouhi M, Abolhassani M, Arezumand R, et al. Inhibition of angiogenesis in human endothelial cell using VEGF specific nanobody. *Mol Immunol* (2015) 65(1):58–67. doi: 10.1016/j.molimm.2015.01.010

36. Arbabi-Ghahroudi M. Camelid single-domain antibodies: Promises and challenges as lifesaving treatments. *Int J Mol Sci* (2022) 23(9):5009. doi: 10.3390/ijms23095009

37. Jovčevska I, Muyldermans S. The therapeutic potential of nanobodies. *BioDrugs* (2020) 34(1):11–26. doi: 10.1007/s40259-019-00392-z

38. Xia A, Zhang Y, Xu J, Yin T, Lu XJ. T Cell dysfunction in cancer immunity and immunotherapy. *Front Immunol* (2019) 10:1719. doi: 10.3389/fimmu.2019.01719

39. Spranger S. Mechanisms of tumor escape in the context of the T-cell-inflamed and the non-t-cell-inflamed tumor microenvironment. *Int Immunol* (2016) 28(8):383–91. doi: 10.1093/intimm/dxw014

40. Pan MG, Xiong Y, Chen F. NFAT gene family in inflammation and cancer. *Curr Mol Med* (2013) 13(4):543–54. doi: 10.2174/1566524011313040007

41. Li X, Xiang Y, Li F, Yin C, Li B, Ke X. WNT/β-catenin signaling pathway regulating T cell-inflammation in the tumor microenvironment. *Front Immunol* (2019) 10:2293. doi: 10.3389/fimmu.2019.02293

42. Park YJ, Yoo SA, Kim M, Kim WU. The role of calcium-Calcineurin-NFAT signaling pathway in health and autoimmune diseases. *Front Immunol* (2020) 11:195. doi: 10.3389/fimmu.2020.00195

43. Goebeler ME, Bargou R. Blinatumomab: a CD19/CD3 bispecific T cell engager (BiTE) with unique anti-tumor efficacy. *Leukemia lymphoma* (2016) 57(5):1021–32. doi: 10.3109/10428194.2016.1161185

44. Goebeler ME, Knop S, Viardot A, Kufer P, Topp MS, Einsele H, et al. Bispecific T-cell engager (BiTE) antibody construct blinatumomab for the treatment of patients with Relapsed/Refractory non-Hodgkin lymphoma: Final results from a phase I study. *J Clin Oncol* (2016) 34(10):1104–11. doi: 10.1200/JCO.2014.59.1586

45. Moradi-Kalbolandi S, Sharifi KA, Darvishi B, Majidzadeh AK, Jalili N, Sadeghi S, et al. Evaluation the potential of recombinant anti-CD3 nanobody on immunomodulatory function. *Mol Immunol* (2020) 118:174–81. doi: 10.1016/j.molimm.2019.12.017

46. Khatibi AS, Roodbari NH, Majidzade AK, Yaghmaei P, Farahmand L. *In vivo* tumor-suppressing and anti-angiogenic activities of a recombinant anti-CD3ε nanobody in breast cancer mice model. *Immunotherapy* (2019) 11(18):1555–67. doi: 10.2217/imt-2019-0068

47. Harwood SL, Alvarez-Cienfuegos A, Nuñez-Prado N, Compte M, Hernández-Pérez S, Merino N, et al. ATTACK, a novel bispecific T cell-recruiting antibody with trivalent EGFR binding and monovalent CD3 binding for cancer immunotherapy. *Oncoimmunology* (2017) 7(1):e1377874. doi: 10.1080/2162402X.2017.1377874

48. Mølgaard K, Harwood SL, Compte M, Merino N, Bonet J, Alvarez-Cienfuegos A, et al. Bispecific light T-cell engagers for gene-based immunotherapy of epidermal growth

factor receptor (EGFR)-positive malignancies. *Cancer immunol immunother CII* (2018) 67(8):1251–60. doi: 10.1007/s00262-018-2181-5

49. Mandrup OA, Ong SC, Lykkemark S, Dinesen A, Rudnik-Jansen I, Dagnæs-Hansen NF, et al. Programmable half-life and anti-tumour effects of bispecific T-cell engager-albumin fusions with tuned FcRn affinity. *Commun Biol* (2021) 4(1):310. doi: 10.1038/s42003-021-01790-2

50. Khalique H, Baugh R, Dyer A, Scott EM, Frost S, Larkin S, et al. Oncolytic herpesvirus expressing PD-L1 BiTE for cancer therapy: Exploiting tumor immune suppression as an opportunity for targeted immunotherapy. *J immunother Cancer* (2021) 9(4):e001292. doi: 10.1136/jitc-2020-001292

51. Zhu X, Wang L, Liu R, Flutter B, Li S, Ding J, et al. COMBODY: one-domain antibody multimer with improved avidity. *Immunol Cell Biol* (2010) 88(6):667–75. doi: 10.1038/icb.2010.21

52. Liu J, Wu X, Lin L, Pan H, Wang Y, Li Y, et al. Bp-bs, a novel T-cell engaging bispecific antibody with biparatopic Her2 binding, has potent anti-tumor activities. *Mol Ther oncol* (2019) 14:66–73. doi: 10.1016/j.omto.2019.03.009

53. Xing J, Lin L, Li J, Liu J, Zhou C, Pan H, et al. BiHC, a T-Cell-Engaging bispecific recombinant antibody, has potent cytotoxic activity against Her2 tumor cells. *Trans Oncol* (2017) 10(5):780–5. doi: 10.1016/j.tranon.2017.07.003

54. Pan H, Liu J, Deng W, Xing J, Li Q, Wang Z. Site-specific PEGylation of an anti-CEA/CD3 bispecific antibody improves its antitumor efficacy. *Int J nanomed* (2018) 13:3189–201. doi: 10.2147/IJN.S164542

55. Tapia-Galisteo A, Sánchez Rodríguez Í, Aguilar-Sopeña O, Harwood SL, Narbona J, Ferreras Gutierrez M, et al. Trispecific T-cell engagers for dual tumor-targeting of colorectal cancer. *Oncoimmunology* (2022) 11(1):2034355. doi: 10.1080/2162402X.2022.2034355

56. Zhai T, Wang C, Xu Y, Huang W, Yuan Z, Wang T, et al. Generation of a safe and efficacious llama single-domain antibody fragment (vHH) targeting the membrane-proximal region of 4-1BB for engineering therapeutic bispecific antibodies for cancer. *J immunother Cancer* (2021) 9(6):e002131. doi: 10.1136/jitc-2020-002131

57. Mikkelsen K, Harwood SL, Compte M, Merino N, Mølgaard K, Lykkemark S, et al. Carcinoembryonic antigen (CEA)-specific 4-1BB-Costimulation induced by CEA-targeted 4-1BB-Agonistic trimerbodies. *Front Immunol* (2019) 10:1791. doi: 10.3389/fimmu.2019.01791

58. Compte M, Harwood SL, Muñoz IG, Navarro R, Zonca M, Perez-Chacon G, et al. A tumor-targeted trimeric 4-1BB-agonistic antibody induces potent anti-tumor immunity without systemic toxicity. *Nat Commun* (2018) 9(1):4809. doi: 10.1038/s41467-018-07195-w

59. Bachmann M. The UniCAR system: A modular CAR T cell approach to improve the safety of CAR T cells. *Immunol lett* (2019) 211:13–22. doi: 10.1016/j.imlet.2019.05.003

60. Han L, Zhou J, Zhou K, Zhu X, Zhao L, Fang B, et al. Safety and efficacy of CAR-T cell targeting BCMA in patients with multiple myeloma coinfected with chronic hepatitis b virus. *J immunother Cancer* (2020) 8(2):e000927. doi: 10.1136/jitc-2020-000927

61. Han L, Gao Q, Zhou K, Zhou J, Fang B, Zhang J, et al. The phase I clinical study of CART targeting BCMA with humanized alpaca-derived single-domain antibody as antigen recognition domain. *J Clin Oncol* (2019) 37(15_suppl):2535. doi: 10.1200/JCO.2019.37.15_suppl.2535

62. Han L, Zhang JS, Zhou J, Zhou KS, Xu BL, Li LL, et al. Single VHH-directed BCMA CAR-T cells cause remission of relapsed/refractory multiple myeloma. *Leukemia* (2021) 35(10):3002–6. doi: 10.1038/s-01269-021-41375

63. Zhao WH, Liu J, Wang BY, Chen YX, Cao XM, Yang Y, et al. A phase 1, open-label study of LCAR-B38M, a chimeric antigen receptor T cell therapy directed against b cell maturation antigen, in patients with relapsed or refractory multiple myeloma. *J Hematol Oncol* (2018) 11(1):141. doi: 10.1186/s13045-018-0681-6

64. Xu J, Chen LJ, Yang SS, Sun Y, Wu W, Liu YF, et al. Exploratory trial of a biepitopic CAR T-targeting b cell maturation antigen in relapsed/refractory multiple myeloma. *Proc Natl Acad Sci United States America* (2019) 116(19):9543–51. doi: 10.1073/pnas.1819745116

65. An N, Hou YN, Zhang QX, Li T, Zhang QL, Fang C, et al. Anti-multiple myeloma activity of nanobody-based anti-CD38 chimeric antigen receptor T cells. *Mol pharm* (2018) 15(10):4577–88. doi: 10.1021/acs.molpharmaceut.8b00584

66. De Munter S, Van Parys A, Bral L, Ingels J, Goetgeluk G, Bonte S, et al. Rapid and effective generation of nanobody based CARs using PCR and Gibson assembly. *Int J Mol Sci* (2020) 21(3):883. doi: 10.3390/ijms21030883

67. Zhang T, Wang T, You F, Li Z, Chen D, Zhang K, et al. Nanobody-based anti-CD22-chimeric antigen receptor T cell immunotherapy exhibits improved remission against b-cell acute lymphoblastic leukemia. *Transplant Immunol* (2022) 71:101538. doi: 10.1016/j.trim.2022.101538

68. Nix MA, Mandal K, Geng H, Paranjape N, Lin YT, Rivera JM, et al. Surface proteomics reveals CD72 as a target for *In vitro*-evolved nanobody-based CAR-T cells in KMT2A/MLL1-rearranged b-ALL. *Cancer discov* (2021) 11(8):2032–49. doi: 10.1158/2159-8290.CD-20-0242

69. Zhang M, Fu X, Meng H, Wang M, Wang Y, Zhang L, et al. A single-arm, open-label, pilot trial of autologous CD7-CAR-T cells for CD7 positive relapsed and refractory T-lymphoblastic Leukemia/Lymphoma. *Blood* (2021) 138(Supplement 1):3829. doi: 10.1182/blood-2021-149999

70. Pan J, Tan Y, Wang G, Deng B, Ling Z, Song W, et al. Donor-derived CD7 chimeric antigen receptor T cells for T-cell acute lymphoblastic leukemia: First-in-Human, phase I trial. *J Clin Oncol* (2021) 39(30):3340–51. doi: 10.1200/JCO.21.00389

71. Khaleghi S, Rahbarizadeh F, Ahmadvand D, Rasaee MJ, Pognonec P. A caspase 8-based suicide switch induces apoptosis in nanobody-directed chimeric receptor expressing T cells. *Int J hematol* (2012) 95(4):434–44. doi: 10.1007/s12185-012-1037-6

72. Bakhtiari SH, Rahbarizadeh F, Hasannia S, Ahmadvand D, Iri-Sofla FJ, Rasaee MJ. Anti-MUC1 nanobody can redirect T-body cytotoxic effector function. *Hybridoma (2005)* (2009) 28(2):85–92. doi: 10.1089/hyb.2008.0079

73. Iri-Sofla FJ, Rahbarizadeh F, Ahmadvand D, Rasaee MJ. Nanobody-based chimeric receptor gene integration in jurkat cells mediated by φC31 integrase. *Exp Cell Res* (2011) 317(18):2630–41. doi: 10.1016/j.yexcr.2011.08.015

74. Rajabzadeh A, Rahbarizadeh F, Ahmadvand D, Kabir Salmani M, Hamidieh AA. A VHH-based anti-MUC1 chimeric antigen receptor for specific retargeting of human primary T cells to MUC1-positive cancer cells. *Cell J* (2021) 22(4):502–13. doi: 10.22074/cellj.2021.6917

75. Hassani M, Hajari Taheri F, Sharifzadeh Z, Arashkia A, Hadjati J, van Weerden WM, et al. Construction of a chimeric antigen receptor bearing a nanobody against prostate a specific membrane antigen in prostate cancer. *J Cell Biochem* (2019) 120 (6):10787–95. doi: 10.1002/jcb.28370

76. Hassani M, Hajari Taheri F, Sharifzadeh Z, Arashkia A, Hadjati J, van Weerden WM, et al. Engineered jurkat cells for targeting prostate-specific membrane antigen on prostate cancer cells by nanobody-based chimeric antigen receptor. *Iran BioMed J* (2020) 24(2):81–8. doi: 10.29252/ibj.24.2.81

77. Hajari Taheri F, Hassani M, Sharifzadeh Z, Behdani M, Arashkia A, Abolhassani M. T Cell engineered with a novel nanobody-based chimeric antigen receptor against VEGFR2 as a candidate for tumor immunotherapy. *IUBMB Life* (2019) 71(9):1259–67. doi: 10.1002/iub.2019

78. Sharifzadeh Z, Rahbarizadeh F, Shokrgozar MA, Ahmadvand D, Mahboudi F, Jamnani FR, et al. Genetically engineered T cells bearing chimeric nanoconstructed receptors harboring TAG-72-specific camelid single domain antibodies as targeting agents. *Cancer lett* (2013) 334(2):237–44. doi: 10.1016/j.canlet.2012.08.010

79. Jamnani FR, Rahbarizadeh F, Shokrgozar MA, Mahboudi F, Ahmadvand D, Sharifzadeh Z, et al. T Cells expressing VHH-directed oligoclonal chimeric HER2 antigen receptors: towards tumor-directed oligoclonal T cell therapy. *Biochim Biophys Acta* (2014) 1840(1):378–86. doi: 10.1016/j.bbagen.2013.09.029

80. De Munter S, Ingels J, Goetgeluk G, Bonte S, Pille M, Weening K, et al. Nanobody based dual specific CARs. *Int J Mol Sci* (2018) 19(2):403. doi: 10.3390/ijms19020403

81. Wang H, Wang L, Li Y, Li G, Zhang X, Jiang D, et al. Nanobody-armed T cells endow CAR-T cells with cytotoxicity against lymphoma cells. *Cancer Cell Int* (2021) 21 (1):1–12. doi: 10.1186/s12935-021-02151-z

82. He X, Feng Z, Ma J, Ling S, Cao Y, Gurung B, et al. Bispecific and split CAR T cells targeting CD13 and TIM3 eradicate acute myeloid leukemia. *Blood* (2020) 135(10):713–23. doi: 10.1182/blood.2019002779

83. Zhou Z, Han Y, Pan H-B, Sang C-J, Shi D-L, Feng C, et al. Tri-specific CD19xCD20xCD22 VHH CAR-T cells (LCAR-AIO) eradicate antigen-heterogeneous b cell tumors, enhance expansion, and prolong persistence in preclinical in vivo models. *Blood* (2021) 138(Supplement 1):1700. doi: 10.1182/blood-2021-150650

84. Hazelton W, Ghorashian S, Pule M. Nanobody based tri-specific chimeric antigen receptor to treat acute myeloid leukaemia. *Blood* (2020) 136:10–1. doi: 10.1182/blood-2020-141214

85. Albert S, Arndt C, Feldmann A, Bergmann R, Bachmann D, Koristka S, et al. A novel nanobody-based target module for retargeting of T lymphocytes to EGFR-expressing cancer cells *via* the modular UniCAR platform. *Oncoimmunology* (2017) 6 (4):e1287246. doi: 10.1080/2162402X.2017.1287246

86. Albert S, Arndt C, Koristka S, Berndt N, Bergmann R, Feldmann A, et al. From mono- to bivalent: improving theranostic properties of target modules for redirection of UniCAR T cells against EGFR-expressing tumor cells *in vitro* and in vivo. *Oncotarget* (2018) 9(39):25597–616. doi: 10.18632/oncotarget.25390

87. Jureczek J, Feldmann A, Bergmann R, Arndt C, Berndt N, Koristka S, et al. Highly efficient targeting of EGFR-expressing tumor cells with UniCAR T cells *via* target modules based on cetuximab(®). *OncoTargets Ther* (2020) 13:5515–27. doi: 10.2147/OTT.S245169

88. Mo F, Duan S, Jiang X, Yang X, Hou X, Shi W, et al. Nanobody-based chimeric antigen receptor T cells designed by CRISPR/Cas9 technology for solid tumor immunotherapy. *Signal Transduct Target Ther* (2021) 6(1):80. doi: 10.1038/s41392-021-00462-1

89. Shankland KR, Armitage JO, Hancock BW. Non-Hodgkin lymphoma. *Lancet (London England)* (2012) 380(9844):848–57. doi: 10.1016/S0140-6736(12)60605-9

90. Mihara K, Yanagihara K, Takigahira M, Imai C, Kitanaka A, Takihara Y, et al. Activated T-cell-mediated immunotherapy with a chimeric receptor against CD38 in b-cell non-Hodgkin lymphoma. *J immunother (Hagerstown Md 1997)* (2009) 32(7):737–43. doi: 10.1097/CJI.0b013e3181adaff1

91. Bostwick DG, Pacelli A, Blute M, Roche P, Murphy GP. Prostate specific membrane antigen expression in prostatic intraepithelial neoplasia and adenocarcinoma: a study of 184 cases. *Cancer* (1998) 82(11):2256–61. doi: 10.1002/(SICI)1097-0142(19980601)82:11<2256::AID-CNCR22>3.0.CO;2-S

92. Nguyen A, Johanning G, Shi Y. Emerging novel combined CAR-T cell therapies. *Cancers* (2022) 14(6):1403. doi: 10.3390/cancers14061403

93. Xie YJ, Dougan M, Jailkhani N, Ingram J, Fang T, Kummer L, et al. Nanobody-based CAR T cells that target the tumor microenvironment inhibit the growth of solid tumors in immunocompetent mice. *Proc Natl Acad Sci United States America* (2019) 116 (16):7624–31. doi: 10.1073/pnas.1817147116

94. Derniame S, Vignaud JM, Faure GC, Béné MC, Massin F. Comparative T-cell oligoclonality in lung, tumor and lymph nodes in human non-small cell lung cancer. *Oncol Rep* (2005) 13(3):509–15. doi: 10.3892/or.13.3.509

95. Shah NN, Johnson BD, Schneider D, Zhu F, Szabo A, Keever-Taylor CA, et al. Bispecific anti-CD20, anti-CD19 CAR T cells for relapsed b cell malignancies: a phase 1 dose escalation and expansion trial. *Nat Med* (2020) 26(10):1569–75. doi: 10.1038/s41591-020-1081-3

96. Zah E, Nam E, Bhuvan V, Tran U, Ji BY, Gosliner SB, et al. Systematically optimized BCMA/CS1 bispecific CAR-T cells robustly control heterogeneous multiple myeloma. *Nat Commun* (2020) 11(1):2283. doi: 10.1038/s41467-020-16160-5

97. Zhao J, Lin Q, Song Y, Liu D. Universal CARs, universal T cells, and universal CAR T cells. *J Hematol Oncol* (2018) 11(1):132. doi: 10.1186/s13045-018-0677-2

98. Sutherland AR, Owens MN, Geyer CR. Modular chimeric antigen receptor systems for universal CAR T cell retargeting. *Int J Mol Sci* (2020) 21(19):7222. doi: 10.3390/ijms21197222

99. Liu D, Zhao J, Song Y. Engineering switchable and programmable universal CARs for CAR T therapy. *J Hematol Oncol* (2019) 12(1):69. doi: 10.1186/s13045-019-0763-0

100. Minutolo NG, Hollander EE, Powell DJJr. The emergence of universal immune receptor T cell therapy for cancer. *Front Oncol* (2019) 9:176. doi: 10.3389/fonc.2019.00176

101. Loureiro LR, Feldmann A, Bergmann R, Koristka S, Berndt N, Máthé D, et al. Extended half-life target module for sustainable UniCAR T-cell treatment of STn-expressing cancers. *J Exp Clin Cancer Res CR* (2020) 39(1):77. doi: 10.1186/s13046-020-01572-4

102. Shimasaki N, Jain A, Campana D. NK cells for cancer immunotherapy. *Nat Rev Drug discov* (2020) 19(3):200–18. doi: 10.1038/s41573-019-0052-1

103. Zheng F, Zhou J, Ouyang Z, Zhang J, Wang X, Muyldermans S, et al. Development and characterization of nanobodies targeting the kupffer cell. *Front Immunol* (2021) 12:641819. doi: 10.3389/fimmu.2021.641819

104. Behar G, Sibéril S, Groulet A, Chames P, Pugnière M, Boix C, et al. Isolation and characterization of anti-FcgammaRIII (CD16) llama single-domain antibodies that activate natural killer cells. *Protein eng des select PEDS* (2008) 21(1):1–10. doi: 10.1093/protein/gzm064

105. Dong B, Zhou C, He P, Li J, Chen S, Miao J, et al. A novel bispecific antibody, BiSS, with potent anti-cancer activities. *Cancer Biol Ther* (2016) 17(4):364–70. doi: 10.1080/15384047.2016.1139266

106. Zhao Y, Li Y, Wu X, Li L, Liu J, Wang Y, et al. Identification of anti-CD16a single domain antibodies and their application in bispecific antibodies. *Cancer Biol Ther* (2020) 21(1):72–80. doi: 10.1080/15384047.2019.1665953

107. van Faassen H, Jo DH, Ryan S, Lowden MJ, Raphael S, MacKenzie CR, et al. Incorporation of a novel CD16-specific single-domain antibody into multispecific natural killer cell engagers with potent ADCC. *Mol pharm* (2021) 18(6):2375–84. doi: 10.1021/acs.molpharmaceut.1c00208

108. Rothe A, Sasse S, Topp MS, Eichenauer DA, Hummel H, Reiners KS, et al. A phase 1 study of the bispecific anti-CD30/CD16A antibody construct AFM13 in patients with relapsed or refractory Hodgkin lymphoma. *Blood* (2015) 125(26):4024–31. doi: 10.1182/blood-2014-12-614636

109. Pahl JHW, Koch J, Götz JJ, Arnold A, Reusch U, Gantke T, et al. CD16A activation of NK cells promotes NK cell proliferation and memory-like cytotoxicity against cancer cells. *Cancer Immunol Res* (2018) 6(5):517–27. doi: 10.1158/2326-6066.CIR-17-0550

110. Arvindam US, van Hauten PMM, Schirm D, Schaap N, Hobo W, Blazar BR, et al. A trispecific killer engager molecule against CLEC12A effectively induces NK-cell mediated killing of AML cells. *Leukemia* (2021) 35(6):1586–96. doi: 10.1038/s41375-020-01065-5

111. Vallera DA, Oh F, Kodal B, Hinderlie P, Geller MA, Miller JS, et al. A HER2 tri-specific NK cell engager mediates efficient targeting of human ovarian cancer. *Cancers* (2021) 13(16):3994. doi: 10.3390/cancers13163994

112. Liu T, Wu Y, Shi L, Li L, Hu B, Wang Y, et al. Preclinical evaluation of [(99m)Tc]Tc-labeled anti-EpCAM nanobody for EpCAM receptor expression imaging by immuno-SPECT/CT. *Eur J Nucl Med Mol imaging* (2022) 49(6):1810–21. doi: 10.1007/s00259-021-05670-z

113. Roshan R, Naderi S, Behdani M, Cohan RA, Ghaderi H, Shokrgozar MA, et al. Isolation and characterization of nanobodies against epithelial cell adhesion molecule as novel theranostic agents for cancer therapy. *Mol Immunol* (2021) 129:70–7. doi: 10.1016/j.molimm.2020.10.021

114. Felices M, Lenvik TR, Kodal B, Lenvik AJ, Hinderlie P, Bendzick LE, et al. Potent cytolytic activity and specific IL15 delivery in a second-generation trispecific killer engager. *Cancer Immunol Res* (2020) 8(9):1139–49. doi: 10.1158/2326-6066.CIR-19-0837

115. Gleason MK, Verneris MR, Todhunter DA, Zhang B, McCullar V, Zhou SX, et al. Bispecific and trispecific killer cell engagers directly activate human NK cells through CD16 signaling and induce cytotoxicity and cytokine production. *Mol Cancer Ther* (2012) 11(12):2674–84. doi: 10.1158/1535-7163.MCT-12-0692

116. Banihashemi SR, Hosseini AZ, Rahbarizadeh F, Ahmadvand D. Development of specific nanobodies (VHH) for CD19 immuno-targeting of human b-lymphocytes. *Iranian J basic Med Sci* (2018) 21(5):455–64. doi: 10.22038/IJBMS.2018.26778.6557

117. Schmohl JU, Felices M, Todhunter D, Taras E, Miller JS, Vallera DA. Tetraspecific scFv construct provides NK cell mediated ADCC and self-sustaining stimuli *via* insertion of IL-15 as a cross-linker. *Oncotarget* (2016) 7(45):73830–44. doi: 10.18632/oncotarget.12073

118. González C, Chames P, Kerfelec B, Baty D, Robert P, Limozin L. Nanobody-CD16 catch bond reveals NK cell mechanosensitivity. *Biophys J* (2019) 116(8):1516–26. doi: 10.1016/j.bpj.2019.03.012

119. Schmidt P, Raftery MJ, Pecher G. Engineering NK cells for CAR therapy-recent advances in gene transfer methodology. *Front Immunol* (2020) 11:611163. doi: 10.3389/fimmu.2020.611163

120. Zhang C, Hu Y, Shi C. Targeting natural killer cells for tumor immunotherapy. *Front Immunol* (2020) 11:60. doi: 10.3389/fimmu.2020.00060

121. You F, Wang Y, Jiang L, Zhu X, Chen D, Yuan L, et al. A novel CD7 chimeric antigen receptor-modified NK-92MI cell line targeting T-cell acute lymphoblastic leukemia. *Am J Cancer Res* (2019) 9(1):64–78.

122. Hambach J, Riecken K, Cichutek S, Schütze K, Albrecht B, Petry K, et al. Targeting CD38-expressing multiple myeloma and burkitt lymphoma cells in vitro with nanobody-based chimeric antigen receptors (Nb-CARs). *Cells* (2020) 9(2):321. doi: 10.3390/cells9020321

123. Zhang G, Liu R, Zhu X, Wang L, Ma J, Han H, et al. Retargeting NK-92 for anti-melanoma activity by a TCR-like single-domain antibody. *Immunol Cell Biol* (2013) 91(10):615–24. doi: 10.1038/icb.2013.45

124. Gong L, Li Y, Cui K, Chen Y, Hong H, Li J, et al. Nanobody-engineered natural killer cell conjugates for solid tumor adoptive immunotherapy. *Small (Weinheim an der Bergstrasse Germany)* (2021) 17(45):e2103463. doi: 10.1002/smll.202103463

125. Polgárová K, Otáhal P, Šálek C, Pytlík R. Chimeric antigen receptor based cellular therapy for treatment of T-cell malignancies. *Front Oncol* (2022) 12:876758. doi: 10.3389/fonc.2022.876758

126. Cendrowicz E, Sas Z, Bremer E, Rygiel TP. The role of macrophages in cancer development and therapy. *Cancers* (2021) 13(8):1946. doi: 10.3390/cancers13081946

127. Poh AR, Ernst M. Targeting macrophages in cancer: From bench to bedside. *Front Oncol* (2018) 8:49. doi: 10.3389/fonc.2018.00049

128. Miyake M, Tatsumi Y, Gotoh D, Ohnishi S, Owari T, Iida K, et al. Regulatory T cells and tumor-associated macrophages in the tumor microenvironment in non-muscle invasive bladder cancer treated with intravesical bacille calmette-guérin: A long-term follow-up study of a Japanese cohort. *Int J Mol Sci* (2017) 18(10):2186. doi: 10.3390/ijms18102186

129. Yusa T, Yamashita YI, Okabe H, Nakao Y, Itoyama R, Kitano Y, et al. Survival impact of immune cells infiltrating peri-tumoral area of hepatocellular carcinoma. *Cancer sci* (2022) 113(12):4048–58. doi: 10.1186/s12885-020-6613-1

130. Najafi M, Hashemi Goradel N, Farhood B, Salehi E, Nashtaei MS, Khanlarkhani N, et al. Macrophage polarity in cancer: A review. *J Cell Biochem* (2019) 120(3):2756–65. doi: 10.1002/jcb.27646

131. Kashfi K, Kannikal J, Nath N. Macrophage reprogramming and cancer therapeutics: Role of iNOS-derived NO. *Cells* (2021) 10(11):3194. doi: 10.3390/cells10113194

132. Navegantes KC, de Souza Gomes R, Pereira PAT, Czaikoski PG, Azevedo CHM, Monteiro MC. Immune modulation of some autoimmune diseases: the critical role of macrophages and neutrophils in the innate and adaptive immunity. *J Trans Med* (2017) 15(1):36. doi: 10.1186/s12967-017-1141-8

133. Biswas SK, Mantovani A. Macrophage plasticity and interaction with lymphocyte subsets: cancer as a paradigm. *Nat Immunol* (2010) 11(10):889–96. doi: 10.1038/ni.1937

134. Celik M, Labuz D, Keye J, Glauben R, Machelska H. IL-4 induces M2 macrophages to produce sustained analgesia via opioids. *JCI Insight* (2020) 5(4):e133093. doi: 10.1172/jci.insight.133093

135. Kumari N, Choi SH. Tumor-associated macrophages in cancer: recent advancements in cancer nanoimmunotherapies. *J Exp Clin Cancer Res CR* (2022) 41(1):68. doi: 10.1186/s13046-022-02272-x

136. Nuhn L, Bolli E, Massa S, Vandenberghe I, Movahedi K, Devreese B, et al. Targeting protumoral tumor-associated macrophages with nanobody-functionalized nanogels through strain promoted azide alkyne cycloaddition ligation. *Bioconjugate Chem* (2018) 29(7):2394–405. doi: 10.1021/acs.bioconjchem.8b00319

137. Wang Y, Tiruthani K, Li S, Hu M, Zhong G, Tang Y, et al. mRNA delivery of a bispecific single-domain antibody to polarize tumor-associated macrophages and synergize immunotherapy against liver malignancies. *Adv mater (Deerfield Beach Fla)* (2021) 33(23):e2007603. doi: 10.1002/adma.202007603

138. Cioffi M, Trabulo S, Hidalgo M, Costello E, Greenhalf W, Erkan M, et al. Inhibition of CD47 effectively targets pancreatic cancer stem cells *via* dual mechanisms. *Clin Cancer Res* (2015) 21(10):2325–37. doi: 10.1158/1078-0432.CCR-14-1399

139. Schürch CM, Roelli MA, Forster S, Wasmer MH, Brühl F, Maire RS, et al. Targeting CD47 in anaplastic thyroid carcinoma enhances tumor phagocytosis by macrophages and is a promising therapeutic strategy. *Thyroid* (2019) 29(7):979–92. doi: 10.1089/thy.2018.0555

140. Velliquette RW, Aeschlimann J, Kirkegaard J, Shakarian G, Lomas-Francis C, Westhoff CM. Monoclonal anti-CD47 interference in red cell and platelet testing. *Transfusion* (2019) 59(2):730–7. doi: 10.1111/trf.15033

141. Ma L, Zhu M, Gai J, Li G, Chang Q, Qiao P, et al. Preclinical development of a novel CD47 nanobody with less toxicity and enhanced anti-cancer therapeutic potential. *J nanobiotechnol* (2020) 18(1):12. doi: 10.1186/s12951-020-0571-2

142. Dougan M, Ingram JR, Jeong HJ, Mosaheb MM, Bruck PT, Ali L, et al. Targeting cytokine therapy to the pancreatic tumor microenvironment using PD-L1-Specific VHHs. *Cancer Immunol Res* (2018) 6(4):389–401. doi: 10.1158/2326-6066.CIR-17-0495

143. Bolli E, Scherger M, Arnouk SM, Pombo Antunes AR, Straßburger D, Urschbach M, et al. Targeted repolarization of tumor-associated macrophages *via* imidazoquinoline-linked nanobodies. *Adv Sci (Weinheim Baden-Wurttemberg Germany)* (2021) 8 (10):2004574. doi: 10.1002/advs.202004574

144. Rao L, Zhao SK, Wen C, Tian R, Lin L, Cai B, et al. Activating macrophage-mediated cancer immunotherapy by genetically edited nanoparticles. *Adv mater (Deerfield Beach Fla)* (2020) 32(47):e2004853. doi: 10.1002/adma.202004853

145. Klichinsky M, Ruella M, Shestova O, Lu XM, Best A, Zeeman M, et al. Human chimeric antigen receptor macrophages for cancer immunotherapy. *Nat Biotechnol* (2020) 38(8):947–53. doi: 10.1038/s41587-020-0462-y

146. Chen HM, van der Touw W, Wang YS, Kang K, Mai S, Zhang J, et al. Blocking immunoinhibitory receptor LILRB2 reprograms tumor-associated myeloid cells and promotes antitumor immunity. *J Clin Invest* (2018) 128(12):5647–62. doi: 10.1172/JCI97570

147. Bono P, Pasanen A, Verlingue L, Jonge M, Miguel M, Skytta T, et al. Promising clinical benefit rates in advanced cancers alongside potential biomarker correlation in a phase I/II trial investigating bexmarilimab, a novel macrophage-guided immunotherapy. *J Clin Oncol* (2022) 40(16_suppl):2645. doi: 10.1200/JCO.2022.40.16_suppl.2645

148. Finn OJ. Immuno-oncology: understanding the function and dysfunction of the immune system in cancer. *Ann Oncol* (2012) 23 Suppl 8(Suppl 8):viii6–9. doi: 10.1093/annonc/mds256

149. Pardoll DM. The blockade of immune checkpoints in cancer immunotherapy. *Nat Rev Cancer* (2012) 12(4):252–64. doi: 10.1038/nrc3239

150. Gun SY, Lee SWL, Sieow JL, Wong SC. Targeting immune cells for cancer therapy. *Redox Biol* (2019) 25:101174. doi: 10.1016/j.redox.2019.101174

151. Tang Z, Mo F, Liu A, Duan S, Yang X, Liang L, et al. A nanobody against cytotoxic T-lymphocyte associated antigen-4 increases the anti-tumor effects of specific CD8(+) T cells. *J Biomed nanotechnol* (2019) 15(11):2229–39. doi: 10.1166/jbn.2019.2859

152. Salvador JP, Vilaplana L, Marco MP. Nanobody: outstanding features for diagnostic and therapeutic applications. *Anal bioanal Chem* (2019) 411(9):1703–13. doi: 10.1007/s00216-019-01633-4

153. Rotte A. Combination of CTLA-4 and PD-1 blockers for treatment of cancer. *J Exp Clin Cancer Res CR* (2019) 38(1):255. doi: 10.1186/s13046-019-1259-z

154. Zhang F, Wei H, Wang X, Bai Y, Wang P, Wu J, et al. Structural basis of a novel PD-L1 nanobody for immune checkpoint blockade. *Cell discov* (2017) 3:17004. doi: 10.1038/celldisc.2017.4

155. Broos K, Lecocq Q, Keersmaecker B, Raes G, Corthals J, Lion E, et al. Single domain antibody-mediated blockade of programmed death-ligand 1 on dendritic cells enhances CD8 T-cell activation and cytokine production. *Vaccines* (2019) 7(3):85. doi: 10.3390/vaccines7030085

156. Xian Z, Ma L, Zhu M, Li G, Gai J, Chang Q, et al. Blocking the PD-1-PD-L1 axis by a novel PD-1 specific nanobody expressed in yeast as a potential therapeutic for immunotherapy. *Biochem Biophys Res Commun* (2019) 519(2):267–73. doi: 10.1016/j.bbrc.2019.08.160

157. Fang T, Li R, Li Z, Cho J, Guzman JS, Kamm RD, et al. Remodeling of the tumor microenvironment by a Chemokine/Anti-PD-L1 nanobody fusion protein. *Mol Pharm* (2019) 16(6):2838–44. doi: 10.1021/acs.molpharmaceut.9b00078

158. Hao S, Xu S, Li L, Li Y, Zhao M, Chen J, et al. Tumour inhibitory activity on pancreatic cancer by bispecific nanobody targeting PD-L1 and CXCR4. *BMC Cancer* (2022) 22(1):1092. doi: 10.1186/s12885-022-10165-7

159. Zhong Z, Zhang M, Ning Y, Mao G, Li X, Deng Q, et al. Development of a bispecific antibody targeting PD-L1 and TIGIT with optimal cytotoxicity. *Sci Rep* (2022) 12(1):18011. doi: 10.1038/s41598-022-22975-7

160. Wan R, Liu A, Hou X, Lai Z, Li J, Yang N, et al. Screening and antitumor effect of an anti–CTLA–4 nanobody. *Oncol Rep* (2018) 39(2):511–8. doi: 10.3892/or.2017.6131

161. Wang W, Wang X, Yang W, Zhong K, He N, Li X, et al. A CTLA-4 blocking strategy based on nanoboby in dendritic cell-stimulated cytokine-induced killer cells enhances their anti-tumor effects. *BMC Cancer* (2021) 21(1):1029. doi: 10.1186/s12885-021-08732-5

162. Xie YJ, Dougan M, Ingram JR, Pishesha N, Fang T, Momin N, et al. Improved antitumor efficacy of chimeric antigen receptor T cells that secrete single-domain antibody fragments. *Cancer Immunol Res* (2020) 8(4):518–29. doi: 10.1158/2326-6066.CIR-19-0734

163. Yu S, Xiong G, Zhao S, Tang Y, Tang H, Wang K, et al. Nanobodies targeting immune checkpoint molecules for tumor immunotherapy and immunoimaging (Review). *Int J Mol Med* (2021) 47(2):444–54. doi: 10.3892/ijmm.2020.4817

164. Homayouni V, Ganjalikhani-Hakemi M, Rezaei A, Khanahmad H, Behdani M, Lomedasht FK. Preparation and characterization of a novel nanobody against T-cell immunoglobulin and mucin-3 (TIM-3). *Iranian J basic Med Sci* (2016) 19 (11):1201–8.

165. Morris EC, Neelapu SS, Giavridis T, Sadelain M. Cytokine release syndrome and associated neurotoxicity in cancer immunotherapy. *Nat Rev Immunol* (2022) 22(2):85–96. doi: 10.1038/s41577-021-00547-6

166. Liu Y, Fang Y, Chen X, Wang Z, Liang X, Zhang T, et al. Gasdermin e-mediated target cell pyroptosis by CAR T cells triggers cytokine release syndrome. *Sci Immunol* (2020) 5(43):eaax7969. doi: 10.1126/sciimmunol.aax7969

167. Tosato G, Jones KD. Interleukin-1 induces interleukin-6 production in peripheral blood monocytes. *Blood* (1990) 75(6):1305–10. doi: 10.1182/blood.V75.6.1305.1305

168. Dick MS, Sborgi L, Ruhl S, Hiller S, Broz P. ASC filament formation serves as a signal amplification mechanism for inflammasomes. *Nat Commun* (2016) 7:11929. doi: 10.1038/ncomms11929

169. Schmidt FI, Lu A, Chen JW, Ruan J, Tang C, Wu H, et al. A single domain antibody fragment that recognizes the adaptor ASC defines the role of ASC domains in inflammasome assembly. *J Exp Med* (2016) 213(5):771–90. doi: 10.1084/jem.20151790

170. Bertheloot D, Wanderley CW, Schneider AH, Schiffelers LD, Wuerth JD, Todtmann JM, et al. Nanobodies dismantle post-pyroptotic ASC specks and counteract inflammation in vivo. *EMBO Mol Med* (2022) 14(6):e15415. doi: 10.15252/emmm.202115415

171. Guile SD, Alcaraz L, Birkinshaw TN, Bowers KC, Ebden MR, Furber M, et al. Antagonists of the P2X(7) receptor. from lead identification to drug development. *J Med Chem* (2009) 52(10):3123–41. doi: 10.1021/jm801528x

172. Chrovian CC, Rech JC, Bhattacharya A, Letavic MA. P2X7 antagonists as potential therapeutic agents for the treatment of CNS disorders. *Prog Med Chem* (2014) 53:65–100. doi: 10.1016/B978-0-444-63380-4.00002-0

173. Sun H, Li M. Antibody therapeutics targeting ion channels: are we there yet? *Acta Pharmacol Sin* (2013) 34(2):199–204. doi: 10.1038/aps.2012.202

174. Wesolowski J, Alzogaray V, Reyelt J, Unger M, Juarez K, Urrutia M, et al. Single domain antibodies: promising experimental and therapeutic tools in infection and immunity. *Med Microbiol Immunol* (2009) 198(3):157–74. doi: 10.1007/s00430-009-0116-7

175. Danquah W, Meyer-Schwesinger C, Rissiek B, Pinto C, Serracant-Prat A, Amadi M, et al. Nanobodies that block gating of the P2X7 ion channel ameliorate inflammation. *Sci Trans Med* (2016) 8(366):366ra162. doi: 10.1126/scitranslmed.aaf8463

176. Le RQ, Li L, Yuan W, Shord SS, Nie L, Habtemariam BA, et al. FDA Approval summary: Tocilizumab for treatment of chimeric antigen receptor T cell-induced severe or life-threatening cytokine release syndrome. *Oncologist* (2018) 23(8):943–7. doi: 10.1634/theoncologist.2018-0028

177. Rose-John S. IL-6 trans-signaling *via* the soluble IL-6 receptor: importance for the pro-inflammatory activities of IL-6. *Int J Biol Sci* (2012) 8(9):1237–47. doi: 10.7150/ijbs.4989

178. Van Roy M, Ververken C, Beirnaert E, Hoefman S, Kolkman J, Vierboom M, et al. The preclinical pharmacology of the high affinity anti-IL-6R Nanobody(R) ALX-0061 supports its clinical development in rheumatoid arthritis. *Arthritis Res Ther* (2015) 17 (1):135. doi: 10.1186/s13075-015-0651-0

frontiers | Frontiers in Immunology

TYPE Original Research
PUBLISHED 16 February 2023
DOI 10.3389/fimmu.2023.1063838

OPEN ACCESS

EDITED BY
Mohammad Ali Shokrgozar,
Pasteur institute, Iran

REVIEWED BY
Tolga Sutlu,
Boğaziçi University, Türkiye
Kailin Xu,
Xuzhou Medical University, China

*CORRESPONDENCE
Fatemeh Rahbarizadeh
rahbarif@modares.ac.ir

SPECIALTY SECTION
This article was submitted to Cancer Immunity and Immunotherapy, a section of the journal Frontiers in Immunology

RECEIVED 07 October 2022
ACCEPTED 23 January 2023
PUBLISHED 16 February 2023

CITATION
Nasiri F, Safarzadeh Kozani P and Rahbarizadeh F (2023) T-cells engineered with a novel VHH-based chimeric antigen receptor against CD19 exhibit comparable tumoricidal efficacy to their FMC63-based counterparts.
Front. Immunol. 14:1063838.
doi: 10.3389/fimmu.2023.1063838

T-cells engineered with a novel VHH-based chimeric antigen receptor against CD19 exhibit comparable tumoricidal efficacy to their FMC63-based counterparts

Fatemeh Nasiri[1], Pooria Safarzadeh Kozani[1] and Fatemeh Rahbarizadeh[1,2]*

[1]Department of Medical Biotechnology, Faculty of Medical Sciences, Tarbiat Modares University, Tehran, Iran, [2]Research and Development Center of Biotechnology, Tarbiat Modares University, Tehran, Iran

Background: Chimeric antigen receptor (CAR)-T cell therapy has established itself as a potent therapeutic option for certain patients with relapsed/refractory (R/R) hematologic malignancies. To date, four CD19-redirected CAR-T cell products have been granted the United States Food and Drug Administration (FDA) approval for medical use. However, all of these products are equipped with a single-chain fragment variable (scFv) as their targeting domains. Camelid single-domain antibodies (VHH or nanobody) can also be used as alternatives to scFvs. In this study, we developed VHH-based CD19-redirected CAR-Ts, and compared them with their FMC63 scFv-based counterpart.

Methods: Human primary T cells were transduced to express a second-generation 4-1BB-CD3ζ-based CAR construct whose targeting domain was based on a CD19-specific VHH. The expansion rate, cytotoxicity, and secretion of proinflammatory cytokines (IFN-γ, IL-2, and TNF-α) of the developed CAR-Ts were assessed and compared with their FMC63 scFv-based counterpart as they were co-cultured with CD19-positive (Raji and Ramos) and CD19-negative (K562) cell lines.

Results: VHH-CAR-Ts showed an expansion rate comparable to that of the scFv-CAR-Ts. In terms of cytotoxicity, VHH-CAR-Ts mediated cytolytic reactions against CD19-positive cell lines, comparable to those of their scFv-based counterparts. Moreover, both VHH-CAR-Ts and scFv-CAR-Ts secreted remarkably higher and similar levels of IFN-γ, IL-2, and TNF-α upon co-cultivation with Ramos and Raji cell lines compared with while cultured alone or co-cultured with K562 cells.

Conclusion: Our results demonstrated that our VHH-CAR-Ts could mediate CD19-dependent tumoricidal reactions as potently as their scFv-based counterparts. Moreover, VHHs could be applied as the targeting domains of CAR constructs to overcome the issues associated with the use of scFvs in CAR-T therapies.

KEYWORDS

chimeric antigen receptor, CD19, cancer immunotherapy, hematologic malignancy, VHH, scFv

1 Introduction

Cancer immunotherapy has changed the face of the fight against cancer in the past decades. The advent of different platforms of cancer immunotherapy has proven its effectiveness for the treatment of a wide range of immunological and oncological indications (1, 2). Monoclonal antibodies (mAbs), T-cell-redirecting bispecific antibodies (TRBAs), antibody-drug conjugates (ADCs), tumor-infiltrating lymphocytes (TILs), and chimeric antigen receptor T cells (CAR-Ts) are now known as revolutionary second-, third-, fourth-, and fifth-line treatments for special groups of patients. CAR-T therapy has experienced a rapid progress in the past decade as the US Food and Drug Administration (FDA) approved six products for five different malignancies (3–15). So far, CAR-Ts have been granted approval for the treatment of patients with hematologic malignancies which include B-cell precursor acute lymphoblastic leukemia (B-ALL; *tisagenlecleucel* and *brexucabtagene autoleucel*), diffuse large B-cell lymphoma (DLBCL; *tisagenlecleucel*, *axicabtagene ciloleucel*, and *lisocabtagene maraleucel*), follicular lymphoma (FL; *tisagenlecleucel* and *axicabtagene ciloleucel*), mantle cell lymphoma (MCL; *brexucabtagene autoleucel*), and multiple myeloma (MM; *ciltacabtagene autoleucel* and *idecabtagene vicleucel*) (16). It is interesting to mention that four of the approved CAR-T products target CD19 as their target antigen while the other two (namely, *ciltacabtagene autoleucel* and *idecabtagene vicleucel*) target B-cell maturation antigen (BCMA).

CD19 has been an interesting target antigen for immunotherapy (17, 18). To date, aside from four FDA-approved CD19-redirected CAR-T products, one TRBA (*Blinatumomab*), two humanized mAbs (*Tafasitamab* and *Inebilizumab*), and one humanized ADC (*Loncastuximab tesirine*) have also been granted FDA approval against CD19, which accentuates its potential as one of the most, if not the most, successful target antigens of cancer immunotherapy. Also, numerous clinical trials are currently investigating the safety and efficacy of different CD19-redirected CAR T cells in Phase II and III (NCT05281809, NCT04605666, NCT04257175, etc.).

The production of a conventional CAR-T product entails blood sampling from the patient, isolation of peripheral blood mononuclear cells (PBMCs), genetic engineering of the isolated T cells for the expression of CAR molecules, and reinfusion of the generated CAR-Ts into the patient (19). A CAR molecule is topologically made from three domains; the extracellular domain, the transmembrane domain, and the intracellular domain. The intracellular domain of CARs is where the signaling domains are incorporated (4-1BB-CD3ζ or CD28-CD3ζ in the case of the FDA-approved CAR-Ts) while the extracellular domain redirects the cytotoxicity of CAR-Ts against cells expressing the target antigen (for which the targeting domain of CAR is specific) (16). CAR targeting domains are usually derived from the single-chain fragment variable (scFv) of mAbs; however, researchers have recently applied other targeting domains such as single variable domain on a heavy chain (VHH; also referred to as nanobodies), peptides, and ligands (20). Of note, the targeting domain of Janssen's *ciltacabtagene autoleucel* is based on BCMA-specific single-domain antibodies (20). Such efforts alongside successful clinical records prove that CAR-T products could be developed using targeting domains other than scFvs (20). In this research, we constructed a VHH-based CD19-redirected CAR molecule using a CD19-specific VHH previously isolated in our laboratory, and developed VHH-based CD19-redirected CAR-Ts (hereafter referred to as VHH-CAR-Ts) (21). Then, we assessed the tumoricidal efficacy of the VHH-CAR-Ts against CD19-positive cell lines to demonstrate that they can be as potent as FMC63 scFv-based CAR-Ts *in vitro*.

2 Materials and methods

2.1 Cells

All of the cell lines used in this study were purchased from National Cell Bank of Iran (NCBI), and Pasteur Institute (Tehran, Iran), and were cultured in a humidified condition at 37°C (5% CO_2). Human embryonic kidney 293T (HEK293T) cells were cultured in high glucose Dulbecco's Modified Eagles Medium (DMEM; Gibco, Life Technologies, USA) supplemented with 10% (v/v) fetal bovine serum (FBS; Gibco, Life Technologies, USA), 1 mM sodium pyruvate, 4 mM L-glutamine, and 1% penicillin-streptomycin (100 IU/mL). HEK293T cells were used for the production of lentiviral particles and the titration of the produced lentiviruses. Burkitt's lymphoma cell lines Raji and Ramos were used as CD19-positive human blood cancer cells, and K562 was used as CD19-negative human blood cancer cells, and were cultured and maintained in Roswell Park Memorial Institute (RPMI) 1640 (Gibco, Life Technologies, USA) supplemented with 4 mM L-glutamine, 1 mM sodium pyruvate, 1% penicillin-streptomycin (100 IU/ml), and 10% (v/v) FBS. Raji, Ramos, and K562 cells were applied for evaluating the specific cytotoxicity, proliferation, and cytokine secretion of VHH-CAR-Ts and scFv-CAR-Ts upon co-cultivation.

Human blood samples were collected from healthy donors (HD; n = 3) after obtaining written informed consent according to the guidelines and the approval of *Tarbiat Modares University Research Ethics Committee*. PBMCs were isolated using density gradient centrifugation by diluting the obtained blood in phosphate-buffered saline (PBS; with a ratio of 1:1 v/v) and slowly layering it over Ficoll-Hypaque (Lymphodex, Inno-Train, Germany) followed by centrifugation at 800 × g for 20 minutes at room temperature. Then, the PBMC layer was harvested carefully and washed twice with PBS. Ultimately, the obtained primary T cells were cultured in complete RPMI 1640 media (10% FBS v/v) supplemented with 50 IU/mL interleukin (IL)-2 (MACS, Miltenyi Biotec, BIOTEC GmbH, Germany). Dynabeads™ Human T-Activator CD3/CD28 (Gibco, Thermo Fisher Scientific, USA; catalog No. #11131D) were used to activate primary T cells at a bead-to-cell ratio of 2:1. Lentiviral transduction with the desired multiplicity of infection (MOI) was carried out on the activated T cells after three days of incubation at 37°C (5% CO_2).

2.2 Plasmids and reagents

The pLJM1 lentiviral vector encoding the green fluorescent protein (*PLJM1-EGFP*; Cat. No. #19319; Addgene, MA, USA) was used as the GFP control transfer vector (lentiviral control used for the transduction of T cells without CAR expression, hereinafter referred to as CAR-negative cells) in this study for virus production, titration steps, and functional assays. Two other versions of this vector were also generated; one encoding "anti-CD19.VHH.CAR-4-1BB-CD3ζ" as our main transfer vector (called *pLJM1VHH19*), and the other one encoding "anti-CD19.scFv.CAR-4-1BB-CD3ζ" (called *pLJM1scFv19*) applied as the positive control. Of note, pLJM1scFv19 harbors the same CAR construct as pLJM1VHH19 with the only exception that the targeting domain of pLJM1scFv19 is composed of the CD19-specific scFv, FMC63, rather than our CD19-specific VHH. To transfer the CAR transgenes into T cells, third-generation lentiviruses were used. In this regard, two packaging plasmids, "*pMDLg/pRRE*" and "*pRSV/Rev*", and one envelope plasmid, "*pMD2G*", were used alongside the transfer vector in the co-transfection process for the encapsulation of the third-generation lentiviruses. Moreover, polyethylenimine (PEI; 25 kDa; Cat. No. #9002-98-6, Sigma-Aldrich, Merck KGaA, Germany) was used as the transfection enhancer/reagent during the process of plasmid co-transfection and lentiviral packaging.

2.3 CAR construct

The VHH-based CD19-redirected CAR cassette contained the coding sequences for a CD19-specific VHH along with CD8α, followed by the 4-1BB costimulatory domain and the CD3ζ signaling domain, all of which were synthesized by Genscript (Piscataway, NJ, USA). This construct was PCR-amplified using the following oligonucleotide primers 5' GCTAGCATGGCCTTACCAGTG 3' and 5' TTCGAACTAGCGAGGGGGCAG 3' as forward and reverse primers, respectively. The forward and reverse primers were designed to introduce NheI (New England Biolabs, MA, USA) and BstbI (New England Biolabs, MA, USA) restriction sites at the 5' and 3' end of the CAR construct, respectively. The resultant CAR construct was subcloned into the pLJM1-EGFP vector using the mentioned restriction enzymes and T4 DNA ligase (Thermo Fisher Scientific, MA, USA). Finally, plasmid extraction was carried out using the Geno pure Plasmid Maxi Kit (Roche; Cat No. #03143422001) as an endotoxin-free kit for large-scale plasmid DNA isolation with sufficient high-quality.

2.4 Co-transfection and lentiviral packaging

12 hours prior to co-transfection, HEK293T cells (1.5×10^6; at a confluency rate of ~80%) were seeded in 6-well treated tissue culture plates. 10 hours later, the media was replaced with fresh media containing 2% v/v FBS. Next, the polyplex supernatant for lentiviral production was prepared by co-transfecting a lentiviral transfer vector (PLJM1-EGFP, pLJM1VHH19 or pLJM1scFV19), and two lentiviral packaging vectors and one envelope vector at a ratio of 4:(2:2):1, respectively, using PEI as the transfection reagent. Four different ratios of PEI:DNA (w/w; 1:1, 2:1, 3:1, and 4:1) were tested during co-transfection to determine the PEI:DNA mixture ratio with lowest toxic effects yielding the maximum viral titration. The GFP-expressing cells were detected under a fluorescence microscope, 24 to 72 hours after transfection. Furthermore, the transfection efficiency for the optimal non-toxic ratio of PEI:DNA was determined using flow cytometry analysis (BD FACSCalibur flow cytometer, BD Biosciences, San Jose, California, USA) 24 hours after transfection. For this aim, the cells were stained with propidium iodide (PI; Sigma-Aldrich, Merck KGaA, Germany) before flow cytometry analyses. For data analysis, the population of cells were first gated on PI-negative cells (live cells) and then the expression of GFP was assessed in that population. Also, the titration of the produced lentiviral particles was assessed using flow cytometry analysis and quantitative PCR (qPCR) 72 hours after transduction in every sample. Of note, the virus-containing supernatant was collected 24, 48, and 72 hours after transfection, concentrated using ultracentrifugation, and stored at -80°C for the further steps of the study.

2.5 Genome integration analysis for determining viral titration

To analyze the quality and quantity of the recombinant viral particles, the flow cytometry assay was used for the assessment of GFP and CAR expression in the relative groups, and quantitative PCR (qPCR) to determine vector copy numbers. For this aim, HEK293T cells (2×10^4 per well) were seeded into a treated 96-well tissue culture plate with incomplete DMEM media overnight prior to transduction. In the following step, the supernatant samples containing lentiviral particles were thawed on ice, and multiple serial dilutions of them were prepared (10^{-1}, 30^{-1},10^{-2}, 30^{-2}, 10^{-3}, and 30^{-3}) in DMEM high glucose media containing 8 µg/mL polybrene (hexadimethrine bromide, Sigma-Aldrich, Merck KGaA, Germany), and then they were incubated 30 minutes at 37°C (5% CO_2). Seeded HEK293T cells were transduced with lentivirus serial dilutions and were incubated for 12 hours at 37°C (5% CO_2), followed by an exchange of fresh complete DMEM media, and incubation. For the flow cytometry assay, the transduced cells were trypsinized 72 hours after transduction (to ensure gene expression), then the cells were

suspended in PBS. Finally, the expression of the transgene of each group (GFP, scFv-based CARs, and VHH-based CARs) was evaluated by flow cytometry for determining viral titers in transduction units (TU)/mL. Moreover, the genomic DNA was extracted from the transduced HEK293T cells using a High Pure PCR Template Purification Kit (Roche, Mannheim, Germany) for calculating the copy number of the integrated transgenes using a concentration standard curve (with known titers). To verify that free plasmid was removed from the media, q-PCR was performed after two passages (every three days over the course of 10 days) with primers specific for the puromycin gene (the viral resistance gene as an integrated sequence). qPCR was conducted on a Corbett Rotor-Gene 6000 instrument (Corbett Life Science; Sydney, Australia) using the following materials: 10 µL of Taq DNA Polymerase 2x Master Mix RED (Ampliqon; Cat. No. #A190303), 0.4 µM of each primer, template and distilled nuclease-free water to reach the final volume of 20 µl. The qPCR was performed in two steps with the following thermal settings: 15 minutes at 95°C for an initial Taq DNA polymerase activation step with hot start followed by 40 amplification cycles (30 seconds at 95°C and 30 seconds at 60°C). The test samples, standards, and negative and positive controls were all performed in duplicate. The cycle threshold (Ct) was set at 37 ± 2 since it does not adversely affect detection sensitivity. Of note, the forward and reverse puromycin primers were 5' GCAGCAA CAGATGGAAGG 3' and 5' GAGGTCTCCAGGAAGGC 3', respectively.

2.6 T cell lentiviral transduction

Primary T cells were activated using Dynabeads™ Human T-Activator CD3/CD28 and 100 IU/mL IL-2 while being incubated for 3 days prior to lentiviral transduction. Next, the media of the activated cells were replaced with concentrated lentiviral supernatant supplemented with polybrene at a concentration of 6 µg/mL of culture media. Next, the cells were centrifuged for 60 minutes at 1200 × g at 25°C. The stimulation beads were removed after 6-8 days of culture following transduction. Also, T cell culture media was supplemented with 50 IU/mL IL-2 three times per week. For flow cytometry analysis, the population of the cells were first gated on CD3-positive cells, and then the percentage of CAR-positive cells was analyzed in each cell population.

2.7 Target antigen-triggered activation and proliferation of CAR-Ts

The target cell-triggered expansion capability of the CAR-Ts was analyzed using the carboxyfluorescein succinimidyl ester (CFSE; BioLegend, San Diego, CA; Cat No. 423801) cell staining assay (22). Briefly, 10^6 - 10^7 effector T cells were labeled with 1 µL of 5 mM CFSE per mL of PBS. After a 20-minute incubation in a dark condition at 37°C (5% CO_2), the stained cells were resuspended in PBS, washed twice, and incubated overnight in culture media. The CFSE-stained effector cells were co-cultured with stimulator target cell lines without IL-2 at an effector-to-target (E:T) ratio of 6:1. After 72 hours of incubation, the effector cells were stained with APC-conjugated anti-human CD3 antibody and the CFSE signal reduction through the CD3+ cells division was assessed by flow cytometry. Also, the Mitomycin C inactivation protocol was used for inhibiting the proliferation of target cells. Briefly, 10^6 target cells were incubated with 50 µL of 1 mg/mL mitomycin C for 1 hour before co-culturing with the respective effector cells.

2.8 Cytotoxicity assessment

A cytotoxicity test was conducted by staining the target cells of CAR-Ts with PI while gating on CFSE-labeled target cells. In detail, CAR-Ts were co-cultured with CFSE-stained (in accordance with the previous protocol) K562, Raji, and Ramos target cells at different E:T ratios (3:1, 6:1, and 10:1) for 16 hours followed by PI staining to measure cell death *via* flow cytometry. Target cells included the CD19-negative cell line K562 (used as negative control) and the CD19-positive cell lines Raji and Ramos. For flow cytometry analysis, the population of cells was first gated on CFSE-positive cells, and then the percentage of apoptotic cells was assessed in that population (as PI-positive cells).

2.9 Inflammatory cytokine production of CAR-Ts

The level of CAR-T-secreted cytokines including human IFN-γ (human IFN-γ ELISA Kit; ab46025, Abcam, MA, USA), human TNF-α (human TNF-α ELISA Kit; ab46087; Abcam, MA, USA), and human IL-2 (human IL-2 ELISA Kit; ab100566; Abcam, MA, USA) was measured in the supernatant of the cells *via* enzyme-linked immunosorbent assay (ELISA) according to the manufacturer's instructions. Briefly, CAR-Ts were co-cultured with the target cells at an E:T ratio of 6:1, and the supernatant was collected 24 hours after incubation.

2.10 Flow cytometry antibodies and antigens

FITC-conjugated human CD19 antigens (Cat. No. CD9-HF2H2; Acro Biosystems, Newark, NJ, USA) were used for determining the expression rate of the VHH-based and scFv-based CAR molecules on the surface of VHH-CAR-Ts and scFv-CAR-Ts, respectively, in the flow cytometry assay. The concentration of the FITC-conjugated CD19 antigen and the number of cells used for the flow cytometry assay were according to the manufacturer's instructions. APC-conjugated anti-human CD3 antibody (BD Pharmingen™, USA; Cat No. #555335) was used to assess the percentage of CD3-positive cells in a given population of PBMCs, according to the manufacturer's instructions.

2.11 Statistical analyses

Statistical analyses were performed using GraphPad Prism version 8.01 (Graph Pad Software, Inc., USA). The mean values for each group were calculated, and the error bars indicate the standard deviation. Statistical significance was determined using one-way ANOVA with Tukey's multiple comparison test. Significances are

represented as * for p values < 0.05, ** for p values < 0.01, *** for p values < 0.001, and **** for p values < 0.0001.

3 Results

3.1 PEI:DNA ratio optimization and lentiviral packaging

The percentage of living cells as well as the percentage of cells expressing GFP were quantified 24 hours after transfection to determine the most appropriate PEI:DNA ratio. As presented in Figures 1A, B, PEI:DNA ratios of 1:1 and 2:1 did not result in a remarkable decline in the level of living HEK293T cells; however, the 3:1 and 4:1 ratios mediated significant cytotoxicity against these cells, resulting in 68.5 and 52.4% living cells, respectively. In terms of GFP expression, the highest proportion of GFP-expressing cells was detected in the 2:1 and 1:1 PEI:DNA ratio groups with 74.1 and 58.2%, respectively. Overall, the PEI:DNA ratio of 2:1 resulted in the highest percentage of GFP-expressing HEK293T cells and the lowest rate of cells damaged by the cytotoxic effects of PEI; therefore, this ratio was selected as the optimized PEI:DNA ratio. Also, according to the statistical analysis (presented in Figure 1B), the PEI:DNA ratio of 2:1 mediated a significantly higher rate of transfection in comparison with other PEI:DNA ratios (p value < 0. 01 for PEI:DNA ratio of 1:1 and 2:1, and p value < 0.0001 for PEI:DNA ratio of 3:1 and 4:1). Furthermore, in terms of post-transfection cell viability, the viability of HEK293T cells was significantly higher in the PEI:DNA ratio of 1:1 and 2:1 group in comparison with other PEI:DNA ratios (p value < 0. 001 for PEI:DNA ratio of 3:1 and p value < 0.0001 for PEI:DNA ratio of 4:1). Moreover, GFP expression rate in the transfected HEK293T cells was also detected under a fluorescence microscope. The different PEI:DNA ratios resulted in different GFP expression levels in the transfected cells (data not shown).

3.2 Viral titration and transduction optimization

In the process of CAR-T manufacturing, it is important to know the concentration of the produced viral particles. In addition, determining the MOI of the produced viral particles helps optimize

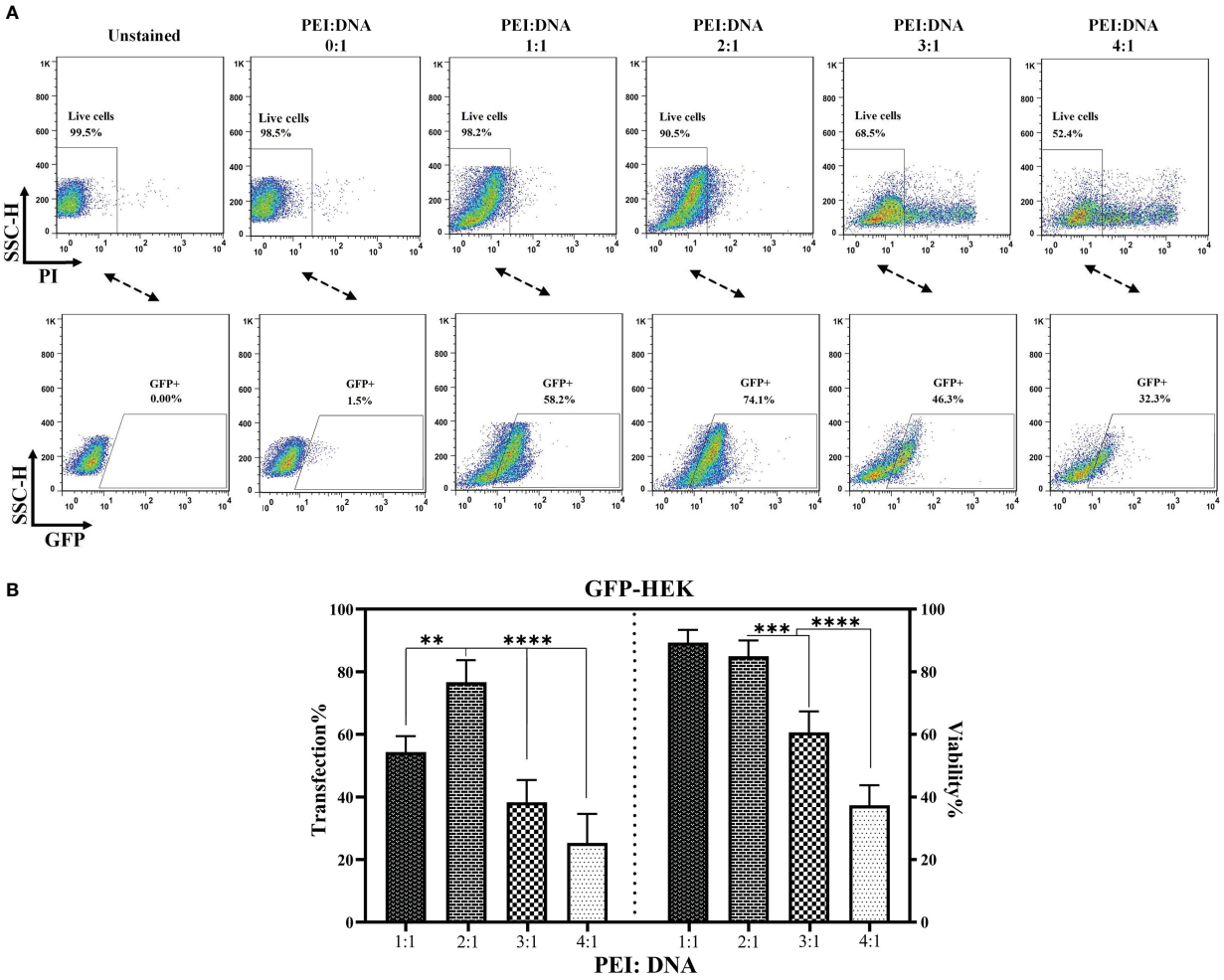

FIGURE 1
PEI:DNA ratio optimization for lentiviral packaging. **(A)** Flow cytometry plots for GFP-expressing cells and the post-transfection viability of HEK293T cells. **(B)** Statistical analysis between different groups of HEK293T cells transfected using four different PEI:DNA ratios. Data are expressed as the mean ± SD. **p < 0.01, ***p < 0.001, and ****p < 0.0001. All experiments were carried out in triplicate.

gene delivery into T cells during CAR-T production. To ensure maximum accuracy and compensate for multiple transduction events per cell, the viral particle titers were calculated by two practical assessments: flow cytometry analysis for the cells that express the integrated transgene and qPCR to assess the relative copy number of the produced lentiviral particles. As the results indicated, there was a close correlation between the expression of GFP, VHH-based CAR molecules, and scFv-based CAR molecules in the corresponding groups and the amount of the produced lentiviral particles as TU/mL (data not shown). MOI of 1, 5, 10, 15, 25 were considered for the transduction of T cells. As the results indicated (Figure 2), MOI of 10 mediated the highest rate of transduction alongside the lowest rate of rate of cytotoxicity; therefore, this MOI was selected for the transduction of T cells for the rest of the experiments. In reference to the flow cytometry result analysis, the population of cells were first gated on PI-negative cells (live cells). Next, the PI-negative cells were gated on the expression of CD3 (CD3-positive cells), and then the population of CAR-positive cells was assessed in each cell population.

3.3 Lentiviral transduction and assessment of CAR expression rate on the surface of CAR-Ts

Lentiviral transduction of the activated primary T cells resulted in the efficient surface expression of VHH- and scFv-based CARs. In this experiment, we used five different MOI for the lentiviral transduction step. We considered MOI of 1, 5, 10, 15, and 25 for T cell transduction to determine the optimized MOI which could result in the lowest rate of cytotoxicity and highest rate of lentiviral transduction and CAR surface expression. An MOI of 10 was selected as the optimized MOI

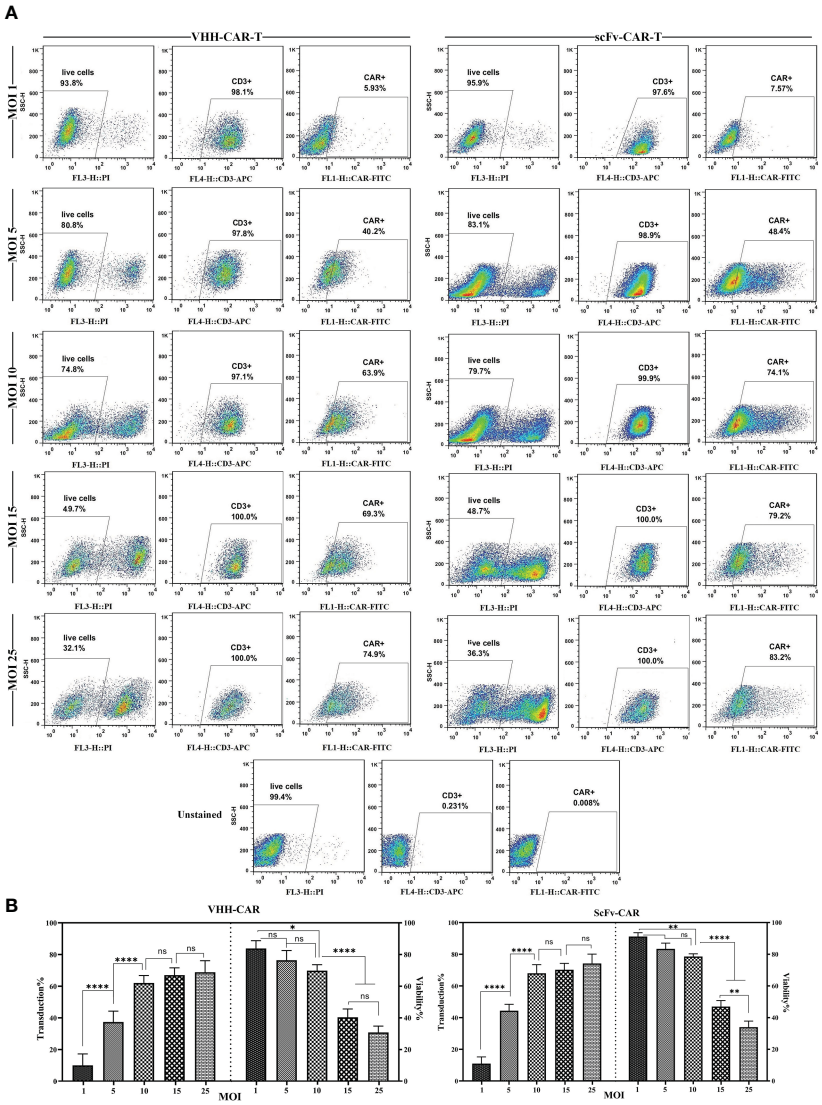

FIGURE 2
Effects of different MOI on the viability and transduction rate of T cells. **(A)** Flow cytometry plots of the effects of different MOI (1, 5, 10, 15, and 25) on the viability and transduction rate of T cells. **(B)** Statistical analyses of how different MOI result in different viability and transduction rates of T cell in the process of CAR-T production. Data are expressed as the mean ± SD. *p < 0.05, **p < 0.01, and ****p < 0.0001; ns, not significant. Each experiment was carried out in triplicate (n = 3).

for the transduction procedures in this study. Flow cytometry was used to evaluate the efficacy of lentiviral transduction by analyzing the surface expression of different CARs. According to the flow cytometry plots presented in Figure 3, around 59% of the cells in the VHH-CAR-T group were positive for the expression of VHH-based CARs, whereas about 60% of the cells in the scFv-CAR-T group were positive for the expression of scFv-based CARs.

3.4 VHH-CAR-Ts exhibited target antigen-dependent expansion upon co-cultivation with CD19-positive cell lines

Durable disease remission in cancer patients receiving CAR-T therapy is highly dependent on the *in vivo* persistence and expansion of the adoptively transferred CAR-Ts (23). The cytolytic activity or cytokine release of CAR-Ts does not necessarily guarantee that CAR-Ts can have efficient proliferation upon encountering their target cells. Herein, CAR-negative T cells, VHH-CAR-Ts, and scFv-CAR-Ts were labeled with CFSE before co-cultivation with K562, Raji, and Ramos target cells. Of note, the effector cells were not supplemented with IL-2 to be able to assess target antigen-dependent effector cell expansion. 72 hours after co-cultivation, the proportion of CAR-Ts divided was assessed using flow cytometry. According to the results presented in Figures 4A, B, VHH-CAR-Ts and scFv-CAR-Ts exhibited a comparable proportion of cells divided over 72 hours of co-cultivation with Raji and Ramos target cells in comparison with the same effector cells co-cultured with K562 cells. Moreover, CAR-negative control cells demonstrated significantly lower expansion rates after 72 hours of co-cultivation with K562, Raji, and Ramos target cells in comparison with VHH-CAR-Ts and scFv-CAR-Ts (p value < 0.0001 for both groups).

3.5 VHH-CAR-Ts meditated selective cytolytic reactions against CD19-positive cell line upon co-cultivation

Effector cells (VHH-CAR-Ts and scFv-CAR-Ts, and CAR-negative control T cells) were co-cultured with target cells at three different E:T ratios (3:1, 6:1, and 10:1). Target cells included K562 cells (as CD19-negative cells), and Raji and Ramos cells as (CD19-positive cells). The target-specific cytotoxic activity of the effector cells was assessed after 16 hours of co-cultivation with the target cells. According to the results presented in Figures 5A, B, all three types of effector cells demonstrated almost similar rates of cytotoxicity against K562 cells at each of the E:T ratios. In the Raji group, VHH-CAR-Ts mediated a rate of around 20, 55, and 69% damaged target cells at 3:1, 6:1, and 10:1 E:T ratios, respectively. In the same group, scFv-CAR-Ts mediated similar cytotoxicity rates with around 27, 66, and 79% damaged target cells at 3:1, 6:1, and 10:1 E:T ratios, respectively. These number were at least two-fold higher than what was observed in the CAR-negative control cells group except for VHH-CAR-Ts at 3:1 E:T ratio.

In the Ramos group, all three types of effector cells demonstrated cytotoxic behavior similar to the Raji group. In detail, VHH-CAR-Ts mediated a rate of around 22, 40, and 78% damaged target cells at 3:1, 6:1, and 10:1 E:T ratios, respectively. Furthermore, scFv-CAR-Ts mediated similar cytotoxicity rates with around 32, 42, and 79% damaged target cells at 3:1, 6:1, and 10:1 E:T ratios, respectively. Similar to the Raji group, these numbers were almost two-fold higher

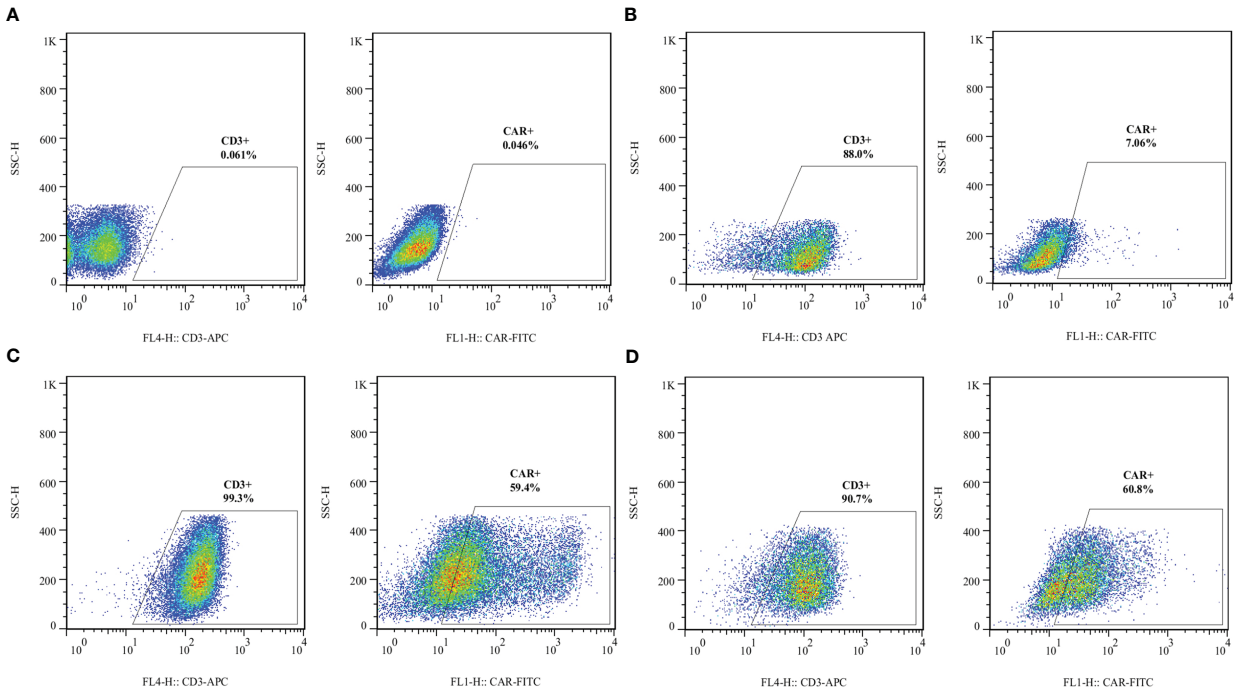

FIGURE 3
Transduction efficacy of the developed CAR-Ts as assessed by staining surface-expressed CARs in different experimental groups. **(A)** Unstained. **(B)** Non-transduced T cells. **(C)** The expression rate of VHH-based CARs on the surface of VHH-CAR-Ts. **(D)** The expression rate of scFv-based CARs on the surface of scFv-CAR-Ts. Each experiment was carried out in triplicate (n = 3).

10.3389/fimmu.2023.1063838

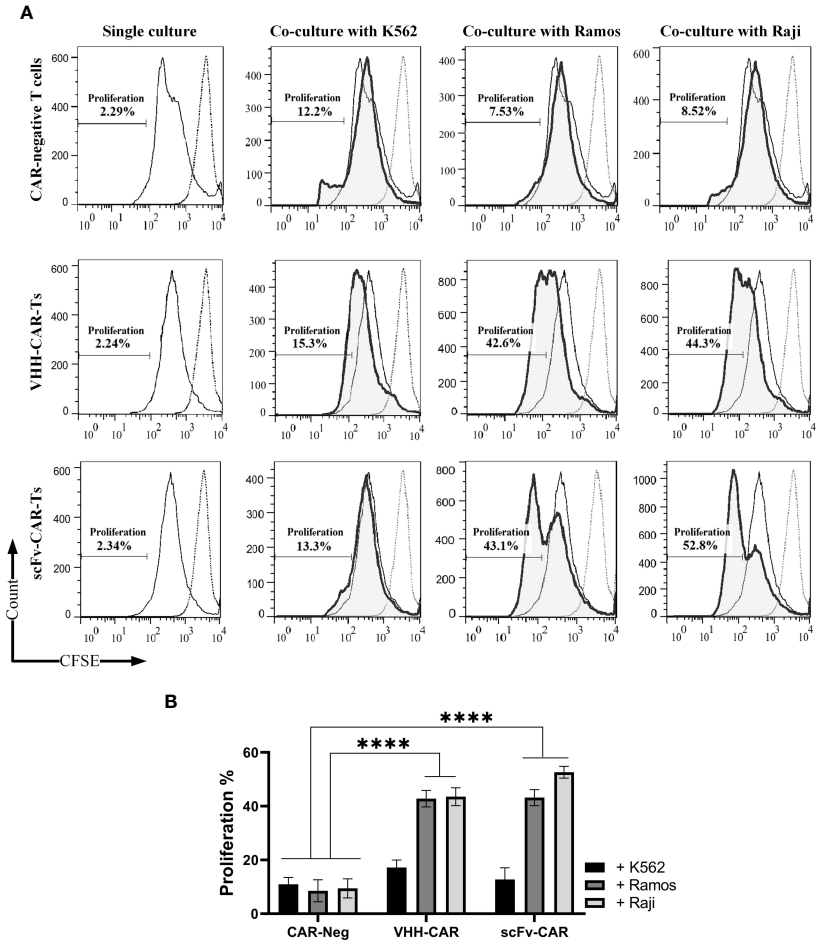

FIGURE 4
Target antigen-specific activation and expansion of CAR-Ts. **(A)** Flow cytometry assessment of CFSE in CAR-negative T cells, VHH-CAR-Ts, and scFv-CAR-Ts upon their co-cultivation with the CD19-positive target cell lines Ramos and Raji and the CD19-negative cell line K562. **(B)** Statistical analysis between the expansion rate of CAR-negative T cells, VHH-CAR-Ts, and scFv-CAR-Ts upon their co-cultivation with the CD19-positive target cell lines Ramos and Raji and the CD19-negative cell line K562. Data are expressed as the mean ± SD. ****p < 0.0001. Each experiment was carried out in triplicate (n = 3).

than what was observed in the CAR-negative control cells group except for VHH-CAR-Ts at 3:1 E:T ratio. Overall, it can be stated that scFv-CAR-Ts mediated slightly stronger target-specific cytotoxicity than VHH-CAR-Ts against Raji and Ramos target cells. Of note, it was also discovered that efficient antitumor activity of CAR-Ts could be achieved at higher E:T ratios.

3.6 VHH-CAR-Ts secreted almost similar levels of IFN-γ, IL-2, and TNF-α upon encountering CD19-positive cell lines as their FMC63-based counterparts

Target-antigen dependent cytokine production and secretion of VHH-CAR-Ts, scFv-CAR-Ts, and CAR-negative control cells were measured using ELISA after 24 hours of co-cultivation with K562, Raji, and Ramos target cells at 6:1 E:T ratio. As presented in Figure 6, separate analyses showed that both scFv-CAR-Ts and VHH-CAR-Ts secreted higher levels of human IFN-γ, human IL-2, and human TNF-α in comparison with CAR-negative T cells upon co-cultivation with the CD19-positive Raji and Ramos cells but not upon co-cultivation with the CD19-negative K562 cells or during single culture of the effector cells. The secretion of human IFN-γ, human IL-2, and human TNF-α by VHH-CAR-Ts upon co-cultivation with Raji and Ramos cells were significantly higher than their levels upon co-cultivation with K562 cells or during single culture of the VHH-CAR-Ts as negative control (p value < 0.0001, for all of the groups). The same pattern was observed in regards to the secretion of IFN-γ, IL-2, and TNF-α by scFv-CAR-Ts upon co-cultivation with Raji, Ramos, and K562 cells or during their single culture as negative control (p value < 0.0001, for all of the groups). Moreover, VHH-CAR-Ts and scFv-CAR-Ts secreted almost similar levels of IFN-γ, IL-2, and TNF-α while co-cultured with the CD19-negative cell line K562 and the CD19-positive cell lines Raji and Ramos. This could accentuate the fact that VHH-CAR-Ts can be as potent as scFv-CAR-Ts in terms of secreting certain proinflammatory cytokines in response to the presence of CD19-positive cell lines.

4 Discussion

CAR-T therapy has been considered a revolution in the treatment of patients with certain hematologic malignancies. B-ALL, DLBCL,

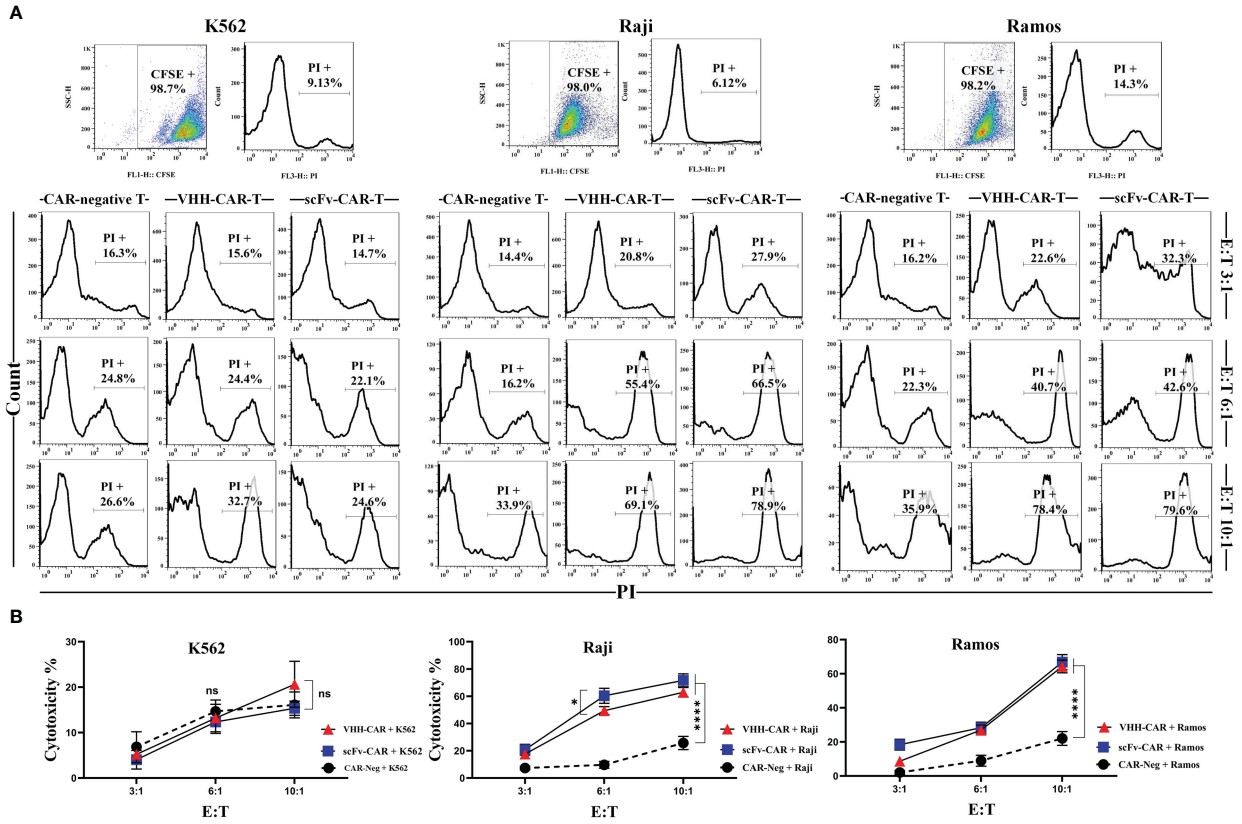

FIGURE 5
Cytotoxicity of CAR-Ts against the CD19-positive target cell lines Ramos and Raji and the CD19-negative cell line K562. **(A)** Flow cytometry assessment of PI staining in K562, Raji, and Ramos target cells after co-cultivation with CAR-negative T cells, VHH-CAR-Ts, and scFv-CAR-Ts at three different E:T ratios (3:1, 6:1, and 10:1). Each pair of dot-plot and histogram relating to any of the target cell lines at the upper panel of the figure represents their CFSE signal level and viability, respectively, before co-cultivation. **(B)** The linear plot of the cytotoxicity rate of CAR-negative T cells, VHH-CAR-Ts, and scFv-CAR-Ts against the CD19-negative cell line K562 and the CD19-positive target cell lines Raji and Ramos. Data are expressed as the mean ± SD. *p < 0.05 and ****p < 0.0001; ns, not significant. Each experiment was carried out in triplicate (n = 3).

FL, MCL, and MM patients are now the beneficiaries of this cancer treatment modality that is itself a result of intricate protein engineering and cancer immunotherapy. Since 2017 that the first CAR-T product was granted approval for medical use by the US FDA, numerous clinical trials have started assessing the antitumor efficacy and safety of this treatment method for patient with different oncological and immunological indications. Among those CAR-T therapy clinical trials that aim to investigate such products for the treatment of patients with blood-based cancer, CD19, CD20, CD22, and BCMA are the most frequent target antigens. In this study, we constructed a CD19-redirected CAR whose targeting domain was based on a VHH. Currently, most of the CAR-Ts being assessed in clinical trials harbor scFvs as their targeting domains. The light chain (V_L) and heavy chain (V_H) of an scFv are fused together by the means of a flexible linker. Due to the fact that scFvs are recombinant fragments derived from full-length mAbs, there have been reports of their inherent tendency to aggregate on the surface of CAR-Ts (24–26). This occurrence, termed "*tonic signaling*", leads to the antigen-independent activation and downstream singling of CAR-Ts, resulting in their exhaustion (24–26). For instance, Landoni et al. conducted an experiment to modify the amino acid sequences of the frameworks regions of CAR targeting domains to overcome the issue of CAR tonic signaling (26). Tonic signaling debilitates the antitumor efficacy of the infused CAR-T cells, leaving room for disease progression (23). As a solution, single-domain antibodies could be applied as the antigen-recognition domain of CAR constructs, since there have not been any reports regarding the tonic signaling of VHH-based CAR-Ts. However, broader investigations are warranted in this regard to clearly assess whether VHH-based CAR constructs tend to aggregate on the surface of CAR-Ts to mediate tonic signaling. This topic could be a direction for future research.

Most of the antigen-recognition fragments of CAR-Ts are derived from animal-origin antibodies which might be considered immunogenic while administered to human subjects (23, 27, 28). Several investigations have reported anaphylaxis in patients receiving CAR-T products whose targeting domains were based on murine scFvs (27, 28). Such reactions result in the production of neutralizing antibodies in the body of the recipients, impairing the antitumor efficacy of the infused CAR-Ts and the consequent abrogation of all CAR-T-related therapeutic benefit as a result of their elimination from circulation (23, 27, 28). To overcome this issue, scientists proposed the strategy of humanizing such CAR targeting domains for the generation of humanized CAR-Ts or using targeting domains derived from fully-human mAbs (23, 29–32). To date, several humanized CAR-Ts are being assessed for their safety and antitumor potential in various clinical trials (NCT02782351,

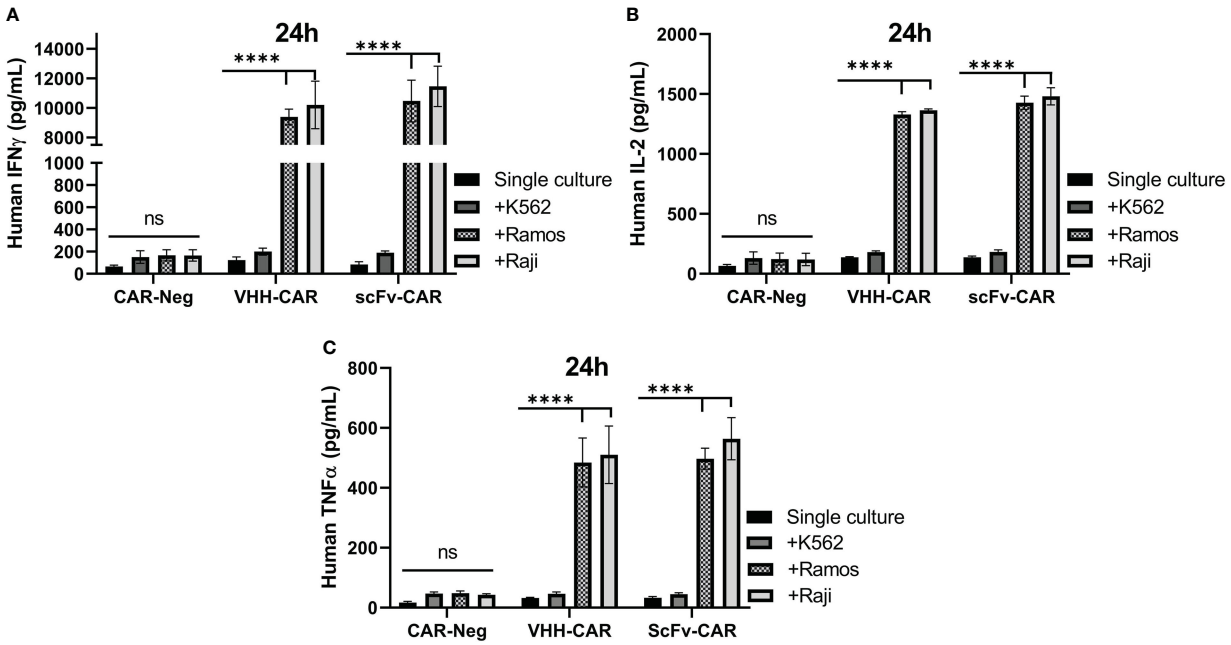

FIGURE 6
The cytokine production and secretion of CAR-negative T cells, VHH-CAR-Ts, and scFv-CAR-Ts upon their co-cultivation with the CD19+ target cell lines Ramos and Raji and the CD19- cell line K562 at an E:T ratio of 1:1. **(A)** Human INF-γ. **(B)** Human IL-2. **(C)** Human TNF-α. Data are expressed as the mean ± SD. ****p < 0.0001; ns, not significant. Each experiment was carried out in triplicate (n = 3).

ChiCTR1800017401, etc.) (18, 23, 29–31). Since the antigen-recognition domain of our VHH-CAR-Ts was derived from a camelid heavy-chain-only antibody, the issue of immunogenicity might be one of the limitations of this study which warrants further investigations.

Aside from the CD19 antigen, VHH-based CAR-Ts could also be used for the simultaneous targeting of other hematologic malignancy-associated target antigens such as CD20, CD22, CD123, CD30, etc (17, 20). Of note, two VHHs could be fused and engineered into the construct of any given CAR to enable CAR-Ts to target two different antigens or two different epitopes of a single antigen. In particular, our laboratory experience demonstrated that oligoclonal CAR-Ts, equipped with oligoclonal anti-HER2 nanobodies, exhibit higher proliferation, cytokine secretion, and tumoricidal capacity in comparison with CAR-Ts harboring each of the single nanobodies that constitute the oligoclonal CAR (33). To date, several clinical investigations are assessing the safety and antitumor efficacy of CD19/CD20- or CD19/CD22-redirected CAR-Ts for the treatment of individuals with blood-based cancers (NCT03233854, NCT03019055, and NCT03196830). The importance of such applicability is accentuated in the case of CD19 downregulation or loss as reported by various recent investigations (34–36). As accumulating evidence suggests, malignant cells undertake intricate mechanisms to escape immune surveillance (34–36). Such mechanisms entail alternative splicing of the target antigen (such as CD19) recognized by CAR-Ts in a way that the epitope recognized by the targeting domain is no longer present in the target antigen (35, 36). In such cases, a CAR-T product equipped with a different targeting domain whose epitope is still present in the alternatively-spliced target antigen should be taken into consideration (34). This occurrence further highlights the importance of having different CD19-redirected CAR-T products, so that patients with CD19-positive malignancies can still continue to benefit from this treatment modality as long as they have not experienced CD19 loss. In this regard, a pilot study was conducted (NCT02975687) to assess the safety and feasibility of CAR-Ts that target a different CD19 epitope, rather than that recognized by FMC63, in pediatric and adult R/R B-ALL patients (34). The results demonstrated that 18 out of 20 patients (90%) achieved complete remission (CR)/incomplete count recovery (CRi) within 28 days, thus highlighting the fact that the antileukemic potential of these CAR-Ts can be as satisfactory as those of conventional CD19-redirected CAR-T products (34).

scFv development requires the use of synthetic linker peptides for fusing V_H and V_L domains (37). The presence of such linkers in the construct of scFvs can be immunogenic and may trigger host immunological defensive reactions through the production of neutralizing antibodies (35, 38). In the case of nanobodies, the absence of these synthetic linker peptides leaves no room for the mediation of host immune responses. Similarly, VHH-based CAR-Ts have been investigated in various clinical stages and there have not been any reports regarding their immunogenicity and post-infusion production of neutralizing antibodies against them. Also, limited studies have indicated that nanobodies might be immunogenic in a negligible way when used as the targeting domain of CAR-Ts redirected against HER2 (39). It is worth mentioning that some researchers have pointed out the fact that nanobodies are more well-tolerated and less immunogenic for in-human use since their sequences are highly similar to those of human V_H (40). Another

structural difference between scFvs and VHHs is the long CDR3 of nanobodies enabling them to bind specific epitopes that are not accessible to human or mouse mAbs, or scFvs (41–43). Additionally, the humanization process of nanobodies is considered to be much simpler than that of scFvs due to the fewer amino acid residue substitutions required for the humanization of nanobodies (44). Such fewer number amino acid residue substitutions can reduce the risk of affinity loss after humanization (18, 23). Also, unlike nanobodies, the large DNA fragments of scFvs can adversely affect the efficiency of transfection and viral packaging in the process of CAR-T generation (45–47).

Moreover, studies have also reported mutations in the genes encoding the target antigens which lead to antigen loss, to overcome which CAR-Ts should be programmed to target different antigen(s) (35). In addition to antigen loss, Ruella et al. have reported a rare incidence in the manufacturing process of CD19-redirected CAR-Ts which rendered a patient resistant to CD19-based CAR-T products, despite the consistent expression of this antigen (48). In detail, a single leukemic cell was accidentally transduced in the process of CAR-T manufacturing which resulted in the expression of CAR molecules on its surface, and their consequent engagement with CD19 on the surface of the malignant cell (48). Following administration into the patient, this single leukemic cell expanded and resulted in a vast population of CD19-positive leukemic cells resistant to CD19-redirected CAR-T products (48). In such cases, different target antigens should be taken into consideration. According to the findings of a Phase I dose-escalation study (NCT04088890), three patients with large B-cell lymphoma achieved CR following treatment with CD22-redirected CAR-Ts after they experienced relapse from their previous treatment with CD19-redirected CAR-Ts (49).

One of the benefits of developing potent CD19-redirected CAR-T products is that they can be applied for the eradication of a wide range of hematologic malignancies owing to the constitutive expression of CD19. For instance, Novartis' *Kymriah* has been granted permission by the US FDA as a third-line treatment for B-ALL, DLBCL, and FL. Aside from the mentioned oncological indications, CD19-redirected CAR-T products are currently being assessed against various CD19-positive hematologic cancers. As an example, Juno Therapeutics' *JCAR017* is currently being evaluated in an open-label Phase I/II clinical trial (NCT03331198) for the treatment of 259 individuals with R/R chronic lymphocytic leukemia (CLL) or small lymphocytic lymphoma (SLL). According to a study by Xue et al., a patient with R/R classical Hodgkin's lymphoma (cHL) was treated with low doses and repeated infusions of CD19- and CD30-redirected CAR-Ts which resulted in the prolonged progression-free survival (PFS) of the patients without any severe treatment-related toxicities (50). Xue and colleagues further highlighted the importance of combination CAR-T therapy for the treatment of cHL (50). CD19 might also be considered a suitable target antigen in particular subtypes of MM cells, despite being absent from the dominant MM cells (51). According to a clinical study by Garfall and colleagues (NCT02135406), 2 out of 10 patients (20%) with R/R MM underwent CD19-redirected CAR-T therapy (CLT019) following autologous stem cell transplantation (ASCT) and melphalan-based salvage therapy, and experienced remarkably more prolonged PFS than when they only underwent ASCT as prior therapy (479 versus 181 days for one patient, and 249 versus 127 days for the other, respectively) (51). Based on the findings of a clinical investigation by Zhou et al., CD19 might also be considered as a suitable target antigen even for the treatment of patients with Burkitt's lymphoma (52). In detail, 3 out of 6 patients with Burkitt's lymphoma, who underwent CD19- and CD22-redirected CAR-T therapy, achieved an objective response (two partial responses; one CR) (52). Clinical investigations, such as those exemplified here, accentuate the suitability of CD19 as a target antigen in a wide range of blood-based cancers alongside the applicability of CD19-redirected CAR-T products as possible treatment options.

VHH-based CAR-Ts were first introduced as alternatives to overcome the limitations of scFv-based CAR-Ts. In the early days, concerns were raised regarding the effectiveness of VHH-based CAR-Ts (53). So far, numerous studies have demonstrated that VHH-based CAR-Ts are capable of mediating specific target antigen-dependent cytotoxicity against various types of malignancies both in preclinical and clinical investigations (53, 54). In detail, the antitumor activity and efficient effector function of VHH-based CAR-Ts have been highlighted in both hematologic malignancies and solid tumors (20). To our knowledge, this is the first study comparing the antitumor activity of VHH-based CD19-redirected CAR-Ts with their FMC63-based counterparts. To date, other hematologic malignancy target antigens such as CD20, CD7, CD33, CD38, and BCMA have also been targeted using VHH-based CAR-Ts, and it has been demonstrated that these engineered effector cells can mediate target antigen-dependent antitumor activity and efficient cytokine secretion, and they have also been proven to be well-tolerated and capable of mediating satisfactory CR rates in clinical studies (53–59). Our *in vitro* results of the antitumor activity of VHH-CAR-Ts are consistent with these clinical trials even though some of the mentioned studies target non-B cell-specific target antigens (20). It is also worth mentioning that *ciltacabtagene autoleucel* (also known as *cilta-cel* or *CARVYKTI*) is a CAR-T product based on two single-domain antibodies which was approved on February 28, 2022 by the US FDA for the treatment of certain adult patients with R/R MM [12]. This was the first single-domain antibody-based CAR-T product approved for medical use in the US. Though this product targets BCMA, such favorable clinical approvals can highlight the potential of single-domain antibody-based CAR-Ts, at least in hematologic malignancies.

5 Conclusion

CAR-T therapy has proven to be a highly effective treatment modality for certain patients with particular blood cancers who have failed to respond to prior conventional therapies. To date, four CD19-redirected CAR-T products have been granted the US FDA approval for the treatment of certain patients, which highlights the potential applicability of this cancer treatment modality and the suitability of CD19 as a target antigen for the treatment of CD19-positive malignancies. In this study, we developed and characterized VHH-based CD19-redirected CAR-Ts, and demonstrated that these engineered effector cells could be as potent as their FMC63 scFv-

based counterparts *in vitro*. Future studies will be focused on assessing the safety and antitumor efficacy of our VHH-CAR-Ts in xenograft animal models to further validate the findings of this investigation.

Data availability statement

The original contributions presented in the study are included in the article/supplementary material. Further inquiries can be directed to the corresponding author.

Ethics statement

The studies involving human participants were reviewed and approved by Tarbiat Modares University Research Ethics Committee. The patients/participants provided their written informed consent to participate in this study.

Author contributions

FN: Data curation, Formal analysis, Investigation, Methodology, Project administration, Validation, Visualization, Writing - original draft, Writing - Review and Editing. PSK: Data curation, Formal analysis, Investigation, Methodology, Validation, Visualization, Writing - original draft, Writing - Review and Editing. FR: Conceptualization, Data curation, Formal analysis, Funding acquisition, Methodology, Project administration, Resources, Software, Supervision, Validation. All authors contributed to the article and approved the submitted version.

Acknowledgments

This work was partly supported by the National Institute for Medical Research Development (NIMAD) [Grant No. 984179] and by the Faculty of Medical Sciences, Tarbiat Modares University, Tehran, Iran.

Conflict of interest

The authors declare that the research was conducted in the absence of any commercial or financial relationships that could be construed as a potential conflict of interest.

Publisher's note

References

1. Safarzadeh Kozani P, Safarzadeh Kozani P, Rahbarizadeh F. CAR-T cell therapy in T-cell malignancies: Is success a low-hanging fruit? *Stem Cell Res Ther* (2021) 12:527. doi: 10.1186/s13287-021-02595-0

2. Safarzadeh Kozani P, Safarzadeh Kozani P, Rahbarizadeh F. CAR T cells redirected against the tumor-specific glycoforms of antigens: Can low sugar antigens guarantee a sweet success? *Front Med* (2022) 16:322–38. doi: 10.1007/s11684-021-0901-2

3. Bouchkouj N, Kasamon YL, de Claro RA, George B, Lin X, Lee S, et al. FDA Approval summary: Axicabtagene ciloleucel for relapsed or refractory large b-cell lymphoma. *Clin Cancer Res* (2019) 25:1702–8. doi: 10.1158/1078-0432.Ccr-18-2743

4. Mullard A. FDA Approves first BCMA-targeted CAR-T cell therapy. *Nat Rev Drug Discovery* (2021) 20:332. doi: 10.1038/d41573-021-00063-1

5. Voelker R. CAR-T therapy is approved for mantle cell lymphoma. *JAMA* (2020) 324:832. doi: 10.1001/jama.2020.15456

6. Mullard A. FDA Approves first CAR T therapy. *Nat Rev Drug Discovery* (2017) 16:669. doi: 10.1038/nrd.2017.196

7. Mullard A. FDA Approves fourth CAR-T cell therapy. *Nat Rev Drug Discovery* (2021) 20:166. doi: 10.1038/d41573-021-00031-9

8. FDA Approves second CAR T-cell therapy. *Cancer Discovery* (2018) 8:5–6. doi: 10.1158/2159-8290.Cd-nb2017-155

9. Prasad V. Immunotherapy: Tisagenlecleucel - the first approved CAR-t-cell therapy: Implications for payers and policy makers. *Nat Rev Clin Oncol* (2018) 15:11–2. doi: 10.1038/nrclinonc.2017.156

10. Mullard A. FDA Approves second BCMA-targeted CAR-T cell therapy. *Nat Rev Drug Discovery* (2022) 21:249. doi: 10.1038/d41573-022-00048-8

11. Schuster SJ, Bishop MR, Tam CS, Waller EK, Borchmann P, McGuirk JP, et al. Tisagenlecleucel in adult relapsed or refractory diffuse Large b-cell lymphoma. *New Engl J Med* (2018) 380:45–56. doi: 10.1056/NEJMoa1804980

12. Fowler NH, Dickinson M, Dreyling M, Martinez-Lopez J, Kolstad A, Butler J, et al. Tisagenlecleucel in adult relapsed or refractory follicular lymphoma: The phase 2 ELARA trial. *Nat Med* (2022) 28:325–32. doi: 10.1038/s41591-021-01622-0

13. Jacobson CA, Chavez JC, Sehgal AR, William BM, Munoz J, Salles G, et al. Axicabtagene ciloleucel in relapsed or refractory indolent non-Hodgkin lymphoma (ZUMA-5): A single-arm, multicentre, phase 2 trial. *Lancet Oncol* (2022) 23:91–103. doi: 10.1016/s1470-2045(21)00591-x

14. Frey NV. Approval of brexucabtagene autoleucel for adults with relapsed and refractory acute lymphocytic leukemia. *Blood* (2022) 140:11–5. doi: 10.1182/blood.2021014892

15. Nasiri F, Kazemi M, Mirarefin SMJ, Mahboubi Kancha M, Ahmadi Najafabadi M, Salem F, et al. CAR-T cell therapy in triple-negative breast cancer: Hunting the invisible devil. *Front Immunol* (2022) 13:1018786. doi: 10.3389/fimmu.2022.1018786

16. Safarzadeh Kozani P, Safarzadeh Kozani P, Ahmadi Najafabadi M, Yousefi F, Mirarefin SMJ, Rahbarizadeh F. Recent advances in solid tumor CAR-T cell therapy: Driving tumor cells from hero to zero? *Front Immunol* (2022) 13:795164. doi: 10.3389/fimmu.2022.795164

17. Safarzadeh Kozani P, Safarzadeh Kozani P, Rahbarizadeh F. Novel antigens of CAR T cell therapy: New roads; old destination. *Trans Oncol* (2021) 14:101079. doi: 10.1016/j.tranon.2021.101079

18. Safarzadeh Kozani P, Safarzadeh Kozani P, O'Connor RS. Humanized chimeric antigen receptor (CAR) T cells. *J Cancer Immunol (Wilmington)* (2021) 3:183–7.

19. Safarzadeh Kozani P, Safarzadeh Kozani P, Rahbarizadeh F. Optimizing the clinical impact of CAR-T cell therapy in b-cell acute lymphoblastic leukemia: Looking back while moving forward. *Front Immunol* (2021) 12:765097. doi: 10.3389/fimmu.2021.765097

20. Safarzadeh Kozani P, Naseri A, Mirarefin SMJ, Salem F, Nikbakht M, Evazi Bakhshi S, et al. Nanobody-based CAR-T cells for cancer immunotherapy. *biomark Res* (2022) 10:24. doi: 10.1186/s40364-022-00371-7

21. Banihashemi SR, Hosseini AZ, Rahbarizadeh F, Ahmadvand D. Development of specific nanobodies (VHH) for CD19 immuno-targeting of human b-lymphocytes. *Iran J Basic Med Sci* (2018) 21:455–64. doi: 10.22038/ijbms.2018.26778.6557

22. Fulcher D, Wong S. Carboxyfluorescein succinimidyl ester-based proliferative assays for assessment of T cell function in the diagnostic laboratory. *Immunol Cell Biol* (1999) 77:559–64. doi: 10.1046/j.1440-1711.1999.00870.x

23. Safarzadeh Kozani P, Safarzadeh Kozani P, O'Connor RS. In like a lamb; out like a lion: Marching CAR T cells toward enhanced efficacy in b-ALL. *Mol Cancer Ther* (2021) 20:1223–33. doi: 10.1158/1535-7163.Mct-20-1089

24. Ajina A, Maher J. Strategies to address chimeric antigen receptor tonic signaling. *Mol Cancer Ther* (2018) 17:1795–815. doi: 10.1158/1535-7163.Mct-17-1097

25. Calderon H, Mamonkin M, Guedan S. Analysis of CAR-mediated tonic signaling. *Methods Mol Biol* (2020) 2086:223–36. doi: 10.1007/978-1-0716-0146-4_17

26. Landoni E, Fucá G, Wang J, Chirasani VR, Yao Z, Dukhovlinova E, et al. Modifications to the framework regions eliminate chimeric antigen receptor tonic signaling. *Cancer Immunol Res* (2021) 9:441–53. doi: 10.1158/2326-6066.Cir-20-0451

27. Lamers CH, Willemsen R, van Elzakker P, van Steenbergen-Langeveld S, Broertjes M, Oosterwijk-Wakka J, et al. Immune responses to transgene and retroviral vector in patients treated with ex vivo-engineered T cells. *Blood* (2011) 117:72–82. doi: 10.1182/blood-2010-07-294520

28. Turtle CJ, Hanafi LA, Berger C, Gooley TA, Cherian S, Hudecek M, et al. CD19 CAR-T cells of defined CD4+:CD8+ composition in adult b cell ALL patients. *J Clin Invest* (2016) 126:2123–38. doi: 10.1172/jci85309

29. Zhao Y, Liu Z, Wang X, Wu H, Zhang J, Yang J, et al. Treatment with humanized selective CD19CAR-T cells shows efficacy in highly treated b-ALL patients who have relapsed after receiving murine-based CD19CAR-T therapies. *Clin Cancer Res* (2019) 25:5595–607. doi: 10.1158/1078-0432.Ccr-19-0916

30. Cao J, Cheng H, Shi M, Wang G, Chen W, Qi K, et al. Humanized CD19-specific chimeric antigen-receptor T-cells in 2 adults with newly diagnosed b-cell acute lymphoblastic leukemia. *Leukemia* (2019) 33:2751–3. doi: 10.1038/s41375-019-0516-7

31. Cao J, Wang G, Cheng H, Wei C, Qi K, Sang W, et al. Potent anti-leukemia activities of humanized CD19-targeted chimeric antigen receptor T (CAR-T) cells in patients with relapsed/refractory acute lymphoblastic leukemia. *Am J Hematol* (2018) 93:851–8. doi: 10.1002/ajh.25108

32. Shams N, Khoshtinat Nikkhoi S, Gu Z, Rahbarizadeh F. Isolation and characterization of human anti-CD20 single-chain variable fragment (scFv) from a naive human scFv library. *Med Oncol* (2022) 39:177. doi: 10.1007/s12032-022-01757-1

33. Jamnani FR, Rahbarizadeh F, Shokrgozar MA, Mahboudi F, Ahmadvand D, Sharifzadeh Z, et al. T Cells expressing VHH-directed oligoclonal chimeric HER2 antigen receptors: Towards tumor-directed oligoclonal T cell therapy. *Biochim Biophys Acta* (2014) 1840:378–86. doi: 10.1016/j.bbagen.2013.09.029

34. Gu R, Liu F, Zou D, Xu Y, Lu Y, Liu B, et al. Efficacy and safety of CD19 CAR T constructed with a new anti-CD19 chimeric antigen receptor in relapsed or refractory acute lymphoblastic leukemia. *J Hematol Oncol* (2020) 13:122. doi: 10.1186/s13045-020-00953-8

35. Shah NN, Fry TJ. Mechanisms of resistance to CAR T cell therapy. *Nat Rev Clin Oncol* (2019) 16:372–85. doi: 10.1038/s41571-019-0184-6

36. Fischer J, Paret C, El Malki K, Alt F, Wingerter A, Neu MA, et al. CD19 isoforms enabling resistance to CART-19 immunotherapy are expressed in b-ALL patients at initial diagnosis. *J Immunother* (2017) 40:187–95. doi: 10.1097/cji.0000000000000169

37. Völkel T, Korn T, Bach M, Müller R, Kontermann RE. Optimized linker sequences for the expression of monomeric and dimeric bispecific single-chain diabodies. *Protein Eng* (2001) 14:815–23. doi: 10.1093/protein/14.10.815

38. Gorovits B, Koren E. Immunogenicity of chimeric antigen receptor T-cell therapeutics. *BioDrugs* (2019) 33:275–84. doi: 10.1007/s40259-019-00354-5

39. Ackaert C, Smiejkowska N, Xavier C, Sterckx YGJ, Denies S, Stijlemans B, et al. Immunogenicity risk profile of nanobodies. *Front Immunol* (2021) 12:632687. doi: 10.3389/fimmu.2021.632687

40. Muyldermans S. Nanobodies: Natural single-domain antibodies. *Annu Rev Biochem* (2013) 82:775–97. doi: 10.1146/annurev-biochem-063011-092449

41. Vu KB, Ghahroudi MA, Wyns L, Muyldermans S. Comparison of llama VH sequences from conventional and heavy chain antibodies. *Mol Immunol* (1997) 34:1121–31. doi: 10.1016/s0161-5890(97)00146-6

42. Bannas P, Hambach J, Koch-Nolte F. Nanobodies and nanobody-based human heavy chain antibodies as antitumor therapeutics. *Front Immunol* (2017) 8:1603. doi: 10.3389/fimmu.2017.01603

43. Gulati S, Jin H, Masuho I, Orban T, Cai Y, Pardon E, et al. Targeting G protein-coupled receptor signaling at the G protein level with a selective nanobody inhibitor. *Nat Commun* (2018) 9:1996. doi: 10.1038/s41467-018-04432-0

44. Vincke C, Loris R, Saerens D, Martinez-Rodriguez S, Muyldermans S, Conrath K. General strategy to humanize a camelid single-domain antibody and identification of a universal humanized nanobody scaffold. *J Biol Chem* (2009) 284:3273–84. doi: 10.1074/jbc.M806889200

45. Kumar M, Keller B, Makalou N, Sutton RE. Systematic determination of the packaging limit of lentiviral vectors. *Hum Gene Ther* (2001) 12:1893–905. doi: 10.1089/104303401753153947

46. Bos TJ, De Bruyne E, Van Lint S, Heirman C, Vanderkerken K. Large Double copy vectors are functional but show a size-dependent decline in transduction efficiency. *J Biotechnol* (2010) 150:37–40. doi: 10.1016/j.jbiotec.2010.07.010

47. Yacoub N, Romanowska M, Haritonova N, Foerster J. Optimized production and concentration of lentiviral vectors containing large inserts. *J Gene Med* (2007) 9:579–84. doi: 10.1002/jgm.1052

48. Ruella M, Xu J, Barrett DM, Fraietta JA, Reich TJ, Ambrose DE, et al. Induction of resistance to chimeric antigen receptor T cell therapy by transduction of a single leukemic b cell. *Nat Med* (2018) 24:1499–503. doi: 10.1038/s41591-018-0201-9

49. Baird JH, Frank MJ, Craig J, Patel S, Spiegel JY, Sahaf B, et al. CD22-directed CAR T-cell therapy induces complete remissions in CD19-directed CAR-refractory large b-cell lymphoma. *Blood* (2021) 137:2321–5. doi: 10.1182/blood.2020009432

50. Xue Y, Lai X, Li R, Ge C, Zeng B, Li Z, et al. CD19 and CD30 CAR T-cell immunotherapy for high-risk classical hodgkin's lymphoma. *Front Oncol* (2020) 10:607362. doi: 10.3389/fonc.2020.607362

51. Garfall AL, Stadtmauer EA, Hwang WT, Lacey SF, Melenhorst JJ, Krevvata M, et al. Anti-CD19 CAR T cells with high-dose melphalan and autologous stem cell transplantation for refractory multiple myeloma. *JCI Insight* (2019) 4:e127684. doi: 10.1172/jci.insight.127684

52. Zhou X, Ge T, Li T, Huang L, Cao Y, Xiao Y, et al. CAR19/22 T cell therapy in adult refractory burkitt's lymphoma. *Cancer Immunol Immunother* (2021) 70:2379–84. doi: 10.1007/s00262-021-02850-6

53. Mo F, Duan S, Jiang X, Yang X, Hou X, Shi W, et al. Nanobody-based chimeric antigen receptor T cells designed by CRISPR/Cas9 technology for solid tumor immunotherapy. *Signal Transduction Targeted Ther* (2021) 6:80. doi: 10.1038/s41392-021-00462-1

54. De Munter S, Van Parys A, Bral L, Ingels J, Goetgeluk G, Bonte S, et al. Rapid and effective generation of nanobody based CARs using PCR and Gibson assembly. *Int J Mol Sci* (2020) 21:883. doi: 10.3390/ijms21030883

55. Xu J, Chen L-J, Yang S-S, Sun Y, Wu W, Liu Y-F, et al. Exploratory trial of a biepitopic CAR T-targeting b cell maturation antigen in relapsed/refractory multiple myeloma. *Proc Natl Acad Sci* (2019) 116:9543. doi: 10.1073/pnas.1819745116

56. Zhao WH, Liu J, Wang BY, Chen YX, Cao XM, Yang Y, et al. A phase 1, open-label study of LCAR-B38M, a chimeric antigen receptor T cell therapy directed against b cell maturation antigen, in patients with relapsed or refractory multiple myeloma. *J Hematol Oncol* (2018) 11:141. doi: 10.1186/s13045-018-0681-6

57. An N, Hou YN, Zhang QX, Li T, Zhang QL, Fang C, et al. Anti-multiple myeloma activity of nanobody-based anti-CD38 chimeric antigen receptor T cells. *Mol pharmaceutics* (2018) 15:4577–88. doi: 10.1021/acs.molpharmaceut.8b00584

58. Pan J, Tan Y, Wang G, Deng B, Ling Z, Song W, et al. Donor-derived CD7 chimeric antigen receptor T cells for T-cell acute lymphoblastic leukemia: First-in-Human, phase I trial. *J Clin Oncol* (2021) 39:3340–51. doi: 10.1200/jco.21.00389

59. Zhang M, Fu X, Meng H, Wang M, Wang Y, Zhang L, et al. A single-arm, open-label, pilot trial of autologous CD7-CAR-T cells for CD7 positive relapsed and refractory T-lymphoblastic Leukemia/Lymphoma. *Blood* (2021) 138:3829–. doi: 10.1182/blood-2021-149999

Frontiers in Immunology

Explores novel approaches and diagnoses to treat immune disorders.

The official journal of the International Union of Immunological Societies (IUIS) and the most cited in its field, leading the way for research across basic, translational and clinical immunology.

Discover the latest Research Topics

See more →

Frontiers

Avenue du Tribunal-Fédéral 34
1005 Lausanne, Switzerland
frontiersin.org

Contact us

+41 (0)21 510 17 00
frontiersin.org/about/contact